SOVIET PHYSICS

JETP

A translation of the Journal of Experimental and Theoretical Physics of the USSR.

SOVIET PHYSICS JETP VOL. 34 (7) NO. 4, pp. 541-722 October, 1958

POLARIZATION OF ELECTRONS IN BETA-DECAY

A. I. ALIKHANOV, G. P. ELISEEV, V. A. LIUBIMOV and B. V. ERSHLER

Academy of Sciences, U.S.S.R.

Submitted to JETP editor February 3, 1958

J. Exptl. Theoret. Phys. (U.S.S.R.) **34**, 785-799 (April, 1958)

In connection with the revision of the law of conservation of parity, experiments to observe the longitudinal polarization of electrons in β-decay were carried out. It was found that the β-electrons were emitted with spin opposite to the direction of motion. The degree of longitudinal polarization is consistent with the value $-v/c$.

In a short communication[1] published in JETP, experiments were described which established the longitudinal polarization of β-electrons, predicted by the theory following from the hypothesis of nonconservation of parity in weak interactions.[2]

In this article we shall describe the experimental conditions and controls in detail, and introduce corrections in the calculation of the degree of longitudinal polarization of the electrons from the experiments, since, (1) in calculating the amount that the spin was turned in crossed electric and magnetic fields, which was necessary for calculation of the expected azimuthal asymmetry, an incorrect formula was used in Ref. 1, (2) in connection with this, several simplifications and neglects were made, which influence the final result substantially at the high-energy end of the experiment, and (3) several corrections were increased. These corrections in the value of the polarization of electrons of energy near 300 kev amounted to 10 — 25%.

In order to establish the longitudinal polarization of electrons in β-decay and to measure its value, we used the azimuthal asymmetry in the single scattering of electrons at an angle near 90°. Since azimuthal asymmetry occurs only for electrons with spin component perpendicular to the direction of motion, it was necessary to change the longitudinal polarization of the electrons into a transverse one. For this purpose, a beam of electrons from a radioactive source was sent through crossed electric and magnetic fields which, while not changing the direction of the electrons in the first approximation turns the spin with respect to the direction of motion of the electrons.

DESCRIPTION OF THE APPARATUS

The apparatus consisted of an arrangement for turning the spin and an arrangement for measuring the intensities of electrons scattered at a large angle for different azimuthal angles in the range 0 — 360°. A longitudinal cross section of the apparatus is shown on Fig. 1, and, on Fig. 2, a transverse cross section of the counting part of the apparatus, where two Geiger-Müller counters acting in coincidence are placed for the registration of scattered electrons.

The arrangement for turning the spin consisted of a longitudinal electrical condenser, placed in an evacuated metal tube which, in turn, was placed between poles of a permanent magnet. The condenser was formed of two plexiglass sheets of thickness 6 mm and length 30 cm with deep notches (4 mm). The notches in the plexiglass sheets, between which there remained only cross pieces of width 3 mm, acted as traps for electrons in order to diminish the number of electrons in the beam scattered from the walls of the condenser.

A thin (10μ) aluminum foil glued on the inner surface served as facing for the condenser. The distance between the plates of the condenser was 12 ± 0.15 mm. The length of the condenser was 25 cm; however, the effective length of the electric field was somewhat greater, since the scattered

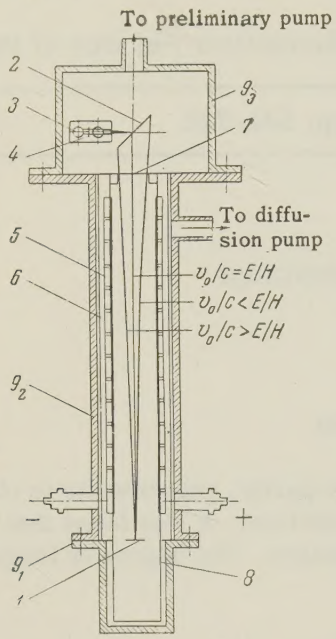

FIG. 1. Cross section of the apparatus in the plane perpendicular to the magnetic field. 1 – source, 2 – scatterer (gold), 3 – Geiger counters, 4 – absorbing filter, 5 – aluminum electrodes of the condenser (foil of 10 μ), 6 – plexiglass, 7 – collodion film (0.3 mg/cm^2), 8 – plexiglass container, $9_{1,2,3}$ – brass body.

electric field extended beyond the edges of the condenser. In addition, the length of the plexiglass sheets was 50 mm greater than the length of aluminum foil, and its surface, owing to surface conduction, acted as an extension of the surface of the condenser. This effective increase in length of the condenser lay between 0.4 and 1.4 cm.

The magnetic field was produced by a permanent magnet made from an alloy of magnico with poles of armco-iron of length 25 cm and width 6 cm. The gap between poles was equal to 4 cm. The permanent magnet was furnished with coils which made it possible to magnetize and remagnetize the magnet. The topography of the magnetic field was plotted in three dimensions; in the region traversed by the electron beam it turned out to be uniform within the limits of accuracy of the measurements (1 – 1.5%).

In order to limit the scattered magnetic field in the upper part of the apparatus where the electron scattering took place, an iron shield was mounted at a distance of 0.8 cm from the end of the condenser. Measurement of the topography of the field showed that the scattered magnetic field was well shielded and, near the scatterer, was not more than 1.5% of its value in the gap. From the curve of fall off of the magnetic field at the upper edge, it was established that the effective length of the magnetic field here was increased by 0.5 cm. At the lower edge of the magnet the scattered field was substantially more extended, dropping to half its value at a distance of 2 cm from the edge of the pole. This scattered field increased the effective length of the magnetic field by 1.5 cm. Thus, the effective length of the whole system of fields which turned the spin exceeded the geometrical dimensions of the magnet by 2 cm, i.e., was equal to 27 cm.

In the method of crossed fields in the form we were able to employ it, the electrons are not focussed and therefore a high intensity can be reached only at the expense of resolution with respect to energy. The effect of azimuthal asymmetry falls off slowly with increasing electron energy; the degree of polarization of β-electrons, according to the theory, rises slowly with energy ($\sim v/c$), the β-spectrum of heavy elements is a slowly decreasing function of electron energy and, finally, the angle of turning of the spin is also a slowly changing function. Therefore, the measurements of polarization of β-electrons were all carried out with a wide spectrum of electron energies.

Thus, the main purpose of the crossed electric and magnetic fields in our experiments, which influenced the spectral composition of the electrons falling on the scatterer only slightly, was to turn the spin. The sharp falloff of the scattering with electron energy, $\sigma \sim (pv/c)^{-2}$ was essential in determining the form of the energy spectrum of electrons which underwent scattering.

Calculation of the curves of resolution in the crossed fields by analytic means turned out to be difficult. Therefore, they were obtained by numer-

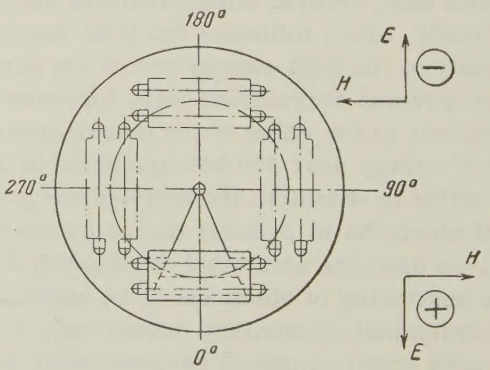

FIG. 2. Counting part of the apparatus. Electrons move out of the paper. The combinations of fields are denoted + and –.

ical calculations. Two such curves of resolution for two different values of v_0/c and values of the field, close to those used in this work, are shown on Fig. 3.

ACCURACY OF MEASUREMENT OF THE ELECTRIC AND MAGNETIC FIELDS

The electric field was measured by an electrostatic apparatus to an accuracy of 1.5%. The gap in the condenser had a tolerance of ~0.15 mm, and thus the value of the voltage of the electric field was determined to an accuracy of ~2%.

The magnetic field was measured in the usual way by a ballistic galvanometer and a coil, calibrated by use of standard mutual inductances. The error in the direct measurement of the magnetic field, that in the calibration and measurement of the ratio of the mean magnetic field to the field at the point of measurement, constituted about 3%. Thus, the overall error in the measurement of the ratio of fields E/H was ~3.5%.

SOURCE OF BETA-ELECTRONS

The source of β-electrons was in the form of a spot of uniform thickness and diameter 1 cm on an aluminimum backing of thickness 10 μ, which was attached by its edges to an aluminum ring. The ring was fixed in the container — a brass cylinder of diameter 32 mm and length 84 mm, put inside a layer of plexiglass to exclude the scattering back of electrons.

The source was Sr^{90} with an admixture of Sr^{89} made up from fragment solutions; in the course of

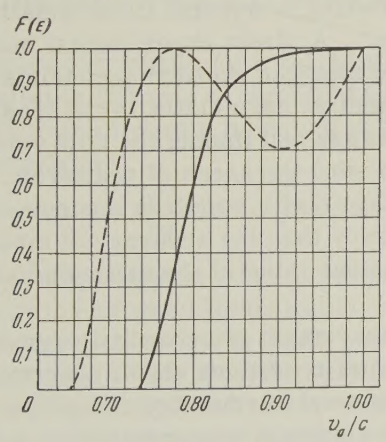

FIG. 3. Resolving power of the apparatus. F(E) is the probability of traversal of electrons of energy E through the apparatus: the continuous curve is for $v_0/c = E/H = 0.925$, the dashed one, for $v_0/c = 0.775$.

time Y^{90} was formed in the source, with an amount reaching equilibrium in almost all experiments. The mixture of Sr^{89} was 35% of that of Sr^{90}. The composition of the source was determined by the decay curve.

The electron energy spectrum of such a source is shown on Fig. 4. All of the elements making up

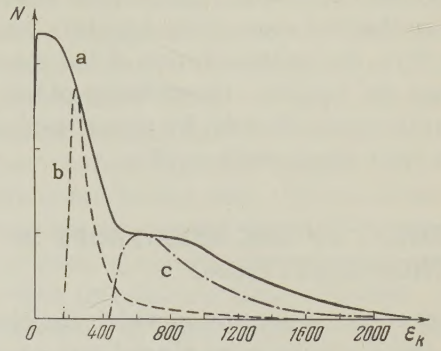

FIG. 4. Energy spectra of electrons in arbitrary units; ε_K is the kinetic energy of the electron in Kev, a is the original spectrum of the source, b is the spectrum of electrons incident on the counter in the experiment with energy 300 Kev, c, the same, at energy 750 Kev.

the source have unique transitions (that is, their β-transitions all have $\Delta j = 2$ and change of parity). For unique transitions, one can expect that the degree of electron polarization is close[3] to v/c.

The source thickness plays an essential role in such measurements. Longitudinally polarized electrons traversing layers of the source material and undergoing multiple scattering in them, are depolarized, since the electrons change their direction of flight in scattering, whereas the spin retains its direction. The correction for depolarization was introduced into the calculation of the azimuthal symmetry through the factor $\cos\theta \approx 1 - \frac{1}{2}\theta^2$, where θ^2 is the mean square angle of multiple scattering.

In order to calculate the quantity $\overline{\theta^2}$, we employed the formula given by Bethe and Ashkin[4]

$$\overline{\theta^2} = 0.157 \frac{Z(Z^2+1)t}{A(pv/c)^2} \ln[1.13 \cdot 10^4 Z^{4/3} A^{-1} t],^*$$

where Z is the atomic number, A is the atomic weight, p is the momentum in Mev/c, and t is the thickness in g/cm^2.

In this work sources of two thicknesses were employed, 4 and 1.5 mg/cm^2. For both thicknesses the correction for depolarization in the source, according to the formula of Bethe and

*For calculation of the quantity $\overline{\theta^2}$ in Ref. 1, we used the formula of Rossi and Greisen $\overline{\theta^2} = \left(\frac{21.3}{pv/c}\right)^2 t'$, where p is the momentum in Mev/c, t' the thickness in $X_0 = 10$ g/cm^2). However, the formula of Rossi and Greisen is incorrect and gives values 5–7 times larger than those that follow from the formula given by Bethe and Ashkin.[4]

Ashkin, was small. It is to be expected that the depolarization depends not only on the mean thickness of the source, but also on the dimensions of the individual crystal aggregates and, in the limit, on the individual crystals. The second source was prepared so that the size of the crystals was minimal. For this, the sedimentation of the solution was carried out quickly. Observation of the source under a microscope showed, by visual estimate, that the crystal sizes were $\sim 10\,\mu$.

MEASUREMENT OF THE ANISOTROPY IN ELECTRON SCATTERING

The part of the apparatus in which the electron scatterer and counters were placed was separated from the condenser by a thin film of collodion on netting.

The electron beam traversed the film and fell on the scatterer, joined to the frame at an angle of 45° to the axis of the beam. Two selfquenching counters with windows cut out were prepared on the same frame for counting electrons in coincidence and were placed at the angle of $(90 \pm 4)°$ (and also, in one of the experiments, at 105°) to the axis of the electron beam. The vertical dimensions of the window in the counters were such that the solid angle subtended by them included only part of the scatterer and certainly did not include the frame of the scatterer. The frame of the scatterer had dimensions larger than the cross section of the beam, as was easy to ascertain by carrying out measurements with only the frame and without it at all.

The first window of the counter was covered by a film of collodion of thickness 0.5 mg/cm^2, supported by a thin net. The window between counters was covered by aluminum foils of different thicknesses, depending on the part of the electron spectrum, but was not less than $40\,\mu$ for the filtering of electrons of energy less than 50 Kev. The counters were joined through a rubber tube, which was fitted hermetically through the apparatus, to a balloon of large volume with a given mixture pressure and, thus, a constant mixture pressure was maintained in the counters, even with a small current in the vacuum.

The counters, together with the frame of the scatterer, were rotated around the axis of the beam so that the scatterer was placed in strictly the same relationship to the counters for all azimuthal angles. The scattered electrons were always counted "in traversal". As is well known, this differs from "on reflection" by the substantially fewer electrons having undergone multiple scattering.

Multiple scattering is the main obstacle to the measurement of single scattering and, correspondingly, in the measurement of azimuthal asymmetry. In the work of Alikhanian, Alkihanov and Vaisenberg[5] studying the scattering of electrons at 90°, experimental results relating to the role of multiple scattering were obtained and in the work of Artsimovich[6] an attempt to estimate this effect theoretically on the basis of these data was made. According to the data,[5] in the scattering of 680-Kev electrons at 90° "on reflection" in the interval of thickness $0.34 - 0.81$ mg/cm^2 of Au, the intensity of scattered electrons was proportioned to the thickness. That showed that the admixture of multiple scattering was small.

Starting from these data and the well known dependence $\sigma \sim (c/pv)^2$, it is possible to estimate the allowed thickness of scatterer for electrons near 300 Kev. This turned out to be close to 0.5 mg/cm^2. According to Artsimovich's criterion, at the scattering angle of 90°,

$$I = I_0 (1 + 7\overline{\theta^2})\, t,$$

where I is the intensity of scattered electrons, I_0 is the intensity of singly-scattered electrons per unit thickness of the target, t is the thickness of the scatterer and $\overline{\theta^2}$ is the mean square angle for multiple scattering. For 0.5 mg/cm^2 and energy 300 Kev, the admixture of multiple scattering, according to this criterion, is 30%. This estimate gives an upper limit for the proportion of multiple scattering, since (1) the criterion of Artsimovich is larger than the multiple scattering in heavy elements and (2) in the position "in traversal" the multiple scattering is several times smaller than "on reflection". A direct experimental means of evaluating the multiple scattering consists of measuring the azimuthal asymmetry for at least two different thicknesses and finding the true value by extrapolating to zero thickness of scatterer. This has the disadvantage that it requires measurements of greater accuracy than the accuracy of measurement of the actual value of the azimuthal asymmetry.

In the measurement of azimuthal asymmetry, the experimental conditions should guarantee no purely instrumental asymmetry and give a control on this. Such a control was provided by substituting for the scatterer consisting of a heavy element (gold) a light element (aluminum) for which the asymmetry for scattering through such an angle is an order of magnitude less. However, we considered this control insufficient, since it was difficult to carry it out in a continuous fashion. In order to substitute one scatterer for another, the apparatus

had to be opened, the vacuum destroyed, then renewed, the condenser readjusted, etc. After such changes it would not be possible to be sure that instrumental asymmetries did not occur in the apparatus which escaped observation.

In the method employed, we arranged a second independent and uninterrupted control. It is easy to see that by reversing the field we excluded all types of asymmetry except for that coming from the sign of the field. In this last case the instrumental asymmetry should show up very distinctly in the direction perpendicular to the direction of measurement of the physical asymmetry, because it is in precisely this direction in which the field deflects the particles (i.e., has a maximum effect on the beam) and in which the physical asymmetry vanishes.

This control, which was very convenient, did not, however (in the case of asymmetries coming from the fields), determine the sign and magnitude of the necessary corrections. These could be obtained only by using the control with the scatterer of a light element.

Using both control methods, we could exclude instrumental asymmetry with complete certainty.

CALCULATION OF THE EXPECTED AZIMUTHAL ASYMMETRY EFFECT AND POLARIZATION OF ELECTRONS

In calculating the expected azimuthal asymmetry, it is necessary to know the angle through which the spin of the electron was turned in the crossed fields and the dependence of the azimuthal asymmetry on the scattering angle and energy of the polarized electrons.

For a monochromatic ($v = v_0$) beam of electrons parallel to the axis of the apparatus, the angle through which the spin is turned is determined by the expression*

$$\varphi = \frac{300Hl}{p_0 e}\sqrt{1-(v/c)^2},$$

where H is the magnetic field in oersteds, l is the length of the crossed fields in cm, p is the electron momentum in ev/c; $v_0/c = E/H$, where E is the strength of the electric field.

In our experimental conditions, we are dealing with an essentially non-monochromatic and non-parallel beam. The task of calculating the rotation of the spin in this case turned out to be quite complicated, and was carried out by Ter-Martirosian (see the appendix).

Usually, the quantity entering into theoretical calculations of the magnitude of azimuthal asymmetry is the spin-component in the rest system of the electron perpendicular to the direction of motion of the electron in the laboratory system. The tables of Sherman,[7] which we used, for the value of the azimuthal asymmetry for various scattering angles and various electron energies for $Z = 80$ were calculated in this way. To calculate the turning of the spin in crossed fields, it is convenient to go to a system of coordinates moving with velocity v_0, in which the electric field vanishes. After this transformation, an expression for the rotation of the spin for an arbitrary value of v/c and angle α between the axis of the apparatus and the direction of motion of the electron was obtained, the transformation to the laboratory system was carried out, and then to the system of rest for the spin and the laboratory for the velocity.

As a result (see Appendix), a rather complicated expression was obtained for $\sin\varphi$, where φ is the angle of rotation of the spin. Neglecting terms containing the small angle α, we obtain

$$\sin\varphi = \sin\varphi_0\left\{\frac{[\{(v/v_0)-1\}+\{1-(vv_0/c^2)\}\cos\varphi_0]^2}{[1-(v^2/c^2)][1-(v_0^2/c^2)]}+\sin^2\varphi_0\right\}^{-1/2},$$

and for small φ

$$\varphi = \frac{300Hl}{pc}\frac{v_0}{v}\sqrt{1-v^2/c^2}.$$

In the formulas given (and in Table 7) one can see the magnitude of $\sin\varphi$ depends rather strongly on the energy of the electrons, in particular, for large energies. To obtain the correct value φ for v_0/c near to 1, it is necessary, as far as possible, to calculate the form of the electron spectrum accurately.* The spectrum of scattered electrons with energy near 300 Kev was determined in the following way. For each energy interval the source spectrum (from Fig. 4) was multiplied by the resolving power (from Fig. 3) and then by the relative value of the scattering cross section. For the experiment with electron energy 750 Kev the resolving power played no role and the form of the spectrum was determined by the scattering cross section and the curve of absorption of electrons in the filter between the I and II counters, the thick-

*In our first communication, the factor $\sqrt{1-(v/c)^2}$ was left out of this formula and the calculation of the expected effect and polarization were carried out with an incorrect formula. We thank Prof. L. Rosenfeld for calling our attention to this.

*In the work of Ref. 1 we did not consider this necessary, since the expected effect calculated from the incorrect formula depended very weakly on energy.

TABLE I. E = 18.3 Kev/cm; H = 80.5 Oe; t = 0.537 mg/cm^2 Au; T = 4 mg/cm^2 Sr+Y

0°	180°	90°	270°	Sign of the field
98.5±6.2 98.6±4.8	101.7±6.3 108.7±4.2	118.8±4.0 99.1±2.0	101.0±4.1 118.4±2.4	— +
100.1±3.9 103.5±3.6		99.5±1.8 118.6±2.1		Weighted mean

TABLE II. t = 0.537 mg/cm^2 Au; T = 1.5 mg/cm^2 Sr+Y

0°	180°	90°	270°	Sign of the field
12.8±1.4 11.2±0.8	13.9±1.0 8.9±0.9	15.6±0.6 8.9±0.5	10.8±0.6 14.7±0.6	— +
12.5±0.6 10.8±0.7		9.8±0.4 15.2±0.4		Weighted mean
Scatterer t = 5.4 mg/cm^2 Al				
33.0±2.1 35.8±2.2	37.3±2.2 32.0±2.5	36.5±1.2 32.9±1.4	33.4±1.2 37.8±1.5	— +
36.5+1.5 32.5±1.6		33.1±0.9 37.1±0.9		Weighted mean

TABLE III. E = 20 Kev/cm; H = 86 Oe; t = 0.17 mg/cm^2 Au; T = 1.5 mg/cm^2 Sr+Y

0°	180°	90°	270°	Sign of the field
120.0±7.0 112.5±4.0	120.2±5.8 121.5±4.0	135.0±5.6 113.3±2.3	106.0±7.0 136.0±2.7	— +
116.3±3.2 120.7±3.3		109.6±2.2 135.5±2.1		Weighted mean

TABLE IV. E = 20 Kev/cm; H = 71 Oe; t = 1.9 mg/cm^2; T = 4 mg/cm^2 Sr+Y

0°	180°	90°	270°	Sign of the field
29.5±0.7 29.4±1.0	29.8±0.8 28.9±1.0	31.3±0.4 27.6±0.5	28.7±0.5 29.6±0.5	— +
29.6±0.6 29.2±0.6		28.1±0.3 30.4±0.3		Weighted mean
28.9±1.0	29.9±0.9	29.7±0.8	29.2±0.8	Field off

TABLE V.* Expected value of the azimuthal asymmetry $\delta_{exp} = 21.8\%$

ε_K	200	250	300	350	400	450	500	600	750	900	1050	1200	1350	1500	1650
v/c	0.70	0.74	0.78	0.81	0.83	0.84	0.86	0.89	0.91	0.93	0.94	0.95	0.96	0.97	0.97
$\sin\varphi$	0.840	0.714	0.585	0.492	0.433	0.379	0.327	0.256	0.196	0.147	0.125	0.102	0.082	0.063	0.056
Δ, %	53.0	51.6	49.8	47.4	45.6	44.5	43.2	39.0	36.4	32.6	29	27	25	23	22
$\Delta \frac{v}{c} \sin\varphi$	31.2	27.2	22.7	18.9	16.3	14.1	12.1	8.9	6.3	4.45	3.4	2.6	2.0	1.5	1.20
N	33	39	26	15	9	6	4	8	5	4	2	2	1	1	0
$\Delta \frac{v}{c} \sin\varphi \cdot N$	1028	1060	590	284	147	85	48	71	32	18	7	5	2	1	0

*ε_K is the kinetic energy of the electrons in Kev, φ is the angle between the direction of the spin in the rest system of the electron and the direction of the velocity of the electron in the laboratory system after traversal of the crossed fields, Δ is the azimuthal asymmetry for electrons 100% polarized in the transverse direction,[7] N is the number of electrons incident on the counter, in relative units; N is the product of the curve of resolution of the apparatus with respect to energy times the probability of traversal of an electron of given energy through the absorber between the counters times the cross section for scattering of the electrons through the angle considered in the scatterer times the energy spectrum of the source.

TABLE VI. Expected value of the azimuthal asymmetry $\delta_{exp} = 31.7\%$

ε_K	200	250	300	350	400	450	500	600	750	900	1050	1200	1350	1500	1650	1800
v/c	0.70	0.74	0.78	0.81	0.83	0.84	0.86	0.89	0.91	0.93	0.94	0.95	0.96	0.97	0.97	0.975
$\sin\varphi$	0.892	0.776	0.643	0.547	0.473	0.420	0.364	0.281	0.219	0.165	0.140	0.114	0.091	0.071	0.064	0.060
Δ, %	73.0	71.3	69.1	67.2	64.5	63.8	61.6	57.0	53.6	49.0	46.0	41.2	34.6	27.4	25.0	24.0
$\Delta \frac{v}{c} \sin\varphi$	45.6	40.9	34.7	29.8	25.3	22.5	19.2	14.3	10.7	7.51	6.05	4.46	3.02	1.88	1.55	1.40
N	42	72	52	31	21	12	8	15	10	7	5	3	2	2	1	0
$\Delta \frac{v}{c} \sin\varphi N$	1914	2942	1804	924	532	270	154	214	107	52	30	13	6	4	2	0

TABLE VII. Expected value of the azimuthal asymmetry $\delta_{exp} = 6.8\%$

ε_K	500	600	700	800	900	1000	1100	1200	1300	1400	1500	1600	1700	1800	1900	2000
v/c	0.86	0.89	0.91	0.92	0.93	0.94	0.95	0.95	0.96	0.96	0.97	0.97	0.97	0.97	0.98	0.98
$\sin\varphi$	0.359	0.281	0.222	0.195	0.170	0.153	0.122	0.115	0.095	0.088	0.070	0.067	0.063	0.061	0.046	0.045
Δ, %	43.2	39.0	36.4	34.5	32.6	29	27	27	25	25	22	22	22	21	16	16
$\Delta \frac{v}{c} \sin\varphi$	13.3	9.75	7.35	6.19	5.15	4.17	3.14	2.95	2.28	2.11	1.50	1.43	1.34	1.24	0.72	0.71
N	24.0	30.6	29.0	24.5	19.4	15.0	11.6	8.9	6.3	4.6	3.3	2.5	1.6	1.0	0.6	0.3
$\Delta \frac{v}{c} \sin\varphi N$	319	298	213	152	100	62	36	26	14	10	5	4	2	1	1	0

ness of which was 0.08 g/cm^2 Al + 0.08 g/cm^2 Cu. The absorption curves were taken for the case of bad geometry.*

The dependence of the scattering cross section on energy in the range 600 — 2500 Kev was taken from the experimental data of Ref. 5. Since the table of Sherman finishes at $v/c = 0.9$, for large v/c the necessary theoretical values for the magnitude of the asymmetry for scattering at 90° were obtained from the curve, also given by Sherman.

EXPERIMENTAL RESULTS

The experimental results for three series of measurements at energies near to 300 Kev are given in Tables 1, 2 and 3, and in Table 4, for an energy of 750 Kev.† The measurements corresponding to Tables 1 — 4 were carried out with a source of thickness $T = 4$ mg/cm^2, and the others with a thickness of 1.5 mg/cm^2. In experiment II, the control experiment with an aluminum scatterer was carried out, showing the absence of instrumental asymmetry to an accuracy of ±3.5%.

We consider first the data of the tables for the experiments I and II, since these measurements differ only by the target thickness.

From the tables it is evident that, in the plane going through the spin direction and the electron velocity, the asymmetry is almost absent for both signs of fields. At the same time, in the plane perpendicular to the spin, the asymmetry significantly exceeds the errors of measurement and changes sign with change of sign of the field.

In experiment I the value of the azimuthal asymmetry from measurements with both signs of the field was equal to $\delta_1 = (17.4 \pm 2.6)\%$ and in experiment II $\delta_2 = (21.0 \pm 2.5)\%$. As noted above, these two experiments differed only by the thickness of the source. Corrections for depolarization in the first source were ~3.5%, in the second, ~1%, i.e., very small. Therefore the results of the two experiments can be put together, whereupon

$$\delta_{mean} = (19.2 \pm 1.8)\%.$$

Including in the error the inaccuracy in determining the instrumental asymmetry ± 3.5%, we obtain

$$\delta_{mean} = (19.2 \pm 3.8)\%.$$

All intermediate numbers for the calculation of the expected values of azimuthal asymmetry and the corresponding electron polarization are given in Table 5. (The expected azimuthal asymmetry is, from Table 5:

$$\delta_{exp.} = \sum_i \Delta_i (v_i/c) \sin\varphi_i N_i \Big/ \sum_i N_i = 21.8\%.)$$

As a result we obtain

$$P_{mean} = (0.88 \pm 0.18)(v/c).$$

We will return to the correction that must be introduced into these results as a result of multiple scattering after consideration of experiment III.

The conditions of experiment III were different in that (1) the scattering angle was equal to 105 ± 4°; (2) the thickness of the scatterer was equal to 0.17 mg/cm^2; (3) the background was diminished; however, since the intensity of scattering fell by a factor of 3, it constituted ½ of the intensity with the scatterer present.

From Table 3 it can be seen that there is an asymmetry in the directions 0 — 180° which changes sign with change in the sign of the fields. Its mean value is (14.5 ± 8.5)%. In the directions 90 — 270°, the asymmetry — both physical and instrumental — was (42.8 ± 4.8)%. Results of the measurements with the aluminum scatterer, which are given in the same table, make is possible to determine the magnitude and sign of the correction which must be introduced to obtain the value of the physical asymmetry. The instrumental asymmetry has the same sign as the physical, and is equal to (11.3 ± 3.7)%. However, in the scattering with the aluminum foil of thickness 20 μ, a 2% physical asymmetry should be present. With this in view, we obtain from experiment III

$$\delta_3 = (33.6 \pm 6.0)\%.$$

From Table 6, the expected $\delta_{exp} = 31.7\%$, and thus

$$P = (1.06 \pm 0.19)(v/c).$$

The data obtained for the polarization are necessary for the correction due to multiple scattering in the scattering foils. As we said above, this correction can be obtained by extrapolating to zero scatterer thickness the inverse of the azimuthal asymmetry obtained from the measurements with different thicknesses of scatterer. However, since this correction is not larger in magnitude than the statistical errors, it cannot be determined in this way from two experimental values of the polarization obtained by us with two different thicknesses of scatterer — 0.17 and 0.537 mg/cm^2. Therefore, we used experimental data obtained in our

*In the work of Ref. 1 we determined the lower limit of the spectrum by the extrapolated mean free path and, in addition, did not take into account the presence of Sr^{89}, which greatly increases the number of electrons in the energy range 500-800 Kev.

†In Ref. 1, Tables 1-4 were given.

laboratory with different apparatus, on which Vishnevskii et al. also measured the polarization of electrons in scattering at 90° from gold foils of different thicknesses and for different electron energies from 100 to 200 Kev. According to these data, for electrons in the energy interval 160 — 200 Kev and scattering "in transmission" in gold, the correction to the azimuthal asymmetry because of multiple scattering is determined by the expression

$$\delta_0 = \delta(t)\left[1 + \frac{(0.022 \pm 0.004)}{(pv/c)^2}\, t\right],$$

which in our case at a mean energy of 300 Kev and foil thickness 0.17 mg/cm^2 gives the magnitude of the correction as 4%, and for a foil 0.537 mg/cm^2, 13.5%.

Introducing these corrections, we have:

$P = (1.00 \pm 0.20)(v/c)$ for the first two experiments;
$P = (1.10 \pm 0.19)(v/c)$ for the third experiment.

The mean of these is

$$P = (1.05 \pm 0.14)(v/c).$$

We note one circumstance common to all three experiments. In the directions 0 — 180° the sum of counts is somewhat less than the sum of counts at 90 and 270°. This difference scarcely exceeds the limits of error, and is even sometimes less than these; however, it has a systematic character and, in the mean, is 5%. The origin of this difference is easy to understand. The deflecting field acts in the direction 0 — 180°. Thus, the dimensions of the beam in these directions are somewhat larger than in the direction 90 — 270°, owing to the fact that part of the scattered electrons in the direction 0 —180° does not fall into the angle of acceptance of the counters in the vertical direction.

In experiment IV, measurements of the electron polarization were carried out at a higher energy — 750 Kev. In this case the electrons emitted by Sr^{90} are almost all filtered out and only the electrons emitted by Sr^{89} and Y^{90} remained. The limit of the Sr^{89} spectrum is 1460 Kev and, of the Y^{90} one, 2260 Kev. Since the number of electrons of high energy after scattering drops sharply according to the law $\sim \sigma = B(pv/c)^{-2}$, the electrons with energy > 1500 Kev hardly contribute to the azimuthal asymmetry. Thus, the decay electrons of Sr^{89}, having a softer spectrum than those of Y^{90}, play a large part in this measurement.

The experimental conditions are indicated in Table 4. Data of the control experiment with fields turned off are presented there in the same way. As noted above, the resolving power of the apparatus in this energy region is low. The field does not have a deflecting action on the electrons, but only turns their spin. The spectrum of electrons is determined by the scattering law and the filter between the counters. In fact, it is evident from the table, that, with the fields turned off, the number of counts in the 0 — 180° plane and the mean number of counts in the 90 — 270° plane do not change within the limits of error of the measurements (~2%). Therefore it is impossible to conceive of any asymmetry connected with the switching of the fields, larger than this quantity. This can be seen from the equality of intensities in the directions 0 — 180° with the fields turned off.

Geometrical asymmetry is excluded by the switching of the fields and, besides, from the identities shown for all four angles with the field absent, it is clear that it is practically absent.

From Table 4 we obtain

$$\delta_4 = (7.85 \pm 1.4)\%.$$

Assuming that the absence of instrumental asymmetry is known to us to an accuracy of 2%, we obtain

$$\delta_4 = (7.85 \pm 2.5)\%.$$

From Table 7, the expected value of the asymmetry is

$$\delta_{exp.} = (6.8 \pm 0.8)\%.$$

The error in the expected value arises from its great sensitivity to the mean energy of the electron spectrum, which cannot be accurately determined. Thus,

$$P = (1.16 \pm 0.4)(v/c).$$

CONCLUSIONS

In the present work the polarization of electrons of energy 200 — 1500 Kev emitted in β-decay was observed by the method of electron scattering. It was shown that the degree of polarization was near to v/c to an accuracy of 15% for mean energy 300 Kev and 40% for mean energy 750 Kev. Similar experiments with results near to ours have been communicated simultaneously in a series of papers.

Frauenfelder et al.[8] observed the polarization for electrons near 70 Kev emitted by Co^{60} using the deflection of electrons in an electric field and electron scattering. Nikitin et al.,[9] using the same method, showed the same effect for electrons of energy 120 Kev emitted by Cu^{64}. Cavanagh et al.[10] using the same method as we of crossed fields to turn the spin, observed the polarization of β-electrons of energy 120 Kev emitted by Co^{60}. Later, the polarization of β-electrons has been observed

by other means than measurement of the azimuthal asymmetry in the scattering.

The establishment of the polarization of β-electron was, together with the experiments of Wu et al.[11] and Lederman et al.,[12] a strong experimental proof of the violation of parity in weak interactions.

In conclusion, we should express our gratitude to K. A. Ter-Martirosian for deriving the formula for the turning of the spin in the crossed fields, to L. Ia. Suvorov, M. P. Anikina and V. D. Laptev for separating and preparing the source of Sr, to A. S. Kronrod for calculating the intensity and to M. E. Vishnevskii for helpful information on the role of multiple scattering.

[1] Alikhanov, Eliseev, Liubimov and Ershler, J. Exptl. Theoret. Phys. (U.S.S R.) **32**, 1344 (1957). (Communicated at the Rochester Conference, 1957.) Soviet Phys. JETP **5**, 1097 (1957).

[2] T. D. Lee and C. N. Yang, Phys. Rev. **104**, 254 (1956); L. D. Landau, J. Exptl. Theoret. Phys. (U.S.S.R.) **32**, 405, 407 (1957); Soviet Phys. JETP **5**, 336, 337 (1957).

[3] Berestetskii, Ioffe, Rudik and Ter-Martirosian, Nuclear Phys. **5**, 464 (1958).

[4] Experimental Nuclear Physics, edited by E. Segrè (New York, 1953), Russian Translation, 1955, pp. 239-241; B. Rossi and K. Greisen, Interaction of Cosmic Rays with Matter, (Russ. Transl.) IIL, Moscow 1948, p. 41.

[5] Alikhanian, Alikhanov and Vaisenberg, J. Phys. (U.S.S.R.) **9**, 280 (1945).

[6] L. A. Artsimovich, J. Exptl. Theoret. Phys. (U.S.S.R.) **9**, 927 (1939).

[7] N. Sherman, Phys. Rev. **103**, 1601 (1956).

[8] Frauenfelder et al., Phys. Rev. **106**, 386 (1957).

[9] Vishnevskii et al., Nuclear Phys. **4**, 271 (1957).

[10] Cavanagh et al., Nuclear Phys. **5**, 11 (1958).

[11] Wu et al., Phys. Rev. **105**, 1413 (1957).

[12] Garwin, Lederman and Weinrich, Phys. Rev. **105**, 1415 (1957).

APPENDIX

On the Turning of the Spin in Crossed Electric and Magnetic Fields

Below we present considerations derived by K. A. Ter-Martirosian on the motion of the spin upon the traversal of the electron through crossed electric and magnetic fields.

Let an electron, the spin of which is parallel to its initial velocity* β, go into constant and uniform fields $\mathbf{E}$ and $\mathbf{H}$ ($\mathbf{E}$ parallel to the y-axis, and $\mathbf{H}$, to the z-axis). The vector $\boldsymbol{\beta}$ lies in the x,y-plane† and makes angle α with the x-axis. It is not assumed that $\beta = \beta_0$, where $\beta_0 = E/H$. The fields act in the region between two parallel planes ($x = 0$ and $x = l$), the distance between which is l.

It is required to find the angle φ through which the spin of the electron is turned after it has traversed the region in which the field acts, that is, the angle between the direction $\mathbf{n}(n^2 = 1)$ of the spin of the electron after traversing the field in the system of reference K^0, in which the electron is at rest, and the direction $\boldsymbol{\nu} = \boldsymbol{\beta}_1/\beta$ of its final velocity.‡

For a covariant description of the spin, it is convenient to introduce a 4-vector $(\boldsymbol{\sigma}, \sigma_0)$ defined in such a way** that in the rest system K^0 its spatial part coincides with $\mathbf{n}$, and its time-like part is equal to zero. According to definition, $\sigma^2 = \boldsymbol{\sigma}^2 - \sigma_0^2 \equiv \mathbf{n}^2 = 1$ in an arbitrary system. Under a Lorentz transformation from the laboratory system to the system K^0, the perpendicular component $\boldsymbol{\sigma}_\perp = [\boldsymbol{\nu}(\boldsymbol{\sigma}\boldsymbol{\nu})]$ of the spin does not change, i.e., $\boldsymbol{\sigma}_\perp = \mathbf{n}_\perp$. Therefore $\sin\varphi = |\mathbf{n}_\perp|/|\mathbf{n}| \equiv |\boldsymbol{\sigma}_\perp| = \boldsymbol{\sigma}_\perp = \boldsymbol{\nu} \times [\boldsymbol{\sigma} \times \boldsymbol{\nu}]$, $|\boldsymbol{\sigma} \times \boldsymbol{\nu}|$. Since $\boldsymbol{\sigma}$ and $\boldsymbol{\nu}$ lie in the x,y plane, then

$$\sin\varphi = \left| \frac{\sigma_x\beta_y - \beta_x\sigma_y}{\sqrt{\beta_x^2 + \beta_y^2}} \right|_{t'=\tau}, \qquad (1)$$

where it is noted that all quantities relate to the instant $t' = \tau$ of exodus of the electron from the region of the field.

For calculation of the components of the vectors $\boldsymbol{\sigma}$ and $\boldsymbol{\beta}$ it is convenient to go to the system of reference K' which moves along the x axis with velocity $\beta_0 = E/H$ (it is assumed that $E < H$, i.e., $\beta_0 < 1$) with respect to the laboratory system. The quantities relating to the system K' will be denoted by primes.

In the system K' the electric field vanishes

$$\mathbf{E}' = 0, \quad \mathbf{H}' = \mathbf{H}\sqrt{1 - \beta_0},$$

*It will be assumed everywhere that the spin is measured in units of the light velocity, i.e., $\beta = v/c$.

†The generalization to the case in which β_z is different from zero can be carried out in an elementary fashion.

‡The magnitude of this angle determines the magnitude of left-right asymmetry of the subsequent scattering of the electron in the Coulomb field.

**To do this, as is well known, one should set $i\sigma_\mu = \varepsilon_{\mu\nu\lambda\rho}\sigma_{\nu\lambda}u_\rho$, where $\varepsilon_{\mu\nu\lambda\rho}$ is the completely antisymmetric unit matrix ($\varepsilon_{1234} = 1$), $\sigma_{\nu\lambda}$ is the antisymmetrical spin tensor (in the rest system K^0, $\sigma_{12} = s_3$, $\sigma_{31} = s_2$, $\sigma_{23} = s_1$, with s the spin-vector), and u_ρ is the 4-vector electron velocity.

Therefore, in it the spin $\sigma'(t')$ and velocity $\beta'(t')$ of the electron rotates uniformly in the x', y' plane:

$$\beta'_x(t') = \beta'_x \cos\varphi' - \beta'_y \sin\varphi', \quad \sigma'_x(t') = \sigma'_x \cos\varphi' - \sigma'_y \sin\varphi',$$
$$\beta'_y(t') = \beta'_x \sin\varphi' + \beta'_y \cos\varphi', \quad \sigma'_y(t') = \sigma'_x \sin\varphi' + \sigma'_y \cos\varphi'; \tag{2}$$

here $\varphi' = \omega' t'$

$$\omega' = ecH'/\varepsilon' = (eH/m_e c)\sqrt{(1-\beta^2)(1-\beta_0^2)}, \tag{3}$$

and β'_x, β'_y and σ'_x, σ'_y are the velocity and spin of the electron at the moment of exodus from the region of the fields.

Using the Lorentz transformation from the laboratory system to the system K', it is clearly possible to express $\sin\varphi$ in Eq. (1) in terms of the spin components and velocities in the system K':

$$\sin\varphi = \frac{\sigma'_y(\tau)[\beta'_x(\tau)+\beta_0] - [\sigma'_x(\tau)+\beta_0\sigma_0]\beta'_y(\tau)}{\sqrt{[\beta'_x(\tau)+\beta_0]^2 + \beta'^2_y(\tau)(1-\beta_0^2)}}, \tag{4}$$

and the projections β'_x, β'_y and σ'_x, σ'_y of the velocity and spin at $t' = 0$ through α, β and β_0. A simple calculation and substitution in Eq. (2) give

$$\sigma'_x(\tau) = \frac{(\cos\alpha - \beta\beta_0)\cos\varphi_0 - \sqrt{1-\beta_0^2}\sin\alpha\sin\varphi_0}{\sqrt{(1-\beta^2)(1-\beta_0^2)}},$$

$$\sigma'_y(\tau) = \frac{(\cos\alpha - \beta\beta_0)\sin\varphi_0 + \sqrt{1-\beta_0^2}\sin\alpha\cos\varphi_0}{\sqrt{(1-\beta^2)(1-\beta_0^2)}},$$

$$\beta'_x(\tau) = \frac{(\beta\cos\alpha - \beta_0)\cos\varphi_0 - \beta\sqrt{1-\beta_0^2}\sin\alpha\sin\varphi_0}{1-\beta\beta_0\cos\alpha},$$

$$\beta'_y(\tau) = \frac{(\beta\cos\alpha - \beta_0)\sin\varphi_0 + \beta\sqrt{1-\beta_0^2}\sin\alpha\cos\varphi_0}{1-\beta\beta_0\cos\alpha}. \tag{5}$$

The substitution of Eq. (5) into Eq. (4) gives a very long expression, which we won't reproduce here. The formulae (5) and (4) solve the required problem, if the quantity $\varphi_0 = \omega'\tau$ is found, i.e., the time τ in the system K' of movement of the electron through the region of the fields. In this system, the length of the projection l' of the path of the electron on the x' axis will be $l = l\sqrt{1-\beta_0^2}$, therefore, τ is determined by the condition

$$l' = \tau\beta_0 + \int_0^\tau \beta'_x(t')\,dt'. \tag{5'}$$

Using Eqs. (3) and (5), this condition leads to the following equation for φ_0:

$$\varphi_0 - \frac{1-(\beta_0/\beta\cos\alpha)}{1-\beta_0^2}(\varphi_0 - \sin\varphi_0) - \frac{(1-\cos\varphi_0)\tan\alpha}{\sqrt{1-\beta_0^2}} = \frac{eHl}{cp\cos\alpha}\sqrt{1-\beta_0^2}, \tag{6}$$

where $p = m_e\beta c/\sqrt{1-\beta^2}$ is the initial momentum of the electron. In practice to a high accuracy one can consider that φ_0 is equal to the right-hand side, since the second and third terms on the left-hand side are very small* in comparison with φ_0.

In the case $\alpha < 1$ and $\varphi_0 < 1$, neglecting terms of order α^2, φ_0^2 and $\alpha\varphi_0$, the simple formula

$$\varphi \approx \frac{eHl}{cp}\frac{\beta_0}{\beta}\sqrt{1-\beta^2}. \tag{7}$$

follows from Eqs. (4) — (6).

A relatively simple formula can be obtained also in the important case of small α and arbitrary φ_0. For this, expansion of Eq. (5) in powers of α and substitution into Eq. (4) gives

$$\sin\varphi = \sin\varphi_0\left[\sin^2\varphi_0 + \frac{[(\beta/\beta_0) - 1 + (1-\beta\beta_0)\cos\varphi_0]^2}{(1-\beta^2)(1-\beta_0^2)}\right]^{-1/2} \times [1 + \alpha\Delta_1 + \alpha^2\Delta_2 + \ldots], \tag{8}$$

where Δ_1, Δ_2, etc. — of the order of magnitude unity — are some functions of β_0, β and φ_0 which are easy to calculate.

For $\alpha = 0$ and $\beta = \beta_0$ the electron trajectory is rectilinear and Eq. (7) or Eq. (6) and Eq. (8) lead to the well-known equation:

$$\varphi = (eHl/cp)\sqrt{1-\beta^2}.$$

Translated by G. E. Brown
163

*These terms determine the correction to φ_0 connected with the curvilinear nature of the trajectory of the electron. For $\alpha = 0$ and $\beta = \beta_0$, the trajectory is rectilinear; as can be seen, the terms vanish in this case.

INVESTIGATION OF MULTIPLE SCATTERING OF PROTONS

F. R. ARUTIUNIAN

Physics Institute, Academy of Sciences, Armenian S.S.R.

Submitted to JETP editor September 17, 1957

J. Exptl. Theoret. Phys. (U.S.S.R.) **34**, 800-806 (April, 1958)

Multiple scattering of protons with energies from 90 to 200 Mev and with energies from 40 to 60 Mev was investigated respectively in lead and copper plates of various thicknesses. The experimental data are compared with the multiple Coulomb scattering curves for a point and extended nucleus. A consequence of diffraction scattering is that the experimental results do not agree with the theoretical values for a finite sized nucleus and exceed them. The effect of nuclear scattering depends on the relation between the angle $\theta = \lambda\!\!\!^{-}/R$ and the mean square angle of multiple Coulomb scattering. The integral cross section for nuclear scattering of protons $\sigma = (0.0755 \pm 0.0375)\sigma_{geom}$ has been obtained in the angle region in which Coulomb scattering is small compared with nuclear scattering. This value is in good agreement with the optical model of an "absolutely black" nucleus.

1. INTRODUCTION

WE have investigated the scattering of protons with energies of 90 to 200 Mev in lead plates 7 and 4 mm thick, and from 40 to 60 Mev in 5 and 2 mm copper plates, located in a Wilson chamber. Cosmic ray protons, stopped by ionization in the Wilson chamber plates, were selected, and their momentum prior to entering the chamber was measured with a magnetic mass spectrometer. A detailed description of the experimental setup is given in Ref. 1.

The conditions for selecting particles for the scattering investigation were such that it was possible to observe elastic scattering only. The mass of an inelastically-scattered proton, determined from its momentum and range, is not the true proton mass, and such cases are not investigated. However, there is a spread in the proton masses, because of the errors in measuring the momentum and range. If one assumes that a particle corresponds to the selected upper limit of the interval for the proton masses, equal to 2300 m_e, not because of errors but on account of inelastic scattering, then the value of the transferred momentum will be $\Delta p_{inel} = 0.8 \times 10^8$ ev/c, which constitutes 15% of the particle momentum itself. The proton mass spectrum is well approximated by a Gaussian distribution which shows that the spread of masses is due to the errors of measuring momentum and range and not to some inelastic processes. Besides, the relatively small value of Δp_{inel} gives reason to believe that the investigated scattering is elastic.

The projections of scattering angles in plates were investigated from zero to the maximum observable. The angles were measured independently by two observers, from photographs, by means of a protractor. A large number of measurements were averaged. The mean-square error in measuring the angle was 0.6°.

It is to be noted that only those scattering angles were investigated which corresponded to the residual tracks, equal to two or more plates; thus, if the plate in which the particle has stopped is assigned the number $k = 0$ and the plates are numbered consecutively upward from this plate, then the investigated scattering pertains only to plates with numbers $k \geq 2$. The scattering was not investigated in the plate $k = 1$, since in this case the large uncertainty in the track lowered considerably the precision of the momentum determination.

The protons were divided according to their residual tracks into four groups (I, II, III, and IV). Groups I, II, and III correspond to plates with numbers $k = 2$, 3, and 4. Group IV corresponds to plates with numbers $k = 5$ and 6.

Inasmuch as the curves of multiple Coulomb scattering are dependent very strongly on the momentum p (more accurately, on the quantity $\pi = p\beta c$), it was measured by two methods for a more precise determination. The momentum was determined, on one hand, from the residual track and on the other hand, from the momentum measured in a magnetic field and from the amount of matter

traversed by the particle up to the scattering point. For each group, the average momenta calculated by both methods agree well with each other (with a precision to 2%). The momenta and energies of investigated protons for each group are shown in Table I.

TABLE I

Group	Momentum p, 10^8 ev/c	Energy E, Mev
I	4.6±0.25	104±13
II	5.15±0.24	132±11
III	5.6±0.21	152±10
IV	6.17±0.16	186±9

The average momentum for each individual group has an uncertainty Δp, determined by the finite plate thickness in which the particle stops. Corrections were made for the multiple Coulomb-scattering curves, plotted with the average value of π, which take into account the existing uncertainty in the momentum determination.

The elastic proton scattering in plates, in the region of small angles, is determined primarily by multiple Coulomb scattering. Only for large angles ($\theta \gg \lambda\!\!\!^{-}/R$) does the scattering have in practice a purely nuclear aspect. The presence of nuclear scattering for protons leads to the conclusion that the experimental curves differ from the curve of Coulomb scattering.

2. ON THE THEORY OF MULTIPLE SCATTERING OF NUCLEAR-ACTIVE PARTICLES

The distribution function of multiple Coulomb scattering for a point nucleus was calculated by Moliere.[2,3] The nuclear dimensions begin to show up when the momentum change of the scattered particle is of the order of the "nuclear momentum," $\Delta p = p\theta \sim \hbar/R$, i.e., for angles $\theta \gtrsim \lambda\!\!\!^{-}/R$.

Scattering curves that take into account the finite nuclear dimensions, applicable to the scattering of μ mesons with momenta $p = (1.0 - 2.0) \times 10^8$ ev/c, were obtained and communicated to us by M. L. Ter-Mikaelian. The differential Coulomb scattering cross section (neglecting the atomic form factor) has the form

$$\sigma_C(\theta)\, d\Omega = \sigma_R(\theta)\, F(y) d\Omega, \quad y = \theta R/\lambda\!\!\!^{-}, \qquad (1)$$

where $\sigma_R(\theta) = 4\alpha^2\lambda\!\!\!^{-2}/\theta^4$ — the Rutherford scattering cross section, $\alpha = Ze^2/\hbar v$, and F is a nuclear form factor which drops off rapidly with $\theta R/\lambda\!\!\!^{-} \gg 1$ and which equals 1 for $y \ll 1$. Its values for intermediate values of y, according to Hofstadter's data,[4] are: $y = 0.5$; $F(y) = 0.91$; $y = 1.0$; $F(y) = 0.64$; $y = 2.0$; $F(y) = 0.294$.

From the comparison of the multiple Coulomb scattering curves for the point and extended nucleus it can be seen that the smaller the angle $\theta = \lambda\!\!\!^{-}/R$ in relation to the mean square of Coulomb scattering $\chi_c\sqrt{B}$ (Ref. 2, 3), i.e., the larger the atomic number Z and the thickness of the scattering substance, the greater the influence of the nuclear dimensions. However, if there is also a nuclear interaction, then for the same momentum change $\Delta p = \hbar/R$ one must also take into account the nuclear forces; therefore the calculation of the finite nuclear dimensions in Coulomb scattering and of the nuclear field must be done simultaneously. It is clear that the nuclear scattering must be taken into account if its cross section is (for some scattering angles) comparable to the Coulomb scattering cross section. For the differential nuclear scattering cross section we shall use the data on neutron scattering for an "absolutely black nucleus."[5]

$$\sigma_{nuc}(\theta)\, d\Omega = R^2 |J_1(y)/\theta|^2\, d\Omega. \qquad (2)$$

The nuclear and Coulomb cross sections become equal at angles $\theta_1 = 2\alpha\lambda\!\!\!^{-}/R$ for $\alpha \gtrsim 1$ and $\theta_2 = 2\sqrt{\alpha\lambda\!\!\!^{-}}/R$ for $\alpha \ll 1$. If angles θ_1 and θ_2 exceed significantly the mean-square angle of multiple scattering ($\alpha \gg 1$), then the Coulomb interaction predominates over the nuclear one in the angle region of interest to us. It is then valid to take into account the nuclear dimensions which manifest themselves at deviation angles $\lambda\!\!\!^{-}/R$, and disregard nuclear scattering which becomes of the order of Coulomb scattering for angles much larger than $\lambda\!\!\!^{-}/R$. When $\alpha \approx 1$, the effects of nuclear dimensions and nuclear scattering are of the same order, but when $\alpha \ll 1$ the nuclear scattering shows up considerably earlier than the nuclear form factor in Coulomb scattering. The thicker the scattering substance and the higher its Z, the larger the mean-square angle of multiple Coulomb scattering $\chi_c\sqrt{B}$ and the greater the effect of nuclear scattering.

The total differential scattering cross section is

$$\sigma_{total}(\theta)\, d\Omega = \sigma_R(\theta)\, N(y, \alpha)\, d\Omega, \qquad (3)$$

where $N(y, \alpha)$ is the coefficient which accounts simultaneously for the effects of the finite nucleus dimensions and of nuclear scattering.

Following the calculations of Ref. 5, we can simply use the coefficient $N(y, \alpha)$, which must be multiplied by the Rutherford scattering cross section in order to obtain the correct formula for the single scattering cross section, which in turn yields the curve of multiple scattering. This coef-

ficient, for $\alpha \lesssim 1$, is everywhere larger than unity and only for $\alpha \gg 1$ is it smaller than unity. This is well illustrated by a series of experimental curves in Ref. 6, which give the dependence of $N(y, \alpha) = \sigma_{total}/\sigma_R$ on the scattering angle for 22-Mev protons for a large number of elements. For light elements $\alpha < 1$ and $N(y, \alpha) > 1$, and $N(y, \alpha) < 1$ only for very heavy elements. We shall use these experimental curves for comparison with our experimental data.

As follows from calculations in Ref. 5, the experimental curves for the dependence of $N(y, \alpha)$ on the scattering angle, cited in Ref. 6, depend only on the magnitude of α. Having the interval of velocities for protons under consideration ($\beta = 0.44 - 0.55$ for lead and $\beta = 0.3 - 0.35$ for copper), we determine the corresponding values of α for our conditions:

$$\alpha_{Pb} = 1.37 - 1.1 \text{ and } \alpha_{Cu} = 0.723 - 0.625.$$

We next determine the equivalent elements which correspond to our values of α_{Pb} and α_{Cu} for 22-Mev protons.

TABLE II

θ°	$y = \theta R/\chi$	N(y) Ref. 5 α = 0.2	N(y) Ref. 5 α = 1.73	N(y) Ref. 6
0	0	1	1	1
2	0.705	3.8	1.6	1
4	1.41	7.10	3.5	1.1—1.4
6	2.11	12.5	6.7	1.1—1.3
8	2.82	12.1	6.4	1.4
10	3.53	6.0	4.0	1.3
12	4.23	5.0	2.60	1.2
14	4.92			1.05
16	5.63			1.0
18	6.34			0.95

TABLE III

θ°	$y = \theta R/\chi$	N(y) Ref. 5 α = 0.2	N(y) Ref. 5 α = 1.73	N(y) Ref. 6
0	0	1	1	1
2	0.208	1	1	1
4	0.416	1	1	1
6	0.624	3.4	1.6	1
8	0.832	4.0	1.4	1.05
10	1.04	4.2	1.5	1.15
12	1.248	5.6	2.0	1.20
14	1.456	6.5	3.4	1.17

Tables II and III show the values of $N(y, \alpha)$ for lead (from the graph for Nb) and copper (from the graph for Fe), respectively, in the region of angles investigated by us. The same tables show the coefficients $N(y, \alpha)$ as calculated in Ref. 5 for $\alpha = 0.2$ and $\alpha = 1.73$. These coefficients, in the region of scattering angles investigated by us, are always greater than unity, whether obtained from the experimental data[6] or from the theoretical calculations.[5] Note, however, that the use of the experimental data of Ref. 6 for $N(y, \alpha)$ is based on Ref. 5 and that the coefficients $N(y, \alpha)$ according to theoretical calculations[5] are considerably higher than the same coefficients according to the experimental data of Ref. 6. It is possible that the coefficients $N(y, \alpha)$ as calculated in Ref. 5 have higher values because no account was taken of the diffuseness of the nuclear edge or of its transparency. However, there are no experimental and theoretical papers covering the energies and substances of interest to us.

As far as the degree of blackness is concerned, since the range in nuclear matter, for neutrons and consequently for protons with energies of 20 to 140 Mev, is approximately constant, (it varies from 3×10^{-13} to 4×10^{-13} cm in the interval of proton energies investigated by us, i.e., 90 to 200 Mev for lead and 40 to 60 Mev for copper), then, to a first approximation, one can consider the nuclei of lead and copper as "absolutely black."

We can thus conclude that allowance for the nuclear interaction and nuclear dimensions leads to an increase in the Rutherford scattering cross-section for the point nucleus, in the angle region of interest to us, and not to a decrease due to finite nuclear dimensions, as occurs for particles which undergo only Coulomb interactions. The experimental data for protons must lie above the Molière curve, or at least coincide with it when $N(y, \alpha)$ is close to unity.

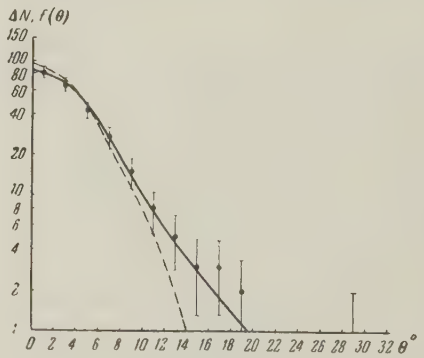

FIG. 1. Differential distribution of scattering angles for protons in 7 mm lead plates for group I. Solid line – curve of multiple Coulomb scattering for a point nucleus, dotted line – for extended nucleus; n = 254.

3. EXPERIMENTAL RESULTS AND THEIR EVALUATION

In Fig. 1 are shown the experimental distribution of scattering angles for one of the groups (group I) for scattering by 7 mm Pb, and the

corresponding theoretical curves of multiple Coulomb scattering for a point and an extended nucleus. The scattering-angle distributions for the remaining groups are similar in nature and are therefore not shown. Since the projections of scattering angles are under study, all theoretical relationships and curves, used for comparison with experimental data, pertain to scattering-angles projections.

The "χ^2 criterion" can be used to check the agreement between the experimental data and the theoretical curves. For group I $(P_{\chi^2})_{extend} = 10^{-5}$ and $(P_{\chi^2})_{point} = 0.94$. It follows from all these curves that the experimental data agree with the scattering curve for the point nucleus, but differ markedly from the curve for an extended nucleus.

In Fig. 2 are shown the combined scattering-angle distributions for all the groups (I, II, III, IV). The scattering angles are given in units of φ, where φ is the relative scattering angle ($\varphi = \theta/\chi_c\sqrt{B}$). The superiority of such a construction lies in the fact that we can combine all of the groups, by previously constructing the distributions according to φ for each group separately, and then summing them up.

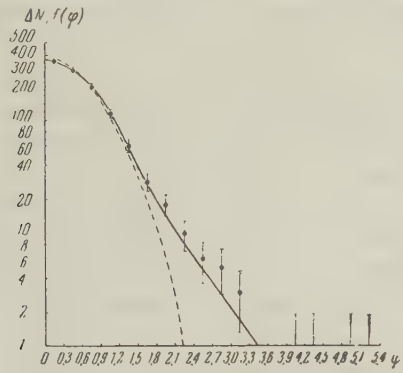

FIG. 2. Differential distribution of scattering angles for protons in 7 mm lead plates for all the groups combined. Solid line – curve of multiple Coulomb scattering for a point nucleus, dotted line – for extended nucleus; n = 1060.

The experimental curves for angles $\varphi > 1.8$ (Fig. 2) are less steep than the scattering curve for the point nucleus. This is explained by the fact that with large angles, the diffraction scattering cross-section is on the average inversely proportional to the cube of the scattering angle [Eq. (2)], whereas the pure Coulomb scattering cross section is to its fourth power [Eq. (1)].

There are relatively few experimental data on proton scattering in 4 mm lead plates. They are therefore not subdivided into groups and the combined graph for all the groups is shown (Fig. 3), although the construction of the experimental and theoretical distributions was made by intervals, and the data were summed afterwards. It is seen

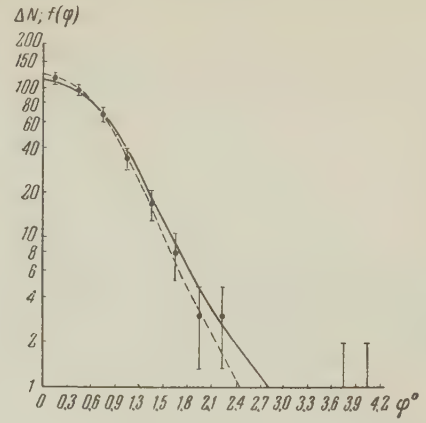

FIG. 3. Differential distribution of scattering angles for protons in 4 mm lead plates. Solid line – curve of multiple Coulomb scattering for a point nucleus, dotted line – for extended nucleus; n = 349.

from Fig. 3 that the experimental data agree equally well with the point nucleus and with the curve of the extended nucleus $[(P_{\chi^2})_{point} = 0.94]$ and $[(P_{\chi^2})_{extend} = 0.93]$.

Comparing scattering curves for two different thicknesses of scattering plates (7 mm Pb and 4 mm Pb), we see that the effect of nuclear scattering increases with the increase in plate thickness. In the region of large scattering angles, where the Coulomb scattering is very small, and consequently the interference of Coulomb and nuclear scattering plays no role, all the scattering cases can be considered to be purely nuclear. The experimental scattering cross-section for angles $\varphi > 3.3$ for 7 mm Pb plates (Fig. 2) was found to be

$$\sigma = (0.0755 \pm 0.0375)\,\sigma_{geom}.$$

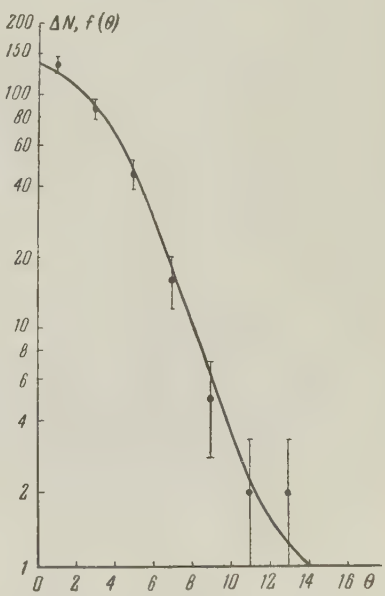

FIG. 4. Differential distribution of scattering angles for protons in 5 mm copper plates; n = 290.

From the asymptotic expression for the diffraction scattering formula[2] for large angles one can obtain the integral diffraction scattering cross section for projections of scattering angles larger than θ_0:

$$\sigma = (4\lambda / \pi^2 R\theta_0)\sigma_{geom}, \quad (4)$$

which gives for angles $\varphi > 3.3$ a cross section $\sigma = 0.06\ \sigma_{geom}$, in good agreement with its experimental value.

The experimental data on proton scattering in

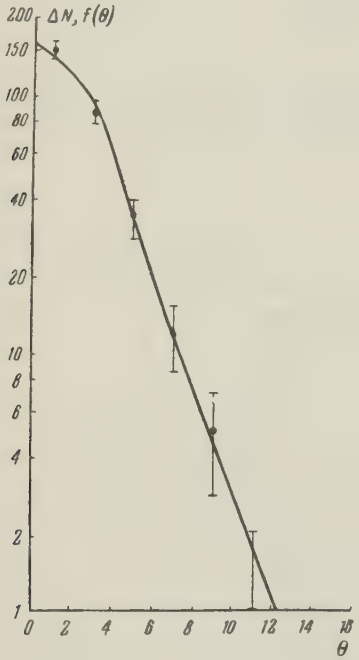

FIG. 5. Differential distribution of scattering angles for protons in 2 mm copper plates; n = 290.

copper, with scattering plates 5 and 2 mm thick, are shown in Figs. 4 and 5 respectively. These data are compared only with the curve of multiple-scattering by a point nucleus because the effect of finite nucleus dimensions is negligible for the copper nucleus and the investigated momentum range.

While the mean-square angles $\chi_c\sqrt{B}$ (averaged over all groups) for lead and copper are almost identical ($\sim 5°$), the value of $\theta = \lambda\!\!\!^{-}/R$ for copper ($\sim 7°$) is 2.7 times larger than the same value for lead (2.6°). One concludes from this that the effect of diffraction scattering is also small, and the experimental points must agree well with the curve of multiple Coulomb scattering for the point nucleus. This is clearly seen in the curves shown in Figs. 4 and 5 and Table III, where the coefficients $N(y, \alpha)$ are very close to unity.

It follows from the above that, depending on the energies of the protons, the plate thickness, and substance in which scattering is being investigated, the nuclear scattering takes place in a diverse manner. If $\lambda\!\!\!^{-}/R < \chi_c\sqrt{B}$, then the nuclear scattering shows up in the region of multiple scattering; if, however, $\lambda\!\!\!^{-}/R \gtrsim \chi_c\sqrt{B}$, then the nuclear scattering is apparent only at angles considerably larger than the mean-square angle of multiple scattering. The larger the effect of finite nuclear dimensions, the larger is the effect of the nuclear scattering, and vice versa. This, in the final analysis, leads us to the conclusion that the elastic proton scattering in the region of multiple scattering can be approximated artificially by the curve of Coulomb scattering for a point source.*

The author expresses his thanks to Prof. A. I. Alikhanian for his interest in the problem and for his participation in its discussion, and to W. L. Ter-Mikaelian for developing the scattering theory given in this paper and for his participation in the discussion of the data.

[1] Daion, Fedorov, Merzon, and Shostakovich, Приборы и техника эксперимента (Instruments and Meas. Engg.) **1**, 3 (1957).

[2] G. Z. Molière, Naturforsch, **3A**, 78 (1948).

[3] H. A. Bethe, Phys. Rev. **89**, 1256 (1953).

[4] R. Hofstadter, Revs. Mod. Phys. **28**, 214 (1956).

[5] A. I. Akhiezer and I. Ia. Pomeranchuk, Некоторые вопросы теории ядра (Certain Problems in Nuclear Theory), Moscow, 1950.

[6] D. C. Peaslee, Annual Rev. Nucl. Sci. **5**, 126 (1955).

Translated by H. Kruglak
164

*Note added in proof (March 31, 1958). We have established recently that in a scattering investigation by experimental setups of this type it is necessary to take into account the geometry of the apparatus. For mesons this calculation would lead to a substantial change in the scattering curve; for protons the change is several percent.

YIELD OF ELECTRONS FROM GAMMA-RAY BOMBARDMENT

M. V. KHATSKEVICH and E. M. TSENTER

Submitted to JETP editor October 5, 1957

J. Exptl. Theoret. Phys. (U.S.S.R.) **34**, 807-810 (April, 1958)

The absolute yield of electrons produced by 2.62 Mev γ-quanta in an aluminum target of effective thickness is determined experimentally and computed theoretically.

INTRODUCTION

VARIOUS experimenters have studied the relative yield of electrons emitted in bombardment with γ-rays of different energies of targets of various materials[1-8] having an effective thickness.* At the same time, there are actually no data in the literature on absolute values of these yields. Papers on the determination of the efficiency of cylindrical γ-counters, for example that of Bradt et al.,[9] do not give such data directly† since the broad divergent beams used in these experiments lead to a multiplicity of angles of incidence of γ-rays on the walls of the counter (from 0° to 90°). As is well known, this gives a comparatively complicated relation between the value of the counter efficiency obtained and the yield of electrons from a flat target of the same material which is, instead, irradiated by a beam along the normal.[10]

Since data on relative yields are available, it is sufficient to determine the absolute yield for any one material at one γ-ray energy, in order to convert to absolute values for other materials and energies. The present paper is devoted to this problem.

Aluminum was chosen as the target material and the yield of electrons was determined for the hard component of the radiation from ThC″ (2.62 Mev). The quantity to be determined was found by experimental and computational methods.

COMPUTATION

Let us consider an aluminum target of infinite thickness (cf. Figure 1), where A-B is the front face at which the γ-rays enter, and a-b is a plane parallel to this face at a distance r from A-B. The general expression for the flux through

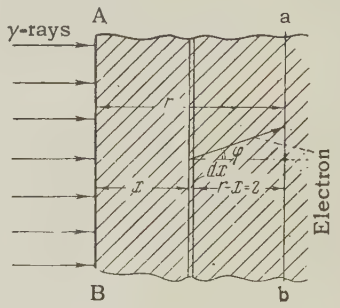

FIG. 1.

the plane a-b of electrons with initial energy in the interval from E to E + dE, which are produced in the elementary layer dx at distance x from the front face of the target is

$$dN = \sigma e^{-\sigma x} D(E)_\alpha f\left\{E, \frac{r-x}{\cos\varphi(E)}\right\} dx\, dE, \qquad (1)$$

where σ is the linear Compton scattering coefficient, $D(E)_\alpha$ is the energy distribution function for the Compton electrons for a given value of $\alpha = E_\gamma/mc^2$, and is given by the Klein-Nishina formula; $f\{E, (r-x)/\cos\varphi(E)\}$ is the function which gives the probability that a Compton electron emerging at an angle φ (relative to the initial direction of the quantum) will penetrate to depth $r-x$ in the target. For this function we took the experimental curves for absorption of monochromatic electrons of various energies in aluminum,

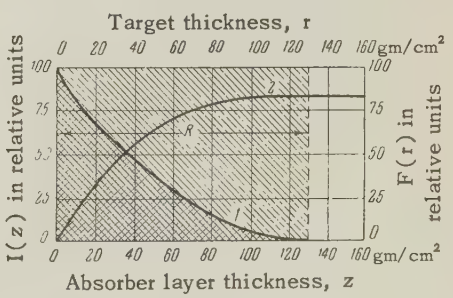

FIG. 2. Results of integration of expression (1). 1 – I(z) (ordinate scale on the left); 2 – F(r) (ordinate scale on the right).

*I.e. a target thickness of the order of the range of the secondary electrons of maximum energy.

†This is the case even when one takes into account the yield of electrons from the back wall, using for example the data of Hine.[7]

which were obtained by Sinel'nikov, Val'ter et al.[11]

To find the total flux of electrons passing through the plane a-b, expression (1) was integrated over the whole range of energies and then over x. The integration was done numerically. The result is shown on an arbitrary scale in Fig. 2. The first integration gives the curve I(z), where $z = r - x$ (cf. Figure 1). This is just the absorption curve of the electrons produced in the layer dx. The second integration gives the curve F(r),* which shows the dependence of the flux of electrons through a-b on the distance from the front face, or in other words, the dependence of electron yield on target thickness.

It is not hard to see that the ratio of the area under the curve I(z) to the total area of the shaded rectangle gives the ratio of the electrons emitted from the back face of a target of effective thickness to the total number of Compton electrons formed in the body of the target. Denoting this ratio by ξ, we determine η — the number of electrons per quantum incident on the target, from the simple relation

$$\eta = \xi \sigma R,$$

where R is the effective thickness of the target. Taking $R = 0.048$ cm (cf. Figure 2), $\sigma = 0.098$,[12] and substituting the value of $\xi = 0.33$ found from the graph, we get finally

$$\eta = 1.6 \cdot 10^{-2} \text{ electrons}/\gamma\text{-quantum}.$$

EXPERIMENTAL DETERMINATION OF η

For the experimental determination of η, a special aluminum counter tube was prepared. Its construction is shown in Figure 3. In the middle of the body of the counter, on the outer wall, there is a cylindrical projection 13 mm in diameter. The wall thickness of the tube at the position of the projection is 6 mm, i.e., a little greater than the effective thickness. There is a fine channel 1 mm in diameter at the center of the projection, and its outer end is covered by a thin (30 μ) cellophane window. In the diametrically opposite wall of the tube there is a circular opening 15 mm in diameter, also covered with cellophane. A constant pressure of 40 — 60 mm Hg was maintained in the tube, and the operating voltage was 2000 V. The tube plateau was 40 — 50 V, which is entirely adequate.

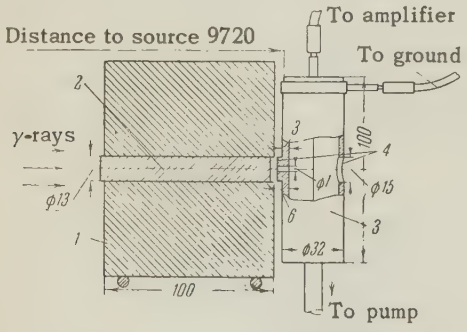

FIG. 3. Counter tube with lead collimator-shield. 1) Shield, 2) collimator channel, closed by lead plug, 3) counter tube, 4) cellophane windows. All dimensions given in mm.

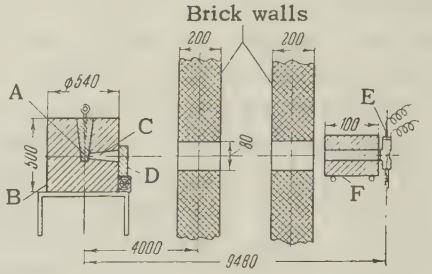

FIG. 4. Arrangement of apparatus (dimensions in mm).

The overall geometry of the experiment is shown in Figure 4. The source A (RdTh with an intensity of 896 ± 20 mC) was placed in the lead container B at a distance of 948 cm from the center of the tube. The preliminary collimation of the γ-rays was done by the channel C in the container and a pair of brick walls with 80 mm diameter holes. The radiation was filtered by a 5 cm lead filter D at the exit of the channel C. In front of the counter tube E we placed the main collimator F, consisting of a lead shield 100 mm thick, with a cylindrical channel whose cross section precisely matched that of the projection on the tube (13 mm diameter). The channel could be closed throughout its length by means of a tight-fitting lead plug (cf. Figure 3).

The experiment was carried out as follows. A small lamp was placed at the position of the source, and its light was used to align the whole apparatus visually, so that the source, the axis of the channel in the shield, the projection on the tube and the cellophane window opposite it were in a straight line. With the shield channel closed by the lead plug, we measured the tube background and the effect of scattered radiation from the source. Then the plug was removed, and the collimated beam of γ-rays passed through the projection into the counter tube and emerged from it through the cellophane window. The excess count thus obtained above the effect of background and scattered radiation was attributed

*The factor $\exp\{-\sigma(r - x)\}$, which is unimportant for the thicknesses used, was set equal to unity.

to electrons produced in the tube by the γ-rays. The effect of the action of the γ-rays on the rear cellophane window was assumed to be equal to zero.

Three series of measurements were made, with repeated counting of background and effect. Between series of measurements the apparatus was readjusted to eliminate possible systematic errors resulting from inexact alignment. The measurements gave the value

$$\eta = 1.3 \pm 0.2 \cdot 10^{-2} \text{ electrons/quantum.}$$

Here it is assumed that only quanta with energy 2.62 Mev are effective.* This result is in satisfactory agreement with the computed value.

From this value and the data of Hine[8] we can compute, for example, the absolute values of the yields of electrons per 2.62 Mev quantum for other materials (cf. the table).

Yield of electrons per quantum of energy 2.62 Mev for various materials

Element	Atomic number of element	Relative yield according to Hine	Absolute yield (electrons/quantum)$\times 10^2$
C	6	2.1	1.6
Al	13	1.7	1.3 ± 0.2
Cu	29	1.2	0.9
Sn	50	0.92	0.7
Pb	82	1	0.8

Comparing these data with the values found in Bradt's experiments for the efficiency of copper and lead counters for γ-rays of the same energy (1.45 electrons/quantum for copper, and 1.94 ± 0.07 for lead), we see that, as was to be expected, Bradt's data are higher than the values in our table, by factors of 1.6 and 2.4, respectively. This excess is completely reasonable, since in the geometry of Bradt's experiment, there should be an appreciable effect of small angles of incidence in the irradiation of the cylindrical surfaces of the counters, while for the lead counter there is in addition the yield of electrons from the back wall, which is known to amount for lead to about $\frac{1}{3}$ of the yield of electrons from the front wall.[7]

*For the fraction of quanta with energy 2.62 Mev in the spectrum of the radiation, cf., for example, Reference 13.

CONCLUSION

We have made an experimental determination of the yield of electrons from an aluminum target bombarded by 2.62 Mev γ-rays. The value 1.3 ± 0.2 electrons/quantum which was found is in satisfactory agreement with the value 1.6 electrons/quantum which was computed using data from the literature on absorption of monochromatic electrons.

On the basis of these data and values in the literature for relative yields of electrons from various materials at various energies, one can find absolute values of these quantities.

[1] W. H. Bragg and J. P. V. Madsen, Phil. Mag. **16**, 918 (1908).

[2] K. W. F. Kohlrausch and E. Schrödinger, Wiener Ber. **123**, 1319 (1914).

[3] W. V. Mayneord, Proc. Roy. Soc. (London) **A130**, 63 (1930).

[4] E. J. Workman, Phys. Rev. **43**, 859 (1933).

[5] Quimby, Marinelli and Blady, Amer. Jour. Roentgenology **41**, 804 (1939).

[6] C. W. Wilson, Proc. Phys. Soc. (London) **53**, 613 (1941).

[7] G. J. Hine, Phys. Rev. **82**, 755 (1951).

[8] G. J. Hine, Nucleonics **10**, 9 (1952).

[9] Bradt, Gugelot et al., Helv. Phys. Acta **19**, 77 (1946).

[10] K. W. F. Kohlrausch and E. Schrödinger, Wiener Ber. **123**, 1319 (1914).

[11] Sinel'nikov, Val'ter et al., J. Exptl. Theoret. Phys. (U.S.S.R.) **9**, 127 (1939).

[12] C. M. Davisson and R. D. Evans, Rev. Mod. Phys. **24**, 79 (1952).

[13] J. Surugue, Journ. Phys. et Rad. **8**, 145 (1946).

Translated by M. Hamermesh
165

INTERNAL CONVERSION ELECTRON STUDY OF THE LOWER EXCITED LEVELS OF U^{235}

E. F. TRET'IAKOV, G. I. GRISHUK and L. L. GOL'DIN

Submitted to JETP editor November 15, 1957

J. Exptl. Theoret. Phys. (U.S.S.R.) **34**, 811-819 (April, 1958)

The internal conversion electrons emitted by excited U^{235} nuclei after α decay of Pu^{239} were investigated. Multipolarities of the transitions were established and the spins and parities of the first 6 levels were determined by comparing the results with the theoretical internal conversion coefficients for the L_I, L_{II} and L_{III} shells. It was shown that the first 5 levels form a rotational band with $K = \frac{1}{2}$. More precise values of the energies of the excited states were obtained.

INTRODUCTION

THE α spectrum of Pu^{239} is very well known at present and indicates that the daughter nucleus U^{235} possesses a number of excited levels. Table I is a list (taken from Refs. 1 to 3) of the first few excited levels of U^{235} as known from α decay and the probabilities of α decay to these levels.

TABLE I

No. of level	Excitation energy (kev)	Intensity of α decay (%)
0	0	72
I	13.2	16.8
II	51.7	10.5
III	84	$3.7 \cdot 10^{-2}$
IV	151	$1.3 \cdot 10^{-2}$
V	172	$5 \cdot 10^{-3}$
VI	234	$5 \cdot 10^{-3}$

These excitation energies are computed from the "zero" level of U^{235} (the lowest U^{235} level to which α decay goes). As was shown by Novikova et al.,[3] this level does not coincide with the ground level of U^{235}. α spectroscopy provides a reliable determination of the energies of the excited levels but does not generally establish their spins and parities. The γ transitions between levels must be studied for additional information.

The conversion and γ emission of U^{235}* have not been studied as thoroughly as the α decay of Pu^{239}. In Refs. 4 and 5 the internal conversion electrons of U^{235} were investigated by means of electron-sensitive plates. Only the most intense transitions of 35 and 53 kev were found (II — I and II — 0 in our notation). West and Dawson[6] obtained strong L lines, and also γ lines with the energies 37.7, 52.3, and 59.2 kev. The first two lines are due to the transitions II — I and II — 0; the origin of the last line is uncertain. Freedman, Wagner and Engelkemeir[7] observed only conversion electrons with the energies 31.4, 35.3, 47.1, and 50.2 kev, i.e., L_{II}, L_{III}, M and N + 0 electrons from the II — 0 transition. They also found γ rays with energies of 17.5 kev (100%), 35 kev (0.4%), 100 kev (1.1%), 124 kev (0.5%) and 384 kev (0.3%). These will be discussed later. Finally, Shliagin[8] detected a number of U^{235} conversion lines which can be explained completely by the transitions I — 0, II — I and II — 0. He also found strong 2.2-kev emission which he erroneously ascribed to K conversion of a 117-kev γ transition.

It is thus clear that we have extremely incomplete data as well as poor agreement in the case of weak lines. This induced us to make a detailed investigation of the conversion electron spectrum which accompanies the α decay of Pu^{239}

EXPERIMENTAL METHOD

The internal conversion electrons which accompany the α decay of Pu^{239} were studied by means of an iron-free β spectrometer with a toroidal magnetic field.[9] We studied the spectrum of electrons ejected immediately following α emission ($\alpha - \beta$ coincidences). The transmission of the instrument for electrons is 7% with resolution of 1% (the transmission for $\alpha - \beta$ coincidences is 2.5%).

In the study of low-energy electrons a potential of 10 kev was applied to the source. Acceleration did not cause broadening of the lines of even the slowest electrons. The α detector was a stilbene crystal placed directly behind the source and con-

*Here and hereinafter we are concerned with the radiation from U^{235} nuclei left in excited states after the α decay of Pu^{239}.

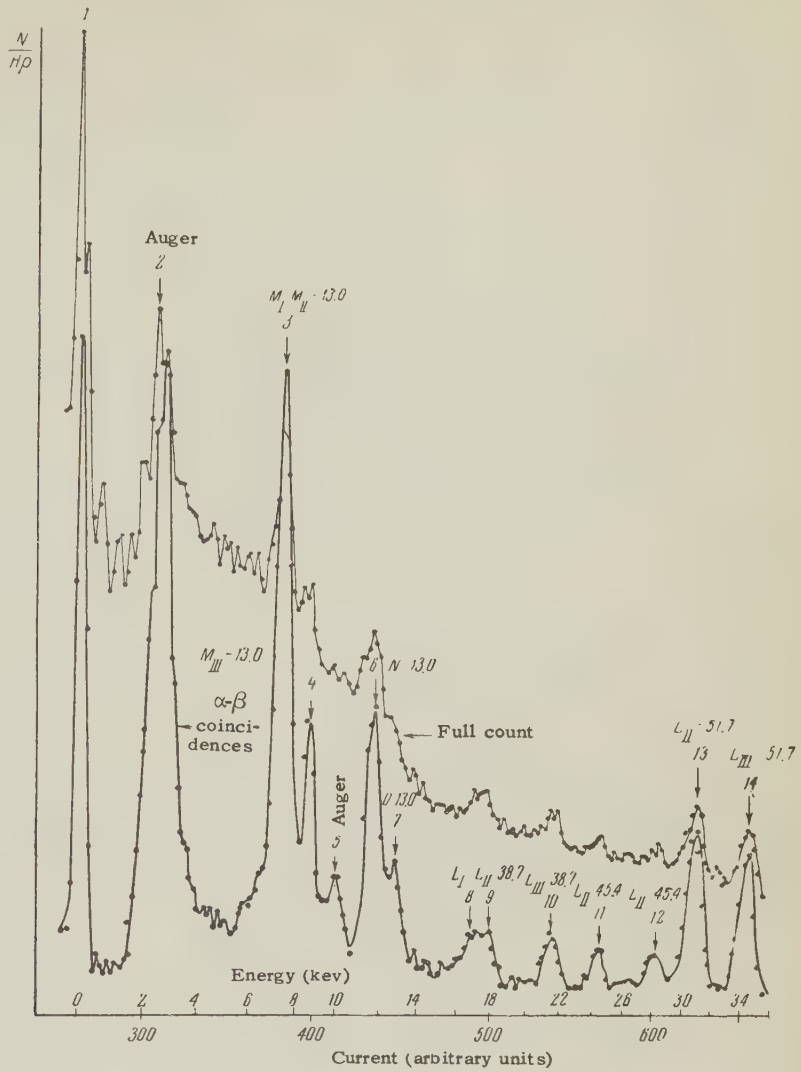

FIG. 1. Electron spectrum of U^{235} in the range 0 – 35 kev with accelerating voltage 7.0 kev.

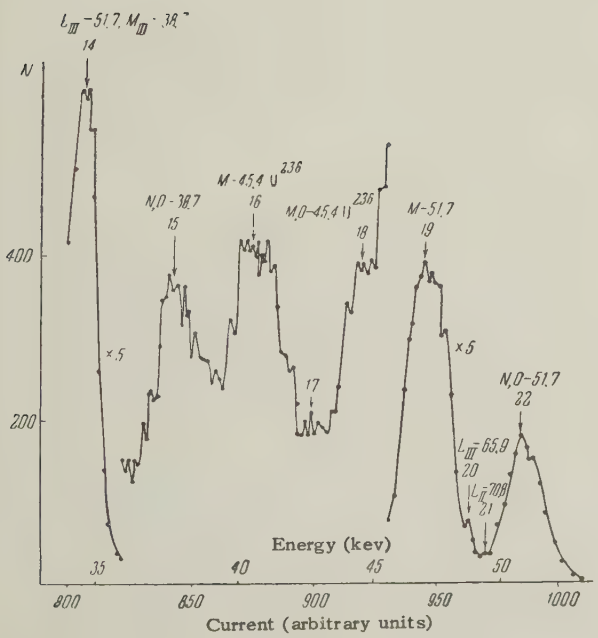

FIG. 2. Electron spectrum of U^{235} in the range 35 – 52 kev.

nected by a light pipe to a FEU-29 photomultiplier. We also used a scintillation counter to detect electrons, with a CsI(T1) crystal for electrons with energies below 20 kev and stilbene at higher energies.

The source was prepared by vacuum deposition of the active material on a thin mica backing (0.8 mg/cm^2) which was coated with aluminum on the reverse side.

EXPERIMENTAL RESULTS

We investigated the conversion spectrum of U^{235} up to electron energy of 350 kev, but only in the 0 — 105 kev range were conversion lines found which appreciably exceeded the background energy level.

Figures 1, 2 and 3 show portions of the conversion spectrum, which was not fully corrected for the counter efficiency. We measured the counter efficiency in the range 0 — 35 kev and assumed it to be unity above 35 kev.

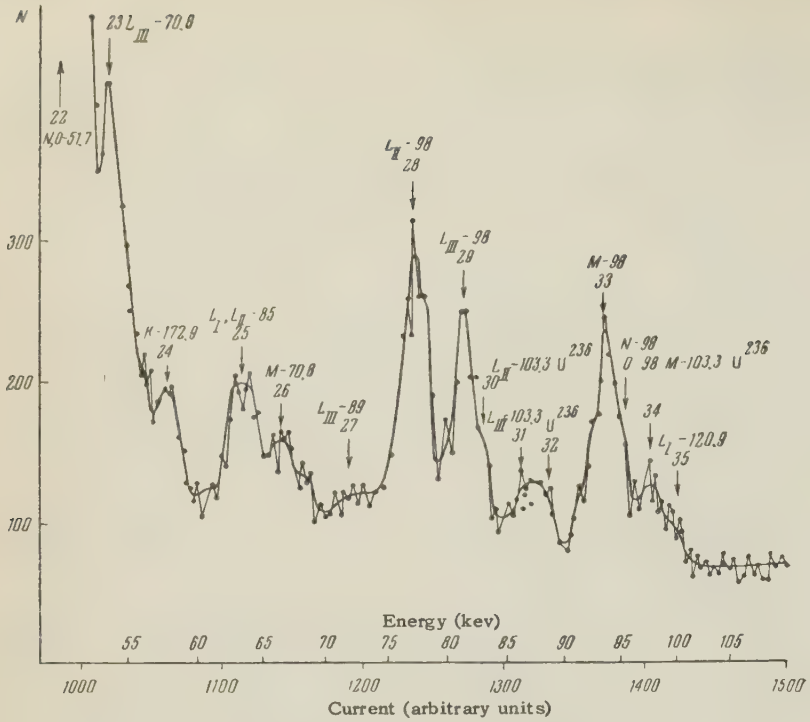

FIG. 3. Electron spectrum of U^{235} in the range 52 – 105 kev.

The electron energies and conversion line intensities are given in Table II. The line intensities were corrected for counter efficiency and are expressed as percentages relative to the number of Pu^{239} α decays. In determining conversion electron energies our reference lines were the L_{II} and L_{III} lines from the II – 0 transition with energy taken to be 51.7 kev and the L_{II} and L_{III} lines from the γ transition between the 143.3 and 43.5-kev levels of U^{234} (the daughter nucleus of Pu^{238}).

I. Levels I and II (13.0 and 51.7 kev)

Novikov et al.[3] have shown that levels I and II with excitation energies 13.0 and 51.7 kev (relative to the "zero" level of U^{235}) can be regarded as the first excited levels of a rotational band with $K = \frac{1}{2}$, beginning with the "zero" level. With this interpretation levels 0, I and II must have spins $\frac{1}{2}$, $\frac{3}{2}$, and $\frac{5}{2}$ and identical parity.

Almost all of the conversion lines corresponding to the transitions II – 0, II – I and I – 0 are clearly seen in the spectrum (Figs. 1 and 2). We determined the multipole orders of these γ transitions. Our experimental ratio of the conversion coefficients of the II – 0 γ transition in the L_{III} and L_{II} subshells is 0.88, which is in excellent agreement with the theoretical value of 0.87 (private communication from L. A. Sliv) for an E2 transition at the given energy. The II – I transition is mixed: 87% M1 + 13% E2 (for γ-emission probability). The multipole orders of the transitions provide acceptable confirmation of the rotational nature of levels II, I and 0

The M-conversion coefficients are unknown, but if we make the usual assumption that the conversion ratio for M subshells is equal to the corresponding ratio for L subshells it is possible to calculate the M1 and E2 contributions to the I – 0 transition. (In this case L radiation cannot be excited because the γ-ray energy is below the electron binding energy in the L shell.) For the I – 0 transition the experimental ratio is $(M_I + M_{II})/M_{III} = 10\%/3.6\%$, which corresponds to 99.5% M1 + 0.5% E2. (The L-conversion coefficients supplied to us by Sliv were extrapolated to 13 kev.)

II. Level III (83.8 kev)

According to Ref. 3, the 83.8-kev level is the third excited rotational level of a band with $K = \frac{1}{2}$. The spin must be $\frac{7}{2}$ and the parity must agree with that of the other levels of the same band.

We detected only one transition beginning at this level (the III – I transition). The transition energy of 70.8 ± 0.2 kev was determined from the L_{III} line (peak 23, Fig. 3). We were unable to determine the multipole order of this transition because its weak L peaks fall on the slope of the strong N + 0 peak of the II – 0 transition and reliable measurements could not be obtained. We were also unable to detect III – II transitions; this is

TABLE II. Internal conversion electrons which accompany the α decay of Pu^{239}

No. of peak	Electron energy (kev)	Intensity*	Transition type and energy		Levels between which transition occurs
1	0	~100	"Zero" peak		
2	2.59	~15	Auger M – 2N		
3	7.48	10	$M_I M_{II}$	13.0	13.0—0
4	8.62	3.6	M_{III}	12.92	13.0—0
5	9.79	1.0	Auger M – 2N		
6	11.68	4.4	N	13.1	13.0—0
7	12.88	1.6	O	13.2	13.0—0
8	16.70	0.65	L_I	38.5	51.7—13.0
9	17.83	0.76	L_{II}	38.8	51.7—13.0
10	21.63	0.76	L_{III}	38.8	51.7—13.0
11	24.43	0.61	L_{II}	45.4	45.4—0 U^{236}
12	28.28	0.54	L_{III}	45.4	45.4—0 U^{236}
13	30.82	2.8	L_{II}	51.7	51.7—0
14	34.47	2.46	L_{III}	51.6	51.7—0
15	37.5	0.14	N, O	38.8	51.7—13.0
16	40.7	0.19	M	45.4	45.4—0 U^{236}
17	42.8	0.01	?		
18	44.5	0.07	NO	45.4	45.4—0 U^{236}
19	47.0	1.4	M	51.7	51.7—0
20	48.7	0.02?	L_{III}	65.9	149.7—83.8
21	49.4	0.02?	L_{II}	70.3	83.8—13.0
22	51.0	0.6	N, O	51.7	51.7—0
23	53.6	0.0050	L_{III}	70.8	83.8—13.0
24	57.9	0.002	K	172.9	172.6—Ground level of U^{235}
25	63.3	0.003	$L_I L_{II}$	85	234.7—149.7
26	66.6	0.002			
27	71.9	0.0007	L_{III}	89	172.6—83.8
28	77.0	0.006	L_{II}	97.9	149.7—51.7
29	81.0	0.004	L_{III}	98.2	149.7—51.7
30	82.7		L_{II}	103.6	148.7—45.4 U^{236}
31	85.9	0.001	L_{III}	103.1	148.7—45.4 U^{236}
32	87.9	0.0008			
33	93.6	0.004	M	98.0	149.7—51.7
34	97.4	0.002	N, O	98.0	149.7—51.7
35	99.2	0.001?	L_I	120.9	172.6—51.7

*The intensity is corrected for the transition of the counter in the 0 – 35 kev region and given in percentages relative to the total number of P^{239} α decays.

easily explained by the fact that the conversion lines of these transitions fall in the region of the strong peaks of Fig. 1.

There is a noteworthy absence of the III – 0 transition, which we would easily have observed if its intensity were comparable with that of the III – I transition. This absence provides strong confirmation that the spin of level III is $\frac{7}{2}$. Indeed, the III – 0 transition must thus be of the M3 type and cannot compete with the E2 and M1 transitions from level III to levels I and II.

III. Level IV (149.7 kev)

This level, like the preceding level, was first found by Novikova et al.[3] through α rays and was interpreted as the fourth excited level of a rotational band with $K = \frac{1}{2}$. Its spin must be $\frac{9}{2}$ and its parity must agree with the parity of lower-lying levels.

We have found two transitions beginning at this level. Fig. 3 shows the L_{II} (peak 28) and L_{III} (peak 29) conversion lines which belong to the transition IV – II. From these lines the transition energy was determined to be 98.0 ± 0.3 kev. The experimental L_{III}/L_{II} intensity ratio is 0.76, which is somewhat higher than the theoretical ratio of 0.56 for an E2 transition but fits no other transition. The absence of conversion in the L_I subshell is additional evidence favoring an E2 transition.

Figure 2 shows a weak line (peak 20) of the IV – III transition (L_{III} with 65.9 kev). By a fortunate coincidence this line falls into the valley between the M and N peaks of the II – 0 transition. The other L lines of this transition are hidden by the M peak of II – 0. We cannot see conversion lines corresponding to IV – I and IV – 0 transitions, and if they exist their intensity is less than $\frac{1}{10}$ of the IV – II intensity. On the basis of the foregoing data, we can confidently

state that level IV belongs to the rotational band which we are considering and has spin $^9/_2$.

As already mentioned, a 100-kev γ line in the γ spectrum of U^{235} was reported in Ref. 7. This line is easily explained by the IV — II transition; its intensity compared with the 17.5-kev line is highly exaggerated in Ref. 7.

IV. Level V (172.6 kev)

This level was first observed by Asaro and Perlman through $\gamma-\gamma$ coincidences (private communication). According to Ref. 3, the intensity of the α transition to level V is 5×10^{-3}%. We observed a few weak conversion lines which can be ascribed to transitions from this level, which has an energy of 172.6 ± 0.5 kev. In considering transitions from level V, we are struck by the absence of L-conversion electrons from V — I transitions and the considerable number of such electrons from V — II. The absence of L electrons from V — I cannot be explained by reduction of the L-conversion coefficient with increasing transition energy; higher probabilities of γ transitions with increasing energy compensate the reduction of the conversion coefficient. The most reasonable explanation is the large spin of level V.

Our results can be interpreted clearly by assigning spin $^7/_2$ to level V and a parity which is opposite to that of the rotational band and agrees with the parity of the ground level (but not zero level) of U^{235}. The transition to level I must then be of type M2 and cannot compete with the E1 transition to levels II and III. We interpret peak 27 to be an L_{III} peak of the V — III transition. The L_I and L_{II} lines fall into the region occupied by peak 26 and cannot be seen. Peak 35, which is on the slope of peak 34, can be ascribed to a V — II transition (a L_I line). In the E1 transition the L_{II} and L_{III} lines are considerably weaker than L_I and are thus not observed. The small conversion coefficient for E1 transitions (K + L = 0.27) explains the strong 120-kev γ radiation which has been noted by a number of investigators (Ref. 7 and a private communication from Asaro and Perlman).

We ascribe peak 24 to the K conversion of the transition from level V to the ground level of U^{235}. E0 and M1 transitions are possible here, and estimates show that the first of these possesses considerable probability. The large conversion coefficient for M1 transitions and, possibly, the considerable contribution of the 100% converted E0 transition explain why no one has observed thus far the corresponding γ rays. The absence of L electrons is due to the large K/L ratio for E0 and M1 transitions.

We note in conclusion that our argument in favor of spin $^7/_2$ is based on an interpretation of very weak and inadequately investigated transitions. This interpretation cannot therefore be considered final.

V. Level VI (234.7 kev)

Peak 25 of Fig. 3 (electron energy 63.4 kev) cannot be ascribed to any one of the foregoing transitions. This peak is wider than the peaks of single lines. It could be explained as resulting from a transition between level III (83.8 kev) and the ground level (not the zero level) of U^{235}. However, this seems very unlikely since the intensity of this transition must be small as a result of nuclear readjustment and peak 25 is only one-half smaller than peak 23 (of the L_{III} transition III — I).

We believe that peak 25 is most probably associated with a transition between levels VI and IV. The energy obtained for level VI is 234.7 kev. We find no transitions from level VI to other levels of the rotational band; this may be ascribed to a large spin of level VI (such as $^{11}/_2$).

SEARCH FOR AN ISOMERIC TRANSITION

We know from Ref. 10 that the spin of U^{235} in the ground state is $^7/_2$, whereas the α decay of Pu^{239} goes to the "zero level" of U^{235}, which undoubtedly has spin $^1/_2$. The large spin difference and close energies of the ground and zero levels suggest that the "zero state" is an isomeric state of U^{235} (Ref. 3).

In Shliagin's[8] study of the conversion spectrum of U^{235}, he found an intense 2.2-kev line which he ascribed to γ radiation of 3 kev. On the basis of Shliagin's work, Novikova et al.[3] suggested that the "zero peak" of U^{235} is separated by 3 kev from the ground level.

We have carefully investigated the conversion radiation from U^{235} in the soft energy region and have actually found a strong peak in the region 2.4 — 2.6 kev. However, we have found similar peaks with comparable intensities for Pu^{238}, Cm^{242}, Am^{241} and even Po^{210}, where there are certainly no 3-kev transitions. This peak is undoubtedly associated with the Auger effect, which occurs in emission from excited levels (the larger part of the effect) and in auto-ionization of atoms accompanying α decay (the smaller part of the effect).

We were unsuccessful in our search for electrons from the isomeric transition. These electrons are most likely concealed by the strong (~100%) peak of "zero"-energy electrons which

was always present in our experiments and was even observed in control sources lacking the active material (aluminum-coated mica). The energy of electrons from the isomeric transition is probably so small that they practically do not emerge from our sources of 0.8 mg/cm^2 thickness. This was confirmed by Asaro and Perlman, who reported[12] that they succeeded in finding soft radiation from U^{235} which was almost completely absorbed in a source of 0.7 mg/cm^2 thickness.

EXCITED LEVELS OF U^{236}

An admixture of Pu^{240} (6.5% of the activity) in our sources enabled us to investigate the conversion electrons emitted by the daughter nucleus U^{236} The L_{II} and L_{III} lines (peaks 11 and 12, Fig. 1) permit a reliable determination of the energy and spin of the first excited level of U^{236}. The energy of the level is 45.4 ± 0.2 kev. The emission in question is of type E2, so that the 45.4-kev level has spin 2 and positive parity. The L_{III} line for the transition from the second to the first excited level gives 148.7 ± 0.4 kev for the energy of the second excited level.

Our source also contained some Pu^{241}. We observed only a continuous β spectrum associated with the β transition $Pu^{241} \rightarrow Am^{241}$.

CONCLUDING REMARKS

Our results definitely show that the zero, I, II, III, and IV levels of U^{235} (see Fig. 4) belong to a rotational band with $K = 1/2$. We observed a number of electromagnetic transitions between these levels and transitions from the nonrotational level V ($7/2^-$) to various levels of the rotational band.

The probabilities of transitions of the same multipole order to levels in a single rotational band are related by the simple theoretical formula:[13]

$$\frac{B(L,\ I_i - I_f)}{B(L,\ I_i - I_f')} = \frac{\left| C^{I_f K_f}_{I_i K_i;\ L,\ K_f - K_i} \right|^2}{\left| C^{I_f' K_f;}_{I_i K_i;\ L,\ K_f - K_i} \right|^2},$$

where B is the reduced probability of a γ transition, which depends on the multipole order L of the γ radiation and the difference between the spin I_i of the initial nucleus and I_f of the final nucleus. The right-hand side of this equation contains the Clebsch-Gordan coefficients C. The probabilities B are related to ordinary probabilities by the formula

$$T = \frac{8\pi\,|\,L+1\,|}{L\,[(2l+1)!!]^2} \frac{1}{\hbar} \left(\frac{\omega}{c}\right)^{2L+1} B(L).$$

Our experimental results permit a comparison

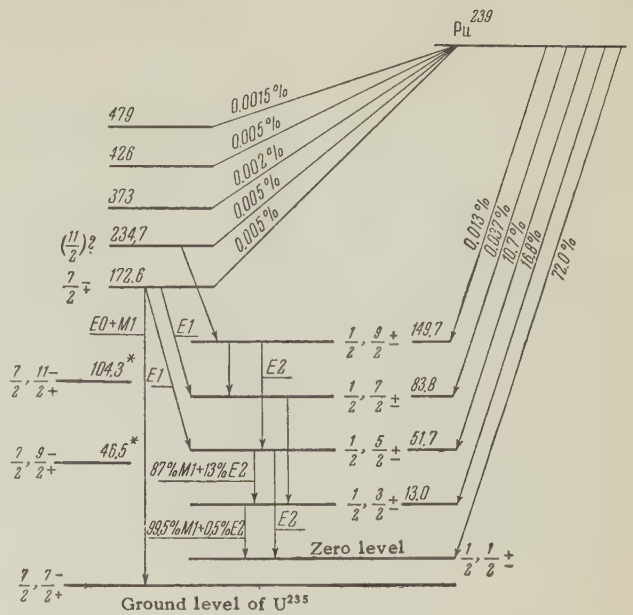

FIG. 4. Low-lying excited levels of U^{235} (from α decay data in Ref. 3). * – marks levels known from the Coulomb excitation of U^{235}. The energies of all levels are expressed in kev and computed from the "zero level."

with the theoretical intensities of E2 transitions from level II to levels I and 0. The theoretical ratio is

$$B\left(E2;\ \frac{5}{2} - \frac{3}{2}\right) \Big/ B\left(E2;\ \frac{5}{2} - \frac{1}{2}\right) = \frac{2}{7} = 0.29.$$

The experimental ratio is

$$\frac{B(E2;\ {}^5/_2 - {}^3/_2)}{B(E2;\ {}^5/_2 - {}^1/_2)} = \frac{N_{L_{III}}(38.7)}{N_{L_{III}}(51.7)} \frac{\alpha_{L_{III}}(51.7)}{\alpha_{L_{III}}(38.7)} \left(\frac{51.7}{38.7}\right)^3 = 0.36.$$

The good agreement of the theoretical and experimental intensity ratios is additional confirmation of the rotational nature of levels 0, I, and II. Transitions from level V to levels of the rotational band cannot be compared with the foregoing theory because these transitions involve violation of the rules of K forbiddenness, making the formulas inapplicable.

We note, finally, that the investigation of the α spectrum of Pu^{239} points to the existence of a series of higher excited levels of U^{235}, although electromagnetic transitions between these levels have thus far escaped detection.

Figure 4 summarizes the present data on the lower excited levels of U^{235}.

In conclusion we gratefully acknowledge assistance with the measurements by L. N. Kondrat'ev, I. I. Agapkin, and G. Chernov. We also wish to thank L. A. Sliv for values of the L-conversion coefficients which he supplied to us before publication.

[1] F. Asaro and I. Perlman, Phys. Rev. **88**, 828 (1952).

[2] Gol' din, Tret' iakov and G. I. Novikova, Reports of Conference of the U.S.S.R. Academy of Sciences on the Peaceful Uses of Atomic Energy, Div. of Phys. and Math. Sciences, p. 266, 1955.

[3] Novikova, Kondrat' ev, Sobolev, and Gol' din, J. Exptl. Theoret. Phys. (U.S.S.R.) **32**, 1018 (1957); Soviet Phys. JETP **5**, 832 (1957).

[4] D. Dunlavey and G. T. Seaborg, Phys. Rev. **87**, 165 (1952).

[5] G. Albouy and I. Teillac, Compt. rend. **232**, 326 (1951).

[6] D. West and J. K. Dawson, Proc. Phys. Soc. (London) **A64**, 586 (1951).

[7] Freedman, Wagner, and Engelkemeir, Phys. Rev. **88**, 1155 (1952).

[8] K. N. Shliagin, J. Exptl. Theoret. Phys. (U.S.S.R.) **30**, 817 (1956), Soviet Phys. JETP **3**, 663 (1956).

[9] Tret' iakov, Gol' din and Grishuk, Приборы и техника эксперимента (Instruments and Meas. Engg.) **6**, 22 (1957).

[10] K. L. Van der Sluis and J. R. McNally, J. Opt. Soc. Am. **45**, 65 (1955).

[11] Bohr, Froman and Mottelson, Kgl. Danske Videnskab. Selskab, Mat.—fys. Medd., **29**, 10 (1955).

[12] F. Asaro and I. Perlman, U.C.R.L. 3774 (1957).

[13] Alaga, Alder, Bohr and Mottelson, Kgl. Danske Videnskab. Selskab, Mat.—fys. Medd., **29**, 9 (1955).

Translated by I. Emin
166

SOVIET PHYSICS JETP VOLUME 34(7), NUMBER 4 OCTOBER, 1958

STRUCTURE OF SUPERCONDUCTORS: XII
INVESTIGATION OF BISMUTH — RUBIDIUM ALLOYS

N. N. ZHURAVLEV, T. A. MINGAZIN, and G. S. ZHDANOV

Moscow State University

Submitted to JETP editor November 15, 1957

J. Exptl. Theoret. Phys. (U.S.S.R.) **34**, 820-826 (April, 1958)

A provisional melting diagram is constructed for the Bi — Rb system on the basis of thermal, microscopic, and x-ray data. Four compounds have been established for the Bi — Rb system: Bi_2Rb, $BiRb_3$, and two others which presumably are Bi_2Rb_3 and $BiRb_2$. The superconducting compound Bi_2Rb crystallizes in the cubic system with a lattice constant a = 9.609 A and has a structure of the Cu_2Mg type.

ACCORDING to data obtained by Alekseevskii,[1] heterogeneous alloys of bismuth with rubidium, having a large excess of bismuth, go over into the superconducting state at a temperature of 4.25°K. In spite of the non-uniformity of the alloys, the curves showing the superconducting transition displayed relatively little scatter, thus indicating the existence of a superconducting bismuth — rubidium compound. One of the purposes of the present investigation was to ascertain the composition and the atomic-crystalline structure of this compound.

The study of the bismuth — rubidium system involved the solution of a series of experimental problems. The principal difficulties were conditioned by the large chemical activity of metallic rubidium and by the markedly different physiochemical natures of bismuth and rubidium. All the investigations were carried out with a small quantity of rubidium (~3 gm), so that we had to develop micromethods for preparing the alloys and for analyzing them physiochemically. A certain quantity of metallic rubidium was obtained by one of the authors from the vacuum reduction of rubidium — iodide by calcium.[2]

PREPARATION OF THE ALLOYS

The large chemical activity of metallic rubidium required the creation of conditions which would prevent the oxidation of the metal during the proc-

ess of preparing a charge, putting it into an iron crucible or a quartz capsule, and melting it. The methods of preparing alloys which are described in the literature relate principally to the less active alkali metals — lithium, sodium, and potassium, and were designed to be used for the separate melting of comparatively large quantities of metal, of the order of several grams or more. Our attempts to find methods described in the literature for preparing small quantities of bismuth — rubidium alloys (of the order of tenths of grams) gave no positive results. After an entire series of experiments carried out by one of the authors,[3] we arrived at the following method of preparing the alloys. A special pipette was made from a quartz tube (Fig. 1).

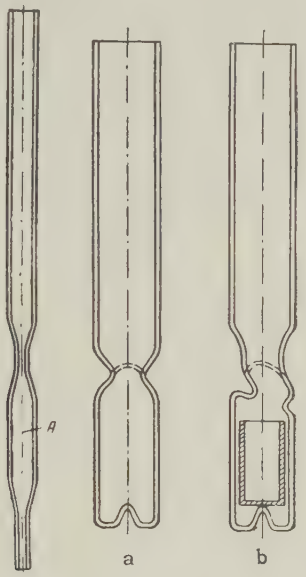

FIG. 1. FIG. 2.

Liquid rubidium was drawn into the volume A, which was terminated at both ends by capillaries. After the rubidium had hardened, the pipette was weighed on an analytical balance and the weight of rubidium was determined from the difference in the weights of the pipette with and without the rubidium. In such a pipette the surface area of the rubidium in contact with the atmosphere was small (the capillary diameter was 0.2 — 0.6 mm). The loss of rubidium during the time necessary to prepare a charge (2 — 3 minutes) was negligible. The error in the determination of the composition of an alloy did not exceed 0.1%. A known weight of bismuth was placed in the quartz capsule, or into an iron crucible placed in the quartz capsule (Fig. 2a, b). By means of a specially-made apparatus the rubidium, under a pressure of helium, was run off into the quartz capsule or into the iron crucible located in the capsule, and the capsule was removed.

A diagram of the apparatus used for fusing the rubidium and sealing off the capsule is shown in Fig. 3. The whole assembly is fastened to a common laboratory stand 1. The brass capsule holder 3 is made fast to the pillar of the stand by means of a sleeve 2. The quartz capsule 4 with the iron crucible 5, in which there is a known weight of bismuth, is connected to the holder through a length of vacuum hose 6. The pipette 19 containing the rubidium projects down into the capsule through a hole in the center of the holder, which is sealed off by means of a rubber packing 7, a collar 8, and a nut 9. The lower end of the pipette (the capillary) leads into the iron crucible. The upper end is connected through a piece of vacuum hose 10 to a forepump and to a helium cylinder 11. The capsule holder is attached to the forepump through a connecting pipe 12. Valves 13 and 14 are opened, and the air is pumped out of the capsule and the pipette. Then valves 13 and 14 are closed and helium from the cylinder is let into the upper end of the pipette through valve 15. The rubidium is melted with the aid of a resistance oven 16 and flows into the crucible under the pressure of the helium gas. The pipette is carefully raised upward so that its lower end is beyond the vicinity of the capsule neck 17. The lower end of the capsule, containing the charge, is wrapped with wet cotton wads and the capsule is sealed off at the neck with

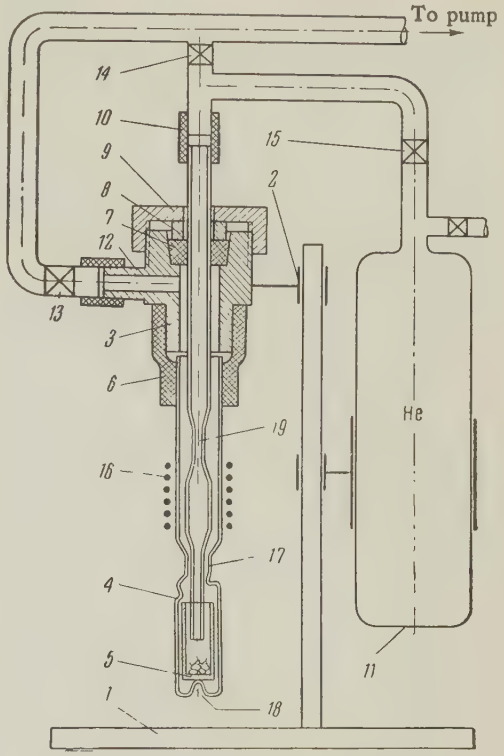

FIG. 3. Arrangement of the apparatus for fusing the rubidium and sealing off the capsule.

the flame of an oxygen torch. An indentation 18 is provided in the capsule for the insertion of a thermocouple junction.

Chemically pure bismuth and rubidium with a calcium impurity of about 3% were used for preparing most of the alloys. Some of the alloys were made with chemically pure rubidium and bismuth. Within the limits of error of the experiment, no appreciable difference was observed between the alloys of bismuth with pure rubidium and with rubidium containing a calcium impurity.

The melting was carried out in a small-gauge resistance oven specially constructed for the purpose. For the alloys containing small amounts of rubidium, quartz capsules of small volume (2 — 5 cm^3) were used for melting the samples and for recording their cooling curves. The alloys containing large amounts of rubidium were melted in iron crucibles placed inside the small-volume quartz capsules. The recording was carried out inside the capsules as follows. The capsule with its iron crucible was placed in the oven and the charge was melted down in the crucible. Then, after the alloy had soaked, the oven was turned over so that the alloy could run into the end of the capsule, where there was an indentation provided for a thermocouple, and the cooling curve was recorded. The preparation directly in the capsule of alloys with a large rubidium content led to a change in the composition of the alloy, since at high temperatures rubidium reacts with the surface of the quartz; a layer is formed thereby which inhibits the further loss of rubidium from the alloy. The preliminary alloying of bismuth with rubidium in the iron crucibles with the subsequent recording of cooling and heating curves inside the quartz capsules makes it possible to obtain alloys with a composition practically corresponding to that of the given charge.

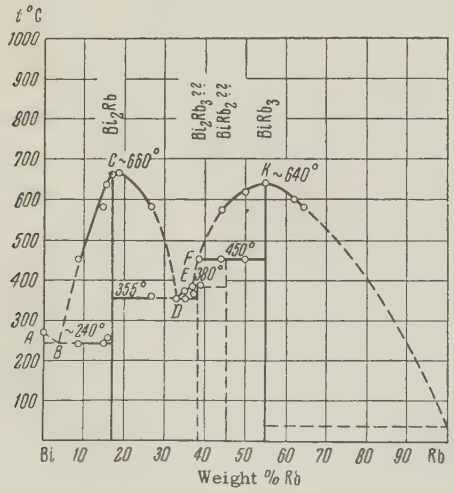

FIG. 4. Melting diagram of the Bi-Rb system.

THERMAL ANALYSIS OF THE ALLOYS

Heating and cooling curves were recorded with an electronic automatic potentiometer EPP-09 down to a temperature of 50 — 100°C. The weight of the alloys varied from 0.3 to 1 gm. The results obtained from the thermal analysis are displayed graphically in Fig. 4.

The melting temperature of bismuth with rubidium added decreases along the line AB down to ~240 — 250°C. A eutectic point lies at about 2 — 4% by weight Rb. From the eutectic point the melting curve gradually increases along the line BC, reaching a maximum at ~660°C at point C for 17% by weight Rb, which corresponds to the compound Bi_2Rb. A further addition of rubidium is accompanied by a falling melting curve, and on the cooling curves a eutectic stop occurs at ~355 — 360°C. An increase in the rubidium content of the alloy leads to a rising melting curve along the line DEFK. At the point K the curve achieves a maximum at ~640°C for an alloy of composition 55% by weight Rb, corresponding to the compound $BiRb_3$. Alloys in the range of compositions from the eutectic point D up to the point K revealed temperature stops at ~380° and ~450°C. The presence of these stops permits us to consider the possibility that two compounds, presumably Bi_2Rb_3 and $BiRb_2$, crystallize out in a peritectic reaction. From the point K on, the melting curve falls as the rubidium content increases.

MICROSCOPIC INVESTIGATION OF THE ALLOYS

A metallographic study was carried out for alloys rich in bismuth with compositions up to that of Bi_2Rb. This study showed that as the rubidium content of the metal increases, the number of crystals of the compound Bi_2Rb increases. In Fig. 5a, b are shown microphotographs of alloys with rubidium contents of 9 and 15% by weight, in which the dark etched spots are crystals of Bi_2Rb, and the light field is the eutectic Bi + Bi_2Rb. As can be seen from the microphotographs, alloys with 15.8% by weight Rb, which are close in composition to the compound Bi_2Rb (17% by weight), contain a small amount of eutectic and are almost homogeneous. Since the preparation of microsections of alloys enriched with rubidium presented experimental difficulties, we studied cross-sections of the alloys microscopically at magnifications of 35, 70, and 120. The phases in the bismuth — rubidium system differed in color. This difference made it possible to estimate the phase composition of an

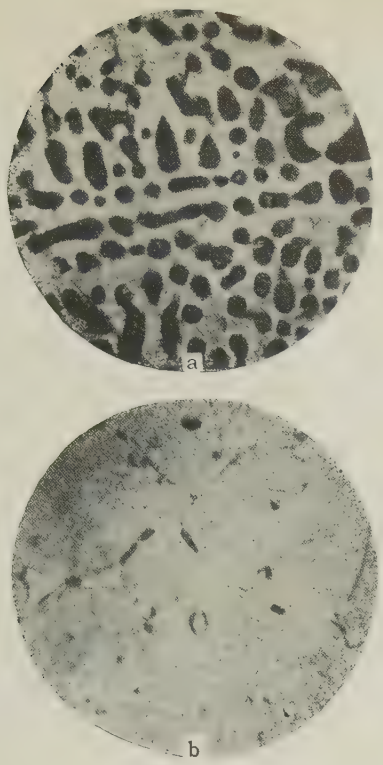

FIG. 5. a) etched with HCl, magnified 200×, b) etched with HCl, magnified 200×.

alloy from its cross-section. Such microscopic studies of the phase composition of alloys rich in rubidium supported the data obtained by thermal analysis.

DETERMINATION OF THE STRUCTURE OF THE SUPERCONDUCTING COMPOUND Bi_2Rb

A comparison of the results of the present investigation with data from low temperature measurements on alloys rich in bismuth 1 shows that the compound Bi_2Rb is a superconductor. An x-ray study of this compound was carried out to determine its atomic structure. This investigation was complicated by the chemical activity of the alloy and by the difficulty of obtaining an alloy of a uniform stoichiometric composition from the alloying of small quantities of charge. At the end of a long experimental program, several satisfactory x-ray photographs were obtained which were of use in determining the structure of the compound Bi_2Rb.

The samples to be used for x-ray photographs were prepared in the following way. A bead of the alloy was crushed up in kerosene which had first been treated with sodium (by maintaining it at a temperature of 110 — 130°C and stirring it for 2 hours, and then filtering it). The alloy powder in the kerosene was drawn into a piece of quartz capillary, and the open end of the capillary was sealed with picein.

Using CuKα radiation and a RKU-86 camera, we obtained x-ray photographs of alloys with compositions close to that of Bi_2Rb (15.8%, 16.6%, etc.). Alloys with such compositions consist mostly of crystals of the compound Bi_2Rb and a small amount of the eutectic Bi + Bi_2Rb. Bismuth gives a large number of lines in x-ray powder patterns. In order to separate the bismuth lines from the compound lines in the x-ray photographs, we used a different size of crystal of Bi_2Rb and bismuth (the crystals of bismuth in the eutectic were considerably small then the crystals of the principal phase, Bi_2Rb). While the x-ray film was being exposed, the sample was rotated, but not with the customary large velocity; it performed only one or two revolutions during the whole time of exposure. As a result of such a process it was easy to separate the weak diffusion lines of the bismuth from the punctuated lines of the compound. The slow rotation of the sample was necessary in order that the points on the lines would be nearly in position and would permit the line intensities to be estimated. From x-ray diagrams obtained with a stationary sample it was difficult to estimate not only intensities of the lines but their location on the diagram as well.

From the x-ray powder patterns of the alloys, the intensities I and the displacements of the lines were measured, and the values of the interplanar distances d were calculated. All the lines of the x-ray photographs of Bi_2Rb crystals are indexed in the cubic system. Laue patterns obtained from single crystals of Bi_2Rb also served to assign these crystals to the cubic system.

The single crystals of Bi_2Rb were separated by mechanical means from alloys composed of 25% by weight Rb. During the exposure the crystal was immersed in a cellulose-nitrate varnish; consequently the surface of the crystal was covered with a thin film of the product of the interaction between the rubidium and the varnish. The Laue patterns were obtained with hard radiation (tungsten). Attempts to obtain x-ray patterns of the waves with copper radiation gave no positive results, and molybdenum radiation is unsuitable, since it gives a strong background due to the excitation of the L-series of bismuth.

The value $a = 9.590 \pm 0.002$ kX is obtained as the result of an accurate determination of the period of the Bi_2Rb cell. Calculations of the interplanar distances using this figure agree well with the measured values.

The most probable type of structure for Bi_2Rb is that of Cu_2Mg,[4] since the compound Bi_2K of

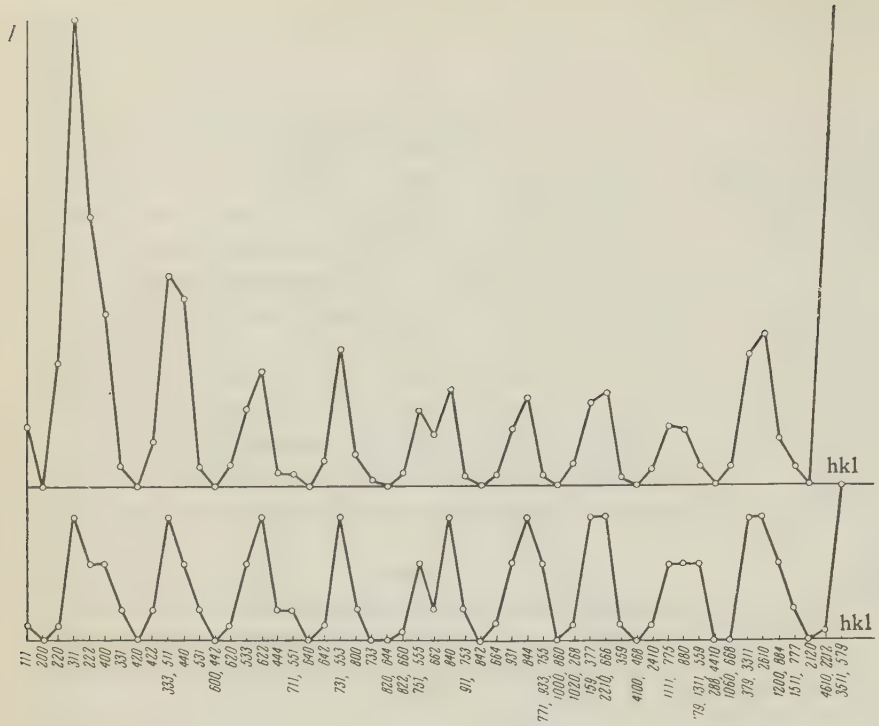

FIG. 6. Curves of I_{exper} (below) and $I_{theoret}$ (above) for Bi_2Rb.

bismuth with calcium — the chemical analog of rubidium — crystallizes in a structure of the Cu_2Mg type[5] and its cell has a cubic parameter a close to that for the Bi_2Rb cell. The results of the indexing and a comparison of x-ray photographs of Bi_2K and Bi_2Rb reveal their similarity and show that these compounds are isomorphs. Using the method of hydrostatic suspension[6] in kerosene and carbon tetrachloride, we measured the density of an alloy with a 16.6% rubidium content, which is close to that of Bi_2Rb (17% by weight Rb), and found it to be equal to 7.1 gm/cm^3. In the first approximation the density of this alloy can be taken to be the pycnometric density of Bi_2Rb crystals.

For Z = 8 we obtain $\sigma_x = 7.54$ gm/cm^3. In a structure of the Cu_2Mg type the atoms occupy positions a and d (space group O_h^7 — Fd3m):

$$\text{Rb } 8(a): 0\ 0\ 0 \ldots\ldots$$
$$\text{Bi } 16(d): \tfrac{5}{8}\ \tfrac{5}{8}\ \tfrac{5}{8} \ldots\ldots$$

For the structural amplitudes:

$$F_{hkl} = f_{Rb} \cos 2\pi \frac{h-k}{4} \cos 2\pi \frac{k-l}{4} \times \cos 2\pi \frac{l-h}{4} \cos 2\pi \frac{h+k+l}{8} + f_{Bi} \cos 2\pi \frac{h-k}{4} \cos 2\pi \frac{k-l}{4} \cos 2\pi \frac{l-h}{4} \times \left\{ \cos 2\pi \frac{h+k+l}{8} \cos 2\pi \frac{5}{8} h \cos 2\pi \frac{5}{8} k \cos 2\pi \frac{5}{8} l - \sin 2\pi \frac{h+k+l}{8} \sin 2\pi \frac{5}{8} h \sin 2\pi \frac{5}{8} k \sin 2\pi \frac{5}{8} l \right\}.$$

The line intensities were calculated from the formula

$$I \sim L_p p F^2,$$

where L_p is the Lorentz factor or the polarization and p is the recurrence factor. Comparison of the calculated and the measured intensities (Fig. 6) shows good agreement and supports the assignment of a structure of the Cu_2Mg type to crystals of Bi_2Rb.

The rubidium atoms in the Bi_2Rb structure are situated according to the diamond law.

In each empty octant, a regular tetrahedron of bismuth atoms is located in such a way that the edges of the small tetrahedron are parallel to the edges of a large one of rubidium atoms, and the center of gravity of the small tetrahedrons is located at the center of the octant. Each atom of rubidium is surrounded by 12 atoms of bismuth at distances of 3.98 A and by 4 atoms of rubidium at distances of 4.16 A. Each atom of bismuth has as nearest neighbors 6 atoms of bismuth at distances of 3.40 A and 6 atoms of rubidium at distances of 3.98 A.

CONCLUSIONS

1. A provisional melting diagram of the bismuth — rubidium system has been constructed.

2. The existence of four compounds in the bismuth — rubidium system has been discovered: Bi_2Rb, $BiRb_3$, and two compounds which presumably are Bi_2Rb_3 and $BiRb_2$. The compounds Bi_2Rb and $BiRb_3$ correspond to maxima on the melting diagram. In the alloying of the components these compounds are formed with a large evolution of

heat. The other two compounds are formed in a peritectic reaction.

3. The superconducting compound Bi_2Rb crystallizes in the cubic system with $a = 9.590 \pm 0.002$ kX and has a structure of the Cu_2Mg type.

4. An increase of the minimum interatomic spacing in Bi_2Rb relative to the isomorphic compound Bi_2K (Ref. 5) leads to an increase of the superconducting transition temperature from 3.58°K up to 4.25°K, analogous to the increase in T_c observed with increasing interatomic distances for compounds of bismuth with palladium,[8,9] rhodium, and nickel.[10]

In conclusion we express our thanks to Professor N. E. Alekseevskii for valuable advice during the performance of the present research and to R. N. Kuz' min for aid in carrying out the experiments.

[1] N. E. Alekseevskii, J. Exptl. Theoret. Phys. (U.S.S.R.) **23**, 610 (1952).

[2] T. A. Mingazin, Zhurnal Neorgan. Khimii **2**, 995 (1957).

[3] T. A. Mingazin, Uch. Zap. Turkmen. Gos. Un-ta **10**, 350 (1957).

[4] G. B. Bokii, Введение в кристаллохимию (Introduction to Crystal Chemistry) Izd. MGU, 1954.

[5] E. Zintl and A. Harder, Z. Phys. Chem. **16**, 206 (1932).

[6] E. M. Bronshtedt-Kupletskaia, Определение удельного веса минералов (Determination of the Specific Gravity of Minerals), U.S.S.R. Acad. Sci. Press 1956, pp 43-55.

[7] Alekseevskii, Brandt, and Kostina, J. Exptl. Theoret. Phys. (U.S.S.R.) **21**, 951 (1951).

[8] N. N. Zhuravlev and G. S. Zhdanov, Izv. Akad. Nauk SSSR, Ser. Fiz. **20**, 708 (1956).

[9] N. N. Zhuravlev, J. Exptl. Theoret. Phys. (U.S.S.R.) **32**, 1305 (1957); Soviet Phys. JETP **5**, 1064 (1957).

[10] N. N. Zhuravlev, Dissertation, MIFI (1954).

Translated by W. M. Whitney
167

SOVIET PHYSICS JETP VOLUME 34 (7), NUMBER 4 OCTOBER, 1958

STRUCTURE OF SUPERCONDUCTORS: XIII

INVESTIGATION OF BISMUTH — CESIUM ALLOYS

N. N. ZHURAVLEV

Moscow State University

Submitted to JETP editor November 15, 1957

J. Exptl. Theoret. Phys. (U.S.S.R.) **34**, 827-829 (April, 1958)

A provisional melting diagram is constructed for the Bi — Cs system. Three compounds were found: Bi_2Cs, $BiCs_3$, and one which probably is $BiCs_2$. The superconducting compound Bi_2Cs crystallizes in the cubic system with a lattice constant $a = 9.746 \pm 0.005$A and is isomorphic with the superconducting compounds Bi_2K and Bi_2Rb.

ACCORDING to experimental data,[1] certain bismuth — cesium alloys become superconductors at $T_c = 4.75$°K. It is assumed that a bismuth — cesium compound which is rich in bismuth is responsible for the superconductivity of these alloys. The principal goal of the present study of bismuth — cesium alloys was to ascertain the composition and the atomic-crystalline structure of this compound.

The investigation of bismuth — cesium alloys was accompanied by certain difficulties connected with the large chemical activity of metallic cesium. Having located a small quantity of metallic cesium (~2 gm) we used the micromethods developed for an experimental study of bismuth — rubidium alloys[2] to prepare the samples and to analyze them physiochemically.

PREPARATION AND THERMAL ANALYSIS OF THE ALLOYS

In preparing the alloys we used chemically pure bismuth and 99.99% pure cesium (the principal impurity was calcium). The melting was done in a small-gauge resistance oven. For the melting and for recording the cooling curves of the alloys with small cesium content we used quartz capsules of small volume (2 — 5 cm^3). Samples with a large cesium content were melted in iron crucibles enclosed in the quartz capsules, just as was done for the bismuth — rubidium alloys.[2]

The heating and cooling curves were recorded with an electronic automatic potentiometer EPP-09 down to a temperature of 50 — 100°C. The weight of the alloys ranged from 0.2 to 1.0 gm. The results of the thermal analysis are presented in the figure in the form of a tentative melting diagram for the bismuth — cesium system.

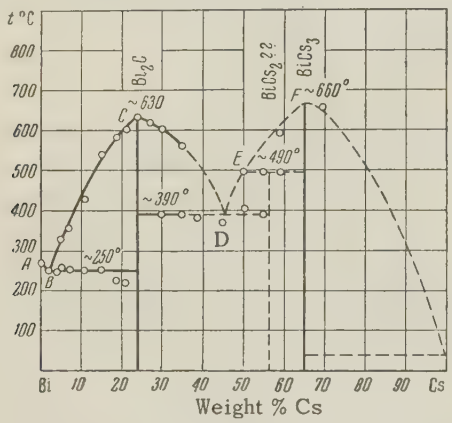

Melting Diagram for the Bismuth-Cesium System

As cesium is added, the melting temperature of bismuth decreases along the line AB, reaching a minimum at about 250°C. The eutectic point lies at ~1 — 3% by weight Cs. From the eutectic point B the melting curve increases steadily along the line BC, reaching a maximum at about 630°C at the point C for 24.1% by weight Cs, which corresponds to the compound Bi_2Cs. An increase in the cesium content is accompanied by a falling melting curve; a eutectic stop appears on the cooling curves at ~390°C. Further increase in the cesium content of the alloy brings about a rise in the melting curve along the line DEF. At the point F the curve reaches a maximum at a temperature of about 660°C for an alloy composed of 65.6% by weight Cs, which corresponds to $BiCs_3$. For alloys with compositions lying in the region between the eutectic point D and the point F, temperature stops were observed at ~500°C. In our opinion these stops are related to a peritectic reaction of formation of a compound which presumably consists of $BiCs_2$. Further increase of cesium in the alloy leads to a falling melting curve.

DETERMINATION OF THE STRUCTURE OF THE SUPERCONDUCTING COMPOUND Bi_2Cs

Samples of alloys with compositions close to that of Bi_2Cs were prepared for x-ray analysis in the same way as in the study of the structure of the compound Bi_2Rb,[2] except that as a protective liquid we used dekaline treated with cesium (maintained at a temperature of 150 — 170°C and stirred for 3 hours) in place of kerosene.

X-ray powder patterns were obtained with a RKU-86 camera by CuKα radiation of samples consisting of ~23% by weight Cs. According to microscopic data, such a sample contains mostly crystals of the compound Bi_2Cs and a small quantity of the eutectic Bi + Bi_2Cs. In order that the bismuth lines could be separated from the lines of the compound in the x-ray photograph, the sample was viewed with a slow rotation (one or two revolutions during the time of exposure), just as for the x-ray study of Bi_2Rb crystals.

From the x-ray photographs, the intensities I and the displacements of the lines were measured, and values of the interplanar distances d were calculated. All the lines of the x-ray photographs of Bi_2Cs crystals are indexed in the cubic system. A value of $a = 9.726 \pm 0.005$ kX was obtained for the period of the elementary cell of Bi_2Cs. The interplanar distances calculated from these data agree well with the measured values. As a result of the indexing and of a comparison of x-ray photographs of Bi_2Cs, Bi_2K, and Bi_2Rb, it is established that these three compounds are isomorphs. A comparison of the calculated and measured intensities shows good agreement and supports the assignment to Bi_2Cs crystals of a structure of the Cu_2Mg type. Below are given the minimum interatomic distances for crystals of Bi_2Cs:

Compound	Bi — Bi, Å	Bi — Cs, Å	Cs — Cs, Å
Bi_2Cs	3.44	4.04	4.22

The research which has been carried out permits us to perform a crystallochemical analysis of the group of superconducting compounds established as isomorphs: Bi_2K, Bi_2Rb, and Bi_2Cs. Considering the change of the period of the unit cell and the minimum interatomic spacings in these compounds as the atomic number of the alkali metal increases, it can be noted that an increase in the atomic number (atomic radius) of the alkali metal leads to an increase in the period of the unit cell of the compound and is accompa-

nied by an increase in T_c. This fact supports the correlation, mentioned in reference 3, between the temperatures at which the superconducting transition occurs and the position in the Mendeleev table of the metal forming the compound with the bismuth.

It is probable that the other group of compounds BiK_3, $BiRb_3$, and $BiCs_3$ are also isomorphs and have a structure of the Na_3As type.[4] A series of compounds of arsenic, antimony, and bismuth with the alkali metals crystallizes in this type of structure: Li_3As, Na_3As, K_3As, α-Li_3Sb, Na_3Sb, K_3Sb, Na_3Bi, and K_3Bi.

According to one author,[6] the compound $BiCs_3$, obtained by the method of successive precipitation of layers of bismuth and cesium by vacuum sublimation, can serve as a photo-cathode like the compound $SbCs_3$, but among the group of compounds $SbCs_3$, $SbRb_3$, SbK_3, and $BiCs_3$ it is the one least sensitive to light.

CONCLUSIONS

1. A tentative melting diagram has been constructed for the bismuth — cesium system.

2. Three compounds crystallize in the bismuth — cesium system: Bi_2Cs, $BiCs_2$, and a compound which presumably consists of $BiCs_2$. The compounds Bi_2Cs and $BiCs_3$ correspond to maxima on the melting diagram; the third compound is formed in a peritectic reaction.

3. The superconducting compound Bi_2Cs crystallizes in a cubic lattice with $a = 9.726 \pm 0.005$ kX and has a structure of the Cu_2Mg type.

4. Crystallochemical analysis shows that for the isomorphic group Bi_2K, Bi_2Rb, and Bi_2Cs, an increase in the period of the unit cell is accompanied by an increase in T_c.

We take this opportunity to express our deep gratitude to Professor G. S. Zhdanov and to Professor N. E. Alekseevskii for valuable discussions and for guidance during the performance of the present research, and to V. A. Smirnov for assistance in conducting the experiments.

[1] N. E. Alekseevskii, J. Exptl. Theoret. Phys. (U.S.S.R.) **23**, 610 (1952).

[2] Zhuravlev, Mingazin, and Zhdanov, J. Exptl. Theoret. Phys. (U.S.S.R.) **34**, 820 (1958) p 566 (this issue).

[3] Alekseevskii, Zhdanov, and Zhuravlev, Uch. Zap. MGU, Jubilee Collection of the Physics Faculty (in press).

[4] G. B. Bokii, Введение в кристаллохимию (Introduction to Crystal Chemistry), Izd. MGU, 1954.

[5] N. S. Khlebnikov, J. Tech. Phys. (U.S.S.R.) **17**, 333 (1947).

[6] R. Sommer, Proc. Phys. Soc. **55**, 145 (1943).

Translated by W. M. Whitney
168

SOVIET PHYSICS JETP VOLUME 34(7), NUMBER 4 OCTOBER, 1958

ANGULAR CORRELATIONS OF $\pi^+ - \mu^+ - e^+$ - DECAYS IN A PROPANE BUBBLE CHAMBER

V. V. BARMIN, V. P. KANAVETS, B. V. MOROZOV, and I. I. PERSHIN

Submitted to JETP editor November 15, 1957

J. Exptl. Theoret. Phys. (U.S.S.R.) **34**, 830-835 (April, 1958)

The result of projective treatment of 6760 $\pi^+ - \mu^+ - e^+$ -decay events photographed in a two liter propane bubble chamber is discussed. Assuming the angular distribution of decay positrons to be described by the formula $1 + a\cos\theta$, it is found that $a_{prop} = -0.19 \pm 0.03$. This result confirms the hypothesis of Lee and Yang of nonconservation of parity in weak interactions.

1. INTRODUCTION

THE hypothesis of Lee and Yang[1,2] of non-conservation of parity and charge conjugation in weak interactions has been confirmed by a series of experiments on β-decay and angular correlations in $\pi^+ - \mu^+ - e^+$ -decay. If parity is not conserved in the consecutive stages of the $\pi^+ - \mu^+ - e^+$ -decay, the angular distribution of the positrons will be given by the formula

$$dN = (1 + a\cos\theta)\, d\Omega/4\pi, \qquad (1)$$

where θ is the angle between the original direction of motion of the μ^+-meson and the positron.

The value of the factor of asymmetry a depends on the relation between the various types of interactions in the μ^+-decay. The experimental energy spectrum of decay positrons is in best agreement with the vector and pseudovector variants of the theory. The asymmetry factor can assume (over the whole spectrum) values from $-\frac{1}{3}$ to $+\frac{1}{3}$ depending on the type of interaction. An accurate determination of the factor a for the whole spectrum of decay positrons and measurements of the energy dependence of the asymmetry factor may provide information about other types of interaction present.

The use of a propane bubble chamber in such an investigation is especially advantageous since it combines the desirable characteristics of photographic emulsion (good angular definition, constant sensitivity for electrons of various energies) with higher statistical accuracy due to the lesser degree of μ^+-meson depolarization in propane and the possibility of fast reduction of a large number of $\pi^+ - \mu^+ - e^+$ decay events.

The present work is devoted to the study of angular distribution of positrons in $\pi^+ - \mu^+ - e^+$ decay and determination of the factor a in propane over the whole energy spectrum of positrons.

2. EXPERIMENTAL ARRANGEMENT AND METHOD OF DATA REDUCTION

A two liter propane bubble chamber[3] was used in conjunction with the π^+-beam of the United Institute of Nuclear Studies synchrocyclotron.

Positive pions were produced in a polyethylene target bombarded by 650 Mev protons. π^+-mesons of ~ 170 Mev were selected by means of a deflecting magnet, focussing devices, and a collimator. A Cu — Al absorber, with thickness so chosen that a maximum number of $\pi^+ - \mu^+ - e^+$-decays was observed in the chamber, was used for slowing the π^+-mesons. The chamber was shielded from the magnetic field of the synchrocyclotron by a laminated screen of soft sheet iron of Armco type and Permalloy. The complicated shape of the chamber made it difficult to shield it properly and in the first series of pictures the stray field amounted to 1.8 gausses. Addition of a second shield in the second series of pictures reduced the stray field to 0.35 gausses.

Tracks in the bubble chamber were photographed with a stereoscopic camera having an average reduction of 4.5 and distance between lenses equal to 70 mm. High-speed 35 mm motion picture film was used. Pictures of the $\pi^+ - \mu^+ - e^+$-decays were projected and the angle between the projections of the μ^+-meson and positron tracks on the film plane measured. The mean error of angle measurement was $\leq 5°$.

There are two ways of comparison of the measured angular distribution with Eq. (1) and of determination of the asymmetry factor a. The first method can be used for the case of $\pi^+ - \mu^+ - e^+$-decays when the μ^+-meson track is at a small angle to the film plane. Assuming then that the track lies in that plane, one can easily pass from the distribution of angle projections on a plane to the distribution in space.[4] This method was used by us as an independent check of the form of the angular distribution (Fig. 1).

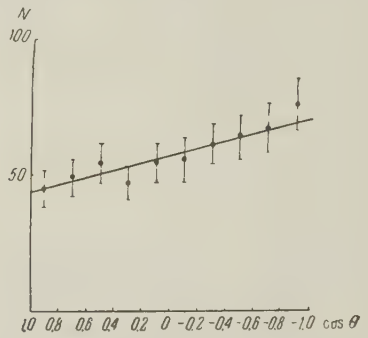

FIG. 1. Angular distribution of $\pi^+ - \mu^+ - e^+$-decay positrons calculated for space angles θ. Events with track projections of the μ^+-meson > 3 mm and perpendicular to the axis of π^+-meson beam were selected. n = 607, a = 0.20 ± 0.075.

The second method is based on an expression for the distribution of angle projections equivalent to Eq. (1). It can be shown that the expression is of the form

$$dN = (1/\pi)\,[1 + (a\pi/8)\, f(\alpha)\cos\varphi]\, d\varphi, \qquad (2)$$

where φ is the angle between the projections of the μ^+-meson and positron tracks, and α is the maximum angle between the μ^+-meson track and the plane of projection. The function $f(\alpha)$ is defined by the following relation:

$$f(\alpha) = \frac{\alpha}{\sin\alpha} + \frac{\sin 2\alpha}{2\sin\alpha}. \qquad (3)$$

It has been assumed in the derivation of Eq. (2) that the μ^+-mesons produced in π^+-decay are isotropic. The function $f(\alpha)$ varies from 2 to 1.57 for α varying from 0 to $\pi/2$. The values $\alpha = 0$ and $\alpha = \pi/2$ correspond to the two limiting cases: for $\alpha = 0$ the tracks of μ^+-mesons lying in the plane of projection are selected, while for $\alpha = \pi/2$ all decay events are taken into account.

It follows from Eq. (2) that the use of the pro-

jective method of treatment reduces the asymmetry. In fact, if a track is inclined at a large angle to the plane of projection, then positrons propagating both in the forward and backward directions with respect to the direction of motion of the μ^+ -meson will fall into the angle interval $\Delta\varphi$ in the plane of projection and the distribution of the projections of positron tracks with respect to the projections of μ^+ -mesons tracks will be almost isotropic.

Events with length of the projected μ^+ -meson track < 1 mm were disregarded in view of the low accuracy of angle measurements. This corresponds to the angle $\alpha = 73°$. Such a selection causes the loss of 4.5% of the decay events.

The asymmetry factor a was determined from the "backward-forward" ratio, i.e., the ratio of the number of positrons with track projection between $\pi/2$ to π to the number of positrons with track projection in the interval 0 to $\pi/2$, according to the formula

$$a = 4(1 - R)/f(\alpha)(1 + R), \qquad (4)$$

where R is the backward-forward ratio. For $\alpha = 73°$, $4/f(\alpha) = 2.465$ and we have, therefore,

$$a = 2.465(1 - R)/(1 + R). \qquad (4a)$$

It should be noted that the standard deviation of the asymmetry factor a is, in the method used, larger by 23% than that of spatial angle measurement. However, the ease and simplicity of the above method compensate fully for that disadvantage.

3. ANALYSIS OF RESULTS

Angular distribution of positrons for the first and second series of pictures is shown in Fig. 2a

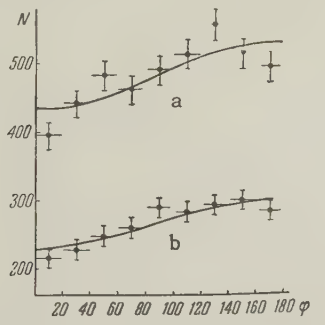

FIG. 2. Angular distribution of $\pi^+ - \mu^+ - e^+$-decay positrons in the plane of projection. a – first series of measurements, n = 4353, a = −0.175 ± 0.04. b – second series, n = 2408, a = −0.214 ± 0.05.

and b for 4353 and 2408 cases, respectively. The asymmetry factor was determined according to Eq. (4).

For the first series it was found that $a = -0.163 + 0.037$. The stray magnetic field of 1.8 gausses caused a slight depolarization of μ^+ -mesons due to precession of their magnetic moment. Calculations showed that for an isotropic distribution of μ^+- mesons the decrease in the value of a amounted to 7. After introducing a correction it was found that $a = -0.175 + 0.04$. In the second series it was found that $a = -0.214 + 0.03$. The average of the two series is $a = -0.19 + 0.03$.

Experimental errors in reading the film are basically due to conical projection in photography and to the loss of a small fraction of $\pi^+ - \mu^+ - e^+$ -decays, either because of the absence of the positron track or poor identification due to the general background. Equation (2) was obtained under the assumption that the projection is perpendicular. In the fact, conical projection takes place in photography. It can be shown, however, that if the inspected region of the chamber forms a cone with axis coinciding with the optical axis of the camera, and if the angle between track projections equals φ in the perpendicular projection, then, in conical projection, the number of cases when the angle is found to be $\varphi + \Delta\varphi$ will be equal to the number of cases with $\varphi - \Delta\varphi$.

Conical projection is therefore equivalent to perpendicular projection with certain symmetrical error of angle measurements and does not change the angular distribution. The error $\Delta\varphi$ can be minimized by selecting cases with small photographic angle. For the events analyzed, this angle was $\leq 5°$. Absence of distortion of the angular distribution due to conical projection or imperfections of the optical system is illustrated by the histograms of the angular distribution of μ^+ -mesons about the axis of the π^+ -meson beam (Fig. 3a) and the direction of π^+ -meson tracks (Fig. 3b).

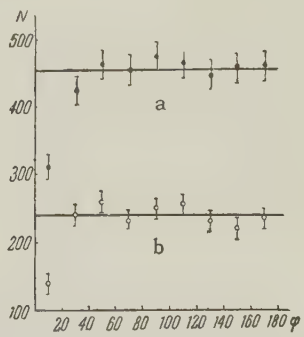

FIG. 3. Angular distribution of μ^+-mesons in the plane of projection: a – about the π^+ beam axis, n = 3953, R = −1.01 ± 0.032; b – about the direction of π^+-meson tracks, n = 2078, R = 1.01 ± 0.045.

Both distributions are in a good agreement with the assumption of isotropic distribution of μ^+ -

mesons in $\pi^+ - \mu^+$ -decay. Deficiency of particles in the interval $0° - 20°$ can be easily explained by the difficulty in separating evnnts with small angles of emission of μ^+ -mesons from decays of μ^+ -mesons contained in the beam.

Our results show that $\sim 3.9\%$ of $\pi^+ - \mu^+$ -decays are not accompanied by a visible positron track and, besides, tracks of positrons in $\sim 1\%$ of the events are unsuitable for angle measurements due to the small length of the projected track.

A simple calculation leads to the conclusion that the number of μ^+ -mesons from $\pi^+ - \mu^+$ -decays stopping in the glass and the walls of the chamber amounts to 2.4%. It can be shown that these do not introduce any change in the shape of the distribution and the value of the asymmetry factor, assuming the validity of Eq. (1).

Distortion of the angular distribution of positrons due to omission of some decay events can occur only when the probability that an event is omitted depends on the angle between the tracks of the positron and the μ^+ -meson. We identified all events by the characteristic kinks in the tracks of $\pi^+ - \mu^+ - e^+$ - or $\mu^+ - e^+$ decays. The most probable omissions in fast scanning in the presence of a considerable chamber background occur for events in which the tracks of the two mesons and the positron differ little in direction. In other words, positrons moving forwards or backwards at small angles to the direction of the μ^+ -meson are most likely to be overlooked. Considerations given below make it possible to avoid this.

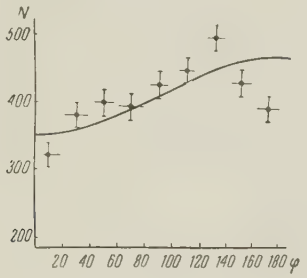

FIG. 4. Angular distribution of $\pi^+ - \mu^+ - e^+$-decay positrons in the plane of projection obtained in the first series of measurements (preliminary result)

The histogram in Fig. 4 was obtained as the result of the first scanning, and that in Fig. 2a — of the second. Variation in the number of positrons in the extreme angle intervals and better agreement between the theory and the experimental result in the second histogram are clearly visible.

The above mentioned errors can be avoided if we choose a different characteristic of the decay for its identification, namely, (as it is the practice in emulsion work) the presence of a kink corresponding to the $\pi^+ - \mu^+$ -decay of a stopped π^+ -meson, and do not look for the presence of a positron. In that case, possible omissions of some events will not change the form of the angular distribution of positrons about the direction of μ^+ -mesons.

The analysis shows that a marked distortion of the shape of the angular distribution can occur in our experiment by omission of the $\pi^+ - \mu^+ - e^+$ -decay events in scanning the film.

4. DISCUSSION OF RESULTS

The value for the asymmetry factor a found in our experiment, $a = -0.19 + 0.03$, is in good agreement with the results of the Liverpool group ($a = -0.17 + 0.03$),[5] the group of the Physical Institute of the Academy of Sciences, U.S.S.R. ($a = -0.21 + 0.035$)* and of the work of Pless et al. ($a = -0.18 + 0.05$).[6] The mean weighted value of all the experiments is $a = -0.187 + 0.017$. This value is determined not only by the relation between theoretical variants but also by the depolarization of μ^+ -mesons in propane. The asymmetry factor for the elementary process a_e is obtained accounting for the depolarization factor. This can be done using the data of the Chicago group[7,8] which obtained for the asymmetry factor in C (and in metals) the value $a_c = -0.244 + 0.01$ and for $a_{prop} = -0.175 + 0.015$.

It has been shown[7,8] that the time of depolarization is much shorter than the half-life of the μ^+ -meson. The ratio a_{prop}/a_c determines the degree of depolarization of μ^+ -mesons in propane. It is clear that the above ratio is independent of positron energy and the degree of polarization of the μ^+ -meson beam. The asymmetry factor for the elementary process, obtained from the mean experimental value of a given above equals $-0.256 + 0.033$.

Under the assumption that μ^+ -mesons originating in the decay of stopped π^+ are totally polarized and decay according to the scheme $\mu^+ \to e^+ + \nu + \bar{\nu}$, the ratio ξ between the interaction variants[1,2] equals $-3a_e$. In the case of a partial polarization of the μ^+ -meson the value $-3a_e$ represents the lower limit of ξ. The value $\xi \geq 0.77 \pm 0.10$, calculated from the mean value of the asymmetry coefficient, is in a very good agreement with the results of emulsion work, $\xi \geq 0.8 \pm 0.15$.[9]

In conclusion the authors would like to thank Academician A. I. Alikhanian for suggesting the theme and discussing the results, G. P. Eliseev

*Private communication of A. I. Alikhanian.

and V. A. Liubimov for valuable advice, V. P. Dzhelepov for taking part in the work with the accelerator, and V. G. Zaitseva, N. S. Konoplev, I. A. Sosunov, V. M. Golubchikov, and V. N. Luzin for taking part in reducing the data.

[1] T. D. Lee and C. N. Yang, Phys. Rev. **104**, 254 (1956); **105**, 1671 (1957).

[2] L. Landau, Nucl. Phys. **3**, 127 (1957).

[3] I. I. Pershin, Приборы и техника эксперимента (Instr. and Meas. Engg.), **1**, 39 (1957)

[4] V. A. Ostroumov and R. A. Filov, Prib. i Tekhn. Eksper. **2**, 44 (1957).

[5] Alston, Evans, Morgan, et al., Phil. Mag. **2**, 1143 (1957).

[6] I. Pless et al., Phys. Rev. **108**, 159 (1958).

[7] Swanson, Campbell, Garwin, et al., Bull. Amer. Phys. Soc. **2**, 205 (1957).

[8] S. C. Wright, Proceedings of the Rochester Symposium, 1957.

[9] M. F. Kaplon, Proceedings of the Rochester Symposium, 1957.

Translated by H. Kasha
169

SOVIET PHYSICS JETP VOLUME 34(7), NUMBER 4 OCTOBER, 1958

TEMPERATURE ANOMALY IN THE RESISTANCE AND THE HALL EFFECT IN GOLD

Iu. P. GAIDUKOV

Institute of Physical Problems, Academy of Sciences, U. S.S.R.

Submitted to JETP editor November 26, 1957

J. Exptl. Theoret. Phys. (U.S.S.R.) **34**, 836-842 (April, 1958)

The dependence of the Hall effect on temperature and magnetic field was studied in samples of gold with normal and abnormal temperature dependence of the resistance. A jump was observed in the Hall constant of an "anomalous" sample at a field of 8 kOe. The magnitude of the jump increased with decreasing temperature. A field strength of 8 kOe is the value at which the anomalous temperature dependence of the resistance vanishes.

1. INTRODUCTION

As is well known (see the references to the literature in Ref. 1) the Ohm's-law resistance in a series of metals (Au, Cu, Ag, Mg and, apparently, Mo)[2] shows an anomalous temperature dependence, consisting in the fact that as the temperature is lowered, the resistance of these metals falls, reaches a minimum at some temperature denoted by T_{min}, and then begins to rise. It was noticed in a series of articles[2-5] that the dependence of this rise on temperature could be satisfactorily represented in the form

$$\frac{\Delta r}{r_{min}} = \frac{r(T) - r_{min}}{r_{min}} = \text{const} + a \log(1/T) \quad \text{for } T < T_{min},$$

where r_{min} is the resistance at T_{min}. In the work of Ref. 5 carried out by us on gold samples, it was shown that $\Delta r/r_{min}$ decreased in a magnetic field and reached zero for some value H_k. In the same work it was noticed that, for a value of the field equal to H_k, a discontinuous change in the slope of the Hall electric field $E_y(H)$ was observed.

It was of interest to carry out a more detailed investigation of the Hall effect in dependence on temperature and magnetic field using gold samples with both normal and anomalous-type resistances, which allowed us to clarify the connection between anomalous resistance and the Hall effect.

2. METHOD OF MEASUREMENT

To prepare samples we had at our disposal two batches of gold naturally occurring: a foil of 0.05 mm and a plate 1 mm thick. Both batches were 99.99% pure. A spectral analysis of the gold is given in Table I.

The sample Au-1, together with current and potential leads was cut out of the foil, as shown in

Fig. 1. The thick plate was rolled to a thickness of 0.05 mm. A sample Au-4 was prepared from this foil. The samples had identical geometrical dimensions $0.05 \times 14 \times 30$ mm^3. To get rid of surface dirt, the samples were immersed in aqua regia.

TABLE I

Admixtures	Samples	
	Au-1	Au-4
Ag	$8 \cdot 10^{-5}$	$7.5 \cdot 10^{-5}$
Cu	$1 \cdot 10^{-5}$	$2.4 \cdot 10^{-5}$
Fe	$4.4 \cdot 10^{-7}$	$5 \cdot 10^{-7}$
Bi	$< 3 \cdot 10^{-7}$	$< 3 \cdot 10^{-7}$
Pb	$2.5 \cdot 10^{-7}$	$5 \cdot 10^{-7}$
Ni	$1.2 \cdot 10^{-7}$	$1.6 \cdot 10^{-7}$
Mg	$3 \cdot 10^{-7}$	$5 \cdot 10^{-7}$
Sb	$2 \cdot 10^{-7}$	$2 \cdot 10^{-7}$
Si	$1.5 \cdot 10^{-7}$	$2 \cdot 10^{-7}$

The value of the residual resistance r_{min}/r_{295} for Au-1 was equal to 0.00971 and for Au-4, 0.00893.

Measurement of the Hall electric field was carried out at room temperature, temperatures of liquid nitrogen, hydrogen and helium and in the very low temperature region, reached by the method of adiabatic demagnetization of ferric-ammonium alums. Construction of the apparatus for obtaining very low temperatures, making it possible to carry out galvanomagnetic measurements at these temperatures, was described previously[5] by us. In the present work, the only change introduced was in the mounting of the sample (Fig. 1). To the

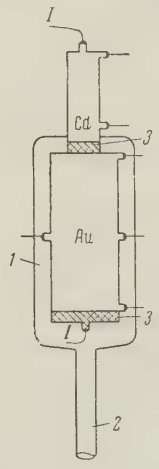

FIG. 1. Mounting of the gold and cadmium specimens.

copper plate 1, which ended at the cooling system 2, we soldered BiCd* 3 to one of the ends of the sample studied. To the other end of the gold sample we fixed a specimen of cadmium of the same origin as those in Refs. 6 and 7. It was used in determining the temperature of gold in the region 0.05 — 0.5°K, in which it was assumed that the curve of critical fields of this specimen coincided with the analogous curves previously measured for the other specimens.[6,7] The critical fields of cadmium were determined from the curves of the appearance of resistance upon destruction of superconductivity in a magnetic field. Measurements were carried out with a potentiometer set up. The current through the sample was equal to 0.1 amp, with the specimen of cadmium in series with that of gold. Comparison of the curve of critical fields with the data of Refs. 6, 7 made it possible to determine the difference in temperature between the cadmium and the alum block. This difference was negligible for a current of 0.1 amp. Therefore, in our measurements the temperature of the gold sample was taken equal to the temperature of the alum block. The inaccuracy introduced in this way did not influence the results of the measurements essentially. The temperature of the alum block was determined by measuring its susceptibility, carried out by a ballistic method.

In the study of the Hall effect in metals of group I, the essential difficulty is the small magnitude of the measured electric field, connected with the small value of the Hall constant. In order to increase the Hall electric field, higher currents and stronger magnetic fields are usually used. However, in our case such a way was not possible because use of currents ($I > 0.3$ amp) led to considerable overheating of the sample and to a rapid rise in temperature of the alum block, and the need to study the dependence of the Hall effect on magnetic field required that the measurements be carried out in both strong and weak fields. As a consequence, it was necessary to increase the sensitivity of the measuring scheme. For this, a two-cascade photoelectric multiplier FEOU-15 of the Kozyrev type[8] was used.

In order to increase the sensitivity and stability of the work still further, this multiplier was subjected to several changes. Thus, for example, the low power illumination lamp (0.5 W) was replaced by a stronger one (2 W). The zeroing apparatus was completely changed, and the insulation of the chassis wiring was improved. The multiplier was included in a KL-48 potentiometer set up. Measurement of the Hall electric field in the very low temperature region was carried out with a sensitivity of 2×10^{-19} V/(mm/m) of the scheme and a field through the sample of 0.1 amp. At temperatures

*A eutectic alloy 60% Bi + 40% Cd; $T_{melt} \approx 140$°C, $T_k = 0.55$°K.

above 1°K it was possible to carry out the measurements at a higher current (0.3 amp) which made it possible to decrease the sensitivity of the scheme to 3×10^{-9} v/(mm/m).

At such high voltage sensitivities of the measuring apparatus, random electric fields began to show up strongly. The largest of these was the electric field induced on the potential ends of the sample by fluctuation in the magnetic field. In order to attain sufficient accuracy in the measurement of the Hall electric field, a number of special measures were taken. Thus, in order to exclude large fluctuations, a stabilizer of the magnetic field* was worked out, which was distinctive because of the following. Fluctuations in the current of the generator feeding the electromagnet, produced a change in the difference of potentials on a resistor placed in series with the windings of the electromagnet. These changes, after considerable amplification, corrected the current of the generator, making it possible to keep up the feeding current (up to 150 amp) with an accuracy of 0.01%.

In order to get rid of the influence of small fluctuations of the magnetic field, an additional loop was placed in series with the Hall potential leads. This loop was outside the air Dewar, between the poles of the electromagnet. The turning of this loop relative to the magnetic field made it possible to compensate almost completely for the induced alternating electric fields.

In order to exclude from the measured electric field the thermoelectric field and the difference of potentials $E_x(H)$ arising because of the asymmetrical disposition of the Hall potential terminals, the usual commutation of the measuring current and magnetic field was carried out.

The relative error of measurement, beginning with a field of 8 kOe, did not exceed 1%.

3. RESULTS OF THE MEASUREMENTS

Study of the temperature dependence of the resistance showed that, whereas the resistance of the Au-1 sample rose noticeably with the lowering of the temperature (Fig. 2), the growth of the resistance of the Au-4 sample in the region $4.2 - 1.4$°K was less than the error of measurement (0.2%). In the study of the depth of the temperature minimum resistance with respect to its dependence on magnetic fields, $[r_{0.07;H} - r_{min;H}]/r_{min;H}$, it turned out that for Au-1 it became zero for a value of the field $H = 8 \pm 0.5$ kOe, in good agreement with the values H_k obtained in Ref. 5. Measurements of the dependence of the Hall effect on magnetic field were carried out for temperatures of 295.77; 20.4; 10.1; 4.2 and 0.07°K. Relative to the final temperature, it should be remarked that in the region below 1°K measurements took place with a slow rise in temperature of the gold sample, as a consequence of which, we took the mean between the initial and final temperatures as the temperature of the experiment. Usually, during the time in which the dependence of $E_y(H)$ on fields of 1.5 to 18.3 kOe was obtained, the temperature of the sample rose from 0.05°K to 0.1°K.

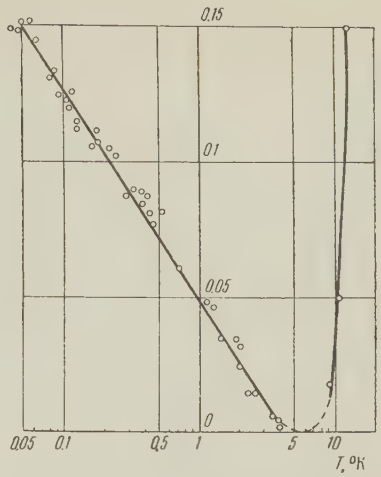

FIG. 2. Specimen Au-1. Dependence of $\frac{r(T) - r_{min}}{r_{min}}$ on temperature.

Results of the dependence of the Hall electric fields on magnetic fields for the samples Au-4 and Au-1 are given in Figs. 3 and 4 for a series of temperatures. The Hall constant $R(H)$ for Au-1 is given on Fig. 5, where

$$R = E_y d / HI \quad \text{for } H < 8 \text{ kOe},$$

$$R = E_y d / (H - 8000) I \quad \text{for } H > 8 \text{ kOe},$$

where d is the thickness of the sample and I is the current through the sample.

In Table II the numerical values of the Hall constant for Au-1 and Au-4 are given in the CGSM system for all temperatures studied.

Analogous results were obtained with a series of other gold samples.

4. DISCUSSION OF RESULTS

Measurements showed that the Hall constant of the sample Au-4, which did not have an anomaly in the curve $r(T)$, did not depend on the magnetic field up to 18 kOe at all temperatures. In the region from 77 to 20.4°K its value rose 25% and then remained constant with further decrease in temperature. For the sample Au-1, having an anoma-

*The author is grateful to A. N. Vetchinkin for working out the stabilizing scheme.

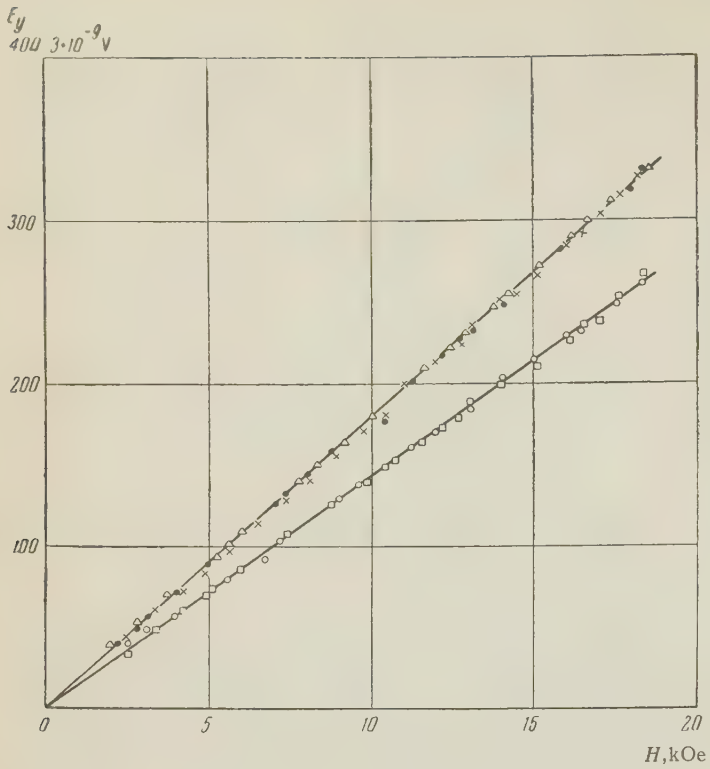

FIG. 3. Sample Au-4. Dependence of $E_y(H)$: ○ – T = 295°K; □ – T = 77°K; △ – T = 20.4°K; ● – T = 4.2°K; × – T = 1.45°K.

lous resistance, in fields of less than 8 kOe, the Hall constant also did not depend on magnetic field and here the Hall constants for Au-1 and Au-4 coincided within the limits of error for all temperatures.

In a field equal to 8 kOe, the Hall constant of the sample Au-1 underwent a jump, the magnitude of which increased with decreasing temperature. The dependence of these jumps $\Delta R = R(H > 8\,\text{kOe}) - R(H < 8\,\text{kOe})$ on temperature is shown in Fig. 6.

Thus, in the gold sample which had an anomaly in the curve $r(T)$, an anomaly was also observed in the Hall effect. In comparing the anomaly in the resistance with the anomaly in the Hall effect, one cannot help but notice that ΔR, upon extrapolation with respect to temperature, becomes zero for $T \approx 140°K$, where T_{min} lies between 4 and 6°K. However, T_{min} may be a characteristic point for an anomalous branch of resistance. One can imagine a temperature at which the sum of two processes — one connected with the fall and the other with the rise of the resistance with decreasing temperature — has a minimum. From this point of view, the temperature at which ΔR becomes zero, it seems to us, may definitely characterize anomalous galvanomagnetic properties of the metal.

It is of interest to compare results of this work with those of other workers.[9,10] In these works, measurements of the Hall effect have been carried out for gold samples for a wide range of temperatures. But in both Ref. 9 and Ref. 10 these measurements were carried out for only one value of the magnetic field.

TABLE II. $R \times 10^{-4}$ CGSM

T°K	Au - 1		Au - 4	
	H < 8 kOe	H > 8 kOe	H < 8 kOe	H > 8 kOe
295	6.7	6.7	6.75	6.75
77	6.7	6.95	6.75	6.75
20.4	8.5	9.3	8.4	8.5
10	8.5	10.1		
4.2	8.5	10.6	8.4	8.4
1.4	8.5	11.15	8.35	8.5
0.075	8.5	12.5		

Comparing results of these two works with results of this work, it may be assumed that the anomalous rise in the Hall constant with decreasing temperatures observed in Ref. 9 is connected with the fact that these authors used a field of 20 kOe, larger than H_k. That is, in that region of fields, where an anomalous change in the Hall constant with temperature was observed in our case. The fact that the anomalous behavior of the Hall constant was not observed by the authors of Ref. 10 is connected with the fact that their measurements took place in a field of 8 kOe, where there is not yet an anomalous temperature dependence of the Hall constant.

In conclusion, it is my pleasant duty to express sincere gratitude to Academician P. L. Kapitza for the interest that he showed in this work, to N. E.

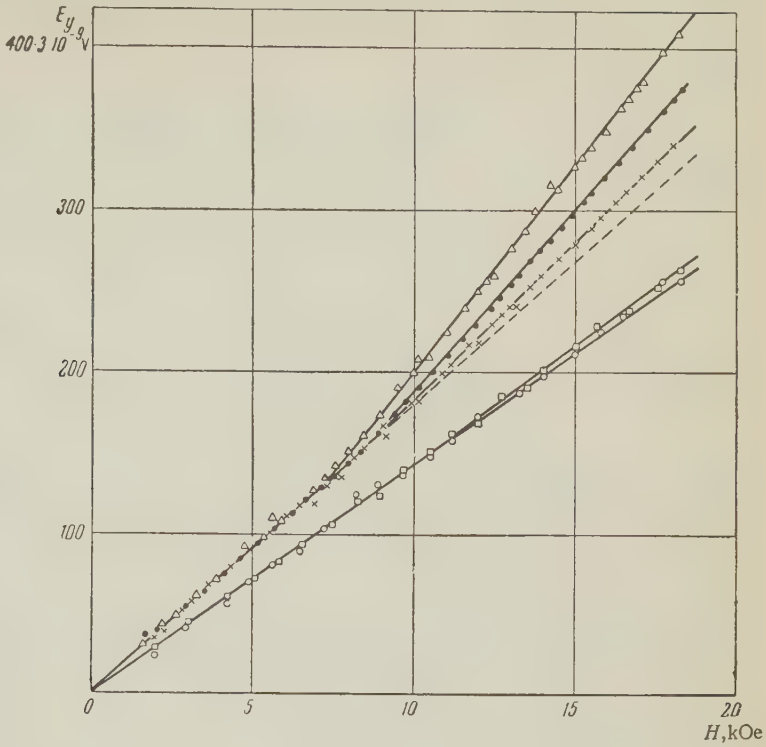

FIG. 4. Sample Au-1. Dependence of $E_y(H)$: ○ – T = 295°K; □ – T = 77°K; × – T = 20.4°K; ● – T = 4.2°K; △ – T = 0.07°K.

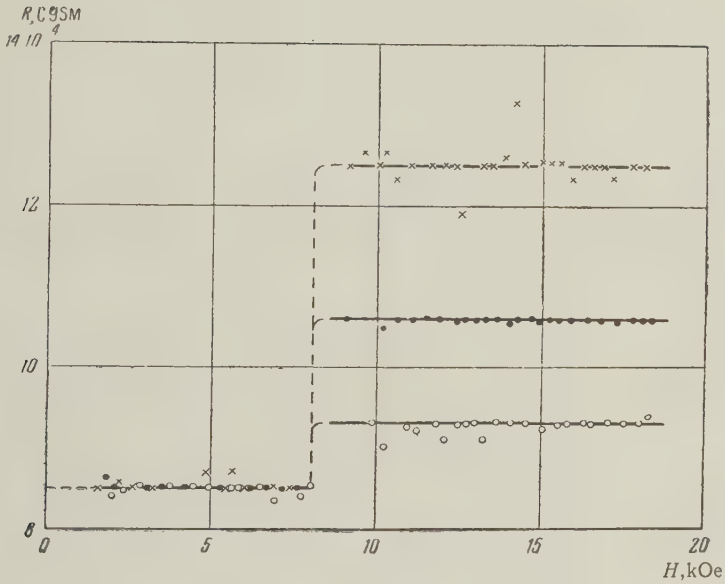

FIG. 5.

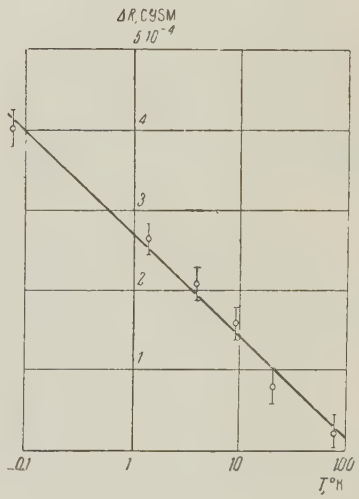

FIG. 6.

FIG. 5. Sample Au-1. Dependence of R(H): ○ – T = 20.4°K; ● – T = 4.2°K; × – T = 0.07°K.
FIG. 6. Sample Au-1. Dependence of ΔR(T).

Alekseevskii for valuable advice and suggestions and to G. E. Karstens for carrying out the spectral analysis of the samples.

[1] D. K. C. MacDonald, Phys. Rev. **88**, 148 (1952).
[2] E. Mendoza and J. G. Thomas, Proc. Conf. Low-Temp. Phys., p. 39 (1951).
[3] Croft et al., Phil. Mag. **44**, 289 (1953).
[4] G. K. White, Canad. J. Phys. **33**, 119 (1955).
[5] N. E. Alekseevskii and Iu. P. Gaidukov, J. Exptl. Theoret. Phys. (U.S.S.R.) **31**, 947 (1956); Soviet Phys. JETP **4**, 804 (1957).
[6] B. N. Samoilov, Dokl. Akad. Nauk SSSR **81**, 791 (1951).

[7] N. E. Alekseevskii and Iu. P. Gaidukov, J. Exptl. Theoret. Phys. (U.S.S.R.) **29**, 898 (1955); Soviet Phys. JETP **2**, 762 (1956).

[8] B. P. Kozyrev, Usp. Fiz. Nauk **44**, 173 (1951).

[9] T. Fukuroi and T. Ikeda, Sci. Repts. of Tokyo Univ. **8**, 205 (1956).

[10] W. B. Teutsch and W. F. Love, Phys. Rev. **105**, 487 (1957).

Translated by G. E. Brown
170

SOVIET PHYSICS JETP VOLUME 34 (7), NUMBER 4 OCTOBER, 1958

NUCLEAR INTERACTION IN PHOTOGRAPHIC EMULSION ACCOMPANIED BY LARGE ENERGY TRANSFER TO THE ELECTRON—PHOTON COMPONENT

G. B. ZHDANOV, E. A. ZAMCHALOVA, M. I. TRET' IAKOVA, and M. N. SHCHERBAKOVA

P. N. Lebedev Physical Institute, Academy of Sciences, U.S.S.R.

Submitted to JETP editor November 26, 1957

J. Exptl. Theoret. Phys. (U.S.S.R.) **34**, 843-848 (April, 1958)

A nuclear interaction event with primary energy $E_0 = 250^{+250}_{-125}$ Bev in which about 200 Bev was carried away by one of the π^0-mesons is investigated in detail. The lower limit of energy transferred to the soft component is approximately 30% of the total shower energy.

DATA on interactions between particles with energy of the order of few hundred Bev and atomic nuclei obtained by means of a cloud chamber[1] indicate the existence of very large fluctuations of the fraction of energy carried away by photons. The minimum value of the energy transferred to photons was found to be equal to a few tenths of a percent of the primary energy. The problem of the maximum energy transfer to the soft component is also of considerable interest.

In a stack of stripped Ilford G-5 emulsions exposed at the altitude of 2.5 km during the Italian expedition of Prof. C. F. Powell in 1955, we found and studied in detail an interaction event of the type 1 + 12n characterized by an unusually large fraction of the energy carried away by the electron-photon component. The path length of particles in each emulsion layer was ~1.5 cm and the total

TABLE I. Angular distribution of penetrating particles

No. of particles	θ (first method) $\theta_i \cdot 10^3$, radians	θ (second method) $\theta_i \cdot 10^3$, radians	No. of particles	θ (first method) $\theta_i \cdot 10^3$, radians	θ (second method) $\theta_i \cdot 10^3$, radians
1	40	2.5	9	245	235
2	40	11	10	280	265
3	40	32	11	430	420
4	80	67	12	510	525
5	104	95	$\theta_{1/2}^{-1}$	6	7
6	140	135	$1/\theta_{min}$	25	400
7	190	160	$\Sigma 1/\theta_i$	125	580
8	218	220			

length of the electronic cascade observed in the stack ~12 cm. A microprojection of the shower and the subsequent electronic cascade is shown in Fig. 1.

1. ANGULAR DISTRIBUTION OF PENETRATING PARTICLES AND MEASUREMENT OF THE ENERGY OF PRIMARY PARTICLE

In spite of the fact that the primary particle was neutral, it was possible to use two methods of measurement of the emission angles θ of penetrating particles with respect to the axis of the electron-nuclear shower. In the first method shower axis was identified with the center of circular symmetry of the angular distribution of penetrating particles. Such a procedure is based upon the assumption that the transverse momentum of all those particles is equal. Corresponding data are given in Table I. In the second method the shower axis was found from the direction of the first electron pair which initiated the large electronic cascade. Since that pair is situated in the same emulsion layer as the center of the star, and the energy of the electron cascade, according to estimates given below, is much greater than that of any penetrating particle we consider the second method to be much more accurate. The angular distribution of penetrating particles according to the second method is given in the third column of Table I, and has been adopted as the basis of subsequent considerations. The angle between the axes directions given by the two methods is small (~0.04) and, therefore, the estimates of energy of the primary particle given below for the different axes differ little (by not more than a factor of 1.5).

Analysis of the data of Table I indicates first of all that the angular distribution of penetrating particles is nearly isotropic in the coordinate system having a Lorentz factor $\gamma_c = 7$; e.g., about 85% of the particles should be emitted, for isotropic distribution, within the limits of the ten-fold range of values of θ_{lab} near $\theta = 90°$, which is in a good agreement with the experiment. However, the presence of an asymmetrically placed group of two penetrating particles emitted, in c.m.s., in the direction of the primary particle within a cone with opening angle $\theta_0 \leq 0.1$ radian, should be noted. It can be easily seen that the probability that any of those particles will be found in such a cone, for a random and isotropic emission, is less than 25%. Analysis of the angular and energy distribution of the particles of soft component* strengthens the

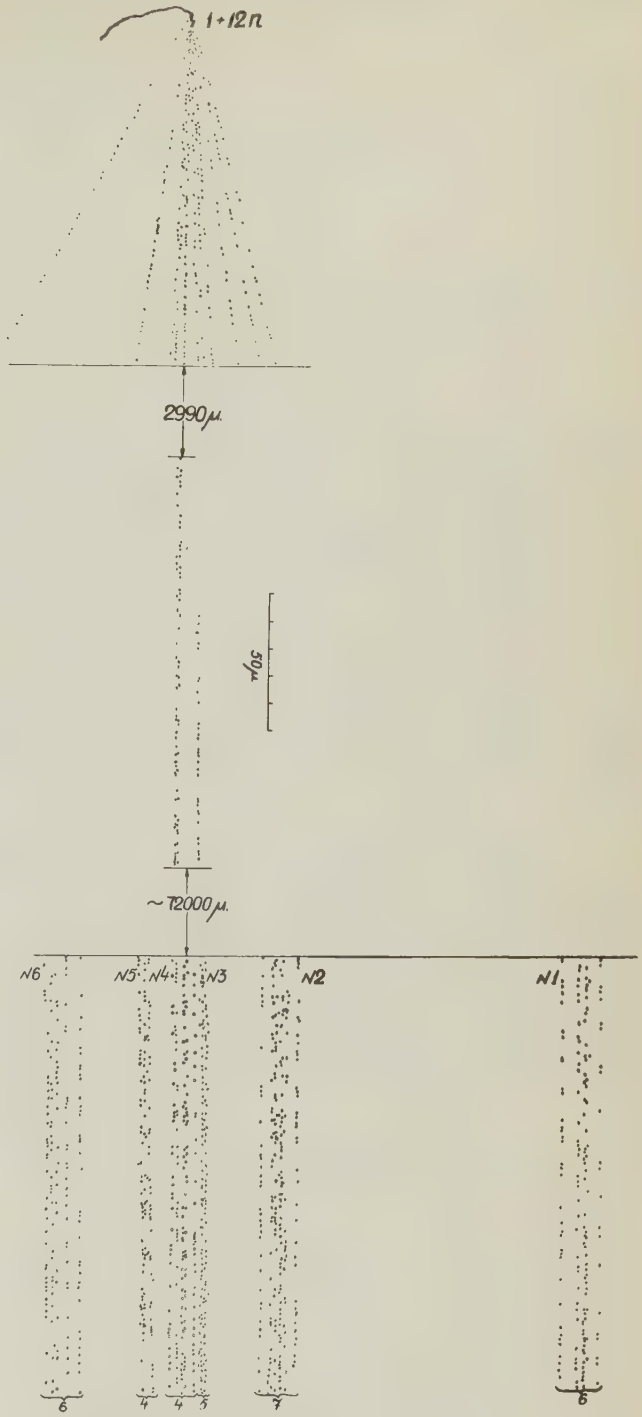

FIG. 1. Microprojection of star of the type 1 + 12n with subsequent electronic cascade.

conclusion about the existence of an anomalously narrow beam of secondary particles and, in consequence, about the absence of total isotropy of the angular distribution of secondary particles in c.m.s.

The probable relative error $\delta\gamma_c$ for isotropic distribution and for $n_s = 12$ amounts to ~30% (assuming that the fluctuations of the angular distribution are Poissonian). In determining the energy of the primary particle (a neutron, evidently), the tunnel effect should be taken into account.[2] The

*It will be seen in the following that also 2–3 π^0-mesons are found in the cone.

TABLE II. Lateral distribution of electrons

R, μ		<25	25–50	50–100	100–200	Penetrating particle	ΣN_e
$N_e(R)$	$t = 1.6$	15	9	3	2	$R_{min} = 110\mu$	28
	$t = 3.1$	5	7	12	14	$R_{min} = 210\mu$	38
	$t = 4.5$	6	2	16	21	$R_{min} = 305\mu$	45

tunnel length found from the multiplicity of the event is $n_T = 2.5+1$. The primary energy, finally, is

$$E_0 = 250^{+250}_{-125}\ \text{Bev}. \qquad (1)$$

The above value could be strongly underestimated if the angular distribution in c.m.s. were substantially asymmetric. In that case all usual methods of finding γ_c from the angular distribution would not be applicable and the only remaining possibility would be to assume that the transverse momentum $p_\perp$ of all particles is the same and known to us. C.m.s. can then be found from the condition that the total longitudinal momentum of all (relativistic) charged particles must vanish. Assuming that $p_\perp = 2\mu c$ (cf. Ref. 3) we obtain that $\gamma_c = 20^{+8}_{-5}$ and, consequently,*

$$E_0 = 2\gamma_c^2 n_\tau (n_s, \gamma_c) = 1300^{+700}_{-300}\ \text{Bev}. \qquad (1a)$$

Adding the longitudinal momenta we find, however, that the total longitudinal momentum of charged particles of the backward cone amounts to $\frac{1}{3}\,Mc\gamma_c$, while the corresponding estimate of the tunnel length $n_T = 1.5$ calls for a value of 1.5 $Mc\gamma_c$. This means that among the particles of the backward cone there must be a number of slow nucleons (not mentioned by us) each with longitudinal momentum of $\sim Mc\gamma_c$ (in c.m.s.). The presence of even one such nucleon in the backward cone first, lowers immediately the estimated value of γ_c to 10 and the energy E_0 to 400 Bev and, second, renders improbable the hypothesis of substantial asymmetry of the angular distribution between the forward and backward cones.

In view of all that has been said above, we think that it is improbable that E_0 exceeds 800 Bev (taking into account both the fluctuations in the angular distribution and the errors of finding γ_c, assuming a symmetrical emission of particles in c.m.s.)

An estimate of the energy of the penetrating component, which is independent of the tunnel length and, in general, of the interaction mechanism, can be obtained from the following relation which is based upon the fact that the transverse momentum is approximately constant:

$$E_{pen} = \bar{p}_\perp \sum (1/\theta_i). \qquad (2)$$

Assuming that $\bar{p}_\perp = 2\mu c$ (cf. Ref. 3), we find that $E_{pen} = 150$ Bev and, for the energy of the most energetic penetrating particle, we obtain $E_{max} = p_\perp/\theta_{min} = 110$ Bev.

2. LATERAL AND ENERGY DISTRIBUTIONS OF THE PARTICLES OF SOFT COMPONENT

The distribution of particles in planes perpendicular to cascade axis at the depth $t = 1.6$, 3.1, and 4.5 cascade units is given in Table II. Only the particles within the cone with opening angle of 1° about the shower axis were taken into account, thus excluding practically all particles not connected with the shower. At the same time, for electrons of the core (at distances up to 0.01 cascade units from the axis) such a selection does not represent a serious limitation of the (lower) energies, especially at small depths ($t \leq 2$ cascade units). Linear deviations from the axis of the nearest penetrating particle calculated from the relation $R_{min} = t\theta_{min}2.5$ cm are given for comparison in the last column of the table. In all cases, the axis was chosen so as to pass through the center of circular symmetry of the lateral distribution of electrons in a given plane. In the mean, symmetry was conserved in spite of the presence of at least six

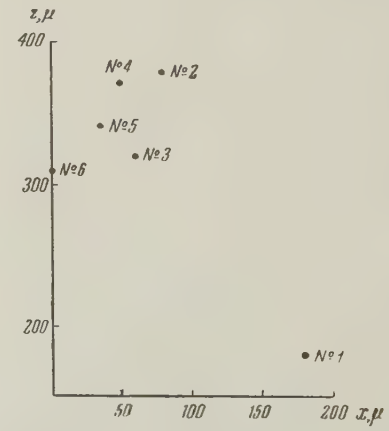

FIG. 2. Lateral distribution of cores of the electronic cascade at the depth of three cascade units.

*The given error of γ_c corresponds to twice the error of $p_\perp/\theta$ for the fastest particle. The influence of errors of $p_\perp$ and θ for the remaining particles is relatively small.

TABLE III.* Lateral and energy distributions of electron pairs

Opening angle $\alpha \cdot 10^3$	<0.32	0.32—2.2	0.83—2.2	2.2—6.2	>6.2	Number of photons with energy
Photon energy E_0, Bev	>32	32—10	10—3.2	3.2—1	<1	>1 Bev
$t \leqslant 1$	2(a, b)	0	0	0	0	2/0.77 = 3
$1 < t \leqslant 2$	3*	0	3	1	5	7/0.77 = 9
$2 < t \leqslant 3$	0	1	2	4	5	7/0.77 = 9
$3 < t \leqslant 4$	0	1	4	2	5	7/0.77 = 9

*Angular distances between adjacent pairs a—b: $\theta = (1.2 + 0.2) \cdot 10^{-3}$. The three pairs denoted by * may possibly be of bremsstrahlung origin.

sharply defined cores of the electronic cascade (cf. Figs. 1 and 2 where the positions of cores is shown in the plane perpendicular to the cascade axis at the depth t = 3.)

We also studied the lateral energy distribution of electron pairs (cf. Table III). The energies of corresponding photons were found from the opening angle of the corresponding pair (following Reference 4). In a few cases these estimates could be checked by direct energy measurements of the pair components from their scattering.

The width of energy intervals given in Table III were chosen so as to be equal to, or slightly narrower than, the mean relative errors of the energy of individual pairs.

Lateral and energy distributions of electrons and pairs given in Tables II and III permit us to estimate the total energy of soft component using one of the following four methods:

(a) by comparing the data of Table II* with cascade theory calculations[5] giving (for each section of the shower) the dependence of the total number of particles in the core on the universal parameter $Z_0 = E_0 R$, where E_0 is the initial photon energy and R the radius of the core.

(b) by comparing the data of Tables II and III with the cascade curves $N(y,t)$ for photons and electrons, where $y = \ln(E_0/E_{min})$ and E_{min} is the effective lower limit of energy of detectable particles.

(c) by adding the energies of all pairs of non-bremsstrahlung origin.†

(d) from the relation

$$\Delta\theta_{min} = 2\mu c^2 / E_{\pi^0} \qquad (3)$$

between the minimum angle of emission of photons in π^0-decay and the energy E_{π^0} of the pion (μ denotes the mass of π^0-meson). The required estimate of the π^0-meson energy follows after substituting in Eq. (3) the angular distances θ between adjacent pairs of non-bremsstrahlung origin given in Table III.

In general, the first method seems to us to be the most accurate. In this method random errors are due to uncertainty in the initial number of photons and statistical fluctuations of cascade processes, and systematic — to the omission of a certain number of particles because of angle limitation. In the second method, the error is, in addition to the above factors, substantially influenced by the indeterminacy of E_{min} increased by geometry effects which are not accounted for. Lastly, in the third method the inaccuracy of the measurement of the primary photon energy is most essential, since for a small number of those both the systematic and random errors may become very large.* It should be taken into account that the assumption of equipartition of energy between the primary photons,

TABLE IV. Estimates of the energy E_M of the central electronic cascade

Method of estimate*	E_M, Bev	E_M/E_0
Cascade curves with lateral limitations (table 2) (cf. ref. 5)	240	⩾50%
Cascade curves with energy limitations	~150	~30%
Total energy of pairs of non-bremstrahlung origin	225	~45%
Angle of emission of photons in π^0-decay	⩾200	⩾40%

*E_0 — probable energy of the primary particle (under the assumption of a symmetrical angular distribution).

*It should be borne in mind that only the particles of the central, most intensive cascade are included in Table II.

†Since the total observed length of the cascade is sufficiently large the correction for photon conversion can be neglected.

*The systematic error is connected here with the possibility of including photons of bremsstrahlung origin. We excluded the latter following the method of Ref. 6.

underlying the two first methods, can cause an apparent decrease of the total cascade energy. In actual experimental conditions this effect, however, is not large, corresponding roughly to the difference between the mean geometric and arithmetic value of the energies of primary photons, amounting to less than a factor of 1.5.

The number of photons n_0 produced in the nuclear interaction by means of π^0-mesons was found comparing the various methods of estimating the electronic cascade energy; for $n_0 = 2$ the agreement is satisfactory, for $n_0 = 4$ there is a marked discrepancy with the results of cascade theory.

Final estimates of the energy of the main core of soft component E_M by means of all four methods are given in Table IV where the values of the ratio E_M/E_0 are also given. Roughly similar estimates (smaller by a factor of $1.5-2$) were obtained for the additional cascade (core 1 in Fig. 2) which started to develop at a greater depth.

It must be concluded therefore that at any rate not less than 30% of the total energy of the star is carried away by the soft component (accounting even for the errors mentioned at the end of section 1). At the same time, attention is drawn to the distinct concentration of high-energy photons near shower axis as compared with the angular distribution of penetrating particles. The bulk of energy of the electronic cascade is emitted within a cone with opening angle $\theta_{max} \approx 1/500$ while the deviation of the penetrating particle closest to the axis of the same cone is $\theta_{min} \approx 1/400$.

Referring to the result of Ref. 1 mentioned earlier, our results indicate that the energy fraction carried away by the soft component may fluctuate by a factor of ten or more. It should be noted also that the energy estimates given above confirm again (cf. Ref. 2) the inadequacy of the explanation of all jets (i.e., high-energy interactions with a small number of slow charged particles) by the $n-n$ collision model.

The authors would like to thank R. M. Gruzinov, L. V. Kruglov, M. N. Pachkov, and Iu. F. Sharapov for taking part in reducing the data, and Prof. N. A. Dobrotin and I. L. Rozental' for discussion of results.

[1] Baradzei, Rubtsov, et al., J. Exptl. Theoret. Phys. (U.S.S.R.) **33**, 17 (1957); Soviet Phys. JETP **6**, 12 (1958).

[2] I. A. Ivanovskaia and D. S. Chernavskii, Nucl. Phys. **4**, 29 (1957).

[3] United Japanese Emulsion Group, paper presented at the Varenna Conference, 1957.

[4] Gramenitskii, Zhdanov, Zamchalova, and Shcherbakova, J. Exptl. Theoret. Phys. (U.S.S.R.) **32**, 936 (1957); Soviet Phys. JETP **5**, 763 (1957).

[5] R. Pinkau, Phil. Mag. **2**, 1389 (1957).

[6] F. A. Brisbout, C. Dahanayake, et al., Phil. Mag. **1**, 605 (1956).

Translated by H. Kasha
171

SPECTROSCOPIC INVESTIGATION OF INTENSE PULSED DISCHARGES IN HYDROGEN. II

S. Iu. LUK'IANOV and V. I. SINITSYN

Submitted to JETP editor, November 26, 1957

J. Exptl. Theoret. Phys. (U.S.S.R.) 34, 849-855 (April, 1958)

The spectral properties of the radiation from the hydrogen plasma in a low-pressure gas discharge at currents up to 500 kiloamperes have been studied by means of a mirror-sweep method. Using this method it is possible to study the behavior of the gas discharge in the visible region as a function of time. During contraction of the plasma pinch a continuous-spectrum "flash" is observed. Results obtained in experiments in which nitrogen and helium were added indicate a high electron temperature in the plasma when contraction takes place. An estimate of the charged particle concentration is made on the basis of the broadening of the H_α line.

1. INTRODUCTION

THE presently available spectroscopic data for pulsed, low-pressure, high-current discharges (approximately 10^5 amperes[1]) yield comparatively scanty information on the development of the discharge. These data are relatively incomplete because they are obtained over the entire duration of the discharge, thereby yielding the "integrated" characteristics of the process. Valuable additional information can be obtained from a knowledge of the intensity of the spectral lines as a function of time; the appropriate measurements can be easily carried out using a photoelectric cell in conjunction with a monochromator. However, this method is inconvenient because of the impossibility of simultaneous photometric measurements of all the spectral lines. Moreover, in experiments of this kind, it is difficult to study another important parameter — the width of the spectral line. Among other things, a knowledge of the half width of the spectral line is extremely important for establishing the time variation of the density of charged particles in the plasma. It should also be kept in mind that without some sort of time-sweeping arrangement it is difficult to observe the extremely short-lived lines due to multiply charged ions which are produced in the discharge when atoms of other materials are introduced artificially.

The identification and time variation of the intensity of these lines can be extremely important in estimating the electron temperature in the plasma at various instants of time.

These considerations were the motivation for carrying out an investigation of the time variation of spectra of pulsed discharges. Time sweep was obtained by use of the rotating-mirror method.[2] A Kerr cell would be less effective because the emission from the discharge at times long after the initiation of the discharge is tens and even hundreds of times greater than that which obtains when the discharge is initiated; the latter is of greatest interest in studying the development of the discharge.

Since the transmission of a Kerr cell cannot be reduced to zero even when it is "closed", the intense and long-lived emission characteristic of the later stages of the discharge would tend to mask the weak spectrum characteristic of the initial stages.

2. APPARATUS AND METHOD OF MEASUREMENT

The experimental conditions were essentially the same as those described earlier in Ref. 1. The pulsed system consisted of a condenser bank with a capacity of 86 μfd and a discharge chamber made from a porcelain tube with inner diameter of 400 mm. The distance between the copper electrodes of the discharge chamber was 900 mm. The discharge chamber was furnished with a side port covered with a quartz plate. The central region of the discharge could be ovserved through the window in the port (see Fig. 1).

The discharge chamber was filled from a measured volume; the hydrogen was first passed through a palladium filter. In the experiments in which gaseous mixtures of hydrogen and helium were used the helium was spectrally pure.

A Rogovskii loop was used to measure the current; with an initial voltage of 40 kv across the condenser bank the maximum current strength was 460

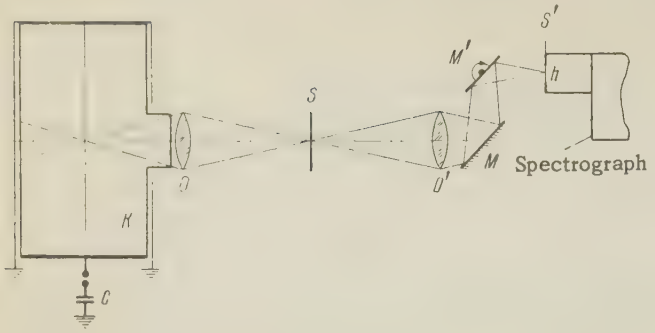

FIG. 1. Optical diagram for the spectral sweep system. D) discharge chamber; O and O') objectives; S) intermediate slit, the image of which is obtained as a band in the plane S'; M and M') fixed mirror and rotating mirror respectively; h) height of the slit of the spectrograph.

kiloamperes. The stray inductance in the discharge circuit was small and under the conditions indicated the initial rate-of-rise of the current was 1.5×10^{11} amps/sec. The first contraction started 3 — 4 microseconds after the discharge was initiated.

The method of obtaining the time sweep for the spectrum is as follows. The optical system forms a light beam from the visible radiation emitted from a definite section of the luminous volume of the discharge chamber; in the plane of the entrance slit of the spectrograph, this beam forms an image of the intermediate slit in the form of a narrow band. If this band is perpendicular to the entrance slit of the spectrograph, its width determines the wavelength of the spectral lines which are observed in the focal plane of the camera of the spectrograph. By using a rotating mirror it is possible to displace the luminous band along the entrance slit of the spectrograph. Thus the entire spectrum is swept in wavelength as a function of time. A schematic diagram of the optical system is shown in Fig. 1. The optical system is designed so that there are no limiting apertures for the light beam as the luminous band is displaced along the input slit.

The sweep speed is determined by the distance from the rotating mirror to the plane of the input slit and by the rotational velocity of the mirror. In the present scheme, with $n = 15{,}000$ rpm and $h = 12$ mm, the total sweep time was 20 microseconds. The time required for the luminous band to be displaced by a natural line width (the resolving time) was approximately 0.7 microsecond in the experiments described here. The rotational velocity of the mirror was controlled to within 0.1 per cent by means of a special electron-beam tachometer unit.

The spectral time-variation pattern can be synchronized with the discharge current. For this purpose a cross hair is placed across the input slit of the spectrograph; this cross hair produces a fiduciary mark on all the spectral lines. A small mirror is placed at the level of the cross hair; when the luminous band passes through the cross hair light is reflected on to the cathode of a photomultiplier. Thus, one beam of the oscilloscope is used to display the discharge current curve while the signal obtained from the photomultiplier is applied to the other beam and serves as an indication of the point in the discharge which corresponds to the fiduciary mark on the spectral sweep.

3. RESULTS OF THE MEASUREMENTS

In Fig. 2 are shown time-swept discharge spectra for several typical cases; these spectra were obtained with a condenser-bank voltage of 35 kv. The first two spectra (2a and 2b) were obtained using a discharge in pure hydrogen at initial pressures $p_0 = 0.05$ mm Hg and 0.1 mm Hg. In the spectrum marked 2c are shown data obtained by photographing the spectrum of a discharge in a mixture of hydrogen and nitrogen (95 per cent H_2 + 5 per cent N_2), 2d was obtained with a mixture of hydrogen and helium (70 per cent H_2 + 30 per cent He). For convenience, the current oscillogram corresponding to each spectrogram is also shown. The sweep speeds are the same for the spectra and oscillograms.

Under the conditions being considered here the intensity of the H_α line is 15 — 20 times greater than the intensity of the H_β line and greater still than the H_γ line (cf. for example, Fig. 4 of Ref. 1).

The spectra were photographed with panchromatic aerial plates with a sensitivity of 1,000 GOST units, having maximum sensitivity in the red portion of the spectrum; hence of all the lines of the Balmer series only the H_γ line was recorded.

An interesting characteristic of several of the spectrograms is the coninuum flash which occurs at maximum contraction of the plasma pinch (first break in the current oscillogram). The continuous background is small for the hydrogen discharge (with $p_0 = 0.05$ mm Hg it is generally not noticeable) and fairly small when helium is added; however, when even small amounts of nitrogen are added the background becomes very pronounced (cf. Spectrogram 2c). In addition to the continuum, on Spectrograms 2c and 2d there are observed lines, which as a rule, fade out in later stages of the discharge. The origin of these lines is considered below.

In the red region of the spectrum, the spectrograph dispersion is small so that a reliable analysis of the line shape can be made only for well separated lines. In Fig. 3 is shown the time be-

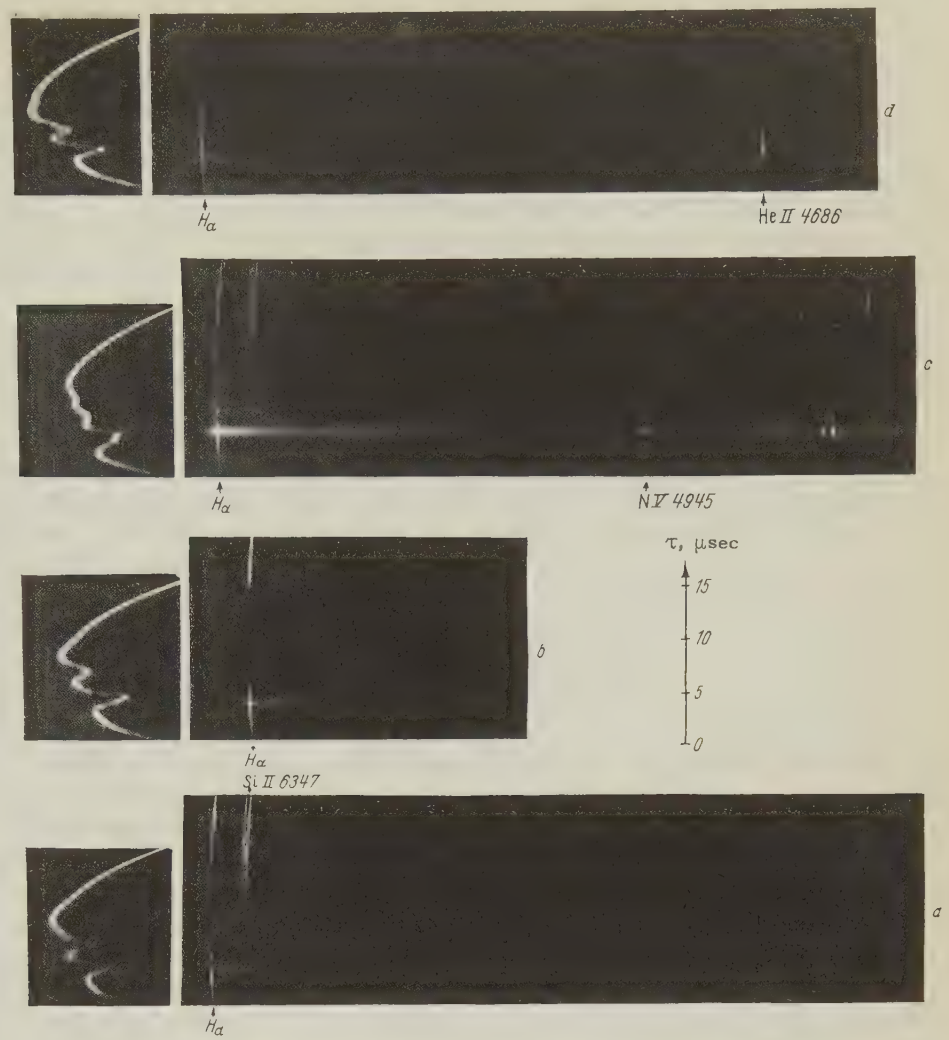

FIG. 2. Spectrogram of the pulsed discharge under various conditions. a) pure hydrogen, $p_0 = 0.05$ mm Hg; b) pure hydrogen, $p_0 = 0.1$ mm Hg; c) 95 per cent H_2 plus 5 per cent N_2, $p_0 = 0.05$ mm Hg; d) 70 per cent H_2 plus 30 per cent He, $p_0 = 0.05$ mm Hg.

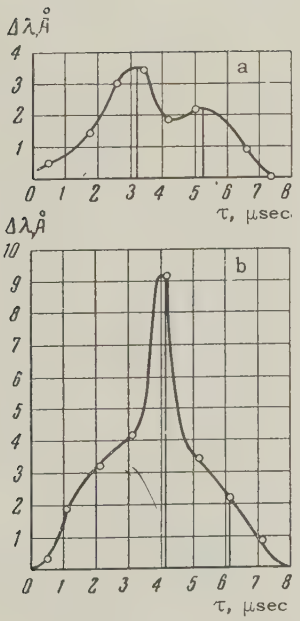

FIG. 3. Time variation of the half-width of the H_α line: a) $p_0 = 0.05$ mm Hg. b) $p_0 = 0.1$ mm Hg. The vertical lines denote the first and second contractions of the pinch.

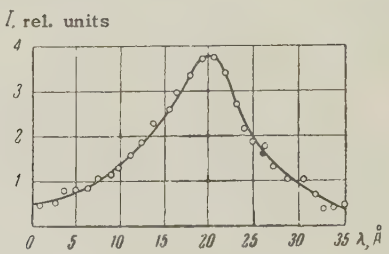

FIG. 4. Shape of the H_α line at maximum contraction, $p_0 = 0.1$ mm Hg, $\tau = 4.2$ microseconds.

havior of the half width of the H_α line for two values of the pressure. In view of what has been indicated the data for $p_0 = 0.1$ mm Hg are much more reliable. As an illustration, in Fig. 4 is shown the line shape for the H_α line at the instant of time corresponding to contraction of the plasma pinch ($p_0 = 0.1$ mm Hg).

4. DISCUSSION OF THE RESULTS

We first consider the spectrograms shown in Fig. 2. On all spectrograms, up to the instant at

which contraction of the pinch takes place, only the H_α line of atomic hydrogen is observed. The absence of other lines in the Balmer series has already been explained. However, it is natural to wonder why the spectrograms do not exhibit nitrogen lines or helium lines in the cases in which the discharge tube is filled with a mixture of hydrogen and these gases. In the nitrogen case the absence of a nitrogen line is explained by the small percentage content of this gas; the fact that the nitrogen content was small was verified in control experiments. In the helium case the absence of He I lines is probably due to the rather high excitation energy (for example, 23 ev for the He I line at 5876 A but 12 ev for the H_α line at 6563 A).

If the discharge takes place in pure hydrogen, lines due to impurity atoms, which enter from the walls of the discharge chamber, are produced after the second contraction (for example, the Si II line at 6347 A in Fig. 2a). This result is in agreement with the data of photoelectric measurements.[1]

If the discharge takes place in a mixture of hydrogen and nitrogen or helium, as has already been noted, at maximum contraction of the pinch there appear short-lived spectral lines which are not observed in the subsequent stages of the discharge. These lines, which can be distinguished from the continuum background, should be assigned to nitrogen or helium (the emission of impurity atoms from the walls of the discharge chamber takes place later). However, these lines do not correspond to lines for neutral nitrogen or helium. Hence the observed lines were assigned to highly excited ionized helium and nitrogen. If the assignment of the N II, He II and N V 4619 lines is granted, the N V 4945 line is open to doubt since the wave length given in the Moore tables[3] is a calculated value which has not been verified experimentally before. The following experiment serves to corroborate this finding: the intensity of the broadened N V 4595 line increases continuously as nitrogen added is increased. Aside from the N V 4945 line the N V 4943 line is also observed in the corresponding part of the spectrum. A microphotogram of this region of the spectrum is

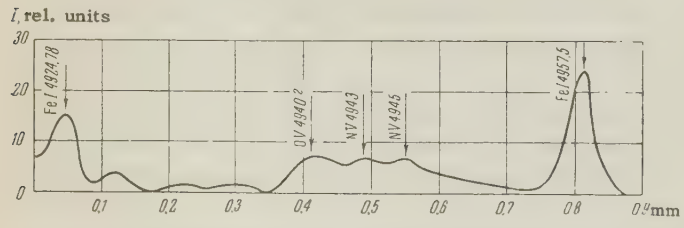

FIG. 5. Microphotogram of the spectrum in the neighborhood of 4950 A. The iron lines Fe I at 4957. 7A and at 4924.78 A are used as references.

TABLE I

Wave length A	Element	Excitation energy,* ev
4945	N V	90
4686	He II	51
4621	N II	21
4619	N V	59
4607	N II	21

*The excitation energy is computed from the ground state of the corresponding ion.

given in Fig. 5. In Table I are shown wave length values for some of the observed lines.

The unexpected appearance of these lines may be taken as an indication of a sudden increase in electron temperature at maximum contraction of the plasma pinch and as an indication of the conversion of the energy associated with the directed motion of the ions into heat. The temperature falls off in the subsequent expansion of the plasma and the lines corresponding to this high excitation vanish. It is interesting to note that in the second contraction these lines are again observed, although their intensities are much weaker.

One further circumstance must be explained in connection with the foregoing. In the initial stages of the discharge there are no nitrogen lines corresponding to small excitation energies; at maximum contraction, however, lines characterized by high excitation energies are observed. The probable cause for this effect is purely geometrical: the conditions for observing emission originating from the center of the discharge chamber are more favorable than those for observing emission distributed uniformly over the volume of the discharge chamber.

Since the electron temperature at the first contraction is sufficient for exciting lines of quadruply ionized nitrogen and lines of neutral helium and nitrogen are not observed, there is little doubt that the hydrogen is completely ionized (at least in certain sections of the inner zones of the discharge). It is clear that the emission of the H_α line observed at this instant is due to those sections of the plasma pitch in which the ionization is less than 100 per cent complete.

If the electron temperature at the first contraction reaches several thousands of electron volts*

*We may recall that the kinetic temperature of the ions, as estimated from the velocity of propogation of the contracting light fronts or magnetic field fronts, reaches 100 – 200 ev at the end of contraction.[1] An estimate of the temperature, obtained from the Doppler broadening of the nitrogen lines during contraction, yields the value $T_i \approx 300$ ev. The authors intend to return to this question.

an important role in the continuum spectrum being considered should be played by the "free-free" transitions, i.e., bremsstrahlung. The bremsstrahlung intensity and recombination radiation can be estimated from the following formulas[4]

$$I_1(\nu, T_e) = A_1 n_i n_e Z_{\text{eff}}^2 T_e^{-1/2} \exp\{-h\nu / kT_e\};$$
$$I_2(\nu, T_e) = A_2 n_i n_e Z_{\text{eff}}^4 T_e^{-3/2} \exp\{-h(\nu - \nu_n) / kT_e\} / n^3.$$

Here n_e and n_i are the electron density and ion density respectively, T_e is the electron temperature, Z_{eff} is the effective charge of the gas ions, n is the principal quantum number of the level from which recombination occurs, $h\nu_n$ is the energy of this level and A_1 and A_2 are universal constants. Applying these to hydrogen for radiation which occurs in the visible region of the spectrum (recombination to the $n = 3$ level) the values shown in Table II are obtained.

TABLE II

T_e, eV		1	3	10	30	100
$1/n_i n_e \int_{\nu_1}^{\nu_2} I_1 d\nu$	Relative units	23.4	60.0	58.7	41.0	25.6
$1/n_i n_e \int_{\nu_1}^{\nu_2} I_2 d\nu$		107	34	6.85	1.41	0.23

As is apparent from the Table, even at an electron temperature of 30 ev, the bremsstrahlung predominates; there is relatively little change in the intensity of this radiation with further increase in temperature. Thus, even if the electron temperature is known with poor accuracy, if it is greater than 20 — 30 ev, the measurement of the intensity of the continuum gives an independent absolute method of determining the density of charged particles in the plasma.

The fact that the bremsstrahlung is proportional to Z_{eff}^2 and, the square of the density of charged particles is probably the explanation for the experimentally observed increase in the intensity of the continuum when helium and nitrogen are introduced and when the initial hydrogen pressure is increased.

As is apparent from Fig. 3, the H_α line is broadened rapidly as the plasma contracts.* The maximum broadening of the line is observed at the first contraction; in the second contraction, the broadening occurs at lower pressures and is scarcely noticeable at all at $p_0 = 0.1$ mm Hg. The line at maximum contraction (cf. Fig. 4) exhibits extended wings; these indicate that the Stark effect is responsible for broadening of the line. If we use the Holtzmark formula[6] to convert from the measured half-widths to ion densities, at the first contraction we obtain values which lie within the limits $0.3 \times 10^{17}\,\text{cm}^{-3}$ to $0.7 \times 10^{17}\,\text{cm}^{-3}$ in the various experiments. In the case being considered ($p_0 = 0.1$ mm Hg), the initial density of neutral atoms is $0.7 \times 10^{16}\,\text{cm}^{-3}$. Thus, there is a five- or ten-fold contraction. Actually, the contraction is greater than this since the ionization is less than 100 per cent complete in the region of the discharge in which the radiating hydrogen atoms are located.

It is obvious that these estimates of ion density cannot be taken too seriously since they were obtained from an application of the Holtzmark formula in a high-temperature plasma. Actually, under these conditions, the theory should not apply. However, as has been shown by Kogan,[7] the relationship between the effective line width and density of charged particles still applies (with certain corrections in the numerical factors).

On the whole the optical data considered give an internally consistent picture of the phenomena which occur in a high-power pulsed discharge.

*A similar result has been obtained recently in Ref. 5.

[1] S. Iu Kukianov and V. I. Sinitsyn, J. Atomic Energy **1**, 88 (1956).

[2] K. S. Vul'fson, Elektrichestvo, Electrical Communication **11**, 16 (1946).

[3] C. E. Moore, Circular of the National Bureau of Standards 467, 43 (1949).

[4] L. H. Aller, Astrophysics (New York, 1954) Russian translation, 1955, p. 158.

[5] Burkhardt, et. al., J. App. Phys. **28**, 519 (1957).

[6] M. Born, Optik (Berlin, 1933). Russian translation, 1937 p. 608.

[7] V. I. Kogan, Dokl. Akad. Nauk SSSR **118**, 5 (1958).

Translated by H. Lashinsky
172

ON THE RELATION BETWEEN THE ANGULAR AND ENERGY DISTRIBUTIONS OF PARTICLES IN HIGH-ENERGY NUCLEAR INTERACTIONS

G. B. ZHDANOV

P. N. Lebedev Physical Institute, Academy of Sciences, U.S.S.R.

Submitted to JETP editor, November 29, 1957

J. Exptl. Theoret. Phys. (U.S.S.R.) **34**, 856-861 (April, 1958)

In continuation of Ref. 1, various experimental data on the magnitude of the transverse momentum component of particles produced in high-energy nuclear interactions are considered. The data are compared with the one-dimensional hydrodynamical theory of multiple particle production.

In study of high-energy nuclear interactions by means of photographic emulsions, it is generally possible to determine the angular distribution of secondary particles with sufficient accuracy, whereas the energy of the particles can be measured only to a limited degree. The knowledge of the energy characteristics of an event is, however, of considerable help not only for the understanding of the interaction process, but also for the correct interpretation of data on the angular distribution, especially in the not very rare cases where there is no frame of reference in which the distribution possesses mirror symmetry with respect to the plane with $\theta = 90°$.

Rozental' and Milekhin[1] were the first to draw attention to the experimental data and theoretical considerations in favor of existence of a connection between the angle of emission θ of a particle and its energy E. They indicate that the projection of momentum on the plane perpendicular to the direction of motion of the primary particle $p_\perp$ vary only slightly over a relatively large region of the angle θ and corresponds roughly to p of particles in thermal motion at the temperature μc^2 (where μ denotes the π-meson mass).* The purpose of the present paper is to consider a much wider sphere of experimental evidence supporting the above view.

2. EXPERIMENTAL DATA ON THE TRANSVERSE MOMENTUM OF SECONDARY PARTICLES OF $10^9 - 10^{13}$ ev.

It is more convenient to consider the distribution of transverse momentum $p_\perp$ in a logarithmic scale, particularly in units of $X = \log_{10}(p_\perp/\mu c)$, since, as a rule the relative error of momentum (or more accurately, energy) measurements (and consequently that of $p_\perp$) does not decrease with its value and even increases in certain cases. We introduce, therefore, a smaller error into the transverse momentum distribution ascribing the same statistical weight to various measurements by using the logarithmic scale. It should be also mentioned that, as it will be seen later, the theoretical and experimental distributions of the variable X can be approximated satisfactorily by the Gaussian curve

$$N(X) = N_0 \exp\{(X - \overline{X})/\sigma\sqrt{2}\}^2, \qquad (1)$$

Any such distribution can be sufficiently well characterized by two parameters: the mean value of X and the dispersion σ.

A. Cloud Chamber Method

Angles of emission of secondary particles with energies up to 10^{11} ev were measured using a cloud chamber placed in a magnetic field. The distributions shown in Fig. 1 (taken from Ref. 2) refer to the angles of emission of secondary particles $\theta_0 =$ 30, 50, and 90° in the center-of-mass system. The primary particles were protons of $E_0 = 2.2$ Bev. Data obtained from cosmic rays[3,4] referring to primary energies of 5 and 30 Bev are shown in Figs. 2 and 3, respectively. The dashed parts of the histograms (which were taken into account in constructing the resulting dashed Gaussian curves) were obtained by an appropriate extrapolation of the events in which only the lower limit of the measured momentum was known.

B. Emulsion Method: Measurements of the Multiple Scattering of Secondary Particles

Besides the 34 measurements of the single event reported by Debenedetti et al.[5] and which was al-

*In the following we call $p_\perp$ simply the transverse momentum, and measure it in units of μc.

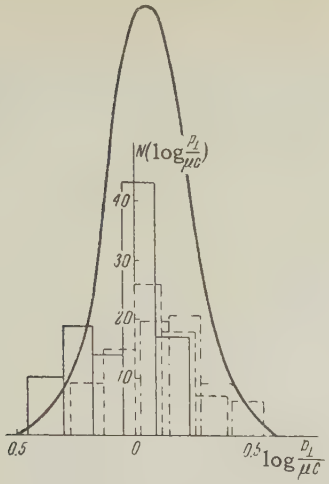

FIG. 1. Distribution of secondary particles with respect to the transverse momentum $p_\perp$ (in units of μc), obtained by means of an accelerator for $E_0 = 2.2$ Bev.[2] Total number of particles $N = 244$. Mean (geometrical) value $(\bar{p}_\perp)_{geom} = 1.1\ \mu c$. Dispersion of the distribution $\sqrt{D(p_\perp)}/\bar{p}_\perp \approx 0.4$. The solid, dot –, and dash-dot histograms of $p_\perp$ distributions correspond to angles $\theta_0 = 30°$, $\theta_1 = 50°$, and $\theta_0 = 90°$ respectively.

ready mentioned in Ref. 1, we had at our disposal additional 46 measurements of 4 events of $10^{12} - 10^{13}$ ev which were partially published in Refs. 6 and 7. The distribution shown in Fig. 4 is based upon all data available. This time we have not included the 8 cases (out of 88) when only the lower limit of the value of $p_\perp$ had been known; the resulting mean value of the transverse momentum is therefore slightly lower.

C. Emulsion Method: Analysis of Secondary Interactions

In the cases when secondary interactions have been observed, it is possible to determine the corresponding value of γ_c from the angular distribution, making use of the fact that the distribution is usually symmetrical in the center-of-mass system. Passing from γ_c to the energy of particles, it is possible to account for the tunnel effect by using the results of Ref. 8. Data on all 15 cases known to us, in which it has been possible to measure the angles of emission and the energies of secondary particles, are given in the table.

It can be seen from the table that both the mean transverse momentum and the spread about the mean are considerably larger than in all previous (and also following) methods of determination of $p_\perp$. There is a reason to think that the large spread in values of $p_\perp$ is in that case connected with large (compared with Poissonian) fluctuations of the angular distribution and that the large value of $p_\perp$ obtained is due to possible deviations from asymmetry in the angular distribution (in

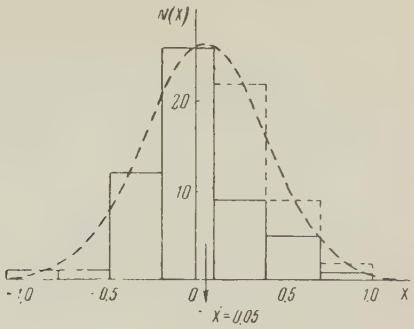

FIG. 2. Distribution with respect to $p_\perp$ of secondary particles for $\bar{E}_0 = 5$ Bev[3] (cloud chamber method). $N = 72$, $(\bar{p}_\perp)_{geom} = 1.1\ \mu c$, $\sqrt{D(p_\perp)}/\bar{p}_\perp = 0.8$.

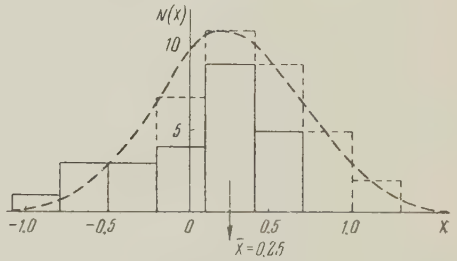

FIG. 3. Distribution of secondary particles with respect to $p_\perp$ for $E_0 = 30$ Bev[4] (cloud chamber method). $N = 41$, $(\bar{p}_\perp)_{geom} = 1.8\ \mu c$, $\sqrt{D(p_\perp)}/\bar{p}_\perp = 1.0$.

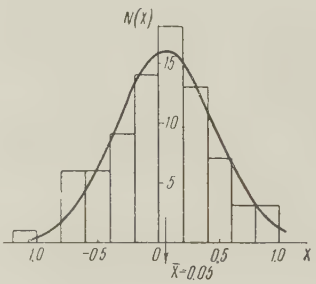

FIG. 4. Distribution of secondary particles with respect to $p_\perp$ for $E_0 \sim 5 \cdot 10^{12}$ ev. Data of Ref. 5–7 and of the author (multiple scattering method, emulsion). $N = 80$, $(\bar{p}_\perp)_{geom} = 1.1\ \mu c$, $\sqrt{D(p_\perp)}/\bar{p}_\perp = 0.9$.

the mean) in interactions between particles with different mass (essentially π-mesons with nuclei).

D. Emulsion Method: Analysis of the Angular and Energy Distributions of Particles of the Soft Component

The study of the electron-photon component of the products of nuclear interactions reveals two possibilities for determination of the transverse momentum of π^0-mesons. Firstly, it is possible to measure the position of electron pairs of non-bremsstrahlung origin* with respect to the axis of the primary star, and to find the energy of those pairs from the opening angle of their components.†

*Bremsstrahlung photons, incidentally, posses a transverse momentum of the order of $m_e c$ only (where m_e is the electron mass).

†The energy determination followed the method of Ref. 13.

Primary interaction	Secondary interactions: Type of star	n_c	Angle with shower axis, θ	Energy in lab. system: a n–n interaction, Bev	Energy in lab. system: b tunnel effect interaction, Bev	$p_\perp/\mu c$: a	$p_\perp/\mu c$: b	Remarks
$1+37_\alpha$, $n_c=200$	$3+10_p$	13 ± 4	$6\cdot10^{-4}$	350^{+250}_{-200}	700^{+500}_{-400}	$1.5^{+1.1}_{-0.9}$	$3.0^{+2.2}_{-1.8}$	
	$9+13_p$	5.5 ± 1.5	$3\cdot10^{-3}$	60^{+40}_{-30}	180^{+120}_{-90}	$1.3^{+0.9}_{-0.6}$	$3.9^{+2.7}_{-1.8}$	
$8+30_n$, $n_c=55$	$4+11_p$	8 ± 2	$5\cdot10^{-3}$	130^{+70}_{-60}	130^{+70}_{-60}	$4.6^{+2.5}_{2.1}$	$4.6^{+2.5}_{-2.1}$	
$1+51_n$, $n_c=22$	$13+10_p$	3.7 ± 1.1	~0.01	30^{+20}_{-12}	60^{+40}_{-25}	~7	~14	
$1+29_Z$, $n_c=20$	$4+5_n$	7 ± 3	~0.05	100^{+100}_{-70}	100^{+100}_{-70}	~35	~35	
	$14+17_p$	3 ± 1	0.025	20^{+15}_{-11}	100^{+75}_{-55}	$3.5^{+2.5}_{-2.0}$	~15	
$21+78_Z$, $n_c=15$	$0+6_p$	~100 (?)	$3\cdot10^{-3}$	$\sim20{,}000$ (?)	$\sim20{,}000$ (?)	~500 (?)	~500 (?)	
	$17+8_p$	20 ± 6	$7\cdot10^{-3}$	760^{+500}_{-420}	760^{+500}_{-420}	35^{+27}_{-18}	35^{+27}_{-18}	
	$4+12_p$	5 ± 1.5	$3.5\cdot10^{-2}$	50^{+35}_{-25}	100^{+70}_{-50}	$1.25^{+0.9}_{-0.6}$	$2.5^{+1.8}_{-1.2}$	
$5+30_p$, $n_c=26$	$3+55_n$	10 ± 1.5	$1.5\cdot10^{-3}$	220 ± 60	1000	2.5 ± 0.75	10	Ref. 9
$20+56_p$, $n_c=70$	$22+22_p$	4	$4\cdot10^{-3}$	30	150	0.85	4	
	$3+9$	13	$4\cdot10^{-3}$	320	500	9	15	Ref. 10
	$23+37_n$	9	$5\cdot10^{-3}$	160	800	6	30	
$0+14_\alpha$, $n_c=420$	$0+16_p$	~30	$1.1\cdot10^{-4}$	~2000	~4000	1.6	3.2	
	$3+18_p$	~20	$5.4\cdot10^{-4}$	~1000	~3000	4	12	Ref. 11
Geometrical mean (of 14 cases) for $p_\perp\mu c$.						~4	~10	

Interactions with $n_s < 5$ are not given. The angles θ are measured in projection on the emulsion plane.

Advantage is taken of the fact that the additional transverse momentum imparted to the photons in the π^0-decay is found to be several times smaller than the initial momentum of the π^0-meson. The second method consists in determination of the photon energy from the development of electromagnetic cascades initiated by them. By a special combination of additional absorbers, it is possible to create such conditions (as it has been done in emulsion chamber experiments of a group of Japanese physicists[12]) that cascades due to different photons are well separated from each other.

In the determination of $p_\perp$ according to the first method we made use of the data of Refs. 13, 14, and 11. The calculated distribution is shown in Fig. 5. The distribution obtained using the second method, and the data of Ref. 2, as well as the theoretical curve for the temperature of evaporation equal to $\mu c^2/k$ calculated according to Ref. 1 are shown in Fig. 6. Comparing Fig. 6 with Figs. 2 — 5, we can see that the last method yields the narrowest distribution which, at the same time, is not in disagreement with the theoretical curve. This distribution of the transverse momentum is based on all available cosmic ray data, and although one cannot exclude the possibility that the result is due to experimental errors, we shall assume the theoretical distribution given in Fig. 6 as the basis for the following discussion.

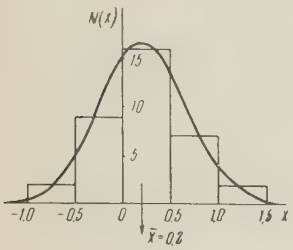

FIG. 5. $p_\perp$ distribution of π^0-mesons obtained from the energy and angle of emission of electron pairs (data of Refs. 12, 14, and 11). N = 36, $(\bar{p}_\perp)_{geom} = 1.6\ \mu c$, $\sqrt{D(p_\perp)}/\bar{p}_\perp$ 1.0.

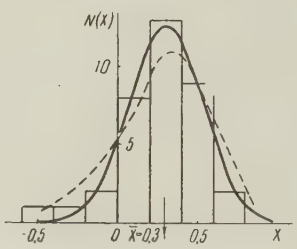

FIG. 6. $p_\perp$ distribution of π^0-mesons obtained from data of Ref. 12, for electromagnetic cascades in emulsion chamber. N = 36, $(\bar{p}_\perp)_{geom} = 2\ \mu c$, $\sqrt{D(p_\perp)}/\bar{p}_\perp = 0.5$. The dotted curve represents distribution according to one-dimensional hydrodynamical theory[1] for disintegration temperature $T_k = \mu c^2/k$.

E. Data from Extensive Air Showers

The multiplicity of processes contributing to the development of extensive air showers makes it impossible to obtain sufficiently accurate data on the transverse momentum of shower particles at the place of production. In view of the considerably higher energies involved, it is nevertheless

interesting to compare even rough estimates of $p_\perp$ with previous results.

The possibility of estimating $p_\perp$ is basically connected with the analysis of the angular distribution of the penetrating component of showers at various depths underground (cf., e.g., Refs. 15, 16). Defining the mean angle of emission of mesons as the ratio of the mean radius of lateral distribution to the effective altitude of shower initiation (about 10 km) and determining the mean energy from the range in ground we found that, for energies up to 10^{12} ev, the mean value of the transverse momentum of π-mesons should be $1-5$ (in units of μc). The same principle of determination of transverse momentum can be used for the soft component of showers, giving results consistent with the above. It can be maintained that, for a primary energy of $10^{12}-10^{14}$ ev, the distribution of secondary particles with respect to transverse momentum is in good agreement with the one-dimensional hydrodynamical theory of multiple particle production if we regard transverse deviation of produced particles solely as a result of their thermal motion at the temperature of evaporation, close to $\mu c^2/k$.

The author wishes to express his gratitude to S. N. Vernov and I. L. Rozental' for the discussion and to E. A. Zamchalov for taking part in the reduction of data.

[1] G. A. Milekhin and I. L. Rozental', J. Exptl. Theoret. Phys. (U.S.S.R.) **33**, 197 (1957), Soviet Phys. **6**, 154 (1958).

[2] Proceedings of the 6th Rochester conference, 1956.

[3] Iu. A. Smorodin, Dissertation, Physical Institute, Academy of Sciences 1957.

[4] Birger, Grigorov, Guseva, Zhdanov, Slavatinskii, and Stashkov, J. Exptl. Theoret. Phys. (U.S.S.R.) **31**, 971 (1956); Soviet Phys. JETP **4**, 872 (1957).

[5] Debenedetti, Garelli, Tallone, and Vigone, Nuovo cim. **4**, 1142 (1956).

[6] Schein, Glasser, and Haskin, Phys. Rev. **99**, 1555 (1955).

[7] Zh. S. Takibaev and E. G. Boos, J. Exptl. Theoret. Phys. (U.S.S.R.) (in press).

[8] I. A. Ivanovskaia and D. S. Chernavskii, Nucl. Phys. **4**, 29 (1957).

[9] E. Lohrmann, Zs. f. Naturforsch. **11a**, 561 (1956).

[10] E. Lohrmann et al., Nuovo cim. **4**, 1473 (1956).

[11] Ciok, Danysz, Gierula, and Jurak, communication at Warsaw international Colloqium, 1957.

[12] United Japanese Emulsion Group, paper presented at the Varenna conference, 1957.

[13] Gramenitskii, Zhdanov, Zamchalova, and Shcherbakova, J. Exptl. Theoret. Phys. (U.S.S.R.) **32**, 936 (1957); Soviet Phys. JETP **5**, 763 (1957).

[14] J. E. Naugle and P. S. Freier, Phys. Rev. **104**, 804 (1956).

[15] E. L. Andronikashvili and M. F. Bibilashvili, J. Exptl. Theoret. Phys. (U.S.S.R.) **32**, 403 (1957); Soviet Phys. JETP **5**, 341 (1957).

[16] Barret, Bollinger, Cocconi, Eisenberg, and Greisen, Rev. Mod. Phys. **24**, 133 (1952).

Translated by H. Kasha
173

PHOTODISINTEGRATION OF HELIUM. II

A. N. GORBUNOV and V. M. SPIRIDONOV

P. N. Lebedev Physical Institute, Academy of Sciences, U.S.S.R.

Submitted to JETP editor December 14, 1957

J. Exptl. Theoret. Phys. (U.S.S.R.) **34**, 862-865 (April, 1958)

The $He^4(\gamma,n)He^3$ reaction was investigated using a Wilson chamber. The method for treating the He^3 track data is described. The dependence of the reaction cross section on γ-ray energy and the angular distributions of the reaction products were measured. σ_{int} and $\sigma_b = \int \sigma(W) W^{-1} dW$ are computed from the curve for $\sigma(W)$.

1. INTRODUCTION

IN the first part of this work[1,*] we gave a detailed description of experiments on photodisintegration of helium using a Wilson chamber in a magnetic field, placed in the beam of the synchrotron of the Physical Institute of the Academy of Sciences, which gives a maximum energy of 170 Mev. We also gave the results of a study of the $He^4(\gamma,p)H^3$ reaction from the analysis of 9000 cloud chamber pictures, including the energy distributions of the protons and tritons and the energy dependence of the cross section for the reaction.

We shall here describe the results of investigation of the $He^4(\gamma,n)He^3$ from processing of the same photographs.

2. PROCESSING OF PHOTOGRAPHS

As was mentioned in I, the $He^4(\gamma,n)He^3$ reaction is characterized by the emission of a single charged particle, the He^3 recoil nucleus, which gives a high density track in the cloud chamber (Fig. 1). A single charged particle with a high density track can also occur from (γ,n) reactions on C and O nuclei, which are contained in the vapor in the cloud chamber. However the mean length of these tracks is $4-5$ mm, and their maximum does not exceed 15 mm, so they can be assigned to events in helium only for photon energies between 20.6 (the threshold for the $He^4(\gamma,n)He^3$ reaction) and 25 Mev. In investigating the energy dependence of the cross section for the $He^4(\gamma,n)He^3$ reaction, we therefore restricted ourselves to the range of photon energies $h\nu \geq 27$ Mev, in which the (γ,n) reaction could be reliably identified.

Since there are only two particles in the final state for the $He^4(\gamma,n)He^3$ reaction, we can, as in the $He^4(\gamma,p)H^3$ reaction, use the conservation laws to determine the energy of the photon which produced the reaction, from a knowledge of the angle of emergence and the momentum of one of the particles (the He^3 nucleus). For the measurement of angles of emergence and momenta of He^3 nuclei, we selected from all the recorded cases of the $He^4(\gamma,n)He^3$ reaction those He^3 tracks which had a sufficient projected length (≥ 53 mm) on the bottom plane of the chamber, and the momenta were determined from the curvature of the tracks in the magnetic field.

The procedure for measuring angles and momenta, as well as the necessary corrections, were described in I. Here we need only add that, since for low energy He^3 nuclei the curvature changed along the track, the measurement gave some average value of the momentum, and a suitable correction was made graphically to find the true momentum. However, if we limited ourselves to only those He^3 tracks which had a large projected length, we would impose a strong limitation on the energy range of the photons for which we could get the energy dependence of the cross section. Actually, if for example the He^3 nucleus is emitted at an angle of 180° to the γ-ray direction and has a range of 5.3 cm in the chamber gas, the energy of the photon responsible for this event is ~ 40 Mev, and this limiting energy depends essentially on the angle of emergence of the He^3 nucleus. Because of this, we also processed short tracks of He^3 nuclei stopping in the chamber gas. For these the path length and spatial angles were measured with a special stereocomparator.* In this case the momenta of the He^3 nuclei were found from the range-

*This paper will be cited as I.

*The stereocomparator was developed in the cosmic ray laboratory of the Physical Institute of the Academy of Sciences by engineer A. G. Novikov.

FIG. 1. $He^4(\gamma, n)He^3$ reaction. The single dense track is a He^3 nucleus.

momentum relation calculated for the mixture of gases in the chamber.

Of the total number of 2685 cases of the $He^4(\gamma, n)He^3$ reaction recorded, 722 tracks of He^3 nuclei were analyzed. As in our study of the $He^4(\gamma, p)H^3$ reaction, all the measured He^3 tracks were incorporated in a nomogram which served as the primary material for further computations of energy dependence and angular distributions.

3. RESULTS

A. Dependence of the Cross Section for the $He^4(\gamma, n)He^3$ Reaction on Photon Energy

The dependence of the cross section for the (γ, n) reaction on photon energy is given in Fig. 2. For the reasons given above, it was not drawn from the reaction threshold (20.6 Mev), but from 27 Mev.

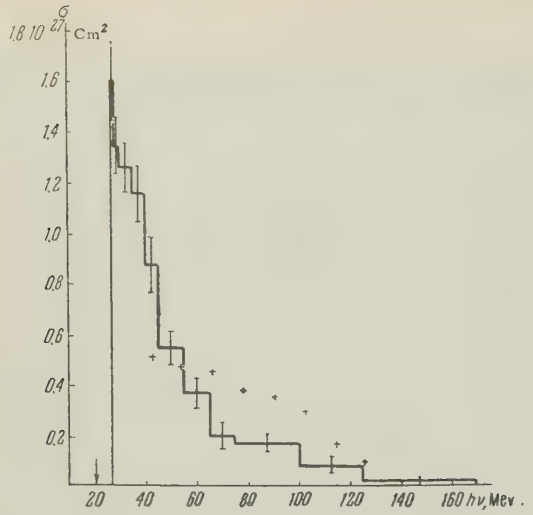

FIG. 2. Dependence of the cross section for the $He^4(\gamma, n)He^3$ reaction on photon energy. Only statistical errors are shown on the figure. The reaction threshold (20.6 Mev) is indicated by the arrow. The points marked with a + are the data of Ref. 2.

As we see from the figure, the (γ, n) reaction on helium has resonant character, with a maximum of $\sim 1.6 \times 10^{-27}$ cm^2 at an energy of 27 – 28 Mev. The position and height of the maximum agree within the limits of error with the corresponding values for the (γ, p) reaction.

Comparison of the curves for the cross sections for the (γ, p) and (γ, n) reactions shows that they have the same shape, although the curve for the (γ, n) reaction runs a little higher for photon energies above 35 Mev. This difference is possibly due to the large corrections made to the measured values of the momenta of He^3 nuclei, of which we spoke before, and also to neglect of multiple scattering. Whether this difference is real will be settled in experiments which are now being done with a magnetic field of twice the intensity and a lower pressure of the gas mixture in the cloud chamber.

In Fig. 2 we include for comparison the results of measurements of the cross section for the (γ, n) reaction on helium which were found in Ref. 2 using thick-layered emulsions. As we see from Fig. 2, these results agree with our data only at ~ 55 Mev, while for higher energies they give cross sections which are approximately twice as large.

TABLE I*

Photon energy E_γ, Mev	$\sigma_{int} = \int_{20.6}^{E_\gamma} \sigma(W)\, dW$, Mev-millibarns
40	21.6±0.9
100	41.3±1.7
170	43.8±1.8

*Only statistical errors are given.

From the cross section curve for the (γ, n) reaction, we calculated the integral cross section $\sigma_{int} = \int \sigma(W)\, dW$ (Table I), and the quantity $\sigma_b = \int_{20.6}^{170} \sigma(W) W^{-1} dW = (1.09 \pm 0.08)$ millibarns.

The value of σ_b agrees exactly with the value of σ_b found in I for the (γ, p) reaction. The values of the integral cross section for the (γ, n) reaction at 100 and 170 Mev are somewhat greater than the corresponding values for the (γ, p) reaction.

B. Angular Distributions

The angular distributions (in the center-of-mass system, c.m.s.) of the neutrons from the $He^4(\gamma, n)He^3$ reaction are given in Fig. 3 for two photon energy ranges: 27 – 30 Mev and 30 – 170 Mev. They were obtained by reflecting the angular distributions of the He^3 nuclei about 90° in the c.m.s. These energy ranges were chosen for convenience of comparison with the angular distributions of protons from the (γ, p) reaction on helium, which were given in I.

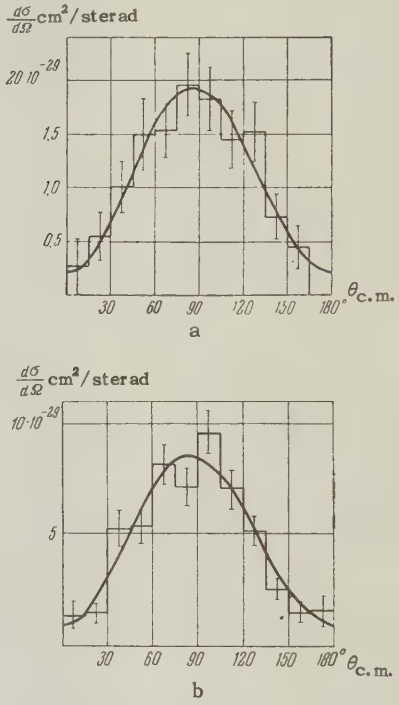

FIG. 3. Angular distributions in the c.m.s. of neutrons from the $He^4(\gamma, n)He^3$ reaction with photons of energy: a) 27 – 30; b) 30 – 170 Mev.

The angular distributions were approximated by curves of the form

$$A(\sin^2\theta + \beta \sin^2\theta \cos\theta + \delta).$$

The values of the coefficients A, β, δ were

fitted by a least squares method, and are given in Table II.

TABLE II

Photon energy E_γ, Mev	$A \cdot 10^{29}$ cm^2/sterad	β	δ
27—30	1.7±0.2	0.11±0.18	0.12±0.07
30—170	7.5±0.6	0.17±0.13	0.12±0.07

From Figure 3 and Table II we see that, in going from photon energies below 30 Mev to energies greater than 30 Mev, the angular distribution of the neutrons remains unchanged within the limits of error of the experiment, and is close to a $\sin^2\theta$ distribution in the c.m.s. On the other hand, as was shown in I, the asymmetry of the angular distribution of the protons from the (γ, p) reaction on helium changes markedly in the photon energy region 30 — 35 Mev, so that in the 30 — 170 Mev range the maximum of the angular distribution in the c.m.s. shifts forward to an angle of 65 — 70°.

It is interesting to note that similar results are found for the angular distributions of photoprotons from more complex nuclei (C, Al, Ni, Mo). In fact[3-6] the angular distributions of the photoprotons have their maximum at an angle of 60 — 70° and contain an appreciable isotropic part. At the same time, the angular distributions of the photoneutrons[3] are well described by curves of the form $a + b\sin^2\theta$, symmetric around 90°. Thus if we disregard the appreciable isotropic part of these distributions (which may be due to evaporation processes and also to internal scattering of the particles inside the nucleus), there is a qualitative similarity of these results to the curves obtained for helium.

These features of the angular distributions of protons and neutrons can be explained from the point of view of a model of direct absorption of the photon by an individual nucleon, as proposed by Courant,[7] supplemented by including electric quadrupole absorption of the photons. Actually, from the point of view of this model, at low energies there is electric dipole absorption, so that the angular distributions of protons and neutrons have the form $\sin^2\theta$. At energies greater than 30 Mev, electric quadrupole absorption begins to appear, which because of interference with the dipole absorption results in a shift of the maximum of the proton angular distribution toward smaller angles. However, the electric quadrupole absorption does not contribute to the neutron yield since the effective charge of the neutron is in this case equal to zero. Thus the angular distribution of the neutrons remains close to $\sin^2\theta$ even at high energies.

The quasideuteron model of photon absorption, proposed in papers of Khokhlov[8] and Levinger[9] cannot be responsible for the observed effects, since for photon energies greater than 30 Mev it would give an angular distribution of the neutrons similar to that for the protons, but with the maximum shifted in the reverse direction.

In conclusion, the authors express their gratitude to Prof. P. A. Cerenkov for continual interest in the work, to Iu. K. Khokhlov, V. V. Daragan and Iu. M. Shirokov for discussion of the results, to A. G. Gerasimov, V. S. Silaev, N. N. Novikov, K. V. Chekhovich and Hu Cheng-Yü for participating in the analysis of photographs, and to the operating group of the synchrotron.

[1] A. N. Gorbunov and V. M. Spiridonov, J. Exptl. Theoret. Phys. (U.S.S.R.) **33**, 21 (1957); Soviet Phys. JETP **6**, 16 (1958).

[2] G. De Saussure and L. S. Osborne, Phys. Rev. **99**, 843 (1955).

[3] S. A. E. Johansson, Phys. Rev. **97**, 434 (1955).

[4] I. V. Chuvilo and V. G. Shevchenko, J. Exptl. Theoret. Phys. (U.S.S.R.) **32**, 1335 (1957); Soviet Phys. JETP **5**, 1090 (1957).

[5] Mann, Halpern and Rothman, Phys. Rev. **87**, 146 (1952).

[6] H. Hendel, Z. f. Physik **135**, 168 (1953).

[7] E. D. Courant, Phys. Rev. **82**, 703 (1951).

[8] Iu. K. Khokhlov, J. Exptl. Theoret. Phys. (U.S.S.R.) **23**, 241 (1952).

[9] J. S. Levinger, Phys. Rev. **84**, 43 (1951).

Translated by M. Hamermesh
174

PHOTODISINTEGRATION OF HELIUM. III

A. N. GORBUNOV and V. M. SPIRIDONOV

P. N. Lebedev Physical Institute, Academy of Sciences, U.S.S.R.

Submitted to JETP editor December 14, 1957

J. Exptl. Theoret. Phys. (U.S.S.R.) **34**, 866-873 (April, 1958)

Results of an investigation of the $He^4(\gamma, pn)D$ reaction, and a summary of results on photodisintegration of He^4 are presented. The dependence of the cross section for the (γ, pn) reaction on γ-ray energy, the angular distributions of the protons and neutrons from this reaction, and the correlations between the directions of emission of protons, neutrons and deuterons were measured. $\sigma_{int} = (95 \pm 7)$ Mev · mbarn and $\sigma_b = (2.4 \pm 0.15)$ mbarn are computed from the cross section curves for the (γ, p), (γ, n) and (γ, pn) reactions on He^4. The results are discussed from the point of view of finding a model for the interaction with He^4 of γ-quanta of varying energies, and are also compared with theoretical computations of the photodisintegration of He^4.

1. INTRODUCTION

IN preceding papers[1,2]* we discussed in detail the properties of the $He^4(\gamma, p)H^3$ (I) and $He^4(\gamma, n)He^3$ (II) reactions, which lead to the emission of two particles — a proton and an H^3 nucleus, and a neutron and an He^3 nucleus. Here we shall consider the third reaction which occurs after absorption of a photon by the helium nucleus — the $He^4(\gamma, pn)D$ reaction, which leads to emission of three particles — a proton, a neutron and a deuteron.

The investigation of this reaction has a special interest from the point of view of testing the validity of the two-nucleon model for the absorption of high energy photons by nuclei, which was proposed in papers by Khokhlov[3] and Levinger.[4] According to this model, high energy photons are absorbed by a pair of nucleons in the nucleus which are located at a relatively small distance from one another. Having absorbed the photon, the high energy proton and neutron either both leave the nucleus or, before emergence, undergo a series of collisions in the nuclear matter and excite the residual nucleus.

Many experimental papers have already been published whose results can be interpreted from the point of view of the quasideuteron model. Among these, we mention papers[5-12] on the angular and energy distributions of high energy photoprotons, in which there were observed characteristic kinks in the energy spectra of the photoprotons at an energy about half the maximum energy of the bremsstrahlung, and a marked forward peaking in the angular distribution of the photoprotons. However no quantitative agreement between the predictions of the quasideuteron model and experiment was found. In addition to this, experiments[13-15] were done to detect directly the correlation in the emission of fast protons and neutrons in the nuclear photoeffect. In these experiments, coincidences between neutrons and photoprotons were observed from lithium, carbon and oxygen, and the kinematics were the same as for the photodisintegration of the deuteron. The angular distributions of the neutron-proton pairs were practically the same as the corresponding distributions in the case of the deuteron. The authors of Ref. 15 arrive at the conclusion that the quasideuteron model is applicable for photon energies from 140 to 300 Mev, but are unable to say whether the quasideuteron process can be responsible for all the high energy photoprotons which are not associated with the production of real mesons.

Since we can, by applying the conservation laws, use the angles of emission and momenta of the proton and deuteron from the $He^4(\gamma, pn)D$ reaction to calculate the energy of the photon and the angle of emission and momentum of the neutron, the study of this reaction enables us to draw conclusions concerning the correlation in the emission of the neutron and proton, and to get some idea of the role of various processes in the photodisintegration of helium.

2. TREATMENT OF PHOTOGRAPHS

We have already said in I that the $He^4(\gamma, pn)D$ reaction is characterized by the appearance of two

*These will be cited as I, II.

tracks of different density in the Wilson chamber (the more dense track being that of the deuteron), and these tracks are at at arbitrary angle to one another and to the direction of the γ-quanta. A cloud chamber photograph of a $He^4(\gamma, pn)D$ reaction was given as Fig. 3 in paper I. We should mention that two arbitrarily oriented tracks of different density can also be formed in the $He^4(\gamma, 2p\,2n)$ reaction. However, as the results of photometering and measurement of momenta showed, almost all cases of a pair of tracks with random orientation are due to the $He^4(\gamma, pn)D$ reaction. In a series of 23,000 photos taken with maximum bremsstrahlung energy from 170 to 260 Mev, the number of cases recorded of the $He^4(\gamma, pn)D$ and $He^4(\gamma, 2p\,2n)$ reactions were 1,370 and 120, respectively. Thus the relative yield of the $He^4(\gamma, 2p\,2n)$ reaction compared to $He^4(\gamma, pn)D$ does not exceed 10%. The yield of reactions of the type of $He^4(\gamma, pn)D$ and $He^4(\gamma, 2p\,2n)$ is 10% compared to that of reactions with two particles in the final state.

To find the energy dependence of the cross section and to construct the angular distributions of the emerging particles, we restricted ourselves to those cases in which both tracks had projected lengths on the plane of the bottom of the chamber at least equal to 53 mm. We could then measure the radius of curvature of the track with sufficient accuracy. Having measured the angles between the γ-ray beam direction and the track projections, as well as the projected momenta, we could, from the projected length of the tracks and the depth of the illuminated region of the chamber, determine by the same method as in I and II the true spatial angles of emission of the particles and their true momenta. Furthermore, by comparing the observed visual densities of the tracks with those expected (assuming we knew the type of particle and using the measured momenta), we checked the correctness of the identification of the particles. After this, using the conservation laws, we found the energy of the photon and the angles of emission and momenta of all three particles in the center of mass system, and the angles between them.

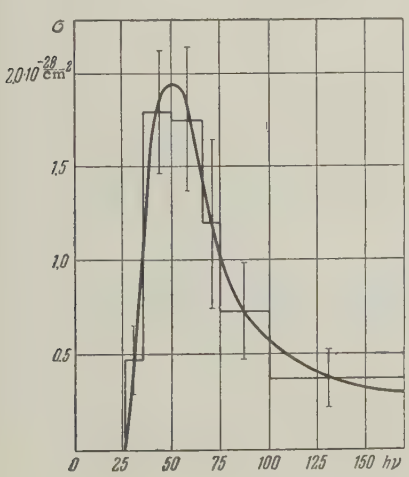

FIG. 1 Dependence of the cross section for the $He^4(\gamma, pn)D$ reaction on photon energy.

In constructing the angular distributions of the emergent particles, we introduced corrections (as described in I) to take account of the limited size of the illuminated region. In constructing the energy distributions, such corrections were not made, but the cross section curve was normalized to the total number of observed cases of the $He^4(\gamma, pn)D$ reaction.

3. RESULTS

A. Dependence of the Cross Section for the (γ, pn) Reaction on Photon Energy

Figure 1 shows the curve for the cross section of the $He^4(\gamma, pn)D$ reaction as a function of photon energy, obtained from analysis of 91 cases of this reaction in a series of 9,000 cloud chamber photographs taken with radiation having a maximum energy of 170 Mev. We see from Fig. 1 that the $He^4(\gamma, pn)D$ reaction has resonance character, with its maximum at an energy around 50 Mev. The cross section at the maximum is of the order of 2×10^{-28} cm^2. Comparison with the cross section curves for the (γ, p) and (γ, n) reactions shows that the cross section for the (γ, pn) reaction becomes approximately the same as those for the (γ, p) and (γ, n) reactions for photon energies of the order of 75 Mev.

To estimate the contribution of the (γ, pn) reaction to the total photon absorption cross section, we give in Table I the integral cross section of this reaction and also the total cross sections for the (γ, p) and (γ, n) reactions.

TABLE I*

Photon energy E_γ, Mev	$\sigma_{int} = \int \sigma(W)\,dW$, Mev·mbarn	
	(γ, pn)	$(\gamma, p) + (\gamma, n)$
$\leqslant 75$	7.2±0.9	71.6±2.2
75—170	4.6±1.2	10.0±1.9
$\leqslant 170$	11.8±1.5	81.6±2.9

*Only the statistical errors are given.

We see from the table that, for energies below 75 Mev, the contribution of the (γ, pn) reaction to the total photon absorption cross section is less than 10%, while in the energy region above 75 Mev its contribution increases to 30%.

The value of $\sigma_b = \int \sigma(W) W^{-1} dW$ found for the

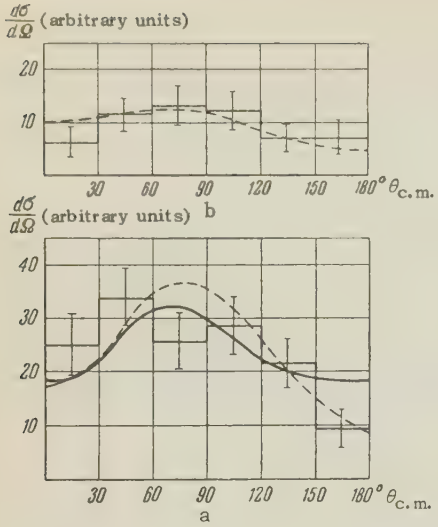

FIG. 2.

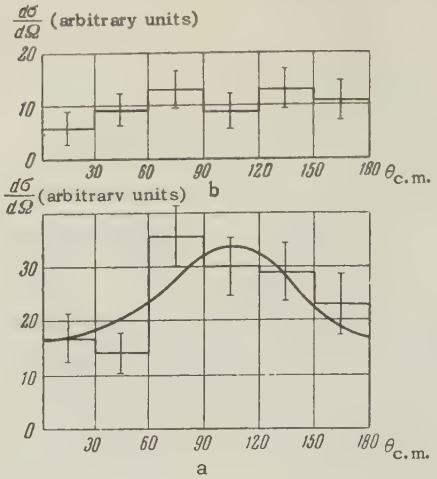

FIG. 3.

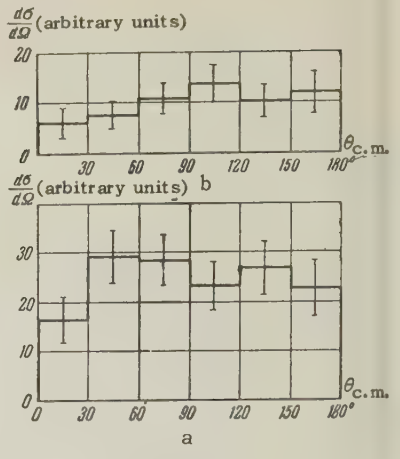

FIG. 4.

FIG. 2. Angular distributions of protons from the He^4 (γ, pn) D reaction, in the center of mass system, integrated over the bremsstrahlung spectrum for photon energies: a) $h\nu = 25.9 - 75$, b) 75 – 170 Mev. The solid curve is a least squares fit of the functional form $\sin^2\theta + \beta \sin^2\theta \cos\theta + \delta$, with $\beta = 1.0 \pm 1.2$; $\delta = 1.6 \pm 1.0$. The dashed curves are angular distributions of protons from photodisintegration of the deuteron, for photon energies of a) 55 Mev, and b) 105 Mev.

FIG. 3. Angular distribution of neutrons from the He^4 (γ, pn) D reaction in the center of mass system, integrated over the bremsstrahlung spectrum for photon energies: a) $h\nu = 25.9 - 75$ Mev, b) 75 – 170 Mev. The solid curve is a least squares fit of the functional form $\sin^2\theta + \beta \sin^2\theta \cos\theta + \delta$, with $\beta = -0.8 \pm 0.8$; $\delta = 1.1 \pm 0.7$.

FIG. 4. Angular distribution of deuterons from the He^4 (γ, pn) D reaction in the center of mass system, integrated over the bremsstrahlung spectrum for photon energies: a) $h\nu = 25.9 - 75$, b) $h\nu = 75 - 170$ Mev.

(γ, pn) reaction was $\sigma_b = 1.8 \times 10^{-28}$ cm^2.

B. Angular Distributions

In Figs. 2 – 4 we give the angular distributions of protons, neutrons and deuterons in the center of mass system, for two ranges of photon energies, from 25.9 Mev (the threshold for the reaction) to 75 Mev and from 75 Mev to 170 Mev. These angular distributions were found from analysis of 207 cases of the He^4 (γ, pn) D reaction, which were recorded in 9,000 pictures at a maximum energy of 170 Mev and in 14,000 pictures at a maximum energy of 260 Mev.

From Figs. 2 and 3 we see that the angular distributions of the protons and neutrons produced in the (γ, pn) reaction are very similar to the angular distributions of the protons and neutrons from photodisintegration of the deuteron. Also, as in the case of the deuteron, they have an appreciable isotropic part at medium energies, and in the c.m.s. system the maximum for the protons is shifted forward to $\sim 75°$ while that for the neutrons is shifted backward to $\sim 105°$. At high energies there is a bigger isotropic part. For comparison, in Fig. 2 the dashed curves are the experimental angular distributions of protons from photodisintegration of the deuteron at photon energies of 55 Mev[16] and 105 Mev,[17] normalized to the area under the histogram.

The angular distribution of the deuterons (Fig. 4) is close to isotropic in both the photon energy intervals $h\nu = 25.9 - 75$ and $76 - 170$ Mev. In Fig. 5 we give the angular distributions of the protons in the laboratory system for approximately the same intervals of photon energy, as constructed from 495 proton tracks. In constructing these curves, we used all cases where the proton track had a projected length ≥ 53 mm. We see from Fig. 5 that the proton angular distribution for $E_p \geq 21$ Mev is in satisfactory agreement with the calculations of Dedrick[18] on the quasideuteron model.

C. Correlation between Particles

To clarify the question of the existence of correlations in the emission of particles from the (γ, pnd) reaction, we constructed distributions of the relative energies of proton and neutron (Fig. 6) and proton and deuteron (Fig. 7), computed in units of the maximum relative energy. In the absence of correlation we should expect the distributions to have the form

$$\text{const}\,[1 - E_{ij}/E_0]^{1/2}\,(E_{ij}/E_0)^{1/2},$$

where E_{ij} is the relative energy of proton and

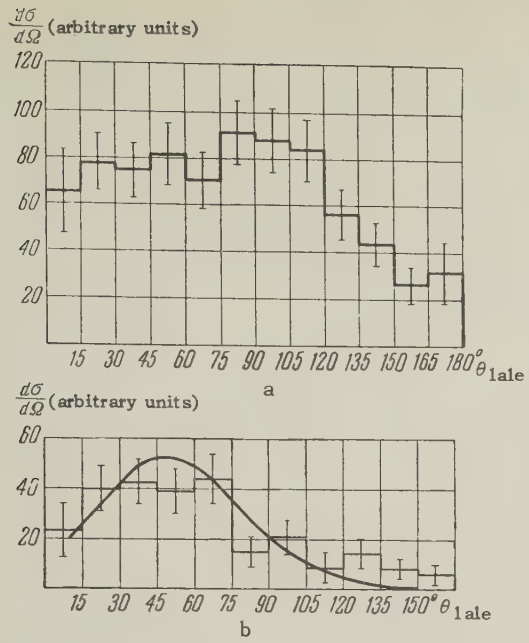

FIG. 5. Angular distribution of protons with energies: a) $E_p \leq 21$ Mev, b) $E_p \geq 21$ Mev, emitted from the He^4 (γ, pn) D reaction, in the laboratory coordinate system. The solid curve is calculated for quasideuteron absorption, from data given in the paper of Dedrick[18] (normalized at $\theta = 30°$).

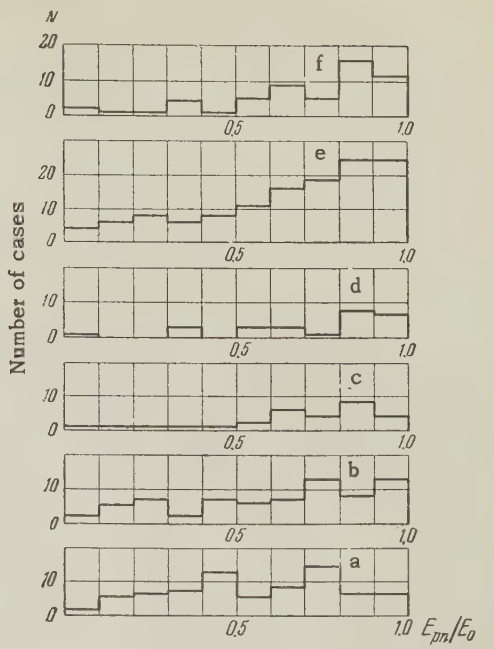

FIG. 6. Distribution of numbers of cases of the He^4 (γ, pn) D reaction as a function of the relative energy (in the c.m.s.) of proton and neutron, for various photon energies: a) $h\nu = 25.9-50$, b) $h\nu = 50-75$, c) $h\nu = 75-100$, d) $h\nu = 100-150$, e) $h\nu = 50-150$, f) $h\nu = 75-150$ Mev.

neutron or of proton and deuteron.

As we see from the graphs, the distributions have approximately this dependence only for photon energies from 25.9 (the reaction threshold) to 50 Mev. In the energy range 50 — 75 Mev, a preponderance of large relative energies of proton and neutron is indicated. The distribution of relative energies of proton and deuteron remains practically the same in the 50 — 75 Mev interval as it was at low energies. For energies above 75 Mev, the preponderance of large relative energies of proton and neutron becomes completely apparent. At the same time a preponderance of small relative energies of proton and deuteron becomes noticeable.

Thus for photon energies greater than 75 Mev, the neutron and proton are emitted preferentially in almost opposite directions, taking away an appreciable part of the energy of the reaction, while the low energy deuteron has a slight preference for being dragged along in the direction of emission of the proton.

Similar conclusions can be drawn from a consideration of the angles between the directions of emission of the particles. For energies up to 75 Mev, all three particles behave equivalently, so that the average angles between them are approximately 120°, whereas for energies > 75 Mev the average angles are

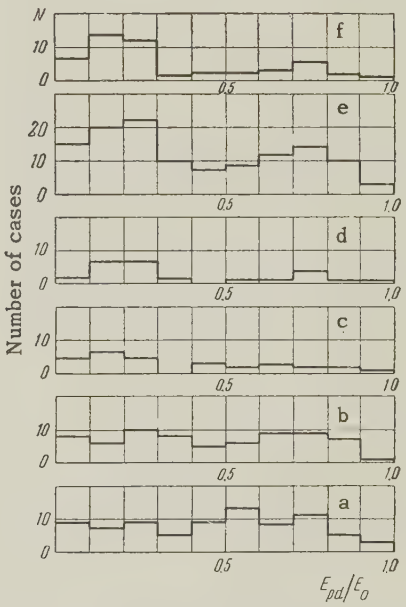

FIG. 7. Distribution of numbers of cases of the He^4 (γ, pn) D reaction as a function of the relative energy (in the c.m.s.) of proton and deuteron, for various photon energies: a) $h\nu = 25.9-50$, b) $h\nu = 50-75$, c) $h\nu = 75-100$, d) $h\nu = 100-150$, e) $h\nu = 50-150$, f) $h\nu = 75-150$ Mev.

$$\alpha_{pn} \sim 139, \quad \alpha_{pd} \sim 94, \quad \alpha_{dn} \sim 127°.$$

Table II gives the average momenta of the emitted particles in units of Mev/c.

TABLE II

Photon energy E_γ, Mev	Proton	Neutron	Deuteron
25.9—75	123	118	124
75—170	214	259	190

CONCLUSIONS

1. On the basis of results reported in papers I, II and III, we may suppose that the process responsible for the $He^4(\gamma, pn)D$ reaction is the quasideuteron absorption of photons, both in the low energy region and in the region above 75 Mev. This is indicated by the angular distributions of the particles and by the presence of correlation between proton and neutron which is clearly evident at high photon energies and is masked by the momentum distribution of the particles in the nucleus at low energies.

2. From comparison of the angular distributions of protons and neutrons from the $He^4(\gamma, p)H^3$ and $He^4(\gamma, n)He^3$ reactions with those from photodisintegration of the deuteron, we can assert that these processes occur as the result of direct single particle absorption of the photon, in which the main process is electric dipole absorption. At energies above 30 Mev, electric quadrupole absorption begins to be important. Its interference with the dipole absorption causes a marked shift of the maximum in the proton angular distribution, but gives no contribution to the yield of the (γ, n) reaction.

3. The relative importance of single-particle and two-particle absorption of photons changes with energy. As was stated above, the total contribution of two-particle absorption to the integral absorption cross section amounts to 12%, or to 14% if we include the $(\gamma, 2p\,2n)$ process which is also apparently related to two-particle absorption. However, in the region above 75 Mev, the contribution of two-particle absorption to the integral absorption cross section is at least 30%. Unfortunately, the poor statistics of the data at high photon energies do not allow us at present to draw conclusions concerning the importance of the two-particle mechanism of photon absorption in (γ, p) and (γ, n) processes for energies above 75 Mev.

4. The cross sections for the three main processes of photodisintegration of helium, (γ, p), (γ, n), and (γ, np) were measured as a function of photon energy. Comparison with the results of calculations of Flowers and Mandl,[19] Gunn and Irving[20] for electric dipole absorption with wave functions of various types (Gaussian, exponential, and the functions introduced by Irving[21]), for a pure central force, and with the calculations of Bransden et al.,[22] which include tensor forces, shows that it is not possible to choose the parameters of wave functions of this type so that one gets simultaneously the correct values of the binding energy and radius of He^4, the energy at which the cross section is a maximum, and the value of the maximum cross section.

5. From the measured values of cross sections for the main reactions in photodisintegration of helium, (γ, p), (γ, n), and (γ, np), we constructed a curve for the absorption cross section of photons in helium (Fig. 8). Using this curve and including

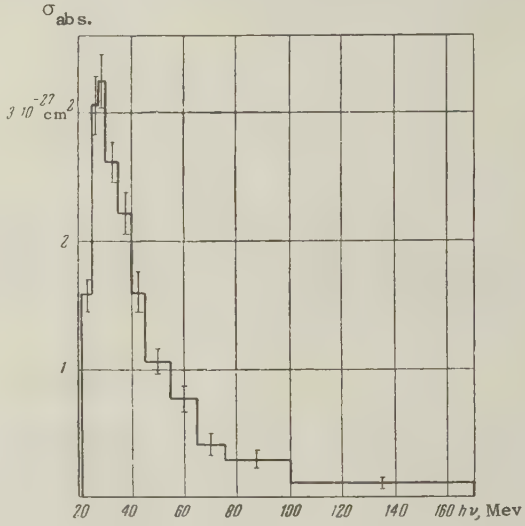

FIG. 8. Dependence of total cross section for absorption of photons by He^4 on photon energy. Only statistical errors are shown on the graph. Errors in absolute values are $\sim 6\%$.

the small contributions from the $He^4(\gamma, 2p\,2n)$ and $He^4(\gamma, 2d)$ reactions, we calculated the integral photon absorption cross section,*

$$\sigma_{int} = \int_{19.8}^{170} \sigma_{abs}(W)\,dW = 95 \pm 7 \text{ Mev·mbarn.}$$

This result is in satisfactory agreement with the calculations of the integral cross section for electric dipole absorption of photons by He^4 which were done by Rustgi and Levinger[23] using sum rules. For central forces, with a 50% mixture of exchange force, these computations give σ_{int} = 89 Mev · mbarn.

*The value 95 ± 7 Mev · mbarn for the integral cross section is somewhat larger than the value $\sigma_{int} = 88 \pm 7$ Mev mbarn given in I, although the difference is within the limits of error. The difference is due to the fact that in I we assumed $\sigma_{int}(\gamma, n) = \sigma_{int}(\gamma, p)$, while here we are using the independently determined value of $\sigma_{int}(\gamma, n)$ from II, and this value was somewhat larger than $\sigma_{int}(\gamma, p)$.

From the photon absorption curve we also calculated

$$\sigma_b = \int_{19.8}^{170} \frac{\sigma_{abs}(W)}{W} dW = 2.4 \pm 0.15 \text{ mbarn.}$$

It is known[24] that σ_b depends only on the mean square radius of the nuclear charge distribution, so that from the experimentally measured value of σ_b we can compute the mean square radius of the He^4 nucleus. We found the value

$$R = (1.57 \pm 0.06) \cdot 10^{-13} \text{ cm}$$
$$(\text{or } r_0 = (1.28 \pm 0.05) \cdot 10^{-13} \text{ cm})^*$$

in satisfactory agreement with the value $R = (1.61 \pm 0.08) \times 10^{-13}$ cm found from electron scattering experiments.[25] This value is markedly different from the values of the He^4 radius calculated using Irving's wave functions, as well as those found with wave functions of Gaussian or exponential type adjusted to give the correct binding energy of He^4.

In conclusion the authors express their gratitude to Prof. P. A. Cerenkov for continual interest in the work, to A. M. Baldin, V. V. Daragan, Iu. M. Shirokov and Iu. K. Khokhlov for discussion of the results, to S. I. Shornikov, A. G. Gerasimov, N. N. Novikov, V. A. Osipov, V. S. Silaev and K. V. Chekhovich who helped in taking and analyzing the photographs, and also to the operating group of the synchrotron.

[1] A. N. Gorbunov and V. M. Spiridonov, J. Exptl. Theoret. Phys. (U.S.S.R.) **33**, 21 (1957); Soviet Phys. JETP **6**, 16 (1958).

[2] A. N. Gorbunov and V. M. Spiridonov, J. Exptl. Theoret. Phys. (U.S.S.R.), this issue, p. 596.

[3] Iu. K. Khokhlov, J. Exptl. Theoret. Phys. (U.S.S.R.) **23**, 241 (1952).

[4] J. S. Levinger, Phys. Rev. **84**, 43 (1951).

[5] C. Levinthal and A. Silverman, Phys. Rev. **82**, 822 (1951).

[6] D. Walker, Phys. Rev. **81**, 634 (1951); **84**, 149 (1951).

[7] J. C. Keck, Phys. Rev. **85**, 410 (1952).

[8] J. W. Rosengren and J. M. Dudley, Phys. Rev. **89**, 603 (1953).

[9] A. M. Perry and J. C. Keck, Phys. Rev. **86**, 629 (1952).

[10] J. W. Weil and B. D. McDaniel, Phys. Rev. **92**, 391 (1953).

[11] Feld, Godbole et al., Phys. Rev. **94**, 1000 (1954).

[12] I. V. Chuvilo and V. G. Shevchenko, J. Exptl. Theoret. Phys. (U.S.S.R.) **32**, 1335 (1957); Soviet Phys. JETP **5**, 1090 (1957).

[13] M. Q. Barton and J. H. Smith, Phys. Rev. **95**, 573 (1954).

[14] Myers, Odian et al., Phys. Rev. **95**, 576 (1954).

[15] Odian, Stein et al., Phys. Rev. **102**, 837 (1956).

[16] L. Allen, Phys. Rev. **98**, 705 (1955).

[17] Whalin, Schriever and Hanson, Phys. Rev. **101**, 377 (1956).

[18] K. G. Dedrick, Phys. Rev. **100**, 58 (1955).

[19] B. H. Flowers and F. Mandl, Proc. Roy. Soc. (London) **A206**, 131 (1951).

[20] J. C. Gunn and J. Irving, Phil. Mag. **42**, 1353 (1951).

[21] J. Irving, Phil. Mag. **42**, 338 (1951).

[22] Bransden, Douglas and Robertson, Phil. Mag. **2**, 1211 (1957).

[23] M. L. Rustgi and J. S. Levinger, Phys. Rev. **106**, 530 (1957).

[24] J. S. Levinger and H. A. Bethe, Phys. Rev. **78**, 115 (1950).

[25] R. W. McAllister and R. Hofstadter, Phys. Rev. **102**, 851 (1956).

*For a model with a uniform charge distribution.

Translated by M. Hamermesh
175

DYNAMIC COMPRESSIBILITY AND EQUATION OF STATE OF IRON UNDER HIGH PRESSURE

L. V. AL' TSHULER, K. K. KRUPNIKOV, B. N. LEDENEV, V. I. ZHUCHIKHIN and M. I. BRAZHNIK

Submitted to JETP editor December 28, 1957

J. Exptl. Theoret. Phys. (U.S.S.R.) **34**, 874-885 (April, 1958)

Two methods for measurement of the dynamic compressibility of solids are described which are based on determination of the kinematic parameters of shock waves, — their velocity of propagation and the mass velocity of the substance behind the front. The adiabates of shock compression of iron possessing various initial densities were determined by these methods in the pressure range from 4×10^5 to 5×10^6 atm. The compressibility curve of iron at absolute zero is derived from the experimental data. The curve is extrapolated to pressures at which statistical atomic models are valid.

INTRODUCTION

THE investigations of the equations of state of elements and compounds at high pressures are of great interest for various branches of experimental and theoretical physics, geophysics, cosmogony and a number of related disciplines.

Until recently, the only experimental method for the high-pressure region was the static measurement of compressibility using piezometers of various designs. Bridgman's well-known work[1-3] covered the range of pressures up to 100,000 atm. At still higher pressures the piezometer vessels were deformed so that exact measurements could not be obtained.

In an entirely different manner, which does not involve the use of mechanical pressure or special piezometers, conditions of high hydrostatic pressure are created for short time intervals behind the front of a strong shock wave. This method can be used to produce pressures of hundreds of thousands and millions of atmospheres, which are unattainable by static methods. The laws of mass and momentum conservation relate pressure and density in a shock compression to the kinematic parameters of the shock wave through two equations:

$$\sigma_1 = v_0 / v_1 = D / (D - U_1), \qquad (1a)$$

$$P_1 = U_1 D / v_0, \qquad (1b)$$

where D is the velocity of propagation of the shock wave, U_1 is the mass (or particle) velocity of the material, v_1 is the specific volume behind the shock front, v_0 is the initial specific volume, σ_1 is the relative compression and P_1 is the pressure of the shock compression. It is assumed that ahead of the front the pressure is zero and the medium is at rest.

By means of Eqs. (1a) and (1b), the problem of determining pressures and densities $p_1 = 1/v_1$ reduces to experimentally feasible measurements of the wave and mass velocities of shock waves.

We now consider the conservation of energy. The total amount of work done on a unit of mass by a passing shock front is represented in Fig. 1 by the area of the rectangle with the sides P_1 and $v_0 - v_1$. According to Eqs. (1a) and (1b), half of

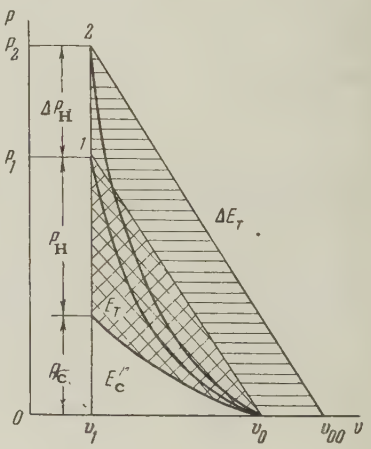

FIG. 1. P – v diagram of shock compressibility.

this work is transformed into kinetic energy, while the remainder increases the specific internal energy by the amount

$$E(P_1;\ v_1) = {}^1/_2 P_1 (v_0 - v_1). \qquad (2)$$

Equation (2) describes the Hugoniot adiabate of the shock compressibility of the medium.

The internal energy acquired through compression is divided into an elastic component E_c represented by the area between the horizontal axis (of volumes) and the curve of P_c, which is the "cold" compressibility at absolute zero, and the thermal energy E_T represented by the area of

the crisscrossed curvilinear triangle. Thus a shock compression is always accompanied by heating of the substance and increase of its entropy, which in turn leads to the appearance of a thermal pressure component P_T. With increasing wave amplitude, the thermal energy and thermal pressure of a shock compression rise progressively.

It is obvious that a single dynamic adiabat does not provide sufficient information for obtaining an equation of state. Ia. B. Zel'dovich has shown that much more complete information regarding the behavior of matter at high pressures can be obtained from two shock adiabats with different initial densities. The shock compression of a porous specimen (of lower density) is associated with large volumetric deformation and a large entropy increase as a result. Thus in the $P-v$ diagram the "porous" shock adiabat is always above the adiabat of the solid material (see Fig. 1). The relative positions of the two adiabates, which correspond to very different degrees of heating, permit the derivation of a semi-empirical equation of state for the test material. Extrapolation leads to the compressibility curve at absolute zero.

The dynamic procedure for the investigation of equations of state was developed by the present authors about ten years ago. The present article describes the principal methods of measuring the dynamic compressibility at high pressures and the results obtained from a study of iron* in the range from 4×10^5 to 5×10^6 atm. One of these methods was independently developed by Mallory,[5] Walsh and Christian,[6] Goranson, Bancroft and others[7,8] in investigations of the compressibility of metals including iron. The range of pressures in these investigations was relatively small and did not exceed a maximum pressure of 4×10^5 atm; the results which are pertinent to the subject of the present article will be mentioned in the section on the equation of state of iron.

1. METHODS OF DETERMINING DYNAMIC COMPRESSIBILITY

The dynamic study of compressibility is based on the experimental determination of wave and mass velocities. Wave velocities are measured relatively simply by contact pins placed in the path of the shock wave. On the other hand, in most cases it is impossible to observe the mass velocity of a substance directly.

We have developed two methods for the complex determination of the kinematic wave parameters, the method of "splitting off" and the method of "deceleration". The first method studies the propagation of a strong discontinuity which appears in an elastic barrier from which a detonation wave is reflected. Figures 2 with the coordinates path and time represents the motion of the shock wave and unloading wave in the barrier plate. The experimentally measurable quantities are the wave velocity D and the velocity of displacement W of the free surface of the plate in the initial portion of its trajectory, which is approximately twice the mass velocity of the material behind the wave front.

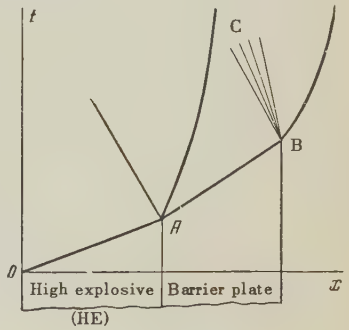

FIG. 2. x – t diagram of the reflection of a detonation wave from an elastic plate. OA detonation wave; AC – shock wave; BC – centered unloading wave.

The velocity W is acquired by the matter of the barrier through two different processes; these are, first, the shock transition from the state $P_0 = 0, v_0$ to the state P_1, v_1 and, secondly, the subsequent isentropic rarefaction in the opposing unloading wave to the state $P_0 = 0,\ v_0' > v_0$.

In the state P_1, v_1, the mass velocity is $U_1 = \sqrt{P_1(v_0 - v_1)}$. The additional velocity acquired through rarefaction to v_0' is

$$U_1' = \int_{v_0'}^{v_1} \sqrt{-dP\,dv}.$$

For very weak shock waves down to sound waves $U_1 = U_1'$ and $W = 2U_1$. In the general case $U_1' \neq U_1$, which with increasing wave amplitude leads to violation of the law of doubled mass velocity. But for a broad class of possible equations of state of solids, with degrees of shock compression $\sigma_1 < 1.4$ the departures from the doubling law are of the order 1 – 2%. Hereinafter for small compressions we shall assume

$$U_1 \approx \frac{1}{2} W. \qquad (3)$$

The same result was obtained in Ref. 6, where the question of violations of the doubling law was regarded under the most general assumptions with respect to the isentropic rarefaction. A special experiment showed that for iron the mass velocity is doubled approximately up to very high shock compressions of 3.5×10^6 atm. The "splitting-off" method is entirely unsuited to the investigation of

*This was actually low-carbon steel with 0.2% carbon.

porous materials, where for weak shock waves U_1' is almost zero.

The "deceleration" method is based on very rigorous premises and can be applied to any materials at pressures and densities as high as desired. In the "deceleration" method a smoothly accelerated "shock driver" strikes a "target" at rest inducing two shock waves which are propagated in opposite directions from the collision surface (Fig. 3). The measurable parameters

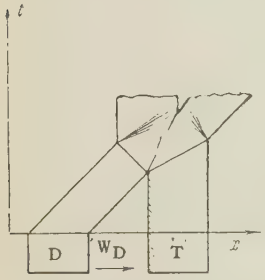

FIG. 3. x – t diagram of shock deceleration. T is the target; D is the shock driver; 1 is the region of shock compression

are the velocity W_H of the driver and the velocity D_T of the shock wave in the "target". In shock compression region 1 on both sides of the driver-target interface equality of velocities and equality of pressures are always established. The first of these equalities follows directly from the continuity of the medium, while the second follows from the law of the equality of action and reaction.

U_1 denotes the velocity of progressive motion of the boundary, which coincides with the jump of mass velocity at the front of the shock wave passing through the "target". The velocity jump at the front of the wave propagating through the driver is $W_D - U_1$. When the driver and target are made of the same material, $W_D - U_1 = U_1$ and thus

$$U_1 = \frac{1}{2} W_D, \qquad (4)$$

The other parameters of the shock wave in the target are obtained by substituting U_1 and D_T into the conservation equations (1). Measurements at different velocities of the shock-producing body determine a number of points on the dynamic adiabat of the tested material and thus on the whole determine the dynamic adiabat of the target and driver material.

Equation (4) superficially resembles Eq. (3). But in the splitting-off method the velocity of the barrier is acquired through two essentially different processes, the shock compression and the subsequent isentropic rarefaction, which furnish approximately identical velocities only for relatively weak shock waves. In the deceleration method, the double reduction of velocity through shock deceleration is exact for velocities of any magnitude and at any pressures and temperatures of shock compression.

When different solids collide, there is no equality of the velocity jumps in the target and driver. This difficulty is easily overcome if the driver is made of a material with a previously determined dynamic adiabat which furnishes a function relationship between shock compression pressure and the velocity jump $W_D - U_1$. In the pressure – velocity diagram (Fig. 4), the dynamic adiabat of

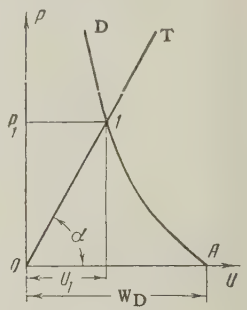

FIG. 4. P – U diagram of shock deceleration. AD is the adiabat of driver deceleration; OT is the wave line of the target; 1 is the state of shock compression.

deceleration of the driver material is represented by a curve whose distance from the coordinate origin is W_D. Measurement of the wave velocity D_T in the target determines the position of the wave line OT of possible shock compression states of the target material, satisfying the equation $P_T = \rho_{OT} D_T U$ (ρ_{OT} is the initial density of the target material). In actuality, state 1 is realized for equal pressures and velocities of the driver and target on both sides of the interface. This state lies at the intersection of the driver adiabat and the target wave line. The intersection coordinates determine the pressure and mass velocity, and also through Eq. (1a) the shock compression density of the target material.

2. METHOD OF INVESTIGATION AND EXPERIMENTAL TECHNIQUE

Measurements of the wave and mass velocities by the splitting-off method were obtained in a series of 6 to 7 experiments which were designed to induce shock waves of identical amplitude in the barriers. Some of the experimental work was de-

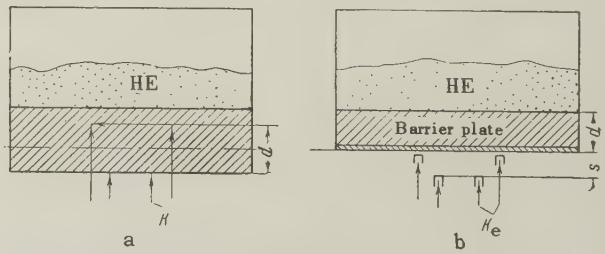

FIG. 5. Scheme of measurements: a – wave velocity; b – splitting-off velocity in the barrier plate. K – electrical contactors; K_e – electrical contactors with protective caps.

signed to determine the wave velocity according to the scheme of Fig. 5a, and the remainder to determine the velocity of the free boundary according to the scheme of Fig. 5b. The wave measurements are performed by means of two groups of electrical pickups K which are acted upon successively by the shock front. The distance between the "upper" and "lower" pickups provides the measuring base distance d, which is usually 5 to 8 mm.

With varying velocity of propagation of shock waves, the recording of time intervals furnishes average velocities for the experimental distance; these agree very accurately with the instantaneous shock velocities at the middle of the base distance. Mass velocities behind the shock front must also be measured at the same distance from the explosive. Figure 5 shows that the latter measurements obtained with thinner barriers whose free surfaces are separated from the HE boundary by the same distance as the center of the base distance in the wave measurements.

The velocity of barrier plate motion is not constant (Fig. 2). This is due to the fact that when the detonation wave is reflected at the boundary between the explosive HE and the plate, the pressure and velocity regime which is established decays with time. For a very strong barrier which remains continuous during the initial period of motion the trajectory of the free surface reproduces accurately to within the doubling coefficient and a certain time shift the velocity decay at the detonation interface.

The pattern of motion is complicated by the presence of disruptive stresses in the region occupied by the unloading wave; these stresses are zero on the free surface and have their maximum value at the boundary of the unloaded zone. The magnitude of the stresses increases as the unloading wave moves farther into the barrier. At a certain distance from the surface the tensile stresses reach the limit of dynamic breaking strength; this leads to the formation of a crack and the splitting off of a thin plate. For matter with vanishingly small strength, the split-off plate is very thin. Under such conditions it can be assumed that its velocity coincides with the free surface velocity at the instant when the shock wave reaches it. For the majority of materials, correct values of the initial velocity can be obtained in barriers with a generated surface of separation between the main plate and a split-off plate a few tenths of a millimeter thick (Fig. 5b). Such plates, which separate freely from the main plate, determine our required maximum mass velocity on the shock front as it reaches the free surface.

In order to obtain undistorted results, the measuring units must be placed close to the explosive axis in a region which is not touched by unloading waves from the lateral surfaces of the explosive charge or the specimen.

Certain limitations are placed on the ratio between the thickness d of the barrier and the distance s which is the base for measurement of the surface velocity (Fig. 5b). During a measurement, the unloading wave after reflection from the boundary between the barrier and explosive products must not again reach the free surface. This condition will be fulfilled if

$$s/W \leqslant 2d/D. \tag{5}$$

In Eq. (5) it is assumed that the velocity of the unloading wave in the barrier is approximately equal to the velocity D of the transmitted shock wave.

In investigations of relatively strong shock waves, which communicate velocities of a few kilometers per second to the free surface, the electrical pickups K outside the barrier must be covered with special protecting caps that are separated from the contact points by a few tenths of a millimeter. These are required to prevent premature shorting of the electrical contacts by the air shock wave which moves ahead of the barrier plate.

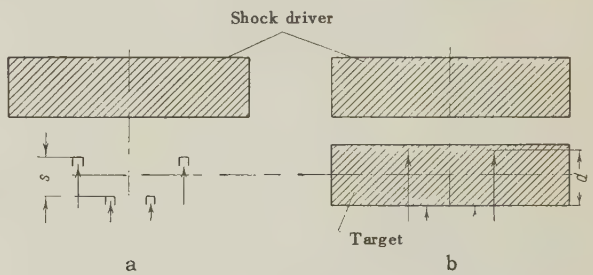

FIG. 6. Arrangement for measurement of wave and mass velocities by the deceleration: a—of the shock driver; b—of the shock wave in the target.

Figure 6 shows the arrangements for determining the velocity of the shock driver and of the wave in the target by the deceleration method. Each of these quantities is determined in an independent series of experiments. With varying, increasing velocity of the driver the wave velocities in the target material and the driver velocities must be measured at an identical point of the trajectory, which is the middle of the measuring base.

Rigorously related values of W_D and D_T could be obtained only if the measuring base were made infinitely small, with the target surface at the midpoint s, and if wave velocities were meas-

ured directly on the surface. This is, of course, impossible. For a finite measuring base distance as shown in Fig. 6b. The motion of the shock driver from the target surface to the center of the base is replaced in wave measurements by the motion of the shock wave in the target. Since the velocity of the driver moving through air and the mass velocity in the shock wave moving through the target do not have identical relative increments, small corrections are made to the measured values of the wave velocities not exceeding one percent of the value of D_T. As in the splitting-off method, during measurements of W_D the electrical contactors must be shielded.

In all of the experiments for the determination of wave and mass velocities, time intervals were measured by means of cathode ray oscilloscopes with high sweep velocity; signals from the contactors were fed to the deflecting plates. Figure 7 is a typical oscillogram as recorded with a twin-beam oscilloscope using a method devised by N. N. Lebedev, E. A. Etingof and M. S. Tarasov. The first

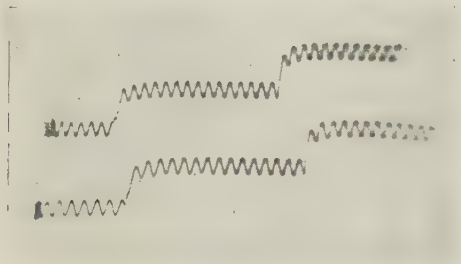

FIG. 7. Oscillogram recording time interval between electrical contacts.

step upward of the traces fixes the time of closing of the upper contacts; the second step upward does the same for the lower contacts. A sine wave with a period of 10^{-7} sec was applied to each beam. Time intervals were recorded with an accuracy of $\pm 5 \times 10^{-9}$ sec.

We can now estimate the accuracy of determination of the dynamic compressibility. Differentiating Eqs. (1a) and (1b) with respect to D and U, and assuming the relative errors of the wave and mass velocities to be independent of each other, we obtain the following expressions for the root mean square relative errors of P and σ:

$$\frac{\Delta P}{P} = \pm\left(\sqrt{\left(\frac{\Delta U}{U}\right)^2 + \left(\frac{\Delta D}{D}\right)^2}\right), \tag{6}$$

$$\frac{\Delta \sigma}{\sigma} = \pm(\sigma - 1)\sqrt{\left(\frac{\Delta U}{U}\right)^2 + \left(\frac{\Delta D}{D}\right)^2} \tag{7}$$

Every value of D and U was obtained by averaging data from 3 to 4 experiments, in each of which the measurements were repeated a few times. The relative error is ± 0.01. When this value of $\Delta U/U$ and of $\Delta D/D$ is substituted in (6) and (7) we find that the density spread at $\rho =$ 1.5 and $2.0\rho_0$ is ± 0.01 and $\pm 0.03\rho_0$, respectively. Pressures were measured with 1.5 — 2% accuracy.

3. DYNAMIC ADIABATE OF IRON

Up to pressure of 1.5×10^6 atm, the dynamic adiabate of iron was obtained by both the splitting-off method and the deceleration method. From 1.5×10^6 to 5×10^6 atm, only the deceleration method was used. Table I contains the parameters of all the experimentally determined points of the shock adiabate of iron. The points are numbered and the methods of measurement are indicated in the first and second column, respectively. The kinematic characteristics of the shock waves are then given: wave and mass velocities in km/sec, pressures in bars, relative shock compressions $\sigma = v_0/v$ and densities in g/cm^3. The initial density of the low-carbon steel specimens was 7.85 g/cm^3. The highest mass velocity U = 5.17 km/sec corresponds to shock wave velocity D = 1200 km/sec, iron density $\rho = 13.79$ g/cm^3 and pressure $P = 4.87 \times 10^{12}$ bars.

In the entire investigated velocity range from

TABLE I

No. of point	Method of measurement	D, km/sec	U, km/sec	$P \times 10^{12}$ bars	$\sigma = v_0/v_1$	ρ, g/cm^3
1	Splitting-off	5.30	0.97	0.40	1.224	9.61
2	"	5.38	1.00	0.422	1.228	9.64
3	Deceleration	5.54	1.14	0.50	1.259	9.88
4	Splitting-off	7.27	2.26	1.29	1.451	11.39
5	"	7.54	2.38	1.41	1.461	11.47
6	Deceleration	8.89	3.25	2.27	1.576	12.37
7	"	9.36	3.56	2.62	1.614	12.67
8	"	9.98	3.83	3.00	1.623	12.74
9	"	10.45	4.20	3.44	1.672	13.13
10	"	10.67	4.32	3.62	1.680	13.19
11	"	11.10	4.59	4.00	1.705	13.38
12	"	11.32	4.83	4.29	1.744	13.69
13	"	12.00	5.17	4.87	1.757	13.79

U = 1.0 to U = 5.17 km/sec the velocities are related linearly:

$$D = 3.80 + 1.58\,U. \qquad (8)$$

The functional relations between D and U, including the form $D = C_0' + \lambda U$, completely determine dynamic adiabates. For the coordinates pressure and velocity Eq. (8) leads to

$$P = \rho_0 (C_0' + \lambda U)\, U.$$

With pressure and the specific volume as coordinates, the linear relation between D and U corresponds to the equation of the adiabates:

$$P = \frac{C_0'^2 (v_0 - v)}{(\lambda - 1)^2 v^2 [(\lambda / \lambda - 1) - (v_0 / v)]^2}, \qquad (9)$$

which is valid for iron from 3×10^5 to 5×10^6 atm.

Figure 8 shows the adiabate of iron in the coordinates P and $\sigma = v_0/v$. It must be mentioned that the parameter C_0' in (9) is an adjusting constant and is not at all related to the actual velocity of propagation of weak acoustic waves.

All of the data refer to the compression of specimens of normal density. Two series of experiments were performed with specimens of reduced density. The results of the latter, which were obtained by the deceleration method, are given in Table II, which also contains for comparison the greatly reduced values of P and E that were obtained through a shock compression to the same densities of solid iron. The dimensionless parameters γ and h are also given; these will be discussed below.

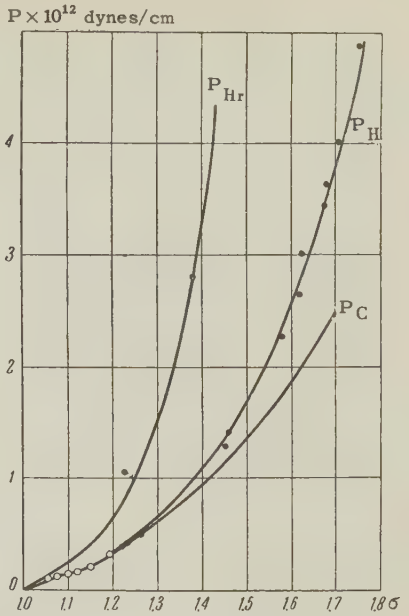

FIG. 8. Shock adiabats and cold compressibility curve of iron. P_H – shock adiabat of iron at normal density; P_{Hr} – shock adiabat of iron at reduced density with $v_{00} = 1.412\, v_0$; PC – isotherm of iron at T = 0°; ● – experimental points; o – data of Goranson, Bancroft et al.[7,8]

TABLE II

ρ_0, g/cm³	v_0, cm³/g	D, km/sec	U, km/sec	v, cm³/g	P, 10^{12} bars	E, 10^{10} erg/g	γ	h
5.52	0.181	6.69	2.82	0.104	1.05	4.04	1.95	2.11
7.85	0.127	—	—	0.104	0.40	0.466		
5.57	0.181	10.17	4.95	0.0923	2.80*	12.14	1.6	2.25
7.85	0.127	—	—	0.0923	1.00*	1.75		

*Calculated using Eq. (9).

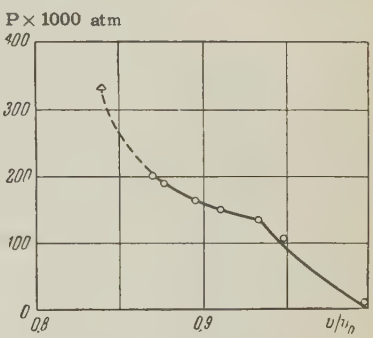

FIG. 9. Compressibility of iron up to 300,000 atm △ – data from Ref. 7; o – data from Ref. 8.

4. COMPRESSION OF IRON AT ABSOLUTE ZERO

There is undoubted interest in the transition from shock compressions where an important part is played by the thermal components of the pressures to the relation $P_c(v)$ at absolute zero.

Goranson and Bancroft and their collaborators[7,8] have studied the compressibility of iron below 300,000 atm. Of special interest are the results of Bancroft et al.,[8] who at 132,000 atm discovered a phase transition accompanied by a kink in the compressibility curve (Fig. 9). Since the thermal components of the pressures are still small at this pressure, the data obtained in Refs. 7 and 8 can be used directly for the purely cold compression relation $P_c(v)$. By treating the curve of Fig. 9 as P_c, we obtain the cold compression energy E_c through a volume integration of this curve. The values of E_c and P_c for $P < 0.3 \times 10^6$ atm are given at the beginning of Table III.

We now turn to the deduction of the equation of state of iron, which we need for the cold compres-

TABLE III

v_0/v	$E_c \cdot 10^{10}$, erg/g	$P_c \cdot 10^{12}$, bars	$P_H \cdot 10^{12}$, bars
1.07	0.0525	0.132*	
1.15	0.181	0.200*	
1.19	0.30	0.332**	
1.25	0.585	0.463	0.484
1.30	0.86	0.600	0.645
1.35	1.18	0.761	0.840
1.40	1.57	0.942	1.07
1.45	1.97	1.154	1.36
1.50	2.42	1.358	1.67
1.55	2.94	1.613	2.08
1.60	3.51	1.880	2.55
1.65	4.12	2.174	3.13
1.70	4.79	2.484	3.82
1.75	5.54	2.822	4.66

*From Ref. 8.
**From Ref. 7.

sibility at high shock compression densities, where the dynamic adiabate differs considerably from the isotherm at absolute zero. Here and hereinafter, we shall not distinguish between isotherms at room temperature and at absolute zero.

We shall write the equation of state and an expression for the internal energy in the form

$$P = -\partial E_c/\partial v + BT/v; \tag{10}$$

$$E = E_c + C_v T. \tag{11}$$

Here $-\partial E_c/\partial v = P_c$ is the compression pressure at $T = 0°K$, B is the thermal pressure coefficient, C_V is the specific heat at constant volume. In general, B and C_V can depend on temperature and density.

When temperature is eliminated we obtain the well-known caloric equation of state[9-10]

$$P + \frac{\partial E_c}{\partial v} = \gamma \frac{E - E_c}{v}. \tag{12}$$

The left member of (12) is the thermal component of the pressure and the ratio $(E - E_c)/v$ in the right member is the volumetric density of thermal energy.

The Grüneisen coefficient $\gamma = B/C_V$ gives the ratio of the thermal pressure to the thermal energy density. We shall consider this quantity to be a constant which like the unknown function $E_c(v)$ must be obtained from experiment. For this purpose, substituting in (12) the expression for E given by the Hugoniot equation (2), we obtain the differential equation

$$v \frac{\partial E_c}{\partial v} + \gamma E_c = -\gamma \frac{P_H(v)\, v}{2}\left(1 + \frac{2}{\gamma} - \frac{v_0}{v}\right). \tag{13}$$

When $v_1 = v_0$, $E_c = \partial E_c/\partial v = 0$. In (13) $P_H(v)$ is the experimental equation of the shock adiabate. The solution of (13) is given by

$$E_c = \frac{1}{(h-1)\, v^{2/(h-1)}} \int_{v_0}^{v} P_H(x)\left(\frac{v_0}{x} - h\right) x^{2/(h-1)}\, dx, \tag{14}$$

$$P_c = -\frac{\partial E_c}{\partial v} = \frac{2}{(h-1)^2 v^{(h+1)/(h-1)}} \times \int_{v}^{v_0} P_H(x)\left(\frac{v_0}{x} - h\right) x^{2/(h-1)} dx - \frac{1}{h-1} P_H(v)\left(\frac{v_0}{v} - h\right). \tag{14a}$$

In (14) $h = (2/\gamma) + 1$ is the so-called maximum density of shock compression.

At pressures from 3×10^5 to 5×10^6 atm, $P_H(v)$ for iron is given by (9). We shall be committing only a very small error if, when calculating E_c in the region $P > 3 \times 10^5$ kg/cm^2, we consider (9) to apply also to the initial portion of the dynamic adiabate.

In order to determine γ and thus h, we shall compare two states 1 and 2 representing the shock compression of solid and of porous iron, respectively, to the same specific volume v_1 (Fig. 1). Since both states have the same energy E_c, which depends only on the volume, the pressure difference $\Delta P = P_2 - P_1 = \Delta P_T$ is accounted for by the thermal energy difference $\Delta E = E_2 - E_1 = \Delta E_T$. From (2)

$$\Delta E_T = \frac{1}{2}[P_2(v_{00} - v_1) - P_1(v_0 - v_1)]. \tag{15}$$

Here v_{00} is the initial volume of the porous iron and P_2 is the shock compression pressure of the porous iron. The constants γ and h are obtained on the basis of (15) from the equations

$$\frac{1}{\gamma} = \frac{\Delta E_T}{v_1 \Delta P_T} = \frac{1}{2}\left[\frac{v_{00}P_2 - v_0 P_1}{(P_2 - P_1)v_1} - 1\right]; \tag{16}$$

$$h = \frac{(v_{00}/v_0)\, P_2 - P_1}{P_2 - P_1}\left(\frac{v_0}{v_1}\right). \tag{16a}$$

The available experimental data on the dynamic compressibility of porous iron (in Table II) permit us to obtain γ and h for two degrees of shock compression. The values of these parameters are given in the last two columns of Table II. For the transition from the dynamic adiabate to the isotherm $T = 0$, h is more important at high compressions, that is, in the region where the thermal components of the pressures are relatively large. In subsequent calculations, we shall assume $h = 2.25$.

The values of the cold compression energy E_c and of the pressure $P_c = -\partial E_c/\partial v$ calculated from (14) are given in Table III for pressures from 0.3 to 5 million atmospheres. Also given are the pressures $P_H(v_0/v)$ of the shock adiabate for the compression of iron of normal density, which were calculated from the interpolation formula (9).

Knowing the function E_c and its derivative, we

can now write an expression for the adiabate of shock compression from a state with the initial volume $v_{00} \geq v_0$. Solving (13) with respect to P_H, we obtain

$$P_H(v_{00};\ v) = -\frac{(h-1)\,\partial E_c/\partial v + 2E_x/v}{h - v_{00}/v} = \frac{(h-1)\,P_c - 2E_c/v}{h - v_{00}/v}. \qquad (17)$$

The curve P_c of cold compressibility, the experimental adiabate of solid iron (9) and the adiabate of porous iron with initial volume $v_{00} = 1.412\,v_0$ are compared in P — v diagrams (Fig. 8). Thermal pressure plays a strikingly large part, especially in the shock compression of porous iron.

We note in conclusion that the equation of state (12) and the expressions that have been found for γ and E_c are valid in the region bounded by the curve for cold compressibility P_c and the shock adiabate of porous iron.

5. EXTRAPOLATION OF THE COMPRESSIBILITY CURVE OF IRON

The compressibility of matter at absolute zero can be studied by quantum statistical methods. However, the Thomas-Fermi and Thomas-Fermi-Dirac statistical models of the atom hold true only at very high pressures of hundreds of millions of atmospheres, when the electronic shells of the atoms are pressed together and lose their individual structure.[11]

At relatively low compression up to 2 or $3\rho_0$ statistical methods yield highly exaggerated values of the pressures. Figure 10 is a logarithmic plot for iron of density-pressure curves which were computed by the Thomas-Fermi method[11] and by the Thomas-Fermi-Dirac method,[11] with an exchange correction. According to Kompaneets and Pavlovskii,[13] the Thomas-Fermi-Dirac results are correct when the exchange correction is small, which undoubtedly occurs for compression close to $\rho = 8 - 10\rho_0$. The lower branch of the compressibility curve up to $\rho = 1.7\rho_0$ has been obtained experimentally by the present authors.

From a knowledge of the upper and lower portions of the function $P_c(\rho)$ we are able to interpolate it satisfactorily for the intermediate region from $\rho = 1.7\rho_0$ to $\rho = 8\rho_0$ (see the dashed line in Fig. 10). The same graph shows Jensen's interpolation,[14] which lies considerably above both the curve for P_c and the dynamic adiabate. The error in Jensen's curve resulted from the lack of experimental information on the compressibility of iron at pressures of several million atmospheres.

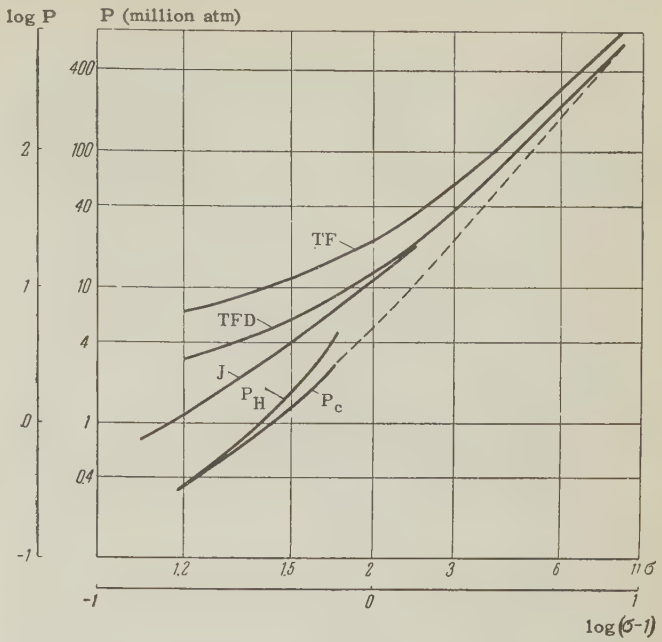

FIG. 10. Extrapolation of the compressibility curve at T = 0°K. TF was computed with the Thomas-Fermi model; TFD was computed with the Thomas-Fermi-Dirac model; P_c is an experimental portion of the isotherm T = 0; J is the isotherm T = 0 according to Jensen; P_H is the experimental dynamic adiabat. The dashed line is the extrapolated portion of the isotherm T = 0.

CONCLUSION

Dynamic methods of investigating compressibility greatly broaden the experimental possibilities in high pressure physics. Our deceleration method is especially promising since it enables us to perform measurements up to a few million atmospheres of pressure. We were thus able to determine the dynamic adiabate of iron with different initial densities from 4×10^5 to 5×10^6 atm.

The dynamic adiabate of porous iron with its reduced initial density lies considerably higher than the adiabate of the solid material in the pressure-density diagram. This is evidence of the large part played by the thermal components of the pressure in shock compression.

On the basis of our experimental findings, we have derived an empirical equation of state for iron and have obtained the cold compressibility curve up to densities $\rho = 1.7\,\rho_0$. The isotherm at T = 0° has been extrapolated to pressures at which quantum statistical methods of computation are applicable.

The present work was undertaken at the suggestion of Ia. B. Zel'dovich. In methodological and instrumental matters the authors were constantly assisted by V. A. Tsukerman and his co-workers E. A. Etingof, N. N. Lebedev and M. S. Tarasov.

The successful conduct of the investigation was greatly assisted by advice and active participation in discussions on the part of E. I. Zababakhin, S. B. Kormer, E. A. Negin and G. I. Gandel'man. In the initial stages some very valuable experimental information was obtained by D. M. Tarasov and A. A. Bakanova. The numerous complicated experiments were performed with the aid of the technicians A. A. Zhiriakov, S. P. Pokrovskii and A. N. Kolesnikova. The authors are extremely gratetul to all of these colleagues.

[1] P. W. Bridgman, The Physics of High Pressure (London, 1931) ONTI, 1936.

[2] P. W. Bridgman, Recent Work in the Field of High Pressures, Revs. Modern Phys. **18**, 1 (1946), Russ. Transl. IIL, 1948.

[3] P. W. Bridgman, Proc. Am. Acad. Arts. Sci. **76**, 3, 55 (1948).

[4] L. D. Landau and E. M. Lifshitz, Механика сплошных сред (The Mechanics of Continuous Media), GITTL, 1953.

[5] H. D. Mallory, J. Appl. Phys. **26**, 555 (1955).

[6] M. Walsh and R. H. Christian, Phys. Rev. **97**, 1544 (1955).

[7] W. Goranson, D. Bancroft et al., J. Appl. Phys. **26**, 1472 (1955).

[8] Bancroft, Peterson and Minshall, J. Appl. Phys. **27**, 291 (1956).

[9] E. Grüneisen, Handbuch der Physik, 1926, Vol. 10, pp. 1-59.

[10] Ia. I. Frenkel', Статистическая физика (Statistical Physics), Acad. Sci. USSR Press, 1948.

[11] P. Gombas, Die statistische Theorie des Atoms und ihre Anwendungen (Wien, 1949).

[12] N. Metropolis and J. R. Reitz, J. Chem. Phys. **19**, 555 (1951).

[13] A. S. Kompneets and E. S. Pavlovskii, J. Exptl. Theoret. Phys. (U.S.S.R.) **31**, 427 (1956); Soviet Phys. JETP **4**, 328 (1957).

[14] H. Jensen, Z. Physik **111**, 373 (1938).

Translated by I. Emin
176

SOVIET PHYSICS JETP VOLUME 34 (7), NUMBER 4 OCTOBER, 1958

DYNAMIC COMPRESSIBILITY OF METALS UNDER PRESSURES FROM 400,000 TO 4,000,000 ATMOSPHERES

L. V. AL'TSHULER, K. K. KRUPNIKOV and M. I. BRAZHNIK

Submitted to JETP editor December 28, 1957

J. Exptl. Theoret. Phys. (U.S.S.R.) **34**, 886-893 (April, 1958)

A method for the determination of pressures and densities of shock compressions is proposed which is based on the measurement of the velocities of propagation of strong shock waves. The dynamic compressibility of copper, zinc, silver, cadmium, tin, gold, lead and bismuth were measured by this method in the pressure range from 400,000 to 4,000,000 atm. The highest degrees of compression (by factors 2.26 and 2.28) were observed in lead and bismuth, which possess the largest atomic volumes. The highest absolute density (32.7 g/cm^3) was recorded for gold.

INTRODUCTION

DYNAMIC methods of investigation in high pressure physics are based on the compression of matter by means of strong shock waves. Experimentally measurable parameters of shock waves are D, the velocity of propagation of a wave front in an undisturbed medium, and U, the velocity of matter behind the wave front. Having determined these parameters, from mass and momentum conservation we obtain the density

$$\rho = \rho_0 D / (D - U) \quad (1)$$

and the pressure of a shock compression

$$P = \rho_0 U D. \quad (2)$$

For the complex determination of shock wave parameters we[1] have developed two methods of in-

vestigation, the "splitting-off" method and the "deceleration" method.

In the "splitting-off" method measurements are obtained of the velocity of a shock wave in an obstacle and of the velocity W of the free surface of the obstacle after the shock wave passes through it. W is approximately twice the velocity of matter behind the wave front. The "deceleration" method, which involves very exact initial premises, is based on the recording of the velocity of a "shock driver" and of the shock wave velocity in the target following the shock. These methods were used[1] to obtain shock compression curves for iron of varying initial density. On the basis of the experimental findings, an equation of state of iron was derived which is valid under pressures of hundreds of thousands or millions of atmospheres.

Knowledge of the shock adiabat of any one material such as iron greatly simplifies measurements of the dynamic compressibility of any other materials. As will be shown below, to obtain points of shock adiabats it is now sufficient to record a single parameter, the velocity of propagation of the shock wave. Measurements of mass velocities, which are considerably more complicated from an experimental point of view, become unnecessary. This method, which was developed by the present authors in collaboration with G. M. Gandel'man, is used to study the decay of a strong discontinuity when a shock wave is reflected from the boundary between two media. This will be designated briefly as the "reflection" method.

The present paper describes the essentials of the method and gives the results obtained for the dynamic compressibilities of copper, zinc, cadmium, tin, silver, gold, lead and bismuth under pressures from 400,000 to 4,000,000 atmospheres.

For each of these substances, the knowledge of only one dynamic adiabat is insufficient to establish the equation of state which relates pressure, temperature and density. Nevertheless, information regarding shock compressibility under pressures of hundreds of thousands and millions of atmospheres is very valuable for the testing of theoretical ideas concerning the behavior of matter under these conditions. Such information also provides a necessary link in the chain of experimental studies which lead to the establishment of empirical equations of state at high pressures.

EXPERIMENTAL METHOD

We shall consider the passage of a shock wave of known amplitude from medium A with a known equation of state into the investigated substance B (see the path-time diagram in Fig. 1). Reflection

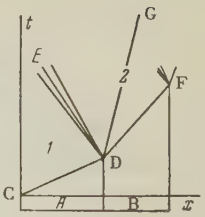

FIG. 1. x – t diagram of the reflection method. CD is the shock wave in medium A; DF is the shock wave in medium B; DE is the reflected wave in medium A; DG is the trajectory of the boundary.

of the shock wave from the interface is accompanied by decay of the discontinuity and the formation of both a transmitted and a reflected wave. The transmitted wave is always a shock compression wave. The reflected wave can be a compression wave if the dynamic rigidity of medium B is greater than the dynamic rigidity of medium A, or it is a rarefaction wave in the opposite case.

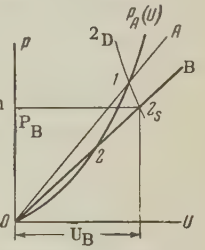

FIG. 2. P – U diagram of the reflection method. $P_A(U)$ is the shock adiabat of medium A; OA is the wave line of medium A; OB is the wave line of medium B; $1-2_s$ is the isentropic rarefaction curve from state 1; $1-2_D$ is the deceleration adiabat from state 1.

In the pressure-velocity diagram (Fig. 2), the dynamic adiabat of a single shock compression of medium A is represented by the parabolic curve $P_A(U)$, and the state in medium A before reflection from the interface by point 1 of this adiabat. After reflection, the new state 2 in medium A lies on the isentropic rarefaction curve $1-2_D$ of substance A or on its double compression shock adiabat $1-2_D$. The geometric locus of the possible states in substance B, in which the shock wave is propagated with velocity D_B, is the straight line OB, $P = \rho_0 D_B U_B$, which satisfies conservation equation (2). In Region 2 (Fig. 1) on both sides of the interface, both in the reflected wave in A and in the transmitted wave in B, the pressures and velocities are equal. In the P – U diagram (Fig. 2) this condition is represented by point 2, the intersection of the $2_s - 2_D$ curve with the "wave line" OB of medium B. The coordinates of the point of intersection determine the pressure P_B and the velocity U_B of one of the points of the dynamic adiabat of substance B. The density is found by substituting the values of U_B and D_B in Eq. (1).

For application of the reflection method, it is necessary to have available at least one substance of known dynamic adiabat and known equation of state, which is required for plotting of the rarefaction and deceleration adiabats of the barrier plate. The experimentally measured quantities in the reflection method are the parameters of state 1 and

the wave velocity D_B which determines the slope of OB. For many materials, including iron, the curve $2_s - 2_D$ is very accurately approximated by the mirror image of the basic adiabat P_A. For the investigated substances whose wave lines pass close to point 1, the error resulting from this approximation is vanishingly small.

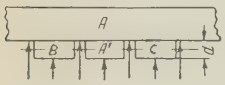

FIG. 3. Measurement of wave velocities by the reflection method. A – iron plate; A' – specimen of iron; B, C – test specimens; d – reference measuring base.

Figure 3 is the schematic drawing of a typical experiment for determining compressibility by the reflection method. A plane shock wave produced by an explosion passes through an iron plate to which samples of iron and of the investigated substances are attached. State 1 in the transmitted wave before reflection is determined in the same experiments as the wave velocities in the test specimens, from the velocity D_{Fe} of the shock wave in the iron specimen. In the pressure-velocity diagram (Fig. 2) D_{Fe} determines the wave line OA, which forms the angle $\alpha = \arctan(\rho_{0Fe} D_{Fe})$ with the horizontal axis. State 1 is given by the point of intersection of OA with the known adiabat $P_A(U)$ of single compression of the iron plate. According to Ref. 1 the equation of the shock adiabat of iron at pressures from 400,000 to 4,000,000 atm is given by the following relation between D and U:

$$D_{Fe} = C_0' + \lambda U, \quad C_0' = 3.8 \text{ km/sec}, \quad \lambda = 1.58. \tag{3}$$

In the coordinates pressure and velocity,

$$P_{Fe} = \rho_{0\,Fe}(C_0' + \lambda U)\, U \cdot 10^{10} \text{ bars} \tag{4}$$

and in the coordinates pressure and relative density,

$$P_{Fe} = \frac{\rho_0 C_0'^2}{(\lambda-1)^2} \frac{\sigma(\sigma-1)}{[\lambda/(\lambda-1)-\sigma]^2} \cdot 10^{10} \text{ bars}. \tag{5}$$

The time required for passage of a shock wave through a test specimen was the difference between the time of shorting of the electrical pickup against the lower surface of the specimen and the average time of shorting of the upper pickups against the iron plate around the specimen. Signals were transmitted to the deflection plates of an oscilloscope with a driven sweep velocity of 50 km/sec. A 10-megacycle sine wave was applied to the oscilloscope beam as a scale. The accuracy of the time intervals was 5×10^{-9} sec. The measuring base, which was equal to the thickness of a specimen, was 6 – 8 mm and the thickness of the iron plate was 6 to 9 mm. The wave velocity was obtained through division of the reference base thickness by the measured time. In order to prevent reduction of the wave velocities by the unloading waves from the edges of the specimens, the specimen diameters were twice their thickness. Specimens were fastened to the plate by pieces of Wood's alloy with the necessary openings for insulated wires. Three specimens (A', B, C in Fig. 3) were used in each trial.

EXPERIMENTAL RESULTS

The dynamic compressibility of the metals was measured in three runs which differed with regard to the shock wave pressure in the iron plate. In the first run the pressures were produced by reflecting a detonation wave from the outer surface of the plate.

In the measurements for zinc, cadmium, lead, bismuth and tin, the plate was 10 mm thick and the specimens were 8 mm thick. Thus the middle of the reference thickness was 14 mm from the first surface. At this distance the velocity of the shock wave in the iron specimens was found to be 5.30 km/sec, corresponding to a pressure of 0.40×10^{12} bars. Measurements on copper, silver and gold were made with a plate of somewhat lesser thickness. Under these conditions at the middle of the reference thickness $D_{Fe} = 5.38$ km/sec and the pressure was 0.42×10^{12} bars.

In the second run the dynamic compressibility of all of the tested metals was determined at a pressure of 1.40×10^{12} bars in the iron plate; in the third run, at 3.60×10^{12} bars. As previously, the characteristics of the shock wave in iron refer to a surface passing through the middle of the reference thickness.

The velocities of propagation of the shock waves are given in Table I, as well as the parameters of the shock waves in the iron plates, the initial densities ρ_0 of the test specimens and the velocities C_0 of the propagation of acoustic waves of volume compression. The latter were calculated by means of the formula $C_0 = 1/\sqrt{\rho_0 \kappa}$, using the initial density of the material and the volume compression coefficient κ taken from Ref. 2.

As was shown in the preceding Section, the data in Table I are sufficient for an unambiguous determination of the pressures and densities of shock compression. Table II contains the corresponding parameters of the shock adiabat points.

The experimental results can be used to determine the shock adiabats by means of Eqs. (1) and (2) with interpolated relations between the wave and mass velocities (Fig. 4). The results of this calculation are given in Table III and are repre-

TABLE I

Metal	Cu	Zn	Ag	Cd	Sn	Au	Pb	Bi	Parameters of shock wave in iron plate			
ρ_0, g/cm³	8.93	7.14	10.49	8.64	7.28	19.30	11.34	9.80				
C_0, km/sec	3.95	2.92	3.08	2.34	2.64	2.98	1.91	1.85	D, km/sec	U, km/sec	P, 10^{12} bars	ρ/ρ_0
I	5.36	—	4.69	—	—	4.27	—	—	5.38	1.00	0.42	1.23
	—	4.70	—	4.10	4.20	—	3.52	3.37	5.30	0.95	0.40	1.23
D, km/sec II	7.13	6.85	6.76	6.32	6.36	5.70	5.33	5.36	7.53	2.36	1.40	1.46
III	10.16	9.90	9.45	9.14	9.02	8.06	7.65	7.94	10.63	4.32	3.60	1.69

TABLE II

Metal	Series I			Series II			Series III		
	ρ/ρ_0	P, 10^{12} bars	U, km/sec	ρ/ρ_0	P, 10^{12} bars	U, km/sec	ρ/ρ_0	P, 10^{12} bars	U, km/sec
Cu	1.21	0.45	0.94	1.47	1.46	2.29	1.70	3.80	4.19
Zn	1.28	0.35	1.04	1.59	1.24	2.54	1.87	3.26	4.61
Ag	1.25	0.46	0.93	1.48	1.55	2.19	1.75	4.01	4.05
Cd	1.33	0.36	1.02	1.63	1.33	2.44	1.94	3.49	4.42
Sn	1.35	0.33	1.08	1.69	1.20	2.59	2.10	3.10	4.73
Au	1.20	0.59	0.71	1.45	1.95	1.78	1.69	5.13	3.30
Pb	1.38	0.39	0.97	1.78	1.41	2.34	2.26	3.70	4.26
Bi	1.45	0.35	1.05	1.86	1.30	2.47	2.28	3.45	4.45

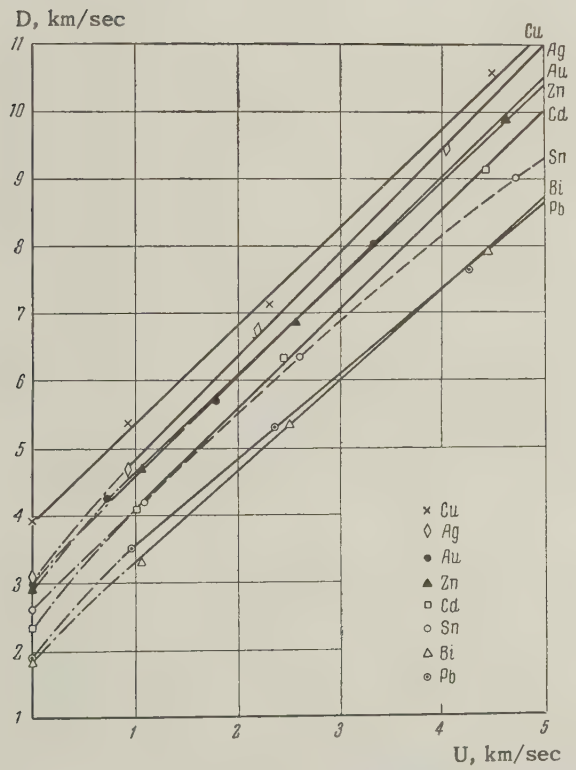

FIG. 4. D – U diagram of the tested metals. The solid lines are portions of curves which are approximately represented by the linear relation $D = C_0' + \lambda U$.

sented graphically in Fig. 5 in the coordinates pressure and relative compression $\sigma = \rho/\rho_0$.

Figure 4 shows that for all of the metals studied except tin the relation between D and U for U > 1 km/sec is approximated with sufficient accuracy by the linear relation $D = C_0' + \lambda U$. The dynamic adiabats can then be represented by Eq. (5). The values of C_0' and λ are given in Table IV. Since the constants C_0' and λ were selected from the requirement of the best possible approximation for the entire investigated velocity range, C_0' differs somewhat from the actual initial sound velocities given in Table I.

We note that at pressures of the order of 400,000 atm the results of the present work agree with the values of the dynamic compressibility of copper and zinc in Ref. 3.

CONCLUSION

Table V gives for zero pressure and 3,500,000 atm the relative compression σ, the gram-atomic volume V_A, the wave velocity D, the mean shock compression modulus $\rho_0 D^2$ and the increment ΔE of internal energy of all of the metals studied including iron.

This table shows a definite relation between the

TABLE III

σ	P, 10^{12} bars							
	Cu	Zn	Ag	Cd	Sn	Au	Pb	Bi
1.1	0.16	0.09	0.12	0.07	0.05	0.25	0.05	—
1.2	0.40	0.21	0.34	0.17	0.14	0.56	0.14	—
1.3	0.71	0.38	0.63	0.32	0.27	1.01	0.26	—
1.4	1.14	0.61	1.04	0.52	0.43	1.63	0.42	0.29
1.5	1.72	0.91	1.61	0.79	0.65	2.45	0.60	0.43
1.6	2.49	1.32	2.40	1.15	0.92	3.57	0.82	0.59
1.7	3.52	1.85	3.51	1.64	1.26	5.06	1.09	0.80
1.8	—	2.57	5.01	2.30	1.65	—	1.40	1.06
1.9	—	—	—	3.22	2.09	—	1.79	1.39
2.0	—	—	—	4.49	2.57	—	2.25	1.80
2.1	—	—	—	—	3.10	—	2.80	2.31
2.2	—	—	—	—	3.77	—	3.46	2.95
2.3	—	—	—	—	—	—	4.26	3.76

degree of compression and the initial atomic volume. Elements with large initial atomic volumes are compressed more strongly that those with smaller atomic volumes. Thus, at 3,500,000 atm the density of bismuth is increased by a factor of 2.28 and that of iron by only 1.67. The ratio of the atomic volumes of these elements, which at atmospheric pressure is 3, reduces to 2.2 at 3,500,000 atm.

TABLE IV

Metal	C_0', km/sec	λ	ρ_0, g/cm³
Cu	3.90	1.46	8.93
Zn	3.20	1.45	7.14
Ag	3.30	1.54	10.49
Cd	2.65	1.48	8.64
Au	3.15	1.47	19.30
Pb	2.30	1.27	11.34
Bi	2.00	1.34	9.80

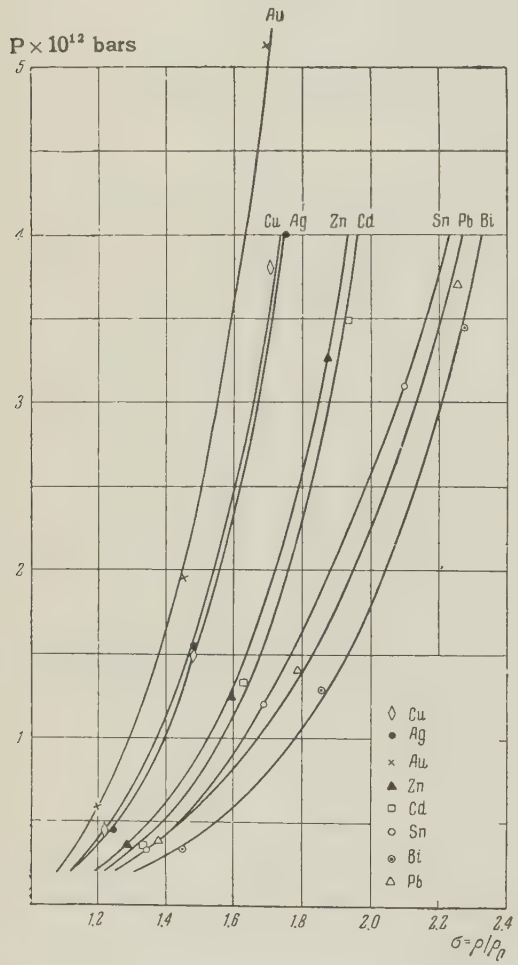

FIG. 5. Dynamic adiabats of copper, zinc, silver, cadmium, tin, gold, lead and bismuth.

With higher pressure there is a many-fold increase in the wave velocity and mean shock compression modulus, which is the ratio of the applied pressure to the relative reduction of volume. The change of the modulus indicates a strong increase in the elasticity of the material with higher densities and temperatures. For copper, the shock wave velocity at 3,500,000 atm exceeds the sound velocity at atmospheric pressure by the factor 2.46, while the modulus $\rho_0 D^2$ increases by about the factor 6. For lead at 3,500,000 atm, the wave velocity increases by the factor 3.93 and the shock compression modulus by the factor 15.

At high pressures there is a large increment of the specific internal energy, which is calculated from the equation

$$E = P(v_0 - v)/2.$$

Thus the internal energy of 1 g of bismuth at 3,500,000 atm exceeds the explosive energy of 1 g of TNT by the factor 2.5. The present paper does not include the question as to what portion of this energy is thermal or the relation between the thermal and elastic pressures.

In conclusion the authors wish to thank the following for their assistance: A. N. Kolesnikova,

TABLE V

Element	σ P = 3.5 × 10^{12} bars	V_A, cm^3/g-atom		D, km/sec		$\rho_0 D^2 \cdot 10^{12}$ bars		$\frac{\Delta E}{10^{10}}$ erg/g
		$P = 0$	$P = 3.5 \cdot 10^{12}$ bars	$P = 0$	$P = 3.5 \cdot 10^{12}$ bars	$P = 0$	$P = 3.5 \cdot 10^{12}$ bars	$P = 3.5 \cdot 10^{12}$ bars
Fe	1.67	7.12	4.26	4.63	10.53	1.68	8.70	9.0
Cu	1.70	7.11	4.18	3.95	9.75	1.39	8.48	8.1
Zn	1.89	9.16	4.84	2.92	10.19	0.61	7.41	11.0
Ag	1.71	10.28	6.01	3.08	8.96	0.99	8.42	6.9
Cd	1.93	13.01	6.72	2.34	9.15	0.47	7.23	10.0
Sn	2.16	16.30	7.54	2.64	9.44	0.51	6.49	13.0
Au	1.59	10.22	6.43	2.98	6.99	1.71	9.43	3.3
Pb	2.21	18.27	8.25	1.91	7.5	0.41	6.38	8.0
Bi	2.27	21.32	9.39	1.85	7.99	0.33	6.25	10.0

S. N. Pokrovskii, A. L. Zhiriakov, M. M. Pavlovskii and V. P. Drakin.

[1] L. V. Al'tshuler, K. K. Krupinkov et al., J. Exptl. Theoret. Phys. (U.S.S.R.) this issue, p. 606.

[2] P. W. Bridgman, The Physics of High Pressure, (London, 1931).

[3] J. M. Walsh and B. H. Christian, Phys. Rev. **97**, 1544 (1955).

Note added in proof (March 10, 1958). The results obtained in the first experimental series also agree with the measurements of the dynamic compression of metals from 150,000 to 400,000 atm [Walsh, Rice, McQueen and Yarger, Phys. Rev. **108**, 196 (1957)], which were brought to the attention of the present authors after this paper was sent to press.

Translated by I. Emin
177

SOVIET PHYSICS JETP VOLUME 34 (7), NUMBER 4 OCTOBER, 1958

EXPERIMENTAL DETERMINATION BY AN OPTICAL METHOD OF THE STRESSES IN AN ANISOTROPIC PLATE UNDER THE ACTION OF A CONCENTRATED FORCE. II

V. M. KRASNOV, A. V. STEPANOV and E. F. SHVEDKO

Leningrad Physico-Technical Institute, Academy of Sciences, U.S.S.R.

Submitted to JETP editor August 8, 1952

J. Exptl. Theoret. Phys. (U.S.S.R.) **34**, 894-898 (April, 1958)

The state of stress in an anisotropic plate made of a 60% TlBr + 40% TlI single crystal of the cubic system was investigated by an optical method. The case of a concentrated force directed along the (110) direction is considered.

1. The present paper is a supplement to Ref. 1, in which an attempt at an optical method of the investigation of stress in anisotropic media was carried out. The theoretical bases of this method was set forth in Ref. 2, while a more detailed methodological instructions were given in Ref. 3. In Ref. 1, the problem of the effect of a concentrated force on an anisotropic plate cut from a single crystal of the alloy TlI + TlBr parallel to the plane of the cube was considered (the crystal belonged to the cubic system). The direction of the force coincided with the direction of the maximum of the modulus E, i.e., with the (100) direction.

According to the method given previously, the stresses at an arbitrary point of an anisotropic plate are determined from the formulas

$$\tan 2\beta = k \tan 2\varphi, \quad (1)$$

$$\tau = C_\beta d (\sigma_1 - \sigma_2), \quad (2)$$

where β is the angle determining the direction of

the semi-axis of the optical ellipsoid and is measured from the (100) direction (the optical parameter of the isocline), φ = the angle defining the direction of the principal normal directions (elastic parameter of the isocline), δ = optical path difference of two rays propagated along the direction of the normal at a given point of the plate considered, $\sigma_1 - \sigma_2$ = difference of the principal normal stresses, k = coefficient equal to the ratio of the two constants A and B which define the photoelastic properties of the material, C_β = a coefficient depending on the angle β. Here, δ and β are quantities which are directly measured by experiment.

These formulas show that in the observation of the stress of an anisotropic plate in polarized light, the optical interference picture (as also the stress distribution) depends on the orientation of the direction of the applied forces relative to the crystallographic axes of the plate. The present research also had the purpose of showing experimentally the difference both in the interference picture and the stress distribution which is produced by a change in the orientation of the plate. Here we consider the same problem as in Ref. 1 — the effect of a concentrated force on the anisotropic plate, except that the direction of the applied force is that of the (110) direction i.e., the direction of the maximum modulus E.

2. The model investigated was prepared from a single crystal of an alloy of 40 mol percent TiBr + 60 mol percent TlI, which belongs to the group of "transparent metals."[4-5] According to Ref. 1, the photoelastic constants of the material of the model are equal to

$$A = +12\cdot10^{-13}\ \text{cm}^2/\text{dyne}, \quad B = -205\cdot10^{-13}\ \text{cm}^2/\text{dyne},$$

and the elastic constants are

$$S_{11} = 37\cdot10^{-13}\,\text{cm}^2/\text{dyne}, \quad S_{44} = 182\cdot10^{-13}\,\text{cm}^2/\text{dyne};$$

$$S_{12} = -11\cdot10^{-3}\ \text{cm}^2/\text{dyne}.$$

FIG. 1. Photograph of a picture of isochromes at a load P = 9.18 kgm.

The model was a rectangular plate of dimensions $40.5 \times 34.0 \times 4.15$ mm. The plate was so cut that its plane coincided, and its side edges made an angle of 45°, with the plane of the cube, i.e., the side edges of the plate run along the (110) direction. Before the measurement, the plate was annealed at a temperature of 190°C to remove the remaining stresses obtained in its processing. For loading the model we made use of a special device, consisting of a stage on which was put a plate and a lever arm, by means of which (making use of a steel cylinder of diameter 2 mm, with its axis located perpendicularly to the plane of the plate) a concentrated pressure was produced on the center of the upper face of the model.

The loading system was put in a polarization apparatus so that rays fell on the model perpendicularly to its surface. Since it was necessary to photograph the entire model and, moreover, to measure the optical path difference δ at separate points of the model, two polarization setups were used: (1) a projection polarization unit (PPU) and (2) a cordinate synchronized polarimeter (KSP) which was prepared in the experimental workshop NIIMM of Leningrad State University. These two units were so set up that it was possible to use them without moving the loading system with the model from one place to another.

The direction of the force coincided with the (110) direction. In this case, it was more suitable to make the measurement of the angles from this direction. Therefore we introduced the angle $\gamma = \beta - 45°$, which changed the fundamental derived formulas to the following form:

$$\tan 2\alpha = k\tan 2\gamma, \tag{1'}$$

$$\delta = C_\gamma d(\sigma_1 - \sigma_2), \tag{2'}$$

where $\alpha = \varphi - 45°$ and C_γ has the value

$$C_\gamma = \frac{AB}{\sqrt{B^2\sin^2 2\gamma + A^2\cos^2 2\gamma}}. \tag{3}$$

The force acting on the model amounted to 4.8 kgm.

3. Figure 1 shows the isochromes obtained on the apparatus PPU for circular polarization and with an interference filter of mean wavelength λ_m = 610 mμ and transmission band width ± 12 mμ. If we compare the given picture of the isochromes with the picture of isochromes given in Fig. 1 of Ref. 1, it is seen how sharply the isochromes are changed in their dependence on the orientation of the plate. Here the pressure is produced in the direction of the largest values of the coefficient

of photoelasticity C_β; there, the direction of the pressure coincided with the direction of the smallest value of C_β.

In addition to the photograph of the isochromes, we carried out measurements of the optical path difference over the horizontal cross section, located at a distance of 5 mm from the upper edge. In the method of measurement of the optical path difference with the aid of a compensator (measurement was carried out on the mica compensator of Krasnov[6]), there enters as a required element the measurement of the angle which determines the position of the plane of polarization of the ray propagated through the plate, i.e., the angle β, or, in our case, the angle γ. Thus, the optical quantities γ and δ were obtained at the points of the particular cross section.

On the basis of Eqs. (1′) and (2′), the quantities φ and $\sigma_1 - \sigma_2$ were calculated according to these data. Consequently, we obtain two quantities φ and $\sigma_1 - \sigma_2$ at any point of the model by the photoelastic method. For the complete solution of the problem, it is also necessary to obtain σ_1 and σ_2 separately. Usually, the method of numerical integration of the equilibrium equation is applied for the separation of the principal normal stresses, making use of data obtained optically. This method is also applied in the case of an anisotropic medium, since the equations of equilibrium are valid for every continuous medium. In this way we would obtain a complete solution of the problem, and for estimates of the roughness of the experiment we compare the data obtained with the theoretical solution. However, in our case, it was desirable to estimate the roughness of the measurement by those quantities which were obtained purely optically. Making use of the same method of numerical integration (which has its own roughness) we could not estimate the accuracy of the photoelastic method. Therefore, for such an estimate we employed a direct comparison of the obtained data with the theoretical data. The theoretical solution of the given problem[7] gives the following results:

(1) the stresses are radial, i.e., the angle α which determines the direction of the principal normal strain, is equal to the central angle θ;

(2) $\sigma_\theta = \sigma_{r\theta} = 0$; $\sigma_r \neq 0$, i.e., that σ_r and σ_θ are the principal normal strains, where $\sigma_r - \sigma_\theta = \sigma_r$;

(3) $\sigma_r r = \text{const}$ for $\theta = \text{const}$, i.e., the strain along the radius changes inversely proportionally to the radius.

These data make it possible to draw the following comparisons.

I. We compare the angle α, computed on the basis of the experimental data, with the angle θ. The data for the comparison are given in the Table, where x is the coordinate of the point measured from the direction of action of the force. The table

x*	θ°	α°
0	—	—
0.5	6	5
1.5	17	19
2.0	22	24
3.0	31	31
4.0	39	36
5.0	45	41
5.5	48	43
5.8	49	45
6.3	52	46
7.0	54	48

*x – coordinate of the point measured from the axis drawn through the direction of action of the force.

shows that there is satisfactory coincidence up to limits of 45°; beyond, there is observed a steadily increasing divergence which can be explained by the finite dimensions of the plate; the radial strains take place in an infinite medium. Detailed comparisons were also carried out on the other cross sections.

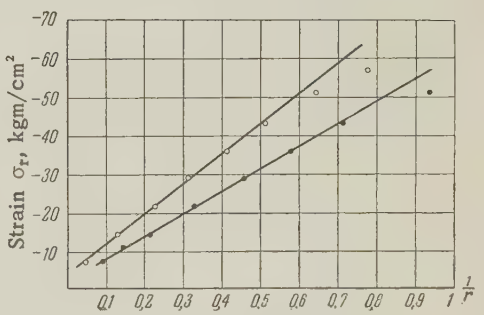

FIG. 2. Dependence of the strain σ_r on the distance for the direction $\varphi = 0$, ○ – P = 8.194, ● – P = 5.784 kgm.

II. Figure 2 shows a graph of the change of $\sigma_1 - \sigma_2$ in dependence on 1/r. The graph shows that the points lie rather well along a straight line, which is also in agreement with theory.

III. Figure 3 shows: (1) a graph of the optical path difference δ, (2) the graph of $\sigma_1 - \sigma_2$, and (3) the graph of σ_2, constructed from theoretical data. All the graphs are given for the cross section h = 5 mm. Taking it into consideration that $\sigma_1 - \sigma_2 = \sigma_r - \sigma_\theta = \sigma_r$, we can state the excellent agreement of theoretical and experimental results.

IV. Figure 4 shows the curve $\sigma_r = \text{const}$, constructed from the theoretical data and the curve $\sigma_1 - \sigma_2 = \text{const}$ drawn from the experimental data, which also agree sufficiently well. On this same

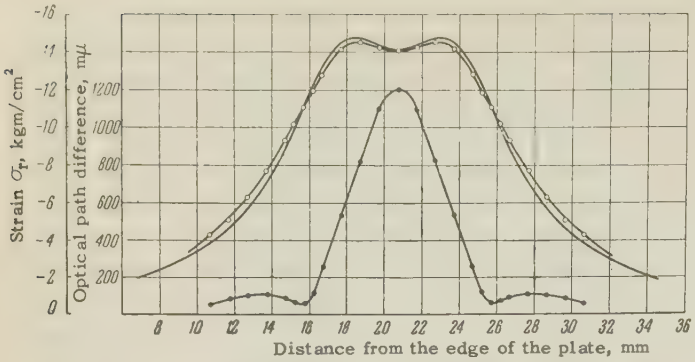

FIG. 3. Distribution of the strain σ_r for the load P = 5.784 kgm at the cross section h = 5 mm; continuous line – theoretical curve, o – experimental results, ● – optical path difference.

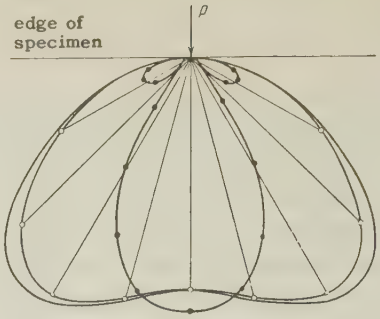

FIG. 4. Curves σ_r = const: continuous line – theoretical curve for σ_r = 16.3 kgm/cm^2 = const; o – experimental values for σ_r = 16.3 kgm/cm^2 = const; ● – isochrome of the first order; P = 5.784 kgm.

curve, there is drawn one of the isochromes which shows clearly that the anisotropy of the photoelastic properties is sharply distinguished from the anisotropy of the elastic properties. In the case of an isotopic body, these curves coincide, as is well known. One must turn one's attention also to the fact that the maximum value of the radial strain σ_2 takes place not on the line of action of the force, but on the two rays located symmetrically relative to this line.

In conclusion, we consider it our pleasant task to thank A. L. Shakh-Budagov for his assistance in carrying out this research.

[1] V. M. Krasnov and A. V. Stephanov, J. Exptl. Theoret. Phys. (U.S.S.R.) **25**, 98 (1953).

[2] V. M. Krasnov. Uch. zap. Leningrad State Univ. No. 13, 97 (1944).

[3] V. M. Krasnov, Dissertation, Leningrad State University, 1953.

[4] A. V. Stepanov, Z. Phys. Sowjetunion **6**, 312 (1934).

[5] A. V. Stepanov, J. Tech. Phys. (U.S.S.R.) **19**, 205 (1949).

[6] V. M. Krasnov, Uc. zap. Leningrad State Univ. No. 8, 108 (1939).

[7] S. G. Lekhnitskii, Теория упругости анизотропного тела (Theory of Elasticity of an Anisotropic Body) GITTL, 1950.

Translated by R. T. Beyer
178

STRANGE-PARTICLE DECAYS IN THE THEORY OF FEYNMAN AND GELL-MANN

I. Iu. KOBZAREV and I. E. TAMM

P. N. Lebedev Physical Institute, Academy of Sciences, U.S.S.R.

Submitted to JETP editor January 16, 1958

J. Exptl. Theoret. Phys. (U.S.S.R.) **34**, 899-901 (April, 1958)

An explanation is given for the equal probabilities of the K_{e3} and $K_{\mu 3}$ decays in the absence of K_{e2} decay, and of the large asymmetry in the decays of polarized hyperons. The assumption used is that of a universal A – V interaction as proposed by Feynman and Gell-Mann.

ONE of the most interesting facts relating to the lepton decays of K mesons is the absence of the decay $K^+ \to e^+ + \nu$ and the presence of the decay $K^+ \to \mu^+ + \nu$, together with the approximately equal probabilities of the decays $K^+ \to \mu^+ + \nu + \pi^0$ and $K^+ \to e^+ + \nu + \pi^0$.

We would like to point out that these facts can be explained in an altogether natural way if one

assumes that all of these decays occur on account of the universal four-fermion interaction proposed by Gell-Mann and Feynman[1] and by Sudarshan and Marshak.[2] If one assumes that such an interaction exists, then the decays $K^+ \to \mu^+ + \nu$ and $K^+ \to e^+ + \nu$ must occur through the conversion of the K meson into a baryon-antibaryon pair and the subsequent conversion of the latter into $e\nu$ or $\mu\nu$, which goes through the weak four-fermion interaction

$$(G/\sqrt{2})\,(\bar{\psi}_N \gamma_\mu (1+\gamma_5)\,\psi_N)\,(\bar{\psi}_\nu \gamma_\mu (1+\gamma_5)\,\psi_e).$$

In its general form, the diagram for such a process can be drawn as in Fig. 1a. Just as in the case

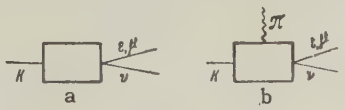

FIG. 1

of the analogous decays of the π meson,[1] the corresponding matrix element has the form

$$F \sim fMG\,(\bar{\psi}_\nu \hat{p}_K (1+\gamma_5)\,\psi_{\mu,e}),$$

where M is the mass of the nucleon and f is a numerical constant which is the same for the μ meson and the electron (in view of the fact that the matrix element for the transition can depend only on p_K).

The corresponding probability w is proportional to $1 + (v_{\mu,e}/c)\cos\vartheta$ where ϑ is the angle between the directions of the momenta of the μ meson (or electron) and the neutrino. For the two-particle decay $\cos\vartheta = -1$, so that the probability is proportional to $1 - v/c$ and is extremely small for the electron case. The ratio of the probabilities of the decays $K \to e + \nu$ and $K \to \mu + \nu$ is given by

$$\frac{K \to e + \nu}{K \to \mu + \nu} \approx \left(\frac{m_e}{m_\mu}\right)^2 \sim 0.25 \cdot 10^{-4}.$$

The situation is decidedly different when a π meson comes off from the baryon loop. The corresponding diagram has the form shown in Fig. 1b. The general form of the corresponding matrix element is

$$F \sim f_1 G\,(\bar{\psi}_\nu \hat{p}_K (1+\gamma_5)\,\psi_{e,\mu}) + f_2 G\,(\bar{\psi}_\nu \hat{p}_\pi (1+\gamma_5)\,\psi_{\mu,e}). \quad (2)$$

Noting that $p_K = p_{e,\mu} + p_\nu + p_\pi$ and using the Dirac equation, we can put Eq. (2) in the form

$$F \sim (f_1 + f_2)\,G\,(\bar{\psi}_\nu \hat{p}_K (1+\gamma_5)\,\psi_{e,\mu}) + f_2 m_{e,\mu} G\,(\bar{\psi}_\nu (1-\gamma_5)\,\psi_{e,\mu}). \quad (3)$$

If we consider the simplest diagrams of the form 1b (see Fig. 2), we find that they lead to logarithmically divergent integrals. If we keep only the logarithmic term, then $f_1 = f_2$, independently of the parity of the K meson.

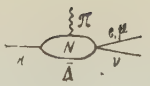

FIG. 2

We shall assume that $f_1 \approx f_2$; then we can neglect the second term in Eq. (3) (which gives for the μ meson an error of the order of 10 percent) and write Eq. (3) in the same form as Eq. (2):

$$F \sim f\,(\bar{\psi}_\nu p_K (1+\gamma_5)\,\psi_{\mu,e}). \quad (4)$$

The probabilities of the decays K_{e3} and $K_{\mu 3}$ are proportional as before to $1 + (v/c)\cos\vartheta$, but since these are three-particle decays, $\cos\theta$ no longer has to be equal to -1. For this reason the forbidden character found for the decay $K \to e + \nu$ is not found for the decay $K \to e + \nu + \pi$, and we get for the ratio of the probabilities

$$\frac{K \to e + \nu + \pi}{K \to \mu + \nu + \pi} \sim 1.$$

This result always holds as to order of magnitude, provided only that $f_1 \neq -f_2$; that precise equality should occur appears improbable. We note that the spectrum of the μ mesons and electrons for the interaction (4) and for other possible types of interaction has been examined by Furiuchi and others;[3] the angular correlations between the momenta of the π meson and electron (which are easily observable in the case of the decay $K^0 \to e^\pm + \nu + \pi^\mp$, which is the analogue of the corresponding K^+ decay) have been obtained by Pais and Treiman.[4]

It must be remarked that the application of analogous considerations to the decays $\pi \to e + \nu$, $\pi \to \mu + \nu$ gives for the ratio of the decay probabilities

$$\frac{\pi \to e + \nu}{\pi \to \mu + \nu} \approx 1.3 \cdot 10^{-4}$$

(see, for example, Ref. 1). The decay $\pi \to e + \nu$ has not been observed. Lattes and Anderson[5] give an upper limit 10^{-5} for this ratio. We believe, however, that the question of the esistence of the decay $\pi \to e + \nu$ calls for further examination.

The question arises as to whether the forbiddenness of the decay $\pi \to e + \nu$ can be removed on account of the emission of a γ-ray quantum in the decay $\pi \to e + \nu + \gamma$, which would give

$$\rho_\gamma = \frac{\pi \to e + \nu + \gamma}{\pi \to \mu + \nu} \sim e^2 \frac{K \to e + \nu + \pi}{K \to \mu + \nu} \sim 10^{-3},$$

This would be in contradiction with the experiments of Cassels,[6] which gave for ρ_γ the upper limit ρ_γ

$< 10^{-5}$. Actually it can be shown that both the A and V types of interaction give $\rho_\gamma \sim 10^{-7}$. For the A interaction this has been shown in a paper by Treiman and Wyld[7] (cf. also Ref. 8); the corresponding calculations for the V interaction have been carried out by V. G. Vaks (private communication).

The existence of the universal A − V interaction also explains in a natural way the large asymmetry in the hyperon decays $Y \to N + \pi$. If we describe such decays by the simplest diagrams of perturbation theory (Fig. 3), we get for the matrix element

$$F \sim fGM(\bar{\psi}_N \hat{k}(1+\gamma_5)\psi_Y),$$

where k is the momentum of the π meson.

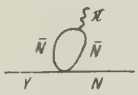

FIG. 3

In the approximation in which the nucleon is nonrelativistic we get

$$F \sim fGM(\psi_N^*(k_0 + \sigma\mathbf{k})\psi_Y).$$

If the decaying hyperon is completely polarized, the probability of emergence of the nucleon at an angle ϑ with the direction of the hyperon spin is proportional to the quantity $1 + \alpha \cos\vartheta$, where

$$\alpha = 2(k/k_0)/[1 + (k/k_0)^2],$$

which for the decay of a polarized Λ hyperon gives $\alpha \sim 0.9$. The latest experimental data on the decay of Λ particles formed in the reaction $\bar{\pi} + p \to \Lambda + K$ lead to the following effective value of the constant α: $\alpha_{eff} = 0.77 \pm 0.16$. From this it must be concluded that the Λ particle produced in this reaction is polarized in the plane of its production, with the average polarization lying in the range between $\frac{2}{3}$ and 1.

The considerably smaller value of the asymmetry in the decay of Σ particles produced in the same reaction $\bar{\pi} + p$ must evidently be ascribed to the fact that the polarization of these hyperons at the time of their production is considerably less than that of Λ particles.

We note that according to the scheme considered here, the ratio of the probabilities for the decays $\Lambda \to p + \pi^-$ and $\Lambda \to n + \pi^0$ is mainly determined by the relative probability for production of a charged or a neutral π meson by a baryon, i.e., is about equal to 2, which is close to the experimental value.

[1] M. Gell-Mann and R. P. Feynman (in press).
[2] R. E. Marshak and E. G. G. Sudarshan (in press).
[3] S. Furiuchi et al., Prog. Theor. Phys. **16**, 64 (1956); **17**, 89 (1957).
[4] A. Pais and S. B. Treiman, Phys. Rev. **105**, 1616 (1957).
[5] H. L. Anderson and C. Lattes. Nuovo cim. **6**, 1356 (1957).
[6] J. M. Cassels et al., Proc. Phys. Soc. **A70**, 729 (1957).
[7] S. B. Treiman and H. W. Wyld, Jr., Phys. Rev. **101**, 1552 (1956).
[8] S. Bludman and M. Ruderman, Phys. Rev. **101**, 910 (1956).

Translated by W. H. Furry
179

NON-STATIONARY PHENOMENA IN NUCLEAR MAGNETIC RESONANCE

V. S. GRECHISHKIN

Submitted to JETP editor September 21, 1957

J. Exptl. Theoret. Phys. (U.S.S.R.) **34**, 902-908 (April, 1958)

The "ringing" of a nuclear spin system produced by a unit pulse, and by a triangular pulse is considered and calculations are made of transient processes caused by jumps in frequency which simulate the phenomenon of the "beating of beats". It is shown that a transient process in a spin system is determined only by the properties of the latter and not by the shape of the radio frequency pulse. Formulas are obtained which may be used to measure relaxation times.

THE application of nuclear magnetic resonance methods to the study of the nature of the liquid state has made it possible to obtain additional information about processes occurring in liquids.

In spite of the fact that recently Bloch[1] succeeded in giving a quantum theory of transient phenomena in nuclear magnetic resonance the most useful description of these phenomena is still the one given within the framework of classical theory also by Bloch[2] who derived on the basis of Ehrenfest's theorem his well known equations describing the behavior of the nuclear magnetization vector in external fields.

Bloch's equations hold sufficiently accurately in the case of liquids[3,4] even though in deriving them no account is taken of the fact that the magnetization of a substance is associated with a decrease in the entropy of the spin system. Taking into account the principle of minimum entropy leads to the appearance in Bloch's equations of only a small additional term.[5]

The solution of Bloch's equations has been investigated by different methods in a number of special cases.[2,6,7] However, these cases do not cover all aspects of the phenomenon since the nuclear induction method has now found a new application. One should first of all refer to the observation of the effect of free nuclear induction in the earth's magnetic field,[8] and also to the use of pulse methods for the measurement of relaxation times. The general solution of the nuclear induction problem has not been given in the literature for the above cases. It is also of considerable interest to investigate the behavior of a spin system when pulsed signals of various shapes are applied to the sample.

In this connection in the present paper we obtain by the methods of operational calculus[9] solutions of Bloch's equations which may be employed for the measurement of relaxation times and also for the simulation of transient processes in a nuclear spin system by processes taking place in certain four terminal networks.

1. FORMULATION OF THE PROBLEM

The system of Bloch's equations is a system of linear differential equations with variable coefficients. In order to observe nuclear resonance signals by the steady state method, a sinusoidal modulation of the magnetic field is used. If the modulation amplitude is small then the variable part of the magnetic field $H(t)$ is small in comparison with the constant component H_0:

$$H(t) = H_0 + H_m \sin \omega_m t, \tag{1}$$

where ω_m is the modulation frequency.

When the weak radiofrequency field which gives rise to the precession of the macroscopic nuclear magnetization vector M is directed at right angles to the strong magnetic field, Bloch's system of equations may be put in the form

$$\begin{gathered} du/dt + \Delta\omega v + u/T_2 = 0, \\ dv/dt - \Delta\omega u + \gamma H_1 M_z + v/T_2 = 0, \\ dM_z/dt - \gamma H_1 v + M_z/T_1 = M_0/T_1, \\ H_x = H_1 \cos \omega t, \quad H_y = \mp H_1 \sin \omega t, \end{gathered} \tag{2}$$

where u is the dispersion mode signal, v is the absorption mode signal, T_2 is the transverse relaxation time, T_1 is the longitudinal relaxation time, M_0 is the static value of nuclear polarization, $\Delta\omega$ is the detuning and γ is the gyromagnetic ratio. If sinusoidal modulation of the magnetic field is employed, the detuning will have the form

$$\Delta\omega(t) = \gamma H_m \sin \omega_m t. \tag{3}$$

Since the amplitude of the modulation of the magnetic field is small, it may be assumed to a sufficient degree of accuracy that $M_0 = \text{const}$. In the

cases of linear detuning $\gamma H_m \omega_m t$, and sinusoidal detuning $\gamma H_m \sin \omega_m t$, the operational method yields respectively integrals of the form

$$\gamma H_m \omega_m \int_0^\infty t v(t) e^{-pt}\, dt = -\gamma H_m \omega_m \frac{dv(p)}{dp},$$

$$\gamma H_m \int_0^\infty \sin \omega_m t v(t)\, e^{-pt}\, dt = \frac{\gamma H_m}{2i} \frac{v(p-i\omega_m)(p+i\omega_m) - v(p+i\omega_m)(p-i\omega_m)}{p^2+\omega_m^2}. \quad (4)$$

Below we discuss the solution of Bloch's equations for certain special cases of practical importance.

2. THE CASE OF ADIABATIC PASSAGE THROUGH THE RESONANCE REGION

We consider the case when $\Delta\omega$ is a slowly varying function, while the relaxation times T_1 and T_2 are sufficiently large that the criterion for rapid passage in Bloch's sense remains satisfied. The condition on the slowness of variation of $\Delta\omega$ is

$$d\Delta\omega/dt \ll \gamma^2 H_1^2. \quad (5)$$

This condition is satisfied more and more accurately as the level of the radio frequency field is raised. The slowness of variation of $\Delta\omega$ does not determine the conditions for the slowness of passage through the resonance region since these conditions also presuppose short relaxation times.[2]

It is well known that the Laplace transformation is applicable to all functions bounded in the interval from zero to infinity or increasing as t^a, or even as e^{at}, where a is some positive number. Any arbitrary physical function satisfies these conditions, and therefore by multiplying Bloch's equations from the left and from the right by e^{-pt} and integrating from zero to infinity we obtain the transformed equations

$$\begin{aligned} (p+1/T_2)\,u(p) + \Delta\omega v(p) &= u(0), \\ (p+1/T_2)\,v(p) - \Delta\omega u(p) + \gamma H_1 M_z(p) &= v(0), \\ (p+1/T_1)\,M_z(p) - \gamma H_1 v(p) &= M_0/T_1 p + M_z(0), \end{aligned} \quad (6)$$

where $u(0)$ is the initial value of the dispersion mode signal, $v(0)$ is the initial value of the absorption mode signal and $M_z(0)$ is the initial value of nuclear polarization along the z axis.

In order to solve this system of equations, we must evaluate its determinant

$$\Delta(p) = (p+1/T_2)^2(p+1/T_1) + (\Delta\omega)^2(p+1/T_1) + (\gamma H_1)^2(p+1/T_2). \quad (7)$$

We limit ourselves to a discussion of the absorption mode signal $v(p)$ and use the inverse Laplace transformation for the determination of $v(t)$. The Riemann-Mellin integral is evaluated by means of residues, and for this we have to find the roots of the characteristic equation

$$\Delta(p) = 0. \quad (8)$$

This is a cubic equation with real coefficients and therefore it has at least one real root; it may be easily shown that the other two roots are imaginary in the present case.

We denote the real root of (8) by α and write the determinant of the system in the form

$$\Delta(p) = (p+\alpha)[(p+\beta)^2 + \eta^2], \quad (9)$$

where β and η are certain arbitrary constants. By decomposing the rational fraction $v(p) = \Delta_2(p)/\Delta(p)$ into the simplest fractions and utilizing the inverse Laplace transformation, we shall obtain the expression for the absorption mode signal:

$$v(t) = Ae^{-\alpha t} + Be^{-\beta t}\cos\eta t + (C/\eta)\, e^{-\beta t}\sin\eta t + D, \quad (10)$$

where A, B, C, D are arbitrary constants. The dispersion mode signal will also have a similar form. The arbitrary constant D may be evaluated from the condition

$$D = v(p)\,p \quad \text{as} \quad p \to 0. \quad (11)$$

D represents the stationary solution of Bloch's equations and its form coincides with the solution obtained by Bloch by a different method.[2]

From a comparison of the coefficients one may easily obtain relations also for the other arbitrary constants:

$$\begin{aligned} A + B + D &= v(0); \\ 2A\beta + B\beta + C + B\alpha + 2\beta D + D\alpha &= v(0)(1/T_1 + 1/T_2) - \gamma H_1 M_z(0) + u(0)\Delta\omega, \\ A\beta^2 + A\eta^2 + B\alpha\beta + C\alpha + D\eta^2 + 2\beta\alpha D + D\beta^2 &= v(0)/T_2T_1 + u(0)\Delta\omega/T_1 - \gamma H_1 M_0/T_1 - \gamma H_1 M_z(0)/T_2; \\ 2\beta + \alpha &= 2/T_2 + 1/T_1; \\ \eta^2 + \beta^2 + 2\beta\alpha &= 1/T_2^2 + 2/T_1T_2 + (\Delta\omega)^2 + (\gamma H_1)^2; \\ \alpha(\eta^2 + \beta^2) &= 1/T_2^2T_1 + (\Delta\omega)^2/T_1 + (\gamma H_1)^2/T_2. \end{aligned} \quad (12)$$

Thus the solution of Bloch's equations consists of terms describing the transient process as well as a stationary term.

Calculations on a molecular basis lead to the conclusion that the relaxation times T_1 and T_2 must be of the same order of magnitude. In practice, because of the inhomogeneity of the magnetic field, considerable deviations from this rule can occur. Since there was no perpendicular polarization before resonance, $u(0) = v(0) = 0$. Then in the case that $T_2 \sim T_1$ we have:

$$v(t) = [\gamma H_1 M_0/((\Delta\omega)^2 T_2 + 1/T_2$$

$$+ (\gamma H_1)^2 T_1)]e^{-t/T_2}\cos\sqrt{(\gamma H_1)^2 + (\Delta\omega)^2}\, t + [\gamma H_1 M_0/((\Delta\omega)^2 T_2 + 1/T_2 + (\gamma H_1)^2 T_1)]e^{-t/T_2}\sin\sqrt{(\gamma H_1)^2 + (\Delta\omega)^2}\, t - \frac{\gamma H_1 M_0}{(\Delta\omega)^2 T_2 + 1/T_2 + (\gamma H_1)^2 T_1}. \quad (13)$$

From this expression it may be seen that the exponential e^{-t/T_2} is the envelope of the transient processes while their frequency is determined by the detuning and increases as the detuning becomes greater.

Similarly in the case of very small detuning we obtain

$$v(t) = \left(v(0) + \frac{\gamma H_1 M_0}{1/T_2 + (\gamma H_1)^2 T_1}\right) \times \exp\left\{-\frac{1}{2}(1/T_2 + 1/T_1)\, t\right\}\cos\eta_1 t + \left[\frac{v(0)}{2}\left(\frac{1}{T_1} - \frac{1}{T_2}\right) + \frac{\gamma H_1 M_0}{1/T_2 + (\gamma H_1)^2 T_1}\left(\frac{1}{T_1} + \frac{2}{T_2}\right) - \gamma H_1 M_z(0)\right] \times \left[(\gamma H_1)^2 - \frac{1}{4}(1/T_2 - 1/T_1)^2\right]^{-1/2} \times \exp\left\{-\frac{1}{2}\left(\frac{1}{T_2} + \frac{1}{T_1}\right) t\right\}\sin\eta_1 t - \frac{\gamma H_1 M_0}{1/T_2 + (\gamma H_1)^2 T_1}. \quad (14)$$

Observation of transient processes enables one to determine the relaxation times. However, in the steady state method their realization in a pure form is associated with considerable experimental difficulties.

3. PULSE METHODS IN NUCLEAR MAGNETIC RESONANCE

Transient phenomena in nuclear magnetic resonance may be realized by means of applying the radio frequency field in the form of pulses. For the case when the signal is observed during pulses of radio frequency field lying within the resonance band ($\Delta\omega = 0$), one can use expression (14). In this case the solution is obtained without any simplifying assumptions since the system of Bloch's equations reduces to a system of equations with constant coefficients. When the radio frequency field is large and the stationary term becomes saturated the nuclear resonance signal during the pulses will have the form

$$v(t) = \frac{-\gamma H_1 M_z(0)}{\sqrt{(\gamma H_1)^2 - 1/4(1/T_2 - 1/T_1)^2}} \exp\left\{-\frac{1}{2}\left(\frac{1}{T_1} + \frac{1}{T_2}\right) t\right\} \times \sin\sqrt{(\gamma H_1)^2 - 1/4(1/T_2 - 1/T_1)^2}\, t. \quad v(0) = u(0) = 0. \quad (15)$$

From the above expression it may be seen that the envelope of the signal is given by the exponential e^{-t/T_0} with $1/T_0 = \frac{1}{2}(1/T_1 + 1/T_2)$, while the oscillation frequency is always given by the nuclear Larmor precession frequency. Since the signal is observed after appropriate detection, the above fact enables one to determine the overall relaxation time T_0.

In the case when the frequency of the r.f. field is not exactly equal to the nuclear Larmor precession frequency expression (13) may be used to describe the absorption mode signal.

Expressions (13), (14) and (15) represent the response of a spin system to an r.f. pulse which may be considered to be a unit pulse. The absorption mode signal will then represent the envelope of the process whose frequency is the nuclear Larmor precession frequency.

Thus the use of the phenomenological Bloch equations as the starting point enables us to calculate the response of a spin system to a unit r.f. pulse, and consequently also to a signal of arbitrary form, since the spin system possesses resonance properties.

In order to investigate the question of the effect of a pulse of triangular shape, we shall use the formula

$$D(t) = E(0)\, v(t) + \int_0^t v(\tau)\, E'(t-\tau)\, d\tau, \quad (16)$$

where $D(t)$ is the envelope of the output signal, $E(t)$ is the envelope of the input signal and $v(t)$ is the response of the system to a unit r.f. pulse. In the present case, it is sufficient to investigate a linearly increasing input voltage $E = at$. We then obtain

$$D(t) = a\int_0^t v(\tau)\, d\tau = A'[e^{-bt}(-b\sin\eta_1 t - \eta_1\cos\eta_1 t) + \eta_1]/(b^2+\eta_1^2). \quad (17)$$

It may be seen from this expression that the envelope of the transient processes remains of the form e^{-t/T_0} also in the case of a triangular pulse, i.e., the "damping" of the transient process is independent of the shape of the r.f. pulse and is determined only by the properties of the spin system.

If the nuclear magnetic resonance signal is observed in the interval between pulses of the r.f. field then the following conditions hold

$$\Delta\omega = \gamma H_0, \quad H_1 = 0. \quad (18)$$

In this case we can obtain for the absorption mode signal

$$v(t) = e^{-t/T_2}(v(0)\cos\gamma H_0 t + u(0)\sin\gamma H_0 t). \quad (19)$$

Similarly, the dispersion mode signal is described by the expression

$$u(t) = e^{-t/T_2}(u(0)\cos\gamma H_0 t - v(0)\sin\gamma H_0 t). \quad (20)$$

Thus observation of nuclear resonance signals both during the pulses and in the interval between the pulses of the r.f. field enables us to determine both the longitudinal and the transverse relaxation

times.

The expressions obtained for the dispersion and absorption mode signals in the interval between pulses may be used for the description of signals of free nuclear induction observed in weak magnetic fields. In order to obtain transverse polarization in this method a sufficiently strong magnetic field perpendicular to the weak one is used. For the perpendicular component of nuclear polarization we obtain

$$M_y = \mp e^{-t/T_2}[v(0)\cos\gamma H_0 t + u(0)\sin\gamma H_0 t]. \quad (21)$$

Then the following nuclear induction signal will appear across the terminals of the receiver coil

$$v(t) = \mp \frac{4\pi}{c} NS\gamma H_0 v(0)\, e^{-t/T_2}\cos\gamma H_0 t, \quad (22)$$

where N is the number of turns in the receiver coil and S is its cross-section area.

Consequently the observation of free nuclear induction signals in the earth's field permits one to determine the transverse relaxation time very accurately since the earth's field has a high degree of natural homogeneity.

In order to carry out calculations for transient processes in a spin system in the case of sudden jumps of frequency we shall assume that initially an r.f. field characterized by the detuning $-\Delta\omega$ was switched on, that it was switched off at the time $T = 0$, and another r.f. field detuned by an amount $+\Delta\omega$ was switched on. Then for large T we can obtain

$$D(t)\, e^{i\omega_0 t} = v(t + T, -\Delta\omega)\, e^{i(\omega_0 - \Delta\omega)t} - v(t, -\Delta\omega)\, e^{i(\omega_0 - \Delta\omega)t} + v(t, +\Delta\omega)\, e^{i(\omega_0 + \Delta\omega)t}. \quad (23)$$

From this we obtain for the nuclear resonance signal

$$D(t) = -[\gamma H_1 M_0 / ((\Delta\omega)^2 T_2 + 1/T_2 + (\gamma H_1)^2 T_1)] \times [1 - 2ie^{-t/T_2}(\cos\eta t + (1/T_2\eta)\sin\eta_1 t)\sin\Delta\omega t]. \quad (24)$$

It may be seen from this that transient processes in the case of frequency jumps are of a more complicated nature, i.e. additional oscillations of the envelope of the nuclear magnetic resonance signals are now observed. Transient processes associated with jumps of frequency remind one by their shape of the phenomenon of "beating of beats" due to the presence in the sample of groups of resonating nuclei with different precession frequencies. This fact makes it much more difficult to observe the "beating of beats". It should be noted that in stationary nuclear resonance methods associated with a deviation of frequency the transient phenomena are always somewhat distorted. Small drifts of the generator frequency sometimes make it possible to observe the pseudo-phenomenon of "beating of beats" even in pure water.

The cases considered above show that transient phenomena in a spin system are similar to transient processes in coupled resonant electrical circuits. The expressions obtained above are simple and may be used for the experimental determination of relaxation times.

[1] F. Bloch, Phys. Rev. **102**, 104 (1956).

[2] F. Bloch, Phys. Rev. **70**, 460 (1946).

[3] A. G. Redfield, Phys. Rev. **98**, 1787 (1955).

[4] P. M. Borodin, Thesis, Leningrad State University (1955).

[5] N. Wangsness, Phys. Rev. **104**, 857 (1956).

[6] H. C. Torrey, Phys. Rev. **76**, 1059 (1949).

[7] S. D. Gvozdover and A. A. Magazanik, J. Exptl. Theoret. Phys. (U.S.S.R.) **20**, 705 (1950).

[8] M. Packard and R. Varian, Phys. Rev. **93**, 941 (1954).

[9] M. Kontorovich, Операционное исчисление и нестационарные явления в электрических цепях (Operational Calculus and Non-Stationary Phenomena in Electric Circuits), Gostekhizdat, 1955

Translated by G. Volkoff
180

CONCENTRATION OF NEGATIVE IONS IN THE PLASMA OF A POSITIVE COLUMN

M. V. KONIUKOV

Tul' skii Pedagogical Institute

Submitted to JETP editor, July 20, 1957; revised version received December 23, 1957

J. Exptl. Theoret. Phys. (U.S.S.R.) **34**, 908-911 (April, 1958)

The concentration of negative ions in a positive column is considered. The effect of recombination of positive ions and negative ions on the concentration of negative ions close to the axis of the discharge is investigated.

THE negative component of the plasma of a positive column in electro-negative gases consists of electrons and negative ions. Although the nature of the discharge depends, to a great extent, on the concentration of negative ions, in the work reported in Refs. 1 — 4 this concentration was not considered and no attempt was made to investigate the effects associated with charged-particle kinetics in the column. It is the purpose of the present paper to consider these questions.

1. In the case of quasi-neutral ambipolar diffusion, when there is surface recombination of electrons and ions at the walls, the relative concentration of negative ions is obtained from the following charged-particle balance equations:

$$\begin{aligned} \frac{1}{r}\frac{\partial}{\partial r}\left\{ r\left[-D_e\frac{\partial N_e}{\partial r} - b_e N_e E_r \right]\right\} &= ZN_e - \beta N_e, \\ \frac{1}{r}\frac{\partial}{\partial r}\left\{ r\left[-D_n\frac{\partial N_n}{\partial r} - b_n N_n E_r \right]\right\} &= \beta N_e, \\ \frac{1}{r}\frac{\partial}{\partial r}\left\{ r\left[-D_p\frac{\partial N_p}{\partial r} + b_p N_p E_r \right]\right\} &= ZN_e, \end{aligned} \tag{1}$$

where N, D and b are the concentration, diffusion coefficient, and mobility of the electrons (subscript "e"), negative ions (subscript "n") and positive ions (subscript "p"), Z is the ionization coefficient, βN_e is the number of negative ions produced in unit volume per unit time and E_r is the transverse field.

Taking

$$N_n = \varkappa N_e, \tag{2}$$

where κ is a constant, after some simple transformations* we obtain

$$\frac{\varkappa - 2\varkappa(1+\varkappa)D_e/D_p}{1+2\varkappa}\,\frac{Z-\beta}{\beta} + 1 = 0. \tag{3}$$

*In carrying out the above simplification the following obvious relations have been used: $D_e b_p \gg D_p b_e$, $D_e b_n \gg D_n b_e$, $b_p \approx b_n$ and $D_n \approx D_p$.

Assuming that

$$(Z-\beta)\,\beta\,(Z+\beta)^{-2} D_p/D_e \ll 1$$

the solution of Eq. (3) is of the form*

$$\varkappa = (D_e/2D_p)(Z+\beta)/(Z-\beta). \tag{4}$$

According to Eq. (4), under the conditions which usually apply in a positive column (non-isothermal) the concentration of negative ions is two orders of magnitude larger than the concentration of electrons. This sharp difference in concentrations is a result of the assumption that surface recombination is the only mechanism for the removal of negative ions. Actually, to have a net transport of negative ions to the walls, it is necessary that the diffusion flow to the walls $\kappa D_n(\partial N_e/\partial r)$ be larger than the flux toward the axis which exists by virtue of the radial electric field

$$\frac{\varkappa D_e b_n}{b_e + b_p + 2\varkappa b_n}\,\frac{\partial N_e}{\partial r},$$

*V. L. Granovskii has called our attention to the fact that the quantity $\varkappa$ as given in Eq. (4) does not approach 0 as $\beta \to 0$. In this limiting process the solution $\varkappa = 0$ should result instead of $\varkappa = D_e/2D_p$ as follows from Eq. (4). It might seem that we are dealing with ambiguous solutions of Eq. (1). However, such is not the case. The only solution of the system for $\beta \to 0$ is $\varkappa = D_e/2D_p$ which corresponds to the stationary state in which the diffusion of negative ions is compensated by motion to the axis by virtue of the existing radial electric field. The absence of the explicit solution $\varkappa = 0$ is due to the approximate nature of Eq. (1), in which no account is taken of volume recombination, the disappearance of negative ions by virtue of decay, and ion transfer to the anode region. As long as β is large, this approximation remains valid; however, when β becomes small, the equations must be supplemented by appropriate additional terms. Taking account of the latter leads to the appearance of the single stationary solution $\varkappa = 0$. From this point of view the limiting transition indicated above is not really valid.

and this situation is possible only when $\kappa > D_e/2D_p$.

2. The existence of high concentrations of negative ions implies small transverse and longitudinal gradients, a situation which is not very probable. Since this is a result of the fact that removal of negative ions has been attributed only to surface recombination at the walls, to obtain the next approximations it is necessary to take account of volume recombination.*

In this case the system of charged-particle balance equations (1) becomes

$$\begin{aligned} \frac{1}{r}\frac{\partial}{\partial r}\left\{r\left[-D_n\frac{\partial N_n}{\partial r}-b_nN_nE_r\right]\right\} &= \beta N_e-\alpha N_nN_p,\\ \frac{1}{r}\frac{\partial}{\partial r}\left\{r\left[-D_p\frac{\partial N_p}{\partial r}+b_pN_pE_r\right]\right\} &= ZN_e-\alpha N_nN_p, \end{aligned} \tag{1a}$$

where α is the volume recombination coefficient. The electron balance, however, remains unchanged.

It is difficult to find a solution for this system of non-linear equation over the entire cross section of the column. Hence we shall limit ourselves to a calculation of the negative-ion concentration only in the region of the discharge axis, where it can be assumed that κ is constant.† If furthermore, ambipolar quasi-neutral diffusion is assumed, after a series of simple transformations, we obtain a system of equations which determines the concentration of negative ions and the distribution of electrons close to the discharge axis:

$$\frac{(1+\varkappa)(D_eb_p+D_pb_e)+\varkappa(D_eb_n-D_nb_e)}{b_e+\varkappa b_n+(1+\varkappa)b_p}\frac{1}{r}\frac{\partial}{\partial r}\left(r\frac{\partial N_e}{\partial r}\right)+(Z-\beta)N_e=0, \tag{5}$$

$$\frac{\varkappa(D_eb_n-D_nb_e)-\varkappa(1+\varkappa)(D_pb_n+D_nb_p)}{b_e+\varkappa b_n+(1+\varkappa)b_p}\frac{1}{r}\frac{\partial}{\partial r}\left(r\frac{\partial N_e}{\partial r}\right)=[\beta-\alpha\varkappa(1+\varkappa)N_e^0]N_e.$$

Eliminating N_e from Eq. (5), we obtain an equation for determining the relative concentration of negative ions at the axis

$$\frac{\varkappa(D_eb_n-D_nb_e)-\varkappa(1+\varkappa)(D_pb_n+D_nb_p)}{(1+\varkappa)(D_eb_p+D_pb_e)+\varkappa(D_eb_n-D_nb_e)}(Z-\beta)+\beta=\alpha N_e^0\varkappa(1+\varkappa), \tag{6}$$

which, since $D_eb_n \gg D_nb_e$, $D_eb_p \gg D_pb_e$, $b_p \approx b_n$, and $D_p \approx D_n$, results in the expression

$$\frac{\varkappa-2\varkappa(1+\varkappa)D_p/D_e}{1+2\varkappa}\frac{Z-\beta}{\beta}+1=\frac{\alpha N_e^0}{\beta}\varkappa(1+\varkappa). \tag{6a}$$

Rather than carry out a general investigation of Eq. (6a) we consider two particular cases:

(a) $\alpha = 0$ and there is no volume recombination. Eq. (6a) becomes Eq. (3) which has already been studied in the first section.

(b) $Z = \beta$ and each electron which appears becomes a negative ion. Equation (6a) assumes the form

$$(\alpha N_e^0/\beta)\varkappa(1+\varkappa)-1=0. \tag{7}$$

Here we are considering the case in which all negative ions are removed by volume recombination. The negative-ion concentration, which is constant over the entire space, is determined by the expression*

$$\varkappa=-{}^1/_2+{}^1/_2\sqrt{1+4\beta/\alpha N_e^0}, \tag{8}$$

which, when $4\beta/\alpha N_e^0 \ll 1$, becomes

$$\varkappa \approx \beta/\alpha N_e^0. \tag{8a}$$

A general investigation of Eq. (6a) is best carried out by graphical methods.† Assuming that

$$D_p/D_e \approx 10^{-2}, \qquad (Z-\beta)/\beta \approx 1$$

(the second condition means that half of all the electrons which are produced lead to the formation of negative ions), we obtain the following table of values of the concentration as a function of the parameter $\alpha N_e^0/\beta$:

$\alpha N_e^0/\beta =$	0	0.001	0.01	0.1	0.5	1
$\varkappa =$	150	34	10.9	3.3	1.15	0.6.

Thus, when volume recombination is taken into account the relative concentration of negative ions at the axis is reduced.‡

3. A direct measurement of the concentration of negative ions is difficult; hence it is easier to examine the variation in the transverse electric

*The small cross section for recombination of electrons and positive ions as compared with the cross section for ion recombination[5] means that the former can be neglected.

†If the entire cross section of the column is considered, $\varkappa = \varkappa(r)$. However, over a small region close to the discharge axis it may be assumed that $\varkappa$ is constant. This assumption is strictly justified in the absence of either volume recombination or surface recombination. Moreover, the assumption concerning the proportionality of the charged components used Refs. 3, 4, 6, leads to reasonable results.

*When $\beta \to 0$, the concentration given by Eq. (8) becomes 0.

†The solutions of Eq. (6) lie between two limiting values: $\varkappa = (D_e/2D_p)[(Z+\beta)/(Z-\beta)]$ corresponding to the case in which only surface recombination is considered and $\varkappa = \beta/\alpha N_e^0$ which applies when only volume recombination is considered.

‡The reduction in the concentration of negative ions is due to the possibility of removal even when the resultant negative-ion flux is toward the discharge axis.

field due to these ions.* Let E_r be the transverse field in the column when there are no negative ions and E_r^0 the transverse field in the case in which only surface recombination is assumed for the negative ions. Using the Schottky boundary condition and computing this ratio we find

$$E_r^0 / E_r = (1 + 2\varkappa b_n / b_e)^{-1}. \quad (9)$$

A measurement of the transverse fields makes it possible to estimate the concentration of charged particles and thus to obtain information on the relative importance of surface recombination and volume recombination.

The destruction of negative ions in collisions should also play a decisive role in negative-ion column kinetics. We propose to examine this question in the future.

*A. A. Zaitsev has indicated a possible method of estimating the transverse field. Since the curvature of the stratum is determined by the magnitude of the transverse gradient, by studying its behavior when electro-negative gases are added it is possible to estimate the relative change in the transverse gradient.

In conclusion we wish to express our gratitude to Professor V. L. Granovskii and Docent A. A. Zaitsev with whom we had a number of illuminating discussions and to E. V. Korotkov for help in carrying out the work.

[1] R. Holm, Z. Physik **75**, 171 (1932).
[2] R. Seeliger and R. Kruschke, Physik Z. **34**, 883 (1933).
[3] A. von Engel and M. Steenbeck, Elektrische gasentladungen, ihre physik und technik, Vol. I, (Berlin, 1934).
[4] R. Seeliger, Ann. Physik **6**, 93 (1949).
[5] V. L. Granovskii, Электрический разряд в газах (Electrical Discharges in Gases) Vol. I (1952).
[6] G. Ecker, Proc. Phys. Soc. (London) **B67**, 485 (1954).

Translated by H. Lashinsky
181

SOVIET PHYSICS JETP VOLUME 34 (7), NUMBER 4 OCTOBER, 1958

MONTE CARLO CALCULATION OF AN ELECTRON-PHOTON CASCADE IN LEAD

V. V. CHAVCHANIDZE, R. S. SHADURI, and V. A. KUMSISHVILI

Institute of Physics, Academy of Sciences, Georgian S.S.R.

Submitted to JETP editor September 23, 1957

J. Exptl. Theoret. Phys. (U.S.S.R.) **34**, 912-915 (1958)

A statistical-probability method, based on random trials, is given for using a model to calculate the effects in an electron-photon cascade initiated in a layer of lead by a γ-ray quantum. This is a modification of the Monte Carlo method. Some typical curves calculated in this way are presented. Two methods are indicated for carrying out this sort of calculations by the use of high-speed electronic calculating machines.

We have used a method of random trials, which is a modification of the well known Monte Carlo method,[1-3] for the calculation of the electron-photon cascade shower produced in a lead plate of thickness 0.5 cm by a γ-ray quantum of energy 500 Mev. The problem reduces to a stepwise reproduction of the picture of the natural process of the production of a cascade shower by a single primary particle. The "feeding in" of a large number of primary particles gives the distributions in energy and angle of the electrons, positrons, and γ-ray quanta emerging from the plate.

We have followed essentially the method of "drawing" given in the papers of Chavchanidze.[4,5] In the drawing we used tables of random numbers,[6] which make it unnecessary to use machines to ob-

tain such data.

Omitting the details,* we shall outline the method for calculating the cascade.

The distance traversed in the lead by the γ-ray quantum before its first interaction is determined by drawing. The drawing is based on the curve of the relation of total cross-section to quantum energy.

Then a drawing is made to determine the "fate" of the quantum. In the case of pair production, the energy of the positron is found by drawing, and this also fixes the energy of the electron. Drawings are made for the distances they traverse before interaction, as in the case of the γ-ray quantum. Then the amount of ionization loss is determined, and thus the energies of the particles at their subsequent collisions. A separate drawing gives the correction for multiple scattering. If the electron and positron have not traveled outside the plate their further fate is traced out.

To find by drawing the energies of Bremsstrahlung quanta, we used a method based on the construction of unnormalized integral curves with nonuniform scales for the arguments.

The drawing of the scattering angles was carried out without including correlation between the scattering angles of quantum and electron.

In the case of annihilation the angle of emission of one of the photons in the center-of-mass system is found by drawing, and this fixes that of the second photon. (The formulas for the angles and energies can be found in the book by Heitler.[7])

The results of the calculation are presented in the form of energy distribution (Fig. 1) and angle distribution (Fig. 2) curves for electrons, positrons, and photons, and also the so-called probability for "zero electrons" as a function of the aperture angle of the cone of observation (Fig. 3). The probability of "zero electrons" is defined as the probability that the developing cascade initiated by a single γ-ray quantum does not give any particle $e^{\pm}$ inside a prescribed cone with aperture angle ϑ. Here it is assumed that an electron or positron having energy less than 10 Mev either does not emerge from the lead plate of thickness 0.5 cm or else is not registered by the apparatus.

The data obtained also make it possible to find these distributions for the intermediate thicknesses 0.1, 0.2, 0.3, and 0.4 cm.

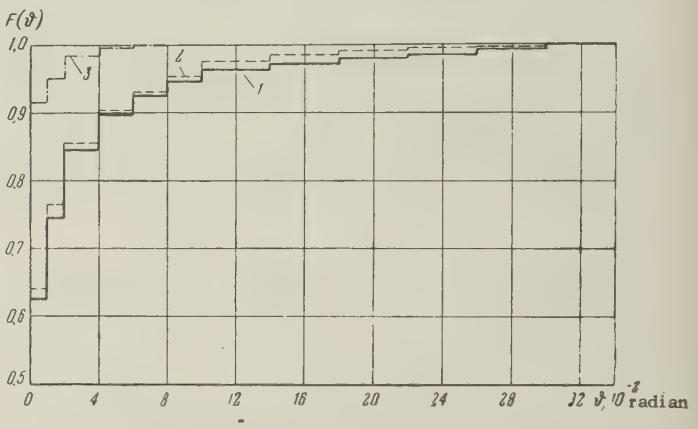

FIG. 2. Integrated angle-of-emergence distributions of electrons 1, positrons 2, and photons 3

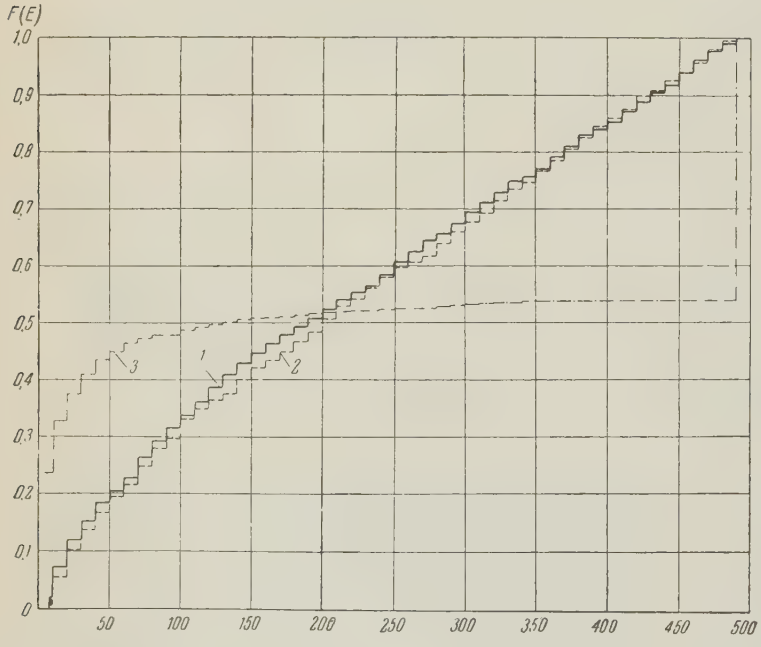

FIG. 1. Integrated energy distributions of electrons 1, positrons 2, and photons 3.

*This research will be published in full in Volume 5 of Trudy Instituta Fiziki Akademii Nauk Gruzinskoi S. S. R.

The amount of work for the calculation of the electron-photon cascade is extraordinarily large.

The largest amount of time is taken by the passage from one set of data obtained by drawing to the input data for the next drawing. The practical carrying out of such calculations requires the use of discrete-action high-speed electronic computing machines. For this purpose it has been found that it is quite unnecessary to remodel the existing machines. All that is required is appropriate programming. We shall state two methods of programming.

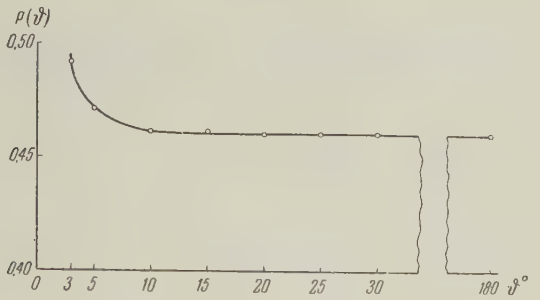

FIG. 3. Probability $P(\vartheta)$ that a cascade initiated by a single γ-ray quantum does not give any electron or positron inside a prescribed cone with aperture angle ϑ.

The distinguishing feature of the first method is that the arguments of the previously prescribed probability functions are stored in the permanent memory in a special order. Let us suppose that we have a diagram of the curve $P = F(x)$. This function can be represented by means of a set of pairs of numbers of the form $x_i, P_i = F(x_i)$, where i ranges from 1 to N. Sufficient accuracy for practical purposes can be obtained with $N \sim 300 - 500$. The statement of one member of a pair uniquely determines the other member. Therefore we need store in a definite section of the permanent memory device (MD) of our electronic computer only the arguments of the function. Suppose that for the storage of the numbers $x_i \epsilon M(x)$ (the set of arguments) we have set aside the counters with addresses beginning with a and ending with $a + 1000$. In the present case the entering of the numbers in the MD is carried out after a preliminary setting up of a certain sequence of values from among the x_i. A random number from the table of random numbers[6] is set equal to $F(x_b)$ and thus we have fixed a value of x_b, the other member of the pair x_b, $F(x_b)$. This number is entered in the MD under the address $a + 1$. The next random number supplies us with a value x_c, which is entered under the address $a + 2$, and so on. In this way 1000 numbers are put into the MD. The command for the use of the next of the random values $x_i \epsilon M(x)$ is taken care of by the use of these addresses in order, i.e., first $a + 1$, then $a + 2$, and so on. After the addresses are used up, the command can call for a displacement of the first address.

The second method of programming allows us to enter the function $F(x)$ in the MD in the usual way. But now the random numbers are stored in a special way in the counters under the various addresses of the MD: each number x_i is stored in the counter of the MD with the address $F(x_i)$. This type of storage is analogous to the storage of previously specified functions. The programming calls for choosing an address by taking a random number out of the table of random numbers. If the addresses take values from α to $\alpha + 1000$, then the program will call for the addresses $\alpha + p_i$, where the p_i are three-figure random numbers obtained by the programmer by reading the table of random numbers in a certain way. Thus a line of the program with a three-address code will have the following form:

$$\text{CRC} \qquad \alpha + p_i \qquad \beta \qquad \gamma$$

Here CRC means "command for a random choice". The CRC takes the number from the address $\alpha + p_i$ (α being a previously fixed number), adds it to the number at address β (this can also be zero) and sends the result to address γ.

It appears to us that the effectiveness of calculations by the method of random trials is fully manifested only when use is made of electronic computing machines, with a special procedure for programming and for entering the data in the memory device.

We take this occasion to express our gratitude to A. V. Tagviashvili, B. I. Bondarev, L. L. Esakiia, G. A. Gogadze, M. E. Pepel' man, and G. A. Almanov, who have taken part in the actual performance of the calculation.

The work presented here was carried out on the suggestion of Professor V. P. Dzhelepov and his group, in connection with the need for an estimate of the probability of failure of electrons and positrons to emerge from a thin layer of lead. The writers thank Professor Dzhelepov and his collaborators for their friendly attitude and their interest in the work.

[1] S. Ulam and J. von Neumann, Bull. Am. Math. Soc. **53**, 1120 (1947).

[2] R. R. Wilson, Phys. Rev. **86**, 261 (1952).

[3] Bernardini, Booth, and Lindenbaum, Phys. Rev. **88**, 1017 (1952).

[4] V. V. Chavchanidze, Izv. Akad. Nauk SSSR, Ser. Fiz. **19**, 629 (1955).

[5] V. V. Chavchanidze, Trudy Inst. Fiz. Akad.

Nauk Gruz. SSR **3**, 105 (1955).

[6] M. Kadyrov, Таблицы случайных чисел (Tables of Random Numbers) Central Asian State University Press, Tashkent 1936.

[7] W. Heitler, The Quantum Theory of Radiation (Oxford, 1953).

Translated by W. H. Furry
182

SOVIET PHYSICS JETP VOLUME 34 (7), NUMBER 4 OCTOBER, 1958

ON THE RELATIONS BETWEEN THE CROSS SECTIONS FOR MULTIPLE PRODUCTION OF PIONS

N. V. DUSHIN

Leningrad Politechnical Institute

Submitted to JETP editor November 8, 1957

J. Exptl. Theoret. Phys. (U.S.S.R.) **34**, 916-921 (April, 1958)

Isotopic relations have been obtained between the cross sections of transformation of a pion and a γ-quantum into three pions during collisions between the pion or γ-quantum and nucleons or deuterons. It is shown that near the threshold of the reaction, and also for production of pions with identical momenta, some auxiliary relations hold.

1. Relations have been obtained previously by the author between the cross sections of transformation of a single pion into two during collisions of pions with nuclei and deuterons.[1] Close to the reaction threshold, and also in the production of two pions with identical momenta, some auxiliary relations hold. In the present note it is shown that some auxiliary relations also hold between the cross sections of the various reactions of production of three pions during collisions of pions with nucleons and deuterons close to the threshold, or in the formation of pions with identical momenta.

Let us consider the collision of pions with nucleons (n) as the result of which the pion is transformed into three pions, i.e., the reaction

$$\pi + n \to n' + \pi' + \pi'' + \pi'''. \qquad (1)$$

The initial state is the superposition of states with isotopic spin T equal to $\frac{1}{2}$ and $\frac{3}{2}$. The wave function of the system of three pions is a superposition of states with isotopic spin t, equal to 0, 1, 2, 3. The wave function of the final state with total isotopic spin $T = \frac{1}{2}$ and $\frac{3}{2}$ can be constructed from the wave function of the nucleon (isotopic spin $\frac{1}{2}$) and from the wave function of the system of three pions with isotopic spin $t = 0$, 1, 2. The state with isotopic spin $t = 3$ is forbidden.

We denote by A_t^T, B_t^T, f_t^T, g_t^T and h_t^T the amplitudes of transitions into states with total isotopic spin T and isotopic spin of the system of three pions t and with a definite (see below) type of symmetry of the coordinate wave function of the pions.

Since the pions obey Bose statistics, then the type of symmetry of the coordinate part of the wave function and isotopic spin for the system of pions is determined by one and the same Young scheme.[2] The symmetry of the amplitude A_t^T is determined by a Young scheme consisting entirely of one row. The symmetric state of the system of three pions relative to an arbitrary pair of permutations of the charge variables is a state with total isotopic spin t equal to unity. Therefore, we have in all two different amplitudes, $A_1^{1/2}$ and $A_1^{3/2}$.

The symmetry of the amplitude B_t^T is determined by a Young scheme consisting of a single column. Since the antisymmetric state of the system of three pions relative to an arbitrary pair of permutations of the charge variables is the state with $t = 0$, then we have just the single amplitude $B_0^{1/2}$

The type of symmetry of the amplitudes f_t^T, g_t^T and h_t^T is determined by a Young scheme consisting of two rows. In his case t can take on the values 1 and 2.

For the differential cross sections σ of the different processes, we have

$$\sigma_1(\pi^+ + p \to p + \pi^+ + \pi^0 + \pi^0) = \left| A_1^{3/2} + f_1^{3/2} + \frac{1}{\sqrt{5}} f_2^{3/2} \right|^2,$$

$$\sigma_2(\pi^+ + p \to p + \pi^+ + \pi^+ + \pi^-) = \left| 2A_1^{3/2} - f_1^{3/2} + \frac{1}{\sqrt{5}} f_2^{3/2} \right|^2,$$

$$\sigma_3(\pi^+ + p \to n + \pi^+ + \pi^+ + \pi^0) = \left| \sqrt{\frac{8}{5}} f_2^{3/2} \right|^2,$$

$$\sigma_4(\pi^- + p \to p + \pi^- + \pi^0 + \pi^0) = \left| -\frac{1}{3}(2A_1^{1/2} + A_1^{3/2}) - \frac{1}{3}(2f_1^{1/2} + f_1^{3/2}) + \frac{1}{\sqrt{5}} f_2^{3/2} \right|^2,$$

$$\sigma_5(\pi^- + p \to p + \pi^- + \pi^+ + \pi^-) = \left| \frac{2}{3}(2A_1^{1/2} + A_1^{3/2}) - \frac{1}{3}(2f_1^{1/2} + f_1^{3/2}) - \frac{1}{\sqrt{5}} f_2^{3/2} \right|^2,$$

$$\sigma_6(\pi^- + p \to n + \pi^0 + \pi^0 + \pi^0) = \left| \sqrt{2}(A_1^{1/2} - A_1^{3/2}) \right|^2,$$

$$\sigma_7(\pi^- + p \to n + \pi^0 + \pi^+ + \pi^-) = \left| \frac{\sqrt{2}}{3}(-A_1^{1/2} + A_1^{3/2}) - \frac{\sqrt{2}}{3} B_0^{1/2} - \frac{\sqrt{2}}{3}(f_1^{1/2} - f_1^{3/2}) - \frac{1}{3}\sqrt{\frac{2}{5}}(f_2^{3/2} + 2g_2^{3/2}) \right|^2,$$

$$\sigma_8(\pi^0 + p \to p + \pi^0 + \pi^0 + \pi^0) = \left| A_1^{1/2} + 2A_1^{3/2} \right|^2,$$

$$\sigma_9(\pi^0 + p \to p + \pi^0 + \pi^+ + \pi^-) = \left| \frac{1}{3}(A_1^{1/2} + 2A_1^{3/2}) - \frac{1}{\sqrt{3}} B_0^{1/2} + \frac{1}{3}(f_1^{1/2} + 2f_1^{3/2}) - \frac{1}{3}\sqrt{\frac{2}{5}}(f_2^{3/2} + 2h_2^{3/2}) \right|^2, \quad (2)$$

$$\sigma_{10}(\pi^0 + p \to n + \pi^+ + \pi^0 + \pi^0) = \left| \frac{\sqrt{2}}{3}(A_1^{1/2} - A_1^{3/2}) + \frac{\sqrt{2}}{3}(f_1^{1/2} - f_1^{3/2}) + \sqrt{\frac{2}{5}} f_2^{3/2} \right|^2,$$

$$\sigma_{11}(\pi^0 + p \to n + \pi^+ + \pi^+ + \pi^-) = \left| \frac{2\sqrt{2}}{3}(-A_1^{1/2} + A_1^{3/2}) + \frac{\sqrt{2}}{3}(f_1^{1/2} - f_1^{3/2}) - \sqrt{\frac{2}{5}} f_2^{3/2} \right|^2.$$

From these we obtain two relations between the cross sections σ^t which are not difficult to obtain by the method laid down in Refs. 3, 4:

$$\sigma_1^t + \sigma_2^t + \sigma_3^t + \sigma_4^t + \sigma_5^t + \sigma_6^t + \sigma_7^t = 2(\sigma_8^t + \sigma_9^t + \sigma_{10}^t + \sigma_{11}^t); \quad (3)$$

$$\sigma_2^t + \sigma_5^t + \sigma_{11}^t = \sigma_1^t + \sigma_4^t + 2(\sigma_6^t + \sigma_8^t) + \sigma_{10}^t. \quad (4)$$

Close to the reaction threshold of (1), the pions are formed in an S state. Since the coordinate part of the wave function of the system of three pions in the final state must be symmetric relative to permutations of the pions, then, close to the reaction threshold, only the amplitudes A_t^T are different from zero.

Substituting $B_t^T = f_t^T = g_t^T = h_t^T = 0$ in (2), we obtain the following relations between the differential cross sections close to the reaction threshold:

$$4\sigma_1 = \sigma_2, \quad 4\sigma_4 = \sigma_5, \quad 9\sigma_9 = \sigma_8,$$
$$\sigma_7 = \frac{1}{9}\sigma_6 = \frac{1}{4}\sigma_{11} = \sigma_{10}, \quad \sigma_1 + \sigma_4 = 2\sigma_9 + \sigma_7, \quad (5)$$

while for the total cross sections,

$$4\sigma_1^t = \sigma_2^t, \quad 4\sigma_4^t = \sigma_5^t, \quad 3\sigma_9^t = 2\sigma_8^t,$$
$$3\sigma_7^t = 2\sigma_6^t = \frac{3}{2}\sigma_{11}^t = 6\sigma_{10}^t, \quad 2\sigma_1^t + 2\sigma_4^t = 2\sigma_9^t + \sigma_7^t. \quad (6)$$

As is seen from (2), the $\pi^+ + p \to n + \pi^+ + \pi^+ + \pi^0$ is forbidden close to the threshold.

The same relations hold away from the reaction threshold if the three pions in reaction (1) are formed with identical momenta ($\mathbf{k}_1 = \mathbf{k}_2 = \mathbf{k}_3$), since in this case also the wave function is symmetric relative to the coordinates of the pions.

Now let us consider the transformation of a pion into three pions during collisions of pions with deuterons, i.e., the reaction

$$\pi + d \to n' + n'' + \pi' + \pi'' + \pi'''. \quad (7)$$

The isotopic spin of the entire system T in the initial and final states of the system is unity. We denote by $A_{t_1t_2}$, $B_{t_1t_2}$, $f_{t_1t_2}$, $g_{t_1t_2}$, $h_{t_1t_2}$ the amplitudes of the transition to a state with isotopic spins of the system of the two nucleons t_1 and the system of three pions t_2, and with a definite type of symmetry of the coordinate part of the wave function of the pions.

For the differential cross sections σ of the different processes, we have

$$\sigma_1(\pi^+ + d \to p + p + \pi^0 + \pi^0 + \pi^0) = \left| \frac{3}{\sqrt{2}} A_{11} \right|^2,$$

$$\sigma_2(\pi^+ + d \to p + p + \pi^0 + \pi^+ + \pi^-) = \left| \frac{1}{\sqrt{2}} A_{11} + \frac{1}{\sqrt{2}} f_{11} - B_{10} + \frac{1}{\sqrt{30}}(f_{12} + 2g_{12}) \right|^2,$$

$$\sigma_3(\pi^+ + d \to p + n + \pi^+ + \pi^0 + \pi^0) = \left| \frac{1}{2} A_{11} + \frac{1}{2} f_{11} - \frac{1}{\sqrt{2}} A_{01} - \frac{1}{\sqrt{2}} f_{01} + \sqrt{\frac{3}{20}} f_{12} \right|^2,$$

$$\sigma_4(\pi^+ + d \to p + n + \pi^+ + \pi^+ + \pi^-) = \left| A_{11} - \sqrt{2} A_{01} - \frac{1}{2} f_{11} + \frac{1}{\sqrt{2}} f_{01} + \sqrt{\frac{3}{20}} f_{12} \right|^2,$$

$$\sigma_5(\pi^+ + d \to n + n + \pi^+ + \pi^+ + \pi^0) = \left| \sqrt{\frac{6}{5}} f_{12} \right|^2,$$

$$\sigma_6(\pi^0 + d \to p + p + \pi^- + \pi^0 + \pi^0) = \left| \frac{1}{\sqrt{2}} A_{11} + \frac{1}{\sqrt{2}} f_{11} - \sqrt{\frac{3}{10}} f_{12} \right|^2, \quad (8)$$

$$\sigma_7(\pi^0+d\to p+p+\pi^-+\pi^++\pi^-)=\left|\sqrt{2}A_{11}-\frac{1}{\sqrt{2}}f_{11}-\sqrt{\frac{3}{10}}f_{12}\right|^2,$$

$$\sigma_8(\pi^0+d\to p+n+\pi^0+\pi^0+\pi^0)=\left|\frac{3}{\sqrt{2}}A_{01}\right|^2,$$

$$\sigma_9(\pi^0+d\to p+n+\pi^0+\pi^++\pi^-)=\left|\frac{1}{\sqrt{2}}A_{01}+\frac{1}{\sqrt{2}}f_{01}+\frac{1}{\sqrt{2}}B_{10}-\frac{1}{\sqrt{15}}(f_{12}+2h_{12})\right|^2.$$

We then obtain two relations between the total cross sections which are also easily obtained with the method outlined in Refs. 3, 4:

$$\sigma_1^t+\sigma_2^t+\sigma_3^t+\sigma_4^t+\sigma_5^t=2(\sigma_6^t+\sigma_7^t)+\sigma_8^t+\sigma_9^t; \quad (9)$$

$$\sigma_4^t+\sigma_7^t=2\sigma_1^t+\sigma_3^t+\sigma_6^t+\sigma_8^t. \quad (10)$$

Close to the threshold of the reaction (7), and also in the formation in this reaction of pions with identical momenta, we have

$$B_{t_1t_2}=f_{t_1t_2}=g_{t_1t_2}=h_{t_1t_2}=0.$$

In these cases the following relations are valid between the differential cross sections:

$$4\sigma_3=\sigma_4,\quad 9\sigma_9=\sigma_8,\quad \tfrac{1}{9}\sigma_1=\sigma_2=\sigma_6=\tfrac{1}{4}\sigma_7, \quad (11)$$

and between the total cross sections:

$$4\sigma_3^t=\sigma_4^t,\quad \tfrac{1}{2}\sigma_9^t=\tfrac{1}{3}\sigma_8^t,\quad 2\sigma_3^t=\sigma_2^t+\sigma_9^t,\quad \tfrac{1}{3}\sigma_1^t=\tfrac{1}{2}\sigma_2^t=\sigma_6^t=\tfrac{1}{2}\sigma_7^t. \quad (12)$$

The reaction $\pi^+ + d \to n + n + \pi^+ + \pi^+ + \pi^0$ is forbidden in the cases under consideration.

For processes of transformation of a single pion into three, for which splitting of the deuteron does not occur, we have

$$\sigma_1(\pi^++d\to d+\pi^++\pi^0+\pi^0)=\sigma_2(\pi^0+d\to d+\pi^0+\pi^++\pi^-)=|A_{01}+f_{01}|^2,$$

$$\sigma_3(\pi^++d\to d+\pi^++\pi^++\pi^-)=|2A_{01}+g_{01}|^2,$$

$$\sigma_4(\pi^0+d\to d+\pi^0+\pi^0+\pi^0)=|3A_{01}|^2. \quad (13)$$

Close to the threshold of the reaction under consideration, and also for $\mathbf{k}_1=\mathbf{k}_2=\mathbf{k}_3$, we obtain the following relations between the differential cross sections:

$$\sigma_1=\sigma_2=\tfrac{1}{4}\sigma_3=\tfrac{1}{9}\sigma_4, \quad (14)$$

and between the total cross sections:

$$\sigma_1^t=\tfrac{1}{2}\sigma_2^t=\tfrac{1}{4}\sigma_3^t=\tfrac{1}{3}\sigma_4^t. \quad (15)$$

2. We consider the reaction of photoproduction of three pions in hydrogen and deuterium. The operator of interaction of the electromagnetic field with the meson-nucleon system consists of two parts $H = S + V_3$,[5] where S is a scalar and V_3 the three components of a vector in isotopic space.

The isotopic spin of the initial state in the reaction $\gamma + p \to n' + \pi' + \pi'' + \pi'''$ is $T = 1/2$, and in the final state, $T = 1/2$ and $3/2$.

The operator S gives the transitions to a state of the meson-nucleon system with isotopic spin $T = 1/2$, the operator V_3, those to the state with $T = 1/2, 3/2$.

We denote by $A^T_{tS(V)}$, $B^T_{tS(V)}$, $f^T_{tS(V)}$, $g^T_{tS(V)}$ and $h^T_{tS(V)}$ the amplitudes of transition (the operator S or V_3 is acting) to a state with total isotopic spin T and isotopic spin of the system of three pions t and with a definite type of symmetry of the coordinate wave function of the pions.

We have for the differential cross sections σ of the different processes:

$$\sigma_1(\gamma+p\to p+\pi^0+\pi^0+\pi^0)=9\left|\frac{1}{\sqrt{3}}A_{1S}^{1/2}-\frac{1}{3}A_{1V}^{1/2}+\frac{\sqrt{2}}{3}A_{1V}^{3/2}\right|^2,$$

$$\sigma_2(\gamma+p\to p+\pi^0+\pi^++\pi^-) \quad (16)$$

$$=\frac{1}{9}\left|-\sqrt{3}(A_{1S}^{1/2}+f_{1S}^{1/2})+(A_{1V}^{1/2}+f_{1V}^{1/2})-\sqrt{2}(A_{1V}^{3/2}+f_{1V}^{3/2})-3B_{0S}^{1/2}+\sqrt{3}B_{0V}^{1/2}+(g_{2V}^{3/2}-h_{2V}^{3/2})\right|^2,$$

$$\sigma_3(\gamma+p\to n+\pi^++\pi^0+\pi^0)=\frac{1}{9}\left|\sqrt{6}(A_{1S}^{1/2}+f_{1S}^{1/2})-\sqrt{2}(A_{1V}^{1/2}+f_{1V}^{1/2})-(A_{1V}^{3/2}+f_{1V}^{3/2})+\sqrt{3}f_{2V}^{3/2}\right|^2,$$

$$\sigma_4(\gamma+p\to n+\pi^++\pi^++\pi^-)=\frac{1}{9}\left|\sqrt{6}(2A_{1S}^{1/2}-f_{1S}^{1/2})-\sqrt{2}(2A_{1V}^{1/2}-f_{1V}^{1/2})-(2A_{1V}^{3/2}-f_{1V}^{3/2})+\sqrt{3}f_{2V}^{3/2}\right|^2.$$

We then obtain the following inequality between the total cross sections σ^t:

$$3\sigma_2^t\geqslant 2\sigma_1^t. \quad (17)$$

Substituting in (16)

$$B^T_{tS(V)}=f^T_{tS(V)}=g^T_{tS(V)}=h^T_{tS(V)}=0,$$

we get the following relation between the differential cross sections σ close to the threshold of the reaction:

$$9\sigma_2=\sigma_1,\quad 4\sigma_3=\sigma_4, \quad (18)$$

and between the total cross sections:

$$3\sigma_2^t=2\sigma_1^t,\quad 4\sigma_3^t=\sigma_4^t. \quad (19)$$

We now determine the cross section of photoproduction of three pions in deuterium. The isotopic spin of the initial state in the reaction $\gamma + d \to n_1 + n_2 + \pi' + \pi'' + \pi'''$ is equal to zero. The isotopic spin of the final state $T = 0$ or 1. The corresponding operators of six transition are S and V_3.

We denote by $A^{t_1}_{tS(V)}$, $B^{t_1}_{tS(V)}$, $f^{t_1}_{tS(V)}$, $g^{t_1}_{tS(V)}$ and $h^{t_1}_{tS(V)}$ the amplitudes of transition to a state with isotopic spin of the system of two nucleons t_1 and of the system of three pions t, and with a definite type of symmetry of the coordinate wave function of the pions.

For the differential cross sections σ of the various processes, we have:

$$\sigma_1(\gamma + d \to p + n + \pi^0 + \pi^0 + \pi^0) = \frac{3}{2}\left| A^1_{1S} - A^0_{1V} \right|^2,$$

$$\sigma_2(\gamma + d \to p + n + \pi^0 + \pi^+ + \pi^-) = \frac{1}{6}\Big| -(A^1_{1S} + f^1_{1S}) + (A^1_{1V} + f^1_{1V}) + B^1_{0V} + \sqrt{3}B^0_{0S} + 2(g^1_{2V} - h^1_{2V}) \Big|^2,$$

$$\sigma_3(\gamma + d \to n + n + \pi^+ + \pi^0 + \pi^0) = \Big| \frac{1}{\sqrt{3}}(A^1_{1S} + f^1_{1S}) + \frac{1}{3}(A^1_{1V} + f^1_{1V}) - f^1_{2V} \Big|^2, \tag{20}$$

$$\sigma_4(\gamma + d \to n + n + \pi^+ + \pi^+ + \pi^-) = \Big| \frac{1}{\sqrt{3}}(2A^1_{1S} - f^1_{1S}) + \frac{1}{3}(2A^1_{1V} - f^1_{1V}) - f^1_{2V} \Big|^2.$$

We then obtain the following inequality:

$$3\sigma^t_2 \geqslant 2\sigma^t_1. \tag{21}$$

Close to the reaction threshold under consideration,

$$B^{t_1}_{tS(V)} = f^{t_1}_{tS(V)} = g^{t_1}_{tS(V)} = h^{t_1}_{tS(V)} = 0.$$

Therefore, close to the threshold of the reaction, the following relations hold between the differential cross sections σ and between the total cross sections σ^t:

$$9\sigma_2 = \sigma_1, \qquad 4\sigma_3 = \sigma_4, \tag{22}$$

$$3\sigma^t_2 = 2\sigma^t_1, \qquad 4\sigma^t_3 = \sigma^t_4. \tag{23}$$

For reactions which take place without splitting of the deuteron, $t = 0$ or 1; therefore, $\sigma(\gamma + d \to d + \pi^0 + \pi^0 + \pi^0) = \frac{3}{2}|A^0_{1V}|^2$,

$$\sigma(\gamma + d \to d + \pi^+ + \pi^- + \pi^0) = \Big| \frac{1}{\sqrt{6}}(A^0_{1V} + f^0_{1V}) + \frac{1}{\sqrt{2}}B^0_{0S} \Big|^2. \tag{24}$$

It then follows that

$$3\sigma^t(\gamma + d \to d + \pi^+ + \pi^- + \pi^0) \geqslant 2\sigma^t(\gamma + d \to d + \pi^0 + \pi^0 + \pi^0). \tag{25}$$

Close to the threshold of the reaction under consideration, $B^0_{0S} = f^0_{1V} = 0$. therefore, the following equations hold between the differential cross sections σ and between the total cross sections σ^t:

$$9\sigma(\gamma + d \to d + \pi^+ + \pi^- + \pi^0) = \sigma(\gamma + d \to d + \pi^0 + \pi^0 + \pi^0); \tag{26}$$

$$3\sigma^t(\gamma + d \to d + \pi^+ + \pi^- + \pi^0) = 2\sigma^t(\gamma + d \to d + \pi^0 + \pi^0 + \pi^0). \tag{27}$$

The relations obtained between the differential cross sections (18), (22) and (26) also hold away from the threshold of the reaction if the three pions in the reactions are formed with identical momenta $\mathbf{k}_1 = \mathbf{k}_2 = \mathbf{k}_3$.

I thank Prof. I. M. Shmushkevich for discussion of the results and advice on completing the present research.

[1] N. V. Dushin, Dokl. Akad. Nauk SSSR **106**, 977 (1956).

[2] L. Landau and E. Lifshitz, Квантовая механика, (Quantum mechanics) Moscow, Gostekhizdat, 1948.

[3] I. Shmushkevich, Dokl. Akad. Nauk SSSR **103**, 235 (1955)

[4] N. Dushin and I. Schmushkevich, Dokl. Akad. Nauk SSSR **106**, 801 (1956).

[5] K. M. Watson, Phys. Rev. **85**, 852 (1952).

Translated by R. T. Beyer
183

TIME REVERSAL AND POLARIZATION PHENOMENA IN REACTIONS INVOLVING GAMMA-QUANTA

L. I. LAPIDUS

Joint Institute for Nuclear Research

Submitted to JETP editor October 11, 1957

J. Exptl. Theoret. Phys. (U.S.S.R.) **34**, 922-930 (April, 1958)

Polarization phenomena in the photoproduction and radiative capture of pions as well as in the Compton effect are treated. Consequences of invariance under time reversal are studied. Wolfenstein's theorems are generalized to the case of reactions involving γ-quanta.

1. INTRODUCTION

ADVANCES in experimental technique lead one to hope that in the near future polarization experiments will become possible in such elementary reactions as the Compton effect on nucleons, photoproduction of pions and photodisintegration of the deuteron. In this connection we meet the problem of treating polarization phenomena in reactions involving γ-rays, delineating independent experiments and setting up a complete set of experiments which would be needed for reconstructing the reaction amplitude. In determining the number of independent experiments, in addition to invariance under rotations and space inversions, the consideration of symmetry under time reversal and the unitarity condition are important.

The present paper treats polarization phenomena in the photoproduction of pions and the Compton effect on nucleons. Invariance of the interaction with respect to time reversal leads to relations not only between unpolarized (spin-averaged) cross sections, but also between the polarization phenomena in inverse reactions. Although it has been asserted[1-4] that Wolfenstein's theorems are valid for elastic scattering and nuclear reactions, they require a separate consideration in the phenomenological analysis of reactions involving γ-rays. Wolfenstein's theorems are generalized to such reactions in the present paper.

The condition of unitarity of the S-matrix, which encompasses elastic scattering of pions by nucleons

$$-p\to -p,\ 0n\to 0n;\ +n\to +n,\ 0p\to 0p;$$

exchange scattering

$$-p\rightleftarrows 0n,\ +n\rightleftarrows 0p;$$

photoproduction and radiative capture

$$+n\rightleftarrows\gamma p,\ -p\rightleftarrows\gamma n,\ 0n\rightleftarrows\gamma n,\ 0p\rightleftarrows\gamma p$$

and the Compton effect

$$\gamma p\to\gamma p,\ \gamma n\to\gamma n,$$

enables us to introduce three real phases and three transformation parameters for each state. This enables us to determine the necessary number of experiments, and this number decreases if we take isotopic invariance into account. The unitarity conditions are treated in the Appendix.

2. PHOTOPRODUCTION OF PIONS AND RADIATIVE CAPTURE

To find the photoproduction amplitude, we first represent it as

$$M = a + \mathbf{b}\sigma. \tag{1}$$

Since the amplitude M must be a pseudoscalar, the quantities **a** and **b** must be a pseudoscalar and a vector, constructed from the polarization vector **e**, and the vectors $\mathbf{n}' = [\mathbf{q}\times\mathbf{k}]$, $\pi' = \mathbf{q}+\mathbf{k}$, $\Delta' = \mathbf{q}-\mathbf{k}$, where **q** and **k** are the momenta of the pion and photon, respectively. The construction of the photoproduction amplitude and the investigation of the consequences of invariance under time reversal for the case of photoproduction of pions on nucleons has been done in many papers.[5-7] By using gauge invariance, the expression for M can be represented as

$$M_{\pi\gamma} = A(\sigma\mathbf{e}) + B(\sigma\mathbf{q})(\mathbf{eq}) + C(\mathbf{en}') + D(\sigma\mathbf{k})(\mathbf{qe}). \tag{2}$$

For the inverse reaction — radiative capture, we find from the same considerations

$$M_{\gamma\pi} = A'(\sigma\mathbf{e}) + B'(\sigma\mathbf{q})(\mathbf{eq}) + C'(\mathbf{en}') + D'(\sigma\mathbf{k})(\mathbf{qe}). \tag{2'}$$

If ω_0 and ω_1 are functions describing one nu-

cleon, and nucleon plus meson, respectively, then, for example,

$$A \equiv (\omega_1, \hat{D}\omega_0), \quad A' \equiv (\omega_0, \hat{D}\omega_1),$$

where the effect of the time reversal operator K on the functions ω_0 and ω_1 reduces to

$$K\omega_0 = \omega_0, \quad K\omega_1 = -\omega_1,$$

and the requirement of invariance under time reversal gives

$$K\hat{D}K^{-1} = \hat{D}^+.$$

Repeating the arguments of Watson,[5] one can show that $A' = -A$. Similarly $B' = -B$, $C' = +C$, $D' = -D$. Thus

$$M_{\pi\gamma} = A(\sigma e) + B(\sigma q)(eq) + C(en') + D(\sigma k)(qe) = M,$$

$$-M_{\gamma\pi} = A(\sigma e) + B(\sigma q)(eq) - C(en') + D(\sigma k)(qe) = M'. \tag{3}$$

From the transversality of γ-quanta, $(ek) = 0$ and

$$B(\sigma q)(eq) + D(\sigma k)(eq) = \delta'(\sigma\pi')(e\pi') + \gamma'(\sigma\Delta')(e\Delta').$$

If we go over to the orthonormal vectors π, Δ and n and use the relation

$$(\sigma e) = (\sigma n)(en) + (\sigma\pi)(e\pi) + (\sigma\Delta)(e\Delta),$$

we obtain finally

$$M = \alpha(en) + \beta(\sigma n)(en) + \gamma(\sigma\Delta)(e\Delta) + \delta(\sigma\pi)(e\pi); \tag{4}$$

$$M' = -\alpha(en) + \beta(\sigma n)(ne) + \gamma(\sigma\Delta)(e\Delta) + \delta(\sigma\pi)(e\pi). \tag{4'}$$

For the cross section for production of mesons by unpolarized γ-quanta on unpolarized protons, we get (omitting the statistical factor, as we shall do throughout the paper)

$$2I_0(\theta) = |\alpha|^2 + |\beta|^2 + |\gamma|^2 \cos^2\frac{\theta}{2} + |\delta|^2 \sin^2\frac{\theta}{2}. \tag{5}$$

In view of the relation ("semidetailed" balancing) between the cross sections

$$I_0(\gamma n \to -p) = I_0(-p \to \gamma n)$$

it may turn out that it is not entirely hopeless to attempt experimental investigation of photoproduction by studying the inverse process — radiative capture of the π^--meson by a proton. Although such experiments are very difficult, their accomplishment will make it possible to get information concerning photoproduction on the free neutron by monochromatic γ-rays.

The relation between the nucleon polarization $\langle\sigma\rangle_f$ in photoproduction, when the γ-quanta and target are unpolarized, and the additional photoproduction cross section I_p

$$I = I_0 + I_p = \tfrac{1}{4}\operatorname{Sp} M^+M + \tfrac{1}{4}\operatorname{Sp} M^+M\sigma_1 \cdot \mathbf{N}, \quad \mathbf{N} \equiv \langle\sigma\rangle_i,$$

when the target is polarized, i.e., a Wolfenstein theorem of the form

$$I_p = I_0 \langle\sigma_1\rangle_f \mathbf{N}$$

follows from representing the amplitude as in (1) and using arguments concerning time reversal.[2] The expression for the polarization of the nucleon can be put in the form

$$2I_0(\theta)\langle\sigma\rangle_f = \mathbf{n}\left\{\alpha^+\beta + \alpha\beta^+ + \frac{i}{2}(\gamma\delta^+ - \gamma^+\delta)\sin\theta\right\}. \tag{6}$$

Let us continue our consideration of photoproduction of mesons by polarized γ-quanta on an unpolarized target.

We know that the state of polarization of a particle of spin 1 can be prescribed by giving the average values of the operators $T_{1,\pm1}$, $T_{1,0}$, $T_{2,\pm1}$, $T_{2,0}$ and $T_{2,\pm2}$, which are constructed from the spin operator.[6] Because of the transversality of γ-quanta, in a completely polarized beam, $\langle T_{1,\pm1}\rangle = \langle T_{2,\pm1}\rangle = 0$,[9] so that the expression for the cross section for photoproduction of mesons by a partially polarized beam of quanta can be written as

$$I(\theta, \varphi) = I_0(\theta) + \langle T_{2,0}\rangle_i \tfrac{1}{4}\operatorname{Sp} MT_{2,0}M^+$$

$$+ \langle T_{2,2}\rangle_i \tfrac{1}{4}\operatorname{Sp} MT_{2,2}M^+ + \langle T_{2,-2}\rangle_i \tfrac{1}{4}\operatorname{Sp} MT_{2,-2}M^+. \tag{7}$$

We note first that, after averaging over the nucleon spin,

$$\operatorname{Sp} MSM^+ = 0 \tag{8}$$

(where S is the spin of the photon). This result is immediately obvious if we use the formula

$$(f\mathrm{S}g) = -i[fg].$$

for functions of the type $f = (fe)$ and $g = (ge)$.

The same result is obtained if we calculate the average value of the spin vector of the photon which is produced in the radiative capture of mesons by unpolarized protons. This result is very general. This is the reason why there is no term proportional to cos φ in the expression for the cross section of a reaction induced by a polarized beam of γ-quanta.

In calculating the remaining terms in (7) and the average values of the tensors $T_{2,\pm2}$, $T_{2,0}$ after radiative capture, we use the formula[4]

$$(S_iS_k + S_kS_i)\,M = 2M\delta_{ik} - (M_ie_k + M_ke_i). \qquad (9)$$

For the tensors which are different from zero, we have

$$\frac{1}{4}\,\mathrm{Sp}\,MT_{2,\pm2}M^+ = \frac{\sqrt{3}}{4}\{(|\alpha|^2 + |\beta|^2)(n_y^2 - n_x^2 \mp 2in_xn_y)$$

$$+ |\gamma|^2(\Delta_y^2 - \Delta_x^2 \mp 2i\Delta_x\Delta_y) + |\delta|^2(\pi_y^2 - \pi_x^2 \mp 2i\pi_x\pi_y)\};$$

$$\frac{1}{4}\,\mathrm{Sp}\,MT_{2,0}\,M^+ = I_0(\theta)/\sqrt{2};$$

$$2T_{2,\pm2} = \sqrt{3}\{(S_x^2 - S_y^2) \pm i(S_xS_y + S_yS_x)\};$$

$$\sqrt{2}T_{2,0} = 3S_z^2 - 2. \qquad (10)$$

If we choose the z axis to be along the momentum of the γ-ray,

$$\frac{1}{4}\,\mathrm{Sp}\,MT_{2,\pm2}M^+$$

$$= \frac{\sqrt{3}}{4}\left\{|\alpha|^2 + |\beta|^2 - |\gamma|^2\cos^2\frac{\theta}{2} - |\delta|^2\sin^2\frac{\theta}{2}\right\}e^{\pm2i\varphi}$$

and the cross section for meson production by polarized quanta finally becomes

$$I(\theta, \varphi) = I_0(\theta)\left[1 + \frac{1}{\sqrt{2}}\langle T_{2,0}\rangle_i\right.$$

$$\left. + \langle T_{2,2}\rangle_i\frac{\sqrt{3}}{2}\left\{|\alpha|^2 + |\beta|^2 - |\gamma|^2\cos^2\frac{\theta}{2} - |\delta|^2\sin^2\frac{\theta}{2}\right\}\cos 2\varphi\right. \qquad (11)$$

We now turn to the polarization of γ-quanta from radiative capture of π^--mesons by unpolarized protons. For the non-zero average values of tensors

$$I_0(\theta)\langle T_{2,m}\rangle = \frac{1}{4}\,\mathrm{Sp}\,M'T_{2,m}M'$$

we obtain expressions which coincide with (10) if we take the z axis along the direction of the emergent γ-rays from the radiative capture. If we write (11) in the form

$$I(\theta, \varphi) = I_0(\theta) + \langle T_{2,0}\rangle I_{2,0} + \langle T_{2,2}\rangle I_{2,2},$$

the result obtained can be written as

$$I_{2,m} = I_0(\theta)\langle T_{2,m}\rangle, \qquad (12)$$

which is the statement of Wolfenstein's theorem for this reaction.

This means that the study of polarization of γ-quanta in the $-p \rightarrow \gamma n$ reaction gives the same information as the study of photoproduction of mesons by polarized γ-rays. We should add to this the result already mentioned concerning the polarization of the nucleon. Study of the nucleon polarization in radiative capture gives the same information as the investigation of photoproduction on polarized target protons, while the proton polarization in photoproduction is related to the cross section for radiative capture by polarized protons.

To conclude the treatment of polarization phenomena in $\gamma N \rightleftarrows \pi N$ reactions, let us compare the expression for the polarization correlation in radiative capture

$$I_0(\theta)\langle(\sigma a)(T_{ik}b_ic_k)\rangle = \frac{1}{4}\,\mathrm{Sp}\,M'^+(\sigma a)(T_{ik}b_ic_k)\,M'$$

with the additional photoproduction cross section I_{pp}, when the γ-rays and the target are polarized:

$$I_{pp} = \frac{1}{4}\,\mathrm{Sp}\,M(\sigma a)(T_{ik}b_ic_k)\,M^+.$$

For the correlation $I_0 < (\sigma a)(Sb) >$, we have

$$-2I_0(\theta)\langle(\sigma a)(Sb)\rangle$$

$$= -i\{(\alpha^+\gamma - \alpha\gamma^+)(a\Delta)(\pi b) - (\alpha^+\delta - \alpha\delta^+)(a\pi)(\Delta b)\}$$

$$+ \{(\beta^+\gamma + \beta\gamma^+)(a\pi)(b\pi)$$

$$+ (\beta^+\delta + \beta\delta^+)(a\Delta)(b\Delta) + (\gamma^+\delta + \gamma\delta^+)(an)(bn)\}, \qquad (13)$$

from which we see, in particular, that

$$\langle(\sigma n)(S\pi)\rangle = \langle(\sigma n)(S\Delta)\rangle = \langle(\sigma\pi)(Sn)\rangle = \langle(\sigma\Delta)(Sn)\rangle = 0$$

$$2I_0(\theta)\langle(\sigma n)(Sn)\rangle = -(\gamma^+\delta + \gamma\delta^+), \text{ etc.} \qquad (14)$$

For the additional photoproduction cross section we find

$$-\frac{1}{4}\,\mathrm{Sp}\,M(\sigma a)(Sb)\,M^+$$

$$= \frac{i}{2}\{(\alpha\gamma^+ - \alpha^+\gamma)(a\Delta)(\pi b) - (\alpha\delta^+ - \alpha^+\delta)(a\pi)(\Delta b)\}$$

$$+ \frac{1}{2}(\beta^+\gamma + \beta\gamma^+)(a\pi)(b\pi)$$

$$+ (\beta^+\delta + \beta\delta^+)(a\Delta)(b\Delta) + (\gamma\delta^+ + \gamma^+\delta)(an)(bn)\}. \qquad (15)$$

From a comparison of (15) and (13) we see that, knowing the results of investigation of the polarization correlation in radiative capture, i.e., knowing

the combinations $(\alpha\gamma^+ - \alpha^+\gamma)$, $(\alpha\delta^+ - \alpha^+\delta)$ etc., we can predict the results of experiments using polarized beams and target. Consequently, these experiments are not independent.

We also see from (13) and (15) that relations like (12) hold whenever one of the vectors **a** or **b** is along the normal **n**. Similar conclusions follow when **S** is replaced by $T_{2,m}$ in (13) and (15).

We note in conclusion that, in the expression for the polarization of the recoil nucleon in photoproduction by polarized γ-quanta on an unpolarized nucleon,

$$4I(\theta, \varphi)\langle\sigma\rangle_f = \mathrm{Sp}\, M^+\sigma M + \langle T_{1,0}\rangle_i \mathrm{Sp}\, T_{1,0}M^+\sigma M$$

$$+ \langle T_{2,2}\rangle_i \mathrm{Sp}\, T_{2,2}M^+\sigma M + \langle T_{2,-2}\rangle_i \mathrm{Sp}\, T_{2,-2}M^+\sigma M \quad (16)$$

the first term is the same as (6), while the second term is proportional to

$$-i[(\alpha\gamma^+ - \alpha^+\gamma)\Delta_z\pi - (\alpha\delta^+ - \alpha^+\delta)\pi_z\Delta]$$

$$+ (\beta\gamma^+ + \beta^+\gamma)\pi_z\pi + (\beta^+\delta + \beta\delta^+)\Delta_z\Delta.$$

From the last expression we see the correspondence with (13) and (15). A similar correspondence exists for the other terms in (16).

3. COMPTON EFFECT

The Compton effect amplitude can be represented in the form of (1), but for elastic scattering M must be a scalar. Using the standard arguments, including symmetry under time reversal, we find that the most general expression for M is

$$M = A(\mathbf{ee'}) + B(\mathbf{n}[\mathbf{ee'}])$$

$$+ C(\sigma\mathbf{n})(\mathbf{ee'}) + D(\sigma\mathbf{n})(\mathbf{n}\cdot\mathbf{e}\times\mathbf{e'}) + F(\sigma[\mathbf{ee'}])$$

$$+ E\{(\pi\mathbf{e'})(\sigma[\Delta\times\mathbf{e}]) + (\pi\mathbf{e})(\sigma[\Delta\times\mathbf{e'}])\}, \quad (17)$$

where **e** and **e'** are the polarization vectors before and after scattering, **n**, Δ and π are constructed, as before, from the (unit) vectors **k** and **k'** along the direction of the γ-ray momentum before and after scattering. Expression (17) contains six terms, as it should. The expression for M can be given another form*

$$M = R_1(\mathbf{ee'}) + R_2(\mathbf{ss'}) + R_3(\sigma[\mathbf{e'e}]) + R_4(\sigma[\mathbf{s's}])$$
$$+ R_5\{(\sigma\mathbf{k})(\mathbf{s'e}) - (\sigma\mathbf{k'})(\mathbf{se'})\} + R_6\{(\sigma\mathbf{k'})(\mathbf{s'e}) - (\sigma\mathbf{k})(\mathbf{e's})\}, \quad (17')$$

*Addition in proof (March 18, 1958). The author recently learned that formula (17') was found earlier by V. I. Ritus, J. Exptl. Theoret. Phys. (U.S.S.R.) **33**, 1264 (1957); Soviet Physics JETP (in press).

if we introduce the vectors $\mathbf{s} = [\mathbf{k}\times\mathbf{e}]$ and $\mathbf{s'} = [\mathbf{k'}\times\mathbf{e'}]$. Under time reversal, $\mathbf{e} \rightleftarrows -\mathbf{e'}$, $\mathbf{s'} \rightleftarrows \mathbf{s}$.

The amplitude for the Compton effect, up to terms linear in the frequency, has been found in various papers:[10-12]

$$M = \frac{e^2}{m}(\mathbf{ee'}) - \frac{ie}{m}\left(2\mu - \frac{e}{m}\right)k(\sigma[\mathbf{e'}\times\mathbf{e}]) -$$

$$- \frac{2\mu^2 i}{k}(\sigma[\mathbf{s}\times\mathbf{s'}]) - i\frac{e}{m}\frac{\mu}{k}[(\mathbf{ek'})(\sigma\mathbf{s'}) - (\mathbf{e'k})(\sigma\mathbf{s})], \quad (18)$$

Here μ is the magnetic moment of the nucleon.

From (17) we find for the cross section for scattering of an unpolarized γ-ray beam by an unpolarized target:

$$2I_0(\theta) = \{|R_1|^2 + |R_2|^2$$

$$+ 4\mathrm{Re}[R_3^+(R_5 + R_6) + R_4^+R_5]\}(1 + \cos^2\theta)$$

$$+ (|R_3|^2 + |R_4|^2)(3 - \cos^2\theta) + 2(|R_5|^2 + |R_6|^2)(3 + \cos^2\theta)$$

$$+ 4\mathrm{Re}\{(R_1^+R_2) + R_4^+(R_3 - R_6) + R_5^+R_6(2 + \cos^2\theta)\}\cos\theta. \quad (19)$$

The condition of unitarity of the S-matrix leads to the optical theorem[13]

$$k\sigma_t = 4\pi\,\mathrm{Im}[R_1(0°) + R_2(0°)], \quad (20)$$

where σ_t is the total interaction cross section, including both elastic scattering and inelastic processes. From (20) we get for the forward elastic scattering cross section $\sigma_s(0^0)$ the inequality*

$$\sigma_s(0°) \geqslant (k\sigma_t/4\pi)^2, \quad (21)$$

as a consequence of which the elastic scattering at high energies is pushed forward and compressed into the small solid angle

$$\Delta\omega = \pi\theta^2 \ll (4\pi/k\sigma_t)^2\sigma_s. \quad (22)$$

The inequalities (21) and (22) show the basic features of elastic scattering at high energies without appealing to an optical model.

The expression for the polarization of the recoil nucleon, when target and beam are unpolarized,

$$2I_0(\theta)\langle\sigma\rangle_f = \mathbf{n}\sin\theta\, 2\mathrm{Re}\{(R_1^+R_4)$$

$$+ [(R_2^+R_4) - (R_1^+R_3)]\cos\theta - R_2^+R_3\cos 2\theta\}, \quad (23)$$

*The existence of the inequality (21) for elastic scattering of particles was shown in Ref. 14 and, in less general form, by Rarita[15] as well as by Karplus and Ruderman (cf. Ref. 15). This inequality was first published in a brief note by Wick,[16] which went unnoticed.

coincides with the expression for the azimuthal asymmetry in the cross section for the Compton effect on a polarized nucleon. We note that the quantities R_5 and R_6 do not appear in (23).

When the target and beam are unpolarized, the average value of the photon spin (and the corresponding addition to the cross section) become zero, as in the case of photoproduction. This result is obvious from dimensional considerations. In these circumstances the average value of the spin can be directed only along the one pseudovector — the normal $\mathbf{n}$. Since $\langle S_x \rangle = \langle S_y \rangle \equiv 0$ for photons propagating along the z axis, we need only consider $\langle S_z \rangle$, but $\langle S_z \rangle \sim n_z = 0$.

For the non-zero average values of the $T_{2,m}$, we find, using (9),

$$2I_0(\theta)\langle T_{2,\pm 2}\rangle = \sqrt{3}\{|R_4|^2 + \mathrm{Re}\,[R_4^+(R_5 + R_6\cos\theta)]\}\, e^{\pm 2i\varphi};$$

$$\sqrt{2}\, I_0(\theta)\langle T_{2,0}\rangle = I_0(\theta). \qquad (24)$$

For the additional Compton effect cross section when the incident quanta are polarized, we get expressions coinciding with (24).

CONCLUSION

The main content of the present paper is the extension of the consequences of invariance under time reversal to reactions involving γ-quanta. We have treated the examples of the Compton effect, photoproduction, and radiative capture of pions. The generalization to the case of any binary reaction (with two particles in the initial and in the final state), is done similarly.

Aside from its theoretical interest, this result is of interest to experiment, for the same reason that in photodisintegration of the deuteron, the study of the polarization of the nucleons gives the same information as the radiative capture by a polarized nucleon, or the study of polarization of γ-quanta from radiative capture of neutrons by protons is equivalent to studying the cross section for photodisintegration of the deuteron by polarized gamma rays.

The relations between polarization phenomena in inverse reactions, as well as the relation between averaged values, are based on invariance of the interaction under time reversal. However, in contrast to detailed balancing, for the Wolfenstein relation it is essential whether or not spatial parity is conserved. For illustration, let us consider the elastic scattering of a neutrino by a spinless particle. If we do not demand invariance under space and time inversion, the most general form for the scattering amplitude is

$$M = a + b(\sigma\mathbf{n}) + c(\sigma\boldsymbol{\pi}) + d(\sigma\Delta). \qquad (25)$$

The last two terms, which are pseudoscalar for space inversions, transform differently under time reversal. If there is no conservation of spatial parity, but we keep the invariance under time reversal (combined parity), the last term in (25) is absent. Though in this case detailed balancing remains valid (trivially), there is no Wolfenstein relation. With $d = 0$, the polarization resulting from the scattering of an unpolarized beam is

$$I_0(\theta)\langle\sigma\rangle_f = (a^+b + ab^+)\,\mathbf{n} + (ac^+ + a^+c)\,\boldsymbol{\pi} + i(b^+c - c^+b)\,\Delta, \qquad (26)$$

while the additional cross section I_p is

$$(a^+b + ab^+)\,\mathbf{n} + (ac^+ + a^+c)\,\boldsymbol{\pi} - i(b^+c - c^+b)\,\Delta. \qquad (27)$$

Although, as before, polarization and azimuthal asymmetry give the same information (since (26) and (27) differ only in the sign of the last term), there is no Wolfenstein relation.

APPENDIX

Unitarity Conditions

The unitarity conditions together with requirements of invariance determine the number of independent parameters necessary for the phenomenological analysis of the experimental data. If we consider the range of γ-ray energies near 300 Mev where, in the interaction of photons with nucleons, only photoproduction of single pions occurs in addition to the elastic scattering, we introduce a 3-by-3 S-matrix to describe the Compton effect, photoproduction and radiative capture, scattering and charge exchange of mesons. To be specific, let us consider the Compton effect on a proton. In this case we can introduce a unitary S-matrix to describe the processes

$$\begin{array}{lll} +n \to +n\,(S_{11}); & 0p \to +n\,(S_{12}); & \gamma p \to +n\,(S_{13}) \\ +n \to 0p\ (S_{21}); & 0p \to 0p\ (S_{22}); & \gamma p \to 0p\ (S_{23}) \\ +n \to \gamma p\ (S_{31}); & 0p \to \gamma p\ (S_{32}); & \gamma p \to \gamma p\ (S_{33}) \end{array} \qquad (A.1)$$

(the elements of the S-matrix are given in parentheses, and $S_{ki} = S_{ik}$).

If to start with we do not consider isotopic invariance, we must introduce another S-matrix for

the processes which include the Compton effect on the neutron,

$$\begin{array}{lll} -p\to -p\ (S'_{11}); & 0n\to -p\ (S'_{12}); & \gamma n\to -p\ (S'_{13}) \\ -p\to 0n\ (S'_{21}); & 0n\to 0n\ (S'_{22}); & \gamma n\to 0n\ (S'_{23}) \\ -p\to \gamma n\ (S'_{31}); & 0n\to \gamma n\ (S'_{32}); & \gamma n\to \gamma n\ (S'_{33}). \end{array} \quad \text{(A.2)}$$

The unitarity conditions enable us to express (separately for (A.1) and (A.2)) the six independent complex quantities S_{ik} in terms of six real quantities by introducing, for example, three scattering phases δ_1, δ_2, δ_3 and three transformation parameters φ, ψ and θ:

$$S_{11} = e^{2i\delta_1}(\cos\varphi\cos\psi - \cos\theta\sin\varphi\sin\psi)^2 + e^{2i\delta_2}(\sin\varphi\cos\psi + \cos\theta\sin\psi\cos\varphi)^2 + e^{2i\delta_3}\sin^2\theta\sin^2\psi;$$

$$S_{12} = e^{2i\delta_1}(\cos\varphi\cos\psi - \cos\theta\sin\varphi\sin\psi)(\sin\psi\cos\varphi + \cos\theta\sin\varphi\cos\psi)$$

$$+ e^{2i\delta_2}(\sin\varphi\cos\psi + \cos\theta\sin\psi\cos\varphi)(\sin\varphi\sin\psi - \cos\theta\cos\varphi\cos\psi) - e^{2i\delta_3}\sin^2\theta\sin\psi\cos\psi;$$

$$S_{13} = e^{2i\delta_1}\sin\theta\sin\varphi(\cos\varphi\cos\psi - \cos\theta\sin\varphi\sin\psi) - e^{2i\delta_2}\sin\theta\cos\varphi(\sin\varphi\cos\psi + \cos\theta\sin\psi\cos\varphi) + e^{2i\delta_3}\sin\theta\cos\theta\sin\psi;$$

$$S_{22} = e^{2i\delta_1}(\sin\psi\cos\varphi + \cos\theta\sin\varphi\cos\psi)^2 + e^{2i\delta_2}(\sin\varphi\sin\psi - \cos\theta\cos\varphi\cos\psi)^2 + e^{2i\delta_3}\sin^2\theta\cos^2\psi; \quad \text{(A.3)}$$

$$S_{23} = e^{2i\delta_1}\sin\theta\sin\varphi(\sin\psi\cos\varphi + \cos\theta\sin\varphi\cos\psi) + e^{2i\delta_2}\sin\theta\cos\varphi(\cos\theta\cos\varphi\cos\psi - \sin\varphi\sin\psi) - e^{2i\delta_3}\sin\theta\cos\theta\cos\psi;$$

$$S_{33} = e^{2i\delta_1}\sin^2\theta\sin^2\varphi + e^{2i\delta_2}\sin^2\theta\cos^2\varphi + e^{2i\delta_3}\cos^2\theta.$$

If we omit reactions with γ-quanta, i.e., set $\delta_3 = \theta = 0$, only S_{11}, S_{12} and S_{22} are different from zero, and we get from (A.3) the familiar expressions for the elements of the 2-by-2 S-matrix, in which the transformation parameter is $\psi + \varphi$. The quantity θ characterizes the effect of radiative processes.

Instead of introducing real scattering phases and transformation coefficients, one can proceed differently and, to determine a complete set of experiments, make use of the unitarity conditions in the form of a generalization of the optical theorem[17,18] analogous to that for the case of elastic scattering alone, as was done in Ref. 19. The unitarity relations then enable one to reduce the number of necessary experiments (from the point of view of completeness of the phenomenological analysis) to the total number of independent terms in the amplitudes of all the reactions included in the unitary S-matrix. If we include radiative processes, additional terms which are not isotopically invariant appear in the amplitudes for meson-nucleon scattering, and in the general case the total number of terms reaches 20. If we take the matrix elements for photoproduction and Compton effect proportional to e and e^2, respectively, and expand (A.3), we find that in processes of the type of meson scattering the inclusion of radiative processes gives rise to small corrections (of order e^2). We shall therefore take the phases δ_1 and δ_2 to be the same as the phases for $\pi - N$ scattering in the states with isotopic spin $T = 3/2$ and $T = 1/2$, respectively (cf. the Appendix to Reference 20). On the other hand, the influence of $\pi - N$ scattering on the Compton effect is large and determines its magnitude.

Various considerations related to the reduction of the number of parameters in the S-matrix have been presented in Refs. 21, 22. We shall therefore not discuss them here.

Expression (18) for the amplitude of the Compton effect is only approximately unitary since, for example, the right side of (20) becomes zero. However, the restriction

$$\mathrm{Im}\,[R_1(0°) + R_2(0°)] \ll \mathrm{Re}\,[R_1(0°) + R_2(0°)],$$

which is necessary for the validity of (18) is satisfied with plenty to spare.

We note in conclusion that when we include considerations related to isotopic invariance, the same $\pi - N$ scattering phases appear in the S-matrix for the Compton effect on a neutron, and this results in various common features of the Compton effect on protons and neutrons.

[1] L. Wolfenstein and J. Ashkin, Phys. Rev. **85**, 947 (1952). R. H. Dalitz, Proc. Phys. Soc. (London) **A65**, 175 (1952).

[2] L. Wolfenstein, Ann. Rev. Nucl. Sci. **6**, 43 (1956).

[3] A. I. Baz', J. Exptl. Theoret. Phys. (U.S.S.R.) **32**, 628 (1957); Soviet Phys. JETP **5**, 521 (1957).

[4] L. I. Lapidus, J. Exptl. Theoret. Phys. (U.S.S.R.) **33**, 204 (1957); Soviet Phys. JETP **6**, 160 (1958).

[5] T. Nakano and K. Nishijima, Progr. Theor. Phys. **8**, 53 (1952). K. M. Watson, Phys. Rev. **95**, 228 (1954).

[6] E. Fermi, Nuovo Cim. Suppl. (Ser. 10) **2**, No. 1, 17 (1955). M. Kawaguchi and S. Minami, Progr. Theor. Phys. **12**, 789 (1954). M. Gell-Mann and K. M. Watson, Ann. Rev. Nucl. Sci. **4**, 219 (1954). E. Coraldinesi, Nuovo Cim. **4**, 1384 (1956). A. A. Logunov and A. N. Tavkhelidze, J. Exptl. Theoret. Phys. (U.S.S.R.) **32**, 1393 (1957); Soviet Phys. JETP **5**, 1134 (1957).

[7] V. I. Ritus, J. Exptl. Theoret. Phys. (U.S.S.R.) **27**, 660 (1954). M. J. Moravcsik, Phys. Rev. **104**, 1451 (1956).

[8] W. Lakin, Phys. Rev. **98**, 139 (1955).

[9] A. Simon, Phys. Rev. **92**, 1050 (1952).

[10] W. Thirring, Phil. Mag. **41**, 1193 (1950).

[11] F. E. Low, Phys. Rev. **96**, 1428 (1954).

[12] M. Gell-Mann and M. L. Goldberger, Phys. Rev. **96**, 1433 (1950).

[13] R. H. Capps, Phys. Rev. **106**, 1031 (1957).

[14] L. I. Lapidus, J. Exptl. Theoret. Phys. (U.S.S.R.) **31**, 1099 (1956); Soviet Phys. JETP **4**, 937 (1957).

[15] W. Rarita, Phys. Rev. **104**, 221 (1956).

[16] G. C. Wick, Phys. Rev. **75**, 1459(A) (1949).

[17] R. Glauber and V. Schomaker, Phys. Rev. **89**, 667 (1953).

[18] R. M. Ryndin and Ia. A. Smorodinskii, J. Exptl. Theoret. Phys. (U.S.S.R.) **32**, 1584 (1957); Soviet Phys. JETP **5**, 1294 (1957).

[19] Puzikov, Ryndin and Smorodinskii, J. Exptl. Theoret. Phys. (U.S.S.R.) **32**, 592 (1957); Soviet Phys. JETP **5**, 489 (1957).

[20] L. I. Lapidus, J. Exptl. Theoret. Phys. (U.S.S.R.) **34**, 453 (1958); Soviet Phys. JETP **7**, 312 (1958).

[21] A. M. Baldin and V. D. Petrun'kin, J. Exptl. Theoret. Phys. (U.S.S.R.) **32**, 1570 (1957); Soviet Phys. JETP **5**, 1279 (1957).

[22] S. Minami and Y. Yamaguchi, Progr. Theor. Phys. **17**, 651 (1957).

Translated by M. Hamermesh
184

SOVIET PHYSICS JETP VOLUME 34 (7), NUMBER 4 OCTOBER, 1958

POLARIZATION AND ANGULAR DISTRIBUTION OF X-RAYS EMITTED AFTER NUCLEAR CAPTURE OF ELECTRONS AND AFTER CONVERSION TRANSITIONS

A. Z. DOLGINOV

Leningrad Physico-Technical Institute, Academy of Sciences, U.S.S.R.

Submitted to JETP editor October 24, 1957

J. Exptl. Theoret. Phys. (U.S.S.R.) **34**, 931-941 (April, 1958)

Results obtained previously[1] are extended to K and L capture of any order of forbiddenness, taking parity nonconservation into account. It is shown that observation of the correlation of the polarization of x-rays emitted after K or L capture with nuclear spin directions or with the polarization of subsequent gamma rays may provide important information concerning β interactions. The angular distribution of x-rays is anisotropic when capture occurs from the L_{III} subshell.

Formulas are presented which permit determination of the spins and parities of nuclear levels from the observation of x-ray polarization following conversion transitions.

1. POLARIZATION AND ANGULAR DISTRIBUTION OF X-RAYS EMITTED FOLLOWING ELECTRON CAPTURE

IN an earlier paper[1] the author proposed observation of the correlation between the angular polarization of x-rays emitted in the filling of atomic shell vacancies following allowed K capture and the orientation of nuclear spins or the polarization of subsequent gamma radiation. It was shown that information might thus be obtained regarding the relative signs of the scalar and tensor β-interaction constants. A number of recent experiments[2] have confirmed Lee and Yang's[3] hypothesis of par-

ity nonconservation in β decay. We have extended the results of Ref. 1 to take the nonconservation of parity into account.

Allowed K and L captures are of greatest interest in connection with the unambiguous interpretation of experimental results. Correlation calculations for these allowed transitions as well as for forbidden transitions are given in Appendix I. At this point we shll present and discuss the final formulas.

We shall first consider the case in which a nucleus before an allowed K capture is located in an external field and we do not study the direction and polarization of the gamma ray which may be emitted after K capture. When an x-ray is emitted in an electronic transition to a vacated K level from a level with a momentum $I = 1/2$ (such as L_{II}) the correlation between the circular polarization of this x-ray and the nuclear spin orientation is given by

$$W_{j\chi}(\theta) = a + b + \sigma_\chi \rho \{1/2 [j_0(j_0+1) - j_1(j_1+1) + 2] b + \varkappa \sqrt{j_0(j_0+1)}\} \cos\theta; \quad (1)$$

$$a = (|c_S|^2 + |c'_S|^2)\,|K_S|^2 + (|c_V|^2 + |c'_V|^2)\,|K_V|^2 - 2\mathrm{Re}\,(c_S c_V^* - c'_S c'^*_V)\,K_S K_V^*;$$

$$b = (|c_T|^2 + |c'_T|^2)\,|K_T|^2 + (|c_A|^2 + |c'_A|^2)\,|K_A|^2 - 2\mathrm{Re}\,(c_T c_A^* - c'_T c'^*_A)\,K_T K_A^*; \quad (2)$$

$$\varkappa = 2\mathrm{Re}\,[(c_S c_T^* + c'_S c'^*_T)\,K_S K_T^* - (c_V c_T^* - c'_V c'^*_T)\,K_V K_T^* - (c_S c_A^* - c'_S c'^*_A)\,K_S K_A^* + (c_V c_A^* + c'_V c'^*_A)\,K_V K_A^*];$$

$$\rho = \sum_{\mu_0} \mu_0 w(\mu_0) / j_0(j_0+1). \quad (3)$$

θ denotes the angle between the direction of the x-ray and the principal nuclear spin orientation; j_0 is the nuclear spin in the initial state, μ_0 is its projection on the z axis, and $w(\mu_0)$ is the probability of a given value of μ_0; ρ gives the degree of polarization of the nuclear spins; $\sigma_\chi = 1$ or -1, respectively, for right or left circular polarization of the x-rays; c_S, c_V, c_T and c_A are the scalar, vector, tensor and axial-vector (pseudovector) β-interaction constants; c'_S, c'_V, c'_T and c'_A are analogous constants in terms which are allowed only when parity is not conserved (containing in addition $\gamma_5 = \gamma_1\gamma_2\gamma_3\gamma_4$, where $\gamma_4 = -\beta$; γ_1, γ_5 and β are Dirac matrices).

In calculating (1) we have used the general form of the β interaction which was proposed by Lee and Yang.[3] K_S and K_T are nuclear matrix elements for the scalar and tensor β interactions, with K_V and K_A for the vector and pseudovector β interactions. In the nonrelativistic approximation for nucleons $K_S = -K_V$ and $K_T = -K_A$. The expression for the correlation does not depend on the magnitudes of K_S and K_T but only on their ratio K_S/K_T:

$$K_S = \int \psi^*_{j_1\mu_1} \beta \psi_{j_0\mu_0}\, d\mathbf{r},$$

$$C^{j_0\mu_0}_{1\Lambda j_1\mu_1} K_T = (-1)^{1+\Lambda} \int \psi^*_{j_1\mu_1} \beta\sigma_{-\Lambda} \psi_{j_0\mu_0}\, d\mathbf{r}; \quad (4)$$

$\psi_{j_0\mu_0}$ and $\psi_{j_1\mu_1}$ are the nuclear wave functions before and after electron capture; $\sigma_0 = \sigma_z$, $\sigma_{\pm1} = \pm\sqrt{1/2}\,(\sigma_x \pm i\sigma_y)$; σ_x, σ_y, σ_z are Pauli matrices; $C^{j_0\mu_0}_{1\Lambda j_1\mu_1}$ is a Clebsch-Gordan coefficient; j_1 and μ_1 are the nuclear spin and its projection after K capture. The matrix elements K_S and K_T are independent of the magnetic quantum numbers μ_0, μ_1 and Λ.

If a gamma ray is emitted after K capture, for the determination of a, b and κ it is possible to study the correlation between the circular polarizations of the x-ray and gamma ray. It is then not necessary to use oriented nuclei. If the x-ray is emitted in an electronic transition to the K shell from a level of mechanical moment $I = 1/2$ and the gamma ray is of multipole order 2^L the correlation is given by

$$W_{\gamma\chi}(\theta) = a + b - \sigma_\chi\sigma_\gamma [j_1(j_1+1) - j_2(j_2+1) + L(L+1)] \times [4j_1(j_1+1)L(L+1)]^{-1} \{[j_1(j_1+1) - j_0(j_0+1) + 2]\, b + 2\varkappa \sqrt{j_1(j_1+1)}\} \cos\theta. \quad (5)$$

Here θ is the angle between the directions of the x-ray and gamma ray, and $\sigma_\gamma = 1$ or -1 for right or left circular polarization of the gamma ray.

For mixed 2^L magnetic and 2^{L+1} electric multipole transitions $[j_1(j_1+1) - j_2(j_2+1) + L(L+1)]$ must be replaced by

$$\{j_1(j_1+1) - j_2(j_2+1) + L(L+1) + f^2(2L+3)^{-1/2} L [j_1(j_1+1) - j_2(j_2+1) + (L+1)(L+2)] - 2fL(L+2)[L(j_2+j_1+L+2)(j_2+j_1-L) \times (j_1-j_2+L+1) \times (j_2-j_1+L+1)/(2L+1)]^{1/2} (2L+3)^{-1}\};$$

f^2 is the ratio of the electric and magnetic radiation intensities, with $f = \pm|f|$.

If the emission of the observed gamma ray does not directly follow K capture, but is separated from the latter by cascade emission of one or more photons which are not observed the curly bracket in (5) must be preceded by the factor[4]

$$\prod_{k=1}^{N-1}\left\{\frac{j_k(j_k+1)+j_{k+1}(j_{k+1}+1)-L_k(L_k+1)}{2[j_k(j_k+1)\,j_{k+1}\,(j_{k+1}+1)]^{1/2}}\right\}, \qquad (6)$$

where L_k is the multipole order of the intermediate photons:

$$j_0(K)\,j_1(L_1)\,j_2(L_2)\,j_3\cdot\cdot\cdot\cdot\cdot j_N(L)\,j_{N+1},$$

while L is the multipole order of the observed photon. If one of the intermediate gamma transitions is mixed, the expressions for magnetic and electric transitions must be added with weights proportional to their intensities. Interference terms drop out upon integration over the angles of gamma emission.

When an electron fills a vacancy in a K shell by a transition from a level with $I = 3/2$ (such as L_{III}), then in (1) and (5) σ_x must be preceded by the factor $-1/2$. Since the transition probability from an $I = 3/2$ level is almost twice as large as from $I = 1/2$ the total correlation is very small. It is therefore necessary to determine the polarization of x-rays coming from $I = 3/2$ and $I = 1/2$, separating them according to their energies. It is most convenient to study the K_{α_1} and K_{α_2} lines. It must be kept in mind that an external magnetic field can change the separations and order of atomic levels. The character of this change for different specific cases is easily established either experimentally or theoretically.

We note that for atoms where the $P_{3/2}$ shell has not been completely built up the polarization of photons coming from the $P_{1/2}$ level is not entirely compensated by the opposite polarization of photons coming from the $P_{3/2}$ level, and it is not necessary to distinguish them energetically. In this case it is best to use the lightest nuclei, where the L shell is not filled. Light nuclei in which K capture occurs possess short lifetimes as a rule and are not easily used in experiments requiring the orientation of nuclear spins. It is then easier to investigate the polarization correlation of x-rays and gamma rays.

For allowed L_I or L_{II} capture, the correlation is of the same character as for K capture. However, in this case there is incomplete compensation of right and left circular polarization for the combined L_β, L_γ, etc. radiation. A theoretical calculation of the remaining degree of polarization is difficult and would require good knowledge of the electronic wave functions.

For K, L_I, and L_{II} capture the correlations (1) and (5) exist only if the nuclei possess dipolar polarization; these correlations do not exist for aligned nuclei, which can be used only to study L_{III} capture. In this case there will be an anisotropic angular distribution of x-rays relative to the orientation of the aligned nuclei. For unoriented nuclei with L_{III} capture followed by gamma-ray emission there exists an angular correlation between x-rays and gamma rays. Only the tensor and pseudovector interactions contribute to allowed L_{III} capture. The x-ray angular distribution is given by

$$W(\theta) = 1 + \sqrt{3(2j_0+1)/10}\,A_I W(j_1 1 j_0 2;\ j_0 1)$$
$$\times\,(3\cos^2\theta - 1)\,P_{20}^{j};$$
$$A_{1/2} = 1/2,\quad A_{3/2} = -2/5,\quad A_{5/2} = 1/10. \qquad (7)$$

The quantities A_I depend only on the total angular momentum I of the electron which fills the vacancy in the L_{III} subshell. W(abcd; ef) is the Racah function. For aligned nuclei without investigation of the possible gamma rays we have

$$P_{20}^{j} = 5\sum_{\mu_0}[3\mu_0^2 - j_0(j_0+1)]$$
$$\times\,w(\mu_0)\,[(2j_0-1)\,j_0(j_0+1)(2j_0+3)]^{-1/2}. \qquad (8)$$

When the angular correlation of x-rays and gamma rays is investigated for unoriented nuclei we have

$$P_{20}^{j} = 5\sqrt{(2j_1+1)(2L+1)}\left[1 - \frac{3}{L(L+1)}\right]$$
$$\times\,W(j_2 L j_1 2;\ j_1 L)\,C_{L020}^{L0}. \qquad (9)$$

Equation (7) does not contain nuclear matrix elements of L capture nor the constants c and c′, which are included within a general factor that goes not influence the angular correlation (7) and is therefore omitted here.

A study of the correlation expressed by (7) does not provide information concerning β interactions, but it can serve for determination of the angular momenta of nuclear levels.

The existing experimental information concerning the constants c and c′ is incomplete and contradictory according to the present theory. There is therefore considerable interest in the determination of combinations of c and c′ which have not yet been investigated. a, b, and κ in (1) and (5)

are among such combinations, and a study of these equations may throw light on the nature of β interactions. We note that the expression for the polarization of β particles emitted by polarized nuclei[5] also contains c and c′ in combinations similar to a, b and κ; but the same expression contains c and c′ in other combinations. Therefore (1) and (5) can be interpreted more simply and unambiguously.

For forbidden K and L capture, the polarization and angular correlations of x-rays can be determined from (25). For first forbiddenness N = 1; L and L′ = 0, 1, 2; i = ½ and ⅜. For $j_1 = j_0 \pm 2$ in capture from the L_{III} subshell the correlation formula agrees with (7) if $\sqrt{3}\, W(j_1 1 j_0 2; j_0 1)$ is replaced by $\sqrt{7}\, W(j_1 2 j_0 2; j_0 2)$. For forbidden K, L_I and L_{II} captures the correlation formulas are more complicated than (1) and (5) as they contain some unknown ratios of nuclear matrix elements which must be determined experimentally.

2. POLARIZATION AND ANGULAR DISTRIBUTION OF X-RAYS FOLLOWING CONVERSION TRANSITIONS

In Ref. 1 it was shown that observation of the circular polarization of x-rays emitted when vacancies in atomic shells are filled following conversion transitions of oriented nuclei can provide the same information regarding nuclear levels that comes from experiments on the angular correlation of conversion electrons and subsequent (or preceding) gamma rays. When gamma rays are emitted following conversion transitions, instead of using oriented nuclei we can study the correlation between the circular polarizations of x-rays and gamma rays.

Appendix II contains the derivation of the general formula for the conversion transition probability of an oriented nucleus with subsequent emission of x-rays and gamma rays of given polarization. We shall here give the final formulas for the most important cases. We first consider a conversion transition by an oriented nucleus when subsequent gamma rays do not interest us. For K-shell conversion, when the vacancy is filled by an electron with I = ½ (let us say $p_{1/2}$), the circular polarization of the x-rays, according to (25), (41) and (42) is given by

$$W_{j_0 X}(\theta) = 1 + \sigma_X \rho \,[j_0(j_0+1) - j_1(j_1+1) + L(L+1)]\, Q_L \cos\theta; \qquad (10)$$

$$Q_L = \frac{1}{2L(L+1)} \frac{(L+1)\left|B_L^-\right|^2 - L\left|B_L^+\right|^2}{(L+1)\left|B_L^+\right|^2 + L\left|B_L^-\right|^2}. \qquad (11)$$

For an EL electric transition

$$B_L^+ = \sqrt{1/L(L+1)}\,[R_3 + R_4 + 2R_6]_{J=L+1/2} M_L^{el}; \qquad (12)$$

$$B_L^- = \sqrt{1/L(L+1)}\,[L(R_3 + R_4) - (2L+1)R_5 - R_6]_{J=L-1/2} M_L^{el}. \qquad (13)$$

For an ML magnetic transition

$$B_L^+ = -(L/L+1)\,[R_1 + R_2]_{J=L+1/2} M_L^{mg}; \qquad (14)$$

$$B_L^- = [R_1 + R_2]_{J=L-1/2} M_L^{mg}. \qquad (15)$$

The quantities $R_1, R_2, \ldots R_6$ are radial integrals which depend on the multipole order of the L conversion transition, on the total and orbital angular momenta of the converted electron in the shell J_0 and $l_0 = J_0 + \lambda_0$; $\lambda_0 = \pm ½$, and on the corresponding angular momenta of the electron after conversion J and $l = J + \lambda$. The explicit form of R_i is given in the book by M. E. Rose.[6] In the deduction it was assumed that a part is played by a conversion transition of a single definite multipole order. There are possible instances in which contributions from E2 and M1 transitions are of comparable magnitude. When the nuclear spin is not changed in conversion ($j_1 = j_0$), comparable contributions can come from E0, M1, and E2 transitions. Formulas (10) and (16) cannot be applied to these cases.

The quantities M_L^{el} and M_L^{mg} in (12) – (15) are reduced matrix elements of the nuclear transition and depend on the structure of the nucleus. In the cases represented by (10) and (16) they drop out and do not affect the correlation.

The correlation between the circular polarizations of an x-ray K_{α_2} quantum (electron transition from I = ½) and a gamma ray after K conversion of an unoriented nucleus is given by

$$W_{j_0 X}(\theta) = 1 - [j_1(j_1+1) - j_2(j_2+1) + L_\gamma(L_\gamma+1)]\,[j_1(j_1+1) - j_0(j_0+1) + L(L+1)]\,[2L_\gamma(L_\gamma+1)\, j_1(j_1+1)]^{-1} Q_L \sigma_X \sigma_\gamma \cos\theta; \qquad (16)$$

θ is the angle between the photon directions $\sigma_X = 1$ or -1 and $\sigma_\gamma = 1$ or -1, depending upon whether the respective photons possess right or left circular polarization.

When an x-ray quantum is emitted through the filling of a K-vacancy by an electron with I = ⅜, in (10) and (16) σ_X must be preceded by the factor $-½$. Therefore all statements made in section 1 concerning the need for distinguishing the energies of the K_{α_1} and K_{α_2} lines remain valid.

When the nuclear spin is not changed through conversion a study of $W_{j_0X}(\theta)$ and $W_{\gamma X}(\theta)$ enables us to determine the contribution and relative phase of the matrix elements of E0 and M1 transitions. According to (25), (41) and (42) the polarization of K_{α_2} photons emitted in the K-conversion transition of a polarized nucleus ($j_1 = j_0$) is given by

$$W_{j_0X}(\theta) = 1 - \sqrt{j_0(j_0+1)}\,\sigma_X \rho Q_{10} \cos\theta; \qquad (17)$$

$$Q_{10} = \frac{B_0^+ B_1^{-*} + B_0^{+*} B_1^-}{\sqrt{3}\sum_L (2L+1)^{-1}\left[L\,|B_L^-|^2 + (L+1)\,|B_L^+|^2\right]}. \qquad (18)$$

In (18) the summation can be taken over $0 \le L \le 2j_0$, but it is usually sufficient to limit this to L = 0, 1, and 2, i.e., to E0, M1, and E2 transitions. B_0^+ and B_1^- in (18) must be taken for E0 and M1 transitions.

The $K_{\alpha_2} - \gamma$ polarization correlation is given by

$$W_{\gamma X}(\theta) = 1 + [j_1(j_1+1) - j_2(j_2+1) + L_\gamma(L_\gamma+1)] \times [2L_\gamma(L_\gamma+1)\sqrt{j_0(j_0+1)}]^{-1} Q_{10}\sigma_X\sigma_\gamma \cos\theta. \qquad (19)$$

The determination of M_0^{el}/M_1^{mg}, which is possible with the aid of (17) and (19), furnishes information concerning the structure of the nucleus.

When conversion occurs in shells with $J_0 > 1/2$, such as L_{III}, the x-ray angular distribution is anisotropic with respect to the nuclear spin orientation or direction of subsequent gamma rays. For L_{III}-conversion the angular distribution is given by

$$W_{jX}(\theta) = 1 + A_j R_{j_1 j_0}(3\cos^2\theta - 1)\,P^j{}_{20},$$

$$R_{j_1 j_0} = \Big[\sum_{LL'J} (2J+1)\sqrt{(2j_0+1)/5}\; W\left(\tfrac{3}{2}J2L', L\tfrac{3}{2}\right) \times W(j_1 L j_0 2;\; j_0 L')\;\; B_L^J B_{L'}^{J*}\Big] \times \Big[\sum_{LJ}(2J+1)(2L+1)^{-1}|B_L^J|^2\Big]^{-1}. \qquad (20)$$

Here B_L^J means $B_{J\lambda L}^{J_0\lambda_0}$ (see Appendix II) for L_{III}-conversion ($J_0 = 3/2$, $\lambda_0 = -1/2$). The sum $R_{j_1 j_0}$ is taken over the possible values: $J = L \pm 1/2$, $L \pm 3/2$. When for the conversion transition it is sufficient to consider only a single multipole order L_0, so that $L = L' = L_0$, the summation over L and L′ in $R_{j_1 j_0}$ vanishes and M_L drops out of the formula.

When an E0 transition is possible, the angular distribution is determined by the interference of E0 and M1. $R_{j_1 j_0}$ contains terms for $L = L' = 0, 1, 2$; $L = 0$ and $L' = 1$; $L = 1$ and $L' = 0$. This case furnishes the same information that can be obtained by investigating Eq. (17) or (19).

APPENDIX I

We shall derive a general formula for the polarization and angular distribution of x-rays emitted after electron capture, for both allowed and forbidden transitions.

Let us consider a nucleus that is oriented in an external field. As heretofore, j_0 and j_1 will denote the spin of the initial and final nucleus, respectively; J_0 and $l = J_0 + \lambda_0$ are the moments of the orbital electron that is absorbed by the nucleus and I and $l_I = I + \lambda_I$ are the moments of the electron which jumps into the vacancy. The wave function of the captured electron is

$$\psi^{(n)}_{J_0 M_0 \lambda_0}(r) = \begin{Bmatrix} -i\,F^{(n)}_{J_0\lambda_0}(r)\;\hat{Y}^{-\lambda_0}_{J_0 M_0}(\vartheta,\varphi) \\ 2\lambda_0\, G^{(n)}_{J_0\lambda_0}(r)\;\hat{Y}^{\lambda_0}_{J_0 M_0}(\vartheta,\varphi) \end{Bmatrix}, \qquad (21)$$

where $F^{(n)}_{J_0\lambda_0}(r)$ is the small and $G^{(n)}_{J_0\lambda_0}(r)$ is the large radial component, and $\hat{Y}^{\lambda}_{JM}(\vartheta,\varphi)$ is a spherical spinor[7] with components equal to the components of the $(h-J)$-vector $Y^{h\tau}_{JM}$ for $h = 1/2$, as follows:

$$\left[Y^{h\tau}_{JM}(\vartheta,\varphi)\right]_\gamma = (-1)^{h-\gamma} C^{JM}_{J+\tau, M+\gamma, h-\gamma}\, Y_{J+\tau, M+\gamma}(\vartheta,\varphi). \qquad (22)$$

The orientation of the initial nucleus is given by the polarization tensor

$$P^{j_0}_{g_0\eta_0} = \frac{2g_0+1}{2j_0+1}\sum_{\mu_0\mu'_0} C^{j_0\mu_0}_{j_0\mu'_0 g_0\eta_0}\,\rho(\mu_0\mu'_0), \qquad (23)$$

where $\rho(\mu_0\mu'_0)$ is the density matrix of the initial state. If the axis of quantization is chosen to be the physically distinguished axis of principal nuclear spin orientation, then

$$\rho(\mu_0\mu'_0) = w(\mu_0)\,\delta_{\mu_0\mu'_0},$$

where $w(\mu_0)$ is the probability of finding the nucleus in a state with the projection μ_0 on the z axis, and $\sum_{\mu_0} w(\mu_0) = 1$. After electron capture the nucleus may remain in an excited state and emit several gamma rays successively. The polarization tensor of this nucleus can be expressed in terms of observed quantities which characterize the subsequent radiative transition:

$$P^{j_1}_{g_1\eta_1} = \frac{2g_1+1}{2j_1+1}\sum_{\mu_1\mu_1'} C^{j_1\mu_1}_{j_1\mu_1' g_1\eta_1} H_{j_1\mu_1} H^{*}_{j_1\mu_1'}, \qquad (24)$$

where $H_{j_1\mu_1}$ is the matrix element of the nuclear gamma transition.

The spin state of the atomic shell after capture is given by the tensor $P^{J_0}_{g\eta}$, which we shall express in terms of quantities that characterize the x-ray that accompanies the filling of the vacated level. Equation (24) remains valid for $P^{J_0}_{g\eta}$ with replacement of j_1, μ_1, g_1, η_1 by J_0, M_0, g, η and replacement of $H_{j_1\mu_1}$ by the x-ray transition matrix element $H_{J_0\mu_0}$.

Thus the state of the atom before the conversion transition is determined by the character of the polarization of the nucleus (the tensor $P^{j_0}_{g_0\eta_0}$) and of the atomic shell. The polarization of the atomic shells which do not participate in the transition is of no interest here. The cases of practical interest are K and L conversion. Since the total angular momentum of a filled K or L shell is zero these shells are not oriented in an external field and the electronic polarization tensor for the initial state can be taken as unity. In the final state the orientation of the nucleus will be given by $P^{j_1}_{g_1\eta_1}$ and the orientation of the shell by $P^{J_0}_{g\eta}$.

Using the method of calculation described in Refs. 1 and 5, we obtain the following expression* for the probability of a conversion transition in an atom:

$$W_{j_0\gamma\chi} = \sum (-1)^{g_0} (2j_0+1)$$
$$\times (2i+1)\sqrt{(2j_0+1)(2j_1+1)(2J_0+1)/(2g+1)}$$
$$\times W(J_0 i g L', LJ_0)\, X(j_1 j_1 g_1,\ j_0 j_0 g_0,\ LL' g)$$
$$\times C^{g\eta}_{g_1\eta_1 g_0\eta_0} P^{j_1^*}_{g_1\eta_1} P^{j_0^*}_{g_0\eta_0} P^{J_0}_{g\eta} B^{J_0\lambda_0}_{i\nu L} B^{J_0\lambda_0^*}_{i\nu L'}. \qquad (25)$$

Here W(abcd;ef) are Racah functions, which are tabulated in Ref. 8, X(abc, def, ghi) are Fano functions, which are tabulated in Refs. 9 and 10, and $C^{c\gamma}_{a\alpha b\beta}$ are Clebsch-Gordan coefficients, which are tabulated in Ref. 11. The total angular momentum carried away by the neutrino is denoted by i and $l_\nu = i + \nu$, $\nu = \pm 1/2$ denotes its orbital angular momentum. The summation in (25) is taken over the permissible values of all indices. The values of j_0, j_1, J_0, λ_0 and the order of forbiddenness of the transition, denoted by N, are given. For a transition of definite order of forbiddenness (25) retains only a few terms of the sum, because the quantities in (25) differ from zero only for definite values of the indices:

$$C^{j_0\mu_0}_{L\Lambda j_1\mu_1} B^{j_0\lambda_0}_{i\nu L} = \sum_{h=0}^{1}\sum_{\tau=-h}^{h}\int \psi^{*}_{j_1\mu_1} S^{L}_{h\tau} Y^{h\tau^*}_{L\Lambda} \psi_{j_0\mu_0}\, d\mathbf{r};$$

$$S^{L}_{h\tau} = \Big\{ [\beta\,(c_S R_1^- + ic'_S R_2^+) + (c_V R_1^+ + ic'_V R_2^-)]\,\delta_{h0} \cdot$$
$$+ [\beta\sigma(c_T R_1^- + ic'_T R_2^+) + \sigma(c_A R_1^+ + ic'_A R_2^-)]\,\delta_{h1}\}\,\delta_{L+\tau,\,N}$$
$$- \{[\gamma_5(ic_A R_2^- + c'_A R_1^+) - \beta\gamma_5(ic_P R_2^+ + c'_P R_1^-)]\,\delta_{h0}$$
$$+ [\alpha\,(ic_V R_2^- + c'_V R_2^+)$$
$$- \beta\alpha(ic_T R_2^+ + c'_T R_1^-)]\,\delta_{h1}\}\,\delta_{L+\tau,\,N-1}. \qquad (26)$$

Here $\psi_{j_0\mu_0}$ and $\psi_{j_0\mu_1}$ are the nuclear wave functions before and after capture. The entire dependence of the right-hand side of (26) on the magnetic quantum numbers μ_0, μ_1 and Λ is contained in the Clebsch-Gordan coefficient while $B^{J_0\lambda_0}_{i\nu L}$ is independent of them.

$$R_1^{\pm} = \sum_{\omega\chi}[\delta_{\omega-\lambda_0}\delta_{\chi-\nu}F^{(n)}_{J_0\lambda_0}(r)$$
$$\pm 4\lambda_0\nu\delta_{\omega\lambda_0}\,\delta_{\chi\nu}\,G^{(n)}_{J_0\lambda_0}(r)]\,N^{h1}_{i\chi J_0\omega}; \qquad (27)$$

$$R_2^{\pm} = \sum_{\omega\chi}[2\lambda_0\,\delta_{\omega\chi_0}\delta_{\chi-\lambda}\,G^{(n)}_{J_0\lambda_0}(r)$$
$$\pm 2\nu\,\delta_{\omega-\lambda_0}\delta_{\chi\nu}\,F^{(n)}_{J_0\lambda_0}(r)]\,N^{hL}_{i\chi J_0\omega}; \qquad (28)$$

$$N^{hL}_{i\chi J_0\omega} = [(qr)^{l_1}/(2l_1+1)!!]$$
$$\times\sqrt{2(2h+1)(2L+1)(2f+1)(2l_1+1)}$$
$$\times\sqrt{2J_0+1}\;C^{l_1 0}_{l0f0}\,X(l_1 l f,\ iJ_0 L,\ \tfrac{1}{2}\,\tfrac{1}{2}\,h), \qquad (29)$$
$$l = J_0+\omega,\ l_1 = i+\chi,\ f = L+\tau,$$
$$-h \leqslant \tau \leqslant h,\ \omega = \pm\tfrac{1}{2},$$

where $\chi = \pm 1, 2$; the parity of $(L+\tau)$ is equal to the parity of $(J_0 + i + \omega + \chi)$; q is the energy of the neutrino.

The angular distribution and polarization of x-rays are given in (25) by the tensor $P^{J_0}_{g\eta}$. Since in this case it is sufficient to consider only electric dipole radiation, following Ref. 1 $P^{J_0}_{g\eta}$ in (24) becomes

$$P^{J_0}_{g\eta} = (2g+1)(-1)^{g+\eta}\sqrt{3(2J_0+1)}\;W(J_0 I g 1;\ 1 J_0)$$
$$\times\sum_{\sigma\sigma'} i^{\sigma-\sigma'}\exp[i(\sigma-\sigma')\alpha]\;C^{1\,\sigma}_{1\,\sigma' g\,\varphi}\,D^{g}_{-\eta\varphi}(\phi,\theta,0). \qquad (30)$$

*Without making specific mention of the fact, we shall always omit general factors which do not affect the correlation.

The angles θ and ϕ give the direction of the x-ray momentum $\mathbf{k}(k, \theta, \phi)$. Its linear polarization is given by the vector ϵ, whose components in a right-handed coordinate system with $\mathbf{k}$ along the z axis are

$$\varepsilon_0 = \varepsilon_z = 0, \quad \varepsilon_{\pm 1} \equiv \pm (\varepsilon_x \pm i\varepsilon_y)/\sqrt{2} = \pm e^{\pm i\alpha}/\sqrt{2}. \qquad (31)$$

The angle α is computed from the x axis in the plane perpendicular to $\mathbf{k}$. $D^{g}_{\eta\varphi}(\phi, \theta, 0)$ is the familiar matrix of the irreducible representation of the rotation group.[12] It is defined here so that

$$\psi_{j\mu}(\theta\phi) = \sum_{\mu'} D^{j}_{\mu\mu'}(\phi, \theta, 0)\, \psi_{j\mu'}(0,0) \qquad (32)$$

and, in particular, $Y_{lm}(\theta, \phi) = \sqrt{(2l+1)/4\pi}\, D^{l}_{m0}(\phi, \theta, 0)$. The spherical harmonic Y_{lm} agrees with Ref. 13 and differs by the factor $(-1)^m$ from Ref. 11. The possible values of g in (30) are 0, 1, and 2.

According to (30), $P^{J_0}_{00} = 1$ and

$$P^{J_0}_{1\eta} = -\frac{\sqrt{3\pi}}{2} \frac{J_0(J_0+1) - I(I+1) + 2}{\sqrt{J_0(J_0+1)}}\, \sigma_X Y^{*}_{1\eta}(\theta, \phi), \qquad (33)$$

where $\sigma_X = 1$ or -1 for right or left circularly polarized light quanta, respectively. If the detector does not distinguish quanta of different circular polarizations, $P^{J_0}_{1\eta}$ is equal to the sum of the right-hand side of (33) for $\sigma_X = 1$ and -1, so that $P^{J_0}_{2\eta} = 0$. $P^{J_0}_{2\eta}$ gives the linear polarization of the x-rays:

$$P^{J_0}_{2\eta} = 2\sqrt{6\pi(2J_0+1)}\, W(J_0 J\, 21;\ 1J_0)\, \{Y^{*}_{2\eta}(\theta, \phi) - \sqrt{15/8\pi}\,(-1)^{\eta}[e^{2i\alpha} D^{2}_{-\eta 2}(\phi, \theta, 0) + e^{-2i\alpha} D^{2}_{-\eta -2}(\phi, \theta, 0)]\}. \qquad (34)$$

If triple correlation is not observed between the x-rays, gamma rays and nuclear spin orientation, and if the Z axis is a physically distinguished direction, then (25) contains no terms for which η, η_1, and η_0 are not zero:

$$P^{J_0}_{20} = 2\sqrt{6\pi(2J_0+1)}\, W(J_0 I\, 21;\ 1J_0)\, \{Y_{20}(\theta, \phi) - \sqrt{6}\cos 2\alpha\, Y_{22}(\theta, 0)\}. \qquad (35)$$

$P^{j_1}_{g_1\eta_1}$, which characterizes the radiative transition of the nucleus, can be represented in a form similar to (30). For a 2^L-multipole transition

$$P^{j_1}_{g_1\eta_1} = (2g_1+1) \times \sqrt{(2j_1+1)(2L+1)} \sum_{\sigma_\gamma \sigma'_\gamma} \xi^{(\sigma_\gamma - \sigma'_\gamma)/2} \exp\{i(\sigma_\gamma - \sigma'_\gamma)\alpha_\gamma\} \times C^{L_\gamma \sigma_\gamma}_{L_\gamma \sigma_\gamma g_1 \varphi} W(L_\gamma j_2 g_1 j_1;\ j_1 L_\gamma) D^{g_1}_{\eta_1 \varphi}(\phi_\gamma, \theta_\gamma, 0). \qquad (36)$$

θ_γ and ϕ_γ are the directional angles of the gamma ray. The angle α_γ for gamma rays is analogous to α for x-rays and is defined in accordance with (31). The term with $\sigma_\gamma = \sigma'_\gamma = 1$ gives $P^{j_1}_{g_1\eta_1}$ for light quanta with right circular polarization; the term with $\sigma_\gamma = \sigma'_\gamma = -1$ does the same for light quanta with left circular polarization; and the sum of the terms with $\sigma_\gamma = 1$, $\sigma'_\gamma = -1$ and $\sigma_\gamma = -1$, $\sigma'_\gamma = 1$ gives $P^{j_1}_{g_1\eta_1}$ for linearly polarized light quanta. $\xi = 1$ or -1, respectively, for magnetic or electric transitions.

If only the gamma-ray angular distribution is observed, by summing (36) with respect to the polarizations we obtain

$$P^{j_1}_{g_1\eta_1} = \sqrt{(2g_1+1)(2j_1+1)(2L_\gamma+1)} \times \left[1 - \frac{g_1(g_1+1)}{2L_\gamma(L_\gamma+1)}\right] W(j_2 L_\gamma j_1 g_1;\ j_1 L_\gamma) \times C^{L_\gamma 0}_{L_\gamma 0 g_1 0} Y_{g_1\eta_1}(\theta_\gamma, \phi_\gamma). \qquad (37)$$

The above formulas can be used to study electron capture of any order of forbiddenness. However, an unambiguous interpretation of experimental findings is obtained most simply and conveniently for allowed transitions, which we shall now consider in detail. For allowed transitions $N = 0$ and the second curly bracket in $S^{L}_{h\tau}$ gives no contribution since $L + \tau \geq 0$. In K capture we have $J_0 = 1/2$, $\lambda_0 = -1/2$ and thus $g = 0$ or 1. For an allowed transition $i = 1/2$, $\chi = -1/2$; therefore L and $L' = 0$ or 1, and, correspondingly, $\tau = 0$ or -1. In $B^{J_0\lambda_0}_{i\nu L}$ we may leave only two indices and write simply $B_{L\nu}$. For $B_{L\nu}$ we obtain

$$B_{0\nu} = (c_S \delta_{\nu -1/2} + ic'_S \delta_{\nu 1/2}) K_S - (c_V \delta_{\nu -1/2} - ic'_V \delta_{\nu 1/2}) K_V; \qquad (38)$$

$$B_{1\nu} = \sqrt{3}\,[(c_T \delta_{\nu -1/2} + ic'_T \delta_{\nu 1/2}) K_T - (c_A \delta_{\nu -1/2} - ic'_A \delta_{\nu 1/2}) K_A]; \qquad (39)$$

$$K_S = \int \psi^{*}_{j_1\mu_1} \beta G^{(1)}_{1/2\,-1/2}(r)\, \psi_{j_0\mu_0} d\mathbf{r}, \quad C^{j_0\mu_0}_{1\Lambda j_1\mu_1} K_T = (-1)^{1+\Lambda} \int \psi^{*}_{j_1\mu_1} G^{(1)}_{1/2\,-1/2}(r)\, \beta\sigma_{-\Lambda}\, \psi_{j_0\mu_0} d\mathbf{r}. \qquad (40)$$

K_V and K_A differ from K_S and K_T, respectively, by the absence of the matrix β. In nonrelativistic approximation for nucleons $K_S = -K_V$, $K_T = -K_A$. In (40) $\sigma_0 = \sigma_Z$, $\sigma_{\pm 1} = (\sigma_X \pm i\sigma_Y)/\sqrt{2}$. The expression for correlation does not depend directly on K_S and K_T but only on their ratio K_S/K_T. Since the electronic wavelength is larger than nuclear dimensions, the function $G^{(n)}_{1/2\,-1/2}(r)$ can be

taken outside of the integral sign and combined in the expression for K_S/K_T. This corresponds to neglecting quantities smaller than $(\alpha Z)^2$ compared with unity. For L capture or forbidden K capture, the correlation expression contains integrals such as (40) with $G^{(n)}_{J_0\lambda_0}(r)$ and $F^{(n)}_{J_0\lambda_0}(r)$. These quantities can be taken outside of the integral sign at a point r on the nuclear boundary. As previously, the error is $\lesssim (\alpha Z)^2$. Since for an allowed K capture $g = 0$ or 1, then, according to (30), the x-rays are not linearly polarized and the angular distribution is isotropic, but circular polarization exists. When the initial nucleus is oriented in an external field and the direction and polarization of gamma rays is not being considered, then we must set in (25) $g_1 = 0$ and thus $g_0 = g = 0.1$. In this case correlation between the circular polarization of the x-rays and the nuclear spin orientations can be expected only when the nucleus possesses dipolar polarization (by the Gorter-Rose method,[14] for example). When the nuclei are aligned (as by the method of Bleaney[15] or Pound[16]), there is no correlation. When triple correlation is observed $g_1 \neq 0$, $g_0 \neq g$ and aligned nuclei can be used.

APPENDIX II

We shall give a general formula for the conversion-transition probability of an oriented nucleus with subsequent emission of x-rays and gamma rays of definite polarization. The only difference from the problem in Appendix I is the fact that an electron jumps from a discrete level to the continuous spectrum and is not captured by the nucleus. As in Appendix I, we are not interested in the direction of emission of the particle (in this case the electron, previously the neutrino). The correlation formula is (25) with the following changes: (1) The neutrino total and orbital angular momenta i and $l\nu = i + \nu$ are replaced by the total and orbital angular momenta J and $l = J + \lambda$ of the ejected electron; (2) L and L′ are understood to mean the multipole order of the conversion transition; (3) Eq. (41) or Eq. (42) is used for $B^{J_0\lambda_0}_{J\lambda L}$. The remaining notation is the same, with the same meaning, as in Eq. (25). For electric conversion transitions we have

$$B^{J_0\lambda_0}_{J\lambda L} = \sqrt{(2J_0+1)(2L+1)/L(L+1)}\ \{\sqrt{2J_0-2\lambda_0+1}$$
$$\times W(LJJ_0-\lambda_0\tfrac{1}{2};\ J_0J-\lambda)$$
$$\times C^{J-\lambda_0}_{J_0-\lambda_0 0L0}[LR_3+(L+(2J_0+1)\lambda_0-(2J+1)\lambda)R_6]$$
$$+\sqrt{2J_0+2\lambda_0+1}\,W(LJJ_0+\lambda_0\tfrac{1}{2};J_0J+\lambda)$$
$$\times C^{J+\lambda_0}_{J_0+\lambda_0 0L0}[LR_4-(L-(2J_0+1)\lambda_0$$
$$+(2J+1)\lambda)R_5]\}\,M^{el}_L. \quad (41)$$

For magnetic conversion transitions we have

$$B^{J_0\lambda_0}_{J\lambda L} = -\sqrt{(2J_0+1)(2L+1)/L(L+1)}$$
$$\times[\lambda(2J+1)+\lambda_0(2J_0+1)]$$
$$\times\{\sqrt{2J_0+2\lambda_0+1}\,W(LJJ_0+\lambda_0\tfrac{1}{2};J_0J-\lambda)$$
$$\times C^{J-\lambda_0}_{J_0+\lambda_0 0L0}R_1+\sqrt{2J_0-2\lambda_0+1}$$
$$\times W(LJJ_0-\lambda_0\tfrac{1}{2};J_0J+\lambda)C^{J+\lambda_0}_{J_0-\lambda_0 0L0}R_2\}\,M^{mg}_L. \quad (42)$$

The radial integrals $R_1, R_2, \ldots, R_6$, used in Rose's book,[6] are taken over all space. A considerable correction is required if it is taken into account that the electronic wave function differs from a Coulomb function inside the nucleus. For K conversion, Sliv and Band[17] calculated the integrals subject to this correction and used them to obtain internal conversion coefficients.

For a conversion transition of a single definite multipole order, say L_0, we must put $L = L' = L_0$ in (25). For a mixture of ML_0 and $E(L_0+1)$, in addition to the terms for which $L = L' = L_0$ and $L = L' = L_0 + 1$ Eq. (25) contains terms with $L = L_0$, $L' = L_0 + 1$ and $L = L_0 + 1$, $L' = L_0$.

M^{el}_L and M^{mg}_L in (41) and (42), which are the matrix elements of the nuclear transition, depend on the structure of the nucleus. The correlation formulas do not contain the M_L but only their ratio $M_L/M_{L'}$. When only one value $L = L'$ plays a part the M_L drop out of the formulas. The corrections[17,18] associated with the interior of the nucleus must depend on its structure, but with the exception of E0 transitions and, in part, M1 transitions this dependence has very little effect on the results.[17]

[1] A. Z. Dolginov, Nucl. Phys. **2**, 723 (1956/1957).

[2] Wu, Ambler, Hayward, Hoppes and Hudson, Phys. Rev. **105**, 1413 (1957); **106**, 1361 (1957).

[3] T. D. Lee and C. N. Yang, Phys. Rev. **104**, 254 (1956).

[4] A. Z. Dolginov, J. Exptl. Theoret. Phys. (U.S.S.R.) **23**, 493 (1952).

[5] A. Z. Dolginov, Nucl. Phys. **5**, 512 (1958).

[6] M. E. Rose, Multipole Fields, Wiley, New York, 1955.

[7] Berestetskii, Dolginov, and Ter-Martirosian, J. Exptl. Theoret. Phys. (U.S.S.R.) **20**, 527 (1950).

[8] Biedenharn, Blatt and Rose, Revs. Modern Phys. **24**, 249 (1952).

[9] H. Matsunobu and H. Takebe, Progr. Theoret. Phys. (Japan) **14**, 589 (1955).

[10] J. W. Stephenson and K. Smith, Proc. Phys. Soc. (London) **A70**, 571 (1957).

[11] E. U. Condon and G. H. Shortley, Theory of Atomic Spectra, Cambridge Univ. Press, 1935.

[12] E. Wigner, Gruppentheorie und ihre Anwendung auf die Quantenmechanik der Atomspektren, Braunschweig, 1931.

[13] H. A. Bethe, Quantenmechanik der Ein- und Zwei-Elektronenprobleme (Russ. Transl), ONTI, 1935.

[14] Simon, Rose, and Jauch, Phys. Rev. **84**, 1155 (1951).

[15] B. Bleaney, Proc. Phys. Soc. (London) **A64**, 315 (1951).

[16] R. V. Pound, Phys. Rev. **76**, 1410 (1949).

[17] L. A. Sliv and I. M. Band, Таблицы коэффициентов внутренней конверсии, (Tables of Internal Conversion Coefficients), Acad. Sci. Press, 1956, part I.

[18] E. L. Church and T. Weneser, Phys. Rev. **104**, 1382 (1956).

Translated by I. Emin
185

SOVIET PHYSICS JETP VOLUME 34 (7), NUMBER 4 OCTOBER, 1958

THE ANOMALOUS SKIN EFFECT IN THE INFRA-RED REGION

L. P. PITAEVSKII

Institute for Physical Problems, Academy of Sciences of the U.S.S.R.

Submitted to JETP editor November 1, 1957

J. Exptl. Theoret. Phys. (U.S.S.R.) **34**, 942-946 (April, 1958)

The surface impedance of metals in the infra-red region at low temperatures has been calculated, taking into account the effect of interelectron collisions. The electrons are considered as a Fermi liquid with an arbitrary dispersion law for the quasi-particles.

THE purpose of this paper is to calculate the effect of interelectron collisions on the optical properties of metals in the infra-red region of the spectrum. To this end we shall assume that the frequency of the incident light satisfies the conditions

$$\omega l / v \gg 1 \qquad (1)$$

(v is the speed of the electrons and l is the free path length) and

$$\omega \delta / v \gg 1, \qquad (2)$$

where δ is the depth to which the field penetrates in the metal. The physical significance of the first condition is obvious, and the second implies that the field in which the electrons are moving may be considered to be uniform. It is also assumed that the metal has a large negative dielectric constant and a small absorption, which can be treated as a perturbation. This condition limits the validity of the formulas to the high-frequency region. The calculations will be carried out for the case of very low temperatures, where $kT \ll \hbar\omega$.

We have made no assumptions at all about the law of dispersion for the electrons, the type of scattering probability which enters into the theory, nor the magnitude of the interactions between electrons. In particular it must be emphasized that we are not assuming either that the electron dispersion is approximately quadratic, or that the electron interaction is weak.

First of all we must consider the current due to a single moving electron (or, strictly speaking, a single Fermi particle) assuming that the electrons form a Fermi liquid. In the same way that the energy $\epsilon(\mathbf{p})$ of each individual particle is given by the formula

$$\delta E = \int \varepsilon(\mathbf{p})\, \delta n(\mathbf{p})\, d\tau$$

[E is the total energy, n the distribution function

of the particles in $\mathbf{p}$-space, and $d\tau \equiv 2\,dp_x dp_y dp_z/(2\pi\hbar)^3]$, the current $\mathbf{j}(\mathbf{p})$ due to a single electron is given by the formula

$$\delta \mathbf{J} = \int \mathbf{j}(\mathbf{p})\,\delta n(\mathbf{p})\,d\tau,$$

where

$$\mathbf{J} = e\int \frac{\partial \varepsilon}{\partial \mathbf{p}}\, n\,d\tau = e\int \mathbf{v} n\,d\tau. \tag{3}$$

Assuming that for some definite function f

$$\delta\varepsilon = \int f(\mathbf{pp}')\,\delta n'\,d\tau'$$

and that $\partial n/\partial \epsilon = -\delta(\epsilon - \epsilon_0)$, we find

$$\mathbf{j}(\mathbf{p}) = e\left(\mathbf{v}(\mathbf{p}) + \int f(\mathbf{p},\ \mathbf{p}')\,\mathbf{v}(\mathbf{p}')\frac{d\tau'}{d\varepsilon'}\right) \tag{4}$$

(Since $kT \ll \hbar\omega$, we can put $T = 0$ in all formulas).

CALCULATION OF THE DIELECTRIC CONSTANT

From the dispersion relation $\epsilon(\omega)$ it follows that in the region of weak absorption in which we are interested the real part of the dielectric constant must be of the form

$$\varepsilon'(\omega) = a - b/\omega^2. \tag{5}$$

(See Landau and Lifshitz,[2] page 338). a and b are to be found in the usual way by calculating the polarization $\mathbf{P}$ of the electrons in the external field. In this case $\dot{\mathbf{P}} = \mathbf{J}$, so that

$$\ddot{\mathbf{P}} = -\omega^2\mathbf{P} = \int \dot{\mathbf{j}} n\,d\tau = e\int \mathbf{j}(\mathbf{n}\cdot\mathbf{E})\frac{d\tau}{d\varepsilon}. \tag{6}$$

Hence for the case of cubic symmetry we find

$$\varepsilon'(\omega) = 1 - \frac{4\pi e^2}{3\omega^2}\int \mathbf{V}\mathbf{v}\frac{d\tau}{d\varepsilon} \approx -\frac{4\pi e^2}{3\omega^2}\int \mathbf{V}\mathbf{v}\frac{d\tau}{d\varepsilon} = -\frac{4\pi e^2}{\omega^2 m}N, \tag{7}$$

where we have introduced the notation $\mathbf{j}(\mathbf{p}) = e\mathbf{V}(\mathbf{p})$. It can be seen that the so-called "number of free electrons" N depends fundamentally on their interaction.

ABSORPTION

The electrons in the metal can absorb light by colliding with impurity atoms (or with lattice defects), with each other, or with the surface of the metal; and also by simultaneously absorbing or emitting a phonon. In our case, the total absorption is the simple sum of terms corresponding to each of the above processes. The formulas describing absorption by collision can be greatly simplified by making use of the fact that in the infra-red region

$$\omega t_{\text{coll}} \ll 1, \tag{8}$$

where t_{coll} is the duration of a collision (e.g., the time during which the electron is directly interacting with an impurity atom). In this case the Fourier components of $\ddot{\mathbf{d}}$ (where $\mathbf{d}$ is the dipole moment) which determine the absorption do not depend on the frequency, and can be expressed easily in terms of the current change due to the collision (See Landau and Lifshitz,[3] page 207):

$$\ddot{\mathbf{d}}_\omega = \frac{1}{2\pi}\int_{-\infty}^{\infty} \ddot{\mathbf{d}} e^{i\omega t}\,dt \approx \frac{1}{2\pi}\int_{-\infty}^{\infty} \ddot{\mathbf{d}}\,dt = \frac{1}{2\pi}(\mathbf{j}' - \mathbf{j}) = \frac{1}{2\pi}\Delta\mathbf{j},$$

$\mathbf{j}$ and $\mathbf{j}'$ being the current before and after the collision. From this we calculate the expression

$$q = 2\pi\frac{\Delta j_i \Delta j_k}{\hbar\omega^3}\frac{\overline{E_i E_k}}{4\pi}. \tag{9}$$

for the energy absorbed in a collision. The derivation of formula (9) is analogous to the derivation of formula (68.10) in Landau and Lifshitz,[3] from which it can readily be obtained by using the principle of detailed balance. In the case of cubic symmetry we obtain

$$dQ = \frac{2\pi}{3}\frac{(\Delta\mathbf{j})^2}{\hbar\omega^3}\frac{\overline{E^2}}{4\pi}\,d\nu, \tag{10}$$

for the energy absorbed per unit time, where $d\nu$ is the number of collisions per unit time in which the quasi-momentum changes by the indicated amount.

COLLISION WITH IMPURITIES

When electrons collide with impurity atoms the number of collisions per second per cubic centimeter is of the form

$$d\nu = N_i\, n(\mathbf{p})(1 - n(\mathbf{p}'))\,\sigma(\mathbf{p}\cdot\mathbf{n}')\,V(\mathbf{p})\,d\tau\,do', \tag{11}$$

where $\sigma\,do$ is the scattering cross-section, $\mathbf{n}'$ is a unit vector in the direction of the scattered electrons, and N_i is the number of scattering centers per unit volume. Since

$$\varepsilon(\mathbf{p}') = \varepsilon(\mathbf{p}) + \hbar\omega, \quad kT \ll \hbar\omega,$$

the expression $n(\mathbf{p})(1 - n(\mathbf{p}'))$ differs from zero only when

$$\varepsilon_0 - \hbar\omega < \varepsilon(\mathbf{p}) < \varepsilon_0$$

(ϵ_0 is the limiting Fermi energy).

By substituting (11) into (10) and integrating with respect to $d\epsilon$, we obtain the energy dissipation per unit volume per unit time

$$Q_{np} = \frac{2\pi}{3}\frac{N_i}{\omega^2}\int (\Delta \mathbf{j})^2 \sigma V \frac{d\tau}{d\varepsilon} d\sigma' \cdot \frac{\overline{E^2}}{4\pi}. \qquad (12)$$

It now becomes easy to find the real part of the impedance. Comparing (12) with the general expression for energy dissipation in a medium with dielectric constant $\epsilon = \epsilon' + i\epsilon''$:

$$Q = \omega \varepsilon'' \overline{E^2} / 4\pi, \qquad (13)$$

we find the imaginary part of the dielectric constant ϵ'', after which we can find an expression for ζ, the surface impedance,* to the corresponding degree of accuracy (since $\epsilon'' \ll \epsilon'$):

$$\zeta = \zeta' + i\zeta'' = -i / \sqrt{\varepsilon' + \varepsilon''/2|\varepsilon'|^{3/2}}. \qquad (14)$$

Therefore

$$\zeta' = \frac{2\pi}{3}\frac{\int (\Delta \mathbf{j})^2 \sigma V \, d\sigma' \, d\tau / d\varepsilon}{2|\varepsilon'|^{3/2}\omega^3}. \qquad (15)$$

As might be expected, equation (15) differs from the well-known light-absorption formulas only in the substitution of $\mathbf{v} = \partial\epsilon/\partial\mathbf{p}$ for $\mathbf{V}$.

COLLISIONS BETWEEN ELECTRONS

This effect is not usually taken into account in calculating the absorption. This is because in the case of an isotropic or quadratic dispersion law, the change of current during the collision process is zero by virtue of the conservation of momentum, since in the first case the current (if we consider the electrons to be non-interacting) is proportional to their momentum, and in the second case the current is a linear function of the momenta which is not altered by the collision.

During the collision of two electrons,

$$d\nu_{el} = w_{el}(\mathbf{p}_1, \mathbf{p}_2; \mathbf{p}_1') n_1 n_2 (1 - n_1')(1 - n_2') d\tau_1' d\tau_2 d\tau_1. \qquad (16)$$

Here w_{el} is the probability of the indicated scattering process, $\mathbf{p}_1$ and $\mathbf{p}_2$ are the momenta of the colliding particles, and $\mathbf{p}'$ is the momentum of one of the scattered electrons (the momentum of the other electron is determined by the conservation of momentum). From the law of conservation of energy,

$$\hbar\omega + \varepsilon(\mathbf{p}_1) + \varepsilon(\mathbf{p}_2) = \varepsilon(\mathbf{p}_1') + \varepsilon(\mathbf{p}_2').$$

Substituting (16) into (10) and then integrating with respect to

(1) $d\varepsilon_1'$ between the limits $\varepsilon_1 + \varepsilon_2 + \hbar\omega - \varepsilon_0 > \varepsilon_1' > \varepsilon_0$,
(2) $d\varepsilon_2$ between the limits $\varepsilon_0 > \varepsilon_2 > 2\varepsilon_0 - \varepsilon_1 - \hbar\omega$,
(3) $d\varepsilon_1$ between the limits $\varepsilon_0 > \varepsilon_1 > \varepsilon_0 - \hbar\omega$,

we obtain

$$Q_{el} = \frac{2\pi}{3}\frac{2\hbar^2}{3}\int (\Delta \mathbf{j})^2 w_{el} \frac{d\tau_1' d\tau_2 d\tau_1}{d\varepsilon_1' d\varepsilon_2 d\varepsilon_1} \frac{\overline{E^2}}{4\pi}, \qquad (17)$$

where

$$\Delta \mathbf{j} = \mathbf{j}(\mathbf{p}_1) + \mathbf{j}(\mathbf{p}_2) - \mathbf{j}(\mathbf{p}_2') - \mathbf{j}(\mathbf{p}_1 + \mathbf{p}_2 - \mathbf{p}_1').$$

It must be kept in mind that because of the energy conservation law w_{el} will contain a factor $\delta[\epsilon_0 - \epsilon(\mathbf{p}_1 + \mathbf{p}_2 - \mathbf{p}_1')]$, and so the integral in (17) will really be five-dimensional instead of six-dimensional. ζ'_{el} can be found from [17] by the method already described.

COLLISION WITH THE SURFACE

Let $W_{surf}(\mathbf{p}, \sigma')\, d\sigma'$ be the probability that an electron with momentum $\mathbf{p}$ is scattered into the solid angle $d\sigma'$. Then the number of impacts on a unit area of surface per unit time is equal to

$$d\nu_{surf} = \mathbf{V}\cdot\mathbf{n}\; w_{surf} n (1 - n')\, d\sigma' d\tau \qquad (18)$$

$\mathbf{n}$ is the unit vector normal to the surface of the metal.

From this we can obtain the energy dissipated in 1 cm^2 of area in 1 second:

$$Q_{surf} = \frac{2\pi}{\omega^2}\int \Delta j_i \Delta j_k \, \mathbf{V}\cdot\mathbf{n}\; w_{surf}\, d\sigma' \frac{d\tau}{d\varepsilon}\frac{\overline{E_i E_k}}{4\pi}. \qquad (19)$$

(It must be borne in mind that the component of ζ' which we have calculated here is in general a tensor quantity, even in the case of cubic symmetry). Comparing this with the formula for energy dissipation

$$Q = c\zeta'_{\alpha\beta}\varepsilon' \overline{E_\alpha E_\beta} / 4\pi,$$

we can find $\zeta'_{\alpha\beta\,surf}$.

If we put $w = \text{const} = 1/2\pi$ into Eq. (19) we get the usual formula for absorption during diffuse reflection of electrons from a surface.[4] In actual fact, however, there is no particular reason to suppose that w is constant. In this paper we do not

*The definition of surface impedance which is used here is different from the usual one. Ordinarily the surface impedance is determined from the equation

$$Z(\omega) = R + iX = (4\pi/c)[E_t / H_t]_{surf}.$$

In this paper, instead of Z we have used the more convenient quantity $\zeta \equiv Zc/4\pi$ (See Landau and Lifshitz[2]).

consider the case of "specular" reflection, i.e., where the integral in (19) becomes identically zero, since this has no physical significance. In this case one would have to consider higher terms in the expansion of ζ'_{surf} in $v/\omega\delta$.

It is interesting to compare the magnitudes of ζ'_{surf} and ζ'_{el}. It stands to reason that they can be estimated only roughly; in any case, no more accurately than the nearest order of magnitude, since at the present time the functions which enter into the formulas are not known. This is particularly true of ζ'_{el}, for which the expression is of an extremely complicated type. The estimates give

$$\zeta'_{surf} \sim v/c \sim 10^{-2}; \quad \zeta'_{el} \sim m^{3/2}\sigma\omega^2/\hbar e n^{3/2} \sim 10^{-30}\omega^2.$$

It can be seen that even up to a frequency of $\omega \sim 10^{14}$, ζ'_{el} is, generally speaking, less than ζ'_{surf}.

As for the absorption of light accompanied by the emission of phonons, Holstein[5] has shown, in the case $\hbar\omega \gg k\Theta$ (Θ being the Debye temperature) that the corresponding component of ζ', like ζ'_{surf}, is independent of ω and is of the same order of magnitude as ζ'_{surf}, and is correspondingly smaller at lower frequencies. It would be very difficult to obtain an exact formula for this, since it depends chiefly on the short wavelength phonons with $\hbar\omega \sim k\Theta$, i.e., with wavelengths of the order of the lattice spacing.

In conclusion I would like to thank Academician L. D. Landau for advice and discussions.

[1] L. D. Landau, J. Exptl. Theoret. Phys. (U.S.S.R.) **30**, 1058 (1956), Soviet Phys. JETP **3**, 920 (1957).

[2] L. D. Landau and E. M. Lifshitz, Электродинамика сплошных сред (Electrodynamics of Continuous Media), Gostekhizdat (1957).

[3] L. D. Landau and E. M. Lifshitz, Теория поля (Theory of Fields) 2nd Ed., Gostekhizdat (1948).

[4] T. Holstein, Phys. Rev. **88**, 1427 (1952). R. B. Dingle, Physica **19**, 311 (1953).

[5] T. Holstein, Phys. Rev. **96**, 535 (1954).

Translated by D. C. West
186

SOVIET PHYSICS JETP VOLUME 34 (7), NUMBER 4 OCTOBER, 1958

SCATTERING OF PARTICLES OF ARBITRARY SPIN

L. D. PUZIKOV

Academy of Sciences, U.S.S.R.

Submitted to JETP editor October 31, 1957

J. Exptl. Theoret. Phys. (U.S.S.R.) **34**, 947-952 (April, 1958)

We study the geometrical consequences for elastic scattering of the fact that nuclear particles possess a spin. The scattering matrix for particles of arbitrary spin is constructed, and those quantities which are experimentally measurable (cross section, polarization, and polarization correlation) are expressed in terms of its matrix elements. We consider the question of the completeness of a polarization experiment. We show that to reconstruct the scattering matrix it is necessary to measure either the cross section for scattering of a polarized beam by a polarized target, or the polarization correlation after scattering (with an initially unpolarized state), or finally measure the change of polarization of the incident particles after scattering (repeated scattering). The last experiments will be sufficient only if the spin of the particles in the beam is not less than the target spin.

THE analysis of angular distributions and polarization in nuclear reactions is done by two methods. The first method, that of phase analysis, has been investigated in detail and generalized to the case of arbitrary spins.[1] The second method, that of Dalitz, Wolfenstein and Ashkin,[2] which constructs the scattering amplitude as a function of the initial and final wave vectors and spin operators, has been investigated for reactions involving particles of spin 0, ½ and 1.[3-6] The present paper gives the

extension of this method to the elastic scattering of particles of arbitrary spin.

1. CONSTRUCTION OF THE SCATTERING MATRIX

The general method for constructing the scattering matrix is to form all possible scalars from the spin operators and the initial and final wave vectors $\mathbf{k}_i$ and $\mathbf{k}_f$. As spin operators, we shall use the irreducible tensor operators T^q_κ, normalized by the condition

$$\mathrm{Sp}\,\{T^q_\varkappa (T^{q'}_{\varkappa'})^+\} = \delta_{qq'}\delta_{\varkappa\varkappa'}.$$

If the spin of the incident particles is s_1 and the target spin s_2, $(s_1, s_2 \neq 0)$ we can use the irreducible combinations of products of tensor operators:

$$T^q_\varkappa (q_1,\ q_2) = \sum_{\varkappa_1\varkappa_2} (q_1 q_2 \varkappa_1 \varkappa_2 \mid q\varkappa)\, T^{q_1}_{\varkappa_1} \times T^{q_2}_{\varkappa_2}. \tag{1}$$

The following functions, which transform according to an irreducible representation of the rotation group, can be formed from the two unit vectors $\mathbf{k}_i$ and $\mathbf{k}_f$

$$\Psi^\varkappa_{q l_1 l_2}(\mathbf{k}_i,\ \mathbf{k}_f) = \sum_{m_1 m_2} (l_1 l_2 m_1 m_2 \mid q\varkappa)\, Y^{m_1}_{l_1}(\mathbf{k}_i)\, Y^{m_2}_{l_2}(\mathbf{k}_f).$$

The spherical harmonics are normalized by the condition $\sum_m |Y^m_l|^2 = 1$. Since the scattering matrix must be even under space inversion, it can contain only those functions $\Psi^\kappa_{q l_1 l_2}$ for which $l_1 + l_2$ is even. If $l_1 + l_2 > q + 1$, the function $\Psi^\kappa_{q l_1 l_2}$ can be written as a linear combination with scalar coefficients of the same functions, but with $l_1 + l_2 = q$ if q is even, or with $l_1 + l_2 = q + 1$ if q is odd. Thus in constructing the scattering matrix we can restrict ourselves to functions of $\mathbf{k}_i$ and $\mathbf{k}_f$ of the form

$$\Psi^\varkappa_{q\lambda}(\mathbf{k}_i,\ \mathbf{k}_f) = \sum_{m_1 m_2} (r + \lambda \quad r - \lambda \quad m_1 m_2 \mid q\varkappa)\, Y^{m_1}_{r+\lambda}(\mathbf{k}_i)\, Y^{m_2}_{r-\lambda}(\mathbf{k}_f), \tag{2}$$

where $r = q/2$ if q is even, and $r = (q+1)/2$ if q is odd. The scattering matrix can thus be written as

$$M(\mathbf{k}_i,\ \mathbf{k}_f) = \sum_{q\varkappa q_1 q_2} [T^q_\varkappa (q_1,\ q_2)]^+ \sum_{\lambda=-r}^{r} a^q_\lambda (q_1,\ q_2)\, \Psi^\varkappa_{q\lambda}(\mathbf{k}_i,\ \mathbf{k}_f). \tag{3}$$

If the spin of one of the particles is zero, the matrix becomes

$$M(\mathbf{k}_i,\ \mathbf{k}_f) = \sum_{q\varkappa} (T^q_\varkappa)^+ \sum_{\lambda=-r}^{r} a^q_\lambda \Psi^\varkappa_{q\lambda}(\mathbf{k}_i,\ \mathbf{k}_f). \tag{3a}$$

The number of independent scalar functions of angle and energy, $a^q_\lambda(q_1, q_2)$, is reduced if we impose the condition of time reversibility of the scattering process. If the time reversal operator is written as UK, where K is the complex conjugation (cf. Ref. 7), the reversibility condition is expressed as:

$$U M^*(\mathbf{k}_i,\ \mathbf{k}_f)\, U^+ = M^+(\mathbf{k}_f,\ \mathbf{k}_i), \tag{4}$$

where $*$ denotes complex conjugation and $^+$ means Hermitian conjugation. We then get

$$a^q_{-\lambda}(q_1,\ q_2) = (-1)^{q_1+q_2+q} a^q_\lambda (q_1,\ q_2); \tag{5}$$

the operator U has the property

$$U T^q_\varkappa (q_1,\ q_2)\, U^+ = (-1)^{q+\varkappa} T^q_{-\varkappa}(q_1,\ q_2).$$

If one of the particles has spin zero, the reversibility condition gives

$$a^q_\lambda = a^q_{-\lambda}. \tag{5a}$$

If the particles are identical, a symmetry condition is imposed on the scattering matrix, giving the relation

$$a^q_\lambda (q_1,\ q_2) = a^q_\lambda (q_2,\ q_1). \tag{6}$$

2. DENSITY MATRIX. CROSS SECTION. POLARIZATION.

The density matrix for the spin state of the two particles, (the incident and target particles) is also conveniently expressed in terms of the tensor operators $T^q_\kappa(q_1, q_2)$:

$$\rho = \sum_{q_1 q_2 q\varkappa} \rho_{q\varkappa q_1 q_2} T^q_\varkappa (q_1,\ q_2).$$

The expansion coefficients are identical with the statistical tensors introduced by Fano, and have the physical significance of being polarization tensors. The final density matrix ρ is related to the initial density matrix $\rho^{(0)}$ by

$$\rho = M\rho^{(0)}M^+ / \sigma, \qquad \sigma = \mathrm{Sp}\,\{M\rho^{(0)}M^+\}. \tag{7}$$

If we go over to the polarization tensors, we get

$$\rho_{q_1\varkappa_1 q_{21} q_{22}} = \frac{1}{\sigma} \sum K^{q_1\varkappa_1 q_{11} q_{12}}_{q_2\varkappa_2 q_{21} q_{22}}(\mathbf{k}_i,\ \mathbf{k}_f)\, \rho^{(0)}_{q_1\varkappa_1 q_{11}\varkappa_{12}}, \tag{8}$$

where

$$K^{q_1\varkappa_1 q_{11} q_{12}}_{q_2\varkappa_2 q_{21} q_{22}}(\mathbf{k}_i,\ \mathbf{k}_f) = \mathrm{Sp}\,\{M(\mathbf{k}_i,\ \mathbf{k}_f)\, T^q_\varkappa (q_1,\ q_2)\, M^+(\mathbf{k}_i,\ \mathbf{k}_f)\, [T^q_\varkappa (q_1,\ q_2)]^+\}. \tag{9}$$

Taking the trace gives the following expression:

$$K^{q_1\varkappa_1 q_{11} q_{12}}_{q_2\varkappa_2 q_{21} q_{22}}(\mathbf{k}_i,\ \mathbf{k}_f) = (-1)^{q_2+\varkappa_2} \sum_z (q_1 q_2 \varkappa_1 - \varkappa_2 \mid z\zeta) \times \sum_{p_i \lambda_i} \varphi^{z\zeta}_{p_i\lambda_1 p_i\lambda_2}(\mathbf{k}_i,\ \mathbf{k}_f) \sum_{p_i h} a^{p_1}_\lambda (p_{11},\ p_{12})\, [a^{p_2}_{\lambda_2}(p_{21},\ p_{22})]^*$$

$$\times \sum_{z_i} \begin{pmatrix} s_1 & s_1 & q_{11} \\ s_1 & s_1 & q_{21} \\ p_{11} & p_{21} & z_1 \end{pmatrix} \begin{pmatrix} s_2 & s_2 & s_{12} \\ s_2 & s_2 & q_{22} \\ p_{12} & p_{22} & z_2 \end{pmatrix} \begin{pmatrix} p_{11} & p_{12} & p_1 \\ p_{21} & p_{22} & p_2 \\ z_1 & z_2 & z \end{pmatrix} \begin{pmatrix} q_{11} & q_{12} & q_1 \\ q_{21} & q_{22} & q_2 \\ z_1 & z_2 & z \end{pmatrix},$$

where (10)

$$\varphi^{z\zeta}_{p_1\lambda_1 p_2\lambda_2}(\mathbf{k}_i,\ \mathbf{k}_f) = \sum_{ll'} (r_1+\lambda_1\ r_2+\lambda_2 \| l)\,(r_1-\lambda_1\ r_2-\lambda_2 \| l')$$

$$\times \begin{pmatrix} r_1+\lambda_1 & r_1-\lambda_1 & p_1 \\ r_2+\lambda_2 & r_2-\lambda_2 & p_2 \\ l & l' & z \end{pmatrix} \Psi^{\zeta}_{zll'}(\mathbf{k}_i,\ \mathbf{k}_f),$$

$$(l_1 l_2 \| L) \equiv (l_1 l_2\, 00 \,|\, L\, 0). \qquad (11)$$

If one of the spins, for example the target spin s_2, is zero, the expression simplifies somewhat:

$$K^{q_1\varkappa_1}_{q_2\varkappa_2}(\mathbf{k}_i,\ \mathbf{k}_f) = (-1)^{q_2+\varkappa_2} \sum_{z} (q_1 q_2 \varkappa_1 - \varkappa_2 \,|\, z\zeta)$$

$$\times \sum_{p_i\ \lambda_i} \varphi^{z\zeta}_{p_1\lambda_1 p_2\lambda_2}(\mathbf{k}_i,\ \mathbf{k}_f)\, a^{p_1}_{\lambda_1} [a^{p_2}_{\lambda_2}]^* \begin{pmatrix} s_1 & s_1 & q_1 \\ s_1 & s_1 & q_2 \\ p_1 & p_2 & z \end{pmatrix} \qquad (11a)$$

The meaning of all the quantities is clear from the way they were introduced. The three-by-three tableaus in parentheses are the coefficients of the unitary transformation between different schemes for coupling of four vectors.

The following important equality follows from time reversibility:

$$K^{q_1\varkappa_1 q_{11} q_{12}}_{q_2\varkappa_2 q_{12} q_{22}}(\mathbf{k}_i,\ \mathbf{k}_f) = (-1)^{q_1+\varkappa_1+q_2+\varkappa_2} K^{q_2-\varkappa_2 q_{21} q_{22}}_{q_1-\varkappa_1 q_{11} q_{12}}(\mathbf{k}_f,\ \mathbf{k}_i). \qquad (12)$$

This is not the only condition which the coefficients $K^{\cdots}_{\cdots}$ satisfy. From the conservation of parity, these coefficients are even functions with respect to simultaneous change of the signs of the vectors $\mathbf{k}_i$ and $\mathbf{k}_f$. Therefore, for example, in the coordinate system in which the z axis is along $[\mathbf{k}_i\mathbf{k}_f]$, the sum $\kappa_1 + \kappa_2$ can take on only even values.

It is not difficult to express all measurable quantities — cross section, polarization, and polarization correlation, in terms of the coefficients $K^{\cdots}_{\cdots}$. We now give these expressions.

A. The cross section for scattering of an unpolarized beam by an unpolarized target is

$$\sigma_0 = K^{0000}_{0000}(\mathbf{k}_i, \mathbf{k}_f). \qquad (13)$$

B. The polarization of the scattered beam under these same initial conditions is

$$\rho_{q\varkappa}(\mathbf{k}_i,\ \mathbf{k}_f) = K^{0000}_{q\varkappa q0}(\mathbf{k}_i, \mathbf{k}_f) / \sqrt{2s_1+1}\ \sigma_0. \qquad (14)$$

As a consequence of the parity condition mentioned above, in the coordinate system in which the z axis is parallel to $[\mathbf{k}_i\mathbf{k}_f]$, κ takes on only even values. In particular, this means that the polarization is always along $[\mathbf{k}_i\mathbf{k}_f]$. In the system in which the z axis is along $\mathbf{k}_i$ or $\mathbf{k}_f$ and the y axis is along $[\mathbf{k}_i\mathbf{k}_f]$, the same condition is expressed differently:

$$\rho_{q-\varkappa}(\mathbf{k}_i,\ \mathbf{k}_f) = (-1)^{q+\varkappa} \rho_{q\varkappa}(\mathbf{k}_i,\ \mathbf{k}_f). \qquad (14a)$$

Thus single scattering gives rise to a state of polarization of a special type. In order to obtain a general state of polarization, double scattering is necessary (if we disregard other means of polarization of particles, such as the use of a magnetic field).

C. The cross section for scattering of a polarized beam by an unpolarized target is

$$\sigma(\mathbf{k}_i,\ \mathbf{k}_f) = \sqrt{2s_1+1} \sum_{q\varkappa} K^{q\varkappa q0}_{0000}(\mathbf{k}_i,\ \mathbf{k}_f)\, \rho^{(0)}_{q\varkappa}. \qquad (15)$$

If follows immediately from (12) that measurement of the polarization gives the same information as measurement of the scattering cross section of a polarized beam. Considerations analogous to those of case B show that the angular distribution is affected by only those $\rho^{(0)}_{q\kappa}$ for which κ is even (in the system with the z axis along $[\mathbf{k}_i\mathbf{k}_f]$). In order to determine the remaining part of the polarization tensor, one must use double scattering (once again assuming that we disregard other methods for analyzing the polarization). If we make use of (12) and (14), the expression (15) can be rewritten as

$$\sigma(\mathbf{k}_i,\ \mathbf{k}_f) = (2s_1+1)\,\sigma_0 \sum_{q\varkappa} (-1)^{q+\varkappa} \rho_{q-\varkappa}(\mathbf{k}_f, \mathbf{k}_i)\, \rho^{(0)}_{q\varkappa}. \qquad (15a)$$

It is also not difficult to obtain the cross section for double scattering of an initially unpolarized beam by an unpolarized target. From (15a) we get immediately

$$\sigma_d = (1/\sigma_0^{(1)}) \sum_{q\varkappa} K^{(1)0000}_{q\varkappa q0}(\mathbf{k}_1,\ \mathbf{k}_2)\, K^{(2)q\varkappa q0}_{0000}(\mathbf{k}_2,\ \mathbf{k}_3), \qquad (16)$$

or

$$\sigma_d = (2s_1+1)\,\sigma_0^{(2)} \sum_{q\varkappa} (-1)^{q+\varkappa} \rho^{(1)}_{q\varkappa}(\mathbf{k}_1, \mathbf{k}_2)\, \rho^{(2)}_{q-\varkappa}(\mathbf{k}_3, \mathbf{k}_2) \qquad (16a)$$

($\mathbf{k}_1$ is the direction of incidence of the beam, $\mathbf{k}_2$ its direction after the first scattering, and $\mathbf{k}_3$ its direction after the second scattering).

In a coordinate system with the z axis along $\mathbf{k}_2$, the double scattering cross section is given by

$$\sigma_d = (2s_1+1)\,\sigma_0^{(2)} \sum_{\varkappa=0}^{2s_1} A_\varkappa \cos \varkappa\varphi;$$

$$A_\varkappa = 2 \sum_{q=\varkappa}^{2s_1} \rho^{(1)}_{q\varkappa}(\vartheta_1)\, \rho^{(2)}_{q\varkappa}(\vartheta_2) \quad (\varkappa \neq 0);$$

$$A_0 = \sum_{q=0}^{2s_1} \rho^{(1)}_{q0}(\vartheta_1)\, \rho^{(2)}_{q0}(\vartheta_2). \qquad (16b)$$

Here $\rho^{(1)}_{q\kappa}(\vartheta_1)$ and $\rho^{(2)}_{q\kappa}(\vartheta_2)$ denote the values of the tensors $\rho^{(1)}_{q\kappa}(\mathbf{k}_1, \mathbf{k}_2)$ and $\rho^{(2)}_{q\kappa}(\mathbf{k}_3, \mathbf{k}_2)$ in the

coordinate systems with the y axis perpendicular to the plane of the first and second scattering, respectively (in both cases the z axis is along $\mathbf{k}_2$); φ is the angle between the planes of scattering.

D. The polarization of the scattered beam when a polarized beam is scattered by an unpolarized target is

$$\rho_{q\varkappa}(\mathbf{k}_i, \mathbf{k}_f) = \frac{1}{\sigma(\mathbf{k}_i, \mathbf{k}_f)} \sum_{q'\varkappa'} K_{q\varkappa q0}^{q'\varkappa' q'0}(\mathbf{k}_i, \mathbf{k}_f)\, \rho_{q'\varkappa'}^{(0)}. \quad (17)$$

E. The cross section for scattering of a polarized beam by a polarized target is

$$\sigma = \sqrt{(2s_1+1)(2s_2+1)} \sum_{q_1 q_2 q\varkappa} K_{0000}^{q\varkappa q_1 q_2}(\mathbf{k}_i, \mathbf{k}_f)\, \rho_{q\varkappa q_1 q_2}^{(0)}. \quad (18)$$

F. The polarization correlation in scattering of an unpolarized beam by an unpolarized target is

$$\rho_{q\varkappa q_1 q_2}(\mathbf{k}_i, \mathbf{k}_f) = K_{q\varkappa q_1 q_2}^{0000}(\mathbf{k}_i, \mathbf{k}_f) / \sigma_0 \sqrt{(2s_1+1)(2s_2+1)}. \quad (19)$$

From (12) it follows immediately that experiments E and F are equivalent from the point of view of the information which they give.

3. COMPLETENESS OF POLARIZATION EXPERIMENTS

The number of independent scalar functions of energy and angle, $a_\lambda^q(q_1, q_2)$, which appear in the scattering matrix (3), is equal (if we disregard time reversibility) to

$$N_0(s_1, s_2) = {}^1/_2 [(2s_1+1)^2 (2s_2+1)^2 + 1], \quad (20)$$

if both spins are integral, and to

$$N_0(s_1, s_2) = {}^1/_2 (2s_1+1)^2 (2s_2+1)^2. \quad (20a)$$

if one or both of the spins are half-integral. If we impose condition (5) on the functions $a_\lambda^q(q_1, q_2)$, their number decrease and becomes

$$N(s_1, s_2) = {}^1/_2 N_0(s_1, s_2) + {}^1/_2 (2s_1+1)(2s_2+1). \quad (21)$$

For identical particles the number of independent functions $a_\lambda^q(q_1, q_2)$ appearing in $M(\mathbf{k}_i, \mathbf{k}_f)$ is decreased still further and becomes ($s_1 = s_2 = s$)

$$N(s) = {}^1/_2 N(s, s) + {}^1/_3 (2s+1)(2s^2 + 2s + {}^3/_2). \quad (22)$$

The functions $a_\lambda^q(q_1, q_2)$ are complex, so that all the numbers we have given should be doubled. However, the scattering matrix satisfies the unitarity condition[8]

$$M(\mathbf{k}_i, \mathbf{k}_f) - M^+(\mathbf{k}_f, \mathbf{k}_i) = \frac{ik}{2\pi} \int M^+(\mathbf{k}_f, \mathbf{n})\, M(\mathbf{k}_i, \mathbf{n})\, d\mathbf{n}, \quad (23)$$

which imposes as many relations on the complex functions $a_\lambda^q(q_1, q_2)$ as the number of such functions appearing in the scattering matrix.

In experiments E and F we find the quantities $K_{0000}^{q\varkappa q_1 q_2}(\mathbf{k}_i, \mathbf{k}_f)$ (or $K_{q\varkappa q_1 q_2}^{0000}(\mathbf{k}_i, \mathbf{k}_f)$ which is the same thing). Their number is $N_0(s_1, s_2)$. Thus each of the groups of experiments E and F gives a sufficient number of equations for reconstructing the scattering matrix.

The experiments B and the equivalent experiments C enable us to study only the quantities $K_{q\varkappa q0}^{0000}$, whose number is in general less than the number of elements in the scattering matrix (though this is not the case for scattering by a spin zero target). Double scattering may thus be insufficient for determining $M(\mathbf{k}_i, \mathbf{k}_f)$, which is the situation we meet when we study nucleon-nucleon scattering.

The number of coefficients $K_{q_2\varkappa_2 q_2 0}^{q_1\varkappa_1 q_1 0}$ which appear in the quantities of group D is $N(s_1, s_1)$, and consequently repeated scattering in principle enables us to reconstruct the scattering matrix, but only when $s_1 \geq s_2$.

In conclusion I should like to express my sincere thanks to Ia. A. Smorodinskii and A. I. Baz' for continued interest in the work and much valuable advice.

[1] A. Simon and T. A. Welton, Phys. Rev. **90**, 1036 (1953); A. Simon, Phys. Rev. **92**, 1050 (1953).

[2] L. Wolfenstein and J. Ashkin, Phys. Rev. **85**, 947 (1952); R. H. Dalitz, Proc. Phys. Soc. (London) **A65**, 175 (1952).

[3] W. Lakin, Phys. Rev. **98**, 139 (1955).

[4] Puzikov, Ryndin and Smorodinskii, J. Exptl. Theoret. Phys. (U.S.S.R.) **32**, 592 (1957); Soviet Phys. JETP **5**, 489 (1957).

[5] L. Wolfenstein, Phys. Rev. **96**, 1654 (1954).

[6] R. Oehme, Phys. Rev. **98**, 147 216 (1955).

[7] E. P. Wigner, Gött. Nachr. **31**, 546 (1932).

[8] R. Ryndin and Ia. Smorodinskii, J. Exptl. Theoret. Phys. (U.S.S.R.) **32**, 1584 (1957); Soviet Phys. JETP **5**, 1294 (1957).

Translated by M. Hamermesh
187

STRONG GRAVITATIONAL WAVES IN FREE SPACE

A. S. KOMPANEETS

Institute of Chemical Physics

Submitted to JETP editor November 11, 1957

J. Exptl. Theoret. Phys. (U.S.S.R.) **34**, 953-955 (April, 1958)

The results of Einstein and Rosen[1] are generalized to the case of two interacting gravitational waves.

STRONG gravitational waves were first considered by Einstein and Rosen,[1] who showed that the equations for the propagation of the strong waves, corresponding in the limit to weak transverse-transverse waves of the $g_{22}-g_{33}$ type, reduce to a linear equation of propagation in the case of a cylindrical wave. It can be shown that even in the more general case, strong gravitational waves corresponding in the limit to incident waves of the types $g_{22}-g_{33}$ and g_{23} show a very similar simplification.

We shall start with integrals of the form

$$-ds^2 = Adx_1^2 + Cdx_2^2 + 2Bdx_2dx_3 + Ddx_3^2 - Adx_4^2. \quad (1)$$

where A, B, C, and D depend only on x_1 and x_4; in the limit this corresponds to a plane wave.

Here the coordinates x_1 and x_4 are so chosen that $g_{11} = -g_{44}$, $g_{14} = 0$ (see Einstein and Rosen[1]). This leads to the following expressions for the Christoffel symbols of the second kind (writing $CD - B^2 \equiv \alpha$, and denoting by lower suffixes on the quantities A, B, C, and D their derivatives with respect to the corresponding coordinates)

$$\Gamma^1_{11} = \Gamma^1_{44} = \Gamma^4_{14} = (2A)^{-1}A_1; \quad \Gamma^4_{11} = \Gamma^1_{14} = \Gamma^4_{44} = (2A)^{-1}A_4;$$
$$\Gamma^1_{22} = -(2A)^{-1}C_1; \quad \Gamma^4_{22} = (2A)^{-1}C_4;$$
$$\Gamma^1_{33} = -(2A)^{-1}D_1; \quad \Gamma^4_{33} = (2A)^{-1}D_4;$$
$$\Gamma^1_{23} = -(2A)^{-1}B_1; \quad \Gamma^4_{23} = (2A)^{-1}B_4;$$
$$\Gamma^2_{12} = (2\alpha)^{-1}(DC_1 - BB_1); \quad \Gamma^2_{42} = (2\alpha)^{-1}(DC_4 - BB_4);$$
$$\Gamma^3_{13} = (2\alpha)^{-1}(CD_1 - BB_1); \quad \Gamma^3_{43} = (2\alpha)^{-1}(CD_4 - BB_4);$$
$$\Gamma^3_{12} = (2\alpha)^{-1}(CB_1 - BC_1); \quad \Gamma^3_{42} = (2\alpha)^{-1}(CB_4 - BC_4);$$
$$\Gamma^2_{13} = (2\alpha)^{-1}(DB_1 - BD_1); \quad \Gamma^2_{43} = (2\alpha)^{-1}(DB_4 - BD_4).$$

Except for the $\Gamma^i_{kl} = \Gamma^i_{lk}$ formed from the above symbols by interchanging their lower indices, the other Γ^i_{kl} are equal to zero.

The only components of the curvature tensor $R_{ik} = R^l_{ikl}$ which do not vanish identically are R_{11}, R_{14}, R_{44}, R_{22}, R_{33}, and R_{23}. This gives six equations for the four quantities A, B, C, and D. It must therefore be proved that there is no contradiction in the equations. This will be done for a particular choice of coordinate system. Here we shall only note that two conditions have already been imposed on the choice of coordinate system: $g_{11} = -g_{44}$ and $g_{14} = 0$. Two other conditions are contained in the two extra equations over and above the four which would be sufficient.

We shall first write down the equations $R_{ik} = 0$ for the components 2 and 3. After some simplification they take the following form:

$$C_{44} - C_{11} + (2\alpha)^{-1}[C_1\alpha_1 - C_4\alpha_4 + 2C(B_1^2 - C_1D_1 - B_4^2 + C_4D_4)] = 0; \quad (2)$$

$$D_{44} - D_{11} + (2\alpha)^{-1}[D_1\alpha_1 - D_4\alpha_4 + 2D(B_1^2 - C_1D_1 - B_4^2 + C_4D_4)] = 0; \quad (3)$$

$$B_{44} - B_{11} + (2\alpha)^{-1}[B_1\alpha_1 - B_4\alpha_4 + 2B(B_1^2 - C_1D_1 - B_4^2 + C_4D_4)] = 0. \quad (4)$$

Now multiply equation (2) by D/2, multiply (3) by C/2, and (4) by $-B$, and add. This gives a linear wave equation for $\sqrt{\alpha}$:

$$(\sqrt{\alpha})_{11} - (\sqrt{\alpha})_{44} = 0. \quad (5)$$

But, as Einstein and Rosen showed,[1] the form of the linear element of distance (1) remains invariant under all coordinate transformations $\bar{x}_1 = \bar{x}_1(x_1, x_4)$ and $\bar{x}_4 = \bar{x}_4(x_1, x_4)$ which satisfy the equation

$$(\bar{x}_1)_{11} - (\bar{x}_1)_{44} = 0. \quad (6)$$

Therefore it is possible, without any loss of generality, to assume

$$\sqrt{\alpha} = \bar{x}_1. \quad (7)$$

This can also be demonstrated in a different way, as follows. The general solution of (5) is $\sqrt{\alpha} = f(x_1 + x_4) + g(x_1 - x_4)$. Let us choose a

coordinate system such that

$$f(x_1 + x_4) = (x_1 + x_4)/2,\ g(x_1 - x_4) = (x_1 - x_4)/2.$$

This choice is compatible with the integral form (1) because of condition (6).

We shall now show that there is no contradiction in the entire system of gravitational equations for the special case $\sqrt{\alpha} = x_1$. (The bars above x_1 and x_4 will be omitted, and we write $\ln\sqrt{A} \equiv L$):

$$2R_{11} = -2[L_{11} - L_{44} - (x_1)^{-1}L_1] - (x_1)^{-2}(B_1^2 - C_1D_1) = 0; \quad (8)$$

$$2R_{44} = 2[L_{11} - L_{44} + (x_1)^{-1}L_1] - (x_1)^{-2}(B_4^2 - C_4D_4) = 0; \quad (9)$$

$$R_{14} = (x_1)^{-1}L_4 - (2x_1)^{-2}(2B_1B_4 - C_4D_1 - C_1D_4) = 0. \quad (10)$$

Half the sum of (8) and (9) gives

$$(x_1)^{-1}L_1 - (2x_1)^{-2}(B_1^2 + B_4^2 - C_1D_1 - C_4D_4) = 0. \quad (11)$$

Differentiating (10) with respect to x_1 and (11) with respect to x_4, it is easy to show, with the aid of (2), (3), and (4), that equations (10) and (11) are compatible, so that the difference in the expressions for L_{14} and L_{41} are proportional to

$$CD_4 + DC_4 - 2BB_4 = (CD - B^2)_4 = (x_1^2)_4 \equiv 0.$$

Finding the second derivatives L_{11} and L_{44} from (10) and (11), we readily see, with the aid of (2), (3), and (4), that equations (8) and (9) are also satisfied. This proves the compatibility of the whole system of equations.

Let us now return to the equations for B, C, and D. Eliminating B by means of $\alpha = x_1^2$ and introducing the new variables

$$\sigma \equiv C(CD - x_1^2)^{-1/2}, \quad \delta = D(CD - x_1^2)^{-1/2}, \quad (12)$$

we have

$$\begin{aligned}[x_1(\sigma\delta - 1)^{-1/2}\sigma_1]_1 - x_1[(\sigma\delta - 1)^{-1/2}\sigma_4]_4 = 0,\\ [x_1(\sigma\delta - 1)^{-1/2}\delta_1]_1 - x_1[(\sigma\delta - 1)^{-1/2}\delta_4]_4 = 0,\end{aligned} \quad (13)$$

corresponding to two non-linear interacting cylindrical waves. In the case studied by Einstein and Rosen[1] a linear cylindrical wave was obtained. A strong plane wave is impossible, because the metric curvature which it produces is incompatible with flat space (see Bergmann[2]).

Nevertheless it is a fact that, in spite of the non-linearity of the system of hyperbolic equations (13), their characteristics are the straight lines $x_1 = \pm x_4$. This shows that the strong gravitational waves propagate with a fundamental velocity equal to the speed of light, just as the weak ones do.* This is much more difficult to deduce from the general gravitational equations $R_{ik} = 0$. Notice further that the characteristics of each family obviously do not intersect. This means that the non-linear hyperbolic equations for gravity in free space do not necessarily lead to the formation of shock waves. In this they differ from the equations of gas dynamics, for example, which belong to the same class.

The space is Riemannian if it admits a continuous group of coordinate transformations. The occurrence of shock waves would contradict the basic hypothesis of continuous transformations; i.e., the Riemannian character of the metric. Thus our investigation has again shown the internal consistency of the Einstein equations for the gravitational field.

In conclusion I should like to thank V. L. Ginsberg for showing me the basic literature sources.

[1] A. Einstein and N. Rosen, J. Franklin Inst. 223, 43 (1937).

[2] P. B. Bergmann, Introduction to the Theory of Relativity (New York, 1942). Russian translation, 1947, p 253.

Translated by D. C. West
188

*It would nevertheless be interesting to study the general case $ds^2 = g_{ik}dx^i dx^k$ where $g_{ik} = g_{ik}(x_1, x_4)$.

ON THE LATERAL DISTRIBUTION OF PARTICLES IN EXTENSIVE AIR SHOWERS

G. B. KHRISTIANSEN

Moscow State University

Submitted to JETP editor November 11, 1957

J. Exptl. Theoret. Phys. (U.S.S.R.) **34**, 956-961 (April, 1958)

The relative role of various factors affecting the lateral divergence of charged particles in extensive air showers is considered. It is shown that the lateral distribution of electrons is completely determined by Coulomb scattering. The lateral distribution of μ mesons is to a large degree determined by Coulomb scattering and deflection in the magnetic field of the earth. The transverse momentum transferred to π and K mesons in an elementary nuclear cascade act is respectively $\leq 1.5 \times 10^8$ ev/c and $\leq 5 \times 10^8$ ev/c.

RECENTLY a number of experiments[1-5] were carried out to study in detail the lateral density distributions of electrons, μ mesons, and nuclear-active particles in extensive atmospheric cosmic ray showers in the lower layers of the atmosphere. In addition, the lateral distribution of electrons and μ mesons was investigaged for distances up to several hundred meters from the shower axis.

In connection with these experiments, it is expedient to consider the question of the relative effect of various factors determining the lateral divergence of shower particles.

Shower particles may deviate from the flight direction of the primary particle which produced the entire shower because of the following reasons:

I. The angular divergence of secondary particles: (a) in the elementary nuclear cascade act and (b) in spontaneous decay acts.

II. Coulomb scattering (of charged particles) by air nuclei.

III. Lorentz forces determined by the earth's magnetic field (acting on the charged particles).

After the discovery of the so-called "anomalous" shower width[6] it was hypothesized[7] that the basic cause of the wide lateral divergence of shower particles is reason I(a). However, a more detailed analysis of the effects of the second and third reasons shows that this notion must be reconsidered.

Let us first consider the lateral distribution of electrons. Electrons in an extensive atmospheric shower originate in electron-photon cascade showers generated by γ-quanta from the decay of π^0 mesons. The latter are formed in the elementary nuclear-cascade acts. As was shown in Ref. 7, from the point of view of the laws of conservation of energy and momentum, the maximum possible π^0-meson emission angles in these acts are sufficiently large, so that the cores of the individual cascade showers could deviate from the axis of the entire shower by a distance on the order of several hundred meters, creating at these distances electron densities which agree with experimental data.

According to the calculations of Moliere[8] and Eyges,[9] available until recently, the electrons in electron-photon cascade showers could not occur in considerable quantities at such large distances. However, during the past few years Nishimura and Kamata,[10] and also Greisen,[10] gave a more accurate solution of the problem on the lateral distribution of electrons in electron-photon cascade showers, which leads to a different qualitative conclusion.

Let us compare the experimental lateral electron distribution[1-5] with theoretical distributions according to Nishimura and Kamata, for the various degrees of s-development of an electron-photon cascade shower. In spite of the fact that the development of the electron-photon component in a real shower is different on the whole than in an electron-photon cascade shower, such a comparison of lateral distributions is justifiable, since the latter are determined primarily by the energy spectrum of electrons and depends quite weakly on the "previous history" of the electron-photon cascade shower.

The lateral distribution of electrons from Refs. 1 — 5 is shown in Fig. 1. The unit of length is $r_1 = E_S X_0/\beta$ (E_S = 19 Mev, β = 72 Mev, and X_0 = 270 m above sea level). The theoretical curves are shown for the parameter s = 1, 1.25, and 1.4. All the curves are normalized for areas under them. The experimental points fit well the theoretical curve for s = 1.25 up to distances r = 3 (Ref. 5) and do not depart appreciably from the curve with

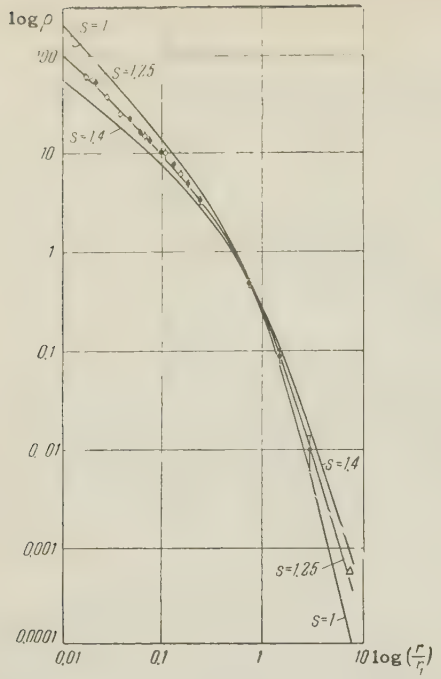

FIG. 1. Comparison of experimental lateral electron distribution in extensive atmospheric showers[1-5] with the theoretical electron distribution in a photon-electron shower according to Nishimura and Kamata.[10] Δ – experimental data of Ref. 1; o, ● – data of Ref. 5.

s = 1.25 for larger distances up to r = 7 (Ref. 4).

The agreement of the experimental and theoretical curves for one definite value of s in such a wide range of distances is, of course, not accidental and it is natural to suppose that this takes place because the energy spectrum of shower electrons coincides with the energy spectrum of the electron-photon cascade shower of age s, whereas the lateral divergence of electrons is determined entirely by Coulomb scattering. Unfortunately, the electron energy spectrum has not been measured to date, but it is worth noting that the electron absorption coefficient, obtained by investigating the barometric effect and altitude behavior of the shower, agrees with the value s = 1.2.[5,11] Thus, if the energy spectrum of the electrons in the shower coincides with the energy spectrum of electrons in an electron-photon cascade shower of age s = 1.2, then the experimentally observed extensive lateral divergence of the electrons can be explained only by the Coulomb scattering of the electrons in the individual electron-photon cascade showers, without assuming that the cores of these showers leave the basic core of the extensive atmospheric shower.*

*As was shown by Cocconi,[12] the earth's magnetic field does not exert any substantial effect on the lateral distribution of electrons for showers observed in the lower layers of the atmosphere.

Let us consider now the lateral distribution of μ mesons. μ mesons originate from the decay of $\pi^{\pm}$ and $K^{\pm}$ mesons in the upper layers of the atmosphere. According to experimental data[13] μ mesons originate in extensive atmospheric showers at altitudes of 5 to 20 km above sea level. μ mesons cover large distances from the place of origin to the observation level, experiencing practically no interactions involving considerable energy losses, and losing energy slowly by ionizing air atoms. The lateral distribution of low-energy μ mesons was investigated by a number of workers.[3-5] According to the experimental data, the meson density falls off considerably slower than the electron current density even over large distances, on the order of hundreds of meters from the shower axis.

The presence of a large free path brings us to the important role played in the lateral divergence of μ mesons both by the Coulomb scattering from air nuclei and by deflections in the earth's magnetic field, even if the muons have a relatively high energy. Inasmuch as $\rho_{\mu}(r)$, even for the maximum distances from the axis investigated in the above references, does not drop off faster than $1/r^2$, we shall not consider quantitatively the Coulomb scattering effect and deflections in the earth's magnetic field. Let us limit ourselves to the evaluation of the mean square deflection $\sqrt{\overline{r_s^2}}$ of μ mesons with energy E by multiple scattering, and to their deflection in a magnetic field r_M. It is obvious that:

$$\overline{r_s^2} = \int_0^H \frac{h^2 E_s^2}{[E + \beta t_0 (1 - e^{-\alpha h})]^2} t_0 \alpha e^{-\alpha h} dh. \qquad (1)$$

Where, H is the altitude above the observation level at which the μ mesons are produced, t_0 the depth of observation level in shower units, E_S the parameter of multiple-scattering theory, β the ionization losses calculated for one shower unit in air (E_S = 21 Mev, β = 72 Mev), α the coefficient in the barometric formula: $\alpha = (1/7000)\ m^{-1}$. For r_m we have the following expression:

$$r_m = \int_0^H h\, dh / \rho; \quad \rho = E + \beta t_0 (1 - e^{-\alpha h}) / 300\, \mathcal{H}, \qquad (2)$$

where $\mathcal{H}$ is the component of the earth's magnetic field perpendicular to the axis of the extensive atmospheric shower. Assuming the altitude of μ meson generation to be H = 10 km above sea level, and considering that the mean energy of the μ mesons at large distances from the shower axis is close to the minimum energy recorded by the detector, equal in the above experiments to 3×10^8 ev, we obtain the values of $\sqrt{\overline{r_s^2}}$ and r_m shown below.* (In doing this we can estimate only the min-

*The data are for sea level.

imum the experimental value of $\sqrt{\overline{r_s^2}}$).

$\sqrt{r^2_{exp.}}$	$\sqrt{\overline{r_s^2}}$	r_m
$\geqslant 400$ m	300 m	200 m.

Thus, the lateral distribution of low-energy μ mesons, ordinarily investigated in experiments, is determined essentially by the Coulomb scattering of the μ mesons and by their deflection in the earth's magnetic field. The angular divergence of the μ-meson "ancestors" in the elementary nuclear cascade acts is also evidently an essential factor in the lateral divergence of the μ mesons. However, the relative role of all these factors cannot be definitely determined at the present time without additional experimental data on the lateral distribution of μ mesons, their energy spectrum, and also the altitude of their production in the atmosphere.*

It is especially interesting to analyze data on the lateral distribution of high-energy μ mesons, since such mesons originate in elementary nuclear-cascade acts of higher energies. Such data were obtained by George[14] and Cocconi.[15] However, these are qualitative in nature, since the lateral distribution of the μ mesons was investigated by the correlation-curve method. Recently Andronikashvili and Bibilashvili,[16] using the method of correlated hodoscopes, obtained the lateral distribution of μ mesons of energy $E \geq 1.5 \times 10^{10}$ ev in extensive showers at sea level. The experimental data[16] are shown in Fig. 2. As can be seen, the lateral distribution is investigated up to distances where the drop-off in the function $\rho_\mu(r)$ becomes $\sim 1/r^3$. Consequently, the experimental data enable one to evaluate the integral $\int \rho_\mu(r) \times 2\pi r dr$, corresponding to the full number of μ mesons in the shower, since the integral does not diverge at the upper limit. Thus, it is meaningful to make a more detailed examination of the effect of Coulomb scattering and of the magnetic field on the lateral divergence of μ mesons.†

Let us find the lateral distribution function $\rho_\mu(r)$ for the case of μ-meson divergence due to Coulomb scattering and the deflection in the earth's magnetic field, neglecting factor I. The lateral distribution of multiply-scattered μ mesons with

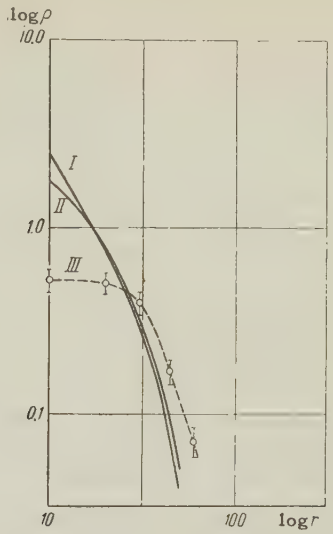

FIG. 2. Lateral distribution of μ mesons in extensive atmospheric showers. I – theoretical curve $\rho_\mu(r_1 > E_{min})$; $\gamma = 0.7$, H = 10 km. II – the same for $\gamma = 1.3$, H = 10 km; III – experimental data of Ref. 16.

energies $E \gg \beta t_0 (1 - e^{-\alpha H})$, has the form of a Gaussian distribution

$$\rho_\mu(r, E)\, dE = C(E) \exp\{-r^2/\overline{r^2}(E)\}\, dE,$$

where $\overline{r^2}(E)$ is determined by the above-mentioned formula. C is determined from the condition

$$\int \rho_\mu(r, E)\, dE\, 2\pi r dr = F(E)\, dE,$$

if

$$F(E)\, dE = AE^{-(\gamma+1)} dE,$$

then

$$C = AE^{-(\gamma+1)}/\pi\overline{r^2}(E) = AE^{-(\gamma-1)}/\pi B(H, t_0),$$

since

$$\overline{r^2} = E^{-2} B(H, t_0).$$

The action of the earth's magnetic field results in a lateral sorting out of the μ mesons according to their energy and charge. If the shower axis is vertical, the positive μ mesons are displaced to the east, and the negative ones in the opposite direction. At the same time, all μ mesons of energy E have the same deflection, $r_m(E) = (H^2/2E) \times 300\mathcal{H}$. Thus, the simultaneous action of the Coulomb scattering and the deflection in the earth's magnetic field can be taken into account in the following expression for $\rho_\mu(r)$, which gives the lateral distribution in the west-east direction.*

$$\rho_\mu(r_1 > E_{min}) = \int_{E_{min}}^{\infty} \frac{A}{\pi B(H, t_0)} E^{-(\gamma-1)} \exp\left\{\frac{-(r - r_m)^2 E^2}{B(H, t_0)}\right\} dE$$

*It is necessary to consider the sensitivity of the values $\sqrt{\overline{r_s^2}}$ and r_m to the altitude H of μ meson production. The value of r_m is quite sensitive to H. According to (2), without taking into account ionization losses, $r_m \sim H^2$. The value of $\overline{r_s^2}$ is considerably less sensitive to H when $\alpha H > 1$: $\overline{r_s^2} \sim |(2/\alpha^2) - H^2 e^{-\alpha H}|$. However, $\overline{r_s^2} \sim (\alpha H)^3$ when $\alpha H < 1$.

†It is impossible to calculate $\overline{r^2}$ from experimental data for this would require us to investigate $\rho_\mu(r)$ up to distances corresponding to a $1/r^5$ drop off.

*The experimental setup was oriented in this direction.

$$+\int_{E_{\min}}^{\infty} \frac{A}{B(H, t_0)} E^{-(\gamma-1)} \exp\left\{\frac{-(r+r_m)^2E^2}{B(H,t_0)}\right\} dE\,.$$

In Fig. 2 are shown the theoretical curves calculated for various assumptions concerning γ (Ref. 17), for $E_{min} = 1.5 \times 10^{10}$ ev, H = 10 km, and the latitude of Tbilisi. The comparison of the theoretical and experimental curves shows that the lateral divergence of high-energy μ mesons is essentially dependent on factors II and III.*

Using the cited data we can estimate of the value of the transverse momentum acquired by the secondary particles, the $\pi^{\pm}$ and $K^{\pm}$ mesons, in elementary nuclear-cascade acts. The transverse momentum of s secondary particle of energy E is $p = (E/c)\vartheta$, where ϑ is the emission angle of the secondary particle in the laboratory system. If the μ-meson energy spectrum has the form $F(E)\,dE = AE^{-(\gamma+1)}\,dE$ for $E > E_{min}$, then, neglecting ionization losses and the μ-meson decay probability (this is true for $E \gg 10^{10}$ ev), one can obtain the differential spectrum of the decayed $\pi^{\pm}$ mesons and $K^{\pm}$ mesons:

$$f_{\pi(K)} = \frac{A}{\left[1-\left(\frac{m}{M}\right)^2\right]\gamma E}\left(E_{\min}^{-\gamma} - E^{\gamma}\right)$$

$$\text{for } E_{\min} \leqslant E \leqslant \left(\frac{M}{m}\right)^2 E_{\min};$$

$$f_{\pi(K)} = \frac{A}{\left[1-\left(\frac{m}{M}\right)^2\right]\gamma}\left[\left(\frac{m}{M}\right)^{-2\gamma} - 1\right]E^{-(\gamma+1)}$$

$$\text{for } E \geqslant \left(\frac{M}{m}\right)^2 E_{\min},$$

Where M is the mass of $\pi^{\pm}$ or $K^{\pm}$ meson, m the mass of the μ meson, and E_{min} the minimum energy of the recorded μ mesons (1.5×10^{10} ev in the experiments of Ref. 16).

Let us determine now the value of energy E* which is possessed by more than half of decayed $\pi^{\pm}$ (or $K^{\pm}$) mesons. For the case of $\pi^{\pm}$ mesons, $E^* = 2E_{min} = 3 \times 10^{10}$ ev. For the case of $K^{\pm}$ mesons, $E^* = 7E_{min} = 10^{11}$ ev, $p^* = E^*\vartheta/c$ and since $\vartheta < 50\ m/10^4\ m = 5 \times 10^{-3}$, then $p_{\pi}^* < 1.5 \times 10^8$ ev; and $p_K^* < 5 \times 10^8$ ev.†

In conclusion it is necessary to note that the Coulomb scattering must also be taken into account in analyzing data for the lateral distribution of charged nuclear-active particles in extensive atmospheric showers.

The author wishes to express his thanks to S. B. Vernov and G. T. Zatsepin for discussion of the above questions.

*The observed discrepancy between the experimental and theoretical curves can be understood if one takes into account the specific geometry of the setup used in Ref. 16. The detector of high-energy μ mesons was placed at a depth of 27 meters underground. The apparatus to locate the shower axis was placed on the surface of the earth. The inclination of the shower axis from the vertical could cause a systematic error in the determination of the distance from the shower axis to the detector, on the order of half of the indicated depth.

†The transverse momentum acquired by the μ meson on account of factor Ib, has an order of magnitude of $\mu_{\pi}c/2$ for the $\pi \to \mu + \nu$ decay; for the $K \to \mu + \nu$ decay, $\mu_K c/2 = 2\mu_{\pi}c$.

[1] Vavilov, Nikol' skii, and Tukish, Dokl. Akad. Nauk SSSR **93**, 233 (1953).

[2] Abrosimov, Bedniakov, Zatsepin, et al., J. Exptl. Theoret. Phys. (U.S.S.R.) **29**, 693 (1955), Soviet Phys. JETP **2**, 357 (1956).

[3] Antonov, Vavilov, Zatsepin, et al., J. Exptl. Theoret. Phys. (U.S.S.R.) **32**, 227 (1957), Soviet Phys. JETP **5**, 172 (1957).

[4] Eidus, Adamovich, Ivanovskaia, et al., J. Exptl. Theoret. Phys. (U.S.S.R.) **22**, 440 (1952).

[5] Abrosimov, Goriunov, Dmitriev, et al., J. Exptl. Theoret. Phys. (U.S.S.R.), (1958), Soviet Phys. JETP (in press).

[6] G. T. Zatsepin and V. V. Miller, J. Exptl. Theoret Phys. (U.S.S.R.) **17**, 939 (1947).

[7] Dobrotin, Zatsepin, Rosental', et al., Usp. Fiz. Nauk **49**, 2 (1953).

[8] G. Moliere, Cosmic Radiation, ed. by W. Heisenberg, N. Y. (1946), p. 26.

[9] L. Eyges, Phys. Rev. **74**, 1801 (1948).

[10] Progress in Cosmic Rays, N. J. (1956) vol. 3, p. 26.

[11] Cranshaw, Oxford Conference of extensive air showers, (1956).

[12] G. Cocconi, Phys. Rev. **93**, 646 (1954).

[13] Rossi, Clark, and Bassi, Phys. Rev. **92** 441 (1953).

[14] E. P. George, Proc. Phys. Soc. **A66**, 345 (1953).

[15] Barrett, Bollinger, Cocconi, et al., Revs. Mod. Phys. **24**, 133 (1952).

[16] E. L. Andrinikashvili and M. F. Bibilashvili, J. Exptl. Theoret. Phys. (U.S.S.R.) **32**, 403 (1957), Soviet Phys. JETP **5**, 341 (1957).

[17] Skarvaralidze, Dissertation, Tbilisi (1956).

Translated by H. Kruglak
189

INFLUENCE OF THE LATTICE VIBRATIONS OF A CRYSTAL ON THE PRODUCTION OF ELECTRON-HOLE PAIRS IN A STRONG ELECTRICAL FIELD

L. V. KELDYSH

P. N. Lebedev Physics Institute, Academy of Sciences, U.S.S.R.

Submitted to JETP editor November 11, 1957

J. Exptl. Theoret. Phys. (U.S.S.R.) 34, 962-968 (April, 1958)

We have evaluated the probability for the production of an electron-hole pair in a semiconductor in a strong electrical field, taking into account the electron-phonon interaction. We have obtained the temperature dependence of this effect which is very appreciable at low temperatures. We have considered qualitatively other processes which may influence the probability of the diffusion of a valence electron into the conduction band, such as the absorption of several phonons and collisions with a slow (non-ionizing) conduction electron or with an impurity. It is pointed out that the first of these processes can play a decisive role in relatively weak fields.

In a previous paper[1] we noted that interactions leading to a change in the quasi momentum of an electron (in particular, the electron-phonon interaction) can play a very essential role in the electron-hole pair production process in a semiconductor when a strong electrical field is present. In the same paper we derived a set of equations (1.12) which determined the probability of the corresponding processes (the 1 denotes here and henceforth the equations of Ref. 1; we use also everywhere, where it is not stated specifically, the notation introduced in that paper). Since their probability is always small, the direct diffusion of a valence electron into the conduction band, considered in Ref. 1, and the transition involving a phonon are to a first approximation independent of one another and can be considered separately. The present paper is devoted to an evaluation of the probability of the latter process.

The initial condition can now be written in the form

$$c_j([N_{\mathbf{k}}],\ \mathbf{p},\ 0) = \delta_{jV} c([N_{\mathbf{k}}]). \tag{1}$$

The integration of equations (1.12) gives then the following expression for the probability of diffusion for one period of oscillation (we assume again for the time being that the field $\mathbf{E}$ is directed along one of the principal axes of the simple cubic lattice)

$$\left|c_c\left([N_{\mathbf{k}}], \mathbf{p}_0, \frac{2\pi\hbar}{eEd}\right)\right|^2 = \frac{\nu}{VN}\frac{1}{(e\hbar E)^2}\sum_{\mathbf{k}'}\left\{N_{\mathbf{k}'}\left|c([N_{\mathbf{k}}] - 1_{\mathbf{k}'})\right.\right.$$
$$\left.\times\int_{-\frac{\pi\hbar}{d}}^{\frac{\pi\hbar}{d}} M_{Vc}(\mathbf{p}, \hbar\mathbf{k}')\, Q^{+}_{Vc}\left(\mathbf{p}, \mathbf{k}', \frac{p_\parallel}{eE}\right) dp_\parallel\right|^2$$
$$+ (N_{\mathbf{k}'}+1)\left|c([N_{\mathbf{k}}] + 1_{\mathbf{k}'})\right.$$
$$\left.\times\int_{-\pi\hbar/d}^{\pi\hbar/d} M_{Vc}(\mathbf{p}, -\hbar\mathbf{k}')\, Q^{-}_{Vc}\left(\mathbf{p}, \mathbf{k}', \frac{p_\parallel}{eE}\right) dp_\parallel\right|^2\Big\}. \tag{2}$$

In deriving Eq. (2) we took it into account that, by virtue of the presence of fast oscillating factors, the terms with different $\mathbf{k}'$ do not interfere with one another. The experimentally observed diffusion probability $D_0(\mathbf{p}_\perp)$ can now be obtained by summation over $[N_{\mathbf{k}}]$, which in the given case leads simply to the substitution

$$N_{\mathbf{k}} \to \overline{N}_{\mathbf{k}} \equiv [\exp\{\hbar\omega_{\mathbf{k}}/kT\} - 1]^{-1}. \tag{3}$$

Here k is Boltzmann's constant and T the absolute temperature. Hence

$$D_0(\mathbf{p}_\perp) = \frac{\nu}{VN}\frac{1}{(e\hbar E)^2}$$
$$\times\sum_{\mathbf{k}}\left\{(\overline{N}_{\mathbf{k}}+1)\left|\int_{-\pi\hbar/d}^{\pi\hbar/d} M_{Vc}(\mathbf{p}, \hbar\mathbf{k})\, Q^{+}_{Vc}\left(\mathbf{p}, \mathbf{k}, \frac{p_\parallel}{eE}\right) dp_\parallel\right|^2\right.$$
$$\left.+\,\overline{N}_{\mathbf{k}}\left|\int_{-\pi\hbar/d}^{\pi\hbar/d} M_{Vc}(\mathbf{p}, -\hbar\mathbf{k})\, Q^{-}_{Vc}\left(\mathbf{p}, \mathbf{k}, \frac{p_\parallel}{eE}\right) dp_\parallel\right|^2\right\}. \tag{4}$$

The presence of the fast oscillating factors $Q^{\pm}_{Vc}(\mathbf{p}, \mathbf{k}, p_\parallel/eE)$ in the expressions under the integral sign in Eq. (4) leads to a very fast decrease of the diffusion probablity with increasing minimum value which the quantity $\epsilon_c(\mathbf{p}) - \epsilon_V(\mathbf{p} \pm \hbar\mathbf{k})$ attains for given $\mathbf{p}_\perp$ and $\mathbf{k}$. The basic contribution to (4) is thus made by terms with values of $\mathbf{k}$ near $\mathbf{k}_0$, which is the difference between the values of the quasi momentum corresponding to the minimum value of the energy in the conduc-

tion band and the one corresponding to the maximum value in the valence band, divided by $\hbar$. As a rule, as we noted already in Ref. 1, $\mathbf{k}_0 \neq 0$. This leads to some changes in the evaluation of the integrals in (4). Indeed, the width Δ of the forbidden band is by definition less than ϵ_0, the minimum value of the function $\epsilon_c(\mathbf{p}) - \epsilon_V(\mathbf{p})$, and the difference $\epsilon_c(\mathbf{p}) - \epsilon_V(\mathbf{p} - \hbar\mathbf{k}_0)$ tends therefore to zero in the complex $\mathbf{p}_\parallel$ plane before any of the energies occurring in it reach a branching point [the latter coincide with the zeroes of the function $\epsilon_c(\mathbf{p}) - \epsilon_V(\mathbf{p})$]. As a result, for the values

$$p_\parallel = [2m^*_\parallel(\varepsilon_{c\min} - \varepsilon_{V\max} \pm \hbar\omega_{\mathbf{k}_0})]^{1/2} \tag{5}$$

the integrands in (4) have not poles, but saddle points. The quantity $m^*_\parallel$ which enters in (5) is the reduced effective mass of the electron and hole, corresponding to motion in the direction of the electrical field.

Evaluating the integrals in (4) by the saddle-point method, and integrating the result obtained with respect to $\mathbf{p}_\perp$, we arrive at the following expression for the number of electrons per unit volume, which get into the conduction band per unit time:

$$n = 2^{3/2}\pi^{7/2}N(2\pi\hbar)^{-6}\left[\prod_i m^*_{ic}m^*_{iV}\right]^{1/2}\Delta^3\Omega_0^2\frac{1}{\hbar\Delta}|M_{Vc}(\mathbf{p}_{\min}, \hbar\mathbf{k}_0)|^2$$
$$\times (e\hbar E/\sqrt{2m^*_\parallel}\Delta^{3/2})^{3/2}\exp\left\{n\gamma_0 - \frac{4\sqrt{2m^*_\parallel}}{3e\hbar E}(\Delta - \hbar\omega_{\mathbf{k}_0})^{3/2}\right\}$$
$$\times\left[\overline{N}_{\mathbf{k}_0} + (1+\overline{N}_{\mathbf{k}_0})\exp\left\{-\frac{4\sqrt{2m^*_\parallel\Delta}}{e\hbar E}\hbar\omega_{\mathbf{k}_0}\right\}\right]. \tag{6}$$

Here $\mathbf{p}_{\min}$ is the value of the quasi momentum corresponding to the lowest electron state in the conduction band, while m^*_{ic} and m^*_{iV} are the principal values of the effective mass tensors of the electrons and holes. Just as was done in Ref. 1, one can easily show that Eq. (6) is valid for lattices of all symmetries and for an arbitrary direction of the field.

Equation (6) contains, generally speaking, an unknown matrix elements $M_{Vc}(\mathbf{p}_{\min}, \hbar\mathbf{k}_0)$. To get a very rough estimate, we can use the fact that the free-flight time τ of an electron in the conduction band is determined by the matrix elements $M_{cc}(\mathbf{p}_{\min}, \hbar\mathbf{k})$ which for $k \approx k_0$ have the same order of magnitude as $M_{Vc}(\mathbf{p}_{\min}, \hbar\mathbf{k}_0)$.

$$\frac{1}{\tau} \sim \frac{\Omega_0}{(2\pi\hbar)^3}\frac{2\pi}{\hbar}$$
$$\times\int|M_{cc}(\mathbf{p}, \mathbf{p}' - \mathbf{p}|^2\delta[\varepsilon_c(\mathbf{p}) - \varepsilon_c(\mathbf{p}') \pm \hbar\omega_{\mathbf{p}'-\mathbf{p}}]\,d^3p'$$
$$\sim \frac{\Omega_0}{(2\pi\hbar)^3\hbar}\overline{|M_{cc}(\mathbf{p}, \hbar\mathbf{k})|^2}\int\delta[\varepsilon_c(\mathbf{p}) - \varepsilon_c(\mathbf{p}')]\,d^3p'$$
$$= \frac{\Omega_0}{(2\pi\hbar)^3\hbar}\overline{|M_{cc}(\mathbf{p}, \hbar\mathbf{k})|^2}\frac{\overline{S[\varepsilon_c(\mathbf{p})]}}{|\operatorname{grad}\varepsilon_c(\mathbf{p})|}, \tag{7}$$

where $S(\epsilon)$ is the area of the surface $\epsilon_c(\mathbf{p}) = \epsilon$, and the bar indicates averaging over that surface. Taking it into account that in a semiconductor the motion takes place at the bottom of the conduction band and that thus

$$S[\varepsilon_c(\mathbf{p})] \approx 8\pi m^*_c\varepsilon_c(\mathbf{p}),\ |\operatorname{grad}\varepsilon_c(\mathbf{p})| \sim (2\varepsilon_c(\mathbf{p})/m^*_c)^{1/2},$$

and substituting $\epsilon_c(\mathbf{p}) \sim kT$ we get

$$\frac{1}{\tau} \sim \frac{\overline{|M_{cc}(\mathbf{p}_{\min}, \hbar\mathbf{k})|^2}}{(\hbar/m^*_c)(\pi\hbar/d)^2}\frac{\sqrt{2m^*_c kT}}{\pi\hbar/d} \tag{8}$$

If the lowest state of the conduction band is degenerate, which apparently is the case for all cases of practical interest, then the transitions with large changes in quasi momentum, will make a considerable contribution to τ^{-1}, i.e., $k \sim k_0$. We then have for the quantity in which we are interested

$$|M_{Vc}(\mathbf{p}_{\min}, \hbar\mathbf{k}_0)|^2 \sim \overline{|M_{cc}(\mathbf{p}_{\min}, \hbar\mathbf{k})|^2}$$

and (6) can be rewritten

$$n \sim \frac{N\tau^{-1}}{(2\pi\hbar)^6}\left(\prod_i m^*_{ic}m^*_{iV}\right)^{1/2}\Delta^3\Omega_0^2\frac{1}{\Delta m^*_c}\left(\frac{\pi\hbar}{d}\right)^2\frac{\pi\hbar}{\sqrt{2m^*_c kT_D}\,d}$$
$$\times\left(\frac{c\hbar E}{\sqrt{2m^*_\parallel}\Delta^{3/2}}\right)^{3/2}\exp\left\{n\gamma_0 - \frac{4\sqrt{2m^*_\parallel}}{3e\hbar E}(\Delta - \hbar\omega_{\mathbf{k}_0})^{3/2}\right\}$$
$$\times\left[\overline{N}_{\mathbf{k}_0} + (1+\overline{N}_{\mathbf{k}_0})\exp\left\{-\frac{4\sqrt{2m^*_\parallel\Delta}}{e\hbar E}\hbar\omega_{\mathbf{k}_0}\right\}\right]. \tag{9}$$

In this equation we have introduced the Debye temperature T_D, since in estimating τ we had assumed $N_{\mathbf{k}} \sim 1$. One can easily verify that relation (9) holds also in the case where the lowest state is non-degenerate. Indeed, the order of magnitude of the quantity of interest to us is given by

$$|M_{Vc}(\mathbf{p}_{\min}, \hbar\mathbf{k}_0)|^2 \sim \overline{|M_{cc}(\mathbf{p}_{\min}, \hbar\mathbf{k})|^2}\,\hbar k_0/\sqrt{2m^*_c kT}.$$

However, if we substitute in Eq. (8) a temperature on the order of the Debye temperature, we must still introduce an additional factor

$$N_{\mathbf{k}} \sim kT_D/\hbar\omega_{\mathbf{k}} \sim kT_D/cp$$
$$\sim kT_D/c\sqrt{2m^*_c kT_D} \sim \hbar k_0/\sqrt{2m^*_c kT_D}, \tag{10}$$

where c is the sound velocity, while the connection between $|M_{Vc}(\mathbf{p}_{\min}, \hbar\mathbf{k}_0)|^2$ and $1/\tau$ remains the same.

The basic qualitative difference between (6) and (1.19) is the explicit temperature dependence which occurs in the last factor. At low temperatures

$$T \ll T_0 \approx e\hbar E/4k\sqrt{2m^*_\parallel\Delta} \sim (E/10^5\ \text{v/cm})\,10^\circ\text{K}$$

the number n of pairs produced is practically independent of the temperature. When the temperature is increased, the current begins to increase exponentially, and does so right up to $T \sim T_D$.

(We assume $\hbar\omega_{\mathbf{k}_0} \sim kT_D$.) For $T > T_D$ one should observe a weak linear dependence of n on the temperature. In the interval from T_0 to T_D the current can change at constant electrical field by a factor $\exp(T_D/T_0)$, i.e., by several orders of magnitude. Of the greatest practical interest is the dependence of the critical field on the temperature. By critical field is customarily meant the value of the field for which the current reaches some well-defined value. In the region of greatest interest, $T_0 \leq T \leq T_D$,

$$\frac{\Delta E}{E_c} = -\frac{\hbar\omega_{\mathbf{k}_0}}{kT}\frac{3e\hbar E_c}{4\sqrt{2m^*_{\parallel}}\Delta^{3/2}}\frac{\Delta T}{T}. \qquad (11)$$

Outside this region there is practically no dependence. We must note, however, that Eq. (6) contains, as is well-known, also an implicit temperature dependence which is connected with the change in character of the crystal parameters (Δ, $m^*_{\parallel}$, and so on) during heating. The relative change in these quantities for a 1°K change in temperature can be of the same order as the coefficient of linear expansion, i.e., $\sim 10^{-5}$. For germanium and silicon a direct measurement gives[2] $\gamma \equiv d\Delta/dT \approx -4 \times 10^{-4}$ ev/degree. The relative shift of the critical field is then expressed by the following formula

$$\frac{\Delta E_c}{E_c} = \frac{3}{2}\frac{\gamma T}{\Delta}\frac{\Delta T}{T}. \qquad (11a)$$

A direct comparison of (11) and (11a) shows that for $T \sim T_D$ the temperature dependence of E_c produced by virtue of the thermal expansion is several times larger than the one following from (11). When the temperature is lowered the reverse situation is produced, since $|dE_c/dT|$ increases sharply according to (11) while the coefficient of linear expansion decreases.[3] At temperatures $T \lesssim 200$°K the temperature dependence is determined on the whole by Eq. (11). For $T \gtrsim T_D$, on the other hand, the thermal expansion is practically the only source of a temperature dependence in Eq. (6).

In the case of a complicated lattice there are always some kinds of phonons with the same wave vector but different frequencies (acoustical and optical). In that case the temperature dependence of the transmission coefficient must clearly have the form of a "staircase" curve, which is a superposition of functions of the form (6). As a consequence, the region where this dependence is appreciable can be extended appreciably. Thus, for germanium $T_D = 360$°K and the frequencies of the optical phonons correspond to a temperature[4]

$$T_{opt} \equiv \hbar\omega_{opt}/k \approx 500°K$$

A direct comparison shows that the factor in front of the exponential in Eq. (9) differs from the corresponding factor in Eq. (1.20) by the quantity

$$\frac{\hbar}{\tau\Delta}\left(\frac{eEd}{kT_D}\right)^{1/2}\left[\frac{1}{\Delta m^*_{\parallel}}\left(\frac{\pi\hbar}{d}\right)^2\right]^{1/4} \sim 10^{-3}.$$

At the same time, a difference between ϵ_0 and Δ, even by a factor two ($\epsilon_0 \sim 2$ ev), makes the exponential factor in Eq. (9) some 10 to 15 orders of magnitude larger than the one in Eq. (1.20), assuming that the quantities $m_{\parallel}$ which enter in these two equations are approximately the same. [We recall that $m^*_{\parallel}$ in Eq. (9) is the effective mass of an electron and a hole, while $m_{\parallel}$ in Eq. (1.20) is some formal quantity which is determined by the expansion (1.18).] If, however, $m^*_{\parallel} \gg m_{\parallel}$, direct diffusion makes a larger contribution to pair-production probability than a process involving the absorption of a phonon $\mathbf{k}_0$. This would merely mean that apparently the transitions involving the absorption of phonons having some other wave vector $\mathbf{k}_{min}$ play the basic role. Indeed, one can see from the general equations (4) and (5) that the probability of pair production involving a phonon $\mathbf{k}$ is determined essentially by the quantity

$$F(\mathbf{E}, \mathbf{k}, \mathbf{p}_\perp) = \mathrm{Re}\left\{\frac{i}{e\hbar E}\int_{}^{q(\mathbf{p}_\perp, \mathbf{k})} [\varepsilon_c(\mathbf{p}) - \varepsilon_V(\mathbf{p} - \hbar\mathbf{k}) - \hbar\omega_{\mathbf{k}}]\, dp_{\parallel}\right\}. \qquad (12)$$

The point $q(\mathbf{p}_\perp, \mathbf{k})$ in the complex $p_{\parallel}$-plane is determined by the condition that the expression under the integral sign tends to zero. For some well-determined values $\mathbf{k} = \mathbf{k}_{min}$ and $\mathbf{p}_\perp = \mathbf{p}_{\perp min}$, which, generally speaking, depend on the direction of the field E, the function $F(\mathbf{E}, \mathbf{k}, \mathbf{p}_\perp)$ reaches a minimum. The neighborhood of this point gives also the main contribution to the pair-production probability. Only in an exceptional case can it be shown that $\mathbf{k}_{min} = 0$ and the decisive fact is then the direct diffusion of the valence electron into the conduction band. For given $\mathbf{p}_\perp = \mathbf{p}_{\perp min}$, the function $\epsilon_c(\mathbf{p}) - \epsilon_V(\mathbf{p} - \hbar\mathbf{k}_{min})$ reaches some minimum value in the neighborhood of which it can be written in the form

$$\varepsilon_c(\mathbf{p}_{\perp\,min}, p_{\parallel}) - \varepsilon_V(\mathbf{p}_{\perp\,min} - \hbar\mathbf{k}_{\perp\,min}, p_{\parallel} - \hbar k_{\parallel\,min}) = \Delta(\mathbf{p}_{\perp\,min}, \mathbf{k}_{min}) + \frac{(p_{\parallel} - p_{\parallel\,min})^2}{2m_{\parallel}(\mathbf{p}_{\perp\,min}, \mathbf{k}_{min})}. \qquad (13)$$

From this it is already absolutely clear that we obtain for the number of electron-hole pairs produced an expression which is completely analogous to Eq. (6), but instead of $\mathbf{k}_0$ we have $\mathbf{k}_{min}$, and instead of Δ and $m^*_{\parallel}$ we have $\Delta(\mathbf{p}_{\perp min}, \mathbf{k}_{min})$ and $m_{\parallel}(\mathbf{p}_{\perp min}, \mathbf{k}_{min})$. Practically, this differ-

ence becomes apparent in the more complicated angular dependence which can no longer be evaluated without giving explicitly the form of the functions $\epsilon_c(\mathbf{p})$ and $\epsilon_v(\mathbf{p})$. Apart from that, as is apparent from what has been said above, an appreciable reduction of the critical field can take place if even one of the functions $\epsilon_c(\mathbf{p})$ and $\epsilon_v(\mathbf{p})$ has sections with anomalously large curvatures.

Finally we consider still one factor which can show an appreciable influence on the form of the function $n(\mathbf{E}, T)$ for relatively weak fields. As can be seen, for instance, from Eq. (6), the probability for a process in which a phonon transfers to an electron not only the necessary momentum, but also an energy ϵ, is essentially determined by the factor

$$\exp\left\{-\frac{4\sqrt{2m_{\parallel}^*}}{3e\hbar E}(\Delta-\varepsilon)^{3/2}\right\},$$

i.e., it increases steeply with increasing ϵ. Collisions in which an electron receives an energy larger than $\hbar\omega_{\mathbf{k}_0}$, even if they have a small probability, can thus influence the number of pairs produced. From the point of view of the framework used by us, such a process must be one in which several phonons are absorbed. It is well-known, however,[5] that the phonon concept itself cannot be used to describe transitions in which the lattice absorbs or emits an energy much larger than kT_D. To ascertain even the qualitative aspects of this influence, we make the apparently very natural assumption that the probability of receiving an energy ϵ from the lattice has the form $a(\epsilon)\exp(-\epsilon/kT)$, where $a(\epsilon)$ is a slowly-varying function compared with the exponent. The total number of pairs produced will then be

$$n=\int_0^\infty b(\varepsilon)\exp\left\{-\frac{\varepsilon}{kT}-\frac{4\sqrt{2m_{\parallel}^*}}{3e\hbar E}(\Delta-\varepsilon)^{3/2}\right\}d\varepsilon. \quad (14)$$

Since the exponent contains a very large number, we can use the saddle-point method to evaluate the integral, whence we get

$$n=b(\varepsilon_m)\frac{e\hbar E}{2\sqrt{m_{\perp}^* kT}}\exp\left\{-\frac{\Delta}{kT}+\frac{1}{24m_{\parallel}^*}\frac{(e\hbar E)^2}{(kT)^3}\right\}, \quad (15)$$

where

$$\varepsilon_m=\Delta-(e\hbar E/kT)^2/8m_{\parallel}^*. \quad (16)$$

Expression (15) is valid provided $\epsilon_m \gg 0$. For strong fields, Eq. (6) remains correct. Thus, right up to fields determined by the condition

$$eEd/kT\sim\sqrt{2m^*\Delta d^2}/\hbar\sim 1, \quad (17)$$

"multiphonon" processes make the main contribution to the probability of transmission of a valence electron into the conduction band, which leads to a completely new dependence of this probability both on the field and the temperature.

As can be seen from the criterion (17), the region of applicability of (15) reaches already at room temperature the experimentally observed range of fields (several times 10^5 v/cm).

The considerations given here can also be fully applied to another mechanism, whereby a valance electron receives an energy ϵ not from the lattice, but from another electron which is already in the conduction band. If the average energy of the conduction electrons is less than the ionization potential, only a very small number of them can produce impact ionization. However, the principal mass also takes part in the ejection of valence electrons, thanks to the process pointed out above, which is a combination of impact ionization and Zener diffusion. A qualitative equation, which can easily be obtained also for this mechanism, will be completely analogous to Eq. (15), only instead of T it will contain an effective conduction-electron temperature T_{eff} which in strong fields is considerably larger than the true temperature.[6] Its region of applicability will, however, be limited by the condition $kT_{eff} \ll \Delta$, i.e., to rather weak fields.

Finally, similar discussions show that collisions with impurities, during which, in general, no energy is transferred, can influence the probability for electron-hole pair production only at very low temperatures, $T \lesssim T_0$.

The most reliable method to distinguish these two mechanisms from one another experimentally is, clearly, the observation of the temperature dependence of the critical field. In the case of an electron-phonon interaction, $dE_c/dT < 0$ according to Eq. (11), while for an electron-electron interaction we must clearly have $dE_c/dT > 0$. Experiments performed on germanium[7,8] give us reasons to assume that electron-electron collisions play the dominant part in not too narrow $p-n$-junctions. There is an indication[9] that the opposite situation holds for narrow silicon $p-n$-junctions.

In conclusion, I should like to use the opportunity to express by gratitude to Professor V. L. Ginzburg for discussing the results of this paper.

[1] L. V. Keldysh, J. Exptl. Theoret. Phys. (U.S.S.R.) **33**, 994 (1957), Soviet Phys. JETP **6**, 763 (1958).

[2] H. Y. Fan, Repts. Progr. Phys. **19**, 107 (1956).

[3] L. D. Landau and E. M. Lifshitz, Статистическая физика (Statistical Physics), M., 1951, § 64.

[4] J. de Launay, Solid State Phys. **2**, 291-303 (1956).

[5] E. I. Adirovich, Некоторые вопросы теории люминесценции кристаллов (Some Problems in the The

ory of Luminescence of Crystals) M., 1951, pp 37-38

[6] V. L. Ginzburg and V. P. Shabanskii, Dokl. Akad. Nauk. SSSR, **100**, 445 (1955); V. P. Shabanskii, J. Exptl. Theoret. Phys. (U.S.S.R.) **31**, 657 (1956), Soviet Phys. JETP **4**, 497 (1957).

[7] A. P. Shotov, J. Tech. Phys. (U.S.S.R.) **26**, 1634 (1956), Soviet Phys. JTP **1**, 1591 (1957).

[8] S. L. Miller, Phys. Rev. **99**, 1234 (1955).

[9] A. G. Chynoweth and K. G. McKay, Phys. Rev. **106**, 418 (1957).

Translated by D. ter Haar
190

SOVIET PHYSICS JETP VOLUME 34 (7), NUMBER 4 OCTOBER, 1958

QUANTUM THEORY OF THE HIGH FREQUENCY CONDUCTIVITY OF METALS

M. Ia. AZBEL'

Institute for Technical Physics, Academy of Sciences, Ukrainian S.S.R.

Submitted to JETP editor November 26, 1957

J. Exptl. Theoret. Phys. (U.S.S.R.) **34**, 969-983 (April, 1958)

A quantum theory of conductivity is developed for metals placed in a high frequency electromagnetic field and a constant magnetic field. The dispersion law of the conduction electrons and the manner in which they are reflected from the surface are assumed to be arbitrary. It is shown that the amplitude of the quantum oscillations in the high frequency case is in general considerably larger than in the static case. The quantum oscillations considered here have not yet been observed experimentally.

1. INTRODUCTION

As is well known, in developing an electronic theory of the conductivity of metals it is possible, to a high degree of accuracy, to limit oneself to a semi-classical investigation which does not take account of the quantization of the energy levels of the conduction electrons. This possibility is related to the fact that, for all real cases, the level splitting $\Delta\epsilon$ is considerably smaller than the limiting Fermi energy ϵ_0 of the electrons. In order to have $\Delta\epsilon \sim \epsilon_0$ it would be necessary to have a magnetic field $H \sim \epsilon_0/\mu \sim 10^9$ oersted, or a metallic sample of width $d \sim \hbar/\sqrt{2m^*\epsilon_0} \sim 10^{-8}$ cm (m^* is the effective mass of an electron and $\mu = e\hbar/m^*c$).

However a semi-classical investigation does not permit one to look into an important effect generally absent in the classical case — purely quantum-mechanical oscillations of the conductivity. At the same time the study of these oscillations is of considerable interest, particularly because it gives a convenient method of reconstructing the form of the Fermi surface from experimental data.[1-3]

The papers of I. M. Lifshitz and Kosevich[2,3] appear to be the only ones in which diamagnetic oscillations of the static conductivity of bulk metal in a constant magnetic field were arrived at in a consistent manner. The essential assumption in their papers was that the current density in the metal was isotropic, which permitted them to regard the statistical operator as not depending explicitly on the coordinates.

In the present work a theory is developed for the general case in which there is spatial anisotropy due to a non-stationary electric field. It is assumed that the anisotropy is substantial, that is, that its characteristic dimension — the skin depth δ — is small in comparison with the Larmor radius r and with the electron mean-free-path l (the so-called anomalous skin-effect), so that the relation between the current density $\mathbf{j}$ and the electric field intensity $\mathbf{E}$ is an integral. At helium temperatures, where the quantum oscillations are observed, this is valid already for meter waves.

The study of this case is of special interest because the amplitude of the quantum oscillations of the resistivity tensor turns out, generally speaking, to be considerably greater (by a factor of $\epsilon_0/\mu H$) than in the static case.

At the same time, specific intrinsic difficulties

arise in the non-uniform case, connected mostly with the fact that it is not clear in what way one can correctly set up the quantum-mechanical problem of determining the energy spectrum and the matrix elements for a finite sample of metal, for which, in the classical case, the reflection of the electrons from the walls is diffuse. The problem can be solved because it turns out that only those electrons which do not collide with the surface make an important contribution to the quantum-mechanical correction to the classical current density.

2. THE COMPLETE SYSTEM OF EQUATIONS FOR THE PROBLEM

The complete system of equations for determining the electrical conductivity of a metal consists of Maxwell's equations

$$\operatorname{curl} \mathbf{E} = -\frac{1}{c}\frac{\partial \mathbf{H}}{\partial t}; \quad \operatorname{curl} \mathbf{H} = \frac{4\pi}{c}\mathbf{j} \tag{2.1}$$

and the kinetic equation for the statistical operator $\hat{f}$

$$\frac{\partial \hat{f}}{\partial t} + \frac{i}{\hbar}[\hat{\mathcal{H}}, \hat{f}] + \hat{W}\hat{f}/t_0 = 0. \tag{2.2}$$

Here $\mathbf{E}$ and $\mathbf{H}$ are the electric and magnetic field intensities; $\mathbf{j}$ is the current density; $\hat{\mathcal{H}}$ is the Hamiltonian; $\hat{W}\hat{f}/t_0$ determines the change of the statistical operator as a result of collisions; and t_0 is the characteristic relaxation time.

The relation between the current density $\mathbf{j}$ and the statistical operator $\hat{f}$ is given in the quasi-classical approximation by the equation*

$$\mathbf{j}(\mathbf{R}) = e \operatorname{Sp} \hat{f}\, \mathbf{v} \cdot \delta(\mathbf{R} - \hat{\mathbf{r}}). \tag{2.3}$$

Here $\mathbf{R}$ is the radius vector, considered as a c-number in contrast to the operator $\hat{\mathbf{r}} = -i\hbar\partial/\partial\mathbf{P}$; $\hat{\mathbf{v}}$ is the velocity operator, corresponding to the classical quantity $\mathbf{v} = \partial\epsilon/\partial\mathbf{P}$; ϵ is the energy; $\mathbf{P}$ is the generalized quasi-momentum of a conduction electron [by "conduction electron" is meant the corresponding quasi-particle with the dispersion law $\epsilon = \epsilon(\mathbf{p})$]; and $\mathbf{p} = \mathbf{P} - e\mathbf{A}/c$ is the kinematic quasi-momentum.

Equation (2.3) can be obtained from the definition of $\mathbf{j}$ with the aid of a variational principle:

$$\delta\bar{\mathcal{H}} = -\frac{1}{c}\int j \delta \mathbf{A} dV, \tag{2.4}$$

where $\hat{\mathcal{H}}$ is the classical Hamiltonian and $\delta\mathbf{A}$ is the variation of the vector potential $\mathbf{A}(\mathbf{R})$; the integral is taken over all space.

In the operation, $\delta\hat{\mathcal{H}}$, it is understood that in the quasi-classical approximation, to an accuracy of order $\hbar^2$, any Hermitian operator is uniquely determined by its classical analogue, and any method of symmetrization leads to a unique result. The latter assertion is easily shown from the consideration that, to an accuracy of order $\hbar^2$,

$$[\hat{a}, \hat{b}] = -i\hbar[a, b],$$

where $[a, b]$ is the classical Poisson bracket.

This one-to-one correspondence between Hermitian operators in the quasi-classical case and the corresponding classical quantities will be used repeatedly in what follows.

We now transform Eq. (2.2). In order to do this, we first of all linearize it with respect to the high frequency field, setting

$$\hat{f} = f^0(\hat{E}) + \hat{f}', \quad \hat{E} = \varepsilon(\hat{\mathbf{p}}) + U = \hat{\mathcal{H}} - e\varphi, \tag{2.5}$$

where φ is the scalar potential, $\hat{\mathbf{p}}$ the kinematic momentum, and U the potential energy (equal to zero inside the bulk metal and to infinity outside it, if emission phenomena are ignored). In the linear approximation in the electric field we obtain

$$\frac{\partial \hat{f}'}{\partial t} + \frac{i}{\hbar}[\hat{E}^0, \hat{f}'] + \hat{W}\hat{f}'/t_0 = -\frac{d}{dt} f^0(\hat{E}),$$
$$\hat{\mathcal{H}} = \hat{E}^0 + \hat{\mathcal{H}}',$$

or, in terms of matrix elements,

$$\partial f'_{kk'}/\partial t + \frac{i}{\hbar}(\varepsilon_k - \varepsilon_{k'}) f'_{kk'} + (\hat{W}\hat{f}')_{kk'}/t_0 = -df^0_{kk'}(\hat{E})/dt. \tag{2.6}$$

Here $\hat{E}^0$ and ϵ_k designate the Hamiltonian and the energy levels in the absence of a varying field, and k stands for the total collection of quantum numbers.

We now transform the right side of equation (2.6), supposing that all classical quantities except $\mathbf{f}^0(\mathbf{E})$ have an even dependence on magnetic field, so that their matrix elements can be calculated quasi-classically, and that the matrix elements of $\mathbf{f}^0(\mathbf{E}^0)$ are known.

In the same linear approximation, which is the only one considered in the present work (it being perfectly clear that non-linear effects are negligibly small for all real cases), we have in the quasi-classical approximation

$$df^0_{kk'}(\hat{E})/dt = \frac{d}{dt}\{f^0(\hat{E}) - f^0(\hat{E}^0)\}_{kk'}$$
$$= \frac{d}{dt}\frac{1}{\varepsilon_k - \varepsilon_{k'}}[\hat{E}^0, f^0(\hat{E}) - f^0(\hat{E}^0)]_{kk'}$$
$$= \frac{1}{\varepsilon_k - \varepsilon_{k'}}\frac{d}{dt}[\hat{E}, f^0(\hat{E}) - f^0(\hat{E}^0)]_{kk'}$$

*This formula could also be obtained from the quantum-mechanical equation $\mathbf{j}(\mathbf{R}) = (\Psi^*\hat{\mathbf{p}}\Psi + \Psi\hat{\mathbf{p}}^*\Psi^*)/m$ (Ψ is the wave function), by replacing $\Psi^*(\mathbf{R})\Psi(\mathbf{R}')$ by $\mathbf{f}(\mathbf{R}, \mathbf{R}')$ and $\mathbf{p}/m$ by $\mathbf{v}$ for an arbitrary law of dispersion.

$$= \frac{1}{\varepsilon_k - \varepsilon_{k'}} \frac{d}{dt} [f^0(\hat{E}^0),\ \hat{E}]_{kk'}$$

$$= \frac{f^0(\varepsilon_k) - f^0(\varepsilon_{k'})}{\varepsilon_k - \varepsilon_{k'}} \left(\frac{d\hat{E}}{dt}\right)_{kk'} = \frac{f^0(\varepsilon_k) - f^0(\varepsilon_{k'})}{\varepsilon_k - \varepsilon_{k'}} (e\hat{\mathbf{v}}\cdot\mathbf{E})_{kk'}.$$

(In these calculations, allowance has been made for the above-mentioned correspondence in the quasi-classical approximation between the operators and their classical analogues).

Thus the complete system of equations has the form

$$\operatorname{curl} \mathbf{E} = -\frac{1}{c}\frac{\partial \mathbf{H}}{\partial t};\ \operatorname{curl} \mathbf{H} = \frac{4\pi}{c}\mathbf{j};$$

$$\frac{\partial f'_{kk'}}{\partial t} + \frac{i}{\hbar}(\varepsilon_k - \varepsilon_{k'}) f'_{kk'} + (\widetilde{W}f')_{kk'}/t_0$$

$$= -\frac{f^0(\varepsilon_k) - f^0(\widetilde{\varepsilon_{k'}})}{\varepsilon_k - \varepsilon_{k'}} (e\mathbf{v}\cdot\mathbf{E})_{kk'}; \qquad (2.7)$$

$$\mathbf{j}(\mathbf{R}) = e f'_{kk'} [\hat{\mathbf{v}}\delta(\hat{\mathbf{R}} - \hat{\mathbf{r}})]_{kk'}. \qquad (2.8)$$

In what follows it will be shown that, under the conditions of the anomalous skin effect ($\delta \ll r, l$), the ratio appearing in the right side of this equation can be replaced by $\partial f^0/\partial \epsilon_k$ for the electrons making the principal contribution to the quantum-mechanical correction. If it is only collisions with impurities which play an essential role, then for these electrons

$$f'_{kk'} = -\frac{\partial f^0}{\partial \varepsilon_k} e\psi_{kk'}.$$

Taking this circumstance into account, we write the current formally as $\mathbf{f}'_{kk'}$ in the form

$$f'_{kk'} = -\frac{f^0(\varepsilon_k) - f^0(\varepsilon_{k'})}{\varepsilon_k - \varepsilon_{k'}} e\psi_{kk'}, \qquad (2.9)$$

where ψ satisfies the classical equation

$$(d\psi/dt)_{\text{field}} + \widetilde{W}\psi/t_0 = \mathbf{v}\cdot\mathbf{E}, \qquad (2.10)$$

which was solved in Ref. 4 for classical boundary conditions. Finally, in the general case, (2.9) and (2.10) will hold with $\widetilde{W} \equiv 1$; this case is also convenient for making all necessary estimates.

As has already been shown,[4] for the anomalous skin effect ($\delta \ll r, l$) it is always possible, at any temperature, to introduce a time of free flight and to set $\widetilde{W} \equiv 1$, taking $t_0 = t_0(\mathbf{p})$.

In terms of the variables E^0, t_1 (the period of revolution of the electron in its orbit), p_z (the projection of the quasi-momentum in the direction z of the constant magnetic field), and ζ (the coordinate in the direction normal to the surface of the metal), we obtain, after setting $\psi = \psi_\omega e^{i\omega t}$ and $\mathbf{E} = \mathbf{E}_\omega e^{i\omega t}$:

$$i\omega\psi_\omega + v_\zeta \frac{\partial \psi_\omega}{\partial \zeta} + \frac{\partial \psi_\omega}{\partial t_1} + \frac{\psi_\omega}{t_0} = \mathbf{v}\cdot\mathbf{E}_\omega. \qquad (2.11)$$

Hence

$$\psi_\omega = \int_\alpha^{t_1} \exp\left(-\frac{t_1 - t'_1}{t_0^*}\right) \mathbf{v}(t'_1)\cdot\mathbf{E}_\omega\left(\zeta - \int_{t'_1}^{t_1} v_\zeta dt_2\right) dt'_1; \qquad (2.12)$$

$$1/t_0^* = 1/t_0 + i\omega. \qquad (2.13)$$

Here we have chosen that solution of Eq. (2.11) which is finite and periodic in t_1. In what follows, j_ω, E_ω, and ψ_ω will always be understood and the index ω will be dropped. The quantity α is the solution of the equation

$$\int_\alpha^{t_1} v_\zeta dt_2 = \zeta. \qquad (2.14)$$

which is closest to, but smaller than, the quantity t_1. In case there is no root it must be assumed $\alpha = -\infty$. Thus

$$\mathbf{j}(Z) = -e^2 \sum_{k,\,l} \frac{f^0(\varepsilon_{k+l}) - f^0(\varepsilon_k)}{\varepsilon_{k+l} - \varepsilon_k} \Big[\int_{\alpha(\zeta, t_1)}^{\infty} \exp\left\{-\frac{t_1 - t'_1}{t_0^*}\right\} v(t'_1)$$

$$\times \mathbf{E}\left(\hat{\zeta} - \int_{t'_1}^{t_1} v_\zeta dt_2\right) dt'_1\Big]_l [v\delta(Z - \hat{\zeta})]_{-l}, \qquad (2.15)$$

where it has been assumed that the quasi-classical matrix elements depend essentially only on the difference of the quantum numbers, and the following notation has been introduced:

$$\Phi_{kk'} \equiv \Phi_{k-k'}(k).$$

Consequently the problem reduces to the calculation of the quasi-classical matrix elements.

If the surface of the metal could be considered as a geometrical plane, on one side of which (inside the metal) the potential energy were zero, apart from emission phenomena, and on the other side infinite, so that there would be a correspondence with the classical case of the specular reflection of electrons from the surface, than finding the quasi-classical energy levels and matrix elements would reduce to the solution of the classical problem. This case is studied in the following paragraph; it is also the only one which has been considered in the literature to date.[5,6]

In itself, specular reflection is of purely academic interest. Actually the reflection of electrons from the surface of a metal is diffuse or nearly so in the classical case (see for instance, Refs. 7, 8), because the potential energy increases from zero to infinity over distances of the order of the interatomic spacing; and, over just such distances, unavoidable distortions of every kind, non-uniformities of the surface of the metal, make the law of the increase of the potential energy a random function. It is thus very difficult simply to formulate correctly the quantum-mechanical problem of determining the electronic energy spectrum even for diffuse reflection. Furthermore, even for mirror

reflection, the task of actually calculating the energy spectrum and the matrix elements is extremely involved, since it requires finding the adiabatic invariants and the angular variables for the motion of electrons in a magnetic field in a potential well.

In Section 4, however, it will be shown that in the case which is of interest to us, that of the anomalous skin effect, only those electrons which do not have any forward motion, do not collide with the surface of the metal, and whose spectrum coincides with the spectrum of electrons in unlimited space, make an essential contribution in the quantum-mechanical correction to the classical current density. Thus the character of the reflection seems to be unimportant for determining the quantum contribution to the impedance, so we are able to obtain the quantum-mechanical formula for the total surface impedance of a metal.

3. SOLUTION OF THE PROBLEM FOR SPECULAR REFLECTION OF ELECTRONS FROM A METALLIC SURFACE

For mirror reflection of electrons from a surface it is convenient to take as quantum numbers (k) the quantum numbers n_1, n_2, n_3 corresponding to the adiabatic invariants I_1, I_2, I_3 (in this section we will for generality treat an arbitrary finite sample of metal). The sets of numbers (n_1, n_2, n_3) and (I_1, I_2, I_3) will for convenience be designated $\mathbf{n}$ and $\mathbf{I}$.

The energy spectrum is obtained from the classical function $E^0(\mathbf{I})$ by replacing $\mathbf{I}$ by $(\mathbf{n}+\boldsymbol{\gamma})h$ (where n_i is integral[6] and $\gamma_i < 1$) and by adding a spin component $\pm e\hbar H/m_0 c$, where m_0 is the mass of a free electron.

In this paper we will ignore the spin component altogether, for the sole purpose of simplifying the writing, and, in conformity with this, apart from the summation over $\mathbf{n}$ in the equation for the current density, will write down spin two:

$$\mathbf{j}(\mathbf{R}) = 2e f'_{\mathbf{nn'}} [\hat{\mathbf{v}}\delta(\mathbf{R}-\hat{\mathbf{r}})]_{\mathbf{n'n}}. \qquad (3.1)$$

It is possible to neglect the spin component because in general the effect mass which enters into μ is not the same as the mass m_0 of a free electron.

In terms of these variables, the quasi-classical matrix elements $\Phi_{\mathbf{nn'}}$ represent the Fourier components of the corresponding physical quantity $\Phi(\mathbf{w}, \mathbf{I})$ with respect to the angular variables:*

$$\Phi_{\mathbf{nn'}} \equiv \Phi_{\mathbf{n}-\mathbf{n'}}(\mathbf{n})$$

$$= \int_0^1\int_0^1\int_0^1 e^{-2\pi i(\mathbf{n}-\mathbf{n'})\mathbf{w}}\,\Phi(\mathbf{w}, (\mathbf{n}+\boldsymbol{\gamma})h)\,dw_1\,dw_2\,dw_3. \qquad (3.2)$$

In order to make calculations one naturally has to know $\Phi(\mathbf{w}, \mathbf{I})$ for all values of the angular variables. For electrons colliding with the surface in the classical case, one has to write down the trajectories taking account of their reflection from the surface. It can be shown that such a description of the trajectories is equivalent to a suitable continuation of the function Φ in the region outside the metal analogous to that developed in Ref. 10, to which, as it was found there, the reflection conditions of the electrons from the metallic surface reduce.

For the choice of quantum numbers which has been made, the final transition to the classical case is particularly graphic.

As seen from (3.2) and (2.7), the equations determining the current density in the quasi-classical approximation have the form

$$\mathbf{j} = 2e\sum_{\mathbf{n}}\sum_{\mathbf{k}} f'_{\mathbf{k}}(\mathbf{n})\,[\mathbf{v}\delta(\mathbf{R}-\hat{\mathbf{r}})]_{-\mathbf{k}}; \qquad (3.3)$$

$$\frac{\partial f'_{\mathbf{k}}(\mathbf{n})}{\partial t} + 2\pi i\frac{\partial E^0}{\partial \mathbf{I}_{\mathbf{n}}}\mathbf{k}f'_{\mathbf{k}}(\mathbf{n}) + \sum_{\mathbf{k'},\,\mathbf{n'}} W_{\mathbf{k},-\mathbf{k'}}(\mathbf{I}_{\mathbf{n}}, \mathbf{I}_{\mathbf{n'}})\,f'_{\mathbf{k'}}(\mathbf{n'})\,\Delta\mathbf{I}_{\mathbf{n'}}$$
$$= -\frac{f^0(\varepsilon_{\mathbf{n}+\mathbf{k}}) - f^0(\varepsilon_{\mathbf{n}})}{\varepsilon_{\mathbf{n}+\mathbf{k}} - \varepsilon_{\mathbf{n}}}(e\mathbf{v}\mathbf{E})_{\mathbf{k}}; \quad \Delta\mathbf{I}_{\mathbf{n}} = \Delta I_{n_1}\Delta I_{n_2}\Delta I_{n_3} = h^3. \qquad (3.4)$$

The classical kinetic equation for the distribution function $\mathbf{f'}$

$$\frac{\partial f'}{\partial t} + [E^0, f'] + \tilde{W}f'/t_0 = -\frac{\partial f^0}{\partial \varepsilon}e\mathbf{v}\cdot\mathbf{E}$$

is written in terms of the canonical variables $\mathbf{I}$, $\mathbf{w}$ in the form

$$\frac{\partial f'}{\partial t} + \frac{\partial E^0}{\partial \mathbf{I}}\frac{\partial f'}{\partial \mathbf{w}} + \frac{\tilde{W}f'}{t_0} = -\frac{\partial f^0}{\partial \varepsilon}e\mathbf{v}\cdot\mathbf{E}.$$

(Here we make use of the fact that E^0 depends only on $\mathbf{I}$, and consequently $\partial E^0/d\mathbf{w} = 0$). Expanding all functions of $\mathbf{w}$ as Fourier series, we obtain

$$f'(\mathbf{w}, \mathbf{I}) = \sum_{\mathbf{k}} f'_{\mathbf{k}}(\mathbf{I})\,e^{2\pi i\mathbf{k}\mathbf{w}};$$

$$\frac{\partial f'_{\mathbf{k}}(\mathbf{I})}{\partial t} + 2\pi i\frac{\partial E^0}{\partial \mathbf{I}}\mathbf{k}f'_{\mathbf{k}}(\mathbf{I})$$
$$+ \frac{1}{t_0}\sum_{\mathbf{k'}}\int W_{\mathbf{k},-\mathbf{k'}}(\mathbf{I}, \mathbf{I'})\,f'_{\mathbf{k'}}(\mathbf{I'})\,d\mathbf{I'} = -\frac{\partial f^0}{\partial \varepsilon}(e\mathbf{v}\mathbf{E})_{\mathbf{k}},$$

which differs from (3.4) only in that $\mathbf{I}$ is considered not as a discrete but as a continuous variable.

We now write down the current density in terms of these same variables. Making use of the fact that the Jacobian of the transformation from one set of canonical variables $(\mathbf{r}, \mathbf{P})$ to another $(\mathbf{I}, \mathbf{w})$ is equal to unity (see, for example, Ref. 11), we have

*This formula is a natural extension of the formula developed in Ref. 9, considering that $\dot{\mathbf{w}} = \partial E^0/\partial \mathbf{I}$.

$$\mathbf{j} = \frac{2e}{h^3}\int \mathbf{v} f' d\mathbf{P} = \frac{2e}{h^3}\int \mathbf{v} f' \delta(\mathbf{R}-\mathbf{r})\, d\mathbf{P} d\mathbf{r}$$
$$= \frac{2e}{h^3}\int \mathbf{v} f' \delta(\mathbf{R}-\mathbf{r})\, d\mathbf{I} d\mathbf{w} = \frac{2e}{h^3}\int [\mathbf{v} f' \delta(\mathbf{R}-\mathbf{r})]_{k=0}\, d\mathbf{I}$$
$$= \frac{2e}{h^3}\int d\mathbf{I} \sum_k f'_k(\mathbf{I}) [\delta(\mathbf{R}-\mathbf{r})\, \mathbf{v}]_{-k},$$

which corresponds to (3.3).

The final transition to the classical equations is now quite apparent. Thus the solution of the quantum mechanical problem for the case of mirror reflection reduces completely to the solution of the classical problem.

4. SOLUTION OF THE PROBLEM FOR AN ARBITRARY LAW OF REFLECTION OF ELECTRONS FROM THE METALLIC SURFACE

As is well known, for the anomalous skin effect, when the smallest characteristic dimension is the penetration depth, the classical magnitude of the surface impedance depends on the way in which electrons are reflected from the surface of the metal. It follows that one must take the boundary conditions at the surface into account in solving the problem.

As already stated, however, the nature of the surface reflection does not show up in the quantum mechanical correction in the zeroth approximation in the "anomalousness" (that is, in δ/l or δ/r, where δ is the penetration depth and l and r are the average mean-free-path and the radius of the Larmor orbit) or in the "quasi-classicalness" (that is, in $\mu H/\epsilon_0$, where μ is the Bohr magneton for a conduction electron and ϵ_0 is the limiting Fermi energy). We will now formulate this statement more precisely. We assume that the width D of the film is not too small, so that the Larmor orbit corresponding to a central cross-section $p_z = 0$ can be "fitted" into it:

$$D > d = \left|\frac{c}{eH}\int_{t_0'}^{t_0''} v_\zeta\, dt_2\right| = \left|\frac{c}{eH}\left(\int_{t_0'}^{t_0''} v_z\, dt_2 \cos\phi + 2p_x^{\max}\sin\phi\right)\right|;$$

$$v_\zeta(t_0') = v_\zeta(t_0'') = 0; \quad v_\zeta'(t_0') > 0, \quad v_\zeta'(t_0'') < 0, \qquad (4.1)$$

where all quantities have their values at $p_z = 0$, $\epsilon = \epsilon_0$. The maximum $p_x(\epsilon_0, p_z, t_1)$ is taken with respect to the time t_1 of an orbital revolution, ϕ is the angle between the direction z of the constant magnetic field and the normal to the surface of the metal, and x lies in the plane of the surface. Then only those electrons which simultaneously satisfy the following conditions make a substantial contribution in the quantum correction to the classical current density:

1. Their average velocity of motion in the interior of the metal during the time of one orbital revolution is small: $|\bar{v}_\zeta| = |\bar{v}_z \cos\phi| \ll |\bar{v}_z| = v_0$.

2. The area S of the cross-sections $\epsilon(\mathbf{p}) = \epsilon_0$, $p_z = \text{const}$ corresponding to their orbits is near an extremum S_{ext}.

If the magnetic field is not parallel to the surface of the metal, $\phi \not\approx 90°$, then only electrons to which there correspond cross-sections close to a central one (where $p_z = 0$) satisfy both conditions. In a magnetic field parallel to the surface of the metal the first requirement for closed cross-sections is satisfied automatically, and only the second one remains.

3. In the course of their motion, the electrons d do not collide with the surface. The division of the electrons into those which do collide with the surface and those which do not can be carried out because of the first condition.

The proof of these assertions is quite simple conceptually, but exceedingly involved even for specular reflection from the surface. Thus we will limit ourselves to illustrations of the corresponding reasons for the simplest cases.

Let us demonstrate the first two assumptions for the example of an unbounded volume, where the electric field is different from zero only in the half-space $\zeta \geq 0$ (obviously this case is in itself of purely academic interest). The energy spectrum of the electrons in unbounded space has been found in Ref. 1: $E^0 = \epsilon(n, p_z)$, where the function ϵ is determined from the condition

$$S(E^0, p_z) = (n+\gamma)\, ehH/c.$$

Since ψ depends on ζ, that is, on both y and z, the matrix elements of ψ in (2.9) will be nondiagonal with respect to n and to p_z, so that from (2.8) and (2.9) we have

$$\mathbf{j} = -\int_{-\infty}^{\infty} dp_z \int_{-\infty}^{\infty} dp_z' \sum_{n=0}^{\infty}\sum_{l=-\infty}^{\infty}$$
$$\times \frac{f^0(\varepsilon_{n+l,\, p_z+p_z'}) - f^0(\varepsilon_{np_z})}{\varepsilon_{n+l,\, p_z+p_z'} - \varepsilon_{np_z}} \mathbf{A}_{lp_z'}(n, p_z), \qquad (4.2)$$

where

$$\mathbf{A}_{lp_z'}(n, p_z) \sim \int_{-\infty}^{\infty} \psi_{lp_z'}(n, p_z)\, [\mathbf{v}\delta(Z-\hat{\zeta})]_{-l,\,-p_z'}\, dP_x; \qquad (4.3)$$
$$\partial\varepsilon_{np_z}/\partial n = \hbar\Omega = \mu H.$$

From (4.2)

$$\mathbf{j} = -\int_{-\infty}^{\infty} dp_z \int_{-\infty}^{\infty} dp_z' \sum_{n=0}^{\infty}\sum_{l=-\infty}^{\infty}$$
$$\times \frac{f^0(\varepsilon_{np_z} + l\hbar\Omega + \bar{v}_z p_z') - f^0(\varepsilon_{np_z})}{l\hbar\Omega + \bar{v}_z p_z'} \mathbf{A}_{lp_z'}(n, p_z); \qquad (4.4)$$

$$\frac{\partial \varepsilon_{np_z}}{\partial p_z} = \frac{\partial}{\partial p_z}\int_0^1 \varepsilon(n, p_z, \tau)\, d\tau = \int_0^1 \frac{\partial \varepsilon}{\partial p_z}\, d\tau = \overline{v_z(\varepsilon_{np_z}, p_z, t_1)};$$

$$\tau = \frac{t_1}{T},\ T = \frac{2\pi m^* c}{eH};\ m^* = \frac{1}{2\pi}\frac{\partial S}{\partial \varepsilon};\ \Omega = \frac{2\pi}{T}. \quad (4.5)$$

Transforming the sum over n by Poisson's formula (see Ref. 12, for example), and keeping only the oscillating quantum-mechanical terms (since they are the only ones of interest to us; the classical part of the current density has been found in Refs. 13, 10, and 4), we have

$$\Delta j^{KB} = \sum_{s=1}^{\infty}\sum_{l=-\infty}^{\infty} G_{sl};$$

$$G_{sl} = -2\int_{-\infty}^{\infty} dp_z \int_{-\infty}^{\infty} dp_z' \int_0^{\infty} e^{2\pi i s n} \times \frac{f^0(\varepsilon_{np_z} + l\hbar\Omega + \bar{v}_z p_z') - f^0(\varepsilon_{np_z})}{l\hbar\Omega + \bar{v}_z p_z'} A_{lp_z'}\, dn. \quad (4.6)$$

Making a shift in n,*

$$n \to n - l - \bar{v}_z p_z'/\hbar\Omega,$$

and assuming that only $\epsilon \sim \epsilon_0$ and $|\bar{v}_z p_z'| \ll \epsilon_0$ play an essential role, we find

$$G_{sl} = -2\int_{-\infty}^{\infty} dp_z \int_0^{\infty} dn \cdot e^{2\pi i s n} f^0(\varepsilon_{np_z}) \int_{-\infty}^{\infty} J_{sl}\, dp_z', \quad (4.7)$$

$$J_{sl} = \frac{1 - \exp(-2\pi i s \bar{v}_z p_z'/\hbar\Omega)}{l\hbar\Omega + \bar{v}_z p_z'} A_{lp_z'} + \exp\left(-\frac{2\pi i s \bar{v}_z p_z'}{\hbar\Omega}\right) \partial A_{lp_z'}/\partial \varepsilon_{np_z}. \quad (4.8)$$

Integrals of the type (4.7) have been calculated by I. Lifshitz and Kosevich,[3] who have also shown that for $\epsilon_0/\hbar\Omega \gg 1$ only those electrons which are near an extreme cross-section $p_z = p_z^{ext}$ of the limiting Fermi surface $\epsilon(\mathbf{p}) = \epsilon_0$ make a significant contribution; this situation corresponds to the second condition for the electrons which are "necessary" for us. A region Δp_z of order

$$|\Delta p_z| \sim [(\hbar\Omega/\varepsilon_0)(2m^*\varepsilon_0)]^{1/2}. \quad (4.7a)$$

near the extremum takes part in this contribution.

We now look into which l, p_z^{ext}, and p_z' make a substantial contribution to G_{sl}, that is, for what values of these quantities J_{sl} is not small.

*It might appear that a convenient shift would be $n \to n - l$, $p_z \to p_z - p_z'$. This is not so, however, because of the divergence with respect to p_z of each separate term in (4.6) for $l = 0$ the divergence occurs for $p_z = 0$).

In doing this we first of all note that from (4.2), (2.9), and (2.7)

$$|A_{lp_z'}| \sim (vE)_{lp_z'} \Big/ \left|\frac{1}{t_0^*} + \frac{i}{\hbar}(\varepsilon_{n+l,\ p_z+p_z'} - \varepsilon_{np_z})\right| \sim (vE)_{lp_z'} \Big/ \left(\frac{1}{t^l} + \frac{1}{\hbar}|\bar{v}_z p_z'|\right);$$

$$1/t^l = 1/t_0 + (\omega + l\Omega). \quad (4.9)$$

Let us designate

$$|\bar{v}_z p_z'|/(\hbar\Omega) = x.$$

Then

$$|J_{sl}| \sim \left[\frac{\hbar\Omega}{\varepsilon_0} + \frac{x}{(1+x)(l+x)}\right] \frac{1}{(\Omega t^l)^{-1} + x} (vE)_{lp_z'}. \quad (4.10)$$

The quantity x is intrinsically different for a central (x_c) and a non-central (x_{nc}) cross-section for one and the same p_z'. For a central section ($p_z = 0$), $\bar{v}_z = 0$, for a non-central one, $|\bar{v}_z| \sim |\overline{v_z}| = v_0$. This means that near a central cross-section, where (4.7a) holds, the quantity $\bar{v}_z$ is of order $|\bar{v}_z| \sim v_0(\hbar\Omega/\epsilon_0)^{1/2}$, while on a non-central section, $|\bar{v}_z| \sim v_0$. Thus, since

$$x \sim \frac{|p_z'|}{\hbar/r_z} \sim \frac{|p_z'|}{\hbar/r}\frac{|\bar{v}_z|}{v_0};\ r \sim v_0 T,\ r_z = |\bar{v}_z| T, \quad (4.11)$$

then

$$x_c \sim \frac{|p_z'|}{\hbar/r}\left(\frac{\hbar\Omega}{\varepsilon_0}\right)^{1/2},\ x_{nc} \sim \frac{|p_z'|}{\hbar/r} \gg x_c. \quad (4.12)$$

The coefficient of $(\mathbf{v}\cdot\mathbf{E})_{lp_z'}$ in J_{sl} is not small if $x \gtrsim 1/(1+\Omega t^l)$, that is, if

$$|p_z'| \lesssim \frac{\hbar}{r_z(1+\Omega t^l)} \sim \frac{\hbar}{r(1+\Omega t^l)}\frac{v_0}{|\bar{v}_z|},$$

$$r_l = r(1 + \Omega t^l). \quad (4.13)$$

However the matrix elements $(\mathbf{v}\cdot\mathbf{E})_{lp_z'}$ differ significantly from zero for $p_z' \sim \hbar/\delta_{eff}^z$, where $\delta_{eff}^z = \delta_{eff}/\cos\phi$ is the effective skin depth in the direction z; δ_{eff} is the effective skin depth (in the direction ζ). Consequently the values which are important are

$$|p_z'| \sim \min\left\{\frac{\hbar}{r_l}\frac{v_0}{|\bar{v}_z|},\ \frac{\hbar}{\delta_{eff}}\cos\phi\right\};$$

$$x \sim \min\left\{\frac{1}{1+\Omega t^l},\ \frac{r_z}{\delta_{eff}^z}\right\}. \quad (4.14)$$

For a central section, this gives

$$|p_z'| \sim \min\left\{\frac{\hbar}{r_l}\left(\frac{\varepsilon_0}{\hbar\Omega}\right)^{1/2};\ \frac{\hbar}{\delta_{eff}}\cos\phi\right\}; \quad (4.15)$$

and for a non-central one,

$$|p_z'| \sim \min\left\{\frac{\hbar}{r_l},\ \frac{\hbar}{\delta_{eff}}\cos\phi\right\}. \quad (4.16)$$

Two cases are possible. If $\delta_{\text{eff}}^{z} \gtrsim r_0$ (that is $\cos\phi \lesssim \delta_{\text{eff}}/r_l$), then relative to the quantity **a**,

$$a = \frac{\delta_{\text{eff}}^{z}}{r_0}\left(\frac{\varepsilon_0}{\hbar\Omega}\right)^{1/3} = \frac{\delta_{\text{eff}}}{r_0\cos\phi}\left(\frac{\varepsilon_0}{\hbar\Omega}\right)^{1/3}, \qquad (4.17)$$

either central sections alone are important (if $a \gg 1$), so that

$$\bar{v}_\zeta = \bar{v}_z\cos\phi \ll \left(\frac{\hbar\Omega}{\varepsilon_0}\right)^{1/3}\frac{\delta_{\text{eff}}}{r_0}v_0 \ll v_0,$$

or else all extreme sections (if $a \lesssim 1$), so that

$$\bar{v}_\zeta \sim \bar{v}_z\cos\phi \ll v_0\delta_{\text{eff}}/r_0 \ll v_0.$$

If $\delta_{\text{eff}}^{z} \ll r_0$ (so that $\cos\phi \gg \delta_{\text{eff}}/r_0$), then only central sections make a substantial contribution to G_{sl} (the contribution of the non-central sections being smaller by a factor of $[\delta_{\text{eff}}^{z}/r_0 + (\hbar\Omega/\epsilon_0)^{1/2}]^{-1}$, or

$$\bar{v}_\zeta = \bar{v}_z\cos\phi \sim v_0\left(\frac{\hbar\Omega}{\varepsilon_0}\right)^{1/3}\cos\phi \ll v_0.$$

(It is obvious that the skin effect was taken to be anomalous, that is $\delta_{\text{eff}} \ll r_0$, at every point of the demonstration).

In this way the first condition is also proved: for all cases $|\bar{v}_\zeta| \ll v_0$.

We note further that, as follows from (4.10) and (4.14), only $x \ll 1$ is important both for $\Omega t^0 \gg 1$ and for $a \gg 1$, which means $l = 0$. Clearly for $a \gg 1$, central sections (or $l = 0$) play the principal role.

The first condition is easily understood physically. It is automatically satisfied in a parallel field ($\phi = 90°$). Let us study an inclined field ($\phi \sim 1$), in which, due to the fact that the electric field **E** depends on z, only $p'_z \sim \hbar/\delta_{\text{eff}}$ is important. However, because of the dependence of the electron energy on p_z, the magnitude of $|p'_z|$ is limited to $|\hbar/\bar{v}_z T|$. Thus for the anomalous skin effect, when $\delta_{\text{eff}} \ll r$, $p'_z \sim \hbar/r$ on a non-central cross-section, and

$$|p'_z| \sim \min\left\{\frac{\hbar}{\delta_{\text{eff}}}, \frac{\hbar}{r}\left(\frac{\varepsilon_0}{\hbar\Omega}\right)^{1/3}\right\},$$

on a central one, so that the non-central sections make a contribution in the next approximation with respect to the anomalousness (δ_{eff}/r) or to $(\hbar\Omega/\epsilon_0)^{1/2}$. For the normal skin effect ($\delta_{\text{eff}} \gg r$) in the bulk metal, however, all extreme cross-sections play the same role, as is to be expected.

We now prove the third assertion in the case when the contribution of electrons colliding with the surface is maximum, as is easily visualized: the constant magnetic field is aligned parallel to the surface ($\phi = \pi/2$), and the reflection of electrons from the surface is specular. The energy spectrum $E^0 = \epsilon(n, P_x, p_z)$ in this case has been found earlier;[5] **A** is non-diagonal only with respect to n; the quasi-classical matrix elements coincide with the Fourier components with respect to the time;[9] the electrons have $\bar{v}_y \sim \overline{dp_y/dt} = 0$ so that they can be separated into those which do and those which do not collide with the surface; and all extreme cross-sections make a substantial contribution to the current density.

The formula for the current density $\mathbf{j}(Y)$ in this case is written in the form

$$\mathbf{j}(Y) = -\int_{-\infty}^{\infty} dp_z \sum_{n=0}^{\infty}\sum_{l=-\infty}^{\infty}\int_{-\infty}^{\infty} dP_x \times \frac{f^0(\varepsilon_{n+l,\,p_z,\,P_x}) - f^0(\varepsilon_{np_zP_x})}{\varepsilon_{n+l,\,p_z,\,P_x} - \varepsilon_{np_z,\,P_x}}\mathbf{D}_l(n,\,p_z,\,P_x), \qquad (4.18)$$

$$\mathbf{D}_l = K\psi_l[\mathbf{v}\,\delta(Y - \hat{y})]_{-l}$$

or, considering that for $\Delta\mathbf{j}^{qu}$ for $\phi = \pi/2$, $a = \infty$, only $l = 0$ is important,

$$\Delta\mathbf{j}^{\text{KB}}(Y) = \sum_{s=1}^{\infty}\mathbf{G}_{s0};\ \mathbf{G}_{s0} \qquad (4.19)$$

$$= -2\int_{-\infty}^{\infty} dp_z \int_{-\infty}^{\infty} dP_x \int_0^{\infty} e^{2\pi isn}\frac{\partial f^0}{\partial\varepsilon_{np_zP_x}}\mathbf{A}_0(n,\,p_z,\,P_x)\,dn.$$

We now separate out from G_{s0} the contribution of electrons which do not collide with the surface $y = 0$. For simplicity, we consider the case of a half-space. In classical mechanics, $y(t) = (P_x - p_x(t)/|eHc|$. An electron does not collide with the surface $y = 0$ if at all times during the motion $y(t) > 0$, that is, if

$$y_{\min}(t) = (P_x - p_x^{\max})\,|c/eH| > 0; \qquad (4.20)$$
$$P_x > P_0 = p_x^{\max},\ p_x = p_x(\varepsilon, p_z, t_1),\ P_0 = P_0(\varepsilon_{np_z}, p_z).$$

(The maximum is taken with respect to t_1). The corresponding inequality in the quasi-classical case is

$$P_x > P_0(\varepsilon_{np_z}, p_z). \qquad (4.21)$$

Here we have considered that the electrons which do not collide with the surface have the same spectrum as in the bulk metal:

$$\varepsilon = \varepsilon(n, p_z), \qquad (4.22)$$

that is, the energy is infinitely degenerate with respect to P_x.

The degeneracy with respect to P_x is removed for electrons colliding with the surface, or $\epsilon = \epsilon(n, p_z, P_x)$.

A calculation analogous to that carried out by Kosevich and Lifshitz[5] shows that, because of the

degeneracy with respect to P_x and the resulting absence of an integration of $\partial f^0/\partial \epsilon_{np_z}$ over P_x, the integral over dP_x from P_0 to ∞ proves, as in Ref. 5, to be $(\epsilon_0/\hbar\Omega)^{1/2} \gg 1$ times larger than the integral from $-\infty$ to P_0. This fact indicates that it is sufficient to give attention only to those electrons which do not collide with the surface.

A case which is more convenient for calculations is naturally one in which

$$a = (\delta_{\text{eff}}/r_0)(\varepsilon_0/\hbar\Omega)^{2/3}/\cos\phi \gg 1, \qquad (4.23)$$

so that the spectrum of the electrons which give a substantial contribution to Δj^{qu} can be regarded as coinciding with the spectrum of the bulk metal, and the relation between the periods of the quantum oscillations and the areas of the extreme cross-sections is the same as in Ref. 1; in the calculation of Δj^{qu} only $l = 0$ is important.

If (4.23) is satisfied, then for the value $l = 0$ which we require the expression for ψ is considerably simplified. From (2.7) for $l = 0$ and according to (4.23), $|\bar{v}_z p'_z t_0^*/\hbar| \ll 1$,

$$\psi = \left(\frac{\bar{1}}{t_0^*}\right)^{-1} vE. \qquad (4.24)$$

As already pointed out, because of the quasi-classicalness only those electrons are important which are near an extreme cross-section $\epsilon(\mathbf{p}) = \epsilon_0$, $p_z = p_z^{ext}$ (and, for $\pi/2 - \phi \gg \delta_{\text{eff}}/r$, near the central cross-section, $p_z = 0$, $\epsilon(\mathbf{p}) = \epsilon_0$).

Because the skin effect is anomalous, only electrons with $|v_\zeta| \ll v_0$, $v'_\zeta(t_1) < 0$ are important (this will subsequently be shown to be analogous to other results[13,14,4]; physically this assertion is related to the fact that only those electrons which spend a maximum amount of time in the skin layer, that is, those having $v_\zeta \approx 0$, play a significant role).

Consequently in the current density in the symbol for a matrix element, it would be possible everywhere to take out $\mathbf{v}$ at the point $\epsilon(\mathbf{p}) = \epsilon_0$, $p_z = p_z^{ext}$ (or $p_z = 0$), $v_\zeta = 0$, $v'_\zeta(t_1) > 0$, and to sum over all extreme cross-sections (or over all non-central ones, in the case of a non-parallel field).

5. CALCULATION OF THE QUANTUM CORRECTION TO THE CURRENT DENSITY

In the preceding paragraph it was shown how one might determine the quantum correction to the classical formula for the current density.

The simplest case is one in which the magnetic field is aligned parallel to the surface. Here the physical quantities depend only on y and consequently are non-diagonal only with respect to one quantum number n; the quantum-mechanical correction to the current density is determined by (4.19), (4.21), and (4.22), where

$$K = 2e^2/h^2, \qquad (5.1)$$

in which it is easy to demonstrate the transition to the classical case.

Evaluating the integrals, we obtain

$$\Delta j_i^{\text{KB}}(Y) = \sum \frac{h^3}{2\pi} H^2 \chi_i(\varepsilon_0, p_z^{\text{ext}}) \left(\frac{d \ln S_{\text{ext}}}{d\varepsilon}\right)^2 \frac{\partial \Delta M_z^{\text{ext}}}{\partial H}, \qquad (5.2)$$

where ΔM_z^{ext} has been found elsewhere;[1] the sum is taken over all extreme sections, and for the film thickness D

$$\chi_i(Y) = \frac{4\pi e^2}{h^3 \overline{t_0^{*-1}}} \left\{ v_i(t) S\left(Y - \frac{p_x^{\max} - p_x(t)}{|eH/c|}\right) \right.$$
$$\times S\left(D - Y - \frac{p_x(t) - p_x^{\min}}{|eH/c|}\right)$$
$$\left. \times \overline{v_j(t') E_j\left(Y + \frac{p_x(t) - p_x(t')}{|eH/c|}\right)} \right\}_{\text{cp}}; \qquad (5.3)$$

$$S(w) = \begin{cases} 1\ (w > 0) \\ 0\ (w < 0) \end{cases}; \quad D > \left|\frac{c}{eH}\right| (p_x^{\max} - p_x^{\min});$$
$$\bar{\varphi} = \varphi_{\text{cp}} = \frac{1}{T}\int_0^T \varphi\, dt,$$

which corresponds to (4.24). The averages are taken over the period t' (designated by a bar) and over t (designated by "av").

Inasmuch as the calculations were actually carried out in terms of the variables ζ_{chem}, H (where ζ_{chem} is the chemical potential), and physically it is not ζ_{chem} but the total number of electrons which is conserved, it would be necessary to allow for oscillations of ζ_{chem}. However, since $\Delta\zeta_{\text{chem}}^{qu} \sim (\hbar\Omega/\epsilon_0)^{3/2}$ and $\Delta j_1^{qu} \sim \hbar\Omega/\epsilon_0)^{1/2}$,[1,3] the oscillations of ζ_{chem} can be ignored. (As will be seen later, this is true for any inclination of the magnetic field). Finding the quantum contribution to the current density for an inclined magnetic field is quite complicated.

We obtain a closed solution of this problem for the case of a strong magnetic field which satisfies the conditions

$$\Omega \gg \omega, \frac{1}{t_0}, \quad \omega \cdot \omega t_0; \quad \frac{\delta_{\text{eff}}}{r\cos\phi}\left(\frac{\varepsilon_0}{\hbar\Omega}\right)^{1/3} = \frac{\delta_{\text{eff}}}{|\bar{v}_z| T} \ll 1 \qquad (5.4)$$

(the second condition allows us to use the spectrum for electrons in the bulk metal).

It is obvious that we would be able to solve this problem without superimpositng this restriction on the size of the magnetic field. Since, as proved in Section 4, the nature of the reflection of electrons from the surface does not influence the result, the

solution of the problem for specular reflection (Section 3) should parallel the solution for any type of reflection. However a similar solution is extremely involved. All the results can be understood in the most important case (5.4), however, when the formula for Δj^{qu} takes a very simple form.

We note that the condition (5.4) leads to an additional reduction of the relative contribution of the electrons corresponding to a central section and colliding with the surface, since these electrons are only accelerated once during the time that the electrons which do not collide with the surface are accelerated many times (since $\Omega \gg \omega$, $1/t_0$). It is this circumstance which facilitates the solution of the problem.

For simplicity let us investigate the case when the Fermi surface is a closed convex surface.

It follows from Section 4 that the quantum contribution to the current density from (5.4) in a film which is not too thin differs from that in an unbounded sample of metal, with the same electric field distribution as in the film, only in that it is necessary to consider only the electrons which do not collide with the surface. Thus we write Δj^{qu} for an unbounded volume of metal in such a form that we can separate the electrons which do intersect the surface $\zeta = 0$, D from those which do not.

In an unbounded metal, j is given by formulas (4.4) and (4.3).

Under the conditions which we have assumed, the oscillating quantum-mechanical part will, according to Section 4, be given just as accurately by the equation

$$\mathbf{j} = -\int_{-\infty}^{\infty} dp_z \sum_{n=0}^{\infty} \frac{\partial f^0}{\partial \varepsilon_{np_z}} \int_{-\infty}^{\infty} \mathbf{A}_{0p'_z}\, dp'_z. \tag{5.5}$$

But from equation (4.9) it is clear that, because of (5.4),

$$\mathbf{A}_{0p'_z} \gg \mathbf{A}_{lp'_z}\ (l \neq 0);\quad A_{0p'_z} \approx \sum_{l=-\infty}^{\infty} A_{lp'_z}, \tag{5.6}$$

or

$$\int_{-\infty}^{\infty} \mathbf{A}_{0p'_z}\, dp'_z \approx \int_{-\infty}^{\infty} dp'_z \sum_{l=-\infty}^{\infty} \mathbf{A}_{lp'_z}$$

$$\sim \int_{-\infty}^{\infty} dP_x \int_{-\infty}^{\infty} dp'_z \sum_{l=-\infty}^{\infty} \psi_{lp'_z} [\mathbf{v}\,\delta(\mathrm{Z} - \hat{\zeta})]_{-l,\,-p'_z}$$

$$= \int_{-\infty}^{\infty} dP_x [\psi\,\mathbf{v}\,\delta(\mathrm{Z} - \hat{\zeta})]_{0,0} \sim \overline{\psi\,\mathbf{v}\,\delta(\mathrm{Z} - \hat{\zeta})}. \tag{5.7}$$

Thus this integral is proportional to the corresponding quasi-classical quantity in a state with $\epsilon = \epsilon(n, p_Z)$ and p_Z. This is to be expected, since if, in the formula

$$\mathbf{j} = -\int_{-\infty}^{\infty} dp_z \sum_{n=0}^{\infty} \frac{\partial f^0}{\partial \varepsilon_{np_z}} \int_{-\infty}^{\infty} dp'_z \sum_{l=-\infty}^{\infty} \mathbf{A}_{lp'_z}$$

we replace the summation over n by an integration and remember that $\partial(n, p_Z)/\partial(\epsilon, p_Z) = 1/\hbar\Omega$, we obtain the classical formula for the current density.

Consequently, the transition from the classical equation for j,

$$\mathbf{j} = -\frac{2|e|^3 H}{ch^3} \int \frac{\partial f^0}{\partial \varepsilon}\, \mathbf{v}\,\psi\, d\varepsilon\, dp_z\, dt_1, \tag{5.8}$$

to the quantum-mechanical one gives

$$\mathbf{j} = -\frac{2|e|^3 H}{ch^3} \int_{-\infty}^{\infty} dp_z \sum_{n=0}^{\infty} \frac{\partial f^0}{\partial \varepsilon_{np_z}}\, \hbar\Omega$$

$$\times \int_0^T \mathbf{v}(\varepsilon_{np_z}, p_z, t_1)\, \psi(\zeta, \varepsilon_{np_z}, p_z, t_1)\, dt_1. \tag{5.9}$$

Substituting the expression (2.12) here for ψ, we write $j_i(\zeta)$ in the form

$$j_i(\zeta) = -\frac{2|e|^3 H}{ch^3} \int_{-\infty}^{\infty} dp_z \sum_{n=0}^{\infty} \frac{\partial f^0}{\partial \varepsilon_{np_z}} \int_{-\infty}^{\infty} d\zeta_0 \tag{5.10}$$

$$\times \left\{ v_i(t_1)\, \delta(\zeta - \zeta_0 - \zeta_1(t_1)) \right.$$

$$\left. \times \int_{-\infty}^{t_1} \exp\left\{ -\frac{t_1 - t'_1}{t_0^*} \right\} v_l(t'_1)\, E_l(\zeta_0 + \zeta_1(t'_1))\, dt'_1 \right\}_{\mathrm{av}},$$

$$\zeta_1(t_1) = \int_{t'_0}^{t_1} v_\zeta dt_2. \tag{5.11}$$

We take t'_0 to be the time when

$$v_\zeta(\varepsilon_{np_z}, p_z, t'_0) = 0;\quad v'_\zeta(t'_0) > 0,\quad t'_0 = t'_0(\varepsilon_{np_z}, p_z). \tag{5.12}$$

Strictly speaking, there are an infinite number of values of t'_0 which are solutions of (5.12). However, only the quantum correction Δj_i^{qu} is of interest to us (the classical part j_i has been determined already[13,14,4]), and for this only the point $\overline{v}_\zeta(\epsilon_{np_Z}, p_Z) = 0$ is important. For electrons in these states, the various values of t'_0 differ by integral numbers of periods, thereby not affecting $\zeta_1(t_1)$; ζ_0 is in this case the minimum distance of an electron from the surface.

It is now a simple matter to separate out the electrons which do not collide with the surface:

$$j_i(\zeta) = -\frac{2|e|^3 H}{ch^2} \int_{-\infty}^{\infty} dp_z \sum_{n=0}^{\infty} \frac{\partial f^0}{\partial \varepsilon_{np_z}} \int_0^Q d\zeta_0$$

$$\times \left\{ v_i(t_1)\, \delta\left(\zeta - \zeta_0 - \int_{t'_0}^{t_1} v_\zeta dt_2\right) \right.$$

$$\times \int_{-\infty}^{t_1} \exp\left(-\frac{t_1-t_1'}{t_0^*}\right) v_j(t_1') E_j\left(\zeta_0 + \int_{t_0'}^{t_1'} v_\zeta dt_2\right) dt_1' \Big\}_{av}; \quad (5.13)$$

$$v_\zeta(t_0') = 0; \quad v_\zeta'(t_0') > 0; \quad v_\zeta(t_0'') = 0;$$

$$v_\zeta'(t_0'') < 0; \quad D > \left| \int_{t_0'}^{t_0''} v_\zeta dt_2 \right|_{p_z=0}, \quad Q = D - \int_{t_0'}^{t_0''} v_\zeta dt_2. \quad (5.14)$$

$\zeta_0 \leq Q$, since the lowest point of the orbit $\zeta_0 + \int_{t_0'}^{t_0''} v_\zeta dt_2$ for electrons which do not collide with the surface lie inside the metal, that is, $\zeta_0 + \int_{t_0'}^{t_0''} v_\zeta dt_2 \leq D$. It is obvious that this formula gives accurately only Δj_i^{qu}, and not the classical value j_i, for which it is essential to make allowances also for the electrons which do collide with the surface.

Evaluating (5.13), with $\bar{v}_\zeta = 0$ and taking note of (5.4), we obtain

$$\Delta j_i^{qu}(\zeta) = \frac{h^3}{2\pi} H^2 \sum \chi_i \left(\frac{d \ln S}{d\varepsilon}\right)^2 \frac{\partial \Delta M_z}{\partial H}\Big|_{\varepsilon=\varepsilon_0,\ p_z=0}; \quad (5.15)$$

$$\chi_i = \frac{4\pi e^2}{h^3 t_0^{*-1}} \Big\{ v_i(t_1) S\left(\zeta - \int_{t_0'}^{t_1} v_\zeta dt_2\right) S\left(D - \zeta - \int_{t_1}^{t_0''} v_\zeta dt_2\right)$$

$$\times \int_{-\infty}^{t_1} \exp\left(-\frac{t_1-t_1'}{t_0^*}\right) v_j(t_1') E_j\left(\zeta - \int_{t_1'}^{t_1} v_\zeta dt_2\right) dt_1' \Big\}_{av}\Big|_{p_z=0}$$

$$\approx \frac{4\pi e^2}{h^3 t_0^{*-1}} \Big\{ v_i(t_1) S\left(\zeta - \int_{t_0'}^{t_1} v_\zeta dt_2\right) S\left(D - \zeta - \int_{t_1}^{t_0''} v_\zeta dt_2\right)$$

$$\times v_j(t_1') E_j\left(\zeta - \int_{t_1'}^{t_1} v_\zeta dt_2\right) \Big\}_{cp}\Big|_{p_z=0}. \quad (5.16)$$

This formula has the same form as (5.3), but it has a considerably narrower range of applicability. The fact that it appears to be exact in a parallel field is connected with the fact that the errors of the two approximations were reduced: in Eq. (5.6) and through the transformation in (5.16).

We note that in the general case in Eqs. (5.15), (5.16), $p_z = p_z^{ext}$ and the sum is carried out over all extreme sections, if $\pi/2 - \phi \ll \delta_{eff}/l$, and over central cross-sections ($p_z = 0$) if $\pi/2 - \phi \gg \delta_{eff}/r$. The form of Eq. (5.16) corresponds completely to what was said at the end of Section 4.

Thus $\Delta j_i^{qu} \sim (\hbar\Omega/\epsilon_0)^{1/2}$ always. The case when $v_i = 0$ at the point indicated in Section 4 might be an exception, also the case of a field aligned perpendicularly for an isotropic dispersion law, when $\bar{v}|_{p_z=0} = 0$ enters into the expression for Δj^{qu}, since at all times during the motion, $v_z = 0$. This leads to a decrease of Δj_i^{qu} by a factor of $\epsilon_0/\hbar\Omega$, but when Δj_i^{qu} increases essentially in conformance with the fact that the electron is at all times located in the skin layer and the normal skin effect occurs. For all cases, the oscillations of the chemical potential $\Delta\zeta_{chem} \sim (\hbar\Omega/\epsilon_0)^{3/2}$ do not have to be taken into account in any way.

Since $|\Delta j_i^{qu}| \ll j_i$, it is a simple matter to obtain the quantum-mechanical correction to the surface impedance. Its determination and also the solution of a series of other questions will be the subject of a separate paper.

I am grateful to L. D. Landau and to I. M. Lifshitz for valuable discussions.

[1] I. M. Lifshitz and A. M. Kosevich, Dokl. Akad. Nauk SSSR **96**, 963 (1954); J. Exptl. Theoret. Phys. (U.S.S.R.) **29**, 730 (1955), Soviet Phys. JETP **2**, 636 (1956).

[2] I. M. Lifshitz, J. Exptl. Theoret. Phys. (U.S.S.R.) **30**, 814 (1956), **32**, 1509 (1957; Soviet Phys. JETP **3**, 774 (1956), **5**, 1227 (1957).

[3] I. M. Lifshitz and A. M. Kosevich, J. Exptl. Theoret. Phys. (U.S.S.R.) **33**, 88 (1957), Soviet Phys. JETP **6**, 67 (1958).

[4] M. Ia. Azbel' and E. A. Kaner, J. Exptl. Theoret. Phys. (U.S.S.R.) **30**, 811 (1956), **32**, 896 (1957); Soviet Phys. JETP **3**, 772 (1956), **5**, 730 (1957); Journ. Phys. Chem. Solids (in press).

[5] A. M. Kosevich and I. M. Lifshitz, J. Exptl. Theoret. Phys. (U.S.S.R.) **29**, 743 (1955), Soviet Phys. JETP **2**, 646 (1956).

[6] I. M. Lifshitz and A. M. Kosevich, Izv. Akad. Nauk SSSR, Ser. Fiz. **19**, 395 (1955). Bull. Acad. Sciences U.S.S.R., Physical Series (Columbia Technical Translations) **19**, 353 (1955).

[7] K. Fuchs, Proc. Camb. Phil. Soc. **34**, 100 (1938).

[8] R. G. Chambers, Proc. Roy. Soc. (London) **215A**, 481 (1952).

[9] L. D. Landau and E. M. Lifshitz, Квантовая механика (Quantum Mechanics), Moscow, GITTL, 1948.

[10] M. Ia. Azbel', Dokl. Akad. Nauk SSSR **99**, 519 (1954).

[11] L. D. Landau and L. M. Piatigorskii, Механика (Mechanics), GITTL, 1940.

[12] R. Courant and D. Hilbert, Methods of Mathematical Physics (New York, 1953), Vol. I.

[13] M. Ia. Azbel' and M. I. Kaganov, Dokl. Akad. Nauk SSSR **95**, 41 (1954).

[14] M. Ia. Azbel', Dokl. Akad. Nauk SSSR **100**, 437 (1955).

Translated by W. M. Whitney
191

EFFECT OF COLLECTIVE INTERACTION OF ELECTRONS IN CYCLIC ACCELERATORS

L. M. KOVRIZHNYKH and A. N. LEBEDEV

P. N. Lebedev Physical Institute, Academy of Sciences U.S.S.R.

Submitted to JETP editor November 26, 1957

J. Exptl. Theoret. Phys. (U.S.S.R.) **34**, 984-992 (April, 1958)

A mathematical technique is developed which permits one to take into account collective interaction of particles in cyclic accelerators. The method is then applied to the problem of electron capture in the betatron acceleration regime. The results obtained are compared with experiment.

IT has been shown in a number of experimental papers[1-4] that in the case of certain processes in cyclic accelerators, particularly during injection, the collective interaction of particles plays a significant and even a dominant role.

Among the various kinds of interaction the following are the most essential ones:

1. Coulomb interaction which in the first approximation leads to a change in the frequency of betatron oscillations associated with a decrease in the effective restoring force, and also to the appearance of azimuthal inhomogeneities. As will be shown below, Coulomb repulsion plays an essential role in the process of the capture of electrons into the acceleration regime.

2. Magnetic interaction which fundamentally reduces to two effects. Firstly, attraction of currents which counteracts Coulomb repulsion; this has to be taken into account only at relativistic energies. Secondly, the effect of beam inductance which was pointed out by Kerst.[5] According to estimates that have been made, such an effect can be significant only in the case of a very rapid change of current in the chamber which never occurs in practice (see, for example, Kerst[5] and Rusanov[2]).

In addition to the above effects one could in principle take into account effects of two-body collisions in the beam which, however, produce an appreciable effect only at such high densities that in practice they can be always neglected.

A typical problem in which the collective interaction plays an essential role is the calculation of the current captured after injection into the betatron acceleration regime.

Recently, a number of papers (primarily by Soviet authors), among which one should particularly note Refs. 1 — 4, have been devoted to the experimental investigation of betatron capture.

The main experimental fact requiring theoretical explanation is the large value of the captured current which does not fit within the framework of the original concepts of Kerst and Serber.[6] Indeed, the slow increase of the magnetic field can produce a displacement of the instantaneous orbit and a change in the amplitude of oscillations only by an amount of the order of 10^{-3} to 10^{-2} cm/turn, which gives a very low value for the captured current since the majority of the particles must be lost on the back side of the injector. Moreover, it has been shown experimentally[1-3] that the value of the captured current within wide limits depends only very little on the distance between the filament of the injector and its edge (the so-called "gap"), which also does not agree with the Kerst and Serber theory. Moreover, recently it has been confirmed experimentally that capture takes place into a field constant in time, with the qualitative picture of the phenomenon being essentially undisturbed.[4]

As a result of the above investigations, it has been definitely established that the capture mechanism is unquestionably a collective mechanism, and that Coulomb interaction plays a fundamental role in it.

Since we are unable to give here even a brief review of the basic experimental facts and hypotheses relating to betatron capture (as was done, for example, by Rusanov[2]) we must merely note that the published papers do not contain any mathematical theory of the above phenomenon which would at all satisfactorily explain the available experimental facts. There exists only a series of unrelated attempts and hypotheses the majority of which is in qualitative disagreement with experiment.

One must, however, note that the above situation exists only for large injection currents when the collective interaction is very pronounced. For

small currents, the theory agrees with experiment satisfactorily.

In dealing with such problems it is most natural to adopt a purely statistical approach making use of the method of the kinetic equation into which the self-consistent interaction has been introduced. This method is used below for the investigation of the injection of non-relativistic electrons into a betatron. The generality of the method employed allows us to extend it to a number of other problems which will be done in subsequent papers. In particular, we shall investigate collective interactions in accelerators with strong focussing, which is of interest from the point of view of obtaining high intensity beams in them.

1. FORMULATION OF THE PROBLEM

We shall describe the state of the system of electrons in the betatron chamber by means of a distribution function $f(p, q, t)$ defined in coordinate and momentum space. We shall take for our starting point the equation

$$\frac{\partial f}{\partial t} + [\mathcal{H} f] = \left(\frac{\partial f}{\partial t}\right)_{\text{coll}} - \frac{f}{\tau} + F_s , \qquad (1.1)$$

which differs from the usual form of the kinetic equation by the terms $-f/\tau$ and F_S which take into account, respectively, the loss of particles on the chamber walls and on the injector, and the appearance of new particles due to the operation of the injector. In this equation, $\mathcal{H}$ is the Hamiltonian of the particle taking the self-consistent field into account. Generally speaking, in order to take the loss of particles into account rigorously one should have included in the Hamiltonian the interaction between the particles and the walls and the injector, but this encounters considerable difficulties. Therefore we take the effect of the walls and the injector into account purely phenomenologically, viz., we characterize the particles by some mean lifetime in the chamber τ which is a function of p, q and t and, generally speaking, a function of $f(p, q, t)$. In other words, we shall consider that the change in the distribution function due to the loss of particles is proportional to $-f/\tau$.

In view of the above remarks we can neglect in the present problem the term $(\partial f/\partial t)_{\text{coll}}$ which takes into account two-body collisions.

In order to demonstrate more explicitly the method being employed, we shall discuss in the present article somewhat idealized conditions of betatron capture which, nevertheless, allow us to obtain the basic qualitative characteristics of the phenomenon and some quantitative estimates. We shall treat the one-dimensional case, i.e., we shall take into account only the radial motion of the electrons whose energy coincides with the equilibrium energy. Then, as is well known, the Hamiltonian may be written in the form:

$$\mathcal{H} = (p^2 + \alpha^4 q^2)/2m, \qquad (1.2)$$

where m is the electron mass, p is the radial component of its momentum, q is the deviation from the equilibrium orbit and α^2 (up to a constant factor) is the frequency of betatron oscillations

$$\alpha = (eH/c)^{1/2}(1-x)^{1/4}(1-n)^{3/4}, \qquad (1.3)$$

where x is the average charge density in the chamber which is to be determined expressed in units of the limiting density.* The self-consistent nature of the problem is already clear from the above since the density x is determined by the function $f(p, q, t)$ which in turn is a solution of Eq. (1.1).

The equation is considerably simplified if we go over to new canonical variables P and Q by means of the generating function

$$V(q, Q, t) = \frac{\alpha^2 q^2}{2}\tan Q + \frac{\dot{\alpha} q^2}{2\alpha}\varepsilon, \qquad (1.4)$$

where we take the quantity $\epsilon = m\dot{\alpha}/\alpha^3$ to be small, which means that the adiabatic invariant is applicable to the betatron oscillations. It may then be easily shown that, up to terms of the second order in ϵ, the new Hamiltonian has the form

$$\mathcal{H}' = \alpha^2(t) P/m \qquad (1.5)$$

and Eq. (1.1) takes on the form

$$\frac{\partial \psi}{\partial t} + \frac{\alpha^2(t)}{m}\frac{\partial \psi}{\partial Q} = -\frac{\psi}{\tau} + F_s(P, Q, t), \qquad (1.6)$$

where $\psi(P, Q, t)$ is the distribution function in terms of the variables P and Q.

The form of the function τ may be chosen on the basis of the following considerations. Since it is physically obvious that particles, which have an oscillation amplitude a greater than the half width of the chamber a_2, are lost during a time shorter than the period of revolution, it is natural to assume that

$$\tau \equiv 0 \quad \text{for} \quad a > a_2. \qquad (1.7a)$$

On the other hand if the amplitude is smaller than the distance a_0 from the centre of the chamber to

*The limiting density is that density at which the force of Coulomb repulsion becomes equal to the magnetic focussing forces so that the effective restoring force becomes equal to zero [cf. (1.3)].

the edge of the injector then the particles have an infinite lifetime, i.e.

$$\tau = \infty \quad \text{for} \quad a < a_0. \tag{1.7b}$$

Finally, within the interval (a_0, a_2) for the variable a the lifetime τ is a function of the amplitude which for the sake of simplifying the calculations we shall assume to be equal to some constant τ.

It may be easily seen from formula (1.4) that the amplitude a is expressed in terms of the canonical momentum P in the following manner:

$$a = \sqrt{2P}/\alpha(t). \tag{1.8}$$

From this it may be easily seen that the quantity $\alpha(t)$ and consequently also $\tau(a)$ are unknown functions of the time determined by the distribution function ψ.

After integration of Eq. (1.6) over the cyclic variable Q and denoting the average value $\overline{\psi(P, Q, t)}$ simply by $\psi(P, t)$ we obtain the equation

$$\frac{\partial \psi}{\partial t} + \frac{\psi}{\tau} = F_s \ (P, t). \tag{1.9}$$

In future we shall assume that the injector cathode has vanishingly small radial dimensions and emits electrons with a certain angular spread so that the source function may be written in the form:

$$F_s \ (p, q, t) = i(t) \frac{\delta(q - a_1)}{\pi} \frac{p_0}{p_0^2 + p^2}, \tag{1.10}$$

where i(t) is the emission current. Substituting into the above in accordance with (1.4) in place of q and p their values in terms of Q and P, and integrating over Q we obtain after neglecting small terms:

$$F_s \ (P, t) = \frac{i(t)}{} \frac{2p_0}{p_0^2 + \alpha^4 (2P/\alpha^2 - a_1^2)} \operatorname{Re}\left(\frac{2P}{\alpha^2} - a_1^2\right)^{1/2}. \tag{1.11}$$

We shall assume the density of the beam to be equal to the total number of particles referred to a certain effective beam dimension a_{eff} which we shall fix later*

$$x = (1/a_{eff}\rho_{lim}) \int_0^\infty \psi(P, t)\, dP, \tag{1.12}$$

where ρ_{lim} is the limiting density equal to Q_{lim}/a_2 and Q_{lim} is the limiting charge.

Thus relations (1.8), (1.7a, b), (1.11), (1.12) and the initial condition

$$\psi(P, 0) \equiv 0 \tag{1.13}$$

completely determine the problem of finding the current or the total number of particles in the chamber at an arbitrary time t.

2. SINGLE ELECTRON CAPTURE

Before proceeding to collective capture we shall first demonstrate how the fundamental features of single electron capture, i.e., capture at low currents, follow from the present treatment.

When the current circulating in the chamber is small the collective interaction is weak and we can take $x \ll 1$. Then assuming that the magnetic field increases linearly with time, we obtain

$$\alpha^2(t) = (eH_i/c)(1 + \gamma t)(1 - n)^{1/2}, \tag{2.1}$$

where $\gamma = H_i^{-1} \partial H/\partial t$ and H_i is the field at injection. Since α and τ now do not depend on ψ we can employ the Green's function method for the solution of Eq. (1.6). As is well known the Green's function G coincides up to a normalization factor with the solution of Eq. (1.9) if in expression (1.11) we set

$$i(t) = \delta(t - t'). \tag{2.2}$$

Further, we assume for the sake of definiteness that the mean exit angle for particles from the injector is much larger than the chamber aperture, i.e., that

$$p_0^2 \gg \alpha^4(0)\,[a_2^2 - a_1^2].$$

Then after some elementary calculations we obtain

$$G(P, t, t') = \begin{cases} \dfrac{\sqrt{2}}{\pi p_0}\, \alpha(t') \exp\left[-\displaystyle\int_{t'}^{t} \frac{dx}{\tau(\sqrt{2P}/\alpha(x))}\right] \\ 0 \qquad \text{for } t < t' \end{cases} \tag{2.3}$$

$$\times \operatorname{Re}\left(P - \frac{a_1^2 \alpha^2(t')}{2}\right)^{1/2} \text{for } t > t',$$

We are interested in the captured current, i.e., in the solution for $t \to \infty$. From expressions (1.7a, b) and (2.1) it follows that the Green's function for the captured current is given by

$$G_\infty(t') = \frac{1}{T} \int_0^\infty \lim_{t \to \infty} G(P, t, t')\, dP$$

$$= \frac{\sqrt{2}}{\pi p_0 T}\, \alpha(t') \int_0^{\alpha^2(t') a_2^2/2} \exp\frac{1}{\tau}\left[t' - \frac{1}{\gamma}\left(\frac{2Pc}{a_0^2 eH_i} - 1\right)\right]$$

$$\times \operatorname{Re}\left(P - \frac{a_1^2 \alpha^2(t')}{2}\right)^{1/2} dP. \tag{2.4}$$

On carrying out the integration we obtain the Green's function $G_\infty(t')$ and then we immediately

*It will be shown below that the results depend only very little on the choice of the parameter a_{eff}.

find the captured current J_c:

$$J_c = \int_{-\infty}^{+\infty} i(t')\, G_\infty(t')\, dt' = \frac{a_0}{p_0 T}\left(\frac{eH_i \gamma\tau}{\pi c}\right)^{1/3}(1-n)^{1/4} \times \int_0^{t_i} i(t')\,\alpha(t') \exp\left\{-\frac{1+\gamma t'}{\gamma\tau}\left(\frac{a_1^2}{a_0^2}-1\right)\right\} \times \Phi\left(\left[\frac{a_2^2-a_1^2}{a_0^2\gamma\tau}(1+\gamma t')\right]^{1/3}\right) dt', \quad (2.5)$$

where Φ is Kramp's function, T is the period of revolution at the end of injection. Since usually $\gamma\tau \ll 1$, $\delta \ll 1$ (where $\delta = 1 - a_0/a_1$), formula (2.5) can be simplified:

$$J_c = \frac{k_i a_0}{a_2 T}\left(\frac{\gamma\tau}{\pi}\right)^{1/3} e^{-2\delta/\gamma\tau} \int_0^{t_i} i(t')(1+\gamma t')^{2/3} e^{-2t'\delta/\tau} dt', \quad (2.6)$$

where t_i is the time when injection ends, and k_i is the ratio of the chamber aperture to the mean angle of spread of the beam leaving the injector: $k_i = (eH_i a_2/cp_0)(1-n)^{1/2}$.

We have thus obtained an expression for the captured current for an arbitrary shape of the injector current pulse [we note that if the rate of increase of the magnetic field H is sufficiently great, i.e., $\gamma\tau > 1$, it is necessary to use the more general formula (2.5)].

We have assumed above that the angle of spread is sufficiently large, i.e., that the coefficient k_i is sufficiently small. We shall quote without giving its derivation the formula for the captured current obtained in the case when the injector gives no angular spread at all and all the particles are injected strictly azimuthally, with the current pulse being of rectangular shape:

$$J_c = \frac{3}{4}\frac{i\tau}{T\delta}\left[1 - e^{-4\delta t_i/3\tau}\right] e^{-4\delta/3\gamma\tau}. \quad (2.7)$$

From formulas (2.6) and (2.7) we obtain the following fundamental characteristics of capture in the case of low current: (1) a low value of the captured current, since the value of the quantity τ/T varies within the limits[4] 5 to 8; (2) exponential dependence of the captured current on the "gap" δ, since in practice always $\gamma\tau \ll 1$; (3) a linear dependence of the captured current on the emission current.

3. COLLECTIVE CAPTURE

In discussing collective capture, we shall neglect the explicit dependence of α on the time, i.e., the variation of field with time, which makes it equivalent to the problem of injection into a constant field. It can be shown that this assumption is quite justified for sufficiently large injector currents. The criterion which determines that collective rather than single-electron capture plays the dominant role will be given below.

Since for $t > t_i$, $F_S = 0$, i.e., Eq. (1.9) reduces to a homogeneous one, the range of variation for the variable t in Eq. (1.9) can be conveniently broken up into two parts: one where $t \le t_i$, and the other where $t \ge t_i$.

We discuss the solution in the first region. On introducing the new variable

$$\varphi = (1-x)^{1/3} \quad (3.1)$$

and taking into account (1.7a, b), (1.9) and (1.11), we obtain the equations which determine the circulating current:

$$\varphi^2 = 1 - \frac{2}{\pi T J_{\lim}} \int_0^t e^{-(t-t')/\tau} i(t') \tan^{-1}\frac{k_i}{\eta}\varphi^{1/3}(t') \times [\eta^2\varphi(t) - \varphi(t')]^{1/3} dt', \quad t \le t_1 \quad (3.2)$$

$$\varphi^2 = 1 - \frac{2}{\pi T J_{\lim}} \int_{\tilde{t}(t)}^t e^{-(t-t')/\tau} i(t') \tan^{-1}\frac{k_i}{\eta}\varphi^{1/3}(t') \times [\eta^2\varphi(t) - \varphi(t')]^{1/3} dt', \quad t \ge t_1 \quad (3.3)$$

where $\eta = a_2/a_1$, $J_{\lim} = Q_{\lim}/T$ is the limiting current, while t_1 and $\tilde{t}(t)$ are determined by the relations

$$\varphi(t_1) = \eta^{-2}, \quad (3.4)$$

$$\varphi(\tilde{t}) = \eta^2\varphi(t). \quad (3.5)$$

In the general case, the solution of these equations is quite a complicated problem, and therefore we shall discuss here the case most important in practice when the injector current reaches a stationary value i after a time $\lesssim \tau$.

In this case the final value of the circulating current will be determined by the equation

$$\varphi_{st}^2 - 1 + \frac{2i\tau}{\pi T J_{\lim}} \tan^{-1}\left[\frac{k_i}{\eta}(\eta^2-1)^{1/3}\varphi_{st}\right] = 0. \quad (3.6)$$

We note that if $t_i \gg \tau$, which always holds in practice, then the captured current does not depend on the way the current behaves during injection, but is determined only by its stationary value $1 - \varphi_{2st}$, or more accurately by the value of x at the time when the injector stops operating: $x_i = x(t_i)$.

We now proceed to determine the captured current. From Eq. (1.9) we obtain

$$x = \frac{a_2}{a_{\text{eff}}} \int_0^\infty \exp\left\{-\int_{t_i}^t \frac{d\xi}{\tau(\sqrt{2P}/\alpha(\xi))}\right\} U(P, t_i)\, dP; \quad (3.7)$$

where

$$U(P, t_i) = \frac{2p_0}{\pi T} \int_0 \exp\left\{-\frac{t'-t_i}{\tau}\right\} \frac{i(t')}{J_{1\lim}} [p_0^2 + 2\alpha^2(t')P - \alpha^4(t')a_1^2]^{-1} \operatorname{Re}\left[\frac{2P}{\alpha^2(t')} - a_1^2\right]^{-1/2} dt', \quad (3.8)$$

Generally speaking, a_{eff} is some monotonic function of the time.

On taking into account the explicit dependence of τ on P equation (3.8) can now be brought into the form:

$$x = x_i e^{-(t-t_i)/\tau}, \quad t \leqslant t_2, \quad (3.9)$$

$$x = \frac{a_2}{a_{eff}} \int_{P_1}^{a_0^2\alpha^2(t)/2} U(P) \exp\left\{-\frac{t''(P)-t_i}{\tau}\right\} dP + \frac{a_2}{a_{eff}} \exp\left\{-\frac{(t-t_i)}{\tau}\right\} \int_{a_0^2\alpha^2(t)/2}^{\eta^2 P_1} U(P)\, dP, \quad t \geqslant t_2, \quad (3.10)$$

where $P_1 = a_1^2\alpha^2(t_i)/2$, $t_2 = t''(P_i)$ and $t''(P)$ is determined by the relation

$$\alpha(t'') = \sqrt{2P}/a_0.$$

We note that if the function $U(P)$ is known Eq. (3.10) allows us to obtain the captured current also in the case that the magnetic field H depends explicitly on the time.

As is shown by calculations made in the two limiting cases $a_{eff} = a_2$ and $a_{eff} = a_0$ the value of the captured current for usual values of the accelerator parameters depends very little on the magnitude of a_{eff} (Fig. 1). Therefore in order to simplify the calculations we shall assume that $a_{eff} = \text{const}$.*

In this case the solution of Eq. (3.10) is obtained from

$$\int_{x(t_2)}^{x} \frac{dx'}{\Psi(x')} = -\frac{a_2}{a_{eff}} \exp\left\{-\frac{t_2-t_i}{\tau}\right\}\left[1 - \exp\left\{-\frac{t-t_2}{\tau}\right\}\right], \quad (3.11)$$

where

$$\Psi(x') = \int_{a_0^2\alpha^2(x)/2}^{\eta^2 P_1} U(P)\, dP,$$

while the value of the captured current is obtained from the equation

$$\int_{x(t_2)}^{x_c} \frac{dx'}{\Psi(x')} = -\frac{a_2}{a_{eff}} \exp\left\{-\frac{t_2-t_i}{\tau}\right\}. \quad (3.12)$$

In the general case of arbitrary p_0 in the expression for the source function in (1.11), the integral on the left hand side of (3.11) is not expressible in terms of elementary functions. Therefore, in order to obtain the final expression in analytic form we shall consider the case most frequently encountered in practice when the mean square exit angle from the injector is much greater than the chamber aperture. Calculations carried out in another limiting case of a sharply focussed beam show that the qualitative picture of the phenomenon is preserved.

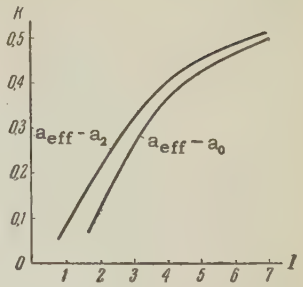

FIG. 1. Dependence of the collective capture coefficient on the emission current.

In the case under discussion, (3.11) is transformed into

$$F\left(\frac{a_0\varphi_3}{a_1\varphi_i}\right) = \frac{a_2}{a_{eff}} \frac{1-(a_1/a_0)^4\varphi_i^2}{2(a_1/a_0)^4\varphi_i^2}\left[1 - \exp\left\{-\frac{t-t_i}{\tau}\right\}\right], \quad (3.13)$$

where

$$F(z) = -2\beta\left[\frac{1}{3}(z-1)^{3/2} + \frac{\beta}{2}(z-1) + (\beta^2+1)(z-1)^{1/2} + \beta(\beta^2+1)\ln\frac{\beta-(z-1)^{1/2}}{\beta}\right], \quad \beta = (\eta_i^2-1)^{1/2}. \quad (3.14)$$

At the beginning of this section we noted that the dependence of the magnetic field on the time can be neglected if the injector current exceeds a certain value equal to i_{cr}. In the case under discussion

$$i_{cr} = \frac{1-(1-\delta)^4}{(1-\delta)^2} \frac{\eta\pi T}{2(\eta^2-1)^{1/2}k_i\tau} J_{1\lim}. \quad (3.15)$$

Thus the condition $i > i_{cr}$ corresponds to the region of collective capture, $i \lesssim i_{cr}$ corresponds to the region of mixed capture, and $i \ll i_{cr}$ to the region of single-electron capture. For example, in the case of the 30 Mev synchroton at the Physics Institute of the Academy of Sciences, we have the value $i_{cr} \approx 10$ ma. The experimental value of the current at which the mechanism of collective capture begins to play a role is approximately equal to 3 ma. This value is less than i_{cr} just as it should be.

In conclusion we indicate the condition of validity of the above formulas which follows from the possibility of writing the Hamiltonian in the form (1.5), i.e., the condition for the existence of an adiabatic invariant for betatron oscillations. It

*It should be noted that similar but more complicated calculations can be carried out in the case that $a_{eff} = a_{eff}(t)$.

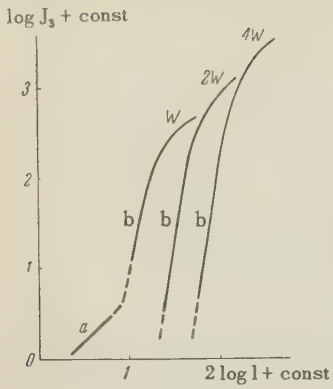

FIG. 2. Dependence of the captured current on the emission current for different injection energies W; a – single electron capture, b – collective capture.

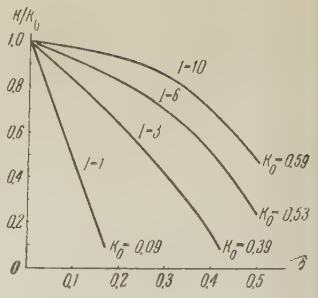

FIG. 3. Dependence of the capture coefficient K on the relative "gap" size:

$$I = \frac{2k_i}{\pi\eta}(\eta^2-1)^{1/2}\frac{\tau}{T}\frac{i}{J_{\lim}}$$

reduces to the requirement $\epsilon < 1$, or taking expression (3.9) into account, to

$$i < \left(\frac{8\pi\tau\sqrt{1-n}}{T}\right)^{1/3}\frac{\eta\pi T}{2(\eta^2-1)^{1/2}k_i\tau}J_{\lim}. \qquad (3.16)$$

4. DISCUSSION OF RESULTS

1. The collective capture coefficient, i.e., the ratio of the captured current to the maximum current circulating in the chamber at first grows rapidly as the injector current increases, and then shows a tendency towards saturation, reaching a value of 0.3 – 0.5 at the boundary of the region of applicability of the adiabatic approximation [see (3.20)]. The characteristic dependence of the capture coefficient on the emission current is given in Fig. 1 for two values of the parameter a_{eff}.

2. Since the maximum current circulating in the chamber is close to the limiting current and depends only slightly on the emission current the dependence of the captured current on the emission current also shows saturation. Figure 2 shows appropriate curves for single electron and for collective capture for different values of the injection energy. These curves show good qualitative agreement with experimental data (see, for example, Refs. 1 – 3). The region of mixed capture for which the theoretical curve has not been calculated is indicated by a dotted line. We note that the ranges of variation of the variables in the graphs shown above all satisfy the condition for the adiabatic approximation (3.16).

3. Figure 3 gives (in relative units) the dependence of the captured current on the "gap", which also agrees well with experiment.[3] As was shown in section 2 for small emission currents the dependence on the "gap" is of exponential nature.

In conclusion the authors express their gratitude to A. A. Kolomenskii, M. S. Rabinovich and P. A. Riasin for fruitful discussions.

Note added in proof (March 18, 1958). Calculations which we have made show that taking into account the deviation of the electron energy from its equilibrium value somewhat reduces the capture coefficient and leads to a lowering of the curves of Fig. 2 for large values of i. In all other respects the description of the phenomenon is preserved.

[1] Logunov, Ovchinnikov and Rusanov, J. Tech. Phys. (U.S.S.R.) **27**, 1135 (1957).

[2] V. D. Rusanov, Thesis, Physics Institute of the Academy of Sciences (U.S.S.R.), 1956.

[3] Iu. N. Lobanov, Thesis, Moscow State University, 1956. Iu. N. Lobanov and V. A. Petukhov, Supplement to Атомная энергия, (Atomic Energy) **4**, (1957).

[4] Iu. S. Korobochko, J. Tech. Phys. (U.S.S.R.) **27**, 745, 1603 (1957).

[5] D. W. Kerst, Rev. Sci. Instr. **21**, 462 (1950).

[6] D. W. Kerst and R. Serber, Phys. Rev. **60**, 53 (1941).

Translated by G. Volkoff
192

Letters to the Editor

DEPOLARIZATION OF MU MESONS IN HYDROGEN

S. S. GERSHTEIN

Institute for Physical Problems, Academy of Sciences, U.S.S.R.

Submitted to JETP editor December 10, 1957

J. Exptl. Theoret. Phys. (U.S.S.R.) **34**, 993-994 (April, 1958)

WE have shown[1] that, in the collision of a μ-mesic hydrogen atom with a free proton, the cross section for transition of the μ-mesic atom from its upper hyperfine structure state (with angular momentum $F = 1$) to the lower ($F = 0$) state is sufficiently large to result in complete depolarization of mesons in hydrogen. We should note that actually in hydrogen this process is determined not by the collision of the mesic atom with a free proton, but rather by collision with an H_2 molecule, since the energy transferred to the proton is considerably less than its binding energy in the molecule.

The collision of a μ-mesic atom with an H_2 molecule can be treated by a method analogous to that proposed by Fermi for calculating the scattering of slow neutrons by molecules. To do this we note that the cross section which was calculated[1] for transition of the μ-mesic atom from the upper to the lower hyperfine structure state:

$$d\sigma = \frac{1}{3} a^2 \frac{k_0}{k} d\Omega; \quad a^2 = \frac{150}{4}\left(\frac{\hbar^2}{m_\mu e^2}\right)^2; \quad k_0 = \sqrt{2m\Delta\varepsilon}/\hbar \gg k$$

($\Delta\epsilon$ is the hyperfine structure splitting in the μ-mesic atom), can be gotten formally from the Born approximation, if the interaction of the μ-mesic atom with a proton is described by the pseudopotential

$$\hat{U} = (2\pi\hbar^2/m)\, a\delta(\mathbf{r} - \mathbf{r}_p)\hat{R},$$

where $\mathbf{r}_p$, $\mathbf{r}$ are the coordinates of the proton and the mesic atom (taken as a point particle); $1/m = 1/M_p + 1/(M_p + m_\mu)$; $\hat{R}$ is an operator which takes the μ-mesic atom from the state with angular momentum 1 to the state with angular momentum 0 (as a result of interaction with the spin of a free proton). It is easy to verify that the operator $\hat{R} = 2(\mathbf{s} - \mathbf{j})\mathbf{i}/\sqrt{3}$ has this property; $\mathbf{s}$, $\mathbf{j}$, $\mathbf{i}$ are spin operators of the μ meson, the proton in the mesic atom, and the free proton, respectively.

The interaction potential of the μ-mesic atom with an H_2 molecule is given by:

$$\hat{V} = \frac{2\pi\hbar^2}{m} a \frac{(\mathbf{s} - \mathbf{j})}{V\,3}\{(\mathbf{i}_1 + \mathbf{i}_2)[\delta(\mathbf{r} - \mathbf{r}_1) + \delta(\mathbf{r} - \mathbf{r}_2)] + (\mathbf{i}_1 - \mathbf{i}_2)[\delta(\mathbf{r} - \mathbf{r}_1) - \delta(\mathbf{r} - \mathbf{r}_2)]\},$$

where $\mathbf{i}_1$, $\mathbf{i}_2$ are the spin operators of the protons in the H_2 molecule.

The hyperfine structure energy of the μ-mesic atom (0.183 ev) is not enough to excite vibrational levels of H_2, but can give excitation of the first four rotational levels. The initial and final states of the system have the form

$$\Psi^{(i)}_{J, M_J, I, M_I, 1, M_F} = e^{i\mathbf{k}\mathbf{r}}\chi_{1, M_F}(s, j) \times \exp\left\{-i\mathbf{k}\frac{(\mathbf{r}_1 + \mathbf{r}_2)}{2}\right\}\Phi_{J, M}(\mathbf{r}_1 - \mathbf{r}_2)\varphi_{I, M_I}(i_1, i_2),$$

$$\Psi^{(f)}_{J', M'_J, I', M'_I, 0, 0} = e^{i\mathbf{k}'\mathbf{r}}\chi_{0, 0}(s, j) \times \exp\left\{-i\mathbf{k}'\frac{(\mathbf{r}_1 + \mathbf{r}_2)}{2}\right\}\Phi_{J', M'_J}(\mathbf{r}_1 - \mathbf{r}_2)\varphi_{I', M'_I}(i_1, i_2),$$

where χ_{1,M_F} and $\chi_{0,0}$ are the spin functions of the mesic atom in states with $F = 1$ and $F = 0$; Φ_{J,M_J} is the wave function of H_2 in the J-th rotational level; φ_{I,M_I} are the spin functions of the H_2 molecule ($I = 1$ for ortho, and $I = 0$ for parahydrogen).

The term in the potential $\hat{V}$ which is symmetric in the proton spins gives rise to transitions between states of the same I, while the antisymmetric term causes transitions between states of different I. The cross section for scattering of the μ-mesic atom (accompanied by a transition $F = 1 \to F = 0$) is:

$$d\sigma^{J', I}_{J, I} = \frac{4a^2}{9(2I+1)(2J+1)}\left(\frac{\mathfrak{M}}{m}\right)^2\frac{k_{JJ'}}{k}\sum_{M_J, M'_J, M_I, M'_I, M_F}\left|\int\cos\frac{(\mathbf{k}_{JJ'} - \mathbf{k})\mathbf{r}}{2} \times \Phi^*_{J', M'_J}(\mathbf{r})\Phi_{J, M_J}(\mathbf{r})(d\mathbf{r})\right|^2 |\langle 0, I, M'_I|(\mathbf{s} - \mathbf{j})(\mathbf{i}_1 + \mathbf{i}_2) \times |M_F, I, M_I\rangle|^2 d\Omega,$$

$$d\sigma^{J', I'}_{J, I} = \frac{4a^2}{9(2I+1)(2J+1)}\left(\frac{\mathfrak{M}}{m}\right)^2\frac{k_{JJ'}}{k}\sum_{M_J, M'_J, M_I, M'_I, M_F}\left|\int\sin\frac{(\mathbf{k}_{J'J} - \mathbf{k})\mathbf{r}}{2} \times \Phi^*_{J', M'_J}(\mathbf{r})\Phi_{J, M_J}(\mathbf{r})(d\mathbf{r})\right|^2 |\langle 0, I', M'_I|(\mathbf{s} - \mathbf{j})(\mathbf{i}_1 - \mathbf{i}_2) \times |M_F, I, M_I\rangle|^2 d\Omega,$$

where $1/\mathfrak{M} = 1/(M_p + m_\mu) + 1/2M_p$; $\hbar k_{JJ'} = \{2\mathfrak{M}(\Delta\epsilon + \epsilon_J - \epsilon_{J'})\}^{1/2} \gg \hbar k$. The calculation of

the integrals over the rotational states of the molecule and the summation over M_J and M'_J were done in Ref. 2.

Summing the spin matrix elements, we get for the transitions in parahydrogen

$$d\sigma_{00}^{J'0} = 0; \quad d\sigma_{00}^{J'1} = {}^4/_3\, a^2 (\mathfrak{M}/m)^2 (k_{J'0}/k)\, \Sigma(0, J')\, d\Omega$$

and in orthohydrogen

$$d\sigma_{11}^{J'0} = {}^4/_9\, a^2 (\mathfrak{M}/m)^2 (k_{J'1}/k)\, \Sigma(J', 1)\, d\Omega;$$
$$d\sigma_{11}^{J'1} = {}^8/_9\, a^2 (\mathfrak{M}/m)^2 (k_{J'1}/k)\, \Sigma(J', 1)\, d\Omega,$$

where

$$\Sigma(J', J) = (2J'+1) \sum_L (2L+1)\, C_{LJJ'} j_L^2 (k_{JJ'} R_0/2),$$
$$L = J + J',\ J + J' - 2, \ldots, |J - J'|,$$
$$C_{LJJ'} = {}^1/_2 \int_0^\pi P_L(\cos\theta)\, P_J(\cos\theta)\, P_{J'}(\cos\theta) \sin\theta d\theta,$$
$$j_L(x) = \left(\frac{\pi}{2x}\right)^{1/2} J_{L+1/2}(x),$$

$R_0 = 1.4\hbar^2/m_e e^2$ is the internuclear separation in the H_2 molecule. Summation over all possible J' gives the total cross section for transition of the μ-mesic atom to the lower hyperfine structure state:

$$d\sigma_{\text{para}} \approx 1.02 a^2 \frac{k_0}{k}\, d\Omega, \quad d\sigma_{\text{ortho}} \approx 0.86 a^2 \frac{k_0}{k}\, d\Omega.$$

We thus confirm the conclusion[1] that there is complete depolarization of μ mesons in hydrogen. This result enables us, in principle, to determine the polarization of the neutrino emitted in the process $\mu^- + p \to n + \nu$, by measuring the polarization of the neutron along its direction of motion, which under these conditions should be complete. At the same time we see that it is not possible to do experiments in hydrogen for studying the $(\mu pn\nu)$ interaction using polarized μ^- mesons.

In conclusion I express my sincere thanks to Ia. B. Zel'dovich and L. D. Landau for valuable comments.

[1] S. S. Gershtein, J. Exptl. Theoret. Phys. (U.S.S.R.) **34**, 463 (1958), Soviet Phys. JETP **7**, 318 (1958).

[2] M. Hamermesh and J. Schwinger, Phys. Rev. **69**, 145 (1946).

Translated by M. Hamermesh
193

NON-CONSERVATION OF PARITY IN PROCESSES OF NEUTRINO CAPTURE BY PROTONS AND DEUTERONS

V. V. ANISOVICH and A. A. ANSEL'M

Leningrad Physico-Technical Institute, Academy of Sciences, U.S.S.R.

Submitted to JETP editor December 9, 1957

J. Exptl. Theoret. Phys. (U.S.S.R.) **34**, 995-997 (April, 1958)

EXPERIMENTAL researches have been reported recently on the capture of neutrinos by nuclei (induced β-decay).[1] In this process, parity is not conserved, inasmuch as the reaction is brought about by β-interaction.[2] Formulas are given below for the cross section of the induced β-decay of protons

$$p + \bar{\nu} \to n + e^+ \tag{1}$$

and deuterons

$$d + \bar{\nu} \to 2n + e^+ \tag{2}$$

with account of the polarization of the incident antineutrinos, wherein the target nuclei are also considered to be polarized.

It is easy to show that the density matrix of a polarized beam of particles of spin $\frac{1}{2}$ and mass zero is

$$\rho = {}^1/_2 (1 + i\gamma_5 (\mathbf{Q}\gamma) \mp \lambda\gamma_5) \frac{(-i\hat{q})}{2q} \gamma_4, \tag{3}$$

where $\mathbf{q}$ is the momentum of the particle $\mathbf{Q}$ = a pseudovector perpendicular to $\mathbf{q}$, λ = pseudoscalar, the upper sign referring to particles, the lower sign to antiparticles.

In experiments on induced β-decay, neutrinos emerging from a reactor were employed. Under these conditions, it is clearly difficult for the polarization of the neutrino to be other than longitudinal. We therefore assume in what follows that $\mathbf{Q} = 0$.* The usual calculations then lead to the following expression for the capture cross section of an antineutrino by protons:

$$d\sigma/d\Omega = Mp\varepsilon/8\pi^2,$$
$$M = \alpha_1 + \alpha_2 m/\varepsilon + \alpha_3 \mathbf{qp}/q\varepsilon + \alpha_4 \mathbf{q}\zeta_n/q + \alpha_5 (m/\varepsilon)\, \mathbf{q}\zeta_n/q + \alpha_6 \mathbf{p}\zeta_n/\varepsilon + \alpha_7 \zeta_n [\mathbf{q} \times \mathbf{p}]/q\varepsilon.$$
$$\alpha_1 = |C_S|^2 + |C'_S|^2 + |C_V|^2 + |C'_V|^2 + 3(|C_T|^2 + |C'_T|^2 + |C_A|^2 + |C'_A|^2) + 2\lambda\, \mathrm{Re}\,(C_S C'^*_S + C_V C'^*_V + 3C_T C'^*_T + 3C_A C'^*_A),$$
$$\alpha_2 = -2\, \mathrm{Re}\,(C_S C^*_V + C'_S C'^*_V + 3C_T C^*_A + 3C'_T C'^*_A)$$

$$- 2\lambda \operatorname{Re}(C_S C_V'^* + C_V C_S'^* + 3C_T C_A'^* + 3C_A C_T'^*),$$

$$\alpha_3 = -|C_S|^2 - |C_S'|^2 + |C_V|^2 + |C_V'|^2 + |C_T|^2 + |C_T'|^2 - |C_A|^2 - |C_A'|^2 + 2\lambda \operatorname{Re}(-C_S C_S'^* + C_V C_V'^* + C_T C_T'^* - C_A C_A'^*),$$

$$\alpha_4 = -2\operatorname{Re}(2C_T C_T'^* + 2C_A C_A'^* + C_T C_S'^* + C_S C_T'^* + C_A C_V'^* + C_V C_A'^*) - 2\lambda(\operatorname{Re}(C_T C_S^* + C_T' C_S'^* + C_A C_V^* + C_A' C_V'^*) + |C_T|^2 + |C_T'|^2 + |C_A|^2 + |C_A'|^2),$$

$$\alpha_5 = 2\operatorname{Re}(2C_A C_T'^* + 2C_T C_A'^* + C_T C_V'^* + C_V C_T'^* + C_A C_S'^* + C_S C_A'^*) + 2\lambda \operatorname{Re}(2C_A C_T^* + 2C_A' C_T'^* + C_T C_V^* + C_T' C_V'^* + C_A C_S^* + C_A' C_S'^*),$$

$$\alpha_6 = 2\operatorname{Re}(2C_A C_A'^* - 2C_T C_T'^* + C_T C_S'^* + C_S C_T'^* - C_A C_V'^* - C_V C_A'^*) + 2\lambda(|C_A|^2 + |C_A'|^2 - |C_T|^2 - |C_T'|^2 + \operatorname{Re}(C_T C_S^* + C_T' C_S'^* - C_A C_V^* - C_A' C_V'^*),$$

$$\alpha_7 = 2\operatorname{Im}(C_T C_S^* + C_T' C_S'^* + C_V C_A^* + C_V' C_A'^*) + 2\lambda \operatorname{Im}(C_T C_S'^* - C_S C_T'^* + C_V C_A'^* - C_A C_V'^*). \quad (4)$$

Here $\mathbf{q}$ and $\mathbf{p}$ are momenta of the incident antineutrino and emitted positron, ϵ = energy of the positron, m = its mass, $\boldsymbol{\zeta}$ = polarization vector of the protons. The cross section is referred to an element of solid angle of the momentum of the positron. The energy of the positron is fixed in (4) by the law of conservation of energy $\epsilon = q - \Delta$, Δ = difference in the masses of the neutron and proton. In this case it is assumed that the Hamiltonian of the interaction has the same form as that of Lee and Yang.[2]

It is easy to see that we can establish whether or not time parity is conserved in the capture of the neutrino by polarized protons. Measuring the total number of electrons emitted to the left and right from the plane $\mathbf{q}$, $\boldsymbol{\zeta}$, we get for the difference in cross section:

$$\sigma_+ - \sigma_- = (\alpha_7 / 4\pi)\, p^2 \zeta \sin\theta,$$

where θ = angle between $\mathbf{q}$ and $\boldsymbol{\zeta}$. If temporal parity (time reversal) is conserved, then $\alpha_7 = 0$, $\sigma_+ = \sigma_-$.

Capture of the antineutrino by unpolarized deuterons was considered by Weneser[4] without account of A and V variants, while the nonconservation of parity was not considered. Taking it into consideration that the neutrons in reaction (2) are in the main formed in the S state, and that $(\mathbf{p}-\mathbf{q})^2/4M\epsilon_0 \ll 1$ ($\mathbf{p}-\mathbf{q}$ is the total momentum transferred by the neutrons, and ϵ_0 is the binding energy of the deuteron), we obtain as a result of the calculations:

$$d\sigma = (|R_f|^2/64\pi^5)\, N p\epsilon d\epsilon\, d\Omega M f\, d\Omega_f,$$

$$N = \beta_1 + \beta_2 \frac{m}{\epsilon} + \beta_3 \frac{\mathbf{pq}}{q\epsilon} + 9\beta_3 (\langle I_z^2\rangle - 2/3)\left(\frac{(\mathbf{pj})(\mathbf{qj})}{q\epsilon} - \frac{1}{3}\frac{\mathbf{pq}}{q\epsilon}\right) + \langle I_z\rangle\left(\beta_4 \frac{\mathbf{qj}}{q} + \beta_5 \frac{m}{\epsilon}\frac{\mathbf{qj}}{q} + \beta_6 \frac{\mathbf{pj}}{\epsilon}\right), \quad (5)$$

$$R_f = \int \psi_f^*(\mathbf{r})\, \psi_d(\mathbf{r})\, d^3r,$$

$$\beta_1 = |C_T|^2 + |C_T'|^2 + |C_A|^2 + |C_A'|^2 + 2\lambda \operatorname{Re}(C_T C_T'^* + C_A C_A'^*),$$

$$\beta_2 = -2\operatorname{Re}(C_T C_A^* + C_T' C_A'^*) - 2\lambda \operatorname{Re}(C_T C_A'^* + C_A C_T'^*),$$

$$\beta_3 = \frac{1}{3}(|C_T|^2 + |C_T'|^2 - |C_A|^2 - |C_A'|^2 + 2\lambda \operatorname{Re}(C_T C_T'^* - C_A C_A'^*)),$$

$$\beta_4 = -2\operatorname{Re}(C_T C_T'^* + C_A C_A'^*) - \lambda(|C_T|^2 + |C_T'|^2 + |C_A|^2 + |C_A'|^2),$$

$$\beta_5 = 2\operatorname{Re}(C_A C_T'^* + C_T C_A'^*) + 2\lambda \operatorname{Re}(C_A C_T^* + C_T' C_A'^*),$$

$$\beta_6 = -2\operatorname{Re}(C_T C_T'^* - C_A C_A'^*) - \lambda(|C_T|^2 + |C_T'|^2 - |C_A|^2 - |C_A'|^2).$$

Here $\langle I_z\rangle$ and $\langle I_z^2\rangle$ are the average values of the projection of the moment of the deuteron on the Z axis and its square, $\mathbf{j}$ = unit vector in the direction of the Z axis, M = mass of the nucleon, f = momentum of the relative motion of the neutrons in the final state, ψ_d = wave function of the deuteron, and ψ_f = wave function of the relative motion of the generated neutrons. The rest of the notation is the same as in (4). The quantity f is determined by the law of conservation of energy $q = (f^2/M) + \epsilon + \Delta$. We note that $(\langle I_z^2\rangle - 2/3)$ vanishes for unpolarized deuterons.

Since R_f is essentially different from zero for $f \lesssim \alpha$, then for $q \gg \alpha^2/M$ in (5) we can carry out the summation over f approximately, making use of the completeness of the functions ψ_f. Then we get

$$d\sigma = (4\pi^2)^{-1} N p\epsilon\, d\epsilon\, d\Omega. \quad (6)$$

In conclusion, we express our deep thanks to I. M. Shmushkevich and V. N. Gribov for useful advice in discussions.

*If we keep terms in (3) proportional to Q, then there arise components in the expression for the cross section of the process under consideration which change sign upon substitution of the primed constant for the unprimed. This apparent contradiction with the work of Pauli[3] is explained by the fact that Q is not a directly observable quantity and, as can be shown, itself changes sign upon substitution of the primed constant for the unprimed in an interaction which corresponds to the creation of a neutrino.

[1] Cowan, Reines, Harrison, Kruse and McGuire, Science **124**, 103 (1956).

[2] T. D. Lee and C. N. Yang, Phys. Rev. **104**, 254 (1956).
[3] W. Pauli, Nuovo cimento **6**, 204 (1957).
[4] J. Weneser, Phys. Rev. **105**, 1335 (1957).

Translated by R. T. Beyer
194

ON THE DETERMINATION OF THE PARITY OF THE K MESON

L. B. OKUN' and I. Ia. POMERANCHUK

Submitted to JETP editor December 11, 1957

J. Exptl. Theoret. Phys. (U.S.S.R.) **34**, 997-998 (April, 1958)

THE determination of the parities of K mesons and hyperons has for some time been one of the central problems of the experimental physics of elementary particles. Since the strong interactions conserve strangeness and the weak interactions do not conserve parity, we can speak only of the relative parity of K mesons and hyperons, i.e., of the signs of $P_K P_N P_\Lambda$, $P_K P_N P_\Sigma$, and so on. We discuss below an experiment which provides a possibility of determining the sign of $P_K P_N P_\Lambda$.

Let us consider the capture of a slow K^- meson from an S state by a proton, according to the reactions

$$K^- + p \to \Lambda^0 + \pi^0 + \pi^0, \tag{1}$$

$$K^- + p \to \Lambda^0 + \pi^+ + \pi^-. \tag{2}$$

Since parity is conserved in the strong interactions, the parity of the system $\Lambda + 2\pi$ must be equal to the parity of the system K + p. Let us consider the two possibilities.

1. Suppose $P_K P_N P_\Lambda = +1$. In this case the transition amplitudes for the two reactions have the forms

$$A_1 = -(a + bp^2 + cq^2)/\sqrt{2} + \cdots,$$

$$A_2 = (a + bp^2 + cq^2) + d\mathbf{pq} + \cdots.$$

Here $\mathbf{q}$ is the difference of the momenta of the two π mesons and $\mathbf{p}$ is the sum of their momenta, equal to the momentum of the Λ particle. The energies released in the reactions (1) and (2), if the K meson had zero kinetic energy, are 47 and 38 Mev, respectively, and the maximum momenta p and q are of the order of μ_π (we use units $\hbar$ = c = 1). If we assume that the dimensions of the region in which the strong interaction occurs are of the order of $1/m_p < r < 1/\mu_\pi$, then we can suppose that $pr < 1$ and $qr < 1$ and confine ourselves to terms independent of p and q. In this case

$$A_1 = -a/\sqrt{2}, \quad A_2 = a \tag{3}$$

and we find that the angular distributions in the reactions (1) and (2) are spherically symmetric, the Λ particle is not polarized, and consequently the angular distribution of the π mesons coming from its decay is isotropic. If the energies released in the reactions (1) and (2) were the same, then from Eq. (3) we would get for the cross-sections of reactions (1) and (2)

$$\sigma_2/\sigma_1 = 2. \tag{4}$$

Inclusion of the effect of the difference of the masses of $\pi^\pm$ and π^0 in changing the volume in phase space gives instead the ratio

$$\sigma_2/\sigma_1 = 1{,}34. \tag{5}$$

2. Suppose $P_K P_N P_\Lambda = -1$. In this case the transition amplitudes must have the forms

$$A_1 = -a\sigma\mathbf{p}/\sqrt{2}, \quad A_2 = a\sigma\mathbf{p} + b\sigma\mathbf{q}, \tag{6}$$

where σ is the vector of the Pauli matrices. Again we have retained the lowest powers of p and q in the expressions for A. Calculating the angular distribution, including effects of the possible polarization of the Λ particle, we get

$$d\sigma_1(p, q, \zeta) = {}^1/_4 |a|^2 p^2 d\rho_f, \tag{7}$$

$$d\sigma_2(p, q, \zeta) = {}^1/_2 \{p^2 |a|^2 + q^2 |b|^2 + 2\mathrm{Re}(a^* b)\,\mathbf{pq} + 2\,\mathrm{Im}(a^* b)\zeta\,[\mathbf{p} \times \mathbf{q}]\}\, d\rho_f, \tag{8}$$

where $\boldsymbol{\zeta}$ is a unit vector in the direction of polarization of the Λ particle, and $d\rho_f$ is the density of states.

We see from Eq. (7) that as before the cross-section of reaction (1) is isotropic and does not depend on the polarization of the Λ particle, but unlike the case $P_K P_N P_\Lambda = +1$ the matrix element is now proportional to p and the probability for emission of low-energy Λ particles is sharply reduced. The cross-section for reaction (2) is in this case anisotropic and depends on the polarization of the Λ particle. Generally speaking, the Λ particle will be polarized in the direction normal to the plane in which the products of the reaction are emitted. In virtue of the nonconservation of parity in the decay, this has as a result that the numbers of π mesons produced in the decay of the Λ par-

ticles and emerging upward and downward relative to the plane of the reaction will be different. The angular distribution of the two π mesons and the Λ particle in reaction (2) turns out to be proportional to $1 + \alpha \cos \vartheta$ (ϑ is the angle between $\mathbf{p}$ and $\mathbf{q}$), where

$$\alpha = 2\mathrm{Re}\,(a^*b)\,pq/(p^2\,|\,a\,|^2 + q^2\,|\,b\,|^2).$$

If we average Eqs. (7) and (8) over angles and energies, we find that the ratio of the total number of charged π mesons to the total number of neutral π mesons is given by

$$\sigma_2 : \sigma_1 = 1.34\,(1 + \bar{q}^2\,|\,b\,|^2/2\bar{p}^2\,|\,a\,|^2).$$

The use of reactions (1) and (2) for the determination of the sign of $P_K P_N P_\Lambda$ is made difficult by the fact that the cross-section for these reactions makes up only a fraction $2 - 3 \times 10^{-3}$ of the total cross-section for inelastic interactions of K^- mesons with protons. Another important difficulty comes from the fact that in order to get an unambiguous interpretation of the distributions obtained for the reactions (1) and (2) one must make sure that the K^- meson was captured by the proton from an S state.

Translated by W. H. Furry
195

PHOTOGRAPHIC METHOD OF DETECTION OF DENSE SHOWERS OF CHARGED PARTICLES

I. D. RAPOPORT

Moscow State University

Submitted to JETP editor December 13, 1957

J. Exptl. Theoret. Phys. (U.S.S.R.) **34**, 998-1000 (April, 1958)

THE emission spectrum of the majority of phosphors used for detection of charged particles coincides, as a rule, with the spectral region of maximum sensitivity of photosensitive materials (λ = 3500 — 4500 A). This fact can be used for detection of showers of charged particles (in particular, electron-nuclear showers initiated in high-energy nuclear processes) by direct contact photography of scintillations.

The method can be used in practice if the density of particles is sufficient to produce an amount of light energy per unit surface of emulsion E which is larger than the sensitivity threshold of the material ϵ_T. If a shower of density σ constant within radius R falls upon luminiscent layer of thickness H and density ρ then, neglecting the absorption of light in the phosphor, we have

$$E_{\max} = 0.5\,\sigma\,\alpha\,(\partial E/\partial H)\,\rho\,\{H + R - \sqrt{H^2 + R^2}\},$$

where $\partial E/\partial H$ is the specific ionization loss of shower particles in the luminiscent medium and α is the relative energy yield of luminiscence. Assuming that $\partial E/\partial H = 2$ Mev $g^{-1}\,cm^2$, $\rho \sim 1$ g/cm^2, $\alpha \sim 0.1$,[1] $\epsilon_T \sim 300$ units GOST[2] (which corresponds to $\sim 3 \times 10^9$ ev/cm^2), R $\sim$ 0.1 cm (for electron-nuclear showers produced in lead[3]), and $H \gg R$ we obtain $N_T \sim 10^4$ for the minimum number of shower particles necessary for photographic detection. Production of such a shower requires a "primary" of $\sim 10^{12}$ ev. The detector might be therefore useful for study of interaction of high-energy cosmic ray particles with matter.

Various luminiscent materials were investigated for their applicability in the proposed detector. Besides the inorganic phosphors NaI, KI and CsI (Thallium activated), plastic scintillators (antracene, terphenyl in polystyrene) which are convenient for use in large-area detectors were tested. Showers were simulated by a collimated electron beam (collimator diameter 3 mm) from radioactive sources (P^{32} and Sr^{90}). The beam was directed perpendicularly to the surface of scintillator. The photographic film (35 mm motion picture film with sensitivity of $\sim$ 350 GOST) was placed in close contact with the scintillator. The most effective position for film without anti-halation backing was between two layers of scintillator. The lowest value of the threshold attained using this method was $\sim 1.5 \times 10^4$ particles. Short-wavelength luminiscence proved to be most active.

Photometric measurements showed that the image density increases with particle density according to the characteristic curve of emulsion.[2] Previous calibration of the detector permits it, therefore, to find the density and the number of particles in a shower. Large latitude of modern high-speed emulsions ($\sim 10^3$) together with the possibility of simultaneous use of several layers of different sensitivity makes it possible to obtain a practically unlimited range of measurement. The experiment shows, furthermore, that the recorded mark is not greatly diffused in comparison with the beam section (within a few tenths of a millimeter). This makes it possible to determine the position of the shower and the particle distribution with a good accuracy.

In practice, the most convenient detector would consist of a "sandwich" of several photographic and luminiscent layers in close contact with each other. Superposition of light marks in several layers increases the total density and excludes errors due to stray light spots.

A similar detector can be used as indicator of electron-nuclear showers produced by high-energy particles in a dense medium. The method may be of value for measurements of the number and distribution of shower particles, having a higher resolving power — for large densities — than ionization methods of detection; it can be used in conjunction with nuclear emulsions (in analogy with the method proposed by Grigorov for ionization chambers[3]) for determination of shower position (more accurately than with chambers). We shall mention also the (limited) possibility of timing the events by the use of moving film.

The author would like to thank N. L. Grigorov for valuable advice.

[1] Furst, Kallman, and Krammer, Phys. Rev. **89**, 416 (1953).

[2] Iu. N. Gorhovskii and S. S. Gilev, (editors) Сенситометрический справочник (Handbook of Sensitometry) Moscow, GITTL, 1955.

[3] Grigorov, Podgurskaia, Shestoperov, and Sobiniakov, Reports of the Session on Thick Emulsion Methods, vol. I, Joint Institute of Nuclear Research, March 1957.

Translated by H. Kasha
196

POLYATOMIC DISTANCES IN FERROMAGNETICS

F. M. GAL' PERIN

Submitted to JETP editor October 25, 1957; corrected manuscript submitted January 29, 1958

J. Exptl. Theoret. Phys. (U.S.S.R.) **34**, 1000-1003 (April, 1958)

IN the present paper we discuss the analogy noted by us between the dependence of the atomic magnetic moments of ferromagnetic metals and alloys on the concentration of electrons (total number of s- and d-electrons) in an atom and the same dependence of some quantity (of the dimensions of length) which, in the case of pure metals, is equal to the difference between the distance of nearest neighbors of the first coordination sphere of the crystalline lattice r_1 and some constant of the metal R. In the case of alloys, this quantity is expressed by an analogous difference.

Let us consider the transition elements with atomic numbers Z from 21 to 29 (see Fig. 1).

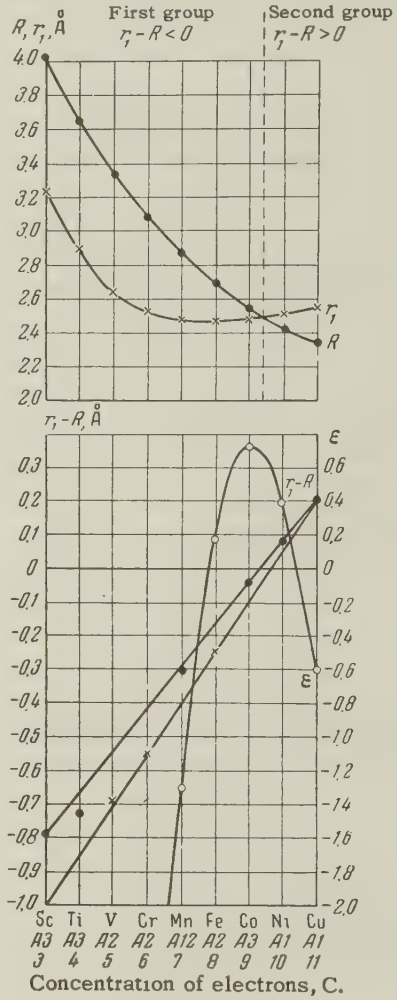

FIG. 1

We find that for these elements,

$$R = 0.13\,[(Z/2)^{\frac{1}{2}} - (13.75 + l)\,Z + 26\,(l-1) + 235.525], \quad (1)$$

where $l = 0$ for $Z \leq 26$, $l = 1$ for $Z \geq 26$.*

In Fig. 1, we have plotted the values of r_1, R, $r_1 - R$, the electronic concentration C, and also the types of metallic lattices. It can be seen from the drawing that the metals separate into two groups: the first includes Co, Fe, etc, for which $r_1 - R < 0$; the second includes Ni and others, for which $r_1 - R > 0$. The value of $r_1 - R$, as a rule, depends linearly on C, in which case the points

for the metals with lattices of type A2 (such as Fe) lie on the lower line, and those of the type A1 (like Ni) and A3 (like Co), on the upper line.

The points for binary disordered alloys lie on the lines 1 — 3 of Fig. 2.

Let us consider the quantity $r_1 - R_{AB}$, where r_1 is the distance between the closest atoms of the transition metals in the lattice of the alloy (it depends on its concentration), $R_{AB} = \lambda_A R_A + \lambda_B R_B$ (λ_A and λ_B are the atomic concentrations of the components of the alloy A and B, respectively, R_A and R_B are computed from Eq. (1).

It is shown in Fig. 2 that the alloys divide into two groups: the first is composed of those for which $r_1 - R_{AB} < 0$, the second, those for which $r_1 - R_{AB} > 0$. The alloys Ni — Fe, Fe — Co, Co — Cu, Fe — Cr, Ni — Cu, FeAl, CoAl, NiAl,† CuZn and others are similar to pure metals: $r_1 - R_{AB}$ and $a - R_{AB}$ (a = parameter of the lattice) depend linearly on the mean electronic concentration per atom of alloy $\bar{C} = \lambda_A C_A + \lambda_B C_B$, where C_A and C_B are the concentrations of electrons of components A and B, respectively. The lines 1 and 3 correspond to these alloys for lattices of the type A2 (CsCl), and the line 2 for lattices of the type A1 (NaCl) and A3. The alloys Co — Mn, Ni — Mn, Fe — V depart from being straight lines.

It is known that atomic magnetic moments of ferromagnetic metals and alloys behave in similar fashion. In particular, the curves 1 — 2 of Fig. 2 are analogous to the Slater-Pauling curve for these moments; the same alloys Co — Mn, Ni — Mn, Fe — V and others depart from these latter lines.[3] It then follows that these moments depend essentially on $r_1 - R$ in the case of pure metals and on $r_1 - R_{AB}$ in the case of alloys. To be more convincing, we shall show, in an example of pure ferromagnetic metals, that the difference $r_1 - R$ enters into the empirical relation assumed by us for the moments m under examination. With this aim, we shall consider the quantity‡

$$\varepsilon = 1 \pm 0{,}642\,[n_1 (r_1 - R) + n_2 (r_2 - R)], \qquad (2)$$

where r_2 = distance of nearest neighbors of the second coordination sphere of the lattice, n_1 and n_2 are the numbers of nearest neighbors of the first and second coordination spheres of the lattice, respectively, the upper sign applying to the first group of metals, the lower, to the second. It was shown in Fig. 1 that $\epsilon > 0$ only for pure ferromagnetic metals. For the latter we get

$$m / M_B = N_d + 0{,}15\,(\varepsilon_0 / \varepsilon - 4)\, n_s, \qquad (3)$$

where M_B is the Bohr magneton, N_d = number of unpaired d electrons in the atom, n_s = number of s electrons in the atom,

$$\varepsilon_0 = -0{,}13 N_d (N_d - n_s + \beta) / (N_d - 1). \qquad (4)$$

Here $\beta = 0$ for the first group of metals, $\beta = 1$ for the second group. The relation (3) is similar

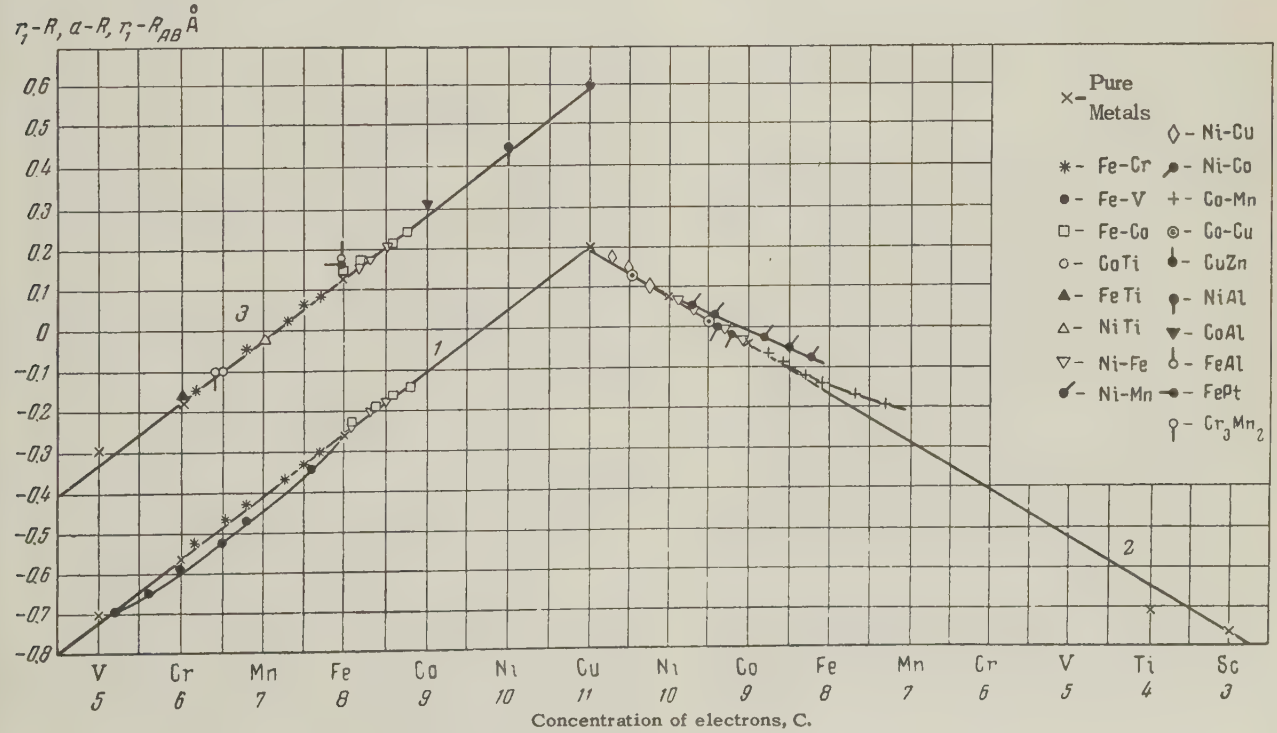

FIG. 2

to the relation

$$m/M_B = N_d + \frac{0.15(I_0/I-4)n_s}{1-2I_s/I},$$

where I_0 and I are the exchange integrals between the s and d electrons for one lattice site and between its neighboring sites respectively, I_S is the transfer integral of the s electron.[4] According to Eqs. (2) and (4), $\epsilon(\epsilon_0) = 0.4, (-0.26)$ for Ni, 0.73 (−0.195) for Co, and 0.18 (−0.347) for Fe. Substituting these values in (3) we find that the computed and experimental values of m are in excellent agreement.

Quantities analogous to (2) also enter into the relation for alloys. For example, for the alloys Fe, Co, Ni (component A) with Cr and V (component B),

$$m_B/M_B = \ldots \mp [1+0.642\sum_i n_i(r_1-R_B)\lambda_B - 0.642\sum_i n_i(r_i-R_{AB})\lambda_A\lambda_B], \quad (5)$$

where i = 1, 2 for lattices A2 and A3, and 1 for lattice A1, while the upper sign applies for Fe — Cr and Fe — V, the lower, for Ni — Cr and Co — Cr. The computed points lie on straight lines which cross the ordinates (moments) −1, 1 and 1, $-1\,M_B$, and abscissas (concentrations) 42 at % Cr, 22.78 cm % Cr, 13.5 at % Cr and 20 at % V, respectively, for Fe — Cr, Ni — Cr, Co — Cr and Fe — V. This is in agreement with experiment.[5] For the observed concentrations, $a = R_{AB}$ for Fe — Cr and Fe — V; above, deviations from linearity are observed. The change of moment (at 100 at % B) is almost the same as in experiments with weak solid solutions.

*It is shown that, with an accuracy to within 1%, $R = R_s + R_d$, where R_s and R_d are the "radii" of the s and d shells of isolated atoms, computed by Slater.[1] The quantity $r_1 - R = r_1 - (R_s + R_d)$ recalls the difference considered in the theory of ionic crystals between the equilibrium minimun interionic distance and the sum of the radii of the neighboring ions of the lattice which characterizes their collision. We note that the numerical values in Eq. (1) are also encounted in Ref. 2 on the ionic structure of spinel; thus, for example, the number 235/60 given the factor u which characterizes the departure of the structure of spinel from the ideal (for the latter case, u = 0.375); the number 13.75 is Madelung's constant, which corresponds to u = 0.385, etc.

†In each of the last three alloys there is one transitional metal; therefore, R for the particular metal is used in place of R_{AB}.

‡The quantity in square brackets in (1) is equal to R/0.13 = 7.7 R. The latter number, divided by 12 (the number of nearest neighbors in a metal with lattice type Al), is equal to 0.642 R. The coefficient 0.642/A obtained in such fashion enters in Eq. (2).

[1] J. C. Slater, Phys. Rev. **36**, 57 (1930).

[2] E. J. W. Verwey and E. L. Heilmann, J. Chem. Phys. **15**, 174 (1947).

[3] R. Bozorth, Ferromagnetism (Van Nostrand N. Y., 1951).

[4] S. V. Vonsovskii and K. B. Vlasov, J. Exptl. Theoret. Phys. (U.S.S.R.) **25**, 327 (1953).

[5] C. G. Shull and M. K. Wilkinson, Phys. Rev. **97**, 304 (1955).

Translated by R. T. Beyer
197

RELATIVISTIC MOTION OF AN ELECTRON IN AN AXIALLY SYMMETRIC FIELD WHICH MOVES ALONG THE AXIS OF SYMMETRY

M. V. KONIUKOV and Ia. P. TERLETSKII

Moscow State University and Tul' skii Pedagogical Institute

Submitted to JETP editor December 16, 1957

J. Exptl. Theoret. Phys. (U.S.S.R.) **34**, 1003-1005 (April, 1958)

1. Since the problem was first studied by Wiederöe[1] a detailed investigation of the relativistic motion of an electron in a varying axially symmetric field has been made in only two cases: motion in a magnetic field which is uniform and parallel to the axis of symmetry[2] and motion in a barrel-shaped magnetic field.[3,4] Below we study a new version of this problem in which a magnetic field which falls off in the direction of the axis of symmetry (bottle-shaped field) is displaced along this axis with variable or fixed velocity. Just as in the earlier cases, the new version of this problem can be used as the theoretical basis for a new type of accelerator — a linear induction accelerator or, as it might be called, a linear betatron.

2. Following Refs. 2 — 4, the equations of motion of the electron are determined from the Lagrangian function

$$L = -m_0c^2\sqrt{1-v^2/c^2} + (e/c)r\dot{\varphi}A$$

and have the form

$$\frac{d}{dt}(m\dot{r}) = \frac{e}{c}r\dot{\varphi}\frac{\partial A}{\partial r} = \frac{e}{c}r\dot{\varphi}\left[H_z - \frac{A}{r}\right],$$
$$\frac{d}{dt}(m\dot{z}) = \frac{e}{c}r\dot{\varphi}\frac{\partial A}{\partial z} = -\frac{e}{c}r\dot{\varphi}H_r, \quad (1)$$
$$mr\dot{\varphi} = -\frac{e}{c}A = -\frac{e}{c}\left(\frac{r\bar{H}}{2} + \frac{b}{r}\right), \quad \frac{d}{dt}(mc^2) = -\frac{e}{c}r\dot{\varphi}\frac{\partial A}{\partial t},$$

where $m = m_0(1-v^2/c^2)^{-1/2}$, A is the A_φ component of the vector potential, b is a constant of

integration, $\overline{H}$ is the mean value of the z component of the magnetic field in a circle of radius r and the remaining notation is obvious. The third equation in (1) can also be written in the form:

$$m^2(\dot{r}^2 + \dot{z}^2 - c^2) + (e/c)^2A^2 + m_0^2c^2 = 0. \quad (2)$$

3. In the quasi-stationary approximation the following solution of the field equation applies in the region of the line $r = R$, $\zeta = z - z(t) = 0$:

$$A = r\left[\frac{H_z^0}{2} - \frac{a}{2}R^2 + \frac{ar^2}{4} - \frac{H_r^0}{R}\zeta - \frac{a\zeta^2}{1-\dot{z}^2/c^2}\right], \quad (3)$$

where H_r^0 and H_Z^0 are the components of the field at $r = R$, $\zeta = 0$, $z(t)$ is an arbitrary function of the time which satisfies the condition $z = c^2 \times (\partial H_Z/\partial r)_0/H_r^0$ and a is a constant. In a field of this kind, when $a = -2H_Z^0/R^2$, Eq. (1) has the particular solutions $r = R$ and $z = z(t)$, i.e., the electron moves in a helix of constant radius if the function $z(t)$ is given by the equation

$$ct = \sqrt{z(t)}\sqrt{\alpha + z(t)} + \alpha \ln\left(\sqrt{z(t)} + \sqrt{\alpha + z(t)}\right), \quad (4)$$
$$\alpha = m_0^2c^4[1 + (eRH_z^0/m_0c^2)^2]/2e^2RH_z^0H_r^0,$$

where the particle energy is

$$E = mc^2 = \sqrt{2e^2H_z^0H_r^0(\alpha + z)}. \quad (5)$$

In the case of relativistic initial energies and $z \gg RH_Z/2H_r$, from Eqs. (4) and (5) we have

$$z = ct, \quad E = E_0\sqrt{2zH_r/RH_z}. \quad (6)$$

4. If the field is displaced along the z axis with constant velocity u, i.e., $A = A(r, z-ut)$, from Eq. (1) we find

$$m(\dot{z} - c^2/u) = -Mc^2/u, \quad M = m_0(1 - r_0^2\dot{\varphi}_0^2/c^2)^{-1/2}, \quad (7)$$

where M is the mass of the particle at $\dot{z} = 0$ and $\dot{r} = 0$.

According to Eqs. (2) and (7), an electron which originally moves in the wide section of the "magnetic bottle," where $H_Z = H_0$ and $A = A_0$, falls into the "neck" of the bottle (where $H_Z = H$) and then again is forced into the wide part, acquiring the following energy in the process

$$E/E_0 = 2[(m_0/M)^2 + (eA/Mc^2)^2] - 1. \quad (8)$$

If it is assumed that the motion is such that the adiabatic invariant $H_Zr^2 = \text{const}$ is conserved, with a relativistic initial energy we have $A = r_0\sqrt{H_0H}$ and Eq. (8) can be written in the form:

$$E/E_0 + 1 = 2(A/A_0)^2 \approx 2H/H_0 \approx L/2l, \quad (9)$$

where L is the length of path over which acceleration takes place, and l is the length of the segment over which the field changes from H_0 to H.

5. Equations (8) and (9) do not hold if $u = c$. In this case the field equation yields

$$A = {}^1/_2rH(z - ct) + b/r, \quad (10)$$

and from Eqs. (1), (2) and (7), for the case $H_Zr^2 = \text{const}$, we have

$$E - E_0 = (e^2/2E_0)(H_0r_0^2)[H - H_0],$$
$$z - z_0 = -\frac{e^2(Hr^2)}{2M^2c^4}\int_{z_0}^{z-ct}(H - H_0)\,d\zeta. \quad (11)$$

For relativistic initial conditions $Mc^2 = -eA_0$ and since $A_0 \approx H_0r_0$, we have

$$E/E_0 - 1 \approx \tfrac{1}{2}(H/H_0 - 1) = L/l. \quad (12)$$

6. According to Eqs. (9) and (12), in a linear accelerator in which the field moves with constant velocity u, we have: $E/E_0 \approx 2H/H_0$ or $E/E_0 \approx H/2H_0$, i.e., the situation is analogous to that in the usual betatron. However, in contrast to the betatron the strong field H can be concentrated in a very small region since $He^2 = \text{const}$.

[1] R. Wiederöe, Arch. Elektrotech. **21**, 387 (1928).
[2] Ia. P. Terletskii, J. Exptl. Theoret. Phys. (U.S.S.R.) **11**, 96 (1941).
[3] D. W. Kerst and R. Serber, Phys. Rev. **60**, 53 (1941).
[4] Ia. P. Terletskii, J. of Phys. (U.S.S.R.) **9**, 159 (1945).

Translated by H. Lashinsky
198

DETERMINATION OF THE VELOCITY OF IONIZING PARTICLES USING A HIGH-FREQUENCY ELECTRIC FIELD FOR TRACK MARKING

G. A. ASKAR'IAN

P. N. Lebedev Physical Institute, Academy of Sciences, U.S.S.R.

Submitted to JETP editor, December 18, 1957

J. Exptl. Theoret. Phys. (U.S.S.R.) **34**, 1005-1007 (April, 1958)

AN interesting method of making direct determinations of the velocities of ionizing particles in a Wilson cloud chamber has recently been proposed by Gabor and Hampton.[1] In this scheme, the tracks are "marked" by a high-frequency (rf) electric field by using the difference in intensity of electron

cascades as a function of field strength at the time the free electrons are produced. This difference is due to the absorption of free electrons and the dissipation of electron energy or other fast processes the duration of which is less than the period of the rf field. In the present paper we present an elementary analysis of the modulation of the ionic density of a track, derive an expression for the track-marking interval for fast particles, and indicate methods by which the effectiveness of this method can be enhanced.

The equation which characterizes the free-electron population

$$dn_e/dt = wn_e - n_e/\tau \qquad (1)$$

contains the probability $w(t)$ of an increase in the number of electrons per unit time and the lifetime τ for the free electrons. Using the solution of this equation

$$n_e = n_0 \exp\left\{\int_{t^*}^{t}\left(w - \frac{1}{\tau}\right)dt\right\}, \qquad (2)$$

we obtain an expression for the number of ions which are produced

$$n_i = \int_{t^*}^{t}\frac{n_e}{\tau}\,dt = \int_{t^*}^{t}\frac{n_0}{\tau}\left\{\exp\left[\int_{t^*}^{t}\left(w - \frac{1}{\tau}\right)dt\right]\right\}dt\,. \qquad (3)$$

Here t^* is the time at which the free electron is produced and n_0 is the initial number of free electrons per unit track length, which depends on the ionizing power of the particle. The function $(w - 1/\tau)$ is of the form $p\{f(|E(t)|/p) - 1/\tau\}$ where p is the pressure of the gas, $E(t)$ is the intensity of the electric field, where we have neglected the weak dependence of τ on the external field, while the function f is an extrapolation of some power function (cf. for example Ref. 2). Because the external field is periodic it is possible to expand the function $w - 1/\tau$ in a Fourier series:

$$w - 1/\tau = \sum_{0}^{\infty} a_k \cos 2k\omega(t - t_k) \qquad (4)$$

(2ω is the modulation frequency of the rf electric field).

For the time being we shall be interested in the case in which the electron avalanches have time to decay, i.e., $(w - 1/\tau)_{ave} = a_0 < 0$; if this condition is not satisfied, extended trains of rf field pulses can lead to "breakdown." (An analysis of increasing electron avalanches is of interest only in the case of short rf field trains, for example pulse trains cut off sharply immediately after the passage of the particle.)

Substituting Eq. (4) in Eq. (3), we have

$$n_i = \int_{t^*}^{t}\frac{n_0}{\tau}\exp\{a_0(t - t^*)\}\exp\left\{\sum_{1}^{\infty}\frac{a_k}{2k\omega} \times [\sin 2k\omega(t - t_k) - \sin 2k\omega(t^* - t_k)]\right\}dt.$$

We expand the second exponential in the integrand in a power series and limit ourselves to the first power; the resulting expression is

$$n_i \simeq \frac{n_0}{\tau\,|a_0|} \times\left\{1 - \sum_{1}^{\infty}\frac{a_k}{\sqrt{a_0^2 + 4k^2\omega^2}}\sin\left[2k\omega(t^* - t_k) + \tan^{-1}\frac{a_0}{2k\omega}\right]\right\}.$$

Substituting the values of t^* and t_k as functions of points along the track $t^* = (l - l_0)/v$, where v is the velocity of the particle and l is the distance along the track) we obtain a function which characterizes the spatial ion distribution. An analysis of the ion distribution function makes it possible to estimate the dependence of $(w - 1/\tau)$ on the instantaneous value of the rf electric field. These results can also be used for choosing the optimum conditions for which the functions $n_i(l)$ change most rapidly, thus making possible a more accurate determination of the positions of the maxima and thus a more accurate determination of the period of the spatial distribution. In particular, the formula which has been obtained exhibits the spatial periodicity of the distribution. For example, at low particle velocities, when the wave properties of the rf field can be neglected (t_k = const), the distribution period is $\Delta l = \pi v/\omega$. For particles with arbitrary velocities, which move as quasi-plane traveling waves ($t_k = z/c' = (l - l_0) \times \cos\theta/c'$ where c' is the velocity of propagation of the wave and θ is the angle between the direction of motion of the particle and the direction of propagation of the wave), the distance between adjacent "condensations" along the track is

$$\Delta l = \frac{\pi}{\omega}\frac{v}{|1 - (v/c')\cos\theta|}$$

(c' may be different from the velocity of light). This same formula can be obtained directly from the expression for the intensity of the wave field at the instant the electrons are produced $E(t^*) = E_0 \sin\omega z(1/v\cos\theta - 1/c')$ using the requirement that conditions be reproduced at the instant the electrons are produced.

In passing, we may note the possibility of reducing the required rf power by superimposing a quasi-uniform base electric field which is constant for a period of time which does not cause significant distortion of the track (the direction of this field is then reversed, etc.). The electron production conditions are satisfied only when the

vector direction of the base field coincides with that of the supplementary rf field; hence the marking intervals become twice as long.

The use of lower rf power, more stable conditions in the excitation of the field, and an investigation of the possibilities of sharp reduction of the rf field after the flight of the particle may all reduce the requirements on stability of the rf amplitude and increase the effectiveness of the marking process.

In addition to synchronous operation with a pulsed accelerator, detection of cosmic particles using triggered rf field trains, and controlled operation of a cloud chamber, it is interesting to consider the possibilities of triggering the rf field from a radiation precursor of a cosmic particle or an early particle in an avalanche of cosmic particles.

[1] D. Gabor and B. Hampton, Nature **180**, 746 (1957).

[2] D. Posin, Phys. Rev. **73**, 496 (1948).

Translated by H. Lashinsky
199

RELAXATION OF DEUTERIUM NUCLEI IN PARAMAGNETIC SOLUTIONS

A. I. RIVKIND

Physico-Technical Institute, Kazan Branch, Academy of Sciences, U.S.S.R.

Submitted to JETP editor, January 3, 1958

J. Exptl. Theoret. Phys. (U.S.S.R.) **34**, 1007-1009 (April, 1958)

AN investigation has been made of spin relaxation of deuterium nuclei in solutions containing Cr^{+++}, Mn^{++}, Fe^{+++} and Cu^{++} in heavy water. The measurements were made by means of a modified saturation-curve method[1,2] in which the degree of nuclear saturation is varied by changing the concentration of paramagnetic ions in the solution rather than by changing the amplitude of H_1, the oscillating magnetic field.[3] All the experiments were carried out at room temperature at $\nu_0 \cong 2.6$ mc/sec. An analysis of the results indicates the following.

1. The nuclear relaxation time for the same concentration of a given paramagnetic salt in D_2O and H_2O obeys the relation

$$T_{1d} / T_{1p} = (\gamma_p^2 / \gamma_d^2)\,\alpha, \qquad (1)$$

where T_{1d} is the longitudinal relaxation time for deuterons in a D_2O solution, T_{1p} is the longitudinal relaxation time for protons in a H_2O solution, γ_p and γ_d are the nuclear gyromagnetic ratios ($\gamma_p^2/\gamma_d^2 \cong 42.4$) and α is a numerical factor. In solutions containing Cr^{+++}, Fe^{+++} and Cu^{++} $\alpha \sim 4.2$, with sizable departures toward lower values for copper. Mn^{++} ions have much less effect on relaxation of deuterium nuclei: $\alpha \sim 6.8$ in solutions of $MnCl_2$ and $Mn(NO_3)_2$.

2. As has been indicated earlier in the case of proton relaxation,[2,4] the time T_1 for deuterons becomes much longer (up to a change of one order of magnitude) as a consequence of the production of complexes in the solution in which the water molecules in the hydrate shells of the paramagnetic ions are replaced by other diamagnetic particles. It may be noted, moreover, that the manganese complex behaves the same as the other ion complexes. Thus, for example, in any of the ion complexes* Cr EDTA$^-$, Mn EDTA^{--}, and Fe EDTA, in Eq. (1) $\alpha \sim 4.2$.

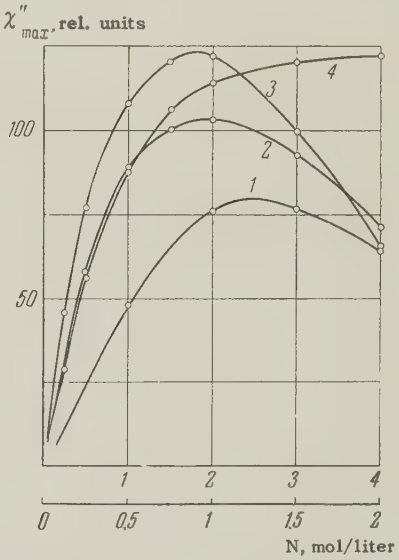

Curves obtained with solutions of nitrate salts: 1) Cu++; 2) Cr+++; 3) Fe+++; 4) Mn++. The upper scale on the absicca axis refers to Curve 1; the lower scale refers to Curves 2, 3 and 4.

3. In the Figure is shown the maximum intensity of the deuteron resonance line χ''_{max} as a function of the molar concentration N of the paramagnetic ion in D_2O. The amplitude of the oscillating field H_1 and the amplitude of the modulating field H_m are fixed. As the quantity N increases the relaxation time T_1 becomes shorter and the line intensity increases, reaching a value which applies in the absence of saturation. However

this is the case only as long as the line width remains constant, being determined by the inhomogeneity of the field. With further increases in N the line width goes beyond the limits imposed by the inhomogeneity of the field, causing a reduction in χ''_{max}. An analysis of the curves using the Bloch equation[6] leads to the conclusion that relaxation of deuterium nuclei in paramagnetic solutions is characterized by the condition $T_1/T_2 \gg 1$ (T_2 is the transverse relaxation time) where the values of T_1/T_2 for the various ions fall in the following order: $(T_1/T_2)_{Cu^{++}} > (T_1/T_2)_{Cr^{+++}} > (T_1/T_2)_{Fe^{+++}} > (T_1/T_2)_{Mn^{++}}$.

These experimental data indicate that the line broadening is due to the displacement of the spin levels of the nuclei by virtue of the interaction of the quadrupole moment of the deuteron with the gradient of the electric field set up by the paramagnetic ion. In this case T_1/T_2 should be approximately proportional to the ratio e^2/μ^2 where e is the charge of the magnetic ion and μ the magnetic moment of the ion. This relation is actually observed in the experiments. In descending order the ratio e^2/μ^2 for the various ions is as follows:

$$(2^2/2^2)_{Cu^{++}} > (3^2/3.8^2)_{Cr^{+++}} > (3^2/5.9^2)_{Fe^{+++}} > (2^2/5.9^2)_{Mn^{++}}.$$

The T_1/T_2 ratios are in exactly the same order (cf. above). If the spin levels of the nuclei are equidistant while the probability for $\Delta m = \pm 1$ transitions is proportional to γ^2, using the general expression for the relaxation time T_1,[7] the expression given in (1) results if we take the value $\alpha = 2$. The values found in the present work ($\alpha \sim 4.2$ for solutions containing Cr^{+++}, Fe^{+++} and Cu^{++}) would also seem to be explained by the existence of unresolved quadrupole structure in the deuteron lines.

Since the anomaly associated with manganese solutions ($\alpha \sim 6.8$) is not observed in complex ions, it is probably due to the nature of the hydration of the Mn^{++} ions in D_2O. It may be assumed that the bonding of the water molecules in the hydrate shell with the paramagnetic ion is slightly covalent. An exception is the $Mn(D_2O)_x^{++}$ ion in which the binding is purely electrovalent. The absence of a covalent bond tends to reduce the magnetic interaction between the neutral ion and the deuterium nuclei in the first coordination sphere, thus increasing T_1.

*EDTA ions are ions of ethylene diamine tetra acetic acid. The EDTA ions form stable complex compounds with a stochiometric ratio of 1:1 with metal ions; the EDTA particle replaces several water molecules in the internal coordination sphere of the central ion.[5]

[1] B. M. Kozyrev and A. I. Rivkind, J. Exptl. Theoret. Phys. (U.S.S.R.) **27**, 69 (1954).

[2] A. I. Rivkind, Zhurn. Neorg. Khimia **2**, 1263 (1957).

[3] Bloembergen, Purcell and Pound, Phys. Rev. **73**, 679 (1948).

[4] A. I. Rivkin, Dokl. Acad. Nauk SSSR **100**, 933 (1955).

[5] K. B. Iatsimirskii, Zav. Laborat. (Industrial Laboratory) **21**, 1149 (1955).

[6] F. Bloch, Phys. Rev. **70**, 460 (1946).

[7] C. J. Gorter, Paramagnetic Relaxation (New York, 1947). Russian translation, 1949, p. 107.

Translated by H. Lashinsky
200

ANISOTROPY IN MAGNETIC SUSCEPTIBILITY AND DEPENDENCE OF HEAT CAPACITY ON FIELD DIRECTION IN AN ANTIFERROMAGNET

E. A. TUROV

Institute for Metal Physics, Ural Branch, Academy of Sciences, U.S.S.R.

Submitted to JETP editor January 3, 1958

J. Exptl. Theoret. Phys. (U.S.S.R.) **34**, 1009-1011 (April, 1958)

1. It is well known that in a magnetic field H smaller than some threshold value H_0 the spin wave energy spectrum in a uniaxial antiferromagnet exhibits a marked anisotropy.[1] Thus, for example, if the characteristic antiferromagnetism direction is along the z axis, in the case $\mathbf{H} \parallel z$ the energies of the two types of spin waves depend on H and the wave vector $\mathbf{k}$ as follows:[2]

$$\varepsilon_k^{(1,2)} = \sqrt{(\mu H_0)^2 + I^2k^2} \pm \mu H, \qquad (1)$$

while in the case $\mathbf{H} \perp z$:[3]

$$\varepsilon_k^{(1)} = \sqrt{(\mu H_0)^2 + I^2k^2}, \quad \varepsilon_k^{(2)} = \sqrt{\mu^2(H^2 + H_0^2) + I^2k^2}. \qquad (2)$$

Here $\mu = ge\hbar/2mc$, $H_0 = M_0\sqrt{J_1(K_1 - K)}$, M_0 is the maximum possible magnetization for the given antiferromagnet, J_1, I, K and K_1 are the constants in the exchange and anisotropy interactions.* It is characteristic that in these two cases the ground states of the antiferromagnet are also considerably different: in the case $\mathbf{H} \parallel z$ the antifer-

romagnetism direction $\Delta \parallel H$ (i.e., this direction corresponds with the natural direction of z) where for $T = 0$, $M_{1z} = -M_{2z} = \frac{1}{2}M_0$ and $\chi_z^{\parallel} = 0$;† while for $H \perp z$, $\Delta \perp H$ (although $\Delta \parallel z$) where for $T = 0$ and $H \parallel y$, $M_{1y} = M_{2y} = M_0H/2H_e$ and $\chi_y^{\perp} = H/H_e$ where $H_e = M_0(J_1 + K_1 - K)$.

Until recently, however, no calculations have been made of the spin wave spectra for the case $H \parallel z$ and $H > H_0$ in which in the ground state $\Delta \perp H$, $M_{1z} = M_{2z} = M_0H/2H_e$ and $\chi_z^{\perp}H/H_e$ where $H_e = M_0(J_1 + K_1 + K)$. This calculation has been carried out by Irkhin and the author.[4] The results are as follows:‡

$$\varepsilon_k^{(1)} = Ik, \quad \varepsilon_k^{(2)} = \sqrt{\mu^2 (H^2 - H_0^2) + I^2k^2}. \qquad (3)$$

A comparison of Eqs. (2) and (3) indicates that the difference in the spectra in the cases $H \parallel z$ and $H \perp z$ remains after rotation of Δ into a position perpendicular to the H field (for $H > H_0$), although the ground states corresponding to (2) and (3) are similar. It is noteworthy that according to (3) one of the branches of the spectrum does not have a break.

In the present work we report on several new results which have been obtained in a calculation of the temperature dependence of the susceptibility χ and heat capacity of the spin waves C from an analysis of all three states listed above. The results apply only for those limiting cases in which the effects which are of interest are most marked.

2. With $\Delta\chi = \chi_T - \chi_0$:

a) $H < H_0$, $\mu H \ll \varkappa T$: $\Delta\chi_z^{\parallel} \approx -4\Delta\chi_y^{\perp} \approx \alpha T^2$,

$\alpha = (\mu\varkappa)^2 / 3I^3$.

b) $H > H_0$, $\mu\sqrt{H^2 - H_0^2} \ll \varkappa T \ll \mu H_0$: $4\Delta\chi_z^{\perp} \approx -\alpha T^2$;

$\Delta\chi_y^{\perp} \approx 0$.

c) $H > H_0$, $\mu\sqrt{H^2 - H_0^2} \gg \varkappa T$: $\Delta\chi_z^{\perp} \approx 0$; $\Delta\chi_y^{\perp} \approx 0$.

The list of formulas given above allows a theoretical explanation of the anisotropy in the temperature dependence of the susceptibility at fields near threshold H_0 observed by van den Handel et al.[7] (our results apply only to the low-temperature region).

3. For C we present the results which apply when $\varkappa T \ll \mu H_0$, in which case there is a marked dependence of spin heat capacity on the magnitude and direction of the field:

a) $H < H_0$, $\mu_1(H_0 - H) \gg \varkappa T$: $C_z^{\parallel} \approx 0$; $C_y^{\perp} \approx 0$.

b) $H < H_0$, $\mu(H_0 - H) \ll \varkappa T$: $C_z^{\parallel} \approx a_1 T^{3/2}$; $C_y^{\perp} \approx 0$.

c) $H > H_0$, $\mu\sqrt{H^2 - H_0^2} \ll \varkappa T$: $C_z^{\perp} \approx aT^3$; $C_y^{\perp} \approx 0$.

d) $H > H_0$, $\mu\sqrt{H^2 - H_0^2} \gg \varkappa T$: $C_z^{\perp} \approx \frac{1}{2}aT^3$; $C_y^{\perp} \approx 0$;

$a = (4\pi^2/15)\varkappa(\varkappa/I)^3$, $\quad a_1 = 15(2\mu H_0\varkappa)^{3/2}\varkappa/32\pi^{3/2}I^3$.

From the examples which have been considered it is apparent that in a uniaxial single crystal the spin heat capacity and its temperature dependence are both functions of the magnitude of the field H[6] [for example in the transition from condition (a) to (b), (c), and (d)] as well as the direction of the crystal axis with respect to the fixed field H [for example in rotation of the crystal axis through 90° from the position $H \perp z$ into the position $H \perp z$ in cases (b), (c) and (d)]. The last result means that if the spin heat capacity comprises a significant part of the total heat capacity of the antiferromagnet, adiabatic rotation of the crystal about an axis which lies in the base plane should result in a noticeable change in the temperature of the sample.

*$J_1 > 0$ and $K_1 - K > 0$ since these are the conditions for the existence of antiferromagnetism with natural direction along the z axis.

†The lower sign denotes the direction of the magnetizing field H while the upper sign denotes the mutual orientation of Δ and H.

‡The application of the phenomenological analysis[5] makes it possible to find the spin wave spectrum for the antiferromagnet for any magnitude and arbitrary direction of H.[4] The approximate formulas used here (1)–(3) are valid only when $H \ll H_e$ $H \ll H_e'$. A phenomenological theory of antiferromagnetism has also been developed by Kaganov and Tsukernik.[6] However, the spectrum for the case $H \parallel z$, and $H > H_0$ has not been studied by these authors.

[1] Antiferromagnetism, Collection of Papers ed. by S. U. Vonsovskii (Russ. Transl.) IL, Moscow (1956).

[2] J. Tessman, Phys. Rev. 88, 1132 (1952).

[3] U. Kanamory and K. Iosida, Prog. Theor. Phys. 14, 423 (1955).

[4] E. A. Turov and Iu. P. Irkhin, Report to the All-Union Conference on the Physics of Magnetic Materials, Leningrad (1957), (Izv. Akad. Nauk, Ser. Fiz., in preparation).

[5] E. A. Turov and V. G. Shavrov, Trudy Inst. Metal Physics, UFAN, (1957).

[6] M. I. Kaganov and V. M. Tsukernik, Report to the All-Union Conference on Low Temperatures, Moscow (1957).

[7] van den Handel, Gijsman and Poulis, Physica 18, 862 (1952).

Translated by H. Lashinsky
201

SOUND EXCITATIONS IN FERMI SYSTEMS

V. M. GALITSKII

Moscow Physico-Technical Institute

Submitted to JETP editor January 9, 1958

J. Exptl. Theoret. Phys. (U.S.S.R.) **34**, 1011-1013 (April, 1958)

IT is well-known that the propagation of sound waves in a degenerate perfect Fermi gas is impossible. The formally evaluated sound velocity ($c^2 = \partial P/\partial\rho = p_0^2/3m^2$) is less than the particle velocity at the Fermi surface which means the possibility of the decay of a sound quantum into a particle and a hole in the Fermi sea. This result remains the same for a Fermi gas with weak repulsions between the particles, since the spectrum in that case has practically the previous character.[1,2] The position changes completely in the case of a Fermi system with attractions. The production of bound pairs of particles on the Fermi surface leads to the appearance of a gap in the spectrum of the one-particle excitations.[3,4] Sound quanta with an energy not exceeding the value of the gap can therefore not decay. It is thus possible in Fermi systems with attractions to have sound excitations with small momenta.

To discuss these excitations it is convenient to use the Green function method. It is well known that sound waves arise from the excitation of particles in the condensed Bose system,[5,6] i.e., in our case from the motion of bound pairs. In that way sound excitations can be considered to be bound states of two elementary excitations with a total momentum different from zero. For our calculation we can thus use the method proposed in Gell-Mann and Low's paper[7] (see also Ref. 8). According to this method, the equation for the bound states is obtained by discarding from the equation for the Green function of two excitations the inhomogeneity (which does not have the frequencies corresponding to the bound states).

To take into account the reshuffling due to the production of a condensed Bose-system of bound pairs, we must transform the original Hamiltonian with direct interactions between the particles, using Bogoliubov's method.[4] In that way we get

$$H = E_0 + H_0 + H', \qquad H_0 = \sum_{\mathbf{p}} \varepsilon(p)\,(\alpha^+_{\rho 0}\alpha_{\mathbf{p}0} + \alpha^+_{\rho 1}\alpha_{\mathbf{p}1}),$$
$$\varepsilon(p) = {}^1\!/_2 \sqrt{\Delta^2 + (p^2 - p_0^2)^2}. \tag{1}$$

Here p_0 is the limiting Fermi momentum, $\Delta = \overline{\omega} e^{-1/\rho}$ is the value of the energy gap, and H' is the Hamiltonian of the interaction between the excitations. Since the result does not depend on the form of the interaction, we took the interaction between the particles in the original Hamiltonian in the most convenient form, analogous to the interactions of electrons in a metal. The Green function of the interaction is constructed in the usual manner from the operators $\alpha_{\mathbf{p}0}$ and $\alpha_{\mathbf{p}1}$. For our purpose it is sufficient to take the zeroth approximation for these functions. The interaction Hamiltonian H' contains in first order only one interaction graph between excitations (graph a).

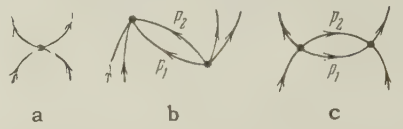

a b c

It is easily seen that nothing is added by a repetition of this graph, since the integration over momentum in the intermediate state, for the case of small total momenta of interest to us, yields $\ln(\overline{\omega}/\Delta)$, cancelling the smallness of the interaction constant. In the second order, graphs b and c also enter. It is easily seen that graph b is of the same order of magnitude as graph a. Indeed, the total momentum of excitations p_1 and p_2 is fixed and equal to the momentum of the excited state k. The integration over these momenta leads thus again to a logarithm that cancels the smallness of the interaction. In contradistinction, in graph c, in which the total momentum of the excitations p_1 and p_2 is not given, the large total momenta are significant and the compensating logarithm is absent. In this way the Green function of two excitations, K, is determined by an infinite sequence of graphs a and b. This sequence is similar to the set of graphs for the one-particle Green function of a Bose gas.[9] Introducing along with the function K the function $\overline{K}$,

$$\overline{K} = \langle T\,\{\alpha^+_{\rho_1 0}\alpha^+_{\rho_2 1}\alpha^+_{\rho_3 0}\alpha^+_{\rho_4 1}\}\rangle,$$

one can construct a set of equations for these functions, similar to the set (5.2) of Beliaev's paper.[9] Dropping the inhomogeneity we go over to the following set of equations for the functions

$$\chi_{\mathbf{k},\omega}(\mathbf{p}) = (\alpha_{\rho+\mathbf{k}/2,0}\alpha_{\rho-\mathbf{k}/2,1})_{0s}, \quad \varphi_{\mathbf{k},\omega}(\mathbf{p}) = (\alpha^+_{\rho-\mathbf{k}/2,0}\alpha^+_{\rho+\mathbf{k}/2,1})_{0s},$$

$$\chi_{\mathbf{k}\omega}(\mathbf{p}) = \frac{1}{\varepsilon(\mathbf{p}+\mathbf{k}/2)+\varepsilon(\mathbf{p}-\mathbf{k}/2)-\omega}\left\{\int d\mathbf{p}'\cdot\gamma_{11}(\mathbf{p},\mathbf{p}')\,\chi_{\mathbf{k}\omega}(\mathbf{p}') - \int d\mathbf{p}'\cdot\gamma_{12}(\mathbf{p},\mathbf{p}')\,\varphi_{\mathbf{k}\omega}(\mathbf{p}')\right\}, \tag{2}$$

$$\varphi_{\mathbf{k}\omega}(\mathbf{p}) = -\frac{1}{\varepsilon(\mathbf{p}+\mathbf{k}/2)+\varepsilon(\mathbf{p}-\mathbf{k}/2)+\omega}\left\{\int d\mathbf{p}'\cdot\gamma_{21}(\mathbf{p},\mathbf{p}')\,\chi_{\mathbf{k}\omega}(\mathbf{p}') - \int d\mathbf{p}'\cdot\gamma_{22}(\mathbf{p},\mathbf{p}')\,\varphi_{\mathbf{k}\omega}(\mathbf{p}')\right\},$$

where $\mathbf{k}$ and ω are the momentum and energy of an excitation, and

$$\gamma_{11} = \gamma_{22} = g^2\theta(p)\theta(p')(u_{p+k/2}u_{p'-k/2} + v_{p+k/2}v_{p'-k/2}) \times (u_{p-k/2}u_{p'+k/2} + v_{p-k/2}v_{p'+k/2}),$$
$$\gamma_{12} = \gamma_{21} = g^2\theta(p)\theta(p')(u_{p+k/2}v_{p'-k/2} - v_{p+k/2}u_{p'-k/2}) \times (u_{p-k/2}v_{p'+k/2} - v_{p-k/2}u_{p'+k/2}). \quad (3)$$

Thanks to the degeneracy of the nuclei (3), the set of integral equations becomes an algebraic system, and the condition that this can be solved gives us an equation for $\omega(k)$. The integrals occurring in the dispersion relation are evaluated for small values of k and ω. The result is $\omega^2 = c^2k^2$, $c^2 = p_0^2/3m^2$.

It is necessary to emphasize that our result cannot be applied to a system of charged particles. In that case, by virtue of the Coulomb interaction, the sound vibrations go over into plasma waves of high frequency ($\omega^2 = 4\pi e^2 n/m$).

The author expresses his gratitude to B. T. Geilikman, L. D. Landau, A. B. Migdal, and I. Ia. Pomeranchuk for valuable advice and interesting discussions.

[1] L. D. Landau, J. Exptl. Theoret. Phys. (U.S.S.R.) **30**, 1058 (1956), Soviet Phys. JETP **3**, 920 (1956).

[2] V. M. Galitskii, J. Exptl. Theoret. Phys. (U.S.S.R.) **34**, 151 (1958), Soviet Phys. JETP **7**, 104 (1958).

[3] Bardeen, Cooper, and Schrieffer, Phys. Rev. **106**, 162 (1957).

[4] N. N. Bogoliubov, J. Exptl. Theoret. Phys. (U.S.S.R.) **34**, 58 (1958), Soviet Phys JETP **7**, 41 (1958).

[5] N. N. Bogoliubov, Izv. Akad. Nauk, S.S.S.R., ser. fiz. **11**, 77 (1947).

[6] S. T. Beliaev, J. Exptl. Theoret. Phys. (U.S.S.R.) **34**, 433 (1958), Soviet Phys. JETP **7**, 299 (1958).

[7] M. Gell-Mann and F. Low, Phys. Rev. **84**, 350 (1951).

[8] V. M. Galitskii and A. B. Migdal, J. Exptl. Theoret. Phys. (U.S.S.R.) **34**, 139 (1958), Soviet Phys. JETP, **7**, 96 (1958).

[9] S. T. Beliaev, J. Exptl. Theoret. Phys. (U.S.S.R.) **34**, 417 (1958), Soviet Phys. JETP **7**, 289 (1958).

Translated by D. ter Haar
202

THE CROSS SECTION OF THE PION—NUCLEON INTERACTION IN THE HIGHER ENERGY REGION

P. B. BEGZHANOV

Physical Institute, Academy of Sciences, Armenian S.S.R.

Submitted to JETP editor January 8, 1958

J. Exptl. Theoret. Phys. (U.S.S.R.) **34**, 1013-1014 (April, 1958)

In a previous paper,[1] it was shown by the author that both for the model of a nucleus with homogeneous density and sharp boundaries, and also for the nuclear model in which the decrease in the density begins at the center of the nucleus, we must renounce the possibility of choosing a value of r_0 in the expression $R = r_0A^{1/3}10^{-13}$ cm (on the basis of these models) that will be the same for all nuclei investigated (R = nuclear radius, A = atomic weight). Also excluded is the Williams density distribution[2] because of the great extension of such a nucleus.

Investigation of the cross section of the interaction of π^- and π^+ mesons of different energies with heavy nuclei[3] has shown that, with an accuracy to within 3%, the radial distribution of the protons and neutrons is identical. On this basis, it can be assumed that the distribution of nucleons in the nucleus coincides with the distribution of protons, which is determined in experiments on electron scattering. Application of the homogeneous, smooth model of the nucleus, obtained from experiments on the scattering of electrons for the analysis of cross sections of nuclear interactions of protons with energies from 0.9 to 34 Bev with nuclei of lead and graphite has given satisfactory results.[1]

In the present work, on the basis of experimental data relative to cross sections of inelastic collision of pions with graphite and lead nuclei[4,5] at the energies mentioned, we have carried out calculations of the cross section of inelastic interaction and the opacity of nuclei, making use of a homogeneous smooth model of the nucleus for this purpose. If we assume for the cross section of the interaction of pions with nucleons $\bar{\sigma}(\pi) = 33$ mbn, then the computed values of the cross section of the interaction coincide with the experimental for values of the radial parameter of the smooth distribution $c = (1.14 \pm 0.04) \times 10^{-13} A^{1/3}$ cm. With consideration of experimental errors, $\bar{\sigma}(\pi) = 33 \pm 4$ mbn. Here it has been assumed that the range of

the fall-off of the density of the nucleons is the same as for protons.[1]

Similar results are obtained in the analysis of the cross section of interaction of negative pions with energies of 0.97 Bev with nuclei under the use of a homogeneous smooth model of the nucleus.[6]

The value of the cross section of the interaction of pions with nucleons $\bar{\sigma}(\pi) = 33 \pm 4$ mbn used by us in this research is, in the region under study, in excellent agreement with the results which follow from a direct measurement of the cross section of pion-nucleon interaction in the region of energy reached by present-day accelerators. Thus, for example, the value of $\bar{\sigma}(\pi) = 31 \pm 2$ mbn was obtained[7] by bombardment of hydrogen targets with pions of energy 1.9 Bev. At an energy of 4.4 Bev, $\bar{\sigma}(\pi) = 30 \pm 5$ mbn.[8] It then follows that for energies higher than 1.9 Bev, the interaction cross section of pions with nucleons does not change with energy, at least up to energies of 34 Bev.

Evidently, the cross section of interaction of pions with nucleons in the region of high energies tends to some limit $\sim 30 - 32$ mbn, which coincides with the cross section of nucleon-nucleon interaction for the energies considered.[1] This can be a consequence of the finiteness of the dimensions of the nucleons. Actually, calculation (see Ref. 9) shows that under the assumption of finite dimensions of the nucleons, the limiting value of the cross section of interaction of pions at high energies is $\bar{\sigma}(\pi) = 30$ mbn.

Thus our data show that the nuclear and electromagnetic radii of nuclei coincide if use is made of a homogeneous smooth distribution.

The author takes this opportunity to extend his thanks to the director of the work, Prof. N. M. Kocharian, and to M. L. Ter-Mikaelian for the interest and help shown in carrying out this research, and also to G. M. Garibian for useful advice.

[1] P. B. Begzhanov, J. Exptl. Theoret. Phys. (U.S.S.R.) **34**, 775 (1958); Soviet Phys. JETP (in press).

[2] R. W. Williams, Phys. Rev. **98**, 1387 (1955).

[3] Abashian, Cool and Cronin, Phys. Rev. **104**, 855 (1956).

[4] Kocharian, Begzhanov, and Pachadzhian, Dokl. Akad. Nauk Armenian SSR **24**, 161 (1957).

[5] N. M. Kocharian, G. S. Saakian et al. Izv. Arm. SSR **10**, 81 (No. 3, 1957).

[6] Cronin, Cool and Abashian, Phys. Rev. **107**, 1121 (1957).

[7] Cool, Piccioni and Clark, Phys. Rev. **103**, 1082 (1956).

[8] Bandtel, Bostick, Moyer et al. Phys. Rev. **99**, 673 (1955).

[9] P. V. Vavilov, J. Exptl. Theoret. Phys. (U.S.S.R.) **32**, 940 (1957); Soviet Phys. JETP **5**, 768 (1957).

Translated by R. T. Beyer
203

ELASTIC SCATTERING OF HIGH ENERGY PARTICLES BY DEUTERONS

A. A. RUKHADZE

Submitted to JETP editor January 8, 1958

J. Exptl. Theoret. Phys. (U.S.S.R.) **34**, 1014-1015 (April, 1958)

THE study of the interaction of high energy particles with deuterons makes it possible to draw some conclusions on the character of the motion of nucleons in the deuteron. In the deuteron the nucleons are preferentially located at great distances from each other; therefore the fast particles interact only with one of the nucleons of the deuteron, leading to breakup of the deuteron or to the reaction of stripping. The theory of these processes has been well studied. However, in the deuteron, the nucleons can be found with some probability at sufficiently small separation distances, and then an incident particle with wavelength $\lambda\!\!\!^{-}$ less than the separation of the nucleons in the deuteron will be scattered elastically. This means that in such collisions, the incident particle transfers a significant part of its momentum to the deuteron.

In recent experiments carried out by Leksin[1] on the scattering of protons of 675 Mev on deuterons, there was observed, along with the scattered nucleons, a small number of undestroyed deuterons with high energies (up to 660 Mev). An explanation of this phenomenon was proposed by Blokhintsev[2] as the elastic scattering of the protons by the deuteron. However, the quantitative estimates given by him appear to us to be insufficiently accurate, the more so as the relative probability of this process, according to Blokhintsev, does not depend on the momentum of the incidence particle. A quantitative estimate is given below of the relative probability of this process with the use of the wave function of the deuteron obtained by the method of Tamm and Dancoff.[3]

The cross section of elastic scattering of fast

particles by deuterons as a whole will be equal to

$$\sigma = \sigma_d w_d(\lambda\!\!\!^{-}), \quad (1)$$

where σ_d is the total cross section of quasi-elastic scattering of particles on the deuteron (with account of the stripping reaction in the case of scattering of nucleons), while the quantity $w_d(\lambda\!\!\!^{-})$ is the probability that the nucleons in the deuteron are found at distances less than $\lambda\!\!\!^{-}$, where $\lambda\!\!\!^{-}$ is the wavelength of the incident particle. In other words, $w_d(\lambda\!\!\!^{-})$ is the relative probability of the process being studied. If we denote by $\psi_d(r)$ the wave function of the deuteron, then

$$w_d(\lambda\!\!\!^{-}) \approx 4\pi \int_0^{\lambda\!\!\!^{-}} \psi_d^2(r)\, r^2 dr \approx \frac{4\pi}{3} \psi_d^2(0)\, \lambda\!\!\!^{-3}. \quad (2)$$

The latter equality holds for sufficiently small $\lambda\!\!\!^{-}$. (For large $\lambda\!\!\!^{-}$, it is necessary to carry out numerical integration of the integral in (2). In the work of Blokhintsev, the integration is carried out up to R, where R is the radius of strong interaction of nucleons, $R \approx (0.3-0.4)\hbar/\mu c$. In the same expression for the relative probability $w_d(R)$ is shown to be independent of the momentum of the incident particle. At small separation distances, the wave function of the deuteron $\psi_d(r)$ contains in practice only the $^3S_1$ wave. Therefore,

$$\psi_d(0) = \lim_{r \to 0} (u(r)/r), \quad (3)$$

where $u(r)$ is a function of the $^3S_1$ state of the deuteron. Making use of the $u(r)$ computed by the Tamm-Dankoff method,[3] we find $\psi_d(0) \approx 0.7$. (in the system of units for which $\hbar = \mu_\pi = c = 1$) and

$$\omega_d(\lambda\!\!\!^{-}) \approx 4\pi\lambda\!\!\!^{-3}/3. \quad (4)$$

For energies of the incident protons of 675 Mev, $\lambda\!\!\!^{-} \approx 0.1$ and, consequently, $w_d(\lambda\!\!\!^{-}) \approx 2 \times 10^{-3}$. The experimental value of this quantity[1,2] amounts to 7×10^{-3}.

Strictly speaking, in the computation of $w_d(\lambda\!\!\!^{-})$, the mutual screening of the nucleons in the deuteron must be taken into account. This increases the relative probability $w_d(\lambda\!\!\!^{-})$ somewhat.

From a comparison of the theoretical and experimental values of w_d, we come to the conclusion that the theory agrees qualitatively with experiment.

There is interest in the experimental investigation of the scattering of fast particles by deuterons and the comparison of the energy dependence of the relative elastic scattering probability of fast particles by deuterons with Eq. (2). It should be noted that the study of the scattering of fast pions by deuterons is preferential in this case in order to separate the stripping reaction, which exists concurrently with the elastic scattering of fast nucleons by deuterons.

In conclusion, I express my thanks to Academician I. E. Tamm for suggesting the topic.

[1] G. A. Leksin, J. Exptl. Theoret. Phys. (U.S.S.R.) **32**, 445 (1957); Soviet Phys. JETP **5**, 371 (1957).

[2] D. I. Blokhintsev, J. Exptl. Theoret. Phys. (U.S.S.R.) **33**, 1295 (1957); Soviet Phys. JETP **6**, 995 (1958).

[3] A. A. Rukhadze, Dissertation, Physical Institute, Academy of Sciences, 1958.

Translated by R. T. Beyer
204

THE INTERACTION OF K-MESONS, PIONS, NUCLEONS AND HYPERONS

V. S. BARASHENKOV

Joint Institute for Nuclear Research

Submitted to JETP editor January 8, 1958

J. Exptl. Theoret. Phys. (U.S.S.R.) **34**, 1016-1017 (April, 1958)

A model was proposed in Refs. 1—3 for the description of the multiple production of strange particles. The structure of the "composite particle," formed in the collision of two fast particles, depends essentially on the assumption of a magnitude of the interaction of particles of different types. In the formulas of the statistical theory of multiple production, the interaction constants do not enter explicitly. "Strong" or "weak" interaction here is understood in the sense of the magnitude of the cross section obtained after establishment of statistical equilibrium between the produced particles. In our view, it is very probable that conclusions on "strong" or "weak" interaction of particles of different types which follow from a comparison of calculations (in terms of the statistical theory) with experiment over a wide range of energies give information on the relative magnitude of the interaction constants between these particles.* Since there are various opinions at the present time concerning the magnitude of the interaction of pions and K mesons with hyperons, and K mesons with nucleons, then even indirect information on these interactions is of great interest. We shall

start out from the very well known experimental fact of the strong interaction of pions and nucleons ($g^2/4\pi\hbar c \gg 1$).

If we assume strong interaction of pions and K-mesons (or K mesons and nucleons), then the following possibilities exist for the choice of the space volumes for the "compound particle."

1. Statistical equilibrium between all the secondary particles is established in one and the same volume V_1.† In this case the fraction of created particles relative to the pions and nucleons exceeds that experimentally observed by us.

2. The statistical equilibrium of nucleons, pions and K-mesons is established in the same space volume V_1, but the equilibrium for hyperons is established in a smaller volume. In this case, the fraction of created strange particles is close to the experimental value;[6,7] however, the ratio of the number of K^- and K^+ mesons produced in nucleon-nucleon collisions at E = 6.2 Bev is $N^+/N^- \cong 3$. In the works of Chapp et al.,[4] values of N^+/N^- of 100 — 150 were obtained for momenta of K-mesons of $p \sim 250 - 350$ Mev/c. Even taking the momentum distribution into account, it is difficult to harmonize these differences of two orders of magnitude.‡

3. The volume in which the equilibrium is established for K-mesons is larger than the corresponding volume for nucleons and pions. In this case, it is not possible to obtain experimental agreement either with the number of strange particles created or with the value of the ratio N^+/N^-.

Agreement can be produced between experiment and the results of the statistical theory of multiple particle production only if weak interaction is assumed between the K-mesons and the pions and nucleons. In this case, the statistical equilibrium for K-mesons is established in a smaller space volume than for pions and nucleons. The best agreement is found if, following Gell-Mann, we assume a symmetric interaction of the pions with nucleons and hyperons ($V = V_2$). Thus, the computed effective cross section σ_s of creation of strange particles in π^--nucleon collisions at 4.3 Bev is equal to 3 mb in this case.** The mean experimental value of this cross section is approximately equal to 2.2 mb.[6] If we assume that all the strange particles interact weakly with pions and nucleons ($V = V_3$), then $\sigma_s = 0.3$ mb. The divergence of the theoretical and experimental values in this case exceeds the experimental error.††

The ratio $N^+/N^- \approx 160$ for $V = V_2$ and $N^+/N^- \simeq 8$ for $V = V_3$, i.e., if we assume that all the strange particles interact weakly with the pions and nucleons, then the results of the calculation of N^+/N^- sharply contradicts experiment.

I thank D. I. Blokhintsev for many discussions, M. A. Markov, B. V. Medvedev, V. I. Ogievetskii for discussions and valuable critical remarks, and K. D. Tolstov for discussion of the experiments.[6]

*A detailed consideration of this question will be given at a later date.

†We use the same notation as in Refs. 1, 2.

‡Exact calculations with account of momentum distribution will be published later in Acta Physica Polonica.

**The calculations were carried out under the assumption that the number of created K^0 and K^+ particles is approximately the same; E = 5 Bev. Taking the Fermi energy in the nucleus into account, this energy is close to the experimental energy of 4.3 Bev.

††The experimental error $\lesssim$ 50%; $\sigma_{tot} = (25 \pm 2.5)$ mb.

[1] Barashenkov, Barbashev, Bubelev and Maksimenko, Nucl. Phys. **5**, 17 (1957); Barashenkov, Barbashev and Bubelev, Nuovo cimento (in press).

[2] V. S. Barashenkov and V. M. Maltzev, Acta Phys. Polon. (in press).

[3] V. S. Barashenkov, Proceedings of the Conference of the Physics of Pions and New Particles; Padua-Venice, 1957.

[4] W. W. Chupp et al., Nuovo cimento, Supplement 2 of vol. 4, 359 (1956).

[5] M. Gell'Mann, Phys. Rev. **106**, 1296 (1957).

[6] C. Besson et al., Nuovo cimento **6**, 1168 (1957).

[7] Proceedings of the seventh Rochester Conference and one of the Conference in Padua-Venice, 1957.

Translated by R. T. Beyer
205

*POLARIZATION OF MU-MESON IN COSMIC RAYS**

I. I. GOL' DMAN

Physical Institute, Academy of Sciences, Armenian S.S.R.

Submitted to JETP editor January 13, 1958

J. Exptl. Theoret. Phys. (U.S.S.R.) **34**, 1017-1019 (April, 1958)

THE recent discovery of nonconservation of parity in weak (decay) interactions leads, in particular, to an asymmetry of the decay of polarized μ-mesons. The measure of asymmetry should then be proportional to the degree of polarization. It can be concluded from the data of Lederman et al.[1]

that μ-mesons emitted by stopped π-mesons are almost totally or even totally polarized in the direction of motion. In the following it will be assumed that the polarization is total in any single event of decay.

It does not follow from the above that the μ-mesons in cosmic rays are totally polarized. In fact, let us consider a vertical flux of μ-mesons with momentum p. A part of these mesons which is injected by decaying π-mesons into the lower hemisphere (in the center of mass system of the pion) is polarized predominantly forwards. The μ-mesons emitted into the upper hemisphere are polarized predominantly backwards. Complete compensation is not attained since the π-meson spectrum is richer in slow particles and, therefore, the probability that after a π-decay process a μ-meson will be found in the lower hemisphere is $> 1/2$.

For calculation of the degree of polarization, let us consider a μ-meson with momentum p and energy E produced as the result of decay of a π-meson (p′, E′). The direction of polarization of the μ-meson forms an angle α with its momentum. The direction of polarization is determined by the direction of spin in the frame of reference in which the μ-meson is at rest. Let us denote the momentum and energy of the π-meson in that system by P′ and $\mathcal{E}'$. It can be easily seen that

$$P' = (m'^2 - m^2)/2m, \quad \mathcal{E}' = (m'^2 + m^2)/2m.$$

Writing the four-dimensional invariants of the momenta of the π- and μ-mesons we find the angle α (which is that between **P′** and **p**):

$$\cos\alpha = (\mathcal{E}'E - mE')/pP'. \qquad (1)$$

We shall note now that the most important region of μ-meson energies (at the moment of production) is ultar-relativistic. We can neglect therefore the difference between p and E and the small angle between the momenta of the π- and μ-meson in the laboratory system. The mean value of polarization η has the direction of p and is equal in its absolute value to the mean value of $\cos\alpha$. Averaging Eq. (1) over the π-meson spectrum, we obtain

$$\eta = \int_{p'_{\min}}^{p'_{\max}} f_\pi(p') \frac{\mathcal{E}'E - mE'}{pP'} \frac{dp'}{p'^2} \Big/ \int_{p'_{\min}}^{p'_{\max}} f_\pi(p') \frac{dp'}{p'^2},$$

where the notation is that of Ref. 2. If we approximate the spectrum of π-mesons in air by power function $f_\pi \sim p^{1-\gamma}$ (the production spectrum of the π-mesons, under certain assumptions,[2] is then $p^{-\gamma}$) we obtain finally

$$\eta = \frac{1}{v} - \frac{\gamma}{\gamma-1}\frac{1-v}{v}\left[1 - \left(\frac{1-v}{1+v}\right)^{\gamma-1}\right] \Big/ \left[1 - \left(\frac{1-v}{1+v}\right)^{\gamma}\right],$$

where

$$v = P'/\mathcal{E}' = (m'^2 - m^2)/(m'^2 + m^2) = 0.26.$$

The above expression is simplified for $\gamma = 2$ ($\eta = v$) and $\gamma = 3$ ($\eta = 4v/(3+v^2)$). The results can be generalized for the case of $K_{\mu 2}$ decay.

The degree of polarization of μ-mesons in cosmic rays is:

	$\gamma = 2$	$\gamma = 3$
$\pi \to \mu + \nu$	0.26	0.34
$K \to \mu + \nu$	0.91	0.96.

The value of γ for π-mesons is $2 - 2.3$.[2] The polarization of μ-mesons produced by K-mesons is almost complete, while for those originating in π-meson decay amounts only to ~ 0.3. Measurements of the degree of polarization of μ-mesons in cosmic rays would make it possible to determine the ratio between the numbers of K- and π-mesons produced in the upper layers of the atmosphere. Since there is much more K^+-mesons than K^-, one should expect also that the degree of polarization of μ^+-mesons is greater than that of μ^-. If the excess of μ^+-mesons in cosmic rays ($N_+/N_- \sim 1.3$)[3] is due only to the excess of K^+, then the degree of polarization of μ^+-mesons in cosmic rays should amount to $40 - 50\%$ at least.

In conclusion, a few remarks concerning the depolarization of μ-mesons. Depolarization in passage through matter is due to multiple scattering and is most marked in the sub-relativistic region where the kinetic energy is of the order of the rest mass. Calculations show that depolarization is proportional to the atomic number of the medium and amounts to $\sim 1\%$ for air.

More important is the case of depolarization after the particle has stopped. The degree of depolarization depends then on the chemical properties of the medium, and can be obtained from the available experimental data on the asymmetry of the $\pi - \mu - e$ decay.

The author takes the advantage to express his gratitude to Prof. A. I. Alikhanian for interesting discussions.

---

*Paper presented at the seminar of the Physical Institute, Academy of Science, Armenian S. S. R., in March, 1957.

---

[1] Garwin, Lederman, and Weinrich, Phys. Rev. **105**, 1415 (1957).

[2] G. M. Garibian and I. I. Gol'dman, J. Exptl. Theoret. Phys. (U.S.S.R.) **26**, 257 (1954).

[3] Kocharian, Aivazian, Kirakosian, and Aleksanian, J. Exptl. Theoret. Phys. (U.S.S.R.) **30**, 243 (1956); Soviet Phys. JETP 3, 350 (1957).

Translated by H. Kasha
206

MAGNETIC DOUBLE REFRACTION OF MICROWAVES IN PARAMAGNETICS

F. S. IMAMUTDINOV, N. N. NEPRIMEROV and L. Ia. SHEKUN

Kazan State University

Submitted to JETP editor January 10, 1958

J. Exptl. Theoret. Phys. (U.S.S.R.) **34**, 1019-1021 (April, 1958)

THE rotation of the plane of polarization of the H_{11} wave was studied at a frequency of 9375 megacycles in a circular waveguide filled with a paramagnetic salt. The directional dependence of the external static magnetic field H_0, applied perpendicularly to the direction of propagation of the radio wave was investigated. As a polarizer, we employed a smooth transition of a standard rectangular waveguide to the circular (d = 23 mm). For an analyzer, we used a rotating turnstile junction, two arms of which were connected to a matched load, while at the two others were placed crystal detectors with approximately equal characteristics, connected in opposition by a bridge circuit. Balancing of the system was observed on a type M-95 galvanometer. Because of the small values of the angles of rotation observed, the mechanical rotation of the turnstile junction was employed only for calibration of the scale of the galvanometer.

2. It was established that the angle of rotation $\Delta\psi$ does not depend on the sign of $\mathbf{H}_0$, but does depend on the angle ψ which the field $\mathbf{H}_0$ forms with the magnetic field $\mathbf{H}$ of the radio wave before establishing it in the paramagnetic according to the law $\Delta\psi \sim \sin 2\psi$, so that the maximum effect was observed for $\psi = 45°$. As an example, we have shown the curve of the specific rotation of a powdered specimen $MnCl_2H_2O$ in the Figure.

3. The observed laws can be understood if we assume that the rotation of the plane of polarization takes place as a consequence of the anisotropy of the magnetic susceptibility μ. There is then a difference of the phenomenon under consideration

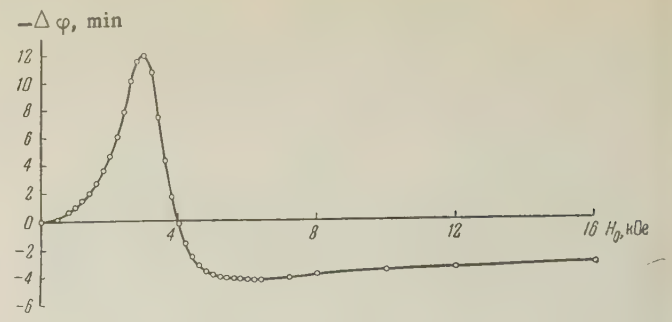

from the ordinary (optical) Cotton-Mouton effect, which is determined by the anisotropy of the constant ϵ.

It is known that the tensor of the high frequency magnetic susceptibility of a paramagnetic magnetized along the z axis has the form:

$$\{\chi\} = \begin{Bmatrix} \chi & -i\delta & 0 \\ i\delta & \chi & 0 \\ 0 & 0 & \chi_z \end{Bmatrix},$$

where χ, δ, χ_Z are complex quantities dependent on H_0, the frequency of the radio wave ω and the relaxation time τ in the paramagnetic. A calculation carried out by one of the authors shows that in the case of wave propagation perpendicular to the applied field, the rotation angle (for not very small ψ) is given by

$$\Delta\psi = -(\pi\omega\sqrt{\varepsilon}/c)\, l\, \{\chi'' - \chi_z''\} \sin 2\psi. \qquad (1)$$

Here l is the thickness of the layer of the paramagnetic, χ'' and χ_Z'' are the imaginary parts of χ and χ_Z. The calculation is carried out for free space; ϵ was considered real. As is known, χ'' and χ_Z'' are the absorption coefficients for the cases $\mathbf{H}_0 \perp \mathbf{H}$ ("perpendicular field") and $\mathbf{H}_0 \parallel \mathbf{H}$ ("parallel field"), respectively, and do not depend on the sign of $\mathbf{H}_0$.

4. Some of the qualitative regularities pointed out in Sec. 2 have already been observed by other authors.[1,2] As concerns the form of the curve $\Delta\psi(H_0)$, it was not observed in sufficient detail.

For $H_0 = 0$, $\Delta\psi = 0$, since $\chi'' = \chi_Z''$. It is also known that at frequencies of the order of 10 kilomegacycles, χ'' has a well-defined maximum at $\gamma H_0 = \omega$ and practically disappears for $\gamma H_0 > (2-3)\omega$, while χ_Z'' decreases slowly and monotonically with increase in H_0.[3] This suffices to explain the observed form of the curve in the Figure. A quantitative estimate on Eq. (1) shows excellent agreement with experimental data.

5. At the present time, the theory does not give precise expressions for χ'' and χ_Z'' in solids. In order to obtain some estimate of these quantities, we can make use of the theory for a paramagnetic gas, consisting of monatomic atoms with spin $\frac{1}{2}$.

We found that in this case,

$$\chi'' = \frac{\chi_0}{2}\left\{\frac{\omega/\tau}{(\omega_0-\omega)^2+\tau^{-2}} + \frac{!\omega/\tau}{(\omega_0+\omega)^2+\tau^{-2}}\right\};\ \chi_z'' = \chi_0\frac{\omega/\tau}{\omega^2+\tau^{-2}} \tag{2}$$

(χ_0 = static susceptibility).

We note that the thermodynamic theory of Shaposhnikov evidently leads to the same formulas (see Ref. 4). If we consider that τ increases with increase in H_0,[3,5] then it is shown that the simple equations (2) provide both a qualitative and a quantitative description of the experimental results.

6. Considerations carried out above show that the magnetic double refraction of microwaves in paramagnetics ("the microwave effect of Cotton-Mouton") is closely connected with the paramagnetic absorption in perpendicular and parallel fields and, together with the paramagnetic resonance rotation,[6-9] enters into a series of phenomena which can now be united under the general title of "paramagnetic resonance."[10]

A more detailed explanation of the results obtained will be published separately.

[1] Battaglia, Gozzini and Polacco, Nuovo cimento **10**, 1205 (1953).

[2] P. Hedvig, Acta Phys. Acad. Sci. Hung. **6**, 489 (1957).

[3] A. I. Kurushin, Izv. Akad. Nauk SSSR, ser. fiz. **20**, 1232 (1956); J. Exptl. Theoret. Phys. (U.S.S.R.) **32**, 727 (1957); Soviet Phys. JETP **5**, 601 (1957).

[4] L. M. Tsirul'nikova and I. G. Shaposhnikov, Izv. Akad. Nauk SSSR, ser. fiz. **22**, 1251 (1956).

[5] C. J. Gorter, Paramagnetic Relaxation (New York, 1957).

[6] N. N. Neprimerov, Izv. Akad. Nauk SSSR, ser. fiz. **18**, 368 (1954); **20**, 1236 (1956).

[7] L. Ia. Shekun, Izv. Akad. Nauk SSSR, ser. fiz. **20**, 1262, 1265 (1956).

[8] P. Hedvig and A. Nagy, Acta Phys. Acad. Sci. Hung. **5**, 529 (1956).

[9] A. Gozzini, Cahier Phys. **79**, 123 (1957).

[10] S. A. Al'tshuler and B. M. Kozyrev, Uspekhi Fiz. Nauk **63**, 533 (1957).

Translated by R. T. Beyer
207

TOTAL CROSS SECTION OF STRIPPING AND DIFFRACTION DISINTEGRATION OF FAST DEUTERONS ON NONSPHERICAL NUCLEUS

V. S. POPOV

Submitted to JETP editor January 14, 1958

J. Exptl. Theoret. Phys. (U.S.S.R.) **34**, 1021-1022 (April, 1958)

LET us consider a nucleus having the form of an ellipsoid of rotation and one that is opaque for incident nucleons. The kinetic energy of the deuterons must be sufficiently large in order that the wavelength of the deuteron be many times smaller than the radius of the nucleus. We shall neglect the effect of the Coulomb field of the nucleus in this note.

With the help of a method developed by Akhiezer and Sitenko,[1] the following expression is obtained for the amplitude of elastic diffraction scattering of deuterons on a nucleus with a fixed orientation of its axis ω:

$$f(\varkappa,\omega) = 2\pi ik\left\{\frac{4p}{\varkappa'}\tan^{-1}\frac{\varkappa'}{2p}\,\Omega(\varkappa',\omega) - \frac{1}{b^2}\int d\mathbf{g}\,\frac{2p}{|2\mathbf{g}-\varkappa'|}\tan^{-1}\frac{|2\mathbf{g}-\varkappa'|}{2p}\,\Omega(\mathbf{g},\omega)\,\Omega(\varkappa'-\mathbf{g},\omega)\right\}, \tag{1}$$

$$\Omega(\varkappa,\omega) = (b^2/2\pi)\,\xi(x)\,J_1(t)/t,$$

$$\cos\vartheta = x;\ t = \varkappa'\left[\xi^2(x)\cos^2(\varphi-\phi) + \sin^2(\varphi-\phi)\right]^{1/2};$$

$$\xi(x) = \left[\left(\frac{a}{b}\right)^2(1-x^2)+x^2\right]^{1/2}.$$

Here a, b = semiaxes of the ellipsoid, while a refers to the axis of rotation; $\omega = (\theta,\varphi)$ = angles defining the orientation of the nucleus in space; $J_1(t)$ is the Bessel function of order 1; κ = transverse momentum obtained by the deutéron upon scattering; $\kappa = k\theta$; (θ,φ) = direction of the momentum of the scattered deuteron; $\kappa' = \kappa b$; $p = b/R_d = 2\alpha b$.

Equation (1) is simplified when the radius of the nucleus is much larger than the radius of the deuteron and the scattering angles are small ($p \gg 1$, $p \gg \kappa'$). In particular, the forward scattering amplitudes are

$$f(0,\omega) = \frac{ika^2\xi}{2}\left[1 + \frac{1}{\pi p}\,E\left(\frac{\pi}{2},\ \frac{\sqrt{\xi^2-1}}{\xi}\right)\right], \tag{2}$$

where E is the complete elliptical integral. Averaging over the various orientations of the nucleus, we obtain the total cross section of all processes:

$$\sigma_t = \frac{4\pi}{k}\overline{\operatorname{Im} f(0,\omega)} = 2\pi b^2\left(1+\frac{\varepsilon}{6}-\frac{\varepsilon^2}{15}\right) + \pi b R_d\left(1+\frac{\varepsilon}{6}-\frac{\varepsilon^2}{40}\right) \tag{3}$$

(with accuracy up to terms $\sim\epsilon^3$); here $\epsilon = (a/b)^2 - 1$. Taking $p \gg 1$, we can neglect the curvature of the surface of the nucleus and use the probability of stripping and of diffraction break up, calculated per unit length of a screen in the form of an infinite half-plane (see Ref. 2). Upon multiplication by the length of the projection of the nucleus, and averaging over all its orientations, we obtain the total cross section of stripping and diffraction disintegration of the deuteron (with accuracy up to ϵ^3):

$$\sigma_p = \sigma_n = \frac{\pi}{2} bR_d \left(1 + \frac{\varepsilon}{6} - \frac{\varepsilon^2}{40}\right);$$
$$\sigma_d = \frac{\pi bR_d}{3}\left(2\ln 2 - \frac{1}{2}\right)\left(1 + \frac{\varepsilon}{6} - \frac{\varepsilon^2}{40}\right). \quad (4)$$

The following relation holds among σ_e, σ_d and σ_t: $\sigma_e + \sigma_d = \sigma_t/2$. This equality, which was established in Ref. 1 for a spherical nucleus, holds also in the case of a black, nonspherical nucleus. Therefore, we can determine the elastic diffraction scattering cross section:

$$\sigma_e = \pi b^2\left(1 + \frac{\varepsilon}{6} - \frac{\varepsilon^2}{15}\right) + \frac{2\pi}{3} bR_d (1 - \ln 2)\left(1 + \frac{\varepsilon}{6} - \frac{\varepsilon^2}{40}\right). \quad (5)$$

For a spherical nucleus, all the formulas reduce to the formula of Akhiezer and Sitenko[1] and of Glauber.[2]

In conclusion, I express my thanks to I. S. Shapiro for discussion of the results.

[1] A. I. Akhiezer and A. G. Sitenko, J. Exptl. Theoret. Phys. (U.S.S.R.) **32**, 794 (1957); Soviet Phys. JETP **5**, 652 (1957).

[2] R. J. Glauber, Phys. Rev. **99**, 1515 (1955).

Translated by R. T. Beyer
208

CERENKOV RADIATION OF LONGITUDINALLY POLARIZED ELECTRONS

A. A. SOKOLOV and Iu. M. LOSKUTOV

Moscow State University

Submitted to JETP editor January 16, 1958

J. Exptl. Theoret. Phys. (U.S.S.R.) **34**, 1022-1023 (April, 1958)

THE discovery of parity non-conservation by Lee and Yang has aroused renewed interest in an investigation of longitudinal (circular) polarization since longitudinally polarized electrons are produced in β-decay.

In investigating the radiation associated with longitudinally polarized electrons, the Casimir formula cannot be used to calculate the matrix elements; instead, use must be made of Eq. (21.12) of Ref. 1 in which the spin state is explicitly taken into account, since the spin quantum number $s = \pm 1$ characterizes the eigenvalue of the operator $(\nabla\sigma)/i\sqrt{-\nabla^2}$. As has already been noted in Ref. 2 (and also in the detailed literature), this same formula can be used conveniently (with different mass values) in investigating the polarization properties of electrons produced in β-decay.

In the present work we extend the results[3] obtained in an investigation of the polarization properties of Cerenkov radiation to the case in which the electrons are longitudinally polarized.

Carrying out the summation indicated in Eq. (21.12) of Ref. 1 over the final spin states s' and fixing the initial value of the spin s we find that the Cerenkov radiation consists of three parts (in analyzing the polarization properties of the Cerenkov radiation, as in the earlier work,[3] we have used Eqs. (10), (11) and (12) of Ref. 4*):

$$W_{s\lambda} = \frac{e^2}{2c^2}\int_0^{\omega_{max}} \tilde{w}_{s\lambda}(\omega)\, d\omega$$
$$= \frac{e^2}{2c^2}\int_0^{\omega_{max}} (w_{class}(\omega) + w_{quant}(\omega) + s\lambda w_{long}(\omega))\, d\omega.$$

Here $w_{class}(\omega) = \omega(1 - \cos^2\theta)$ is the classical component of the radiation (completely linearally polarized);

$$w_{quant}(\omega) = \hbar^2 (n^2\omega^3/2c^2p^2)(1 - n^{-2})$$

is the quantum contribution which is completely unpolarized;

$$w_{long}(\omega) = \hbar \frac{n\omega^2}{cp}\left(1 - \frac{1}{\beta n}\cos\theta\right)$$

characterizes the longitudinally polarized radiated photons (in accordance with conventional classical optics, for $\lambda = -1$ we have right-hand circular polarization while with $\lambda = +1$ we have left-hand circular polarization although the opposite convention would be more natural). It is of interest to note that this part of the radiation is not proportional to $\hbar^2$ (as w_{quant}), but rather to $\hbar$.

The degree of circular polarization is given by the following expression:

$$P = \frac{w_1(\omega) - w_{-1}(\omega)}{w_1(\omega) + w_{-1}(\omega)} \approx s\frac{\hbar n\omega}{cp}.$$

*The notation and a bibliography for this problem are given in Ref. 3.

[1] A. A. Sokolov and D. D. Ivanenko, Квантовая теория поля (Quantum Theory of Fields), Mos – Len (1952).

[2] A. A. Sokolov, J. Exptl. Theoret. Phys. (U.S.S.R.) **33**, 794 (1957); Soviet Phys. JETP **6**, 611 (1958).

[3] A. A. Sokolov and Iu. M. Loskutov, J. Exptl. Theoret. Phys. (U.S.S.R.) **32**, 630 (1957); Soviet Phys. JETP **5**, 523 (1957).

[4] A. A. Sokolov and I. M. Ternov, J. Exptl. Theoret. Phys. (U.S.S.R.) **31**, 473 (1956); Soviet Phys. JETP **4**, 396 (1957).

Translated by H. Lashinsky
209

ELECTRON PARAMAGNETIC RESONANCE OF THE V^{+++} ION IN SAPPHIRE

G. M. ZVEREV and A. M. PROKHOROV

Moscow State University

Submitted to JETP editor, January 16, 1958

J. Exptl. Theoret. Phys. (U.S.S.R.) **34**, 1023-1024 (April, 1958)

THE electronic paramagnetic resonance (epr) spectrum of the V^{+++} ion has been investigated in a sapphire single crystal Al_2O_3.

The ground state of this ion is $^3F_2$. The sevenfold degeneracy of the orbital energy level is split by a crystalline electric field of cubic symmetry into a singlet and two triplets with the triplet found at the lower level. A crystalline field of trigonal or tetragonal symmetry splits this orbital triplet into a doublet and a singlet. The lowest energy level of the V^{+++} ion in a crystalline field of trigonal symmetry is the singlet, which has a triple degeneracy ($S = 1$). In work by Siegert[1] and van Vleck[2] it has been shown that at zero magnetic field the levels with $S_Z = 0$ and $S_Z = \pm 1$ should be separated by approximately 10 cm^{-1}. Hence one would expect to see a line corresponding to the transition from the $S_Z = +1$ level to the $S_Z = -1$ level. Since the number of unpaired electrons is even the $S_Z = +1$ and $S_Z = -1$ levels should be slightly split at zero magnetic field.

To observe the line it is necessary that its width be small, i.e., the spin-lattice relaxation time must be greater than 10^{-11} sec. In the sapphire lattice there is a strong electric field of trigonal symmetry which produces a wide separation in the lower orbital levels of the V^{+++} ion. Hence one would expect that the spin-lattice relaxation time should be sufficiently long at low temperatures. In those crystal lattices in which the axial component of the electric field is weaker there is not much hope of seeing epr lines for V^{+++}. It is for this reason that the V^{+++} spectrum has probably not been studied up to this time.

We have observed one line of the V^{+++} ion in a sapphire single crystal at $T = 4.2°K$ at frequencies ranging from 14 to 38 kilomegacycles/sec. There was a sharp reduction in line intensity when the temperature was reduced to 2°K. When the temperature was increased the line became smeared out and vanished. The line could not be observed at $T = 77°K$. The line comprises eight equidistant components corresponding to a nuclear spin $I = 7/2$ for V^{51}.

The line was observed in the parallel orientation, i.e., with the fixed magnetic field parallel to the z axis of the crystal and vanished, becoming broadened, when the crystal was rotated through an angle greater than 60° with respect to the parallel orientation. The half-widths of the individual components in the parallel orientation were 20 oersteds; the components were 108 oersteds apart.

The spectrum was interpreted by means of the spin Hamiltonian:[3]

$$\hat{\mathcal{H}} = DS_z^2 + g_{\parallel}\beta H_z S_z + g_{\perp}\beta (H_x S_x + H_y S_y) + \Delta S_x + AS_z I_z + B(S_x I_x + S_y I_y),$$

where S_X, S_Y and S_Z are the electron spin projections, I_X, I_Y, and I_Z are the nuclear spin projections, H_X, H_Y and H_Z are the projections of the magnetic field vector, β is the Bohr magneton, D is the spacing between the $S_Z = 0$ and $S_Z = 1$ levels, $g_{\parallel}$ and $g_{\perp}$ are the g-factors for the two orientations, A and B are the hyperfine-splitting constants for the various orientations and the term ΔS_X denotes the small splitting of the $S_Z = +1$ and $S_Z = -1$ levels at zero magnetic field. The spectrum was interpreted under the assumption that $D \gg \Delta$ and $g_{\parallel}\beta H$ and $g_{\perp}\beta H$ were each greater than A or B.

$\Delta M = 1$ transitions were not observed since $D \gg h\nu$. In the case of a $\Delta M = 2$ transition we have:

$$h\nu = (2 - D^{-2}(\Delta + g_{\perp}\beta H \sin\alpha)^2)(g_{\parallel}\beta H \cos\alpha + Am),$$

where α is the angle between the magnetic field and the trigonal axis of the crystal and m is the projection of the nuclear spin on the z axis.

The formula which has been obtained is in good agreement with all the experimental results; the effect of the term $(\Delta + g_{\perp}\beta H \sin\alpha)^2 D^{-2}$ can be neglected for the experimental errors reported here. Hence we can only determine $g_{\parallel}$ and A in the spin Hamiltonian:

$$g_{\parallel} = 1.92 \pm 0.01; \quad A = (1.93 \pm 0.02) \cdot 10^{-2}\ \mathrm{cm}^{-1}.$$

Measurement of the line intensities at various temperatures indicates that $D > 0$ and is approximately $10\ \mathrm{cm}^{-1}$.

The results which have been obtained are in agreement with the values $g_{\parallel} = 1.98$, $g_{\perp} = 1.82$ and $D = 5.0\ \mathrm{cm}^{-1}$, obtained by van der Handel and Siegert[4] from measurements from the susceptibility of vanadium — ammonium alums.

The authors are indebted to S. V. Grum-Grzhimailo and A. A. Popov for preparation of the samples and to Professor A. I. Shal'nikov for participating in the low-temperature experiments.

[1] A. Siegert, Physica **4**, 138 (1937).

[2] J. H. van Vleck, J. Chem. Phys. **7**, 61 (1939).

[3] A. Abragam and M. H. L. Pryce, Proc. Roy. Soc. **205**, 135 (1951).

[4] van den Handel and A. Siegert, Physica **4**, 871 (1937).

Translated by H. Lashinsky
210

DISPERSION OF SOUND IN METALS IN A MAGNETIC FIELD

A. A. GALKIN and A. P. KOROLIUK

Institute of Radio Physics and Electronics, Academy of Sciences, Ukrainian S.S.R.

Submitted to JETP editor, January 14, 1958

J. Exptl. Theoret. Phys. (U.S.S.R.) **34**, 1025-1026 (April, 1958)

DISPERSION effects in the velocity of sound in solid metals, predicted by Alpher and Rubin,[1] have not been observed at the present time; this situation is probably a result of the fact that the effect is so small. In the present paper experiments in which this effect was observed are reported.

A special system was designed and built to investigate small changes in the velocity of acoustic vibrations; under favorable conditions this instrument makes it possible to measure changes of approximately 10^{-6} in the velocity of sound. The operation of the instrument is based on a comparison and measurement of the phase difference between vibrations which pass through the sample being investigated and those which are transmitted directly from an ultrasonic generator.

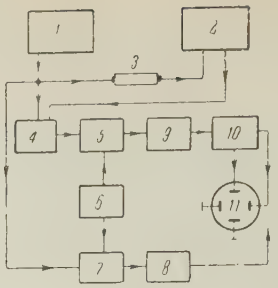

FIG. 1. Diagram of the measuring instrument. 1) 7 mc/sec crystal oscillator, 2) tuned amplifier, 3) sample, 4) electronic switch, 5) mixer, 6) quartz-crystal heterodyne unit, 7) mixer, 8) peeking amplifier, 9) frequency multiplier, 10) circular sweep generator, 11) cathode ray oscilloscope.

A block diagram of the measurement scheme is shown in Fig. 1. The high-frequency voltage from a quartz-crystal oscillator is applied to a quartz radiator which is fastened to one side of the cylindrical sample. A quartz detector is fastened to the second face of the sample; the voltage from the detector is then passed through a tuned amplifier to the phase meter.[2] A voltage obtained directly from the crystal radiator is also applied to the phase meter. Using a frequency multiplication factor of 18, phase differences of the order of 0.2 degrees can be measured.

X-cut quartz slabs 10 mm in diameter were used as ultrasonic radiators. The samples were cylindrical rods 20 cm long and 1.4 cm thick. Because of the high acoustic absorption in polycrystalline tin there was no need to take account of standing waves which could distort the results of the measurements; similarly there was no need to consider reflections from the side surfaces of the sample, produced by the cone-shaped radiation pattern of the quartz radiator. To avoid these effects in aluminum the surface was roughened by cutting to enhance scattering; the face at the receiving end was also cut at a small angle with respect to the axis.

The velocity of sound in a magnetic field is given by the expression:*

$$c_l = c_{l0}\left(1 + \frac{s^2}{2c_{l0}^2}\sin^2\vartheta\right), \qquad c_t = c_{t0}\left(1 + \frac{s^2}{2c_{t0}^2}\cos^2\vartheta\right).$$

Here c_l is the velocity of longitudinal wave while c_t is the velocity of the transverse wave, $s^2 = \mu H^2/4\pi\rho$, ρ is the density, ϑ is the angle between

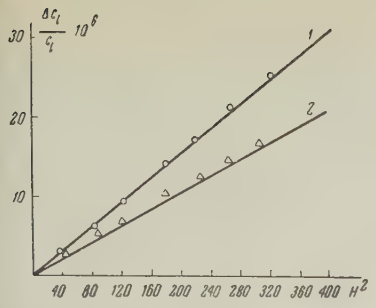

FIG. 2. The velocity of sound as a function of magnetic field.

the wave vector and the magnetic field, H is the magnetic field and μ is the magnetic permeability. These formulas apply when $\sigma \gg c^2\omega/4\pi\mu c_l^2$, where σ is the conductivity, ω is the vibration frequency and c is the velocity of light.

In Fig. 2 are shown the results of experiments carried out at room temperature in a magnetic field perpendicular to the axis of the sample ($\sin\vartheta = 1$). The relative change in velocity c_l is plotted along the ordinate axis while the square of the magnetic field is plotted along the absicca axis. The solid lines are obtained by calculation: (1) for tin ($c_{l_0} = 2630$ meters/sec), (2) for aluminum ($c_{l_0} = 6{,}000$ meters/sec). The absolute values of the velocity were measured by a pulse method. As is apparent from the curves, the experimental points are in good agreement with the theoretical values.

Thus it has been established that the acoustic velocity is proportional to H^2 in a magnetic field and the magnitude of the effect is that predicted by the theory.

It is interesting to note that in bismuth, in which the condition $\sigma \gg c^2\omega/4\pi\mu c_l^2$ is not satisfied, no dispersion in the acoustic velocity at room temperature was found.

In conclusion we wish to express our gratitude to Prof. A. I. Akhiezer and S. V. Peletminskii for calling our attention to this effect.

*These expressions were obtained independently from Alpher and Rubin by A. I. Akhiezer and S. V. Peletminskii.

[1] R. A. Alpher and R. I. Rubin, J. Acoust. Soc. Am. **26**, 452 (1954).

[2] Samoilo, et al., Trudy Moscow Engineering Institute **21**, 89 (1956).

Translated by H. Lashinsky
211

THE NEGATIVE ION H_2^-

V. I. KHVOSTENKO and V. M. DUKEL'SKII

Physical-Technical Institute, Academy of Sciences, U.S.S.R.

Submitted to JETP editor January 15, 1958

J. Exptl. Theoret. Phys. (U.S.S.R.) **34**, 1026-1027 (April, 1958)

ACCORDING to theoretical calculations,[1,2] the molecule H_2 in the lowest electronic state has no affinity for electrons. Nevertheless, the possibility of a stable negative ion H_2^- is not excluded. This unusual situation is due to the fact that, although the fundamental vibrational level of the system H, H^- (which is the H_2^- ion) is higher than the fundamental vibrational level of the H_2 molecule, it has a much larger internuclear separation. The removal of an electron from the H_2^- ion corresponds to an electron transition at an internuclear separation of the order of 3 A, where the potential curve for the H_2 molecule rises higher than the curve for the H_2^- ion. According to Dalgarno and McDowell[2] the "vertical energy of electron removal" from the H_2^- ion is 0.9 ev.

As far as we are aware, the H_2^- ion has never been observed. We have attempted to obtain some evidence for this ion, using the "recharging" method[3] to produce it. Water vapor and antimony vapor were introduced simultaneously into an ion source and bombarded by a beam of electrons (0.3 ma; 80 ev). The resulting negative ions were analyzed in a mass spectrometer connected to an electron multiplier.[4]

When water vapor alone was present in the ion source, the ions H^-, O^- and OH^- were formed. When antimony vapor was subsequently introduced into the source, the additional ions Sb^-, Sb_2^-, and Sb_3^- appeared, together with a negative ion of mass 2. There were also maxima corresponding to mass values of 0.5, ≈ 3, and ≈ 6. These maxima must be assigned to fragmentary ions, arising from the dissociation of primary ions. To suppress the ion fragments, a retarding potential of 1500 volts was applied to the first diode of the multiplier, while maintaining the primary ion energy at 800 ev. When this was done, the peaks corresponding to the masses 0.5, 3, and 6 completely disappeared; the amplitudes of the peaks at mass 1 (H^-) and mass 2 were practically unchanged. This shows that both these maxima were due to primary ions formed in the source. The height of the peak at mass 2 depended on the vapor pressure of the antimony; even under the most favor-

able conditions the ion current at this mass was only 5×10^{-15} amp.

The question may arise whether or not this peak is due to the formation of the negative deuterium ion D^-, which has a mass of two. However, the height of the peak at mass 2 was only 20 — 30 times less than that of the H^- peak, while the ratio H/D in natural water is 6000. Furthermore, the mass 2 ions appeared only when antimony vapor was present in the ion source.

All of the above leads us to the conclusion that the negative ions with mass 2 which we observed were in fact H_2^- ions. The occurrence of fragmentary ions with mass 0.5 can serve as an additional indication of the presence of H_2^- ions within the apparatus. An apparent mass of 0.5 would be carried by an ion formed by the dissociation of an H_2^- ion outside the source.

[1] H. Eyring, J. O. Hirschfelder and H. S. Taylor, J. Chem. Phys. **4**, 479 (1936).

[2] A. Dalgarno and M. R. C. McDowell, Proc. Phys. Soc. (London) **A69**, 615 (1956).

[3] V. M. Dukel' skii, Dokl. Akad. Nauk SSSR **105**, 955 (1955).

[4] V. I. Khvostenko and V. M. Dukel' skii, J. Exptl. Theoret. Phys. (U.S.S.R.) **33**, 851 (1957); Soviet Phys. JETP **6**, 657 (1958).

Translated by D. C. West
212

ON THE DETERMINATION OF THE RELATIVE PARITIES OF ELEMENTARY PARTICLES

CHOU HUAN-CHAO (CHZHOU GUAN-CHZHAO)

Joint Institute of Nuclear Studies

Submitted to JETP editor January 16, 1958

J. Exptl. Theoret. Phys. (U.S.S.R.) **34**, 1027-1028 (April, 1958)

SINCE parity is not conserved in the weak interactions, it is of great interest to determine the parities of elementary particles by means of the strong interactions. We consider below several reactions which can be used for the determination of the relative parities of strange particles. We have in mind the following type of reaction:

$$p\,(n) + \mathrm{He}^4 \rightarrow {}_\Lambda\mathrm{He}^5 + K^+\,(K^0) \qquad (1)$$

with the assumption that the spins of ${}_\Lambda\mathrm{He}^5$ and K are $\frac{1}{2}$ and 0, respectively.

This process is completely described by a spin-space matrix $\mathbf{M}(\mathbf{n}, \mathbf{n}')$ which gives the amplitude of the diverging wave.[1] The most general form of the matrix $\mathbf{M}(\mathbf{n}, \mathbf{n}')$ is

$$M\,(\mathbf{n}, \mathbf{n}') = a + b\sigma\,[\mathbf{n} \times \mathbf{n}'], \qquad (2)$$

when the product I of the parities of all four particles is equal to +1, and

$$M\,(\mathbf{n}, \mathbf{n}') = a\sigma\mathbf{n} + b\sigma\mathbf{n}', \qquad (3)$$

when $I = -1$. Here $\mathbf{n}$ and $\mathbf{n}'$ are unit vectors parallel to the momenta of the incident and emerging particles, respectively; a and b are certain functions of the energy and of the angle between $\mathbf{n}$ and $\mathbf{n}'$. The density matrix ρ_i of the initial state has the form

$$\rho_i = A\,(1 + \sigma\mathbf{P}), \qquad (4)$$

where $\mathbf{P}$ is the polarization vector of the incident particles. If the reaction takes place at threshold, or if we select only the ${}_\Lambda\mathrm{He}^5$ particles emitted forward (i.e., $\mathbf{n} \parallel \mathbf{n}'$), then we can neglect the second term in Eq. (2). At the threshold, Eq. (3) takes the form $M = a\sigma\mathbf{n}$, and for $\mathbf{n} \parallel \mathbf{n}'$ we have $M = (a + b)\sigma\mathbf{n}$. The polarization vector $\mathbf{P}'$ of the ${}_\Lambda\mathrm{He}^5$ particle in the final state is calculated by the formula[1]

$$\mathbf{P}' = \mathrm{Sp}\,(M\rho_i M^+\sigma) \,/\, \mathrm{Sp}\,(M\rho_i M^+). \qquad (5)$$

Substituting Eqs. (2), (3), and (4) into (5), we get

$$\mathbf{P}' = \mathbf{P}, \qquad \text{when } I = +1, \qquad (6)$$

$$\mathbf{P}' = (2(\mathbf{Pn})\,\mathbf{n} - \mathbf{P}), \qquad \text{when } I = -1. \qquad (7)$$

If the parity is not conserved in the decay of the ${}_\Lambda\mathrm{He}^5$, then from the angular asymmetry of the decay one can measure the direction of polarization of the ${}_\Lambda\mathrm{He}^5$ and distinguish between the possibilities (6) and (7). We emphasize that the incident beam must be polarized, and in such a way that the polarization vector is neither parallel nor perpendicular to the direction $\mathbf{n}$. The other reactions of this general type are as follows:

$\Sigma^\pm + \mathrm{He}^4 \rightarrow {}_\Lambda\mathrm{He}^5 + \pi^\pm$ at threshold, or when the ${}_\Lambda\mathrm{He}^5$ emerges forward; (8)

$\Sigma^\pm + \mathrm{He}^4 \rightarrow \Lambda + \mathrm{He}^4 + \pi^\pm$ at threshold; (8′)

$p\,(n) + \mathrm{He}^4 \rightarrow \Lambda + \mathrm{He}^4 + K^+\,(K^0)$ at threshold. (1′)

In the last two reactions He^4 can be replaced by any other nucleus with spin 0 (for example, C^{12}).

We note that, in the reactions (1) and (1′), the polarization vectors of the $_{\Lambda}He^{5}$ and Λ depend only on the vectors $\mathbf{P}$ and $\mathbf{n}$ and the relative parities of K and Λ. Therefore, a case of the reaction (1′) can be simply added in with the cases of reaction (1).

The writer expresses his gratitude to M. I. Shirokov and L. G. Zastavenko for valuable advice and a discussion of the results.

[1] L. Wolfenstein and J. Ashkin, Phys. Rev. **85**, 947 (1952); R. Oehme, Phys. Rev. **98**, 147 (1955).

Translated by W. H. Furry
213

EMISSION OF Λ^0 PARTICLES UPON CAPTURE OF K MESONS BY NUCLEI IN EMULSION

S. A. BUNIATOV, A. VRUBLEVSKII,* D. K. KOPILOVA, Iu. B. KOROLEVICH, N. I. PETUKHOVA, V. M. SIDOROV, E. SKZHIPCHAK* and A. FILIPKOVSKII*

Joint Institute of Nuclear Studies

Submitted to JETP editor January 16, 1958

J. Exptl. Theoret. Phys. (U.S.S.R.) **34**, 1028-1030 (April, 1958)

An Ilford G-5 emulsion stack (each pellicle was 600 microns thick) was exposed at the Bevatron in Berkeley† to K^- mesons with a momentum near 300 Mev/c. In scanning this stack three Λ^0 decays were found in the immediate vicinity of σ_K stars (see Table I, events 1, 2 and 17). Similar events have been observed by others.[1-3] In this connection we attempted to establish a correlation between the parent event and the Λ^0 decay, when it was impossible to observe them in a single field of view of the microscope. The pellicles were area-scanned with a magnification of 225 in a strip 1.5 cm × 10 cm, in which practically all K^- mesons were expected to have been stopped. We recorded σ_K stars, two-prong stars, and all proton tracks starting in the pellicle and longer than 500 microns. The beginning of each track was examined under great magnification in order to find a second track of small ionization, if such exists. This was necessary since some two-prong stars might have been overlooked in scanning with low magnification because of the low sensitivity of the emulsion (g_{min} = 16 grains in 100 microns). All events in which the direction of the fast particle agreed with that of the beam were at once rejected as stars produced by π^- contamination in the K^- beam. The Λ^0 decays were picked out from the set of two-prong stars thus found. First we measured the proton range, the ionization of the fast particle, and the opening angle. Using these data one can select those stars for which the relation between proton momentum, pion ionization, and opening angle in the decay $\Lambda^0 \rightarrow p + \pi^-$ is satisfied. Following the track of the fast particle enables one to determine whether it is a π^- meson; from the range of this particle and the data obtained before one can compute the Q value. Thus 18 Λ^0 decays were found.

A search for parent events was made within cones, whose axes were in the direction of flight of the Λ^0 particles as determined from the proton and pion momenta; the vertex angle of the cones was 5°, and the heights were set by the boundaries of the scanned strip. Parent events were found for 13 Λ^0 particles.

The results of the measurements are given in Table I. Column 4 gives the angle $\Delta\varphi$ between the decay plane and the line joining the point of decay with the parent event; column 5 gives the projection of the angle between this line and the direction of flight of the Λ^0 particle upon the emulsion plane. As is evident from Table I, the actually observed spread of the angles $\Delta\varphi$ and $\Delta\alpha$ is less than the average value of the quoted errors. This is probably connected with the restrictions placed upon the magnitudes of $\Delta\varphi$ and $\Delta\alpha$ in selecting the parent events. For example, if one considered only those events for which $|\Delta\alpha| \leq \sqrt{D}$, where $\sqrt{D}$ is the rms error in the determination of the direction of flight of the Λ^0 particles, then such a "cutoff" leads to $|\overline{\Delta\alpha}| \approx 0.3\sqrt{D}$; a Gaussian distribution of errors is assumed here.

The type of the parent event is given in column 6.

As is evident from Table I, for five events no parent σ_K star was found. The pertinent Λ^0 particle might have been formed in a nuclear explosion produced outside the scanned region by a stopped K^- meson. Nor can we exclude that the parent σ_K star was not found because of nuclear scattering of the Λ^0 particle. Moreover it is possible that the parent event lies outside the scanned cones.

For 18 identified Λ^0 particles (the total volume of the cones was 0.17 cm^3), one could anticipate 4 spurious parent events. In fact one such event was found. Of course, to reduce the number of spurious events one should decrease the density of exposure.

Results of treating the Λ° particles

Decay event number	Q, Mev	Kinetic energy[1] of Λ°, Mev	$\Delta\varphi$,[2] degrees	$\Delta\alpha$,[2] degrees	parent event
1	38.3	3.0	0.8±5.5	2.0±2.9	σ_K
2[3]	42.0	20.9	1.0±2.6	0.5±2.8	σ_K
3	36.0	13.1	1.6±2.3	1.5±1.9	σ_K
4	36.4	10.1	0.2±1.5	0.5±2.1	σ_K
5	38.2	14.5	0.9±1.5	0.0±2.7	ρ_K[6]
6[4]	40.0	48	0.1±2.0	1.5±2.2	σ_K
			1.2±2.0	2.2±2.2	ρ_K[6]
7	38.3	4.9	1±5	0.0±2.1	σ_K
8	37.5	12	1±2.0	0.5±2.1	σ_K
9	38.9	8.8	0.5±1.9	1.5±2.3	ρ_K[6]
10[5]	37.5	3.4	—	—	—
11[5]	36.8	0.9	—	—	—
12[5]	36.5	10.1	—	—	—
13	36.6	6.0	0 4±1.5	0.8±4.5	σ_K
14[5]	37.1	18.4	—	—	—
15	38.2	35.5	2±2.4	2.5±2	ρ_K[6]
16	38.7	23.2	1.7±2.0	2±1.7	σ_K
17	38.3	7.3	2.1±2.5	2.5±2.6	σ_K
18[5]	38.1	10,13	—	—	—

[1]The errors in the energies are 1 to 2 Mev.

[2]Emulsion shrinkage was not considered in estimating the errors for events 1, 2, and 17, since the Λ° decay and the parent event were observed in the same pellicle.

[3]The energy of the π^- meson was estimated from the ionization.

[4]This event has two possible parent events. The energy of the π^- meson was estimated from the ionization.

[5]The parent event (σ_K, ρ_K) was not found.

[6]The mass was determined from multiple scattering and ionization.

One may expect that a juxtaposition of the Λ^0 decays with the parent events will be helpful in the investigation of the diverse types of nuclear interactions associated with the production Λ^0 particles and in the study of the properties of the Λ^0 particles themselves.

The authors express deep gratitude to E. Gerul, Prof. M. Danysz and M. I. Podgoretskii for the statement of the problem and for valuable advice in the course of the work.

*Institute of Nuclear Studies, Warsaw.

†The authors take this opportunity to express gratitude to Prof. Segré for assistance in obtaining the emulsion stack, and to S. Goldhaber for processing the emulsions.

[1] M. Teucher, Suppl. Nuovo cimento **4**, 482 (1956).

[2] George, Herz, Noon, and Solntseff, Nuovo cimento **3**, 94 (1956).

[3] Apparao et al., Suppl. Nuovo cimento **4**, 474 (1956).

[4] Fay, Gottstein and Hain, Suppl. Nuovo cimento **11**, 234 (1954).

Translated by J. Heberle
214

MEASUREMENT OF THE POLARIZATION OF (D + T) — NEUTRONS AT DEUTERON ENERGIES OF 1800 kev

I. I. LEVINTOV, A. V. MILLER and V. N. SHAMSHEV

Academy of Sciences, U.S.S.R.

Submitted to JETP editor January 18, 1958

J. Exptl. Theoret. Phys. (U.S.S.R.) **34**, 1030-1032 (April, 1958)

THE reaction $T(d, n)He^4$ at energy of the deuterons of $E_d = 107$ kev passes through the $3/2^+$ level of the He^5 nucleus, formed by s-deuterons. Consequently, the neutrons obtained at this energy cannot be polarized. At $E_d = 2$ Mev, a significant contribution (about 50%) of the higher states is observed. This is confirmed by the deviation of the total cross section from the Breit-Wigner formula for a single level, and also by the appearance of anisotropy in the angular distribution of reaction products.[1] It is of interest to explain the degree of polarization of the neutrons in this very important reaction.

Measurement of the polarization of (D + T)

neutrons was carried out with the help of a method described previously.[1] In view of the large energy of the neutrons, the pressure of the helium flowing through the proportional counter was raised to 8 — 12.5 atmospheres (depending on the angle of emission of the neutrons from the target). The angular range of the counters was 22°; the cutoff of the discriminator in working measurements amounted to 80% of the cutoff corresponding to the cutoff of pulses from arbitrary collisions of n — He^4.

A thin (~30 kev) tantalum target, saturated with tritium was employed. The apparatus about the target were lightened as much as possible, so that the neutrons in their path to the counter traversed not more than 1 gm/cm^2 of matter. The construction of the target also permitted intense cooling of the target, which made it possible to raise the ion current to 60 μa.

As was shown previously,[2] the worth of this method consists of the complete absence of noise of parasitic pulses from neutrons which do not undergo scattering on the analyzer (helium). In the measurements taken for the reaction D(d, n)He^3,[3] no extraneous pulses were observed. However, in research with neutrons of much higher energy, there arises the danger of the appearance of pulses from α-particles which appear as products of the reaction (n, α) on the walls of the counters. Protons from various (n, p) reactions cannot be registered by the apparatus, since the energy allotted to them in the counters is not sufficient that their pulses be recorded by the amplifier.

A control experiment making evident the extraneous pulses consisted of a rotation of the counters perpendicular to the incident neutron flux. In this case the pulses from nuclei far distant from the helium were absent, since the largest energies from these nuclei, which are recorded in the small angle of rotation of the counter now traversed the counter transversely and entered into its wall, not succeeding in releasing sufficient energy in the gas. The experiment showed that under operation the apparatus registered about 3 — 5% of the extraneous pulses. According to our assumption, these pulses were produced by α-particles from the reaction O^{16}(n, α)C^{13} in the oxygen of the quartz disc which covered the end window of the counter. The presence of this small noise was taken into consideration in the subsequent experiments.

We also verified the possibility of exciting parasitic asymmetry, connected with the non-symmetric location of various pieces of apparatus. This attempt consisted in the measurement of the velocity of counting of the pulses at the upper and lower positions of the counters, and was carried out on a thick tritium target with deuteron energies of 400 kev. In this case the incident part of the neutron flux consisted of neutrons connected with $^3/_2^+$ level of the He^5 nucleus. Such neutrons are unpolarized and, consequently cannot give an azimuthal asymmetry for scattering on helium. As a result of these measurements, it was established that the counting rate in both positions was the same within 0.5%.

It was shown earlier that a strong anisotropy in the angular distribution of the products of the reaction under study for poor geometry of our apparatus noticeably distorts the true azimuthal asymmetry. However, the asymmetry of the angular distribution of neutrons of the reaction D(T, n)He^4 for E_d = 1800 kev does not exceed 30%,[1] and therefore, for calculation purposes the polarization of neutrons was not considered. Computation of the angular distribution can increase the value of the asymmetry several times, and our results must be considered as the lower bound for the polarization of neutrons.

The following data were obtained for the azinuthal asymmetry of scattering R at various angles ϑ_n of emission of the neutrons from the target.

In the Table, we have given only the statistical errors of measurement. The effectiveness of our analyzing apparatus is equal to 0.8 to 0.9. Therefore, the values of R in the Table correspond to the following values of the polarization of the neutrons P_n:

ϑ_n = 45; 67.5; 90; 112.5; 135°

P_n(%) = 7±3; 12±3; 10±3; 2±3; 0±5.

Thus, for E_d = 1800 kev, we observed a noticeable polarization of the (D + T) neutrons. It should be expected that the polarization would increase with increase in the energy of the deuterons. It is especially interesting to determine the

ϑ_n	45°	67.5°	90°	112.5°	135°
Helium pressure (atmos)	12.5	11.3	10.1	8.8	7.1
R	1.12±0.06	1.22±0.08	1.18±0.06	1.03±0.05	1.00±0.08

degree of polarization of the neutrons for deuteron energies of the order of 8 Mev where, according to the data of Galonsky and Johnston,[1] the existence of resonance is assumed, which corresponds to the level of the He^5 nucleus at 22 Mev (probably $D_{5/2}$).

At the present time we are continuing measurements of the polarization of neutrons of the reaction $D(T, n)He^4$ for high energy deuterons.

[1] A. Galonsky and C. H. Johnson, Phys. Rev. **104**, 421 (1957).

[2] Levintov, Miller and Shamshev, J. Exptl. Theoret. Phys. (U.S.S.R.) **32**, 274 (1957); Soviet Phys. JETP **5**, 258 (1957).

[3] Levintov, Miller, Shamshev and Tarumov, J. Exptl. Theoret. Phys. (U.S.S.R.) **32**, 375 (1957); Soviet Phys. JETP **5**, 310 (1957).

Translated by R. T. Beyer
215

SPONTANEOUS RADIATION OF A PARAMAGNETIC IN A MAGNETIC FIELD

V. M. FAIN

Gor'kii Radiophysics Institute

Submitted to JETP editor January 24, 1958

J. Exptl. Theoret. Phys. (U.S.S.R.) **34**, 1032-1033 (April, 1958).

THE problem of spontaneous emission in the radioband was considered in the papers by Dicke[1] and the author.[2,3] It was shown there that if a system of identical quantum objects* that possess two energy levels E_1 and E_2 ($E_1 < E_2$), are situated in a volume, the linear dimensions of which are much smaller than the wavelength, such a system can radiate coherently. The intensity of the radiation of the system may be proportional not to the number of objects, n, but to its square, n^2. States in which the system radiates in proportion to n^2 were called "superradiant." If originally all objects were in the upper energy state then after a time[3]

$$\tau_{r,0} = \ln n / n\gamma_0 \qquad (1)$$

the system goes over into the "superradiant" state. Here γ_0 is the natural line width of one object. After a time $2\tau_{r,0}$ the system goes over into the lower energy state. Here $\tau_{r,0}$ may be sufficiently small.

Using the theory referred to, the following method of exciting electromagnetic radiation by means of a paramagnetic in a magnetic field is proposed.

We place the paramagnetic in a magnetic field. The electrons† of the paramagnetic will then have two energy levels with an energy difference equal to $E_2 - E_1 = \hbar\omega = g\beta H$, where β is the Bohr magneton, g a factor on the order of unity, and H the magnetic field strength. Let the temperature of the paramagnetic be nearly zero (the generalization to the case of finite temperatures is obvious); the magnetic moments of all the electrons are then arranged along the magnetic field. This will be the lowest energy state of the systems. Let us now reverse the direction of the magnetic field. Such a reversal must be sufficiently fast compared to the thermal relaxation time τ and the time $\tau_{r,0}$ of the radiation, and sufficiently slow compared to the period of radiation, $\tau_{rad} = 2\pi/\omega$, i.e., the reversal time τ_H must satisfy the inequalities

$$\tau_H \lesssim 2\tau_{r,0}; \quad \tau_H \ll \tau, \quad \tau_H \gg \tau_{rad}. \qquad (2)$$

After such a reversal, all electrons are in the upper energy state. Let us assume now that the dimensions of the paramagnetic are much smaller than the wavelength of the radiation $\lambda = 2\pi c/\omega$. After a time $\tau_{r,0}$ the system will then go over into the superradiant state. The intensity of the radiation will be equal to

$$I = \omega^4 |\mu_{12}|^2 n^2 / 3c^3, \qquad (3)$$

where μ_{12} is the dipole moment of the transition $1 \rightarrow 2$. It is equal to the Bohr magneton β as far as order of magnitude is concerned.

After the system has radiated, over a period $2\tau_{r,0}$, all the energy, which is equal to $A = n\hbar\omega$, and has gone over into the lower energy state, the magnetic field is reversed anew and the system again starts to radiate.

If we reverse the magnetic field with a frequency $f \approx \frac{1}{2}(\tau_H + 2\tau_{r,0})$ the system will in this way emit an average power on the order of

$$W = n\hbar\omega / (\tau_H + 2\tau_{r,0}). \qquad (4)$$

The peak power must be determined here by Eq. (3).

Let us make some estimates. Let $\omega = 6.3 \times 10^{10}\,\mathrm{sec}^{-1}$ (wavelength $\lambda = 3$ cm) and $n = 10^{17}$ (this is a fully attainable number of electrons in a volume of order $(0.7)^3 \approx 0.35\,\mathrm{cm}^3$). We have then $\gamma_0 \approx |\mu_{12}|^2\omega^3/\hbar c^3 \approx 0.9 \times 10^{-12}$, $2\tau_{r,0} \approx 0.9 \times 10^{-3} \approx \tau_H$, while the average power is equal to $W = 0.7 \times 10^{-3}$ w and the peak power $I \approx 2 \times 10^{-2}$ w.

The line width will be of the order[2,3] $\gamma = n\gamma_0 \approx 10^5\ \text{sec}^{-1}$.

Finally we note that one can use the Stark effect to excite radiation in a similar manner in an electrical field.

The author thanks Professor V. L. Ginzburg for discussing the present paper.

*The role of such objects can be played by molecules in a gas, nuclei or electrons in a paramagnetic, ferromagnetic or ferrite, and so on.

†Below we shall speak about electrons, to fix our ideas, although all this applies equally well to nuclei, ions, and so on.

[1] R. H. Dicke, Phys. Rev. **93**, 99 (1954).

[2] V. M. Fain, J. Exptl. Theoret. Phys. (U.S.S.R.) **32**, 607 (1957), Soviet Phys. JETP **5**, 501 (1957).

[3] V. M. Fain, Usp. Fiz. Nauk **64**, February (1958).

Translated by D. ter Haar
216

SCATTERING OF DEUTERONS BY DEUTERIUM AND TRITIUM AT LOW ENERGIES

Iu. G. BALASHKO and I. Ia. BARIT

P. N. Lebedev Physical Institute, Academy of Sciences, U.S.S.R.

Submitted to JETP editor January 22, 1958

J. Exptl. Theoret. Phys. (U.S.S.R.) **34**, 1034-1036 (April, 1958)

RECENTLY, a remarkable number of measurements were completed on the effective cross sections of the reactions $H_1^3(d,n)He_2^4$ (Ref. 1) and $He_2^3(d,p)He_2^4$, (Ref. 2) which have maximum yield in the low energy region. The experimentally measured values of the cross section are well described by the resonance formula of Wigner and Eisenbud[3] for a single level. In this case, as is to be expected when one starts from the hypothesis of charge invariance, the resonance parameters (obtained from analysis of the reaction) which correspond to the levels of the compound nuclei He_2^5 and Li_3^5 agree within the limits of accuracy with which they are determined. It is natural to expect that the resonance scattering D — T and D — He^3, if the approach of Wigner and Eisenbud is valid for such light nuclei, should be described by the same parameters as the reactions. The scattering of D — He^3 was investigated experimentally by Freier and Holmgren.[4] In the present work, the cross section of D — T scattering was measured at an angle of 90° in the energy interval 30 — 300 kev (center of mass system). In line with this, in the process of working up the method, we measured the scattering cross section of deuterons on deuterium in the energy range for the deuterons from 100 to 600 kev at an angle of 67° in the center-of-mass system. The results obtained for 600 kev agreed with the data of Heydenburg and Roberts.[5]

Utilization of the method possessed certain characteristics which permitted us to complete the measurements at very low energies (down to 70 kev) in the region of resonance of the D — T reaction. The intensity of the beam of bombarding particles was determined by the yield of nuclear reactions which accompany the reaction. In order to be certain of separating the extraneous pulses, coincidences were recorded between the scattered particles and the recoil nucleus. The scattered particles were recorded by proportional counters which were not isolated from the gas target by a small window and were filled, together with the target, to a pressure of 2 — 5 mm of mercury.

The results of the measurement for the D — D scattered are shown in Fig. 1 and those for the D — T scattering in Fig. 2. In both cases, the ratio of the measured cross section to the effective cross section of scattering by a Coulomb field at the same angle is shown.

At small energies, it must be expected that the nuclear D — D scattering will consist of S-scattering in the singlet and quintuplet states. Phase analysis of the data of Eisenbud and Roberts on D — D scattering at 900 kev supports this assumption and allows us to determine the phase for the quintuplet state. This phase essentially determines the scattering cross section.

Measurements of the cross section for a single angle, carried out in the present research, allow only an estimate of the phase in the quintuplet state. The values obtained under the assumption that the phases in both states are the same, corre-

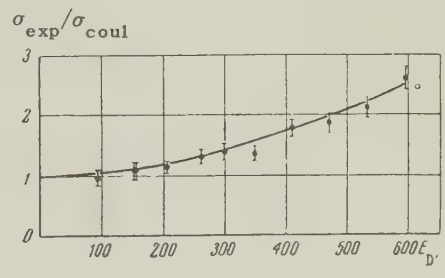

FIG. 1. ● — data of present research; ○ — data of Heydenburg and Roberts.

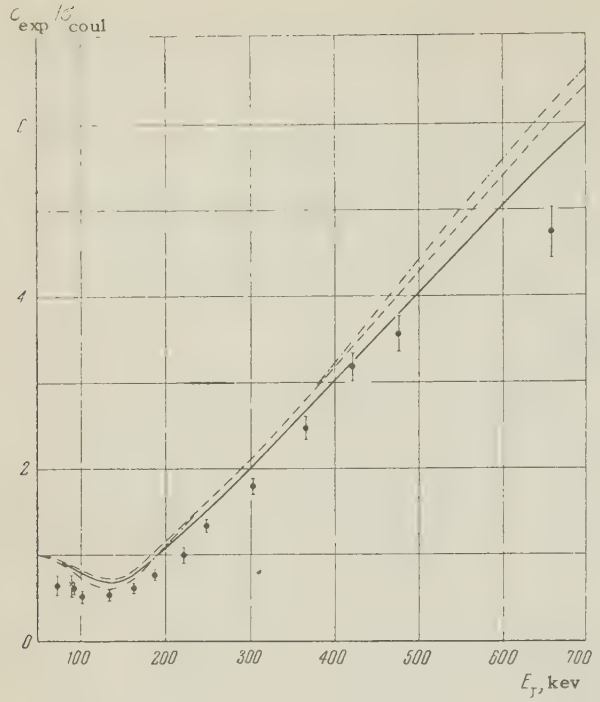

FIG. 2. a – radius of channel, γ_1 – reduced partial width of scattering, γ_2 – reduced partial width of reaction, E_0 – formal resonance energy. Continuous curve: $a = 0.5 \times 10^{-12}$ cm, $\gamma_2 = 2.16 \times 10^{-11}$ kev cm; $E_0 = -444$ kev; dashed curve: $a = 0.7 \times 10^{-12}$ cm, $\gamma_1 = 0.51 \times 10^{-9}$; $\gamma_2 = 1.27 \times 10^{-11}$ kev cm, $E_0 = -130$ kev; dash-dotted curve: $a = 0.7 \times 10^{-12}$ cm, $\gamma_1 = 0.34 \times 10^{-9}$ $\gamma_2 = 1.18 \times 10^{-11}$ kev cm; $E_0 = -55$ kev.

spond to a scattering from an ideally reflecting sphere, surrounded by a Coulomb field, with a spherical radius of 4×10^{-13} cm. The curve is drawn in Fig. 1 for the effective cross section, computed under this assumption. The potential scattering in the quintuplet state is natural, inasmuch as the spins of all the nucleons are parallel in this state.

The character of the dependence of the D – T scattering on the energy in the region of small energies (see Fig. 2) points to the presence of resonance scattering. Computed curves are drawn in the Figure for several values of the resonance parameters, determined from analysis of the reaction. In the computation, potential scattering was also taken into consideration. The experimental values for the cross section of scattering is close to the computed curve; however, it is lower by about 20%.

For energies below 100 kev, the gap between the experimental points and the computed curve is possibly connected with a systematic error in the determination of the energy of the scattered particles. In subsequent research, it is proposed to improve the accuracy of measurements in this region* and to carry out a more detailed analysis of the results with the aim of clarifying the possibility of choice of parameters which would have described equally well both the reaction and the scattering.

*Note added in proof (March 22, 1958). As a result of improving the accuracy of energy measurement of the particles under consideration, we obtained values of 0.98 ± 0.13; 0.79 ± 0.08; 0.63 ± 0.04 corresponding to energies 76, 96 and 140 kev. For high energies, the curve, which we can obtain by means of the experimental points, is not changed.

[1] Argo, Taschek et al., Phys. Rev. **87**, 612 (1952); Conner, Bonner and Smith, Phys. Rev. **88**, 468 (1952); Arnold, Phillips et al., Phys. Rev. **93**, 483 (1954); Davidenko, Pogrebov and Sadukov, Atomic Energy **4**, 386 (1957); Balabanov, Barit et al., Appendix to the journal Atomic energy **5**, 1957).

[2] J. Hatton and G. Preston, Nature **164**, 143 (1949); Bonner, Conner and Lillie, Phys. Rev. **88**, 473 (1952); Arnold, Tuck et al., Phys. Rev. **88**, 159 (1952); Yarnell, Lovberg and Stratton, Phys. Rev. **90**, 292 (1953); W. E. Kunz, Phys. Rev. **97**, 456 (1955).

[3] E. P. Wigner and L. Eisenbud, Phys. Rev. **72**, 29 (1947).

[4] G. Freier and H. Holmgren, Phys. Rev. **93**, 825 (1954).

[5] N. P. Heydenburg and R. B. Roberts, Phys. Rev. **56**, 1092 (1934).

Translated by R. T. Beyer
217

OSCILLATION OF THE ELECTRICAL RESISTANCE OF n-TYPE GERMANIUM IN STRONG PULSED MAGNETIC FIELDS

I. G. FAKIDOV and E. A. ZAVADSKII

Institute of the Physics of Metals, Ural Affiliate, Academy of Sciences, U.S.S.R.

Submitted to JETP editor January 25, 1958

J. Exptl. Theoret. Phys. (U.S.S.R.) **34**, 1036-1037 (April, 1958)

WE have investigated the change in the electrical resistance of three monocrystalline specimens of n-type germanium in a transverse pulsed magnetic field with magnetization up to 120 kG at temperatures of 300, 77 and 20°K.

The magnetic field was produced by the discharge of a condenser stack through a solenoid, in

the opening of which a Dewar was inserted bearing the specimen.

The germanium samples were of different purity and at room temperature (300°K) possessed the following specific resistances: $\rho = 54\,\Omega$ cm (sample No. 1), $\rho = 20\,\Omega$ cm (sample No. 2), and $\rho = 7\,\Omega$ cm (sample No. 3).

In the range of the magnetic field of 25 — 120 kG and at T = 300°K, the dependence of $\Delta R/R_0$ on the field was linear for all three specimens, with a slope of 34×10^{-2}kG^{-1} (No. 1), 1.65×10^{-2}kG^{-1} (sample No. 2) and 1.07×10^{-2}kG^{-1} (sample No. 3). At 77°K, in this same range of fields, the linear dependence of $\Delta R/R_0$ was maintained only for samples 2 and 3; however, the angle of slope of the lines increased in this case. So far as sample No. 1 is concerned, at 77°K, the dependence of $\Delta R/R_0$ on the field, beginning at 25 kG, bore a curvilinear character with a tendency toward saturation; this is seen from the fact that at fields with intensities of 25, 50, 75 and 100 kG, $\Delta R/R_0$ is equal to 2.4; 3.3; 4.6; 5.9, respectively.

The change of the resistance in a magnetic fields $\Delta R/R_0$ of sample No. 1 ($\rho = 54\,\Omega$ cm) was also studied at 20°K in fields up to 110 kG. These measurements gave very interesting results.

When sample No. 1 was at the temperature of liquid hydrogen and the magnetic field was turned on (H = 110 kG), then the resistance of the sample decreased, instead of increasing as it does ordinarily. The magnitude of the decrease in the specific resistance ρ (20°K, H = 0) $-\rho$ (20°K, H = 110) = 670 − 390 = 280 Ω cm. However, the resistance of the sample was reduced in proportion to the decrease in the amplitude of the magnetid field from 110 kG to zero, up to its initial value of ρ (20°K, H = 0).

Moreover, for this sample of n-type germanium ($\rho = 54\,\Omega$ cm), we observed the phenomenon of the oscillation of the electric resistance in the field range from 25 to 110 kG. The period of these oscillations amounted to 0.18 kG^{-1}, while its maximum amplitude was found at a field of H = 55 kG. In the Figure, the dependence of $\Delta R/R_0$ on the reciprocal of the magnetic field intensity is shown for 20°K.

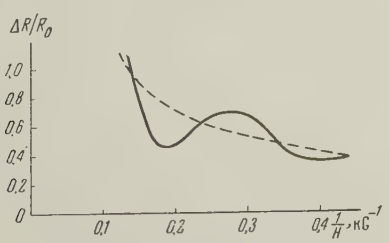

L. Shubnikov and de Haas[1] first discovered the oscillation of the electrical resistance in a transverse static magnetic field, while studying bismuth at low temperatures,[1] and then Frederikse and Hosler,[2] Kanai and Sasaki,[3] and also Busch, Kern and Lüthi,[4] observed this same effect on a specimen of InSb. The latter authors carried out their measurements (as did we) with pulsed magnetic fields.

The theory of the oscillations of galvanometric effects is set forth in the researches of G. E. Zil'berman.[5]

So far as we know, the Shubnikov-de Haas effect has never been observed for germanium up to the present time.

Information on the experimental details and the arrangements for strong magnetic fields will be published in a subsequent paper.

---

[1] L. Schubnicow and W. J. de Haas, Nature **126**, 500 (1930).

[2] H. P. Frederikse and W. R. Hosler, Canad. J. Phys. **34**, 1377 (1956).

[3] Y. Kanai and W. Sasaki, J. Phys. Soc. Japan **11**, 1017 (1956).

[4] Busch, Kern and Lüthi, Helv. Phys. Acta **30**, 471 (1957).

[5] G. E. Zil'berman, J. Exptl. Theoret. Phys. (U.S.S.R.) **29**, 762 (1955), Soviet Phys. JETP **2**, 650 (1956).

Translated by R. T. Beyer
218

ON A FUNCTIONAL RELATION IN QUANTUM MECHANICS

D. A. KIRSHNITS

P. N. Lebedev Physics Institute, Academy of Sciences, U.S.S.R.

Submitted to JETP editor January 30, 1958

J. Exptl. Theoret. Phys. (U.S.S.R.) **34**, 1037-1039 (April, 1958)

WE consider a system of non-interacting particles in a stationary state in some external field with potential $V(\mathbf{r})$.* The density of the number of particles in such a distribution will, generally speaking, be a very complicated function of V and all its derivatives

$$\rho(\mathbf{r}) = \rho(V, \nabla_i V, \nabla_i \nabla_k V \ldots), \qquad (1)$$

where all arguments on the right hand side are taken at the point $\mathbf{r}$.

We shall show below that, independent of the character of the occupation of the levels of the field V, i.e., independent of the statistics and the temperature,† the quantity (1) satisfies the relation

$$D\rho / DV = \partial\rho / \partial V, \tag{2}$$

where the symbol D/DV denotes the Euler derivative,

$$D\rho / DV \equiv \sum_{n=0}^{\infty} (-1)^n \nabla_{i_1} \ldots \nabla_{i_n} \{\partial\rho / \partial (\nabla_{i_1} \ldots \nabla_{i_n} V)\},$$

and $\partial/\partial V$ the derivative with respect to the first argument in (1).

To prove this, we consider first the case of a degenerate Fermi system. The Hamiltonian of a particle has the form, $\hat{H} = \hat{T} - V$, where $\hat{T}$ is the kinetic-energy operator. The density of the number of particles and the kinetic-energy density can be put in operator form,[1,2,3] and the appearance of the gradients of V in (1), is due to the commutators of the operators $\hat{T}$ and V:

$$\rho = \langle \theta (\hat{H} - E_0) \rangle, \quad \mathcal{E} = \langle \theta (\hat{H} - E_0) \hat{T} \rangle, \tag{3}$$

where $\theta(x) = \frac{1}{2}(1 - x/|x|)$, E_0 is the upper bound of the occupied spectrum, and

$$\langle \hat{a} \rangle \equiv (2\pi\hbar)^{-3} \operatorname{Sp} \int d\mathbf{p} \exp(-i\mathbf{pr}/\hbar)\, \hat{a} \exp(i\mathbf{pr}/\hbar).$$

The trace is taken here over the spins and similar variables, and $\hat{a}$ is an arbitrary operator.

Using Eq. (3) and the equation $\langle \hat{a}\delta(\hat{a}) \rangle = 0$ we have

$$\begin{aligned} &\partial [\mathcal{E} - \rho (V + E_0)] / \partial E_0 \\ &= \partial [\mathcal{E} - \rho (V + E_0)] / \partial V = -\rho. \end{aligned} \tag{4}$$

On the other hand, if we transform the equation of the variational principle[4]

$$\delta \int \mathcal{E}\, d\mathbf{r} - \int (V + E_0)\, \delta\rho\, d\mathbf{r} = 0$$

to the functional argument V and take it into account that $\delta \int F d\mathbf{r} = \int (DF/DV)\, \delta V d\mathbf{r}$ for any arbitrary function $F(V)$, we get

$$D [\mathcal{E} - \rho (V + E_0)] / DV = -\rho. \tag{5}$$

If we compare (4) and (5) and take into account the fact that $\partial/\partial V$ and D/DV commute, we are led to the relation (2) which we are trying to prove.

The transition to the case of an arbitrary occupation of the levels, which corresponds to replacing the function θ in Eq. (3) by some other function f, can be realized without difficulty by means of the identity

$$f(\hat{a}) = -\int_{-\infty}^{\infty} f'(\lambda)\, \theta (\hat{a} - \lambda)\, d\lambda.$$

By multiplying both sides of relation (2) by $f'(E_0)$ and integrating over E_0, we can satisfy ourselves that this relation is universally valid.

We shall give as an example the form of the dependence (1), which follows from the Thomas-Fermi model with quantum correction up to the fourth order in $\hbar$ in the degenerate, non-relativistic case.[1,2]‡

$$\begin{aligned} \rho = {} & \frac{1}{3\pi^2\hbar^3} (2MV)^{3/2} - \frac{M^2}{24\pi^2\hbar\, (2MV)^{3/2}} [(\nabla V)^2 - 4V\Delta V] \\ & + \frac{M^4\hbar}{1920\pi^2 (2MV)^{5/2}} \{-64 V^3 \Delta^2 V + 80 V^2 (\Delta V)^2 + 192 V^2 \nabla V \cdot \nabla \Delta V \\ & + 64 (\nabla_i \nabla_k V)^2 V^2 - 200 V \Delta V (\nabla V)^2 \\ & - 240 V \nabla_i V \nabla_k V \nabla_i \nabla_k V + 175 (\nabla V)^4 \}. \end{aligned} \tag{6}$$

The corresponding expression for the case of a finite temperature is of the form (up to terms of the second order in $\hbar$)[2,3]

$$\begin{aligned} \rho = {} & \frac{\sqrt{2} M^{3/2}}{\pi^2\hbar^3} \left\{ \theta^{3/2} I_{1/2}(x) \right. \\ & \left. + \frac{\hbar^2}{24M} [\theta^{-3/2} I''_{1/2}(x) (\nabla V)^2 + 2\theta^{-1/2} I'_{1/2}(x) \Delta V] \right\}; \end{aligned} \tag{7}$$

$$I_{1/2}(x) = \int_0^{\infty} \frac{y^{1/2}\, dy}{\exp(y - x) + 1}, \quad x = \theta^{-1}(V + \mu), \quad \theta = kT,$$

where μ is the chemical potential.

One can easily verify that Eqs. (6) and (7) satisfy, indeed, relation (2). It is important to note that the latter connects only terms of the same order in $\hbar$. In particular, terms of the zeroth order in $\hbar$ satisfy it in a trivial manner.

The relation we have obtained is convenient to use to derive and check the correctness of approximate expressions for the density. The problem whether one can generalize this equation to the case where the interaction V depends on the momentum or on the Dirac matrices, and also whether there exists a similar relation for other quantities (for instance, for the Green function of a particle in an external field) requires a special investigation.

---

*The relation which we obtain below is completely valid also in the case where the interaction between the particles is considered by the Hartree method; we must in that case take for V the sum of the external and the self-consistent field. However, if we take exchange into account, Eq. (2) is violated.

†We restrict ourselves to the case where the number of occupied levels depends on only one energy.

‡Equation (24) of Ref. 1 for the fourth-order corrections contains a mistake, which is corrected in Eq. (6). Corresponding equations for the second-order corrections were also obtained by Kompaneets and Pavlovskii[5] and Golden.[3]

[1] D. A. Kirzhnits, J. Exptl. Theoret. Phys. (U.S.S.R.) **32**, 115 (1957), Soviet Phys. JETP **5**, 60 (1957).

[2] D. A. Kirzhnits, Thesis, Physics Institute, Acad. Sci. (U.S.S.R.), 1956.

[3] S. Golden, Phys. Rev. **105**, 604 (1957).

[4] P. Gombas, Statistical Theory of the Atom (Russian Translation) I L, M., 1951.

[5] A. S. Kompaneets and E. S. Pavlovskii, J. Exptl. Theoret. Phys. (U.S.S.R.) **31**, 427 (1956), Soviet Phys. JETP **4**, 328 (1957).

Translated by D. ter Haar
219

REMARKS ON A NOTE BY F. S. LOS' "PHASE OF A SCATTERED WAVE"[1]

V. V. MALIAROV

Submitted to JETP editor December 16, 1957

J. Exptl. Theoret. Phys. (U.S.S.R.) **34**, 1039-1040 (April, 1958)

LOS' has considered the equation

$$\frac{d^2G}{d\rho^2}+\left[1-\frac{l(l+1)}{\rho^2}-U(\rho)\right]G=0 \qquad (1)$$

and asserts that "it is necessary to find a solution of Eq. (1) which assumes the following form as $\rho \to 0$

$$G = A_0\rho^{l+1} \qquad (2)$$

and the following asymptotic form at large values of ρ

$$G = \text{const}\cdot\sin(\rho-\pi l/2+\delta_l);\quad \delta_l = \text{const}\ldots\text{»} \qquad (3)$$

It should be noted that under the condition $\int_0^\infty U(\rho)\,d\rho < C$, given in the author's note, when $\rho \to \infty$, $G(\rho)$ cannot assume the asymptotic form given in (3). The case $\int_0^\infty |U(\rho)|\,d\rho < C$ is considered in Courant and Hilbert[2] where the same system of equations is obtained, using the method employed by Los'. Equations (6) and (7) given by Los' correspond to Eq. (56) and (57) in Courant and Hilbert.

In Ref. 2, a proof is given for the asymptotic formula (3) which is more detailed than that given in the note by Los'; in this proof it is not shown that $A(\rho) \to$ const. when $\rho \to \infty$ in Eq. (4).

For $\rho \to 0$, Los' has obtained expressions for $\delta(\rho)$ and $A(\rho)$ to which the following remarks apply:

1. It is not meaningful to express $\delta(\rho)$ in terms of $\int_0^\rho \rho\gamma(\rho)\,d\rho$ since in the approximation which is used only the first terms of the series $\gamma(\rho) = \gamma_0 + \gamma_1\rho + \ldots$ should be retained

2. The constant coefficients in (2) and in the expression for $A(\rho)$ are denoted by the same symbol — A_0. These coefficients differ by a factor of $l+1$.

3. Even if these errors are ignored, it should be noted that the title of the note does not reflect its contents.

The use of the supplementary condition (5) is valid for $\rho \to \infty$, when $A(\rho) \to$ const and $\delta(\rho) \to$ const. However, when $\rho \to 0$, in place of (5) any other supplementary condition can be used. The different supplementary conditions correspond to different phases $\delta(\rho)$. The problem becomes indeterminant. By the definition of the phase of a scattered wave it follows that the phase $\delta(\rho)$ found by means of such an additional condition is not the phase of the scattered wave.

Thus, in the form in which it has been published the note given by F. S. Los' is not useful for an analysis of scattering and can only introduce confusion on the part of the reader.

[1] F. S. Los', J. Exptl. Theoret. Phys. (U.S.S.R.) **33**, 273 (1957).

[2] Courant and Hilbert, Methoden der Mathematischen Physik, (Russ. Transl.) 1933, Vol. I, p. 314.

Translated by H. Lashinsky
220

SECOND MOMENT OF THE PARAMAGNETIC ABSORPTION CURVE WHEN THE SPIN MAGNETISM IS NOT PURE

U. Kh. KOPVILLEM

Kazan' State University

Submitted to JETP editor January 21, 1958

J. Exptl. Theoret. Phys. (U.S.S.R.) **34**, 1040-1042 (April, 1958)

IN Refs. 1 — 5, equations were given for the second moment $\langle\nu^2\rangle$ of the curve $f(\nu)$ of paramagnetic absorption in the absence of a static magnetic H_0, and for the second moment $\langle(\Delta\nu)^2\rangle$ of the

curve $\psi(\nu)$ of paramagnetic resonance (ν is the frequency of the variable magnetic field H_t directed along the t-axis). These equations are, however, valid only in the case of absorption in magneto-anisotropic crystals, where the g factor depends strongly on the direction of H_0. The reason for this phenomenon is that when the orbital motion of the electrons is not fully quenched with respect to the intercrystalline electrical field E, the latter changes strongly the character of the internal interactions in the paramagnetic.[6]

We have derived equations for $\langle\nu^2\rangle$ and $\langle(\Delta\nu)^2\rangle$ in magneto-anisotropic crystals which contain only magnetically equivalent ions. We have assumed that for $H_0 = 0$ the energy ground state of magnetic ions possesses a two-fold Kramers degeneracy and that only this doublet is populated. These conditions are, for instance, realized in double nitrates and ethylsulphates of the rare-earth elements at helium temperatures. In our calculations we have found the dependence of $\langle\nu^2\rangle$ and $\langle(\Delta\nu)^2\rangle$ on the direction of H_0 and H_t with respect to the crystal axis, on the spin temperature T, the anisotropic exchange interaction $\mathcal{H}_{\text{exch}}$, the dipole-dipole interaction $\mathcal{H}_{\text{d}}$, and the hyperfine structure interaction $\mathcal{H}_{\text{hfs}}$. Our final equations are expressed in terms of the coefficients of the spin Hamiltonian. This circumstance makes it much easier to evaluate the moments of the $\psi(\nu)$ curves and makes it possible to study the internal interactions in paramagnetics through the plentiful material accumulated recently by paramagnetic resonance methods.[7]

The following is the final expression for

$$\langle(\Delta\nu)^2\rangle = \langle(\Delta\nu)^2\rangle_{\text{d}} + \langle(\Delta\nu)^2\rangle_{\text{exch}} + \langle(\Delta\nu)^2\rangle_{\text{hfs}} + \langle(\Delta\nu)^2\rangle_{\text{d-exch}} \quad (1)$$

for the case where $H_0 \parallel c$ and $H_t \parallel a$, where a, b, and c are the principal axes of the g-tensor; the indices "d", "exch", "hfs", and "d-exch" indicate the contributions to $\langle(\Delta\nu)^2\rangle$ from $\mathcal{H}_{\text{d}}$, $\mathcal{H}_{\text{exch}}$, $\mathcal{H}_{\text{hfs}}$ and the dipole-exchange interactions, respectively:

$$\langle(\Delta\nu)^2\rangle_{\text{d}} = (18Ph^2)^{-1}\sum_{I(\neq j)}\{(B_{aa}^{Ij}+B_{bb}^{Ij})^2K + B_{cc}^{Ij2}D - B_{cc}^{Ij}(B_{aa}^{Ij}+B_{bb}^{Ij})L\}, \quad (2)$$

$$\langle(\Delta\nu)^2\rangle_{\text{exch}} = 2(Ph^2)^{-1}\sum_{I(\neq j)}\{(J_a^{Ij}+J_b^{Ij})^2K + J_c^{Ij2}D - J_c^{Ij}(J_a^{Ij}+J_b^{Ij})L\}, \quad (3)$$

$$\langle(\Delta\nu)^2\rangle_{\text{d-exch}} = \left(\tfrac{3}{2}Ph^2\right)^{-1}\sum_{I(\neq j)}\{(B_{aa}^{Ij}+B_{bb}^{Ij})(J_a^{Ij}+J_b^{Ij})K + B_{cc}^{Ij}J_c^{Ij}D - 0{,}5[B_{cc}^{Ij}(J_a^{Ij}+J_b^{Ij}) + J_c^{Ij}(B_{aa}^{Ij}+B_{bb}^{Ij})]L\}, \quad (4)$$

$$\langle(\Delta\nu)^2\rangle_{\text{hfs}} = (3h^2)^{-1}I(I+1)\textstyle\sum_\nu A_{c\nu}^2, \quad (5)$$

where we have used the notation

$$P = 1 + e^m,\ K = e^m,\ L = 1 + 3e^m,\ m = -g_{cc}\beta H/kT,$$

$$D = 1{,}5 + 2e^m + 0{,}5\,e^{2m},$$

$$J_a^{Ij} = -J^{Ij}B^2,\quad J_b^{Ij} = -J^{Ij}(B^2\cos^2\varphi + F^2\sin^2\varphi),$$

$$J_c^{Ij} = -J^{Ij}(B^2\sin^2\varphi + F^2\cos^2\varphi),$$

$$B_{\alpha\alpha}^{Ij} = -3g_{\alpha\alpha}^2\beta^2 r^{Ij\,(-3)}\left\{\tfrac{3}{2}\gamma_\alpha^{Ij2} - \tfrac{1}{2}\right\},$$

$$B^2 = \langle + - |2S_\xi^I S_\xi^j| - +\rangle,\quad F^2 = \langle + + |2S_\varepsilon^I S_\varepsilon^j| + +\rangle.$$

The superscripts refer here to the particles and the subscripts to the coordinate axes, h· is Planck's constant, k Boltzmann's constant, β the Bohr magneton, $A_{c\nu}$ the components of the tensor of the hyperfinestructure spin interaction of the nucleus with the electrons inside the paramagnetic ion,[8] $g_{\alpha\alpha}$ the components of the g tensor along the α axis, r^{Ij} the radius vector from ion I to ion j, γ^{Ij} the cosine of the angle between r^{Ij} and the α axis (see Ref. 2), ν an index which takes on the values of the principal axes of the tensor $A_{c\nu}$. In deriving Eqs. (3) and (4) it was assumed that the field E has an axis of symmetry ϵ which is a principal axis of the g tensor, like η and ξ. In these equations γ^{Ij} are the usual exchange integrals,[2] $|+\rangle$ and $|-\rangle$ are the correct zeroth order wave functions for the Kramers doublet for the case $H \parallel \epsilon$, φ is the angle between ϵ and H_0, and S is the effective electron spin of the paramagnetic ion. If we put $T = \infty$, $g_{\alpha\alpha} = \text{const}$ in Eq. (2), we obtain the well-known Eq. (11) of Ref. 2 for spin $\frac{1}{2}$. From Eq. (5) we get for $\nu = \alpha$ Eq. (28) of Ref. 4. For $T = \infty$, $g_{\alpha\alpha} = \text{const}$, the contributions (3) and (4) of the exchange interactions vanish, which also agrees with previously obtained results.[2] The lattice sums, which take into account more than 99% of the contribution of all neighbors of the paramagnetic ion in the crystal lattice of the ethyl sulfates of the rare-earth elements, have the values (the symbol $\sum_{I(\neq j)}$ is omitted),

$$B^{Ij2}_{\varepsilon\varepsilon} = 1201 g^4_{\varepsilon\varepsilon}\, d, \quad B^{Ij2}_{\eta\eta} = 514 g^4_{\eta\eta}\, d, \quad B^{Ij2}_{\xi\xi} = 508\, g^4_{\xi\xi}\, d,$$

$$B^{Ij}_{\xi\xi} B^{Ij}_{\eta\eta} = 88 g^2_{\xi\xi} g^2_{\eta\eta}\, d, \quad B^{Ij}_{\eta\eta} B^{Ij}_{\varepsilon\varepsilon} = -603\, g^2_{\eta\eta} g^2_{\varepsilon\varepsilon}\, d,$$

$$B^{Ij}_{\xi\xi} B^{Ij}_{\varepsilon\varepsilon} = -597\, g^2_{\xi\xi} g^2_{\varepsilon\varepsilon}\, d,$$

where the η axis is directed to the nearest neighbor of the paramagnetic ion in the $\xi\eta$ plane which is perpendicular to ϵ, where $d = \beta^4 a^{-6}$, and where a is the largest direction in the elementary cell.[6] For double nitrates of the rare-earth elements[6] $B^{Ij2}_{\epsilon\epsilon} = 32 g^4_{\epsilon\epsilon} d$ and for $H_0 \parallel \epsilon$ we have

$$\langle(\Delta\nu)^2\rangle_d = (18\, Ph^2)^{-1} \sum_{I(\neq j)} \{e^m (x^4 + 3x^2 + 2) + 0.5\, e^{2m} + 1.5 + x^2\} B^{Ij2}_{\varepsilon\varepsilon}, \quad x = g_\perp / g_\parallel, \tag{6}$$

where $g_\perp$ and $g_\parallel$ are the factors of the spectroscopic splitting.

For ethyl sulfates of the rare-earth elements, the term arising from $\mathcal{H}_d$ has the form

$$\langle\nu^2\rangle_d = 4a^{-6}c \{229\, g^4_\perp + \cos^2\psi\,(g^2_\parallel / g^2)(553\, g^4_\perp + 147\, g^2_\perp g^2_\parallel) + \sin^2\psi\,(g^2_\perp / g^2)(101\, g^4_\perp + 534\, g^4_\parallel + 871\, g^2_\parallel g^2_\perp)\},$$
$$c = \beta^4 / 16h^2, \quad g^2 = g^2_\parallel \cos^2\psi + g^2_\perp \sin^2\psi, \tag{7}$$

where ψ is the angle between H_t and ϵ.

In conclusion, the author expresses his thanks to Professor S. A. Al' tshuler for suggesting this topic and considering this paper.

[1] L. J. F. Broer, Physica, **10**, 801 (1943).

[2] J. H. Van Vleck, Phys. Rev. **74**, 1168 (1948).

[3] K. Kambe and J. F. Ollom, J. Phys. Soc. Japan, **11**, 50 (1956).

[4] J. S. van Wieringen, Disc. Faraday Soc. **19**, 118 (1955).

[5] G. Ia. Glebashev, Уч. зап. Казанского гос. ун-та (Scient. Notes, Kazan' State Univ.) **116**, book 1, 121 (1956).

[6] J. M. Daniels, Proc. Phys. Soc. (London) **A66**, 673 (1953).

[7] K. D. Bowers and J. Owen, Repts. Progr. Phys. **18**, 304 (1955).

[8] B. Bleaney and M. C. M. O'Brien, Proc. Phys. Soc. (London) **B69**, 1216 (1956).

Translated by D. ter Haar
221

THERMAL CONDUCTION OF SUPERCONDUCTORS

B. T. GEILIKMAN

Moscow State Pedagogical Institute

Submitted to JETP editor January 27, 1958

J. Exptl. Theoret. Phys. (U.S.S.R.) **34**, 1042-1044 (April, 1958)

THANKS to the presence of a gap in the energy spectrum of superconductors,[1] the number of electronic excitations and hence the electronic thermal conductivity is exponentially small [$\sim \exp(-T_k/T)$] for $T \ll T_k$ (T_k is the temperature of the transition to the non-superconducting state). For $T \ll T_k$ the principal role is therefore played by the lattice thermal conduction, which is connected with the reflection of phonons from boundaries and the scattering of phonons by impurities and lattice defects (the phonon-electron interaction is inappreciable in view of the fact that the number of electronic excitations is very small for $T \ll T_k$), while it is well-known[2] that phonon-phonon interaction does not play a role for $T \ll \Theta_D$, where Θ_D is the Debye temperature).

However, for somewhat higher temperatures, but still appreciably less than T_k, the electronic heat conduction κ_e becomes comparable with the lattice heat conduction and can even exceed it for not very impure specimens. Clearly the largest contribution to κ_e is then given by the scattering of the electrons by impurities. Only for $T \lesssim T_k$ can the interaction of the electrons with the phonons and with one another also play an appreciable role for κ_e.

We consider the scattering of electrons by impurities. Let the Hamiltonian of the interaction of the electrons with the impurity atoms for the normal metal be of the form

$$H' = \sum_{\mathbf{k}} (a^+_{\mathbf{k},\,1/2} a_{\mathbf{k}',\,1/2} + a^+_{\mathbf{k},\,-1/2} a_{\mathbf{k}',\,-1/2}) V_{\mathbf{k},\,\mathbf{k}'}$$

($\frac{1}{2}$ and $-\frac{1}{2}$ are the spin coordinates, and $a_{\mathbf{k},\pm\frac{1}{2}}$ the amplitude in second quantization). According to Ref. 3 the electronic excitations in superconductors can be described by new amplitudes

$$\alpha_{\mathbf{k}0} = u_k a_{\mathbf{k},\,1/2} - v_k a^+_{-\mathbf{k},\,-1/2}; \quad \alpha_{\mathbf{k}1} = u_k a_{-\mathbf{k},\,-1/2} + v_k a^+_{\mathbf{k},\,1/2};$$
$$\left.\begin{matrix} u_k^2 \\ v_k^2 \end{matrix}\right\} = \frac{1}{2}(1 \pm \xi / \sqrt{\Delta^2(T) + \xi^2}); \tag{1}$$

$\xi = (p^2 - p_0^2)/2m \approx v_0(p - p_0)$ is the energy of a

normal electron, reckoned from the Fermi surface ($p = p_0$), and $\Delta(T)$ is the value of the gap in the energy spectrum.

Expressing the $a_{\mathbf{k}}$ in terms of the $\alpha_{\mathbf{k}}$ we find

$$H' = \sum_{\mathbf{k}} (u_k u_{k'} - v_k v_{k'}) (\alpha^+_{\mathbf{k}0}\alpha_{\mathbf{k}'0} + \alpha^+_{\mathbf{k}1}\alpha_{\mathbf{k}'1}) V_{\mathbf{k}\mathbf{k}'}.$$

We have omitted here terms of the kind $\alpha^+_{\mathbf{k}0}\alpha^+_{\mathbf{k}'1}$ and $\alpha_{\mathbf{k}0}\alpha_{\mathbf{k}'1}$, which describe the creation and annihilation of a pair of excitations; these processes are not possible in the case of elastic collisions with impurities. For elastic scattering we have

$$u_k u_{k'} - v_k v_{k'} = u_k^2 - v_k^2 = \xi (\Delta^2 + \xi^2)^{-1/2}.$$

The scattering probability is determined by the equation

$$w_{ab} = \frac{2\pi}{\hbar} |H'|^2_{ab} \rho_E, \quad \rho_E = \frac{p^2 d\Omega}{h^3} \frac{dp}{d\varepsilon}.$$

The energy of an electron excitation ϵ is of the form[1,3] $\epsilon = \sqrt{\Delta^2(T) + \xi^2}$ [$\Delta(T) = 0$ for $T = T_k$], so that $\rho_E \approx d\Omega p_0^2 h^{-3} \epsilon / |\xi| v_0$. We see that for electron excitations in a superconductor the probability of scattering by impurities differs from the scattering probability w_0 in normal metals by the factor $(u_k^2 - v_k^2)^2 = \xi^2/\epsilon^2$ which occurs in $|H'|^2_{ab}$, and by the factor $\epsilon/|\xi|$, which occurs in ρ_E. Thus, $w = (|\xi|/\epsilon) w_0$.

Let us assume that there is a temperature gradient $\partial T/\partial x$ in the superconductor. The electrical field in a superconductor is then, in contradistinction to a normal metal, equal to zero. However, in the equilibrium state the current of the normal component j_n is completely cancelled by the opposing superconducting current j_s ($j = j_n + j_s = 0$) (Ref. 4). We write down the transport equation for the distribution function f of the excitations,

$$\frac{\partial f}{\partial x}\frac{\partial \varepsilon}{\partial p_x} - \frac{\partial f}{\partial p_x}\frac{\partial \varepsilon}{\partial x} = \frac{|\xi|}{\varepsilon}\frac{f_0 - f}{\tau_0};$$

so that

$$\frac{\partial f_0}{\partial \varepsilon}\frac{\varepsilon}{T}\frac{\partial \varepsilon}{\partial p_x}\frac{\partial T}{\partial x} = \frac{|\xi|}{\varepsilon}\frac{f - f_0}{\tau_0}, \qquad (2)$$

where τ_0, the relaxation time for the normal electrons, does not depend on the energy; Ref. 5 gives an expression for τ_0; on the left-hand side, we have substituted for f the equilibrium function f_0; $f_0 = [\exp(\epsilon/\Theta) + 1]^{-1}$ (see Ref. 1); $\Theta = kT$.

From Eq. (2) we can find $f_1 = f - f_0$ and we can evaluate the heat flux

$$Q = 2h^{-3}\int v_x \varepsilon f_1 \, d\mathbf{p}; \quad \varkappa = -Q \Big/ \frac{\partial T}{\partial x} = \frac{2}{3}\frac{p_0^3 \tau_0}{\pi^2 \hbar^3 m} F(T);$$

$$F(T) = \Theta^{-1}\int_{\infty}^{\Delta} \varepsilon^2 \frac{\partial f_0}{\partial \varepsilon} d\varepsilon = \frac{\Delta^2(T)}{\Theta}\left(\exp\left(\frac{\Delta}{\Theta}\right) + 1\right)^{-1} \qquad (3)$$

$$+ 2\Theta \sum_{s=1}^{\infty} (-1)^{s+1} e^{-s\Delta/\Theta}/s^2 + 2\Delta \ln(1 + e^{-\Delta/\Theta});$$

Equation (3) describes satisfactorily the experimental data obtained in Ref. 6. The temperature dependence of $\Delta(T)$ can be found in Ref. 1.

We can estimate the magnitude of the convective heat flux $Q_k = TSv_n = TSj_n/\rho_n$, mentioned in Refs. 4 and 7. Using the expressions for S and ρ_n of Ref. 1, we can easily show that the ratio of Q_k to the normal heat flux Q is of the order of magnitude $k(TT_k)^{1/2}/(p_0^2/m)$, i.e., even for $T \approx T_k$ it is of the order 10^{-5} to 10^{-4}.

In conclusion I want to express my sincere gratitude to L. D. Landau for valuable advice and discussions and to N. V. Zabaritskii for communicating the results of his paper[6] before publication.

[1] Bardeen, Cooper, and Schrieffer, Phys. Rev. **108**, 1175 (1957).

[2] R. Peierls, Ann. Physik. **3**, 1055 (1929); **4**, 121 (1930). R. E. Peierls, Quantum Theory of Solids, Oxford Clarendon Press, 1955.

[3] N. N. Bogoliubov, J. Exptl. Theoret. Phys. (U.S.S.R.) **34**, 58 (1958), Soviet Phys. JETP **7**, 41 (1958).

[4] V. L. Ginzburg, Сверхпроводимость, (Superconductivity) Acad. Sci. Press, 1946, p. 79; J. Exptl. Theoret. Phys. (U.S.S.R.) **21**, 979 (1951).

[5] A. Sommerfeld and H. Bethe, Electron Theory of Metals (Russian translation) ONTI, 1938, p. 227.

[6] N. V. Zavaritskii, J. Exptl. Theoret. Phys. (U.S.S.R.) **33**, 1085 (1957), Soviet Phys. JETP **6**, 837 (1958).

[7] C. J. Gorter, Can. J. Phys. **34**, 1334 (1956).

Translated by D. ter Haar
222

SOVIET TRANSLATION JOURNALS

SUBSCRIPTION AND BACK-NUMBER INFORMATION

THE expanded program of the American Institute of Physics comprises translation of six leading Soviet physics journals, as listed below. These translations, by competent, qualified scientists, provide all research laboratories and libraries with accurate and up-to-date information of the results of research in the U.S.S.R. (For details on editorial content see over.)

Soviet Physics—Technical Physics

A translation of the "Journal of Technical Physics" of the Academy of Sciences of the U.S.S.R. The translation began with the 1956 issues. Twelve issues per year, approximately 3,000 Russian pages. Annually $75.00 domestic, $79.00 foreign. Libraries* $35.00 domestic, $39.00 foreign. Back numbers, all issues $8.00.

Soviet Physics—Acoustics

A translation of the "Journal of Acoustics" of the Academy of Sciences of the U.S.S.R. The translation began with the 1955 issues. Four issues per year, approximately 400 Russian pages. Annually $12.00 domestic, $14.00 foreign. (No library discounts.) Back numbers, all issues $4.00.

Soviet Physics—"Doklady"

A translation of all of the "Physics Sections" of the Proceedings of the Academy of Sciences of the U.S.S.R. The translation began with the 1956 issues. Six issues per year, approximately 1,500 Russian pages. Annually $35.00 domestic, $38.00 foreign. Libraries* $15.00 domestic, $18.00 foreign. Back numbers for Volumes 1 and 2, $5.00 per issue; Volume 3 and subsequent, $7.00 per issue.

Soviet Physics—JETP

A translation of the "Journal of Experimental and Theoretical Physics" of the Academy of Sciences of the U.S.S.R. The translation began with the 1955 issue. Twelve issues per year, approximately 4,000 Russian pages. Annually $75.00 domestic, $79.00 foreign. Libraries* $35.00 domestic, $39.00 foreign. Back numbers, all issues, $8.00.

Soviet Physics—"Crystallography"

A translation of the journal "Crystallography" of the Academy of Sciences of the U.S.S.R. The translation began with the 1957 issues. Six issues per year, approximately 1,000 Russian pages. Annually $25.00 domestic, $27.00 foreign. Libraries* $10.00 domestic, $12.00 foreign. Back numbers, all issues $5.00.

Soviet Astronomy—AJ

A translation of the "Astronomical Journal" of the Academy of Sciences of the U.S.S.R. The translation began with the 1957 issues. Six issues per year, approximately 1,100 Russian pages. Annually $25.00 domestic, $27.00 foreign. Libraries* $10.00 domestic, $12.00 foreign. Back numbers, all issues $5.00.

Subscriptions should be addressed to the American Institute of Physics, 335 East 45th Street, New York 17, N.Y.

---

* For libraries of non-profit degree-granting academic institutions.

INFORMATION ON CONTENTS OF SOVIET TRANSLATION JOURNALS

J. Exptl. Theoret. Phys. The leading physics journal of the Soviet Union. It is edited by Peter Kapitza and is similar to the Physical Review in standards, quality, and range of topics. The articles are about evenly divided between theoretical and experimental, and all represent reports of new research. Outstanding new work in physics is most likely to appear in this journal.

Acoustics Journal. This journal is devoted exclusively to acoustics, principally physical acoustics. Much smaller amounts of electro acoustics, bio- and psycho acoustics are included. Many of the articles are quite mathematical, but experimental work is also covered. The major emphasis is on pure research, rather than on applications.

J. Tech. Phys. Edited by the solid state physicist A. F. Ioffe, this journal has become the primary vehicle for publications on semi-conductors and solid state work in general. The journal also covers a range of topics similar to the AIP Journal of Applied Physics. As an example of coverage, a recent issue contained articles on interface problems, high pressure physics, thermoclastic phenomena, OHF oscillations, telemetric systems, studies of dielectric materials, rupture and creep problems, and diffraction problems involving electromagnetic waves.

Doklady. This is an all-science journal which gives four-page reports of recent new research. Up through 1957, we have translated only articles labeled "physics" by the Journal. Beginning in 1958, however, we shall translate all articles in borderline physics as well. These latter are roughly equal in number to those in "physics" and include such fields as biophysics, crystallography, astronomy, mathematical physics, geophysics, technical physics, hydraulics, elasticity, and oceanography.

Astronomical Journal As the title suggests, this journal covers various problems in astronomy, including solar activity, stellar studies, spectro metric investigations and radio astronomy. The journal is one of over thirty years standing.

Crystallography Journal. This relatively new journal, now in its third volume, publishes both experimental and theoretical papers on crystal structure, lattice theory, diffraction studies, effects of external influences (including radiation damage) on crystalline structure and all other topics of interest to the crystallographer.